

Research Report 6 =

Modern sedimentation and late quaternary evolution of the Magela Creek Plain

Edited by R J Wasson

Supervising Scientist for the Alligator Rivers Region

Supervising Scientist for the Alligator Rivers Region

RESEARCH REPORT 6

MODERN SEDIMENTATION AND LATE QUATERNARY EVOLUTION OF THE MAGELA CREEK PLAIN

Edited by R J Wasson

Australian Government Publishing Service Canberra 1992 Commonwealth of Australia 1992

ISSN 0810-9966 ISBN 0 644 25456 4

The Supervising Scientist for the Alligator Rivers Region manages the Alligator Rivers Region Research Institute, which conducts, coordinates and integrates research relating to the effects on the environment of mining in the Alligator Rivers Region. Research findings of projects carried out under contract to the Supervising Scientist or undertaken by the Supervising Scientist's own staff may be published in the Research Report or Technical Memorandum series. Views expressed by authors do not necessarily reflect the views and policies of the Supervising Scientist, the Commonwealth Government or any collaborating organisation.

This work is copyright. Apart from any use as permitted under the Copyright Act 1968 (Cwlth), no part may be reproduced by any process without written permission from the Director, Publishing and Marketing, Australian Government Publishing Service. Inquiries should be directed to the Manager, AGPS Press, Australian Government Publishing Service, GPO Box 84, Canberra ACT 2601.

Printed in Australia for AGPS by NTU Printing/Publishing Services, Darwin, NT.

MODERN SEDIMENTATION AND LATE QUATERNARY EVOLUTION OF THE MAGELA CREEK PLAIN

Edited by:

R.J. Wasson

Division of Water Resources, CSIRO

With Contributions by:

R.L. Clark

R. Cull

Division of Water Resources, CSIRO

Division of Water Resources, CSIRO

Division of Water Resources, CSIRO

OSS

J. Guppy Division of Water Resources, CSIRO

G. Hancock OSS A. Johnston OSS

F.R. Leaney Division of Water Resources, CSIRO D.A. Mahon Division of Water Resources, CSIRO

R. Marten
OSS
P. Martin
OSS
P. McBride
OSS
A.S. Murray
OSS
B. Noller
OSS
J. Pfitzner
OSS

R.F. Warner University of Sydney

R.J. Wasson Division of Water Resources, CSIRO

I.R. Willett Division of Soils, CSIRO

CONTENTS

Authors listed alphabetically

List of Tal		vii
List of Fig	ures	х
Acknowled	lgements	xx
Abstract		xxi
Preface (T	.J. East, R.J. Wasson)	xxvii
Chapter 1.	Introduction (T.J. East, R.J. Wasson)	1
1.1	Background to this Report — Uranium Mine Rehabilitation	1
1.2	The Geomorphology Feasibility Study	2
1.3	Aims the Present Report	2 2 3 7
1.4	Physical Environment of the Magela Creek Catchment	3
1.5	Seasonal Dependence of the Vegetation	7
1.6	Summary	8
Chapter 2.	The Magela Creek Sediment System (R.F. Warner, R.J. Wasson)	16
2.1	Introduction	16
2.2	Conceptualisation of the Magela Creek Sediment System	16
2.3	Landforms of the Magela Plain	17
2.4	Summary	22
	Late Quaternary Stratigraphy of the Magela Plain (R.L. Clark, J. Guppy, A. Johnston, F. Leaney, P. McBride, R.J. Wasson)	28
3.1	Introduction	28
3.2	Stratigraphic Units	28
3.3	Chemical Properties	31
3.4	Radiocarbon Dating of the Stratigraphic Units	33
3.5	Thorium-Radium Dating in the Mudginberri Corridor	34
3.6	Pollen Analysis and Biostratigraphy	44
3.7	Summary	47
_	. Late Quaternary Evolution of the Magela Plain (R.L. Clark,	
J. Guppy,	D. Mahon, P. McBride, R.J. Wasson)	81
4.1	Introduction	81
4.2	The Stratigraphic Cross-sections	81
4.3	Vegetation History and Implications for Geomorphic	
	Development of the Plain	85
4.4	Geomorphic Evolution of the Magela Plain	89
4.5	Accumulation of the Dark Brown/Black Clay	93
4.6	Environmental Variations during Deposition of the Dark	
	Brown/Black Clay	95
4.7	Palaeoclimate and Change on the Magela Plain	100
4.8	Prediction of Future Climate in the Magela Catchment	106
4.9	The Patterned Ground in the Upstream Basin	107
4 10	Summary	108

Chapter 5.	Soil Materials and their Formation on the Magela Plain (T.J.	
East, B. No	oller, I. Willett)	158
5.1	Introduction	158
5.2	Major Soil Features and Types	159
5.3	Factor Analysis	160
5.4	Down Profile Variation in Factors and Chemical Properties	163
5.5	Spatial Distribution of Factors in Soils of the Plain	164
5.6	Summary	167
Chapter 6.	. Past, Present and Future Sedimentation on the Magela Plain	
	Catchment (R. Cull, G. Hancock, A. Johnston, P. Martin, R.	
Martin, A.	S. Murray, J. Pfitzner, R.F. Warner, R.J. Wasson)	226
6.1	Introduction	226
6.2	Suspended Sediment Loads	226
6.3	A Sediment Budget for the Magela Plain	229
6.4	Determination of Sediment Sources and Sinks using 137Cs	230
6.5	Determination of Sediment Sources and Sinks using U and Th	
	Series Radionuclides	235
6.6	Radionuclide Concentrations in Total and Filterable Samples	
	from Flood Water — Evidence of Sediment Sources, Sinks and	
	Residence Times	237
6.7	Particle Size of Modern Alluvia	238
6.8	A Preliminary Sediment Budget for the Catchments of the	
	Mine Site Tributaries	240
6.9	Quantities of Tailings Reaching the Magela Plain	243
6.10	Pattern of Deposition of Tailings on the Plain	243
6.11	Summary	245
Chapter 7.	Chemical Transformations of Metals in Mixtures of	
Tailings an	d Soil Materials from the Magela Plain (I. Willett	269
7.1	Introduction .	269
7.2	Chemical Properties of Ranger Uranium Mine Tailing	269
7.3	Chemical Transformations of Metals Applied as Tailings	
	under Unsaturated Conditions	271
7.4	Chemical Transformations of Metals Applied as Tailings to	
	Soils Undergoing Saturation and Drying	274
7.5	Summary	276
Chapter 8.	Future Impact on the Magela Plain of Sediment Derived from	
	Site — Summary of Major Conclusions (R.J. Wasson)	300
8.1	The Project Reconsidered	300
8.2	Summary of Conclusions Relevant to Tailings Management	300
8.3	Conclusions Relevant to the Physical and Biological	700
0.3	Environment of the ARR	305
8.4	Concluding Remarks	305
0.4	Concluding itematics	J00
References		307

LIST OF TABLES

Table 2.1	Landform subdivisions (or compartments) of the Magela sediment system	23
Table 3.1	List of sites sampled by either drilling or pit digging for stratigraphic purposes	49
Table 3.2	Summary of chemical characteristics of the stratigraphic units of the Magela Plain at cross-sections	52
Table 3.3	Summary of ¹⁴ C results from MX Pits 1 and 2, Mudginberri Corridor, Cross-section 1	54
Table 3.4	Results of comparison of alkali soluble and insoluble fractions	54
Table 3.5	Results from Pit MX3, Mudginberri Corridor, Cross- section 1	54
Table 3.6	Magela Plain Carbon-14 data	55
Table 3.7	Concentrations (with respect to ash weight) of ²³⁰ Th and ²²⁶ Ra in sub-samples of sediment collected at site MX1	57
Table 3.8	Concentrations (with respect to ash weight) of other long- lived radionuclides in sub-sample sediment collected at site MX1	5 7
Table 3.9	Ratios of the concentrations of selected radionuclides in sub-samples of sediment collected at MX1	58
Table 3.10	Statistical summary of radionuclide concentrations and concentration ratios for site MXI	58
Table 3.11	Results of sedimentation rate and initial excess radium at sites MX1 and MX2	59
Table 3.12	Concentrations (with respect to ash weight) of ²³⁰ Th and ²²⁶ Ra in sub-samples of sediment collected at site MX2	59
Table 3.13	Concentrations (with respect to ash weight) of other long- lived radionuclides in sub-samples of sediment collected at site MX2	60
Table 3.14	Ratios of the concentrations of selected radionuclides in sub-samples of sediment collected at site MX2	60
Table 3.15	Statistical summary of radionuclide concentrations and concentration ratios for site MX2. Samples below 35 cm have been excluded from all analyses.	61

Table 4.1	Heights (AHD) of major stratigraphic boundaries based on pollen	110
Table 4.2	Proportion of major components in the Dark Brown/Black Clay and Grey Clay	112
Table 4.3	Fluxes to the Plain of major sedimentary components	113
Table 4.4	Number of microfossils observed in Magela PPI samples	114
Table 4.5	Concentration of microfossils observed in Magela PP1 samples	116
Table 4.6	Number of microfossils observed in Magela MV1 samples	118
Table 4.7	Concentrations of microfossils observed in MV1 samples	120
Table 4.8	Major pollen taxa, including aquatic macrophytes, in P Pit 1	122
Table 4.9	Spectral peaks recorded in a variety of phenomena	122
Table 4.10	Major correlations of the ENSO phenomenon	123
Table 5.1	Summary description of Grey Clay soils of floodplains of the Alligator Rivers Region (Hooper 1969)	171
Table 5.2	Means for horizons of factor loadings and chemical properties	172
Table 5.3	Varimax-rotated factor score pattern	174
Table 5.4	Squared multiple correlation coefficients (SMCs) and Kaiser's measure of sampling adequacy ((MSAs) (unrotated matrix)	174
Table 5.5	Summary of soil chemistry factors and sedimentary environments occurring at each cross section of the plain	175
Table 6.1	Least squares equations relating sediment loads to discharges	248
Table 6.2	Best estimates of average annual suspended sediments loads in the ARR	248
Table 6.3	Comparison of suspended sediment loads (in tonnes/y) calculated by different methods	249
Table 6.4	Major elements of the sediment budget for the Magela Plain	249
Table 6.5	Concentrations of ¹³⁷ Cs on topographic high points to estimate the atmospheric input	250
Table 6.6	Radionuclide concentrations at sites chosen for variability tests	250

Table 6.7	Particle size distribution of landforms on a cross-section of Magela Creek at the upstream end of Mudginberri Billabong	250
Table 6.8	Sedimentation rates (mm yr ⁻¹) estimated for various parts of the Magela Plain	251
Table 7.1	Summary of SEM-EDX analyses of tailings particles	278
Table 7.2	Chemical properties of Ranger Uranium Mine Tailings	279
Table 7.3	Properties of the soils of the Magela Plain used in experiments 1 and 2	279
Table 7.4	Effects of tailings additions on total metal concentrations (experiment 1): means of duplicates (mg kg ⁻¹)	280
Table 7.5	Total element concentrations in tailings in comparison with four Magela soils	281
Table 7.6	Main effects of tailings on metal fractions: means of duplicates (mg kg ⁻¹)	281
Table 7.7	Main effects of time of incubation on metal fractions: means of duplicates (mg kg ⁻¹)	282
Table 7.8	Total and exchangeable ²²⁶ Ra in tailings amended soils after 4 months of reaction: means of 2 duplicates	282
Table 7.9	Effects of tailings on total metal concentrations, experiment 2: means of duplicates (mg kg ⁻¹)	283
Table 7.10	Main effects of soil saturation on metal fractions, experiment 2 (mg kg ⁻¹)	283
Table 7.11	Effects on exchangeable ²²⁶ Ra of saturated and unsaturated incubation of soils amended with 4% tailings: experiment 2	283

LIST OF FIGURES

Figure 1.1	Location map of the Alligator Rivers Region, showing Kakadu National Park and the Arnhem Land Aboriginal	
	Reserve	9
Figure 1.2	Map of the Ranger Mine Site	10
Figure 1.3	Perspective view of a proposed artificial landform containing tailings, waste rock and BOGUM	11
Figure 1.4	The catchment divide, drainage network and escarpments in the Magela Creek catchment	12
Figure 1.5	Geologic map, partially morphostratigraphic, of the Magela Creek catchment	13
Figure 1.6	Summary of key climatic and hydrologic variations in the Magela Creek catchment	14
Figure 1.7	Mean weekly water surplus at Oenpelli	15
Figure 1.8	Daily rainfall at Jabiru airport and stage hydrographs for the 1978/1979 Wet season for gauging stations located at Mudginberri Homestead (GS 018) and at gauges downstream of the Magela Plain	15
Figure 2.1	Magela catchment drainage net, major sub-catchments and major locations	24
Figure 2.2	Long-profiles of the Magela Plain showing the general level of Low Plain and High Plain	25
Figure 2.3	Geomorphic map of the Magela Plain showing both topographic and landform units, and locations of stratigraphic cross-sections and drill holes	26
Figure 2.4	Idealised cross-section of the Magela Plain, using realistic elevations and shapes, to illustrate the landform units mapped in Figure 2.3	27
Figure 3.1	Longitudinal section of the Magela Plain from just upstream of Mudginberri to the East Alligator River then downstream along the East Alligator Flood Plain showing the distribution of five stratigraphic units approximately along the centreline of the Plain	62
Figure 3.2	Longitudinal pattern of variation of the Cl content of three stratigraphic units of the Magela Plain	63
Figure 3.3	Longitudinal pattern of variation of the organic carbon content of three stratigraphic units of the Magela Plain	63

Figure 3.4	Relationship between pyrite sulfur (S_{py}) and organic carbon in four stratigraphic units of the Magela Plain, averaged for each cross-section	64
Figure 3.5	Carbon Fourteen (14 C) ages plotted against δ^{13} C for all dated samples from the Magela Plain	65
Figure 3.6	Variation with depth of the concentrations of selected long-lived radionuclides in sediment samples at site MX1	66
Figure 3.7	Variation with depth of the ratio of the concentrations of selected long-lived radionuclides in sediment samples at site MX1	66
Figure 3.8	Variation with depth of the ²²⁶ Ra excess in sediment samples at site MX1	67
Figure 3.9	Variation with depth of the concentrations of selected long-lived radionuclides in sediment samples at site MX2	68
Figure 3.10	Variation with depth of the ratio of the concentrations of selected long-lived radionuclides in sediment samples at site MX2	68
Figure 3.11	Variation with depth of the ²²⁶ Ra excess in sediment samples at site MX2	69
Figure 3.12	Correlation between concentrations of ²³⁸ U and ²³⁰ Th in sediment samples from sites MX1 and MX2	70
Figure 3.13	Correlation between concentrations of ²⁸⁰ Th and initial concentrations of ²²⁶ Ra in sediment samples from both sites	70
Figure 3.14	Variation with time of the initial concentration of ²²⁶ Ra in the second sediment component at sites MX1 and MX2	71
Figure 3.15a	The modern vegetation of the Magela Plain with samples from tributary arms that might not be directly affected by Magela water, or that are most affected by local inflows	72
Figure 3.15b	Mean concentration of various pollen types in surface samples at 0.5, 1 or 2 km intervals along the Plain	73
Figure 3.16	Distribution of dominant pollen taxa in surface samples	74
Figure 3.17	Distribution of Barringtonia and Pandanus pollen in surface samples	75
Figure 3.18	Distribution of sites where terrestrial (woodland) taxa dominate surface pollen assemblages	76
Figure 3.19	Percentage of Myrtaceae pollen in relation to the distance of sample sites from the nearest tree of Melaleuca spp	77
Figure 3.20	Longitudinal distribution of the ratio of unidentifiable total pollen in surface samples	77

Figure 3.21	Total pollen and spore concentration versus unidentifiable and unknown pollen concentrations	78
Figure 3.22	Pollen count versus number of identified pollen taxa	79
Figure 3.23a	Lithology and dominant pollen groups for core M8 from near Jabiluka Billabong	80
Figure 3.23b	Biogenic silica fractions from the M8 core	80
Figure 4.1a	Lithostratigraphy and biostratigraphy of cross-section 1	124
Figure 4.1b	Key to the symbols used in Figure 4.1a and 4.2 to 4.11	125
Figure 4.2	Lithostratigraphy and biostratigraphy of cross-section 2	126
Figure 4.3	Lithostratigraphy and biostratigraphy of cross-section 3	127
Figure 4.4	Lithostratigraphy and biostratigraphy of cross-section 4	128
Figure 4.5	Lithostratigraphy and biostratigraphy of cross-section 5	129
Figure 4.6	Lithostratigraphy and biostratigraphy of cross-section 6	130
Figure 4.7	Lithostratigraphy and biostratigraphy of cross-section 7	131
Figure 4.8	Lithostratigraphy and biostratigraphy of cross-section 8	132
Figure 4.9	Lithostratigraphy and biostratigraphy of cross-section 9	133
Figure 4.10	Lithostratigraphy and biostratigraphy of cross-section 10	134
Figure 4.11	Lithostratigraphy and biostratigraphy of cross-section 11	135
Figure 4.12	Lithostratigraphy and biostratigraphy for sites M5, M10 and M12	136
Figure 4.13	Isometric, pseudo-perspective, diagrams showing cross- sections 1 to 11 arranged with respect to elevation (AHD) and distance from Mudginberri	137
Figure 4.14	Stratigraphy, pollen concentration and relative pollen content of the top sections of cores MV2 and M8, with sample depths and the major vegetation/depositional environments indicated	138
Figure 4.15	Ternary diagrams presenting changes in percentages of three groups of pollen taxa and all non-mangrove taxa	139
Figure 4.16	Enlargement of part of the ternary diagrams in Figure 4.15 showing samples in transition phase b with their depths in centimetres in cores MV2 and M8	140
Figure 4.17	A longitudinal section of the Magela Plain showing the major sedimentary environments	141

Figure 4.18	mangrove forest sediments and the 'basal samples' of Woodroffe et al. (1986)	141
Figure 4.19	Age-distance plot of the sedimentary environments of the Magela Plain, projected onto a longitudinal section	142
Figure 4.20	Height-distance plot of the mean ground surface, the base of the Dark Brown/Black Clay, the base of the transition zone and various isochrons	142
Figure 4.21	Palaeogeographic map at 3.5 ka showing the major sedimentary environments then in existence	143
Figure 4.22	Palaeogeographic map at 2.5 ka showing the major sedimentary environments then in existence	144
Figure 4.23	Depth profiles of sites on the Magela Plain showing organic content and bulk density	145
Figure 4.24	Flux to the Magela Plain of detrital mineral sediment and biogenic silica	146
Figure 4.25	Lithostratigraphic diagrams of selected sites on the Magela Plain showing the various kinds of pale layers and their most likely correlations	146
Figure 4.26	Site P Pit 1 on cross-section 2, showing lithostratigraphic subdivisions, colours determined on dry samples, bulk density, particle size and organic C determined by the Walkley-Black method	147
Figure 4.27	Atomic ratios of the major constituents of the organic matter in site P Pit 1, calculated to remove the effect of variations in the amount of organic matter in each sample 147	
Figure 4.28	Site P Pit 1 showing dithionite-citrate and pyrophosphate extractable A1, A1 _D and A1 _p respectively	148
Figure 4.29	Site P Pit 1 showing siliceous microfossil mass % and concentrations, calculated on an organic matter free basis	148
Figure 4.30	Site P Pit 1 showing the major pollen taxa and groups plotted in different ways and an indication of the amount of charcoal in the sediments	149
Figure 4.31	Site P Pit 1 showing: (a) the index VI; (b) the ratio of numbers of siliceous microfossils per gram and organic C content, reduced to an arbitrary scale of 0 - 10; (c) the residuals of the ratio from the linear least squares curve in b, with associated uncertainties; (d) VI plotted against per cent aquatic macrophyte pollen calculated on a Myrtaceae pollen free basis to remove the effect of long-lived plants; (e) VI plotted against per cent Poaceae pollen, also calculated to exclude Myrtaceae pollen.	149
	calculated to eveline Murineana Dollan	1/14

Figure 4.32	Site MC15A showing: a log of colour variations, loss-on- ignition and the proportion of biogenic silica and detrital mineral sediment	150
Figure 4.33	Site MV2/MV1, adjacent cores on cross-section 3	151
Figure 4.34	Site MV1 showing the index VI and the quantity of total siliceous microfossils/organic C	152
Figure 4.35	Palaeoenvironment records for the last 6 ka	152
Figure 4.36	A: Temperature records from central England and New Zealand, B: Supersecular variation in the energy of the secular wave, C: ¹⁴ C content of tree rings, D: the index BS/C for site P Pit 1 on the Magela Plain	153
Figure 4.37	A: BS/C in P Pit 1. B: 618O and an approximate temperature scale obtained from an ice core from Law Dome in East Antarctica. C: New Zealand temperature record. D: Solar activity envelope. E: Glacier advances and retreats in New Zealand.	154
Figure 4.38	Top: New Zealand temperature record, Bottom: Cumulative number of El Niño events since 1523 AD	155
Figure 4.39	Map of the Upstream Basin showing the pattern of ridges and troughs and orthogonals to this pattern which are flow lines	156
Figure 4.40	Trench 1 through a trough and a ridge in the Upstream Basin on cross-section 2	157
Figure 4.41	Trenches 1, 2, 3 and pits dug into ridges and troughs across cross-section 2	157
Figure 5.1	Cross-section of traverse 1 showing soil horizons	176
Figure 5.2	Cross-section of traverse 2 showing soil horizons	177
Figure 5.3	Cross-section of traverse 3 showing soil horizons	178
Figure 5.4	Cross-section of traverse 4 showing soil horizons	179
Figure 5.5	Cross-section of traverse 5 showing soil horizons	180
Figure 5.6	Cross-section of traverse 6 showing soil horizons	181
Figure 5.7	Cross-section of traverse 7 showing soil horizons	182
Figure 5.8	Cross-section of traverse 8 showing soil horizons	183
Figure 5.9	Cross-section of traverse 9 showing soil horizons	184
Figure 5.10	Cross-section of traverse 10 showing soil horizons	185
Figure 5 11	Cross-section of traverse 11 showing soil horizons	186

Figure 5.12	Relationships between factor loadings and soil chemical properties with depth for profile JB3	187
Figure 5.13	Relationships between factor loadings and soil chemical properties with depth for profile NB2	188
Figure 5.14	Relationships between factor loadings and soil chemical properties with depth for profile NB1	189
Figure 5.15 Figure 5.16	Relationships between factor loadings and soil chemical properties with depth for profile LP3 Loadings of factors 1 and 2 for the B horizons of soils of the Magela Plain	190
Figure 5.17	Loadings of factors 1 and 2 for the A horizons of soils of the Magela Plain	192
Figure 5.18	Loadings of factors 3 and 4 for the jarositic horizons of soils of the Magela Plain	193
Figure 5.19	Loadings of factors 3 and 4 for the slightly oxidised pyritic clays of the Magela Plain	194
Figure 5.20	Loadings of factors 3 and 4 for the unoxidised pyritic clays of the Magela Plain	195
Figure 5.21	Loadings of factors 1 and 5 for the slightly oxidised pyritic clays of the Magela Plain	196
Figure 5.22	Loadings of factors 1 and 5 for the unoxidised blue-grey pyritic clays of the Magela Plain	197
Figure 5.23	Loadings of factors 1 and 2 for soils of the East Alligator Flood Plain	198
Figure 5.24	Loadings of factors 1 and 2 for soils of the Downstream Plain	199
Figure 5.25	Loadings of factors 2 and 5 for soils of the East Alligator Flood Plain	200
Figure 5.26	Loadings of factors 2 and 5 for soils of the Downstream Plain	201
Figure 5.27	Loadings of factors 3 and 4 for soils of the Upstream Basin	202
Figure 5.28	Loadings of factors 3 and 4 for soils of the East Alligator River Flood Plain	203
Figure 5.29	Factor loadings in relation to cross-section 1	204
Figure 5.30	Factor loadings in relation to cross-section 2	205
Figure 5.31	Factor loadings in relation to cross-section 3	206
Figure 5 32	Factor loadings in relation to cross-section 4	207

Figure 5.33	Factor loadings in relation to cross-section 5	208
Figure 5.34	Factor loadings in relation to cross-section 6	209
Figure 5.35	Factor loadings in relation to cross-section 7	210
Figure 5.36	Factor loadings in relation to cross-section 8	211
Figure 5.37	Factor loadings in relation to cross-section 9	212
Figure 5.38	Factor loadings in relation to cross-section 10	213
Figure 5.39	Factor loadings in relation to cross-section 11	214
Figure 5.40	Loadings of factors 1 and 2 for soils of the Upstream Basin	215
Figure 5.41	Loadings of factors 1 and 2 for soils of the Central High	216
Figure 5.42	Loadings of factors 2 and 5 for soils of the Upstream Basin	217
Figure 5.43	Loadings of factors 1 and 2 in soils of the Marginal Depressions	218
Figure 5.44	Loadings of factors 1 and 2 in soils of the East Alligator River Flood Plain	219
Figure 5.45	Loadings of factors 3 and 4 in soils of the East Alligator Flood Plain	220
Figure 5.46	Loadings of factors 3 and 4 in soils of the Low Plain	221
Figure 5.47	Loadings of factors 3 and 4 in soils of the Backslopes	222
Figure 5.48	Loadings of factors 2 and 5 in soils of the East Alligator River Flood Plain	223
Figure 5.49	Loadings of factors 2 and 5 in soils of the Backslopes	224
Figure 5.50	Summary of mean factor loadings according to factor and classified by Geographic unit, Landform unit and Horizon	225
Figure 6.1	Specific sediment yield versus catchment area for sites in the Alligator Rivers Region	252
Figure 6.2	Compartment model of the Magela Plain and Catchment showing mean annual fluxes of suspended sediment	253
Figure 6.3	¹³⁷ Cs fallout at Brisbane, shown as both cumulative and annual fallout, corrected to 1985 for radioactive decay	254
Figure 6.4	Australian Geographic Grid and outline of the Magela Plain showing the points sampled for ¹³⁷ Cs measurements	255

Figure 6.5a	Longitudinal profiles of ¹³⁷ Cs activity concentration at 0- 25 cm	256
Figure 6.5b	Longitudinal profiles of ¹⁸⁷ Cs activity concentration at 25 and 35 cm	256
Figure 6.6a	Longitudinal profiles of total bulk density between 0 and 25 cm	257
Figure 6.6b	Longitudinal profiles of total bulk density between 25- 35 cm	257
Figure 6.7	Longitudinal profiles of 137 Cs areal activity density (Bq/m ²) between 0 and 35 cm, averaged as in Fig 6.5	258
Figure 6.8	Variation of the concentrations of uranium series radionuclides in unfiltered water from Magela Creek at 019 during the flood of 19-21/2/85	259
Figure 6.9	Radionuclide concentrations in the sediments of the Magela Creek and Plain as a function of distance downstream and upstream from the arbitrary datum of the sampling grid	259
Figure 6.10	Fraction of sediment, derived from Magela Creek, deposited at various distances from the arbitrary datum, derived from $f(x)$ in Figure 6.9	260
Figure 6.11	Particle size fractions in surface sediments for a cross- section of Gulungul Creek and Magela Creek at Sandy Crossing	260
Figure 6.12a	The <1 μ m particle size fractions for 0-2 cm averaged for northings on the Plain	261
Figure 6.12b	The <2 μ m particle size fractions for 0-2 cm averaged for northings on the Plain	261
Figure 6.13a	The 1-2 μm particle size fractions for 0-2 cm averaged for northings on the Plain	262
Figure 6.13b	The 2-63 μm particle size fractions for 0-2 cm averaged for northings on the Plain	262
Figure 6.14a	The 63-125 μ m particle size fractions for 0-2 cm averaged for northings on the Plain	263
Figure 6.14b	The >125 μ m (b) particle size fractions for 0-2 cm averaged for northings on the Plain	263
Figure 6.15	Map of the Mine Site tributaries and catchments showing the subcatchments most likely to first receive tailings	264
Figure 6.16	Relationships, calculated using simplifying assumptions, showing the dependence upon catchment area of the sediment delivery ratio and sediment storage within catchments	265

Figure 6.17	Calculated relationships between catchment area and sediment yield, channel erosion, total slope erosion and slope storage for the Mine Site catchments	265
Figure 6.18	Sediment budget, depicted as a box model for the Gulungul Creek Catchment	266
Figure 6.19	Calculated curves for Coonjimba Creek, Djalkmarra Creek, Georgetown Creek, Gulungul Creek and the total Mine Site tributaries, showing the relationship between the time taken for total erosion of the tailings and the proportion of tailings that will occur in sediment leaving the Mine Site streams	267
Figure 6.20	Calculated curve showing the variation of the mass of tailings delivered to the Magela Plain each year as the total erosion time increases	267
Figure 6.21	Mass (t/2 km long strip of Plain) of Magela Creek sediment, the minerogenic sediment flux (g/cm ² /y) on the Plain, and flux of Magela Creek sediment to the Plain (g/cm ² /y) at various distances from the arbitrary datum at Mudginberri Billabong	268
Figure 6.22	Calculated curves showing the proportion of tailings in surface Plain sediments at various distances along the Plain for a range of total erosion times	268
Figure 7.1	Examples of a SEM micrograph of tailings and diagram to show the distribution of dominant heavy metals determined by EDX	284
Figure 7.2	Changes in the distribution of copper fractions with time of reaction	285
Figure 7.3	Effects of tailings on soil pH	286
Figure 7.4	Changes in the distribution of iron fractions with time of reaction	287
Figure 7.5	Changes in iron fractions in soil MVPA during incubation	288
Figure 7.6	Changes in manganese fractions with time of reaction	289
Figure 7.7	Changes in lead fractions with time of reaction	290
Figure 7.8	Changes in uranium fractions with time of reaction	291
Figure 7.9	Changes in zinc fractions with time of reaction	292
Figure 7.10	Soil redox potential and pH after 60 days of either unsaturated or saturated conditions	293
Figure 7.11	Effects of saturation on copper fractions and their distribution	294

Figure 7.12	Effects of saturation on iron fractions and their distribution	295
Figure 7.13	Effects of saturation on manganese fractions and their distribution	296
Figure 7.14	Effects of saturation on lead fractions and their distribution	297
Figure 7.15	Effects of saturation on uranium fractions and their distribution	298
Figure 7.16	Effects of saturation on zinc fractions and their distribution	299

ACKNOWLEDGEMENTS

The authors and editor wish to acknowledge the assistance of the following people and institutions:

John McCartnie, Ninon Geier, Heinz Buettikofer, Narelle Dittmer, Colin MacIntosh, Geoff Pickup, Grahaem Chiles, Gary Caitheon, Jim Beattie, Mark Henry, Tony Milnes, Adrian Beech, Carl Shaw, Catriona Turley, Bruce Thom, Shelly Templeman, Bill Neiji, Jimmy Wok Wok, Kate Duggan, Max Finlayson, Bruce Bailey, Ross Rowe, Colin Woodroffe, Gerald Nanson, NT Power and Water Authority, National Mapping Authority, Bureau of Meteorology, NT Department of Mines and Energy, ANSTO, CSIRO Divisions of Soils and Water Resources, Ranger Uranium Mines, ANPWS, Northern Land Council, Gagadju Association, NT Conservation Commission.

ABSTRACT

CONCLUSIONS RELEVANT TO TAILINGS MANAGEMENT FROM RANGER URANIUM MINE

SEDIMENTATION

A sediment budget and routing model has been developed to estimate both the mass and proportion of tailings that might arrive on the Magela Plain in each average year over various time periods after erosion of the tailings has begun. The proportion of tailings in the mixture of sediment passing Mudginberri in each future year is a function of the total time taken to erode the tailings. At a rate close to the natural long-term denudation rate, the tailings would constitute less than 1% of the present-day level of suspended sediment passing Mudginberri. As the total erosion time decreases, the proportion of tailings in sediment reaching the Plain increases. If the total erosion time is ≤ 1800 years, then tailings will be $\geq 50\%$ of the sediment reaching the Plain. The impact of deposition in the Plain's catchment, under conditions of either catastrophic erosion of the tailings or (more likely) slow erosion, has not been assessed in this study.

A sediment budget shows that sedimentation rates on the Plain are approximately constant within large uncertainties using ≤ 3 years of measured suspended sediment loads. The budget further shows that the catchments adjacent to the Plain are of equal importance with Magela Creek as sources of sediment. The pattern of particle size fractions in surface sediments of the Plain supports the conclusion that sediments derived from Magela Creek do not dominate the Plain, although this analysis is confounded by large quantities of silt-size biogenic silica.

By far the most convincing demonstration of the contribution to the Plain of sediment derived from Magela Creek comes from the use of radionuclides of the natural U and Th series. Disequilibrium between ²³⁸U and ²²⁶Ra in modern stream sediments carried by Magela Creek is mirrored in the sediments of the upstream part of the Plain. The presence of disequilibrium in the surface sediments marks the area where sediment carried by Magela Creek, rather than smaller streams adjacent to the Plain, is deposited. It is clear that 90% of Magela Creek sediment is deposited upstream of Jabiluka Billabong, in an area of about 30 km², or about 15% of the Plain. The rest of the Plain's surface sediment comes from other catchments. This conclusion is consistent with the major disjunction between the upstream and downstream parts of the Plain, defined by biogenic silica and organic content of surface sediments, soil chemistry and morphology.

A sediment routing model is derived from ≤ 3 years of measurements. The radionuclide disequilibrium, upon which is based the identification of the pattern of deposition of Magela Creek sediments, has been found in sediments no more than ~140 years old. The predictions are likely to apply only to future conditions like those of today and the last two centuries, unless confidence in extrapolation can be gained by showing that the sedimentary system of the Plain has been stable for many centuries to millennia. The sedimentation rate over the entire Plain has been shown to be approximately constant at about 0.2 mm y⁻¹. This figure holds for time periods from 0.003 to 3.3 ka, implying considerable stability within the relative uncertainties of 6 to 19%.

Extrapolation of sedimentation rates on the Plain, and application of the predicted tailings dispersal, may be appropriate for the next 1000 years, but only if sea level, climate and the sediment delivery system do not change markedly.

IMPACT OF CLIMATE AND SEA LEVEL CHANGES

The most likely futures for the Plain, against which it might be possible to judge the applicability of the predicted patterns of tailings dispersal are:

If the Earth warms with rising atmospheric greenhouse gases the ocean will expand and some glacial ice could melt, raising sea level by between 20 and 140 cm by about the middle of next century. At the same time, the Australian monsoon is likely to intensify, and the Wet season duration and rainfall will increase. Although by no means certain, ENSO may behave as it has during previous warm periods, and so the frequency and intensity of tropical cyclones is likely to increase.

Sedimentation rates on the Plain are not very sensitive to climate change, as shown by their near constancy over a wide range of time periods during which climate change has been detected. If large cyclones are more frequent, however, the tailings may be eroded more rapidly than would be the case under current conditions.

But the Plain is sensitive to changes of sea level, as shown by detailed stratigraphic studies. Absolute sea level is not the only factor that controls the distribution of saline vegetation and sedimentary environments. Connection to tidal channels is just as important, at least for small shifts in the level of the sea. Although not precise, the best prediction is that a sea level rise would reconnect the old tidal channels of the Downstream Plain and possibly the Central High. But it seems highly unlikely that the Upstream Plain would be connected to tidal flows. The Central High, first established between 3 and 2 ka, may offer some resistance to tidal inundation of the Upstream Basin. However, a rise of sea level of several metres, brought about by melting of ice sheets, would inundate the entire Plain.

The Holocene sequence of change from mangrove forest sediments to transition conditions to freshwater sediments is not the inevitable sequence that is to be expected in reverse if sea level rises in the future. The sequence recorded in the sediments is the combined result of a sea level rise and climate change. Estimates of future sea level rise indicate a rate between 0.06 cm y⁻¹ and 2.3 cm y⁻¹. The range 0.06 to 0.15 cm y⁻¹ seems most likely, a rate 13 to 5 times slower than the post-glacial sea level rise of 0.8 cm y⁻¹ during the period 8-6.5 ka. Although the sedimentary sequence deposited on the Plain in the future will not necessarily mirror the sediments of the last 6 ka, because of differences of climate, the relatively slow rate of sea level rise will almost certainly allow time for the establishment of transition-like vegetation and sedimentary environments.

2. Within the next 5 ka the Earth should begin to feel the effects of the next glacial as small insolation variations begin the process of cooling that has repeated itself every ~100 ka for the last 700 ka or so. Within the next 5 ka sea level lowering, as glaciers grow, will probably be a few metres at most. It is possible that some shallow incision of the Plain could occur under these conditions, although this is not likely given the very low gradients of the area. A fall of sea level is likely to follow the superinterglacial which a doubling of atmospheric CO₂ will bring about.

Within the next 1 ka, the period during which any tailings impoundment at Ranger must retain its integrity and protect the tailings from erosion of any kind, the most likely climatic change will be the result of the Greenhouse Effect. It seems highly unlikely that the first effects of the next glacial will be felt in this period.

If global emissions of CO₂ are reduced so that the atmospheric concentration stabilises at twice its pre-industrial value, sea level will probably rise but by less than 1 m. The area of

Magela Plain most likely to receive tailings, or other Mine Site detritus, namely the Upstream Plain and Mudginberri Corridor, will probably not be connected to the sea. Furthermore, this area of the Plain will be some 20 ± 13 cm higher in 1000 years as a result of continuing freshwater sedimentation.

It can be concluded that tailings dispersal on the Plain probably will not be affected by a mild Greenhouse Effect, either by a change of sea level or by climate change directly, other than by the effect of increase cyclone activity on the total time of tailings erosion.

PREDICTABILITY OF CLIMATE AND EXTREME EVENTS

At the natural denundation rate for the tailings dam, there is little evidence that the Plain's biota would be affected by tailings deposition. This is a strong argument for building the tailings impoundment to mimic the natural landscape.

Climatic changes over millennia are relatively slow and seem to be driven by variations of solar insolation, caused by changes in orbital geometry of the solar system, and modulated by CO₂ and the oceans. At shorter time scales, variations of solar output are important, along with volcanic eruptions and changes to oceanic circulation. While these relationships are becoming clear as research proceeds, none of them is strictly periodic and therefore predictable over the next 1000 years.

It is likely, however, that the next 1000 years will include another warm period like the Medieval Warm Period, superimposed on the warming resulting from the Greenhouse Effect. Warm periods are likely to be associated with a more positive Southern Oscillation Index and so are likely to be accompanied by more intense and frequent tropical cyclones. The calculation of the return period of intense rainstorms, caused by tropical cyclones, for the next 1000 years based upon the observations of this century is obviously a hazardous exercise in the face of the almost certain changes just predicted.

The sediments of the Plain do not hold a record of extreme events.

ECOLOGICAL AND GEOCHEMICAL IMPACT OF TAILINGS DEPOSITION

Following massive erosion, deposition of tailings would cause serious problems in the Mine Site catchments for plants and animals, and would have aesthetic implications. Under the more likely conditions of slow erosion of the tailings, the most important effect on the biota will be by mobilisation of metals from tailings.

The heavy metals left in the tailings, after the extraction processes of the mill, occur as inclusions of minerals in silicate fragments and as minerals of the kind found in or near the ore bodies. These metals are in relatively stable forms and are unlikely to be readily mobilised if mixed with soil materials. Sequential extraction of metals from the tailings showed that sulfides of Pb, Cu and Fe were mobilised in the oxidisable fraction, suggesting that, in the long term, the metals occurring as sulfides could be mobilised under oxidising conditions. The reducing agent extracted some Mn, Cu and Pb, suggesting that these elements would be mobilised if added to saturated soils.

Experiments to determine metal transformations in mixtures of tailings and soils were carried out using the major soil material types of the Plain: two varieties of Dark Brown/Black Clay, and one sample each of the jarositic horizon, and the pyritic mud. These soil material types were chosen because they represent the materials most likely to be exposed to tailings. The Dark Brown/Black Clay is the most likely recipient of tailings during the next 1000 years. If the level of the sea rises substantially, however, there is no material currently on the Plain that can represent the pedologically unaltered transition sediments that are likely to accumulate and also receive tailings. In the unlikely

circumstance that sea level falls sufficiently within the next 1000 years to allow incision of the Plain, the jarositic and pyritic materials may receive tailings and so have been included in the experiments.

The tailings have concentrations of Mn, Pb, U and ²²⁶Ra higher than any of the soil materials chosen for the experiments. These metals are therefore the most likely to increase in concentration if tailings reach the Plain. Assuming that the tailings will erode at about the natural long-term denudation rate, then 0.4% of tailings will occur in each average year's load of sediment reaching the Plain. This proportion of tailings in any of the soil materials increases only the Pb and ²²⁶Ra concentration in mixtures of soil and tailings.

Assuming a total erosion time of the tailings of 5×10^4 years, a rate 3.5 times faster than the long-term natural rate, then the Plain's surface sediments should consist of on average 4% tailings. All metals, apart from Zn, increased in their concentrations in the mixtures in all soil materials when 4% tailings was added. The pollution potential of the tailings is highest for Pb and 226 Ra, and lowest for Zn.

Pyrite oxidation appears to produce more changes to the forms of metals than the addition of tailings. There is greater potential for metal mobilisation from native sources of metals within the pyritic mud than from those added as tailings. It is concluded that, up to a concentration of 4% tailings, the effects on the forms of metals is small, and less than that found during pyrite oxidation.

²²⁶Ra in mixtures of tailings and soil materials is either mobilised or immobilised according to the organic content of the soil material. In highly organic material, ²²⁶Ra is mobilised and remains in an exchangeable and hence a bio-available form. Radium is most likely to be available in the first 10 km of the Plain, that is as far as Mine Valley Billabong. Further downstream, availability should fall rapidly.

If sea level rises sufficiently to re-establish tidal connections on the Downstream Plain and Central High, then it is likely that the Upstream Basin will be more poorly drained. The period of inundation of the Basin will increase, aided by a longer Wet season, and aquatic macrophytes will probably become more common. The acid sulfate process will only operate if the water table falls far enough to allow oxygen to penetrate to the pyritic substratum. This oxidation will be less frequent if the length of the period of inundation increases, and so the rate of chemical and mineralogic differentiation, both vertically and horizontally, will decrease.

Given that most changes to the forms and hence bio availability of metals in soil material of the Plain occurs as a result of oxidation of pyrite, a decrease in the rate of this process will slow the release of metals to the interstitial waters. The Al content of the future part of the Dark Brown/Black Clay will probably be lower than it is in existing sediment of this unit.

It is probable that at the natural long-term rate of denundation the tailings would make an undetectable impact on turbidity on the Plain.

CONCLUSIONS RELEVANT TO THE PHYSICAL AND BIOLOGICAL ENVIRONMENT OF THE ARR

The most important conclusions of this report relevant to the general understanding of the natural and human history of the ARR, but not strictly relevant to the problem of sediment management, are:

- 1. The freshwater wetland of the Magela Plain in approximately its current form, appeared between 1500 and 1000 years BP as the influence of the post glacial sea level rise waned, sediment derived from upstream capped the Plain, and climate became slightly wetter.
- 2. The wetlands of the Magela Plain type are seen by many as pristine, affected only by the Asian water buffalo. Yet, the appearance of these wetlands appears to have been the stimulus to a dramatic increase in the population of Aborigines in the vicinity of the Magela Creek and South Alligator River, as judged from the great increase in the number of sites occupied (Jones 1985).
- 3. The wetlands provided resources for many more people who, in their turn, appear to have begun to influence the Plain by burning it, as judged from the large increase in charcoal about half-way through its history. The Asian water buffalo arrived towards the end of this rise in numbers of Aborigines. The idea that a pristine, old and stable wetland was shocked by the arrival of water-buffaloes late in its life is not supported by the evidence. Nor is the often quoted link between species rich ecosystems, such as the Magela Plain, and antiquity.
- 4. The stimulus to human population growth over the last I ka or so has already been described, but there is now the opportunity to make much more detailed comparisons between the history of the Plain as a source of food and natural resources, and human history recorded in archaeological sites. It is also possible to check and fine-tune Chaloupka's (1984) reconstruction of the sequence of rock art in Kakadu National Park.

PREFACE

Two uranium mines are presently operating in the Alligator Rivers Region (ARR) of the Northern Territory, an area broadly defined by the catchments of the East, South and West Alligator Rivers. They are the Ranger Uranium Mine at Jabiru East and Queensland Mines' Nabarlek Mine. Additional major uranium orebodies are located in the Region at Jabiluka and Koongarra. A significant gold and platinum prospect had been proposed for development at Coronation Hill within a Conservation Zone in Stage Three of Kakadu National Park. The Region is rich in cultural and natural resources, and conflict exists between land uses including habitation by traditional Aboriginal landowners, conservation of terrestrial and aquatic ecosystems, tourism, mining, recreation and scientific research.

The special nature of the Region was recognised by the Australian Government in the 1970s with the setting up of a public environmental enquiry (Fox et al. 1976, 1977) into the proposed Ranger project. One of the essential environmental protection measures in the recommendations of the Ranger Uranium Environmental Inquiry (RUEI) was the establishment of the Office of the Supervising Scientist for the Alligator Rivers Region (OSS), set up under the Environment Protection (ARR) Act 1978. The OSS, through the Alligator Rivers Region Research Institute (ARRRI), independently and in collaboration with other agencies, undertakes and promotes research relevant to both the environmental effects of mining operations in the Region and the minimisation of these effects after decommissioning and rehabilitation.

Environmental regulations applying to the Ranger and Nabarlek Mines were introduced to ensure the highest practicable standards of environmental protection. The decommissioning of uranium mines in the region presents a unique set of problems with the potential for environmental consequences far into the future. These problems are mainly associated with the long term stabilisation of large quantities of solid rock material, including radioactive mill tailings, waste rock and below ore-grade uranium material (BOGUM).

Rehabilitation of the waste rock and tailings at Ranger will give rise to artificial landforms square kilometres in area. The presence of long lived radionuclides in these materials means that tailings impoundments and stabilised waste rock dumps will need to resist erosional forces for some thousands of years. A program of research at the ARRI seeks to identify and quantify geomorphic processes relevant to the siting, engineering design and formulation of performance standards for tailings impoundments and other stabilised earth and rock structures, so as to minimise their long-term impact on the environment. In the medium to long-term it is likely that sediment will be eroded from these structures and will be deposited downstream. This report presents the results of one of the studies that aims to predict the likely dispersal patterns, deposition rates and chemical alteration of this eroded sediment under climatic conditions both like those of the present and those that can be reasonably predicted for the next 1000 years.

T.J. East and R.J. Wasson

CHAPTER 1. INTRODUCTION

1.1 BACKGROUND TO THIS REPORT — URANIUM MINE REHABILITATION

Decommissioning of uranium mines in the Alligator Rivers Region presents problems of rehabilitation with long-term environmental consequences. These consequences could include the degradation of downstream ecosystems by sediment eroded and transported by runoff from rehabilitated earth and rock structures and, possibly in the longer term, of radiological hazards to humans through the erosion and dispersal of radioactive mill tailings.

The mill tailings (the crushed ore from which the uranium has been extracted) contain most of the radioactivity of the original ore-body and have special containment requirements. The longest lived major residual isotope is ²³⁰Th with a half-life of about 80 000 years, so the tailings will contain significant quantities of radioactive materials for some hundreds of thousands of years. Because of their low specific activity, tailings do not constitute an acute radiological risk. To produce significant human health risks would require exposure in the vicinity of a tailings pile over many years. However, their large volume, their potential mobility by wind and water, and the persistence of the risk means that they should, as far as practical, be isolated from the environment. Measures should be taken to prevent prolonged human contact with the tailings. Tailings piles at other mines have been abandoned after mining and left unprotected from wind and water erosion. For example, at the old Northern Hercules Mine at Moline near Pine Creek about 60 000 tonnes of radioactive tailings were eroded and deposited on flood plains at least 8 km downstream after earth bunds were breached in the early 1970s (Pickup et al. 1987; East et al. 1988). The management standards at that mine are no longer acceptable and the tailings will need to be buried or otherwise contained in a structure engineered to survive long-term climatic influences, erosion, and weathering.

There are presently two operating uranium mines in the Alligator Rivers Region, with additional major uranium and gold deposits available for development. Ranger Uranium Mines Ltd. is currently mining the Ranger deposit near Jabiru on Magela Creek, the major left bank tributary of the East Alligator River (Fig. 1.1). It is the larger of the two operating mines, containing a total of some 125 000 tonnes of U_3O_8 at an average grade of 0.3%. At Nabarlek, a high grade uranium deposit was completely mined out and stockpiled in 1979, with milling planned for completion by 1989. The tailings were returned to the pit during milling and are presently undergoing rehabilitation by dewatering, consolidation and capping with a multilayered earth and rock cover. Mining proposals for major uranium deposits at Jabiluka, adjacent to the Magela Creek flood plain, and at Koongarra on Nourlangie Creek in the South Alligator River catchment await Commonwealth Government approval. A gold and platinum deposit had been proposed for development at Coronation Hill within Stage Three of Kakadu National Park but the Government has determined that this shall not proceed.

Mining of Orebody No. 1 at Ranger (Fig. 1.2) will produce approximately 10 million tonnes of tailings by the end of 1991. There will be approximately 28 million tonnes of waste rock and very low grade ore (VLG) which will require stabilisation at this time. Current rehabilitation designs proposed by Ranger show that the stabilised waste rock and low grade ore dumps, together with a tailings impoundment (either above or below ground level), could form an artificial landform some two square kilometres in area and 20 metres high. The current proposal is that mining of Orebody No. 3 will be complete in c. 2012 AD. The combined mass of tailings, waste rock and VLG from both orebodies would comprise an artificial landform some 5 km² in area and 20 m high (Fig. 1.3).

One of the Commonwealth's requirements for mining at Ranger is that mill tailings be returned to the pits within 5 years of the end of mining. The possibility of above-grade

containment, such as the stabilisation of the tailings in the existing tailings dam (Fig. 1.2), is allowed for in the Commonwealth Environmental Requirements if the Supervising Scientist is satisfied that the environment will be no less well protected than by transferring the tailings to the mine pits. Above-grade containment also requires the agreement of the Northern Land Council and Ranger. In either case, the capping on the tailings impoundment must protect the tailings from erosion and mass failure for a long period of time.

Containment of uranium mill tailings in Australia is required by the Code of Practice on the Management of Radioactive Wastes from the Mining and Milling of Radioactive Ores (1982). This Code was formulated under the provisions of the Environmental Protection (Nuclear Codes) Act 1978, and Guidelines are developed, as appropriate, to supplement the Code. Under these Guidelines, the 'long-term' nature of tailings containment is defined in terms of a 'design life' and a 'structural life'. A containment structure should achieve a 'design life' of at least 200 years, the period for which the structure is expected to perform fully in accordance with the objectives of its design. The 'structural life' should be not less than 1000 years and is that period over which the structure essentially retains its integrity and during which it is capable of performing the functions of the design, albeit to a reduced extent. It would be expected, for example, that erosion and mass movement of tailings would not be possible during the structural life of the containment. Such performance has not previously been required of engineered earthen structures, particularly in the case of mine rehabilitation.

The stabilisation of large quantities of low level radioactive materials over such time scales in the seasonally-wet tropics presents special problems. A pronounced Dry season with a depleted vegetation cover is followed by often high intensity Wet season rainfall, with the potential for high rates of erosion on disturbed landscapes.

The rehabilitated site and structures at the Ranger mine following decommissioning will almost certainly be characterised by erosion rates higher than are currently occurring on surrounding undisturbed landforms. Increased turbidity and sediment loads could have significant impact on downstream ecosystems. In the longer term there are potential radiological hazards to humans through the dispersion of tailings, mobilised either through the long term erosion of impoundment covers, or by the seepage from impoundments, or by massive failure of the containment. Mines will contribute to the planning for both the design of rehabilitated earth and rock structures and the setting of performance standards for rehabilitated structures (e.g. water quality of runoff).

1.2 THE GEOMORPHOLOGY FEASIBILITY STUDY

In August 1982 a brief was issued by the OSS, commissioning the design of a program of geomorphic research. The objective of the program was to design research projects that would assist the OSS in providing advice on the final method of management and disposal of uranium mill tailings at Ranger. These projects were to identify and, if possible, quantify the geomorphic processes operating or likely to operate in the Alligator Rivers Region, which will be important in choosing this management strategy.

The report of the feasibility study was submitted in May 1983. Minor editing of the report occurred in May 1986 (Pickup et al. 1987).

1.3 AIMS OF THE PRESENT REPORT

The aims of this research project are the result of amalgamation and reconstruction of several projects designed by Pickup et al. (1987). The aims, with detailed justification, are set out in the document which established the collaborative project between OSS and CSIRO. In summary, this project aims to:

- 1. Document and explain the evolution of the Magela Plain downstream of Mudginberri, including sedimentation, vegetation history and pedogenesis, to provide a framework for the substantive aims that follow.
- 2. Describe the nature and quantify the rate of change of sedimentation and vegetation during the last few millennia as a guide to future change both on the Plain and at the Mine Site.
- Identify contemporary sediment transmission zones and sinks to predict likely deposition patterns of sediment eroded from the Mine Site under current climatic conditions.
- 4. Determine the behaviour of tailings reacted with materials of the Plain to predict the mobility of metals in sediments eroded from the Ranger Mine Site under current climatic conditions.
- 5. Estimate likely sediment dispersal patterns and the mobility of metals under plausible future climatic conditions.

These aims form part of a larger effort by ARRI to assess the environmental risk of erosion of the tailings containment structure; that is, to try to predict the rate of erosion of material from the rehabilitated mine site, where the eroded material will end up, and what its environmental and public health consequences might be. Such an assessment requires an estimate of the probability of erosion on the Mine Site, an understanding of the routing of sediment from the Mine Site to the Magela Plain, an estimate of the bioavailability of the pollutants in the sediment, and an assessment of the biological and human health consequences of any sediment deposited in the Plain. This project contributes to answering this question, and therefore belongs to that part of the research program of OSS concerned with Transport Processes, as set out by Riley (1983).

1.4 PHYSICAL ENVIRONMENT OF THE MAGELA CREEK CATCHMENT

The Magela Creek catchment has an area of 1565 km² at the point where it becomes a tidal channel and joins the East Alligator River (Fig. 1.4). The streams of the catchment drain into a plain that is inundated during the Wet season. This, the Magela Plain, is continuous with the flood plain of the East Alligator River. The Ranger Mine lies some 15 km upstream of this Plain.

LANDFORM IN RELATION TO GEOLOGY

Most of the Magela Creek catchment is underlain by rocks of Archaean or Early Proterozoic age (Needham 1984). The Proterozoic rocks form part of the Pine Creek Geosyncline which stretches from slightly west of Darwin to a little east of Oenpelli. The Archaean rocks form the basement to this geosynclinal sequence.

The Archaean Nanambu Complex consists of gneiss, granite, pegmatite, schist and quartzite. The next youngest unit recognised in the catchment is the Cahill Formation, an Early Proterozoic sequence of quartzofeldspathic and mica schist, quartzite, carbonate, and carbonaceous schist. Stratigraphically younger Early Proterozoic rocks of the Nourlangie Schist (quartz and mica schist) and the Koolpin Formation (chert-banded pyritic carbonaceous siltstone and schist with dolomitic lenses) also occur in the catchment (Fig. 1.5).

Either after or near the end of Early Proterozoic sedimention, sills of Zamu Dolerite (metadolerite and amphibolite) were emplaced. The Oenpelli Dolerite (olivine dolerite, quartz dolerite, granophyric dolerite) was emplaced shortly afterwards as a number of

lopoliths. A major period of erosion then occurred, removing 1-2 km of rock in ~50 Ma (R.S. Needham, pers. comm). The lopoliths were relatively resistant to this erosion and formed ridges. Over this irregular surface was deposited the Kombolgie Formation during the Carpentarian. The primary lithologies of this Formation are sandstone, pebbly sandstone, conglomerate, siltstone, with interbedded tuff, rhyolite and ignimbrite.

Since the deposition of this relatively flat-lying sequence there has been chloritisation of both the Kombolgie and Early Proterozoic rocks close to uranium orebodies. Some downfaulting of the Kombolgie Formation has also occurred. The area has not experienced major tectonism for more than 1000 Ma. An escarpment was cut in the Kombolgie Formation, forming sea cliffs during the Early Cretaceous in Arnhem Land. Marine sediments veneered the Proterozoic and Archaean rocks that had once again been exposed as the Kombolgie Formation was stripped.

Sands and earthy sands now extend over large parts of the catchment (Fig. 1.5) and constitute the Koolpinyah Surface (Williams 1969b). On the western side these sands are up to 76 m thick, becoming thinner southwards (Needham 1976). These thick and often lateritised sediments are of Late Tertiary age and, since their deposition, have been dissected into shallow valleys. Needham (1976) and Stuart-Smith (1977) showed that there is up to 81 m of Cainozoic deposits some 20 km west of the Arnhem Highway crossing of the South Alligator River in an area crossed by shallow low-order valleys. By contrast, on the interfluve of the Magela Creek catchment some 20 km west of Jabiru, there is at most 3 m of earthy sands and pisolithic gravels resting on rocks of the Nanambu Complex that have been weathered to a depth of about 30 m.

Fig. 1.4 shows that the upstream and eastern part of the Magela Creek catchment consists of dissected plateau remnants often surrounded by cliffs. This complex of cliffs is known as the Arnhem Land Escarpment and is formed in the Kombolgie Formation. Backwearing of the cliffs has exposed the Archaean and Proterozoic rocks, and near the cliffs has produced sheets of sand of a different character from the generally much thicker and ferruginous Tertiary sands of the Koolpinyah Surface.

LANDFORM, SOILS AND VEGETATION

Mention has already been made of the kinds of soil material that occur on the various rocks and sediments of the Magela Creek catchment. More detail will be given below, along with a brief account of the major structural vegetation types (based on Story et al. 1969) occurring on these soils.

The Arnhem Land Plateau is a block of Kombolgie sandstone dissected along joints and faults and sculpted into planar surfaces, pinnacles and caves. About one third of the Plateau is bare rock. Elsewhere soils are <1 m deep and are sandy and skeletal. There are deeper sandy soils and alluvium in valleys cut into the Plateau. There are also some patches of deep sandy soils on the Plateau top. The vegetation cover consists of eucalypt dominated woodland and scrub (with spinifex grass) with patches of tall open forest.

The footslopes to the cliffs that form the edge of the Plateau consist of sheets of coarse quartzose sand, as mentioned above. Layers of sand are separated by pedogenic features (texture contrast, subsoil colouration) that show a polygenetic origin for these bodies of sediment; that is, episodes of deposition were separated by periods when soil formation dominated. These sheets extend to valley floor alluvia and to the Magela Plain on its eastern side. Eucalypt-dominated tall open forest and woodland dominate.

The alluvial tracts extending from the Plateau and set into the Koolpinyah Surface contain coarse quartzose sands in the areas of active open-channel transport. Earthy sands are common in the upstream parts of the Koolpinyah Surface alluvia. These sediments have

been shifted often only a few hundred metres from the sandy regolith that constitutes the interfluves and slopes of the Koolpinyah Surface, and so mirror the textures of the non-alluvial materials. In the main valleys, and in some valleys of lower-order, there are alluvial terraces of clayey sands, gravelly sands, earthy sands and red massive earths (Wells 1979). These surfaces support grassland and savannah while the smaller alluvial tracts are covered by grassland and woodland.

The Koolpinyah Surface constitutes most of the western part of the catchment where it abuts the Magela Plain. Archaean and Early Proterozoic bedrock crops out as low ridges, boulder piles and 'whalebacks', and structure within bedrock can often be seen on aerial photographs despite a thin cover of sandy regolith. Williams (1969b) has given an account of the evolution of this Surface, updated in 1990. It is thought that epeirogenic uplift rejuvenated the landscape during the Miocene (Noakes 1949), increased the rate of retreat of the Arnhem Land Escarpment, producing more vigorous fluvial deposition to the north. The resulting alluvium is sandy near the Escarpment and clayey more distally, and, as seen earlier, can be up to 80 m thick. Weathering of these sands and clayey sands leached bases and alkali earths to produce residual concentrations of iron and aluminium. This laterite is now being destroyed in some areas leaving a litter of blocks and pisoliths. This erosion has also produced the drainage system briefly discussed above. Some closed depressions, oriented in preferred directions, testify to an earlier drainage system now dismembered (Williams 1969b).

The Koolpinyah Surface, where substantially unmodified, consists of gently undulating surfaces underlain by pisolithic gravels in a matrix of sands, earthy sands and loams. Where dissected there are catenary sequences of soils directly overlying bedrock where the laterite has been stripped. The textures of these soils are of the same kind as found on the interfluves where the Koolpinyah Surface is relatively unmodified. All these soils have low CEC (Wells 1979; Chartres et al. 1988), low clay content (predominantly of kaolinite) and acid character.

The Koolpinyah Surface is covered by woodland and tall open forest, dominated by Eucalyptus tetrodonta and E. miniata above annual sorghum and spiky spear grass. Williams (1990) notes that the apparent monotony of this landscape conceals a subtle variety of soils and plants (see Braithwaite & Werner 1987) as complex and interesting as anywhere on this continent.

The final landscape element is the Magela Plain. The soils will receive complete treatment in Chapter 5 and the vegetation in Chapters 3 and 4. Anticipating the forthcoming descriptions, the Magela Plain is a low gradient accumulation of mostly clay which forms a re-entrant into the Koolpinyah Surface to the west and the Escarpment and its piedmont sands to the east. Using the classification of Story et al. (1969) the Plain is covered by sedgeland and herbaceous swamp vegetation, and by paperbark forest.

CLIMATE AND HYDROLOGY

Climatic summaries for the Alligator Rivers Region have been provided by Christian and Stewart (1953), Australian Bureau of Meteorology (1961) and McAlpine (1969). More recent climatic data have been summarised by us for Jabiru airport where the mean annual rainfall of 1529 mm for the 16 years of record compares with a 46 year mean of 1323 mm at Oenpelli, the climatic station nearest to Jabiru. On the coast at Darwin the mean is higher at 1600 mm.

The rain at these stations is strongly seasonal with the Wet season between late October and early April (Fig. 1.6). This period of floods contrasts with the Dry season, a time of drought. This harsh contrast is between a semi-desert and a land of flowing streams with

inundated flood plains and swamps. This is a highly predictable seasonal pattern and the Wet season is reliable, although the amount of rain received each year is highly variable.

The regional control of this Wet-Dry pattern is the monsoon circulation that straddles the equator from Africa to the Coral Sea (McDonald & McAlpine 1990). Outflow from the Southern Hemisphere subtropical anticyclones during winter forms the S.E. Trades as this air passes across northern Australia towards the Intertropical Convergence Zone (ITCZ) located over the Asian mainland. This is the Dry season circulation that is replaced during the summer Wet season when moist air flows into the ITCZ (also known as the monsoon trough), at this time of year located either over northern or central Australia.

The strength and position of the ITCZ are influenced by the latitudinal migration of the tropical atmospheric circulation, the Hadley cell. They are also influenced by the Walker Circulation, a quasi-periodic circulation between the atmospheric pressures to the north of Darwin and those over the Eastern Pacific. The Walker Circulation has a two or three year quasi-periodicity and has also increased in amplitude in recent decades. McDonald and McAlpine (1990) have shown that the annual rainfall for the Darwin-Daly River rainfall districts has become more variable since this amplitude increased in about 1950. Between 1923 and 1950 the mean annual rainfall for January, February and March (the time when most Wet season rain falls) was 866 mm and has increased to 1066 mm since 1950. This difference is statistically significant.

The seasonal pulse of the monsoon controls the hydrology and sediment transport of Magela Creek, and much of its biology. The Wet season occurs towards the end of December or early in January. This is gudjewg of the Bunitj people of the Magela Plain (Fig. 1.6). Periods of rain are produced by tropical cyclones, monsoon depressions and surges of the moist inflow (Southern 1966). The Bunitj recognise April as bang-gereng when light east winds signal the end of the Wet. Violent storms towards the end of this time knock down the tall native sorghum under the open forests.

The Dry season lasts from May to September and sees little or no rain, even on the coast. Southeasterly winds bring dry air from the anticyclones travelling across southern Australia. A strengthening of these winds occurs when an anticyclone is centred over South Australia and calm conditions follow as the high pressure cell moves eastwards. The Bunitj recognise two periods during the Dry: yegge and the 'cold' season of wurrgeng.

The southeasterlies get warmer in August and September during gurrung. The Transition Season then begins as the influence of the southern anticyclones wanes but the monsoon trough has not yet affected the mainland. Humidity builds up and temperatures rise during October and November, a time called gunumeleng.

McDonald and McAlpine (1990) have modelled the seasonal water balance for stations near the Magela catchment. Mean weekly soil moisture storage at Oenpelli ranges between 100 mm in March in the late Wet season to zero in the mid Dry season. The median start date of plant growth at the same station is 14 November and ends on average on 12 May with an average length of 25 weeks.

Water surplus estimates are derived from the amount by which weekly rainfall is surplus to the needs of evapotranspiration and soil moisture replenishment to field capacity. Surplus water is available for surface runoff and deep percolation. Figure 1.7 shows the estimates for Oenpelli. Year to year variability in these estimates is highest during the transitions from Dry to Wet and vice versa. Kingston (1981) charted a lag of about 2 months between the onset of rainfall in September and the beginning of runoff in November in the Alligator Rivers Region, the delay being the result of water going first into soil moisture stores and evapotranspiration, then being available for runoff.

The end of the Dry season is a time when the Koolpinyah Surface, and other sand plains, are substantially bare of ground vegetation as a result of the death of grasses from fire or the seasonal drought. The surface is protected from rainsplash and overland flow during the early rains only by a residual coarse layer of sands and gravels (Story et al. 1976; Duggan 1983). Williams (1976) and Duggan (1983) have shown that the early rains of the Wet season cause most slope erosion during the year because they occur when grass cover is at a minimum. Extreme events, like Cyclone Max of March 1981, had little effect because it occurred when Wet season vegetation cover was most protective. Had Max occurred early in the 1980/81 Wet season, it would have been a powerful erosive agent. In most years soil loss during the early rains amounts to several hundred cubic metres per square kilometre on gentle slopes but, as the Wet season grass cover establishes, this rate falls to about a fiftieth of the earlier rate (Williams 1969b, 1976).

In the Magela catchment, runoff lags behind the early rains as shown in Fig. 1.6. The stage hydrographs for the gauging stations downstream of Jabiru for the 1978/79 Wet season are shown in Fig. 1.8. Prior to the start of frequent daily rainfall in 1978, a total of 46.4 mm fell at Jabiru airport in September and October. The rainfall of November produced streamflow at GS8210018 (Mudginberri Homestead) towards the end of that month. The stage record at this gauge sensitively reflects the rainfall pattern, with rapid rises and falls of river height. After 398 mm had fallen at Jabiru airport, flow was recorded at GS8210017 (Jabiluka, 14 km downstream of GS8210018) in late December, with evident damping of the rises and falls seen at Mudginberri. In early January, after 592 mm of rainfall since the beginning of rainfall in September, flow was recorded at GS8210022 (Pelican Camp Site No. 3, about 25 km downstream of Mudginberri Homestead). Flow through the outflow channel of Magela Creek (GS8210019, 32 km downstream of Mudginberri Homestead) did not occur until early February, and the individual rainfall periods that resulted in flow are undetectable in this record.

The recession curves of the stage hydrographs for these gauging stations all begin from a peak which is offset by about 7 days between the next upstream site (GS018) and the Magela Creek outflow channel (GS019). The latter stopped flowing first, only 3 months after it started. Flow at GS018, which began first, ended last.

This pattern of flooding can be explained as a wetting phenomenon extending downstream as the Wet season progresses. Flow in the sand tract (represented by GS018 on Fig. 1.8) begins soon after the early rains. Wetting of the Magela Plain by these rains seals the surface and allows ponding of both subsequent direct precipitation and run-on from upstream. Kingston (1981) estimated that 150 mm of rainfall is needed to seal the 'black soil plains' of this region.

The filling of the Magela Plains 'lagoon' by run-on and direct rainfall allowed discharge through the Magela Creek outflow (GS019) some 2 months after flow began at Mudginberri in 1978/79. This flow began early enough to allow the stage at all stations in Fig. 1.8 to peak within a 7 day period, at the end of the Wet season. The outflow dried up first in May and the remainder of the gauges stopped recording some 3 months later.

The hydrologic pattern shown in Fig. 1.8 illustrates the major features of the Magela Creek system. Year to year variations of this pattern are, of course, substantial.

1.5 SEASONAL DEPENDENCE OF THE VEGETATION

It has already been shown that the non-perennial vegetation cover on the 'uplands', that is the area standing higher than the Magela Plain, is strongly seasonal. The timing of rainstorms of varying intensity in relation to this cover is critical in eroding slopes and producing suspended sediment downstream. The generally reliable Wet season also drives the annual flush of growth on the Magela Plain. The floristically poor annual 'mud-flat' and

sedge assemblage of the Dry season is replaced by a floristically rich assemblage in the Wet of about 200 plant species (Finlayson 1988 et al.).

Sanderson et al. (1983) outlined the seasonal cycle of the herbaceous flora on the Magela Plain. Stage 1 (see Fig. 1.6) is marked by saturation of the surface of largely bare ground, and by the germination of annual aquatic herbs and grasses, and increased vigour of existing 'terrestrial' vegetation. Stage 2 is the period of inundation when 'terrestrial' plants are drowned and many annual aquatic herbs germinate and, along with other aquatic species, show maximum growth. Stage 3 is the period of draw down during which aquatic species decline and many annual aquatic herbs and grasses around the edge of the Plain die on the now drying mud. Stage 4 sees the decline and disappearance of the vegetative parts of most aquatic species as the Plain experiences a constant reduction of water level. 'Terrestrial' herbs, grasses and sedges germinate at this time. Stage 5 is the time of minimum water on the Plain, with aquatic plants restricted to permanent water bodies (the billabongs and sometimes the Upstream Basin—see Chapter 2) and the growth and maturation of the 'terrestrial' species.

Three aquatic grasses, Pseudoraphis spinescens, Hymenachne acutigluma and Oryza meridionalis, dominate the herbaceous flora of the Plain, covering on average 14%, 9% and 12% of the Plain respectively (Finlayson et al. 1988). During the 1984-85 Wet-Dry cycle these grasses were highly productive with annual standing crops between 0.51 and 2.09 kg/m². About 34% of the Plain is occupied by Melaleuca spp. woodland and forest. The standing crop of this community is between 235 and 440 t/ha with an annual litter fall of about 14t/ha (Finlayson, pers. comm.). This fall occurs twice a year, during the windy periods of January and June-July.

Based upon Finlayson's measurements, the mean annual rate of supply of organic matter to the Plain's surface from the area of aquatic grasses is about 530×10^3 t, while that under the Melaleucas is about 95×10^3 t. The aquatic grasses contribute about 75×10^3 t of organic C annually to the Plain whereas the Melaleuca forest contributes about 620 t of organic C. Therefore, most of the organic C is contributed by the vegetation that grows during the Wet season.

1.6 SUMMARY

The background to this Report and the aims of the research are set out in the beginning of this Chapter. The history and evolution of the Plain is to be explored in subsequent chapters to provide the framework for an account of contemporary sediment transmission zones and sinks. This information is to be used to predict where sediments eroded from the Ranger Mine Site might lodge and, in conjunction with experiments using tailings reacted with materials of the Plain, will be used to assess the mobility of metals in the eroded sediments. The recent history of the Plain will also provide a guide to likely future change and, in conjunction with other plausible predictions about climatic change, will be used to judge the likely future dispersal patterns of sediments and the chemical mobility of associated metals.

The remainder of this Chapter contains an account of those aspects of the physical environment of the Magela Creek catchment that are of most relevance to the rest of this report. This includes the solid geology, regolith, landforms, a brief account of vegetation, and finally the strong seasonal climatic imprint on the hydrology, slope erosion and biota of the catchment. Each of these components, with the exception of solid geology, will be elaborated in subsequent chapters.

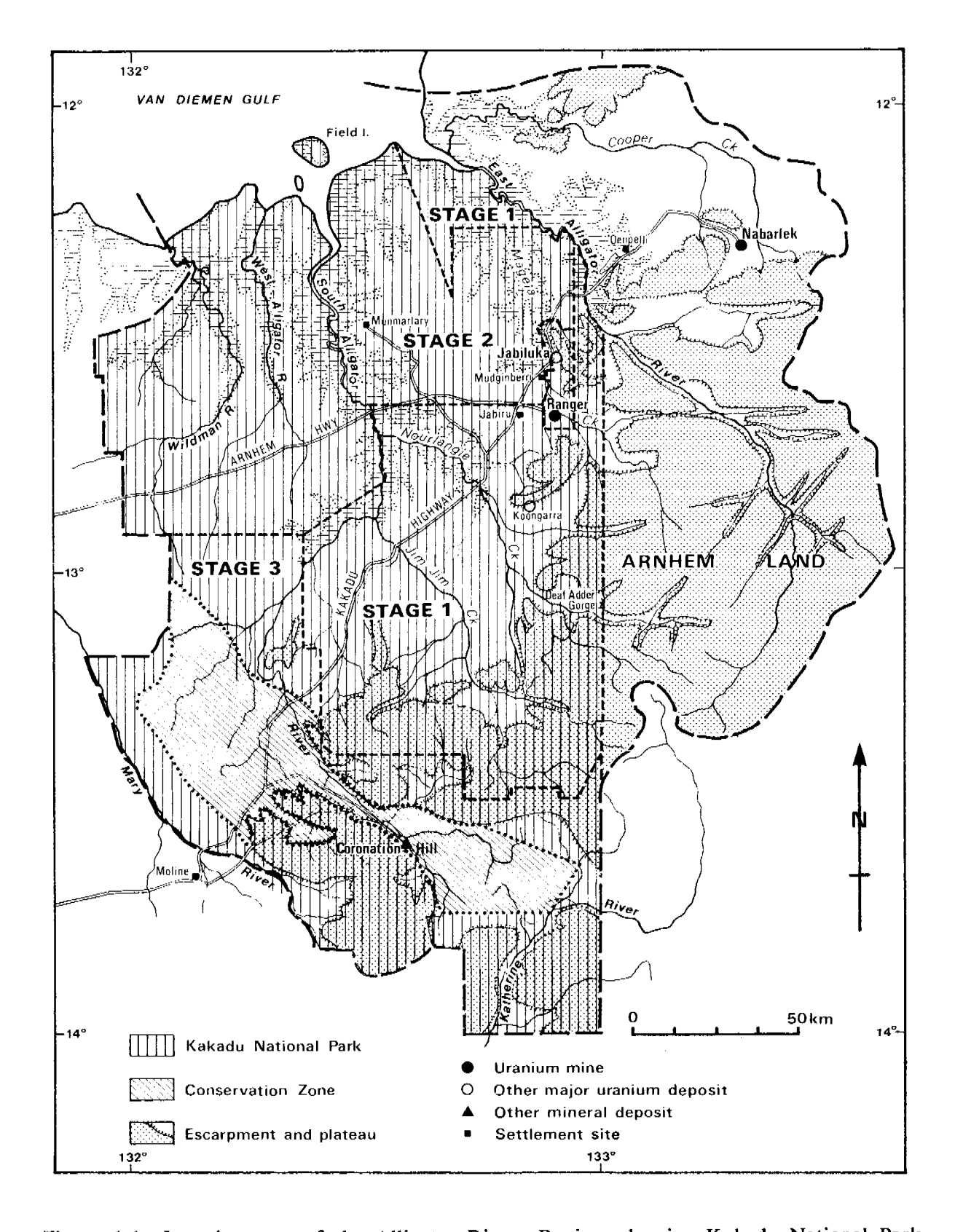


Figure 1.1 Location map of the Alligator Rivers Region, showing Kakadu National Park and the Arnhem Land Aboriginal Reserve

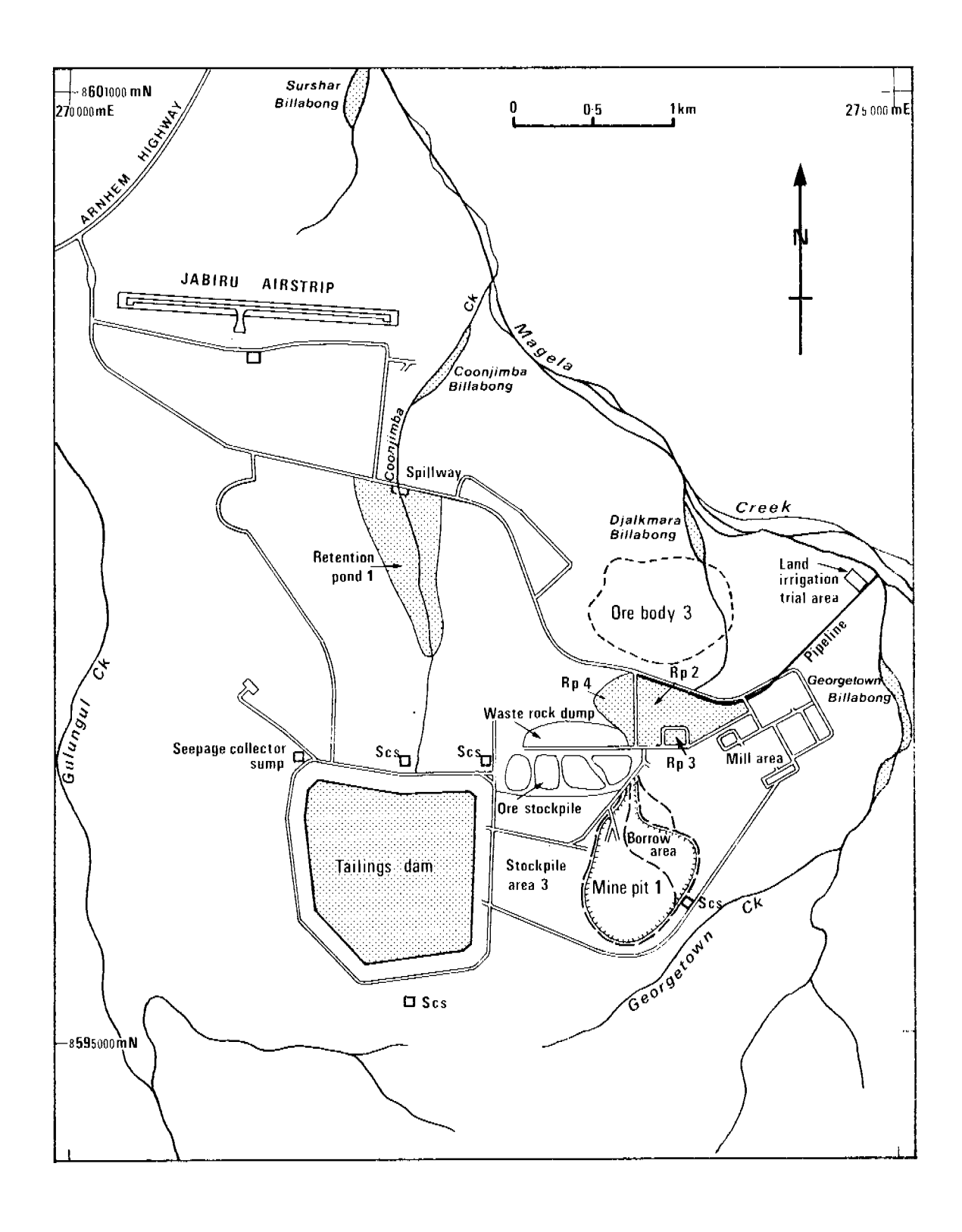


Figure 1.2 Map of the Ranger Mine Site

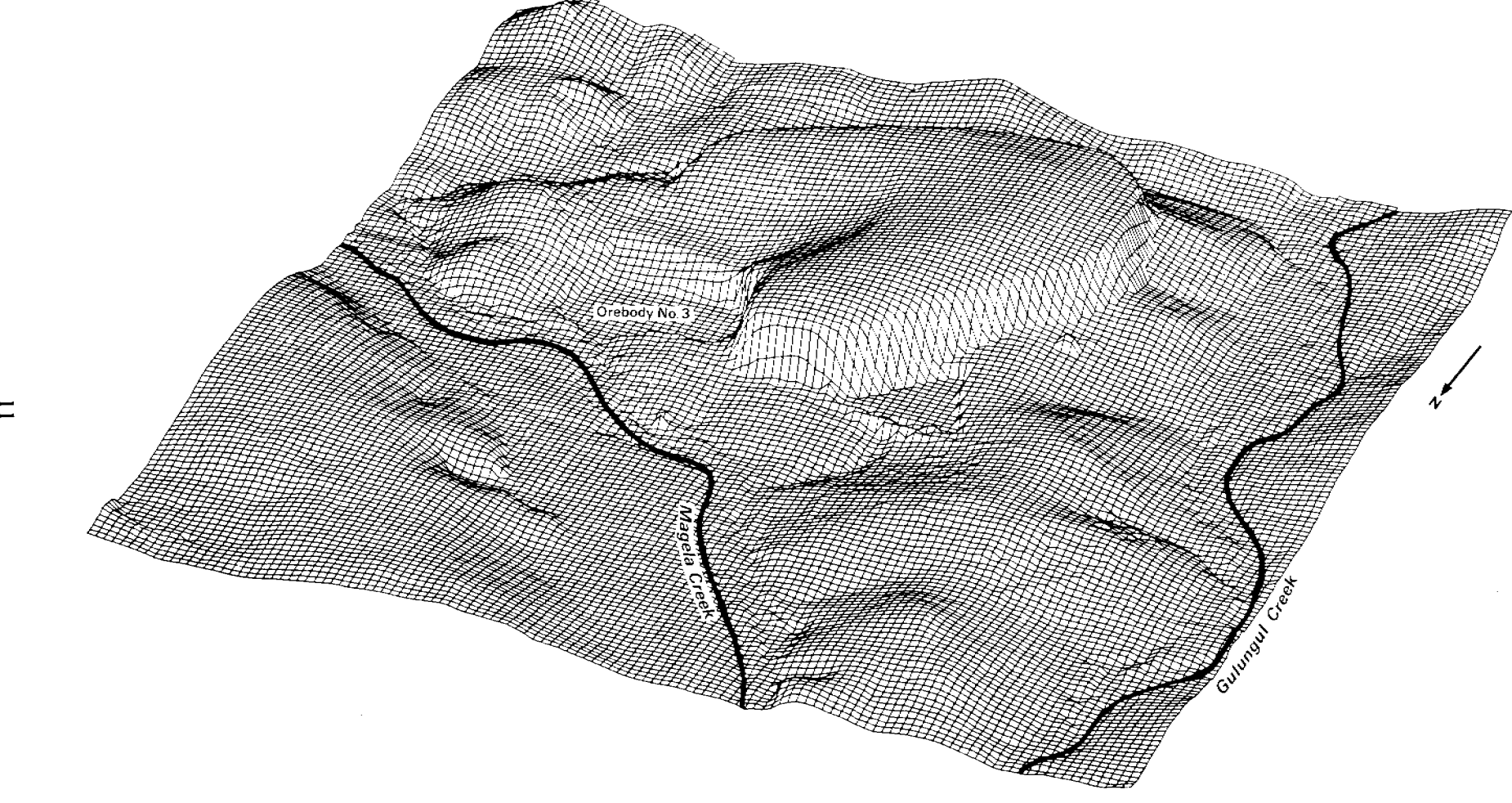


Figure 1.3 Perspective view of a proposed artificial landform containing tailings, waste rock and BOGUM, assuming that these waste materials will be stored above grade

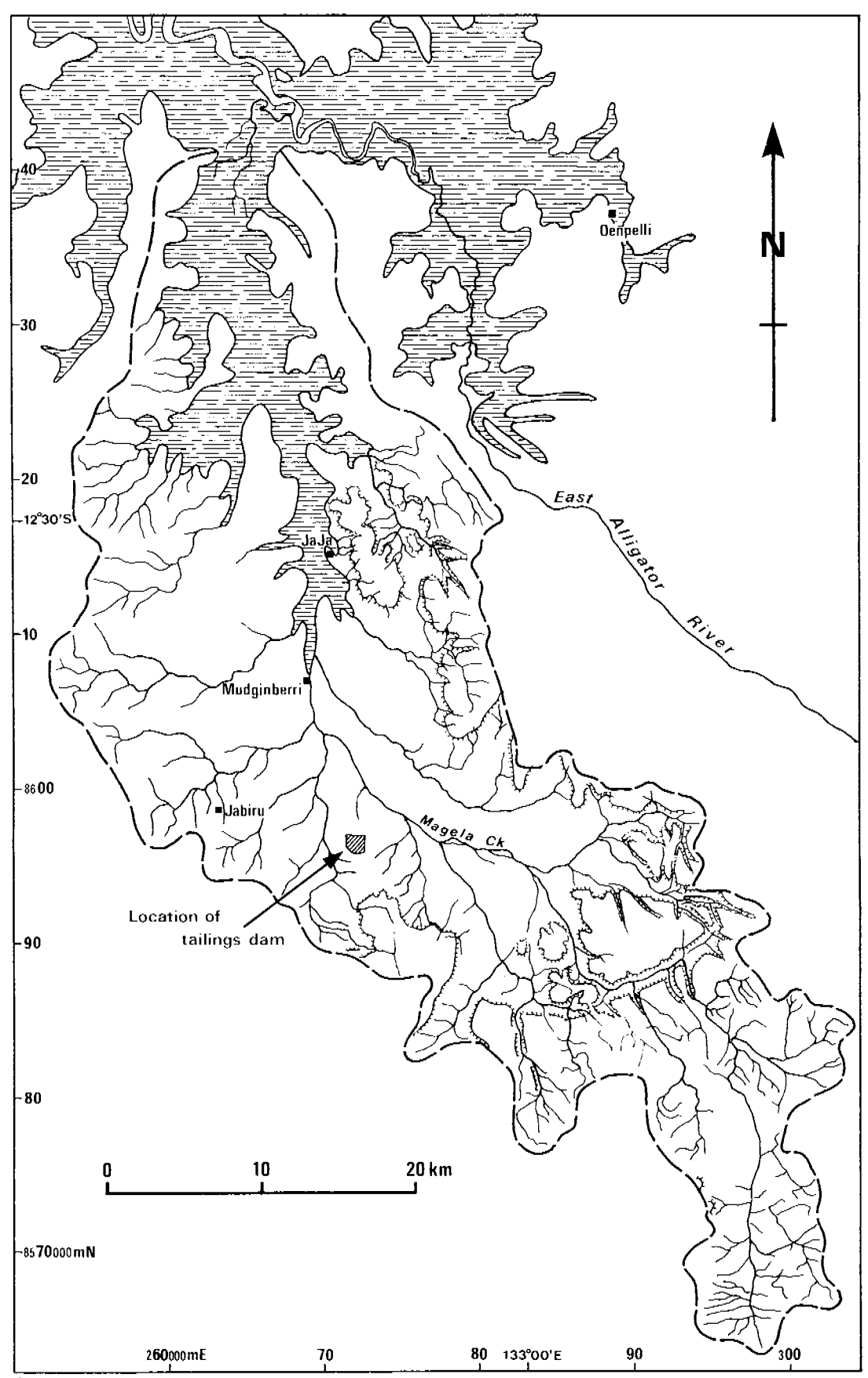


Figure 1.4 The catchment divide, drainage network and escarpments in the Magela Creek catchment

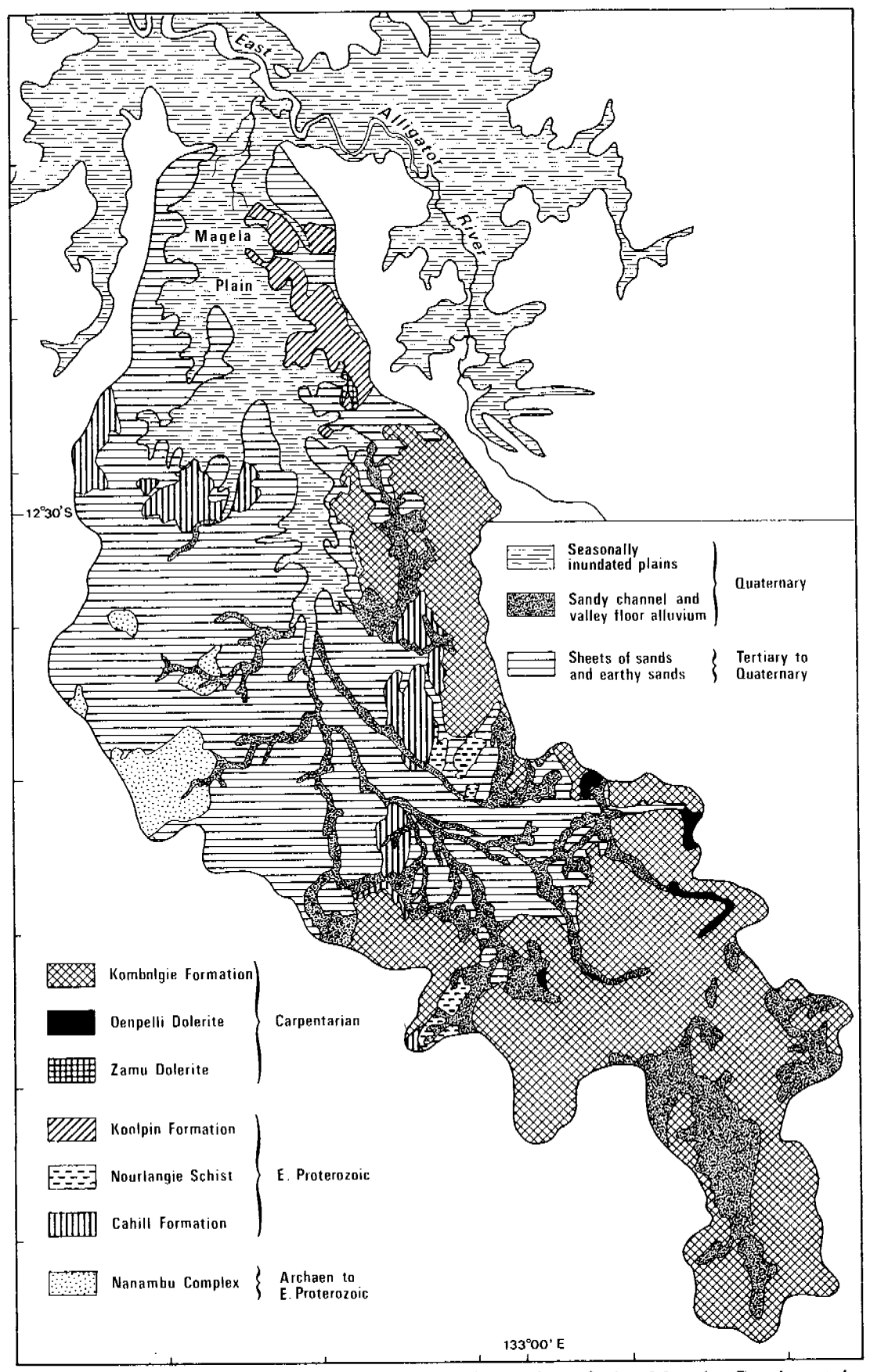
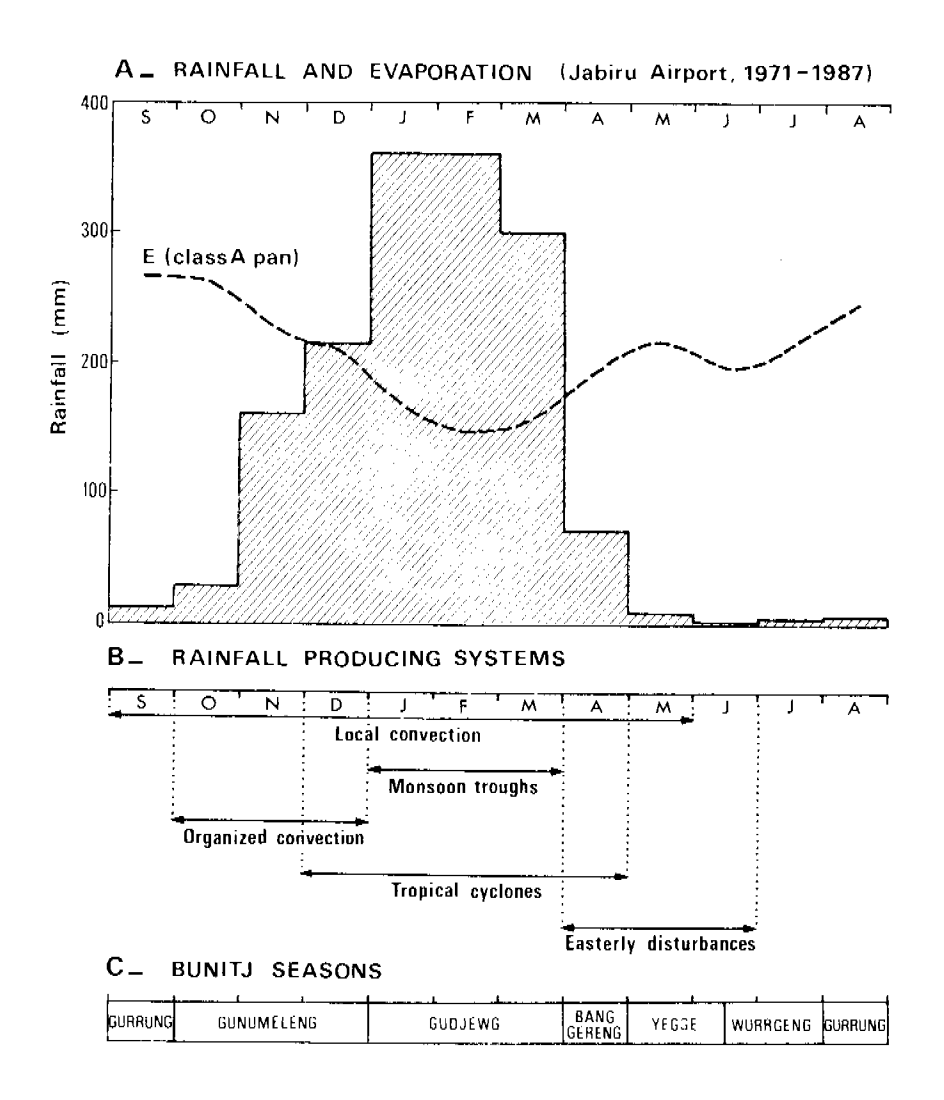


Figure 1.5 Geologic map, partially morphostratigraphic, of the Magela Creek catchment. Simplified after Needham (1984).



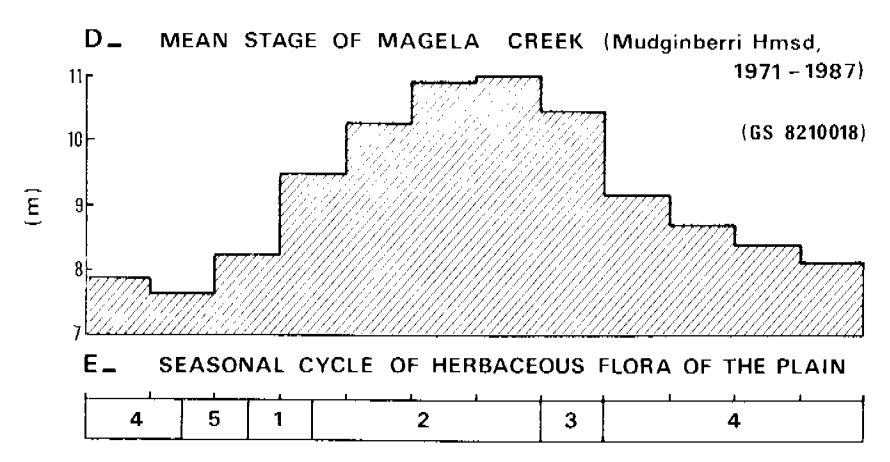


Figure 1.6 Summary of key climatic and hydrologic variations in the Magela Creek catchment.

A: mean monthly rainfall shown as a histogram, with mean monthly evaporation in a Class A pan, at Jabiru airport (1971-1987); B: rainfall producing systems, after Southern (1966); C: the seasons of the Bunitj people; D: mean monthly stage of Magela Creek (1978-1987) at Mudginberri Homestead (GS8210018), from records of the N.T. Power & Water Authority; E: the stages of the seasonal cycle of the herbaceous flora of the Plain (after Sanderson et al. 1983), explained in the text.

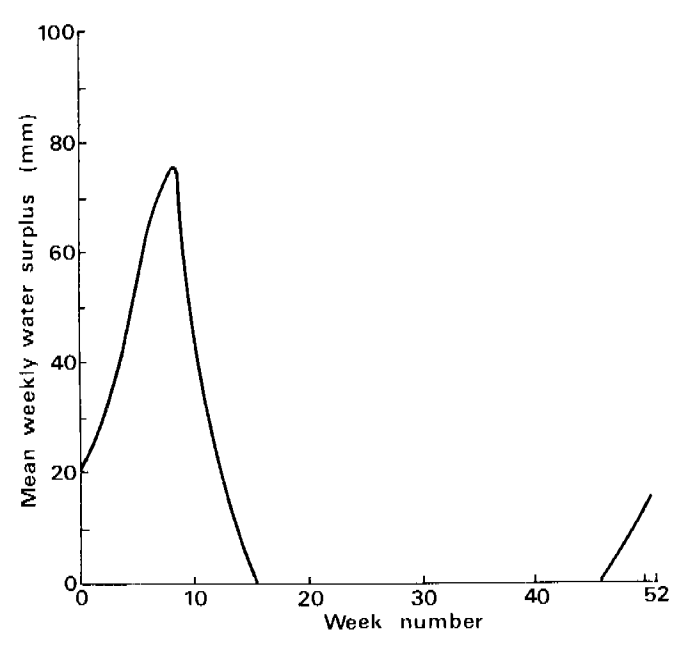


Figure 1.7 Mean weekly water surplus at Oenpelli, after McDonald and McAlpine (1990)

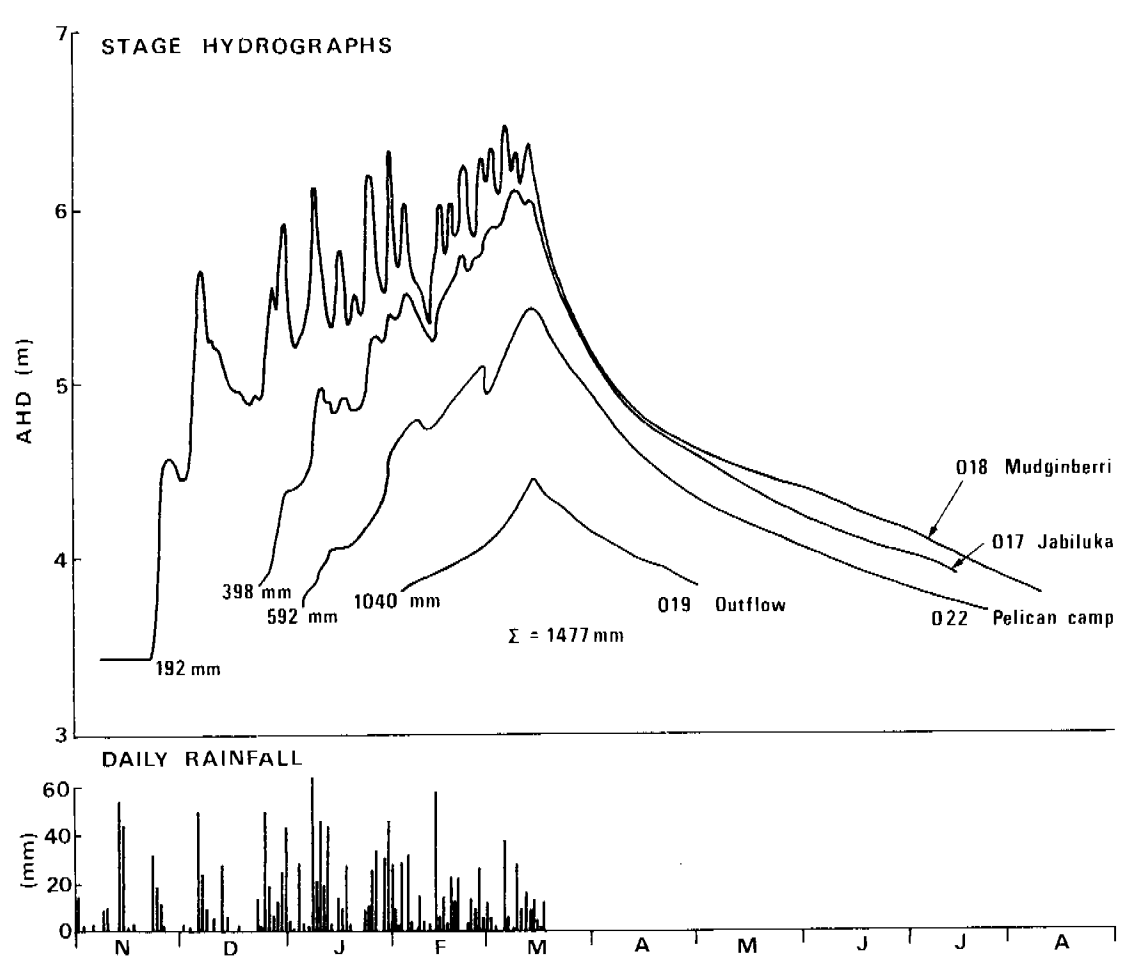


Figure 1.8 Daily rainfall at Jabiru airport and stage hydrographs for the 1978/1979 Wet season for gauging stations located at Mudginberri Homestead (GS 018) and at gauges downstream on the Magela Plain. Rainfall data from the Bureau of Meteorology and gauging data from N.T. Dept. Transport & Works (1979-82).

CHAPTER 2. THE MAGELA CREEK SEDIMENT SYSTEM

2.1 INTRODUCTION

Sediment originating on the Ranger Mine Site (from tailings, waste rock, ore stockpiles, disturbed soils or roads) may be transported downstream. To evaluate the environmental effects of this sediment transport it is necessary to estimate how much sediment will leave the Site and where it will be deposited. In the case of sediments containing radionuclides it is particularly important to estimate changing deposition patterns during the next 1000 years.

Research currently underway at ARRI, in conjunction with Ranger Mines, aims to estimate the amount of sediment that is likely to leave the Mine Site under various conditions. Predicting the fate of this sediment is a problem in routing and may be tackled in various ways. Ideally, any model constructed to simulate the sediment routing system should be process and therefore event based because this would most closely represent the physical system in which it is supposed intense low frequency events (e.g. cyclones) will move most sediment.

Following Pickup (1988), mathematical models of erosion and deposition can be represented as two end points on a continuum: the lumped parameter or black box model, and the distributed process model. It is the latter that is ideally suited to the problem at Ranger. Unfortunately, existing process models are far from adequate representations of the physical system and require as input a large amount of data (e.g. runoff, sediment concentration) that is often not available. In the Magela catchment, where data are limited, it is necessary to use a more empirical box-model approach, often known as compartmental analysis (Jacquez 1972).

2.2 CONCEPTUALISATION OF THE MAGELA CREEK SEDIMENT SYSTEM

The box model that will be developed in Chapter 6 requires a subdivision of the Magela Creek catchment. Sub-catchments represent the first level of subdivision and topographic/landform units are at the second level.

SUB-CATCHMENTS

The Ranger Mine Site may contribute sediment to the sub-catchments of Gulungul Creek, Georgetown Creek, and Coonjimba Creek (Figs 2.1, 6.15). Ideally, the sub-catchments should be subdivided into landforms, each of which can be thought of as a compartment which receives and releases sediment, and through which sediment travels. The upland compartments, relevant to the subcatchment(s) immediately downstream of the Mine Site, are shown in Table 2.1. It is also necessary to identify the backflow billabongs, at the junction of Magela Creek and tributary channels (Galloway 1976), as separate compartments.

The other sub-catchments shown on Fig. 2.1 do not need to be subdivided. It is sufficient to know how much sediment is contributed by them, eventually to mix with any sediment derived from the Mine Site. It is necessary to subdivide the Magela Creek into a sand tract (i.e., the sand bed channels upstream of Mudginberri Billabong, Fig. 2.1) and the Magela Plain (downstream of Mudginberri Billabong).

While the above subdivisions of compartments are ideal, data are not available to quantify the sediment flux through each of them. Therefore, in Chapter 6 a simpler subdivision is used.

SEDIMENT ROUTING

Sediment leaving the Ranger Mine Site will be transported episodically, depending largely upon the nature of rainstorms and antecedent conditions. While the actual transport and deposition events are driven by short term runoff pulses, in the long term it is possible to view the movement of sediment as the aggregate of many pulses both within and between the landform compartments outlined above. Sediment will move from, for example, the tailings dam first onto hillslopes and alluvial valleys of the Mine Site tributaries. Some will be stored on these landforms and the remainder will move into the backflow billabongs. Again, some storage will occur and the rest of the sediment will reach the sand tract of Magela Creek. Eventually, sediment from the tailings dam (or any other Mine Site sediment source) will reach the Magela Plain.

This introduction to a conceptual model of the Magela sediment system will be expanded in Chapter 6. It is sufficient for the moment to note that sediment arriving at the Magela Plain, originating on the Mine Site, has been through a complex route. The elucidation of this upstream route is not properly the concern of this project, yet to make sense of our findings from the Plain it is necessary to take account of processes upstream. We turn now to a detailed account of the landforms of the Magela Plain, to provide a context for the sediment budget of Chapter 6, and the stratigraphically based investigations of Chapters 3 to 5.

2.3 LANDFORMS OF THE MAGELA PLAIN

The Magela Plain (Fig. 2.1) is an area of low gradient and low-lying land of about 220 km² extending downstream from the sand tract of Magela Creek. The Plain merges at its downstream end with the flood plain of the East Alligator River. This flood plain is an example of an Upper Flood Plain within the Deltaic Estuarine Plain as defined by Woodroffe et al. (1986) for the South Alligator River. The same authors would classify the entire Magela Plain as a backwater swamp, while Story et al. (1969) included both the East Alligator Flood Plain and the Magela Plain in their Cyperus land system — a well-drained coastal plain.

TOPOGRAPHIC UNITS

Pickup et al. (1987) relied upon the then available topographic data to draw a long profile of the Magela Plain (their Figs 2 and 3) from which they defined topographic and then landform patterns. Spot heights on the East Alligator Flood Plain are shown as 5 to 6 m AHD (Australian Height Datum) on the N.T. Lands Department 1:25 000 maps. These heights are up to 2 to 3 m above the surface of the Magela Plain immediately to the south. From these topographic relationships, Pickup et al. concluded that a low broad levee (or levee plain) lies along the left bank of the East Alligator River. The Magela Plain was therefore thought of as a backwater swamp, flow across the plain being blocked by the levee plain.

There was always some doubt about the height of the putative levee plain. Three long traverses surveyed in 1980 by the N.T. Water Division showed all heights to be less than 4 m AHD. Pickup *et al.* adopted the more conservative 4 m rather than 5 to 6 m for the height of the levee plain.

The most recent, and most accurate, topographic mapping of both the Magela Plain and East Alligator Flood Plain has been completed by the Australian Survey and Land Information Group (AUSLIG). Benchmarks were established on the East Alligator River Flood Plain and elsewhere, and the centrepoints of aerial photographs levelled by reference to these benchmarks. Spot heights were then determined photogrammetrically and contours drawn by

a numerical interpolation routine. The uncertainty of the spot heights is ± 20 cm and of the photo centrepoints ± 10 cm. In dense ground vegetation the spot heights are accurate to ± 50 cm (A. Spowers, pers. comm.). The maps are drawn at a scale of 1:5000.

These detailed maps show that the Plain's surface (the extensive low gradient areas uninterrupted by channels, billabongs and levees) consists of interconnected areas of low ground, and areas of higher ground that are usually separated by the areas of lower ground. Cross-sections of the Plain were drawn at closely spaced intervals from Mudginberri Billabong to the East Alligator River. The mean levels of the lowest 'low ground' and the highest 'high ground' on each section were calculated from spot heights for areas with widths greater than 100 m, in a direction transverse to flow. This width criterion, in the case of the low ground, selects areas that are connected, whereas areas narrower than ~100 m are often closed depressions on the topographic maps. High areas <100 m in width are often hillocks of no more than local significance.

The levels of the low ground (Low Plain) and high ground (High Plain) are shown, with surveying uncertainties and one standard error of the mean elevation across an area, on Fig. 2.2. Each cross-section is on a northing of the Australian Map Grid (Zone 53) and these grid references are given in Fig. 2.2.

It is now clear that there is no levee plain along the left bank of the East Alligator River. The Plain falls from the sand tract through the Mudginberri Corridor into the Upstream Basin (the Upper Basin of Pickup et al. 1987), then rises to the Central High (Fig. 2.2). Each of these topographic units was recognised by Pickup et al. and has been confirmed by the AUSLIG maps. From the downstream end of the Central High, the Plain undulates but is essentially one topographic unit that will now be known as the Downstream Plain.

A GEOMORPHIC MAP OF THE MAGELA PLAIN

The topographic units of Fig. 2.3 are spatial entities within each of which there is a range of landform units. Each unit is described below and illustrated in an idealised cross-section in Fig. 2.4.

Low Plain

Within each topographic unit the Low Plain (Fig. 2.2) generally remains wet longest after the Wet season. The Low Plain is a low gradient depositional surface which stands at varying altitudes, depending upon which topographic unit it is in. The Low Plain in the Mudginberri Corridor and Downstream Plain is covered by *Melaleuca* forest and woodland. Within the Central High and most of the Upstream Basin it supports a grassland, while in the upstream part of the Upstream Basin the grassland is studded with *Melaleuca*.

High Plain

This landform consists of low gradient depositional surfaces that are up to 50 cm above the Low Plain (Fig. 2.2). The High Plain emerges first from the Wet season inundations and is treeless everywhere but in the Corridor and Downstream Plain. The areas of High Plain are commonly adjacent to channels and are breached by depressions. Levees often flank the channels and surmount the High Plain. Many of the levees cannot be shown on Fig. 2.3 because of limitations of scale.

Levee

Levees are narrow depositional ridges that stand decimetres to metres above adjacent surfaces. They lie adjacent to channels and billabongs. Levees are often absent from the upstream ends of billabongs, begin to appear with distance downstream and reach their

maximum vertical and horizontal extent as prow-shaped accumulations wrapped around the downstream ends of the water bodies. The levees support grassland, *Melaleuca* stands and isolated clumps of *Barringtonia* sp.

Backslope

The surface of the Magela Plain often slopes, linking higher landforms (High Plains, Levees) with lower landforms (Low Plain, Marginal Depressions). As noted earlier, these higher and lower landforms are not at the same altitude in all topographic units (Fig. 2.2), and they vary in height downstream. The Backslopes have times of inundation varying between 3 and 6 months because of their sloping form. This landform type has been mapped by comparing its overall form with that of adjacent land. In some cases, Backslopes and Low Plains are very hard to distinguish on any one cross-section, yet they are distinct planimetrically. The Backslopes are mostly covered by dense *Melaleuca* forest.

Marginal Depression

The valley floors of most of the tributaries that join the Magela Plain are low enough to form flood basins, backed-up by the slightly higher ground that forms a broad low gradient spine to the Central High and the Downstream Plain. These Marginal Depressions fill with water from both the tributaries and from Magela Creek during floods. They are swamps, some of which are perennial supporting a mixed grass and sedgeland vegetation, and others are annual often with a partial cover of *Melaleuca* trees.

Upland Margin

The margins of the Upland, into which the Magela Plain intrudes, are gently sloping sand-rich surfaces that are infrequently inundated. Some sandy slopes gradually merge with the clay-rich plains. Other margins are steep and include alluvial terraces and bedrock slopes, especially in the Mudginberri Corridor. Both colluvial and fluvial processes occur on these margins but the amount of fluvial deposition is small. The orientation of logs deposited on these margins confirm backflow water movements near the entrances to Marginal Depressions. This pattern is well expressed at Magela Point.

Billabong

The billabongs in the Mudginberri Corridor are of the channel type (Hart & McGregor 1980), with sandy beds and muddy banks, and depths of up to 4 m. Flow through these water bodies is like that in a connected channel, to judge from the distribution of sediment particle sizes (Morley 1981; Whitehead & Hickey 1980). The billabongs in the Upstream Basin and Central High are of the so-called floodplain type. They vary in depth from 1 to 4 m with muddy bottoms and banks (Hart & McGregor 1980; Whitehead & Hickey 1980). The billabongs in the Upstream Basin are unconnected and there are no visible signs of former connecting channels. Evidence to be presented in Chapter 3 indicates that they were once connected. Nankeen Billabong, in the Central High, is really a long waterhole in a well-defined channel.

Channel

The Channels of the Magela Plain occur only in the Central High and the Downstream Plain, and some continue across the East Alligator Flood Plain. The channels are of various morphologic types. On the Central High the channels are of meandering form alternating between deep waterholes (e.g. Nankeen Billabong) and infilled reaches dominated by dense vegetation. Ponded reaches coincide with valley margins while infilled reaches are mostly points of inflection on the channel. Water flows freely in the waterholes but is impeded elsewhere.

On the Downstream Plain the channels are straighter, often poorly defined, usually less than 1 m deep, and choked with vegetation. Boundaries between channels and other landforms are often unclear. The channels hold water in most dry seasons. With distance from the Central High, the width of channels increases until they disappear in an area of High Plain. Further north a large arcuate feature (centred on AMG 262500, 8642500) is interpreted as a bend in a palaeochannel of Magela Creek (Fig. 2.3).

The Low Plain at the northern end of the Downstream Plain is drained by a dendritic network of small V-shaped channels which forms the so-called Magela Outflow. Gauging of the Outflow (019) shows that the tidal cycle in the East Alligator River backs-up the Magela water (N.T. Water Division 1980-82). Salt water has reached the gauge, as judged from the death of *Melaleuca* trees adjacent to the main channel. Further downstream V-shaped tidal channels occur on the treeless flood plain of the East Alligator River. Velocities in the larger tidal channels reach 1 m sec-1 as the 6 m tidal range in the East Alligator sets up local pressure heads.

There is some evidence from aerial photographs of various ages that saline conditions are encroaching upstream. Salt scalding is evident above shallow bank tops adjacent to very small tidal channels, and such areas appear to be increasing (cf. Woodroffe *et al.* 1986).

Patterned Ground

Ridges and intervening troughs, with a maximum crest to trough relief of 1 m, are widespread in the Upstream Basin (Fig. 2.3). The ridges interconnect and are mostly flat-topped occurring at about the same elevation over extensive areas. The troughs are of variable altitudes and generally do not interconnect so that the ground surface appears to be planar with depressions set into it. As will be shown in detail in Chapter 4, the ridges and troughs are approximately parallel and are both at right-angles to the direction of water flow. It will be shown that the patterning is caused by deformation of the surface sediment by water movement.

Profiles

The Low Plain begins at the end of the sand tract and continues to the East Alligator Flood Plain. The mean altitude of this landform unit in each topographic unit is shown on Fig. 2.2, and its major features have already been described. The floors of billabongs lie up to 4.5 m below the Low Plain (Morley 1981), and the small tidal channels that extend from the Downstream Plain to the East Alligator Flood Plain are cut about 1.5 m below the Low Plain. The Marginal Depressions lie some 50 cm below the Low Plain in the Central High and are at about the same elevation as the Low Plain elsewhere.

The High Plain approximately parallels the elevation of the Low Plain, in long profile. The margin of the Magela Plain is defined as the downslope edge of the Upland Margin, and it too approximately parallels the other two long profiles (Fig. 2.2).

The maximum recorded stages at gauging stations on the Magela Plain for the period 1971 to 1988 have been plotted on Fig. 2.2, along with the calculated 100 year recurrence interval flood stage (N.T. Water Division 1980-1982; M. Nicholas, pers. comm. 1988). At times of substantial flood the entire Plain is covered with up to 4.5 m of water, dwarfing the small differences in altitude between both topographic units and landform units.

The gradient of the long profile of stage is steep in the sand tract where the talweg is at about the same slope. The stage long profile steepens again in the Downstream Plain where dense stands of *Melaleuca* trees increase resistance to flow. It is noteworthy that the highest stage recorded on the East Alligator River during the period of record (November 1979 to April 1988) is only 50 cm overbank. This is also the only flood that has gone overbank

during that period. This lends support to Kingston's (1981) proposition that 'flooding' of the East Alligator Flood Plain is dominated by precipitation not streamflow. His identical claim for the Central High is not supported by the available hydrologic data.

SPATIAL PATTERN

The topographic units are spatially distinct. Despite their often slight vertical separation, these units play an important part in the behaviour of low flow water movements. The landform units are not restricted to a particular topographic unit, as will be shown in the following descriptions.

The Mudginberri Corridor is a narrow valley that is dominated by Low Plain and channel-type billabongs with prow-shaped levees at their downstream ends. The Corridor, as defined here, is smaller than that defined by Fox et al. (1977) and used by Hart et al. (1986).

The Upstream Basin is wider than the Corridor and is the lowest part of the Magela Plain. The Basin is dominated by Low Plain with extensive areas of patterned ground. The few billabongs are of the floodplain type and, in a few cases, appear to be linked to palaeochannels visible on aerial photographs as oriented patterns of vegetation.

The surface of the Plain rises between 0.5 m and 1 from the Upstream Basin to the Central High. This High also stands above the adjacent Marginal Depressions, two of which are joined by a channel cut in the sandy colluvium and underlying laterite of the Upland Margin. There are in-valley bedrock exposures within the Central High at Sore's Dreaming (Yingindidi). High Plain is common in this topographic unit with adjoining Backslopes extending to both Marginal Depressions and Low Plain. As noted earlier, the Central High ponds low flows in the Upstream Basin and deflects overflow first into the Marginal Depressions then directly down-plain away from the single-thread channel.

The Downstream Plain is essentially flat after the descent from the Central High (Fig. 2.2). The spatial pattern of landform units within the Downstream Plain is like that in the Central High. These two topographic units have a more complicated pattern of landform units than do the Upstream Basin or Mudginberri Corridor, implying some difference of origin of the Plain downstream and upstream of Jabiluka Billabong.

As already noted, the Magela Plain is not backed up by a levee plain built by the East Alligator River (cf. Williams 1979). However, both the Magela Plain and the East Alligator River Flood Plain lie at about the same elevation and are both essentially flat. The impedance to flow in the dense *Melaleuca* forest of the Downstream Plain, in combination with infrequent overbank flooding by the East Alligator River and very low gradients, means that this area of confluence between the Magela Creek and East Alligator River is a zone of very low velocity. Most sediment that reaches this zone settles out.

VEGETATION AND LANDFORMS

Correlation between landform units, defined above, and vegetation communities, defined by Finlayson et al. (1985), is weak. A much stronger correlation exists between topographic units and dominant plant communities.

Melaleuca open forest and woodland dominates the Mudginberri Corridor, covering both High and Low Plain. Pseudoraphis grassland covers the Upstream Basin and, in the area of patterned ground, is mixed with Melaleuca open woodland. The Central High is dominated by Pseudoraphis grassland on Low Plain and Backslopes. There is a tendency for Oryza grassland to dominate on High Plain. The channels are choked by Hymenachne grassland and, where open water appears, there are submerged and floating species and fringe Barringtonia, Pandanus and Melaleuca.

All landform units on the Downstream Plain are dominated by *Melaleuca* open forest and woodland. Once again, a fundamental difference between the topographic units appears: *Melaleuca* forest is far more important downstream of Nankeen Billabong than it is upstream, despite the dense forest in the Mudginberri Corridor.

The Melaleuca of the Downstream Plain gives way to Eleocharis sedgeland on the treeless East Alligator Flood Plain. The Marginal Depressions contain Nelumbo swamps, Hymenachne-Eleocharis swamps, Melaleuca open woodland, Hymenachne grassland mixed with Melaleuca open woodland, and Oryza grassland. The downslope part of the Upland Margin is almost always covered by Melaleuca open forest or woodland.

2.4 SUMMARY

The substance of this chapter is a descriptive account of the morphology of the Magela Plain. This account provides a starting point for an analysis of the nature and origin of the sediments of the Plain, a basis for sampling the Plain, and a basis for the sediment budget and routing model of Chapter 6.

The Plain is morphologically disjunct at the upstream boundary of the Downstream Plain. This disjunction is also reflected in the areally dominant plant communities and, presumably, some animal assemblages.

The pattern of topographic and landform units can be only partially explained by morphology alone. The materials both making up and underlying the various units now need to be considered before a serious discussion of origins can be offered.

Table 2.1. Landform subdivisions (or compartments) of the Magela sediment system.

1. **UPLANDS**

Hillslopes

- upper slope and summit

- lower slope

Alluvial valleys

- unchannelled valley

- channelled valley

- channel bed

- channel bank

- levee

- marginal swamp

- floodout

2. **BACKFLOW BILLABONGS**

Billabong

- delta/apron

- floor - bar/plug

SAND TRACT

Sand-bed channel

- channel

- bar

- marginal swamp

MAGELA PLAIN

- channel

- levee

- palaeochannel

- billabong

- levee

- levee, patterned ground

- high plain

- low plain

- patterned ground

- backslope - marginal depression

- upland margin

5. EAST ALLIGATOR FLOOD PLAIN

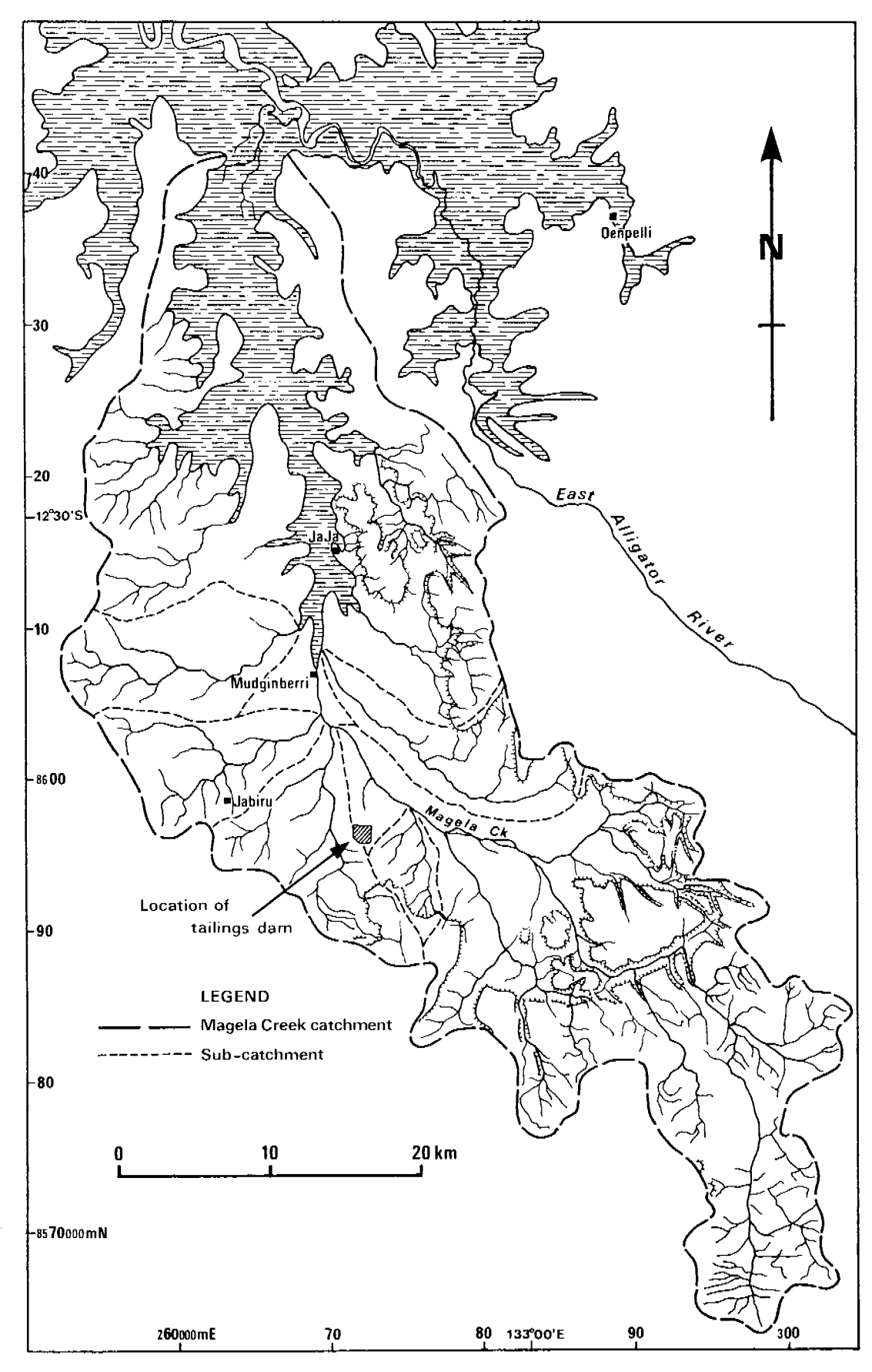


Figure 2.1 Magela catchment drainage net, major sub-catchments and major locations

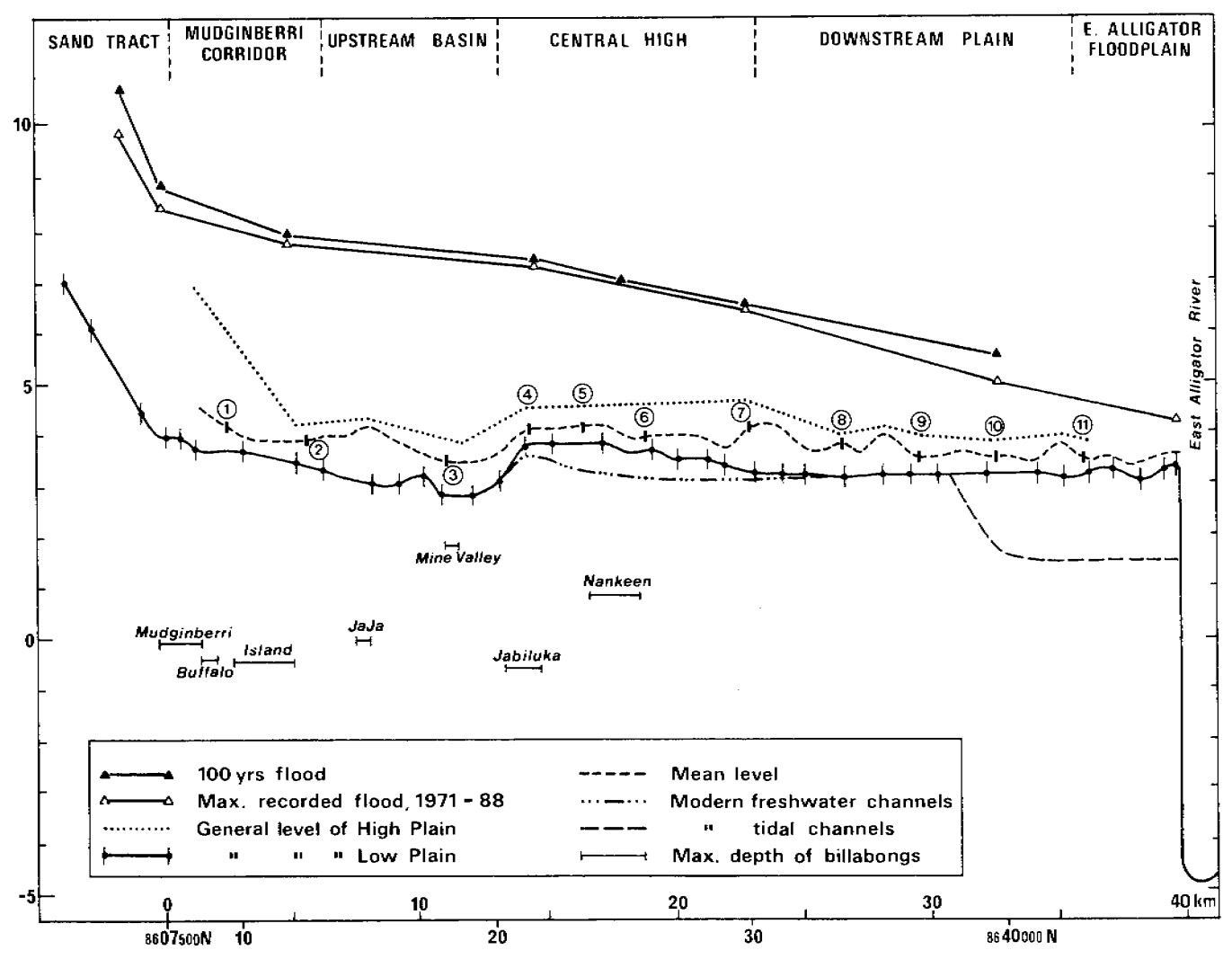


Figure 2.2 Long-profiles of the Magela Plain showing the general level of Low Plain (solid line) and High Plain (dotted line) (as defined in the text). The mean level is shown as a dashed line. The arbitrary datum (0 km) is at northing 8607500 (AMG Zone 53), near the northern end of Mudginberri Billabong. The deepest parts of billabongs are also shown. The circled numbers locate cross-sections located in Figure 2.3.

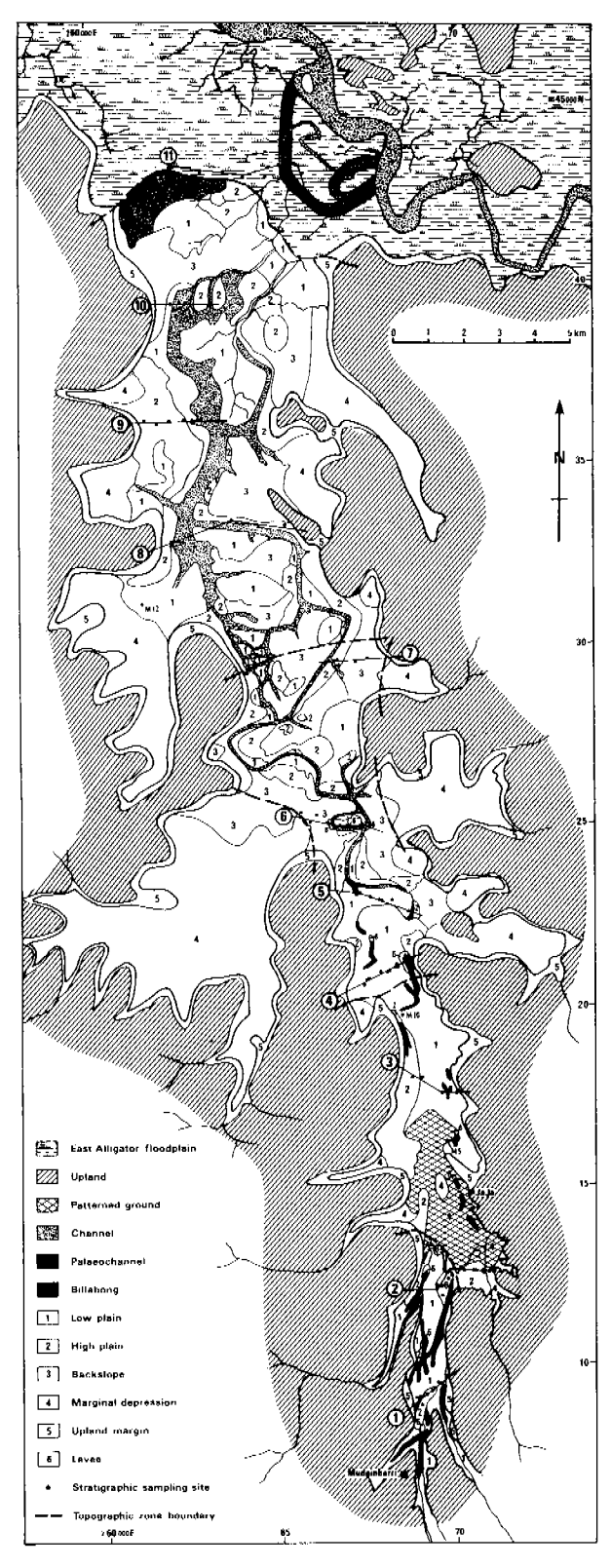


Figure 2.3 Geomorphic map of the Magela Plain showing both topographic and landform units, and locations of stratigraphic cross-sections and drill holes

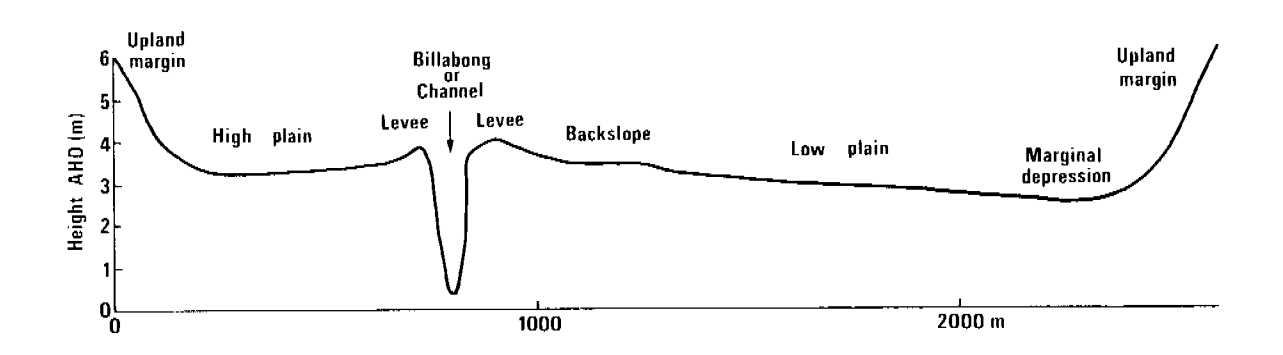


Figure 2.4 Idealised cross-section of the Magela Plain, using realistic elevations and shapes, to illustrate the landform units mapped in Figure 2.3

CHAPTER 3. LATE QUATERNARY STRATIGRAPHY OF THE MAGELA PLAIN

3.1 INTRODUCTION

The geomorphic map of the Plain (Fig. 2.3) contains nothing but morphologic information. Each of the morphologic units (either topographic or landform) consists of materials deposited in a particular sedimentary environment. A deposit that is a surface expression of a discrete subsurface body of sediment is a morphostratigraphic unit (Frye & Willman 1960). Bodies of sediment that have no surface expression are stratigraphic units. Both stratigraphic types are defined sedimentologically, using grain size, sorting, type of stratification, colour and inclusions. The shape and sharpness of boundaries is also used to distinguish stratigraphic units.

Not all of the phenomena listed above are the result of deposition. Some of the inclusions and the colouration, particularly mottling, result from post-depositional alteration by pedogenesis. This will be discussed briefly in this Chapter but will receive extensive treatment in Chapter 5.

The lithostratigraphy of the Plain allows an initial interpretation of the sedimentary environments that have led to the accumulation of both surface and subsurface sediments. In some important cases the sediments alone do not allow an unambiguous interpretation of the environment(s) in which they were deposited. Pollen preserved in the sediments allows further interpretation as does the chemistry of the sediments. The major changes in the Plain's history are dated principally by ¹⁴C and cross-checked by thorium-radium dating.

3.2 STRATIGRAPHIC UNITS

The results of deep drilling (Lau 1980; Needham 1976; B. Williams, Geopeko Pty Ltd, pers. comm.) and shallower drilling (Bettenay et al. 1981; Deutscher et al. 1980), and our own shallow drilling and pit digging (Table 3.1) show that there are five major stratigraphic units lying between the surface and bedrock. Most of the deep holes were near the centreline of Magela Plain (for locations see Fig. 2.3) and these are shown as a longitudinal section in Fig. 3.1, supplemented by the results from our own drilling using only holes near the centreline. Where the deepest part of the Plain has been intersected by a hole not near the centreline, this hole has been used on the longitudinal section. The bedrock surface in Fig. 3.1 is therefore believed to underlie the thickest sediments, although detailed deep drilling may yield extra detail.

The five major stratigraphic units are shown on Fig. 3.1 and are as follows:

BASAL SANDS AND GRAVELS

Lau (1980) describes the unit between 27.4 and 29.3 m below the surface in hole ARH2A as: 'sand, light brown (7.5 yr 6/4), damp; grains clear angular quartz sand to 2 mm diameter muscovite, tourmaline, pyrite'. In hole MC3 (Section 1, Fig. 3.1) the lowermost 5.7 m consists of interbedded medium to coarse sand, muddy fine to medium sand, granule gravel and pebble gravel.

On the basis of this rather meagre evidence, including the briefest description of lithologies in hole RPDDH3, a unit dominated by sands and gravel has been demarcated. This unit may be continuous with similar material upstream of Mudginberri but this is not clear from currently available information.

SANDS AND CLAYS

Lying above, and possibly interdigitating with, the Basal Sands and Gravels is a complex body of interbedded brown to grey brown sandy clay, clayey sand, sand and gravelly clayey sand. In the upstream section of the Plain, these sediments were investigated in pits where they display typical fluvial sedimentary stuctures. Upstream of Mudginberri these sediments form terraces standing at various heights above the modern stream. In the Mudginberri corridor, as will be shown below, sediments belonging to this stratigraphic unit form terraces that are completely buried by younger sediments.

On the East Alligator Flood Plain, in holes ARH2 and ARH2A, Lau (1980) found that this unit consists of pinkish grey (7.5 yr 6/2) clayey sand with pyrite (FeS₂). The top 3 m of this unit consists of brown (7.5 yr 4/2-5/2-5/4) clayey sand with iron staining of quartz grains, soft iron nodules and fine black jarosite (KFe₃ (SO₄)₂(OH)₆) blebs with thin pyrite skins. This sequence is interpreted as a body of clayey sand containing syngenetic pyrite which was exposed at or near the ground surface to oxidation and pedogenesis. The brown layer at the top of the sequence is therefore a palaeosol, forming a significant diastem in the sedimentary sequence.

Between the Mudginberri Corridor and the East Alligator Flood Plain, drill hole intersections with this stratigraphic unit are not common and the lithologies in many of them are poorly described in company logs. It is clear, however, that at some sites the Sands and Clays unit grades vertically into the overlying sediments with no evidence of a palaeosol. For example, in hole MC8 on cross-section 2 (Fig. 4.2) the Sands and Clays unit consists of light grey to cream clayey fine to medium sand. Above this is interbedded grey slightly clayey medium to fine sand and grey poorly sorted coarse and granular sand. The older material is drier and, therefore, tougher to the drill but is otherwise not altered by pedogenesis. At other sites, mottling and iron nodules provide evidence of a diastem of a kind analogous to that found in ARH2 and ARH2A.

The long-section geometry of this stratigraphic unit, shown in Fig. 3.1, is much simpler than its likely three-dimensional terraced form, buried beneath younger sediments on the Plain and rising above the modern depositional surface upstream of Mudginberri.

The sedimentary environment(s) responsible for this unit are only clear in the youngest materials in the vicinity of cross-section 1 (Fig. 3.1) and upstream in the Sand Tract. Here fluvial processes in a freshwater environment produce cross-stratified sands that, in places, interdigitate with the fine-grained sediments that make up the surface of the Magela Plain. Elsewhere, much of the unit is likely to be of fluvial origin, based upon its texture. This matter will be returned to below.

BLUE-GREY CLAY

Lying on top of, and interbedded with, the Sands and Clays unit is a body of essentially blue-grey lithofacies, that is, sub-units with distinctive sedimentologic characteristics believed to reflect the conditions and environment of formation. The lithofacies are:

- 1. Pale blue-grey clay either lacking or containing only minor visible organic fragments.
- 2. Blue-grey clay with abundant visible organic fragments, including wood, twigs, and leaf material. The wood has been identified as 'mangrove' (B. Bailey, pers. comm.).
- 3. Blue-grey clay, silty clay and fine sandy clay. Finely laminated either as silt laminae up to 4 mm thick and clay laminae generally <2 mm thick; or fine sand lenses up to 5 mm thick in weakly laminated clay.

- 4. Black highly organic fibrous peat.
- 5. Clayey sand and sandy clay with visible organic fragments, including 'mangrove' wood.

This unit contains pyrite which has been detected microscopically (using both SEM and light microscopy) and chemically by determining pyrite sulfur (S_{py}) as the difference between EDTA3 Na extractable sulfur and that obtained in an H_2O_2 extract (Willett & Walker 1982; also see Chapter 5). The blue-grey colour (due to ferrous compounds), and the presence of 'mangrove' wood and sedimentary pyrite, point to an estuarine origin for this sedimentary unit. This is a plausible hypothesis because the sediment reaches to -10 m AHD and is recognisable to only +3.5 m AHD, where AHD approximates mean sea level. As will be shown below, this unit is rich in pollen of various mangrove species.

The lithologies of this unit therefore reflect various sedimentary environments within an estuarine environment. The blue-grey clay with abundant organic fragments (facies 2) accumulates within modern mangrove stands in the Alligator Rivers Region (cf. Woodroffe et al. 1986). The pale blue-grey clay with minor organic fragments (1) is similar to lithofacies (2) but has fewer visible organics. The former lithofacies often lies at the top of the stratigraphic unit beneath a zone of oxidation, suggesting loss of organic matter by oxidation. Where facies 2 lies at the top of this stratigraphic unit, organic fragments are common in the overlying oxidised grey clays, suggesting that oxidation has not removed the large store of organic matter that must have been deposited at such sites. However, facies 1 is sometimes found at depth, below facies 2, showing that there were variations in the deposition of organic matter in the palaeo-estuary. Shell fragments appear in both facies 1 and 2 downstream of cross-section 7, that is, beneath the downstream plain and the East Alligator Flood Plain (Fig. 3.1).

Facies 3 is found as veneers and small benches on the sides of modern tidal channels. Well exposed examples occur only along the tidal reach of the East Alligator River, downstream of Cahill's Crossing, and have been described from mid-channel shoals, point bars and channel sites by Woodroffe et al. (1986).

The black organic fibrous peat (facies 4) has been found only in two holes, and is between 10 and 70 cm in thickness. In other holes near-peat has been found, and both kinds of organic-rich material lie on a substrate of sandy clay which is drier than overlying sediments when cored.

The final facies, the clayey sand and sandy clay, also contains 'mangrove' wood and pyrite. This facies occurs most commonly at the base of the estuarine clay stratigraphic unit in what appear to be two distinct bodies (Fig. 3.1). The upstream body is free of shell whereas the downstream body contains shell fragments. Lau (1980) reported finely crystalline pyrite wholly or partially replacing foraminifera and other calcareous tests. Fresh foraminifera also occur. The downstream body is like the 'estuarine sand and mud' described by Woodroffe et al. (1986), which is found in the wide channel and shoals in the lower estuary of the South Alligator River.

GREY CLAY

As already mentioned, lying on top of the blue-grey clay is a stratigraphic unit composed of grey clay, grey-brown clay and light brown clay within which are bright red, orange and yellow mottles. It will be shown in Chapter 5 that the mottling is the result of oxidation and pedogenesis. There are almost no original sedimentary structures remaining in this unit, except in the downstream section of the Mudginberri Corridor where fine sand lenses <1 cm thick occur.

This unit often grades into the underlying unoxidised pyritic estuarine clay. Pyrite occurs in this zone of transition and in the overlying grey clay but in lesser quantities than found in the blue-grey clay. This pattern may be explained as either a transition from estuarine conditions to the freshwater wetland of today where the top of detectable S_{py} marks the uppermost level of an estuarine sedimentary environment. To this hypothesis we must add the role of oxidation and pedogenesis which destroys pyrite (see Chapter 5). The proportionate decline in S_{py} from the reduced estuarine clay to the grey clay is therefore both a sedimentary and pedogenic transition.

DARK BROWN/BLACK CLAY

This stratigraphic unit forms the surface of the Magela Plain, the so-called 'black soil' of the Alligator Rivers Region. This unit, and that part of the Sands and Clays unit upstream of Mudginberri, are the only morphostratigraphic entities. They are also the youngest sediments, with the exception of transitory sediments within the East Alligator River and thin veneers within the billabongs of the Magela Plain.

The Dark Brown/Black Clay is richer in organic carbon than any other stratigraphic unit, and it is its dark colour that distinguishes this unit from the underlying grey clay in the field. This boundary within the Mudginberri Corridor along cross-section 1 is between dark brown clay and clay loam to sand, whereas along cross-section 2 the boundary is very sharp between Dark Brown/Black Clay and Grey Clay. This same sharp boundary continues through the Upstream Basin. In the Central High, Downstream Plain and East Alligator Flood Plain, the boundary at many sites is gradational. Whereas in the upstream parts of the Plain the boundary is like that formed either by a change of sedimentary conditions or by a change of preservation potential of organic matter, in the downstream area the boundary is more like that between A and B horizons of a soil.

This body of sediment varies in its properties along and across the Plain, a subject to be considered in detail below. The sediments on the High Plain are generally lower in organic matter and lighter in colour than the sediments of the Low Plain.

There is little evidence of sedimentary structures in this unit, although in almost all pits and cores there is clear evidence of layering of materials (despite disturbance by buffaloes and magpie geese) with varying texture and organic content. Most often this layering is in dark coloured materials but upstream of Jabiluka Billabong (cross-section 4, Fig. 3.1) very pale layers cut through the organic-rich sediments. These pale layers are the result of marked variations of either sedimentary conditions or of organic matter deposition/destruction. These layers will receive fuller treatment below.

3.3 CHEMICAL PROPERTIES

Samples taken from cores, auger flights and pits were oven dried within 12 hours to stop oxidation of pyrite. These were subjected to a wide range of chemical determinations principally to elucidate the pedogenesis that the sediments of the Plain have undergone. But some of these chemical properties also add to our understanding of the sedimentary environments that have prevailed at various times on and beneath the Magela Plain.

LONGITUDINAL CHANGES

Measurements of Cl and organic C within the three main stratigraphic units have been averaged for each cross-section (Fig. 3.1) and shown as a longitudinal section in Figs 3.2 and 3.3. The values used in these graphs are also given in Table 3.2.

The mean values of Cl concentration vary markedly down the Plain (Fig. 3.2). Although Cl is mobile it should reflect sedimentary environments of widely varying salinity. Cl is most

abundant in the unoxidised estuarine clay rising from 479±53 mg/l to 4254±709 mg/l between cross-sections 2 and 10, with a decrease at cross-section 3. The East Alligator Flood Plain is underlain by estuarine clays of much higher Cl content (cross-section 11). This pattern reflects the normal increase in the salinity of fine-grained estuarine sediments as the open ocean is approached.

There is less CI in the Grey Clay but it shows the same pattern of change as seen in the Blue-Grey Clay. This is consistent with the grey clay being deposited in conditions transitional between estuarine and freshwater, and being oxidised and leached of some of its soluble components.

The Dark Brown/Black Clay has a low Cl content, except in the East Alligator Flood Plain where occasional salt water inundation raises the Cl concentration to values comparable with those in the Grey Clay over most of the Plain.

The pattern of organic C variation down the Plain (Fig. 3.3) shows that the surface Dark Brown/Black Clay has the highest values followed by the unoxidised estuarine clay and then the Grey Clay. The overall pattern of change in the three stratigraphic units is similar, showing a simple decrease down the Plain, with low and steady values across the Downstream Plain and East Alligator Flood Plain. In detail, however, the three curves do not mirror each other.

PYRITE FORMATION

Pyrite has been found using optical microscopy and SEM in all of the stratigraphic units as framboids, isolated crystals and pyritised organic matter. The largest quantity of pyrite (as pyrite sulfur, S_{py}) is found in the unoxidised estuarine clay, followed by the Grey Clay and the Dark Brown/Black Clay (Table 3.2).

Pyrite is formed in most marine sediments under anoxic, sulfate-reducing conditions. In so-called normal marine conditions (i.e. where bottom waters are oxic and usually deep; Raiswell & Berner 1985) pyrite forms during shallow burial of organic matter in the presence of reactive iron minerals. H₂S is produced by the reduction of interstitial dissolved sulphate by bacteria that use organic matter as both a reducing agent and a source of energy (Berner 1984). Reaction of the H₂S with detrital iron minerals produces pyrite by early diagenesis of a series of metastable iron monosulphides. The limiting factors for pyrite formation are therefore sulfate, reactive organic matter, reactive iron, and sulfate-reducing bacteria.

In most normal marine conditions there is no lack of sulphate, and it is rare for there to be a deficiency of reactive iron or sulphate-reducing bacteria. Organic matter can be limiting. The dominant control of organic matter on sulphate reduction and pyrite formation is shown by Berner's (1984) positive linear relationship between organic C and pyrite sulfur (expressed as weight %). This relationship implies that an approximately constant proportion of originally deposited organic matter is used in pyrite formation.

The clays which form the unoxidised blue-grey stratigraphic unit and that part of the oxidised Grey Clays thought to have formed in similar conditions on the Magela Plain, were deposited under shallow oxygenated water. Wada and Seisuwan (1986) show that pyrite forms 20-30 cm beneath the surface in mangrove muds at the boundary between the oxidised upper sediments and the lower strongly reduced sediment. As deposition continues this zone of pyrite formation rises. Pyrite forms by substitution for ferric compounds which are pseudomorphs of micro-organisms which grew within plant debris. As the organic matter decomposes the pyrite is released and may occur as 'free' particles. The conditions on intertidal mangrove flats therefore may mimic normal marine conditions by producing the same relationship between C and S_{py}.

The mean values (\pm standard errors) of S_{py} and organic carbon for each stratigraphic unit on each cross-section of the Magela Plain (from Table 3.2) are shown in Fig. 3.4. Both the unoxidised estuarine clays and the Sands and Clays units fall within the envelope which defines normal marine sediments (Berner 1984, and references therein). The best-fit line ($S_{py}/C = 0.35$) on this graph is from Berner (1982).

This plot confirms the suspicion that both normal marine and intertidal mangrove flat sedimentary environments produce the same relationship between S_{py} and C. Comparing Figs 3.4 and 3.3, it is clear that most pyrite within the unoxidised estuarine clays, and Sands and Clays, was formed in the upstream part of the palaeo-estuary. The pattern of organic C within these units along the Plain is probably a reflection of stillwater accumulation of mangrove-derived organic matter upstream and the loss of organic matter by tidal flushing and reworking by tidal channels downstream.

The mean values of S_{py} and C for the Dark Brown/Black Clay lie along the abscissa of Fig. 3.4, indicating that the very small amounts of pyrite in these sediments are either eroded from other sites and deposited without any correlation with co-deposited organic matter, or have formed in situ under sulphate limiting conditions. Berner and Raiswell (1983) compiled data for organic C and S_{py} for modern freshwater lake muds. These data show the same pattern as the results in Fig. 3.4 for the Dark Brown/Black Clay of the Magela Plain. It is therefore most likely that the pyrite in these Magela sediments has formed in situ under freshwater conditions where sulphate was limited. Widespread redistribution of pyrite by transport is unlikely in the absence of detrital grey clays bedded in the Dark Brown/Black Clay.

The mean values of C and S_{py} for the Grey Clay fall evenly into the normal marine/intertidal mangrove envelope and the freshwater envelope in Fig. 3.4. These means from cross-sections that fall into the first category probably consist of individual samples of pyritic mud deposited under estuarine conditions. Those samples of Grey-Clays on cross-sections that fall within the freshwater envelope in Fig. 3.4 are either a mixture of materials deposited in mangrove and freshwater environments, or they are dominantly freshwater in origin.

3.4 RADIOCARBON DATING OF THE STRATIGRAPHIC UNITS

The stratigraphic units and environmental changes discussed above have been dated principally by the ¹⁴C method. Gupta and Polach (1985) give an excellent account of the method and procedures in common use. Most samples were processed at the CSIRO radiocarbon laboratory, formerly in the Division of Soils and now in the Division of Water Resources, using the methods of Gupta and Polach.

The samples selected for dating are all organic and are believed to be approximately coeval with the clastic sediment in which they are found. However, transported organic matter may have been isolated by death from the contemporary atmospheric ¹⁴C some years before being deposited at the site where it is eventually recovered.

Samples used for dating were selected on the basis of their macroscopic organic content. Fragments of 'mangrove' wood, twigs, leaves and peat were recovered from the unoxidised estuarine clays, while charcoal and fine organic debris (organic clay or clay loam) was recovered from younger sediments. Very little wood, charcoal, or leaf litter has been found in the Dark Brown/Black Clay. It has therefore been necessary to use the disseminated organic matter within these sediments. This organic matter is largely derived from the vegetation that grows on the Plain and so is likely to be of essentially the same age as the mineral sediment with which it has been deposited. However, the chance of contamination by younger carbon (organic acids) is increased when dating such materials.

Contamination from humic acids is normally considered to be unimportant in acid sediments like those of the Magela Plain. Consequently, initial ¹⁴C determinations were made without substantial pretreatment. In the Mudginberri Corridor two pits on cross-section I were sampled for organic fragments from the freshwater clays, and samples taken for thorium-radium dating. The results are shown in Table 3.3 (also see Table 3.6).

The samples taken from MX Pit 1 were too small to provide workable errors. In the case of MX Pit 2, sample CS617 is notionally equivalent to an age of 410±80 years BP. This age is 5 to 6 times less than that estimated by thorium-radium dating (see below).

The small amounts of carbon retrieved from these samples could be more readily contaminated by mobile and younger carbon than is the case for a large piece of wood, for example. In subsequent analyses, before age determination, all alkali soluble material was removed after rootlets had been removed by reworking and hand picking. The alkali treatment follows that of Gupta and Polach (1985).

To test the appropriateness of this procedure, the alkali soluble and insoluble fractions of several samples were compared for their ¹⁴C activity. The results are given in Table 3.4. From these results, it seems that contamination by alkali soluble organics is most important near the groundsurface even in the prevailing acid conditions. The elaborate pretreatment was therefore necessary.

Pit MX 3 was opened beside the former MX Pit 1. Samples from MX 3 were pretreated and only the alkali insoluble fractions dated. The results are shown in Table 3.5. These estimates are very close to those given by the thorium-radium method (see below).

During the pretreatment it is possible to contaminate the sample with atmospheric carbon dioxide, precipitated as sodium carbonate, resulting in a younger measured age. Providing that sufficient time is allowed for the final acid wash then the contaminant will be removed. This can be checked by measuring the 13 C value of the sample. Atmospheric carbon dioxide is readily distinguishable from organic material using values of δ^{13} C.

Measured values of 13 C for each dated sample have been used to calculate ages corrected for isotopic fractionation. Different kinds of organic and inorganic carbon have different values of δ^{13} C (Gupta & Polach 1985). Peat and humus have a mean value of -27 °/.. (rel. PDB standard) whereas freshwater snails have a mean value of -5 °/.. (rel. PDB).

All of the dated samples, for which reliable results exist in Table 3.6, have been plotted in Fig. 3.5. Mangrove wood has a δ^{13} C value of -28 °/... (rel. PDB). The trend to less negative values with decreasing age is evident, reflecting the change in the Magela Plain from estuarine mangrove forests to freshwater seasonal swamps.

3.5 THORIUM-RADIUM DATING IN THE MUDGINBERRI CORRIDOR

The history of the Magela Plain has been derived principally using a chronology based on radiocarbon dating (Section 3.4) of detrital organic remains embedded in sediment. Very little wood or charcoal has, however, been found in the freshwater sediments that make up the surface of the Plain. Dating of these sediments has, therefore, required the use of disseminated organic matter for which there is a high probability of contamination by carbon that is younger than that deposited with the mineral sediment. Alternative methods of dating these sediments have, therefore, been sought.

Since the age of the deepest freshwater sediments is of the order of several thousand years, the only nuclide in the naturally occurring uranium and thorium series of radionuclides that has a suitable radioactive half-life is 226 Ra (T $_{1/2} = 1600$ yr). The observed concentrations of 226 Ra in the surface sediments of the Mudginberri Corridor are considerably greater than

those of 238U (Johnston et al. 1988). If it were established that this disequilibrium between ²²⁶Ra and ²³⁸U reflects a disequilibrium between ²²⁶Ra and its parent ²³⁰Th, sedimentation rates in the Mudginberri Corridor could be determined by measuring the ²²⁶Ra excess as a function of depth in the sediment. The purpose of the work described in this section is to investigate the possible application of thorium-radium dating to sediments of the Mudginberri Corridor.

THE THORIUM-RADIUM DATING METHOD

If the concentration of 226 Ra in the sedimenting material that is now at depth x in the sediment was $R_0(x)$ at the time of deposition and the corresponding concentration of 230 T was $T_0(x)$, then the present day concentrations of 226 Ra at depth x, R(x), is given by:

$$R(x) = R_0(x) e^{-\lambda t(x)} + T_0(x)(1 - e^{-\lambda(x)})$$
3.5.1

where t(x) is the time since deposition at depth x and λ is the radioactive decay probability of 226 Ra. The radioactive decay of 230 Th (T $1/2 = 75\,000$ y) has been neglected in the derivation of this equation, because it is unimportant for the time period being considered.

Hence the time since deposition is given by:

$$t(x) = -\frac{1}{\lambda} \ln[(R(x) - T_0(x))/(R_0(x) - T_0(x))]$$
3.5.2

Both R(x) and $T_0(x)$ can be established by current measurements on a sample collected from depth x but $R_0(x)$ is, in general, unknown. If, however, it is assumed that both $R_0(x)$ and $T_0(x)$ have been constant throughout the period of deposition and that the deposition rate, r, has been constant then

$$\ln E(x) = \ln E_0 - \lambda x/r \qquad 3.5.3$$

where $E(x) = R(x)-T_0(x)$ is the observed radium excess and

$$E_0 = R_0(x) - T_0(x)$$

is the unknown initial radium excess. The sedimentation rate and the time of deposition for depth x (t = x/r) can therefore be derived from a plot of ln E(x) versus x.

The assumptions inherent in the above method of dating are that: the sedimentation rate has been constant throughout the period over which deposition has taken place; the concentrations of ²²⁶Ra and ²³⁰Th have been similarly constant; both ²²⁶Ra and ²³⁰Th have been chemically immobile since deposition; and the sediments have not been disturbed by bioturbation or other processes.

One or two discrete changes in sedimentation rate over the history of a depth profile would not seriously impair the method since such changes would be detected by observed discrete changes in the gradient of $\ln E(x)$ versus x, provided a sufficient number of measurements were taken. The constancy of 230 Th concentrations can be checked by direct observation but the constancy of $R_0(x)$ cannot be directly established. Examination of the constancy of the concentrations of other long-lived nuclides, particularly those of the uranium series, should however give an indication of the constancy expected for $R_0(x)$.

Because of its extremely low solubility in natural waters, ²³⁰Th is not expected to have been mobilised during the period since deposition. It is for this reason that most clastic deposits contain thorium in concentrations similar to source rock (Gascoyne 1982).

Radium is highly mobile in the marine environment. It has been established that the major source of ²²⁶Ra in the oceans is diffusion from sediments on the sea floor (Turekian 1971; Turekian & Cochran 1978). This high mobility of radium in the marine environment has precluded its application to sediment geochronology (Lalou 1982). However, the mobility of radium in the freshwater environment is significantly lower than in the marine environment. Desorption of radium and barium from suspended solids in rivers has been observed to occur as the material crosses the salinity gradient in estuaries (Li et al. 1977; Hanor & Chan 1977; Li & Chan 1979). These observations were responsible for a revised estimate of the significance of the input of radium to the oceans from rivers.

Despite the reduced mobility of radium in the freshwater environment, hardly any attempt has been made to use observations on ²²⁶Ra excess over ²³⁰Th as a means of dating. Inorganic freshwater carbonates and molluscs have been investigated in dating studies by Kaufman and Broeker (1965); discrepancies with ¹⁴C dates were attributed to radium mobility. The short-term mobility of radium can be examined by observations of the ratio of ²²⁸Ra activity to that of its parent ²³²Th. The best method, however, of establishing the significance of radium mobility in a particular environment is to compare the results of thorium-radium dating with those obtained by an independent established technique such as the ¹⁴C dating method. Both procedures have been adopted in the present study. Comparison with ¹⁴C derived dates should also provide a check on the significance of bioturbation and other disturbance mechanisms.

METHODOLOGY

Two samples of sediment profiles were collected at sites in the southern end of Mudginberri Corridor during the 1985 Dry season. One site (MX2) was in the bed of the main-flow channel while the other (MX1) was remote from the channel and in an area that is only inundated during the main flood period of the Wet season. Site locations are indicated on the map in Fig. 2.3.

To enable a careful examination of the stratigraphy at each site and to avoid compression of the sediment during sampling, a coring technique was not used. Rather, at each site a large pit was excavated and a vertical profile of the exposed sediment was removed intact by pressing an aluminium box of rectangular cross-section (30 cm x 15 cm) into the vertical face of the pit.

Stratigraphic details were recorded at each site. At MX1 the sediment consisted of dark brown clays to a depth of about 70 cm with orange-brown mottles appearing below about 15 cm. There were few organic fragments in the clay. A transition to fine-to-medium grained sand occurred at 70 cm. The sediment composition was similar at MX2 but the transition to sand occurred at a depth of about 35 cm. In this case the grain size was medium to coarse and the sands were interspersed with pebbles and mud-balls. Organic material was relatively abundant at MX2.

Each box monolith was subdivided into 2 or 3 cm sections in the laboratory and these sections were dried at 60°C. Roots, gravel (>2 mm) and shell material were removed and, where possible, samples of carbonaceous material were retained for ¹⁴C dating. Each subsample was then homogenised before further subdivision for the measurement of organic content, particle size and radionuclide analysis.

The radionuclides ²²⁶Ra, ²²⁸Ra, ²²⁸Th and ⁴⁰K were analysed by gamma-ray spectroscopy using the methods given by Murray et al. (1987). In summary, after drying and grinding to

a fine powder, samples were mixed with polyester resin and cast in a standard geometry. After a period of 20 days had elapsed to allow for ingrowth of ²²²Rn and daughters, the gamma-ray spectrum was measured using an intrinsic germanium detector. Absolute concentrations were determined by calibration using standard sources of the naturally occurring radionuclides provided by CAMNET (Canadian Bureau of Minerals and Energy Technology) and Amersham. The calibration standards were cast in the same geometry as the sediment samples. Concentrations of ²³⁸U, ²³⁴U, ²³²Th and ²³⁰Th were measured by alpha-particle spectroscopy (Martin & Hancock 1987).

RESULTS FOR SITE MX1

The results obtained for the concentrations (with respect to ash weight) of all the long-lived naturally occurring radionuclides in the sediment profile at site MX1 are given in Tables 3.7 and 3.8. The errors due to counting statistics are given in parentheses. Table 3.7 also lists the radium excess values obtained and several estimates of the associated errors. The error in the excess radium concentration due to counting statistics is σ_1 . The other estimates are discussed below.

The variation with depth of the concentrations of the long-lived nuclides (other than radium) has been used to investigate the validity of some of the assumptions made in deriving equation 3.5.3. Concentrations of ²³⁸U, ²³²Th, ²³⁰Th and ⁴⁰K are shown in Fig. 3.6 as a function of depth. The sample at 80 cm is from the basal sand and clearly does not satisfy the assumption of constant ²³⁰Th concentration and has been excluded from further analysis. The variability of concentrations in samples taken from the clay is not large and the assumption of constancy of concentrations of ²²⁶Ra in the sedimenting material is, therefore, probably a reasonable one.

A statistical summary of the observed radionuclide concentrations is given in Table 3.10. The relative standard deviation (σ/\overline{x}) for the long-lived nuclides varies between 6% and 11%. These results should be compared with the average relative measurement error, $(\overline{\sigma_i/x_i})$, which is about 4% in each case. It can therefore be concluded that concentrations of long-lived nuclides in the sedimenting material have had a true variability of about 9% (the mean of 238 U, 234 U, 232 Th, 230 Th and 40 K results). An estimated error of 9% has been attributed to each value of the excess radium concentration in Table 3.7 to take into account the variability of 226 Ra in the sedimenting material at the time of deposition (σ_3 in Table 3.7).

An estimate of the significance of radium mobility in the sediments over the past few thousand years is difficult to make. Some applicable laboratory techniques exist (e.g. column leaching tests under high pressure) but these have not been carried out. An indication of the significance of mobility over periods of a few years can, however, be obtained by examination of the ratio of concentrations of ²²⁸Ra to those of ²³²Th in the sediment. Since ²²⁸Ra has a half-life of 5.9 years, these nuclides would be expected to be in equilibrium in the sediment if radium mobility is small over a period of time comparable with this half-life.

The ratio of concentrations of ²²⁸Ra to those of ²³²Th in the sediment samples at site MX1 are listed in Table 3.9 and plotted in Fig. 3.7, and the statistical summary is given in Table 3.10. The mean ratio is 1.02 with a standard error of 0.02. This result indicates that radium mobility is small over a period of a few years. However, the relative standard deviation, 7.6%, is significantly greater than the average relative error (4.1%) due to counting statistics. This result could indicate some relative mobility of radium with respect to thorium but, given the mean value of unity, it is more likely that it reflects variability in the analytical procedures. A random error of 6.5% in the relative calibration of the two techniques used (e.g. different and variable recovery efficiencies for the tracer and naturally occurring thorium) could account for the observed standard deviation. For this reason an

error of this magnitude (σ_2 in Table 3.7) has been attributed to the concentrations of ²³⁰Th in estimating the error in the radium excess concentration. The total estimated error in each value of the radium excess, σ_4 , has been obtained from the quadratic sum of σ_1 , σ_2 and σ_3 .

The variation with depth of the 226 Ra excess in sediment samples from site MX1 is shown in the upper graph of Fig. 3.8. The best fit to these data, using expression 3.5.3 and unweighted least squares fitting, is also shown. Results obtained, using this original data set, for the sedimentation rate, initial excess at the time of deposition, R^2 , and chi-square per degree of freedom are given in Table 3.11 for both weighted and unweighted least squares fitting. Statistical errors are given in parentheses. The χ^2 definition adopted is that incorporating the error estimates, namely

$$\chi^{2} = \sum_{i=1}^{n} [(E_{i} - F_{i})/\varepsilon_{i}]^{2} / (n-2)$$
3.5.4

where E_i is the measured excess, F_i is the calculated excess and ε_i is the estimated error in the measured excess. Although the data are quite well represented by a single exponential curve, the value of χ^2 indicates that either the function used is not adequate or that the errors have been underestimated.

Although, as indicated above, the concentrations of the long-lived nuclides are approximately constant, examination of the data in Fig. 3.6 shows that deviations from constancy follow a similar pattern for ²³²Th, ²³⁰Th and ⁴⁰K. Such behaviour could arise from mixing to a variable extent of the mineral sediment (with assumed constant radionuclide concentrations) with inactive material such as sand or biogenic silica. If this were the case, the ratios of observed concentrations would exhibit constancy to a much greater extent than the absolute values of individual concentrations. Results for a number of relevant ratios are given in Table 3.9 and some of these are plotted in Fig. 3.7 as a function of depth in the sediment. The statistical summaries are given in Table 3.10.

In all cases the assumption of constancy is better for the ratios than for the absolute values of concentration. For example, the relative standard deviation is equal to the average relative error in the measurement for $^{234}\text{U}/^{238}\text{U}$, $^{232}\text{Th}/^{230}\text{Th}$ and $^{40}\text{K}/^{228}\text{Ra}$. This is also the case for $^{238}\text{U}/^{230}\text{Th}$ for samples taken below a depth of 10 cm. The result for $^{40}\text{K}/^{230}\text{Th}$ indicates a small residual variance but this is consistent with the previously noted variance associated with the use of two measurement techniques in the case of the ratio $^{228}\text{Ra}/^{232}\text{Th}$.

If f(x) is the fraction (by weight) of the mineral sediment in the sample at depth x, then the observed concentration of 226 Ra is given by:

$$R(x) = f(x)R_0(x) e^{-\lambda t(x)} + f(x)T_0(x) (1 - e^{-\lambda t(x)})$$
3.5.5

where the notation used is the same as in equation 3.5.1. The observed concentration of 230 Th, T(x), is given by:

$$T(x) = f(x)T_0(x)$$
 3.5.6

Hence

$$R(x) - T(x) = f(x) (R_0(x) - T_0(x)) e^{-\lambda t(x)}$$
3.5.7

and

$$ln[E(x)/f(x)] = ln E_0 - \lambda x/r$$
3.5.8

Although the absolute value of $T_0(x)$ is not known, the relative values of f(x) can be obtained by scaling to a chosen reference point, e.g. x = 0. Thus using f(x) = T(x)/T(0), all values of the observed excess should be divided by f(x) before regressing the results against x.

The corrected data obtained in this way are shown in the lower graph of Fig. 3.8. The solid line is the result of an exponential fit to the data using unweighted least squares fitting. Results obtained using these corrected data are given in Table 3.11 for both weighted and unweighted fitting. The quality of the fit is better and the value of χ^2 is reduced compared with that obtained using the original data set.

In each of the four analyses presented, the point at x = 33 cm consistently contributes a value of $\chi_i^2 \simeq 10$ to the total chi-square. The above analyses were repeated using a data set which excluded this point. The results obtained with both the original and the corrected data sets are given in Table 3.11. The final value of chi-square per degree of freedom is about 1.7. A substantial part of the original variance has been accounted for by the above measures.

In conclusion, the sedimentation rate at site MX1 obtained from thorium-radium dating is 0.19±0.02 mm yr⁻¹ and the initial radium excess is 270±30 Bq kg⁻¹. The errors quoted arise from statistical uncertainties but the variation obtained from different methods of data analysis is consistent with these statistical errors.

RESULTS FOR SITE MX2

The results obtained for the concentration (with respect to ash weight) of all the long-lived naturally occurring radionuclides in the sediment at site MX2 are given in Tables 3.12 and 3.13. Table 3.12 also lists the values obtained for the radium excess and various estimates of the error in the excess derived in a similar way to that described for MX1.

The variation with depth in the sediment of the concentration of ²³⁸U, ²³²Th, ²³⁰Th and ⁴⁰K is shown in Fig. 3.9. The variability is much greater than was observed for samples from MX1. The results for the samples at 35 and 43 cm have been omitted from further analysis because the latter was taken from below the transition between clay and sand and the results for the 35 cm sample imply that there is a significant contribution from sand in this sample.

Statistical summaries of the results for each nuclide are given in Table 3.15 for samples collected at depths down to 34 cm. The relative standard deviation for concentrations of each of 232 Th, 230 Th and 40 K is about 15% compared with an average relative measurement error of about 4%. Hence, the assumption of constant concentrations in the sedimenting material is not good in this case. On the basis of these results an estimated error of 15% has been attributed to the values of the radium excess (σ_3 in Table 3.12) to take into account the variation of concentrations of 226 Ra in the sedimenting material. This error dominates all other sources of error in its contribution to the total estimate error, σ_4 . In addition, it should be noted that unlike the results obtained for MX1 the variation of concentrations is not random about the mean value but exhibits a systematic or quasi-cyclic dependence on depth.

The variation with depth of the 226 Ra excess is shown in Fig. 3.11. Also shown is the best fit to the data using unweighted fitting with expression 3.5.3. Results obtained for the sedimentation rate, initial excess radium, R^2 and chi-square per degree of freedom are given in Table 3.11. Although the value of R^2 shows that the regression only accounts for 75% of the variance in the data, the value of χ^2 , 0.87, shows that this result is quite consistent with the estimated errors in the measurements. In the case of MX2 samples an error-weighted analysis has not been carried out because, due to the dominance of σ_3 , the total error is approximately a constant percentage in each case. Since the fitting procedure involves the

logarithm of the measured excess, unweighted and error-weighted analyses will yield identical results.

Results obtained for a number of concentration ratios are given in Table 3.14 and are plotted in Fig. 3.10 against depth in the sediment profile. Statistical summaries are given in Table 3.15. As was observed for site MX1, the assumption of constancy is much better for these ratios than for the absolute values of concentrations. Except for the case of $^{238}\text{U}/^{230}\text{Th}$, which will be considered further below, the relative standard deviation for all ratios is equal to the average relative measurement error. For this reason, a corrected data set was generated by assuming a variable mixing of mineral sedimenting material with inactive material using the same procedure as was adopted for site MX1.

The corrected data and the best fit using expression 3.5.7 are shown in the lower graph of Fig. 3.11. The results obtained for the variables are given in Table 3.11. For MX2 samples, this correction procedure does not give rise to an improvement in the quality of fit. The value of \mathbb{R}^2 is reduced from 0.74 to 0.43 and the χ^2 per degree of freedom increases from 0.9 to 3.1. Hence the residual variance in the fit to the original data set is not explained by this simple mixing model. The origin of the variability of concentrations of radionuclides at this site is discussed in the next section.

The sedimentation rate at site MX2 obtained using the original data set is 0.20 ± 0.04 mm yr⁻¹, a value that is in close agreement with that obtained at MX1. An indication of the magnitude of possible systematic errors is obtained by noting that the use of the above correction procedure, which does not produce a satisfactory fit to the data, only changes the deduced sedimentation rate by 20%.

DISCUSSION

The primary purpose of this research was to investigate the applicability of the thorium-radium dating method to sediments of the Mudginberri Corridor, when samples suitable for ¹⁴C dating are difficult to obtain. While some of the assumptions inherent in the method (including a limited check on radium mobility) have been tested, the best test of the method is a comparison of the results obtained with other techniques. For this reason, a number of samples of organic material were collected from the sediment at sites MX1 and MX2 and ages were determined using the ¹⁴C dating technique.

Unfortunately, most of these samples proved to be too small to provide reliable estimates of age. For site MX2, however, the result obtained for a sample from the depth interval 30-35 mm was 95.0±0.9% modern activity, giving an age of 410±80 BP (CS 617). This age contrasts with that obtained from thorium-radium dating of 1600±300 yr based on the result for MX2 in Table 3.11 and 1710±180 yr based on the more precise data for site MX1.

This discrepancy prompted a review of the methodology used in ¹⁴C dating (see section 3.4). In particular, the possible significance of contamination of dated samples by young carbon was investigated by removal of alkali-soluble material and comparing the results obtained for the alkali-soluble and alkali-insoluble fractions. This investigation showed that contamination by alkali-soluble organics is a significant effect, particularly near the ground surface.

A new pit was opened up at site MX3 close to the former pit at site MX1. Samples collected at site MX3 were pre-treated using a procedure discussed by Gupta and Polach (1985), and only the alkali-insoluble fraction was dated. Ages obtained for two samples at MX3 were 2630±100 BP (CS 688) for a sample at 56-62 cm and 2400±170 BP (CS 698) for a sample at 78-86 cm. These yield a mean sedimentation rate of 0.26±0.04 mm yr⁻¹ in reasonable agreement with that obtained from thorium-radium dating at the nearby site MX1. The

conclusion drawn from this comparison is that the thorium-radium dating technique is applicable to the sediments of the Mudginberri Corridor.

One drawback of the thorium-radium technique is that, in contrast with the ¹⁴C method, the initial activity of the decaying nuclide (226Ra in this case) in any single sample collected at depth is not, in general, known. Application of the thorium-radium method requires the analysis of a number of samples taken from a range of depths in the sediment and, in addition, requires the assumption of constancy of the radium concentration in the sedimenting material as a function of time. The analysis has shown that, after regression using expression 3.5.3, the residual variance can, to a significant extent, be accounted for by attributing to the initial radium concentration a variance equal to that observed for the other long-lived naturally occurring radionuclides. A further reduction in variance was obtained in the case of samples from site MX1 by invoking a simple mixing model in which it was assumed that there are two contributions to the mineral sediment at any depth; an active component in which the specific activity concentrations have been constant and an inactive component such as biogenic silica. This procedure was unsuccessful for MX2. Indeed its use resulted in a considerable increase in the residual variance. Because of the importance of the assumption of constant initial radium activity in the thorium-radium dating method or, in the absence of such constancy, the need for a method of taking it into account in the analysis, the variability observed in the current study was examined further.

The two sites at MX1 and MX2 are separated by about 60 m. However, at this location the width of the flowing waterbody from which deposition of mineral sediment occurs is greater than 1 km for most of the Wet season. Also, although site MX2 is in the main-flow line, the difference in elevation between the two sites is only about 0.7 m and therefore the water velocity at the two sites is very similar for most of the Wet season. It would be expected, therefore, that, apart from the initial part of the Wet season, the composition of the mineral sediment deposited from the water column is identical at the two sites and that this has been the case over most of the period since deposition of freshwater sediments began. The identity of the ratios of the concentrations of different nuclides at the two sites gives strong support to this conclusion. For example, the ratio 232 Th/ 230 Th is 1.23±0.02 and 1.26±0.02 at MX1 and MX2 respectively. The corresponding results for 40 K/ 230 Th are 2.63±0.05 and 2.69±0.04 respectively.

The absolute concentrations of radionuclides are, however, quite different. For example, the mean concentrations of ²³⁰Th are 84.4±1.9 Bq kg⁻¹ and 57.9±2.4 Bq kg⁻¹ at MX1 and MX2 respectively. For ²³⁸U the corresponding mean values are 89.8±1.9 Bq kg⁻¹ and 70.2±1.8 Bq kg⁻¹, respectively. These differences imply that there is (at least) a second component in the mineral sediment at MX2, and this second component may also contribute at MX1. Further, the observed variability of the absolute concentrations with depth at both sites implies that the fractional contribution of the second component has varied over time at both sites although this effect is more marked at MX2.

The observed constancy of the ratios of various concentrations at both sites led to the proposition that the concentrations of all nuclides in the second component were zero or very small. However, although this conclusion applied to ²³²Th, ²³⁰Th and ⁴⁰K, the results for ²³⁸U and ²³⁴U were not as conclusive. For example, using the data given in the previous paragraph, the ratio of the mean ²³⁰Th concentrations at MX2 and MX1 is 0.69±0.03 while the corresponding ratio for ²³⁸U is 0.78±0.03. This difference may imply that the concentration of ²³⁸U in the second component is non-negligible. If this were so there would be no valid reason for assuming that the unknown initial concentration of ²²⁶Ra is negligible in the second component. In the analysis that follows, therefore, the assumption of zero activity in the second component has been avoided except where strong evidence exists in its support.

If X_i and Y_i are the intrinsic concentrations of nuclide i in the first and second components of the mineral sediment and $f_1(x)$ and $f_2(x)$ are the fractional contributions of these components to the sediment at depth x, then the concentration of nuclide i at depth x is given by:

$$C_i(x) = f_1(x)X_i + f_2(x)Y_i$$
 3.5.8

and

$$f_1(x) + f_2(x) = 1 3.5.9$$

The ratio of concentrations of nuclides i and j is then given by:

$$\frac{C_i(x)}{C_j(x)} = \frac{X_i(f_1(x) + f_2(x)Y_i/X_i)}{X_j(f_1(x) + f_2(x)Y_j/X_j)}$$
Thus, this ratio is independent of x, for varying values of $f_1(x)$ and $f_2(x)$, only if

$$Y_i/X_i = Y_i/X_i$$
 3.5.11

or
$$X_i/X_i = Y_i/Y_i$$
 3.5.12

Thus constancy of the ratio of concentrations of different nuclides only occurs if the ratio of these nuclides in the two components is identical or both nuclides have zero concentration in one of the components.

The ratios of nuclides of quite different chemical elements, such as thorium and potassium, exhibit constancy at each site and they have identical values at both sites. It would be remarkable if this arose because of the identical value of the ratio of these concentrations in two different components in the sediment, the one arising from the deposition of particulate matter from the water column and the other possibly arising from in situ development through biological processes. The nuclides ²³⁰Th and ²³²Th are isotopes of the same element but originate in different natural series of radionuclides. It would be similarly unlikely that their ratios were identical in both contributions to the sediment. It is concluded that the probable explanation for the observed constancy of the ratios of the concentrations of ²³⁰Th, ²³²Th and ⁴⁰K is that the absolute concentrations are negligibly small in one of the components, assumed here to be the second component. Thus, for these nuclides $Y_i = 0$, i = 1, 2 and 3, and therefore the fractional contribution of the two components at depth x at each site is given by:

$$f_1(x) = C_i(x)/X_i$$
 3.5.13

$$f_2(x) = 1 - C_i(x)/X_i$$
 3.5.14

where $C_i(x)$ is the observed concentration of one of these nuclides at that site.

If the subscript j is used to identify a nuclide for which the concentration in the second component is assumed to be non-zero, e.g. ²³⁸U, ²³⁴U and ²²⁶Ra, substitution of equations 3.5.13 and 3.5.14 in 3.5.8 gives the following expression for $C_i(x)$:

$$C_{j}(x) = \left\{\frac{X_{j} - Y_{j}}{X_{i}}\right\} C_{i}(x) + Y_{j}$$

$$3.5.15$$

If the above analysis is correct, there should be a linear relationship between the concentration of ²³⁸U and ²³⁰Th, the intercept of which should provide a measure of the concentration of ²³⁸U in the second component. Moreover, if the two components are the same at both sites but simply occur in different percentages, the regression represented by equation 3.5.15 should be common to both sites.

The concentrations of ²³⁸U are plotted against those of ²³⁰Th in Fig. 3.12 using data obtained for all samples collected at both sites. The best fit to the data using equation 3.5.2 is shown as the solid line. This regression clearly gives a good representation of the data for both sites, accounting for 73% of the variance. Results for the coefficients in equation 3.5.15 are:

$$Y_j = 31\pm 3 \text{ Bq kg}^{-1}$$
 3.5.16

$$(X_i - Y_i)/X_i = 0.69 \pm 0.08$$
 3.5.17

Thus the contribution of the second component to the observed concentration of uranium in each of the sub-samples of sediment at sites MX1 and MX2 ranges from 30% to 85%. The absolute concentrations of $^{238}\mathrm{U}$ and $^{230}\mathrm{Th}$ in the first component cannot be established from this analysis. A lower limit for X_i , however, is given by the maximum observed concentration of $^{230}\mathrm{Th}$, namely 95±4 Bq kg $^{-1}$. Taking X_i = 100 Bq kg $^{-1}$, a value is obtained for the concentration of $^{238}\mathrm{U}$ in the first component, X_j , of 100 Bq kg $^{-1}$ from the above results. It would, therefore, appear that $^{238}\mathrm{U}$ and $^{230}\mathrm{Th}$ are in secular equilibrium in the first component, a result that would not be surprising for mineral sediment carried as particulate matter by Magela Creek to the Plain.

The above analysis has established that there are two components contributing to the sediment material at the sites sampled, that the concentrations of ²³⁰Th, ²³²Th and ⁴⁰K are effectively zero in the second component, that the concentration of ²³⁸U (and by implication ²³⁴U) in this component is significant, and that the two data sets obtained for sites MX1 and MX2 constitute a single data set in which the absolute values of observed concentrations arise from different values of the mixing fraction for each component in the sediment. It should be possible to extend this analysis to include ²²⁶Ra concentrations to examine the origin of the variability of the observed values of radium excess.

The values of the initial ²²⁶Ra concentration in each sample from sites MX1 and MX2 were calculated using the expression:

$$R_0(x) = (R(x) - T(x))e^{\lambda x/r} + T(x)$$
 3.5.18

The measured quantities R(x) and T(x) were used for each sample and the sedimentation rate used was r = 0.19 mm yr⁻¹, the best fit value obtained previously. The values of $R_0(x)$ obtained in this way are plotted against ²³⁰Th concentrations in Fig. 3.13. While the variance of the data set is larger than that obtained for ²³⁸U, it would appear that the two data sets for MX1 and MX2 constitute a single data set with a common regression with respect to ²³⁰Th concentrations. The best fit line using equation 3.5.15 is shown in the Figure, but it accounts for only 25% of the variance. The values of the coefficients for the line of best fit are:

$$Y_j = 210\pm 50 \text{ Bq kg}^{-1}$$
 3.5.19

$$(X_j - Y_j)/X_i = 1.8 \pm 0.6$$
 3.5.20

Taking the minimum value of X_i to be about the maximum value of observed ²³⁰Th concentrations, 100 Bq kg⁻¹, gives a value for the concentration of ²²⁶Ra in the first component of 380±80 Bq kg⁻¹.

It is not possible, on the basis of statistical analysis, to associate the residual variance in Fig. 3.13 with either the first or second component of the concentration of ²²⁶Ra in the

sediment. One can speculate, however, that this residual variance could result from the dependence of the second component on some other variable such as the time of deposition. If this were so, one would expect to observe a smooth variation of the ²²⁶Ra concentration with time rather than the random fluctuations about the regression line observed in Fig. 3.13.

The concentration of 226 Ra in the second component, $R_2(t)$, was calculated as a function of time at both MX1 and MX2 using equations 3.5.15 and 3.5.18 and incorporating the result given in 3.5.20. That is:

$$R_2(t) = (R(t) - T(t))e^{\lambda t} - (A-1)T(t)$$
3.5.21

with t = x/r and A = 1.8. Errors in $R_2(t)$ were estimated using only the errors in concentrations due to counting statistics and the error σ_2 in Tables 3.7 and 3.12. That is, use of the correlation in equation 3.5.15 has been assumed to take into account accurately the variability in the excess that is due to fluctuations in the 230 Th concentrations. It is the residual variability without errors of measurement that is being examined here. The results obtained for $R_2(t)$ are shown as a function of time in Fig. 3.14 over the period of 2000 years that is common to both sites. The line shown connects the data points for site MX2. The results for MX2 show a smooth dependence on time in contrast to the random fluctuations observed in the correlation with 230 Th concentrations. There is, perhaps, evidence for a quasi-cyclic pattern with a period of about 800 years. With the exception of the data point at $T \simeq 700$ yrs, the data for MX1, which are less frequent on the time axis, are not inconsistent with this quasi-cyclic behaviour.

From the above analysis, strong evidence has emerged for the existence of two components that contribute to the concentrations of radionuclides in the sediments at MX1 and MX2. The first of these components has high concentrations of all the nuclides examined. The second component contains very low concentrations of ²³²Th, ²³⁰Th and ⁴⁰K, significant concentrations of ²³⁸U and ²³⁴U, and the concentration of ²²⁶Ra is of the same order as that in the first component. About 25% of the residual variance in the data for the radium excess over thorium has been attributed to a correlation between ²²⁶Ra and ²³⁰Th in the first component. Somewhat weaker evidence has been presented that the remaining variance may be attributed to a quasi-cyclic variation with time in the concentration of ²²⁶Ra in the second component.

However, regardless of the veracity of this time dependent second component, it is clear that minimisation of the variance obtained in thorium-radium dating of such sediments will require a choice of sites where there is evidence for a low value of the contribution of the second component. Sites chosen should be those for which the ²³⁸U and ²³²Th concentrations are about 100 Bq kg⁻¹ (as at MX1) rather than about 50 Bq kg⁻¹ (as at MX2). Adoption of this procedure would ensure that concentrations of ²²⁶Ra are dominated by the first component for which corrections can be applied through the correlation with observed concentrations of ²³⁰Th.

3.6 POLLEN ANALYSIS AND BIOSTRATIGRAPHY

THE TECHNIQUE

From the preceding discussion of the lithology, sedimentology and chemistry of the materials that make up the Magela Plain it is possible to ascribe environments of deposition to some of the stratigraphic units and lithofacies. The units can also be dated. The surface morphostratigraphic unit, the Dark Brown/Black Clay (Fig. 3.1) has accumulated under freshwater conditions like those that currently prevail. This conclusion is a straightforward outcome of simple uniformitarianism. Some of the Sands and Clays, and the Basal Sands and Gravel, are of freshwater fluvial origin, as judged by comparisons of their sedimentologic

and textural features with modern fluvial deposits. The Blue-Grey Clay, by contrast, has an estuarine origin while the overlying Grey Clay was deposited under conditions that are not adequately specified by the criteria employed so far (cf. Pickup et al. 1987). The transitions or boundaries between the various stratigraphic units are also hard to specify in some circumstances.

To further define the sedimentary environments of the various bodies of sediment, and so more accurately account for the evolution of the Plain to its current state, a substantial effort has been made to use pollen as an indicator (Clark & Guppy 1988). Pollen assemblages at particular points in a core, and so in time, are generally good indicators of depositional environment. This is so if it can be shown that a consistent and spatially stable relationship can be found in the pollen contents of various modern depositional environments. For mangrove mudflats and chenier plains in northern Australia this relationship has been clearly shown by Grindrod and Rhodes (1984) and by Woodroffe et al. (1986).

While it is clear that mangrove muds can be distinguished from freshwater sediments using pollen analysis, it would also be valuable to use the technique to investigate changes in the vegetation that grew on the Plain during the freshwater phase marked by the Dark Brown/Black Clays. Once again, stable spatial relationships between the distribution of pollen in the surface sediments and the modern vegetation is required before down-core analysis will yield a meaningful vegetation history.

DISTRIBUTION OF 'MODERN' POLLEN

The sampling grid used for determination of the particle size and radionuclide content of the Plain's surface (see Chapter 6) has been used to determine both the distribution and concentration of the pollen taxa. Samples from 0-2 cm were processed in the same way as the subsurface samples. Using the mean sedimentation rates derived from ¹⁴C and thorium-radium dating in the Dark Brown/Black Clay, the upper 2 cm represents about 100 years of sedimentation. However, the surface sediments of the Plain are less compacted than below and so 2 cm is likely to represent <100 years but probably >50 years. A comparison with the modern vegetation may therefore fail to show correspondence for short-lived communities.

The modern vegetation and mean pollen types (at the ground surface) of the Magela Plain are shown in Fig. 3.15a&b (after Finlayson et al. 1985). Figure 3.16 shows the dominant pollen taxa at the surface sampling sites. Comparison of these figures shows that the surface pollen faithfully reflects the dominant modern vegetation. This result indicates that there is limited lateral transport of pollen on the Plain, with the dense aquatic vegetation acting as a substantial barrier to particle movement. This conclusion is supported by the map showing the distribution of Barringtonia and Pandanus pollen in surface sediments (Fig. 3.17). These two taxa occur in almost all the Mudginberri Corridor samples, reflecting a subdominant element of the vegetation in that area. Barringtonia pollen occurs occasionally further downstream near billabongs or channels, and Pandanus pollen near the edge of the Plain. These distributions of pollen once again reflect extant vegetation.

Surface samples dominated by terrestrial (i.e. upland woodland) pollen taxa are shown in Fig. 3.18. Most of this pollen group (and the highest pollen concentrations, Fig. 3.15) occurs in the Mudginberri Corridor where the pollen most likely arrives from upstream. There is no convincing explanation of the downstream pattern. The relationship between percentage Myrtaceae pollen in a surface sample and distance from the nearest Melaleuca tree is plotted in Fig. 3.19, showing a steep decline away from trees. Fig. 3.19, and at least the upstream part of Fig. 3.18, support the hypothesis that the amount of Myrtaceae pollen coming in from the surrounding upland woodland is insignificant compared with local production by Melaleuca on the Plain.

The pollen in the upper 2 cm of the Plain reflects, in the main, the dominant vegetation nearby. This pattern appears to have been stable for at least 50 years, a time period approximately equivalent to the depth interval of the smallest samples taken from cores for pollen analysis. By contrast, a small number of 'exotic' pollen grains occur in the surface samples. These grains are from mangrove taxa that do not occur on the modern Plain. Sonneratia was found in five samples in the Mudginberri Corridor and only one downstream. Rhizophora is also common in the Corridor but there is little Avicennia here. Avicennia was found in almost every sample between 19 and 23 km downstream. An explanation of this pattern will be offered later.

Before turning to the interpretation of pollen preserved in subsurface sediments, preferential preservation or destruction of pollen in surface sediment needs to be considered. Unidentifiable pollen in the surface (and subsurface) samples is mostly too damaged to be identified, rather than unknown. The proportion of unidentifiable pollen is therefore an indication of destruction of pollen by oxidation.

The ratio of unidentifiable to total pollen numbers varies between 0.01 and 0.1 along the Plain (Figs 3.20, 3.21). There is one exceptionally low value 2 km upstream of Jabiluka Billabong. This sample is in a stand of *Melaleuca* near the edge of the Plain and contained abundant *Melaleuca* pollen, a little grass and nothing else.

The ratio is independent of total pollen concentration. A high proportion of damaged grains should result from oxidation in the sediment if the low concentration resulted from pollen destruction. Therefore, nearly a near-constant ratio along the Plain indicates that pollen preservation is approximately constant.

To cope with the large number of sedimentary environments on the modern and former Plain, and the expected degree of time-dependent change of the vegetation, a large number of samples had to be analysed for their pollen content both on the surface and in the subsurface. Less than 100 pollen grains were identified in each sample to allow the processing of large numbers of samples. To check that the number of identified taxa is not an artefact of the number of pollen counted, Fig. 3.22 was constructed.

It is clear from this figure that the number of taxa is independent of the pollen count. The two samples with one taxon contain only *Poaceae* pollen. The nine with two taxa contain only *Poaceae* and *Myrtaceae*. Four of the five highest numbers of taxa are in samples from the Mudginberri Corridor and contain a mixture of grasses, sedges, *Myrtaceae*, *Pandanus*, *Barringtonia*. mangroves, terrestrial species and aquatics. The number of taxa reflects the diversity of pollen sources (grass well out on the Plain and all major taxa in the Corridor) and so the environment of deposition.

The surface pollen have been shown to accurately reflect the vegetation near sampling sites, albeit with some variation in concentration in different geographic areas (Fig. 3.19). Tests for preservation and the dependence of number of taxa on sample size indicate that a pollen count of about 60 per sample will yield a good estimate of the number of taxa, and that this number is essentially independent of pollen destruction.

BIOSTRATIGRAPHY

The results of pollen analyses of a typical core, taken near Jabiluka Billabong, are shown in Fig. 3.23a, along with the litho-stratigraphy of the sediments. Through most of the deposition time, *Rhizophora* pollen predominated over both other mangroves and freshwater taxa. Near the top of the core there is a transition from mangrove dominance to freshwater taxa, particularly grasses and sedges. The mangroves occur principally in the Blue-Grey Clay stratigraphic unit, in this case in variants of the third (channel infill) lithofacies of this

unit (see section 3.2). The transition occurs within the Grey Clay and freshwater taxa were established during deposition of the Dark Brown/Black Clay.

There were marked fluctuations in both the type of sediment being deposited and the mangrove vegetation at the site in the section below 700 cm. Above this, *Rhizophora* mangroves dominated both at this site, and in all samples from the same stratigraphic unit over the entire Plain. There is little variation through the *Rhizophora* forest period in this core and all other cores. This may be due to uniformity of vegetation or to mixing of sediment by tidal suspension and redeposition. Reworking is to be expected in the laminated channel sediments but not in the unlaminated and presumably intra-channel muds. The vegetation was therefore probably uniform.

Towards the surface the Blue-Grey Clay changes gradually to Grey Clay and the pollen shows corresponding vegetation changes. *Rhizophora* decreased while other mangroves, most notably *Avicennia*, paperbarks (*Myrtaceae*) and grasses increased. The very large increase in grass pollen and the disappearance of mangroves in the Dark Brown/Black Clay signals the establishment of freshwater conditions, here about 1650 years BP. At the top, sedges (*Cyperaceae*) became more abundant.

Productivity is high in mangrove vegetation but there are few identifiable plant parts, such as seeds or leaves, preserved in the Blue-Grey Clay, although lenses of wood, leaves and other organic fragments do occur. Only the most resistant plant parts appear to survive organic decay, among which pollen are probably the most resistant.

Siliceous bodies occur throughout the sediments beneath the Magela Plain and probably constitute the second component discussed in section 3.5. Spicules from freshwater sponges, phytoliths produced in cells and cell walls of grasses, sedges and some other plants, and the intricate siliceous shells or frustules of diatoms all occur in varying abundances. All of these have the potential to provide a record of environmental change, if the appropriate reference collections and ecological information are available. Diatoms in particular are used as indicators of water quality, temperature, chemistry and salinity.

Figure 3.23b shows changes with depth in the abundance of biogenic silica. There is little biogenic silica below the Dark Brown/Black Clay unit. Phytoliths and diatoms are rare or absent until the freshwater wetland was established. The species of diatoms present through the *Rhizophora* forest period are estuarine and those towards the surface are freshwater. At this site, sponge spicules make up the largest proportion of the biogenic silica throughout. The coincident increase in all forms of biogenic silica with a change to a freshwater wetland means that most of the silica is autochthonous and is not being washed to the Plain from upstream.

3.7 SUMMARY

The stratigraphic framework of the Magela Plain has been established by describing and analysing both the sediments and their pollen content. This has been achieved by identifying the major litho- and bio-stratigraphic units that constitute the surface and subsurface of the Plain. In both types of stratigraphic units the subsurface units are referable to a particular sedimentary environment by comparison with modern environments — a use of the principle of uniformitarianism.

The sediments have been classified according to environments of deposition by using their stratification, texture and chemistry. Pollen has been shown to be a reliable indicator of modern vegetation on the Plain by investigating the covariation of the pollen and major vegetation types. The pollen is also known to be a reliable indicator of vegetation types that no longer occur on the Plain (e.g. mangroves) by reference to the investigations of other pollen analysts. The combination of lithologic and pollen analytic evidence provides an

accurate classification of the sedimentary environment of a body of sediment beneath the Plain.

The superposition of these sedimentary bodies provides a relative sequence of change from which the evolution of the Plain can be reconstructed. To be able to estimate rates of change to make comparisons with other environmental changes (e.g. climate) an 'absolute' chronology is desirable. A ¹⁴C-based chronology can now be constructed for the Plain using the chemically most stable organic fractions. The appropriate preconditions also exist for the first successful terrestrial use of radium-thorium dating in the Mudginberri Corridor. The two dating methods provide estimates of mean sedimentation rates which are very close. Radium-thorium dating provides an estimate of 0.19±0.02 mm yr⁻¹ at site MX1, and 0.2±0.04 mm yr⁻¹ at MX2, while ¹⁴C dating at MX3, adjacent to MX1, gives 0.26±0.04 mm yr⁻¹.

The major depositional environments of the upper part of the Plain, and some indication of their age, is provided by means of a single core at site M8. Here the Plain was covered by a mangrove forest for most of the time period represented by the core. A transition to freshwater conditions followed, with the establishment of conditions like those of today only in the last 1700 years or so. These three stages (mangrove forest, transition, freshwater) are also reflected in the biogenic silica content of the core.

The techniques and principles that have been documented in this Chapter form the basis of the stratigraphic synthesis, vegetation history and account of the evolution of the Plain that is the substance of the next Chapter.

Table 3.1. List of sites sampled by either drilling or pit digging for stratigraphic purposes.

Cı	ross-section no. and name code	Sample point	Height (AHD) (±0.2 m)	Landform unit
l Mudginberri Corridor		MC1	5.4	5
•	maagoo comao.	MC2	4.6	1
		MC3	5.0	2
		MX2	3.5	Č
		MX1,3	3.9	1
		M1,2	3.6	
		MC4	4.6	1 2
		MX4(+4A)	4.0	1
		MC5	4.3	1
		MC6	5.5	5
	Downstream end of	MC11	4.8	L(F)
	Mudginberri Corridor	MC10	5.6	L
		MC9	5.5	L
		MC8	5.3	L
		M4	5.0	L(F)
		MC12A	3.4	1
		MC12	4.0	2
		MC13	4.1	2
		PPI	4.2	2
		PPit	4.2	2
		M3	4.0	2 2 2
		MC14	4.0	2
		MC14 MC15	3.7	
				1
		MC8 Pit	5.3	L
		MC Pit I	5.0	L(F)
	Mine Valley	M 7	3.6	2
		M6	3.2	1
		M\$1,2	3.0	1
		MV1,2	3.0	1
		MV Pit	3.0	1
		MV Pit A	3.0	1
	Jabiluka Billabong	M9	3.9	1
	THOMAN PHINOONS	M9A	3.8	1
		M9 Pit	3.8	1
		JB7	4,2	1
		JB7 Pit	4.2	J 1
				j 1
		JB6 Pit	4.4	1
		JB6	4.4	1
		M8	4.4	1
		M8A	4.4	! •
		M8 Pit	4.4	l -
		JB4	4.7	L
		JB3	5.0	L
		JB2	5.1	2 2
		JB1	5.0	2
		JB5	4.4	1

Table 3.1. Page 2.

Cross-section no. and name code	Sample point	Height (AHD) (±0.2 m)	Landform unit	
5 Nantson Dillahana Cauth	NIDO	2.0	1	
5 Nankeen Billabong South	NB8	3.9	1	
	NB7	3.9	1	
	NB9 Pit	3.9	1	
	NB6	3.8	1	
	NB5	4.2	L	
	NB9	3.9	l	
6 Nankeen Billabong North	NB1A	3.8	3	
	NB1 Pit	3.9	3	
	NB1	3.8	3	
	Mll	3.8	3	
	NB2	4.2	2	
	NB3	5.1	L	
	NB4	4.4	L	
	NBIA Pit	3.8	3	
7 Downstream Plain	LB23	4.0	2	
	LB22	4.2	2/L	
	LB21	4.0	3	
	LB20	4.1	3	
8 Downstream Plain	ARH3	3.1	2	
	LB6	3.2	2	
	LB5	3.2	2	
	LB Pit 3	3.8	2	
Downstream Plain	LB4	3.8	2	
	LB4A	3.7	2	
	LB3	3.6	2	
	LB2	3.7	2	
	LB Pit 2	3.1	l	
	LB Pit 1	2.9	C	
	LBIA	2.8	C	
	LB1	3.0	1	
10 Downstream Plain	LP3	3.6	1	
	LP2	3.3	P	
	LB Pit 4	3.2	P	
	LP1	3.2	P	
11 East Alligator	IV	3.0	P	
Flood Plain	Palaeo Pit J	3.2	P	

Table 3.1. Page 3.

Cross-section no. and name code	Sample point	Height (AHD) (±0.2 m)	Landform unit
	LP9	3.4	FP
	LP Pit 2	3.4	FP
	LP8	3.2	FP
	LP7	3.3	FP
	M13	3.6	FP
	LP6	3.5	FP
	LP5	3.4	C
	LP Pit 1	3.3	P
	LP4	3.3	P
	LP20	3.2	P
	LP21	3.2	FP
	LP22	3.2	FP
	LP23	3,4	P
Points not on cross-	M5	3.6	1
sections	M10	3.8	1
	M12	3.7	1

l - Low Plain

^{2 -} High Plain

^{3 -} Backslope

C - Channel

P - Palaeochannel

L - Levee

L(F) - Levee Foot

FP - East Alligator Flood Plain

Table 3.2. Summary of chemical characteristics of the stratigraphic units of the Magela Plain at cross-sections.

Cross- section	Strati- graphic	CL	Org. C	Al_D	S_{py}	S_{py}/C
no.	unit	mg/l	%	mg/kg	%S	
2	Black	33.4±5.3	6.65±1.43	6133±1041	0	0
	Grey	(9) 43.3±16.9	(9) 2.8±0.7	(9) 2471±824	(0) 0.89±0.28	0.32±0.183
	·	(9)	(9)	(9)	(2)	
	Blue-Grey	479±53 (14)	5.07±0.61 (14)	781±61 (14)	1.86±0.32 (13)	0.37±0.08
	Sandy clay	68.4±51.2	1.3±0.6	1144±434	0.44±0.06	0.34±0.16
		(3)	(3)	(3)	(3)	
3	Black	28.0±5.4	10.1±1.0	9050±950	0	0
	Canari	(2)	(2)	(2) 3367±241	(0)	0.45.0.15
	Grey	21.6±1.2 (12)	3.8±1.1 (12)	330/±241 (12)	1.7±0.3 (7)	0.45±0.15
	Blue-Grey	20.0±0	1.61±0.29	2572±564	0.53±0.11	0.33±0.09
		(6)	(6)	(6)	(6)	
4	Black	133±38	5.29±1.71	3746±465	0	0
	Grey	(14) 529±56	(14) 1.07±0.23	(14) 1836±250	(0) 0.42±0.12	0.39±0.14
	•	(16)	(18)	(12)	(11)	
	Blue-Grey	1177±209 (10)	2.51±0.20 (14)	1652±180 (14)	0.65±0.16 (9)	0.26±0.07
		(10)		(14)	())	
5	Black	150±30	2.96±0.67	1750±273	0.04±0	0.01±0.002
	Grey	(7) 1120±149	(7) 0.68±0.17	(7) 1200±146	(1) 0.07±0.02	0.1±0.04
	DI C	(16)	(18)	(12)	(11)	0.4.0.10
	Blue-Grey	2084±696 (5)	2.41±0.44 (6)	1032±229 (5)	0.97±0.23 (5)	0.4±0.12
,						
6	Black	43.3±7.6 (4)	4.67±1.7 (5)	2340±388 (5)	0.09±0.03 (2)	0.02±0.01
	Grey	666±204	0.79±0.19	1220±127	0.23±0.18	0.29±0.24
	Blue-Grey	(6) 2399±443	(11) 0.87±0.24	(9) 1354±156	(3) 0.5±0.16	0.57±0.23
	•	(14)	(9)	(14)	(11)	
	Sandy clay	2788±378 (6)	1.38±0.39 (6)	600±142 (6)	0.41±0.16 (6)	0.30±0.14

Table 3.2. Page 2.

Cross- section	Strati- graphic	CL	Org. C	Al_D	S_{py}	S_{py}/C	
no.	unit	mg/l	%	mg/kg	%S		
7	Black	219±87 (8)	1.8±0.36 (8)	2388±266 (8)	0.01±0 (1)	0.01±0.002	
	Grey	1670±270 (20)	0.42±0.08 (20)	1206±73 (20)	0.08±0.02 (12)	0.19±0.06	
	Blue-Grey (6)	2510±331 (6)	1.34±0.23 (6)	827±68 (6)	0.46±0.12	0.34±0.11Y	
8	Black	342±239 (3)	2.18±0.79 (2)	2000±153 (3)	0	0	
	Grey	2237±362 (9)	0.32±0.11 (9)	1188±152 (9)	0.22±0.04 (2)	0.44±0.14	
	Blue-Grey	3876±1030 (2)	1.62±0.08 (2)	1300±100 (2)	1.16±0.56 (2)	0.72±0.38	
9	Black	143±42 (5)	2.45±0.46 (5)	2200±243 (5)	0.01±0 (1)	0.004±0.0008	
	Grey	1893±303 (18)	0.55±0.1 (21)	1285±82 (20)	0.06±0.002 (12)	0.11±0.04	
	Blue-Grey	3483±592 (7)	1.29±0.08 (3)	1171±130 (7)	0.72±0.25 (3)	0.56±0.20	
10	Black	365±152 (6)	1.43±0.39 (6)	1412±118 (6)	0 (0)	0	
	Grey	3223±426 (17)	0.77±0.16 (17)	1293±103 (17)	0.12±0.07 (6)	0.16±0.10	
	Blue-Grey	4254±707 (4)	1.63±0.38 (4)	1325±214 (4)	0.69±0.28 (3)	0.42±0.20	
11	Black	1855±430 (3)	1.22±0.36 (6)	1167±88 (3)	0.06±0 (1)	0.05±0.01	
	Grey	6681±794 (11)	0.35±0.07 (7)	852±97 (10)	0.05±0.01 (8)	0.14±0.04	
	Blue-Grey	11868±828 (6)	1.55±0.15 (5)	1000±140 (6)	0.41±0.16 (6)	0.26±0.10	

Mean \pm standard error. Figure in brackets is the number of samples. Uncertainty in ratio S_{py}/C is calculated in quadrature.

Table 3.3. Summary of ¹⁴C results from MX Pits 1 and 2, Mudginberri Corridor, Cross-section 1.

-	Depth (cm)	%Modern ¹⁴ C activity	Laboratory no.
MX Pit 1	10-14	insufficient sample	<u>-</u>
	21-24	104±6	CS611
	33-36	97±5	CS606
	42-45	97±9	CS610
MX Pit 2	3-8	103±1.3	CS609
	18-24	98.6±0.9	CS615
	30-35	95.0±0.9	CS617

Table 3.4. Results of comparison of alkali soluble and insoluble fractions.

Sample	Depth	Age or % modern activity			
no.	(cm)	Alkali soluble		Alkali insoluble	
LBP3	30- 38	124.6±6.9%	(CS748)	1160±120 BP (CS750)	
MC8	53- 61	1130±60 BP	(CS695)	1380±100 BP (CS669)	
MX4	90-100	2930±270 BP	(CS752)	3570±80 BP (CS755)	

Table 3.5. Results from Pit MX3, Mudginberri Corridor, Cross-section 1.

Depth (cm)	Age	Lab. no.
56-62	2600±100	CS688
78-82	2400±160	CS698

Table 3.6. Magela Plain Carbon-14 data.

Site ident.	Depth (cm)	Lab no.		Age (yr BP) ±1σ	δ^{13} C (°/ rel. PDB ±1 σ)
0 4 1					
Cross-section 1 MX Pit 1	21-24	CS 611	D.W	Madaun	25.1+0.1
WA FIL I	33-36	CS 606	D,W D,W,O	Modern Modern	-25.1±0.1 -27.2±0.1
	42-45	CS 610	D,W,O	Modern	-27.6±0.1
MX Pit 2	3-8	CS 609	D,W	Modern	-26.3±0.1
WIX FIL Z	18-24	CS 615	D,W	Modern	-20.3±0.1 -27.5±0.1
	30-35	CS 617	D,W	410±80	-26.2±0.1
MX Pit 3	56-62	CS 688	D,W D,L	2630±100	-26.58±0.1
WIX III 3	78-86	CS 698	D,L D,L	2400±100	-24.64±0.1
MX Pit 4	90-100	CS 752	C,L	2930±270	-26.89±0.1
WIX III 4	90-100	CS 755	D,L	3570±80	-25.46±0.1
MC 5	274	CS 601	D,O	4380±250	-32.6±0.1
WIC 3	214	C2 001	<i>D</i> ,0	43001230	-32.010.1
Cross section 2	10 35	CE 725	D.I.	3 4!	26.20.0.1
MC Pit 1	18-25	CS 725	D,L	Modern	-26.30±0.1
MC 10	18-25	CS 753	D,L	520±140	-26.90±0.1
MC 10	274	CS 614	D,O	3780±80	-28.1±0.1
MC Pit 8	53-61	CS 695	C,L	1130±60	-20.73±0.1
140.0	53-61	CS 669	D,L	1380±100	-22.21±0.1
MC 8	183	CS 603	D,O	3060±80	-28.8±0.1
	488-549	CS 622	D,O	4630±90	-27.7±0.1
D D'4	914	CS 602	D,O	4890±70	-28.2±0.1
P Pit	35-46	SUA 2593	Н,О	1730±100	-25.0±0.2
Cross-section 3					
MS Pit	18-25	ANU 3515	O (<38 mm)	1300±70	-20.9±0.4
	95	ANU 3512	O (>38 mm)	3590±90	-23.6±0.4
	107	ANU 3513	O (>1 mm)	3830±90	-24.3±0.4
	017	ANU 3514	O (<38 mm, <1 mm)		-23.0±0.4
MV Pit	108	CS 613	D,O	3580±90	-28.0 ± 0.1
MV Pit A	106	CS 681	D,W	870±60	-28.1±0.1
Cross-section 4					
M9	9-16	CS 574	T,H	Modern	-25.88±0.1
	163-169	CS 575	T,W	2760±330	-30.17±0.1
	333-340	CS 576	T,W	3700±370	-27.25±0.1
	440-444	CS 577	T,H (P)	5860±530	-27.85±0.1
	484-488	CS 578	T,H	6540±460	-27.69±0.1
JB6 Pit	23-31	CS 763	D,L	1650±80	-25.40±0.1
M8	30-40	CS 762	D,L	1650±70	-24.14±0.1
	697-700	CS 581	T,L	4300±720	-27.68±0.1
JB3	366	CS 607	D,O	3730±150	-26.2±0.1
Cross-section 5					
NB9	28-35	CS 722	D,L	Modern	-26.22±0.1
			> —		

Table 3.6. Page 2.

Site ident.	Depth (cm)	Lab no.	Material dated	Age (yr BP) ±1σ	δ^{13} C (°/ rel. PDB ±1 σ
Cross-section 6					
NB1A Pit	16-18	CS 759	D,L	630±100	-23.68±0.1
	16-18	CS 764	D,L	770±60	-24,11±0.1
NB1 Pit	28-36	CS 697	D,L	1250±120	-25.79 ± 0.1
Mll	760-770	CS 579	T,O	6640±300	-27.97±0.1
NB3	1067-1128	CS 608	D,O	4330±170	-28.5±0.1
Cross-section 8					
LB Pit 3	30-38	CS 723	D,L	740±100	-25.15±0.1
	30-38	CS 748	C,L	Modern	-24.90±0.1
	30-38	CS 750	D,L	1160±120	-25.0±0.1
Cross-section 9	ı				
LB Pit 2	50-60	CS 726	D,L	1503±170	-21.95±0.1
LB Pit 1	25-30	CS 724	D,L D,L	1720±90	-26.2±0.1
	_		•		
Cross section 10		00.600	T. 1	4.0.00	
LB Pit 4	15-25	CS 699	D,L	510±90	-23.84±0.1
Cross-section 1	1				
LP Pit 1	7-17	CS 700	D,L	1000±110	-17.33±0.1
LP 21	1188-1254	CS 612	D,O	7660+ ⁹⁰⁰ -800	-27.5±0.1
Not on section					
M12	845	CS 580	T,O	7140±170	-27.87±0.1

D - material insoluble in NaOH

C - material soluble in NaOH

T - total, after acid wash

W wood

P peaty organic matter

organic fragments, twigs, leaves O -

L - organic cl H - charcoal. organic clay or clay loam

Table 3.7. Concentrations (with respect to ash weight) of ²³⁰Th and ²²⁶Ra in sub-samples of sediment collected at site MX1.

Errors in concentrations due to counting statistics are given in parentheses. σ_1 is error in the excess due to counting statistics only. σ_2 is error in the excess due to uncertainty in the calibration of alpha-spectroscopy relative to gamma-spectroscopy, equal to $0.065x^{230}$ Th concentration. σ_3 is error in the excess arising from variation in radium concentration at time of deposition, estimated to be 0.09x excess. σ_4 is the quadratic sum of σ_1 , σ_2 and σ_3 .

Sample depth (cm)	²³⁰ Th (Bq/kg)	²²⁶ Ra (Bq/kg)	Excess (Bq/kg)	σ_1 (Bq/kg)	σ_2 (Bq/kg)	σ_3 (Bq/kg)	σ_4 (Bq/kg)
0-2	78.7 (2.8)	296.3 (1.3)	217.6	3.1	5.1	19.6	20.5
4-6	71.1 (2.6)	302.2 (1.1)	231.1	2.8	4.6	20.8	21.5
8-10	71.8 (3.4)	295.8 (1.3)	224.0	3.6	4.7	20.2	21.0
12-14	94.6 (4.3)	287.8 (1.2)	193.2	4.5	6.1	17.4	19.0
14-16	92.8 (4.5)	292.1 (1.3)	199.3	4.7	6.0	17.9	19.5
20-22	83.3 (3.8)	273.9 (1.2)	190.6	4.0	5.4	17.2	18.5
22-24	84.1 (3.8)	284.4 (1.2)	200.3	4.0	5.5	18.0	19.2
32-34	82.2 (3.7)	275.7 (1.2)	193.5	3.9	5.3	17.4	18.6
34-35	89.9 (3.9)	218.3 (1.0)	128.4	4.0	5.8	11.6	13.6
42-44	80.1 (3.9)	175.8 (1.0)	95.7	4.0	5.2	8.6	10.8
44-46	95.4 (4.4)	157.1 (1.8)	61.7	4.5	6.2	5.6	9.5
52-54	86.0 (3.9)	190.6 (1.0)	104.6	4.0	5.6	9.4	11.6
60-62	87.4 (3.8)	150.2 (0.8)	62.8	3.9	5.7	5.7	8.9
68-70	84.7 (4.0)	136.2 (0.8)	51.5	4.1	5.5	4.6	8.2
78-82	16.8 (1.0)	22.7 (0.3)	5.9	1.1	1.1	0.5	1.6

Table 3.8. Concentrations (with respect to ash weight) of other long-lived radionuclides in sub-samples of sediment collected at site MX1.

Sample depth (cm)	²³⁸ U (Bq/kg)	²³⁴ U (Bq/kg)	²³² Th (Bq/kg)	²²⁸ Ra (Bq/kg)	⁴⁰ K (Bq/kg)	Organic content (%)
0-2	94.3 (4.2)	110.6 (4.7)	88.8 (3.7)	103.5 (0.9)	221.3 (7.4)	22.0
4-6	93.0 (3.9)	123.6 (4.8)	85.2 (2.8)	92.6 (0.7)	195.5 (6.1)	15.3
8-10	103.6 (4.0)	145.0 (5.2)	93.8 (4.2)	92.6 (0.9)	201.2 (7.3)	8.5
12-14	96.9 (4.3)	130.8 (5.3)	121.1 (5.1)	104.7 (0.8)	218.7 (7.1)	11.7
14-16	93.0 (4.1)	124.1 (5.1)	107.9 (4.9)	108.9 (0.9)	218.1 (7.8)	10.5
20-22	80.1 (3.1)	103.7 (4.4)	107.2 (4.4)	112.5 (0.8)	230.1 (7.7)	10.1
22-24	80.8 (3.4)	109.5 (4.1)	113.0 (4.7)	112.5 (0.8)	228.6 (7.5)	10.5
32-34	87.1 (3.8)	117.2 (4.8)	112.7 (4.6)	112.2 (0.8)	220.4 (7.3)	10.5
34-36	82.8 (3.3)	104.7 (4.0)	100.8 (4.1)	109.6 (0.7)	228.8 (7.2)	10.1
42-44	81.7 (3.2)	103.4 (3.8)	100.7 (4.5)	109.6 (0.8)	230.2 (7.7)	9.9
44-46	85.1 (3.5)	102.4 (4.1)	121.5 (5.3)	108.0 (0.7)	233.3 (7.1)	9.3
52-54	89.2 (3.4)	112.8 (4.2)	100.5 (4.5)	107.5 (0.9)	207.3 (7.2)	6.1
60-62	89.8 (3.6)	116.8 (4.4)	100.4 (4.2)	99.8 (0.7)	218.1 (6.8)	5.9
68-70	100.4 (4.0)	135.8 (5.1)	102.0 (4.5)	103.9 (0.7)	244.1 (7.7)	5.5
78-82	20.1 (0.9)	23.9 (1.0)	20.7 (1.1)	19.7 (0.3)	37.1 (2.0)	0.7

Table 3.9. Ratios of the concentrations of selected radionuclides in sub-samples of sediment collected at site MX1.

Sample depth (cm)	²³⁴ U/ ²³⁸ U	$^{232}{ m Th}/^{230}{ m Th}$	$^{40}\mathrm{K}/^{230}\mathrm{Th}$	$^{238}{ m U}/^{230}{ m Th}$	²²⁸ Ra/ ²³² Th	⁴⁰ K/ ²²⁸ R
0-2	1.17 (.07)	1.13 (.06)	2.81 (.14)	1.20 (.07)	1.17 (.02)	2.14 (.07)
4-6	1.33 (.08)	1.20 (.06)	2.75 (.13)	1.31 (.07)	1.09 (.04)	2.11 (.07)
8-10	1.40 (.07)	1.31 (.09)	2.81 (.17)	1.44 (.09)	0.99 (.05)	2.17 (.08)
12-14	1.35 (.08)	1.28 (.08)	2.31 (.13)	1.02 (.07)	0.86 (.04)	2.09 (.07)
14-16	1.33 (.08)	1.16 (.08)	2.31 (.13)	1.02 (.07)	0.86 (.04)	2.00 (.07)
20-22	1.29 (.07)	1.29 (.08)	2.76 (.16)	0.96 (.06)	1.05 (.04)	2.05 (.07)
22-24	1.36 (.08)	1.34 (.08)	2.72 (.15)	0.96 (.06)	1.00 (.04)	2.03 (.07)
32-34	1.35 (.08)	1.37 (.08)	2.68 (.15)	1.06 (.07)	1.00 (.04)	1.96 (.07)
34-36	1.26 (.07)	1.12 (.07)	2.55 (.14)	0.92 (.05)	1.09 (.04)	2.09 (.07)
42-44	1.27 (.07)	1.26 (.08)	2.87 (.17)	1.02 (.06)	1.09 (.05)	2.10 (.07)
44-46	1.20 (.07)	1.27 (.08)	2.45 (.14)	0.89 (.06)	0.89 (.04)	2.16 (.07)
52-54	1.26 (.07)	1.17 (.07)	2.41 (.14)	1.04 (.06)	1.07 (.05)	1.93 (.07)
60-62	1.30 (.07)	1.15 (.07)	2.50 (.13)	1.03 (.06)	0.99 (.04)	2.19 (.07)
68-70	1.35 (.07)	1.20 (.08)	2.88 (.16)	1.19 (.07)	1.02 (.05)	2.35 (.08)
78-82	1.19 (.07)	1.23 (.10)	2.21 (.19)	1.20 (.09)	0.95 (.05)	1.88 (.11)

Table 3.10. Statistical summary of radionuclide concentrations and concentration ratios for site MX1.

Nuclide or ratio	Mean (Bq/kg) ^a	Standard deviation (Bq/kg) ^a	Standard error (Bq/kg) ^a	Relative standard deviation (%)	Mean relative error (%)
²³⁸ U	89.8	7.1	1.9	7.9	4.1
²³⁴ U	117.2	12.7	3.4	10.8	3.9
²³⁰ Th	84.4	7.2	1.9	8.6	4.4
²³² Th	104.0	10.4	2.8	10.4	4.2
²²⁸ Ra	105.6	6.4	1.7	6.1	0.8
⁴⁰ K	221.1	12.6	3.4	5.7	3.3
$^{234}\mathrm{U}/^{238}\mathrm{U}$	1.30	0.06	0.02	4.8	5.6
$^{238}{ m U}/^{230}{ m Th}$	1.07	0.15	0.04	14.1	6.1
	1.01 ^b	0.08	0.02	7.5	6.2
$^{232}{ m Th}/^{230}{ m Th}$	1.23	0.08	0.02	6.3	6.1
$^{40}{ m K}/^{230}{ m Th}$	2.63	0.19	0.05	7.3	5.6
²²⁸ Ra/ ²³² Th	1.02	0.08	0.02	7.6	4.1
$^{40}{ m K}/^{228}{ m Ra}$	2.10	0.10	0.03	4.9	3.4
	2.08°	0.08	0.02	3.7	3.4

^aUnits for concentrations (ash) only; ratios are dimensionless; ^bExcluding 3 points at depths less than 10 cm; ^cExcluding 1 point at 69 cm.

Table 3.11. Results for sedimentation rate and initial excess radium at sites MX1 and MX2.

Site	Data set	Fitting mode	Sedimentation rate (mm/year)	Initial excess (Bq/kg)	R ²	Chi- square pdf
MXI	Original (n = 14)	Unweighted Error-weighted	0.19 (.02) 0.21 (.03)	280 (30) 270 (30)	0.84 0.79	3.3 3.6
	Corrected $(n = 14)$	Unweighted Error-weighted	0.18 (.02) 0.20 (.02)	270 (25) 270 (28)	0.88 0.83	2.5 2.6
	Original (n = 13)	Unweighted Error-weighted	0.19 (.02) 0.20 (.02)	270 (25) 265 (25)	0.89 0.88	2.4 2.6
	Corrected (n = 13)	Unweighted Error-weighted	0.18 (.02) 0.19 (.02)	265 (20) 270 (20)	0.93 0.90	1.7 1.8
MX2	Original	Unweighted	0.20 (.04)	240 (25)	0.74	0.9
	Corrected	Unweighted	0.24 (.08)	270 (40)	0.43	3.1

Table 3.12. Concentrations (with respect to ash weight) of ²³⁰Th and ²²⁶Ra in sub-samples of sediment collected at site MX2.

Errors in concentrations due to counting statistics are given in parentheses. σ_1 is the error in the excess due to counting statistics only. σ_2 is the error in the excess due to uncertainty in the calibration of alpha-spectroscopy relative to gamma-spectroscopy, equal to $0.065x^{230}$ Th concentration. σ_3 is the error in the excess arising from variation in radium concentration at the time of deposition, estimated to be 0.15x excess. σ_4 is the quadratic sum of σ_1 , σ_2 and σ_3

Sample depth (cm)	²³⁰ Th (Bq/kg)	²²⁶ Ra (Bq/kg)	Excess (Bq/kg)	$\sigma_1 \ (\mathrm{Bq/kg})$	σ_{2} (Bq/kg)	$\sigma_{f 3}$ (Bq/kg)	$\sigma_{f 4}$ (Bq/kg)
0-3	68.7 (3.2)	260.4 (1.5)	191.7	3.5	4.4	29.	30.
3-6	66.3 (2.8)	261.8 (1.9)	195.5	2.9	4.3	29.	30.
6-8	60.0(2.5)	255.2 (1.4)	195.2	2.9	3.9	29.	30.
8-11	48.6 (2.0)	268.4 (2.3)	219.8	3.1	3.2	33.	33.
11-13	49,4 (1.9)	273.7 (2.3)	224.3	3.0	3.2	34.	34.
13-15	48.7 (2.0)	251.9 (2.3)	203.2	3.1	3.2	31.	31.
15-18	52.1 (2.1)	201.5 (1.8)	149.4	2.8	3.4	22.	23.
18-21	64.6 (2.4)	204.4 (1.7)	139.8	2.9	4.2	21.	22.
21-24	72.0 (4.2)	233.0 (1.1)	161.0	4.3	4.7	24.	25.
24-27	67.3 (3.1)	221.4 (1.4)	154.0	3.4	4.4	23.	24.
27-30	55.9 (2.0)	182.0 (1.6)	126.1	2.6	3.6	20.	21.
30-33	53.5 (2.0)	181.9 (1.4)	128.4	2.4	3.5	19.	20.
33-35	46.1 (2.2)	138.3 (0.7)	92.2	2.3	3.0	14.	14.
35-38	22.2 (1.0)	n.a.	n.a.	n.a.	n.a.	n.a.	n.a.
38-48	7.8 (0.3)	18.0 (1.0)	10.2	1.0	0.5	2.7	3.

Table 3.13. Concentrations (with respect to ash weight) of other long-lived radionuclides in sub-samples of sediment collected at site MX2.

Sample depth (cm)	²³⁸ U (Bq/kg)	²³⁴ U (Bq/kg)	²³² Th (Bq/kg)	²²⁸ Ra (Bq/kg)	⁴⁰ K (Bq/kg)	Organic content (%)
0-3	75.5 (3.2)	95.8 (3.8)	83.3 (3.5)	95.9 (1.0)	188. (8.)	23.9
3-6	70.6 (2.3)	92.8 (3.0)	79.8 (3.0)	86.3 (3.0)	179. (10.)	16.9
6-8	75.4 (3.8)	99.9 (4.7)	78.7 (3.0)	79.7 (0.9)	158. (7.)	23.0
8-11	67.9 (2.8)	86.4 (3.2)	63.3 (2.3)	72.1 (1.6)	130. (11 <i>.</i>)	16.8
11-13	63.8 (2.5)	85.4 (3.0)	66.1 (2.2)	68.6 (1.5)	131. (12.)	17.4
13-15	69.8 (2.6)	92.0 (3.2)	64.7 (2.4)	67.9 (1.4)	130. (12.)	16.7
15-18	63.5 (2.8)	88.2 (3.4)	63.2 (2.4)	71.4 (1.2)	142. (10.)	11.5
18-21	73.8 (3.2)	100.4 (3.9)	82.6 (2.9)	82.7 (1.3)	173. (7.)	10.8
21-24	81.8 (4.0)	111.3 (5.0)	85.3 (4.6)	91.0 (0.8)	195. (7.)	17.3
24-27	80.7 (3.1)	101.4 (3.6)	86.9 (3.8)	86.5 (0.9)	173. (8.)	8.8
27-30	65.7 (2.4)	85.8 (2.8)	69.0 (2.4)	72.6 (1.0)	166. (10.)	8.1
30-33	62.9 (2.4)	83.8 (3.0)	68.3 (2.4)	71.5 (1.0)	154. (7.)	10.1
33-35	61.5 (2.8)	76.2 (3.2)	55.0 (2.5)	54.0 (0.5)	111. (4.)	13.4
35-38	36.2 (1.4)	43.3 (1.6)	28.8 (1.2)	n.a.	n.a.	6.0
38-48	8.7 (0.5)	8.9 (0.5)	10.7 (0.4)	n.a.	n.a.	3.2

Table 3.14. Ratios of the concentrations of selected radionuclides in sub-samples of sediment collected at site MX2.

Sample depth (cm)	²³⁴ U/ ²³⁸ U	²³² Th/ ²³⁰ Th	⁴⁰ K/ ²³⁰ Th	$^{238}\mathrm{U}/^{230}\mathrm{Th}$	²²⁸ Ra/ ²³² Th	⁴⁰ K/ ²²⁸ Ra
0-3	1.27 (.07)	1.21 (.08)	2.74 (.17)	1.10 (.07)	1.15 (.05)	1.96 (.09)
3-6	1.31 (.06)	1.20 (.07)	2.69 (.19)	1.06 (.06)	1.08 (.04)	2.07 (.12)
6-8	1.32 (.09)	1.31 (.07)	2.64 (.17)	1.26 (.08)	1.01 (.04)	1.99 (.10)
8-11	1.27 (.07)	1.31 (.07)	2.68 (.26)	1.40 (.08)	1.13 (.05)	1.81 (.16)
11-13	1.34 (.07)	1.34 (.07)	2.65 (.26)	1.29 (.07)	1.04 (.04)	1.91 (.18)
13-15	1.32 (.07)	1.33 (.07)	2.66 (.26)	1.43 (.08)	1.05 (.04)	1.91 (.18)
15-18	1.39 (.08)	1.21 (.07)	2.72 (.22)	1.22 (.07)	1.13 (.05)	1.98 (.15)
18-21	1.36 (.08)	1.28 (.07)	2.67 (.15)	1.14 (.07)	1.00 (.04)	2.09 (.09)
21-24	1.36 (.09)	1.18 (.09)	2.70 (.18)	1.14 (.09)	1.07 (.06)	2.14 (.08)
24-27	1.26 (.07)	1.29 (.08)	2.57 (.16)	1.20 (.07)	1.00 (.04)	2.00 (.09)
27-30	1.31 (.06)	1.23 (.06)	2.98 (.20)	1.18 (.06)	1.05 (.04)	2.29 (.13)
30-33	1.33 (.07)	1.28 (.07)	2.87 (.16)	1.18 (.06)	1.05 (.04)	2.14 (.10)
33-35	1.24 (.08)	1.19 (.08)	2.42 (.15)	1.33 (.09)	0.98 (.05)	2.06 (.08)
35-38	1.20 (.06)	1.30 (.08)	n.a.	1.63 (.10)	n.a.	n.a.
38-48	1.02 (.08)	1.37 (.07)	n.a.	1.12 (.08)	n.a.	n.a.

Table 3.15. Statistical summary of radionuclide concentrations and concentration ratios for site MX2. Samples below 35 cm have been excluded from all analyses.

Nuclide or ratio	Mean (Bq/kg) ^a	Standard deviation (Bq/kg) ^a	Standard error (Bq/kg)ª	Relative standard deviation (%)	Mean relative error (%)
•••					
²³⁸ U	70.2	6.5	1.8	9.3	4.1
$^{234}\mathrm{U}$	92.2	9.0	2.5	9.7	3.8
²³⁰ Th	57.9	8.6	2.4	14.9	4.3
²³² Th	72.8	9.9	2.8	13.7	3.9
²²⁸ Ra	76.9	10.9	3.0	14.2	1.5
⁴⁰ K	156.2	24.7	6.9	15.8	5.7
$^{234}\text{U}/^{238}\text{U}$	1.31	0.04	0.01	3.2	5.5
$^{238}U/^{230}Th$	1.22	0.11	0.03	8.8	6.0
$^{232}\text{Th}/^{230}\text{Th}$	1.26	0.05	0.02	4.3	5.8
40 K/ 230 Th	2.69	0.13	0.04	4.8	7.2
²²⁸ Ra/ ²³² Th	1.05	0.05	0.02	4.9	4.2
40K/ ²²⁸ Ra	2.03	0.12	0.03	5.9	6.0

^aUnits for concentrations (ash) only; ratios are dimensionless.

Figure 3.1 Longitudinal section of the Magela Plain from just upstream of Mudginberri to the East Alligator River (A-B) then downstream along the East Alligator Flood Plain (C-D), showing the distribution of five stratigraphic units approximately along the centreline of the Plain. The most useful deep drill holes are shown. ACH 22-10 refers to detailed drilling by Geopeko near Sore's Dreaming (Yingindidi). The numbers 1-11 refer to the cross-sections in Figs 4.1 to 4.11.

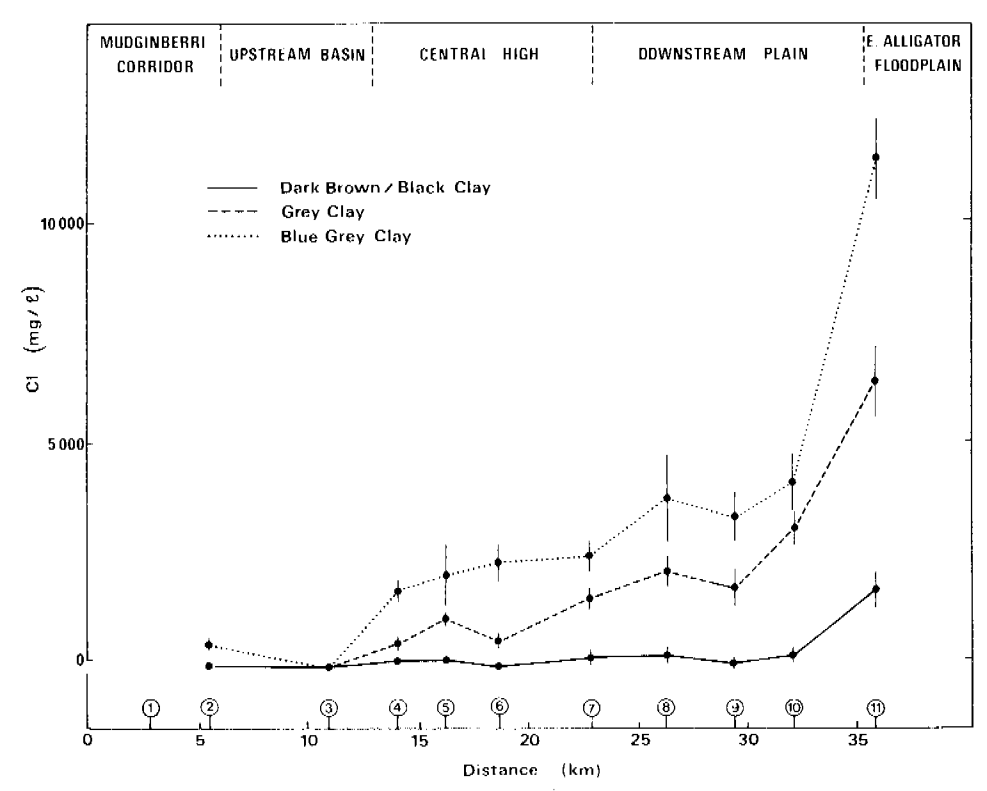


Figure 3.2 Longitudinal pattern of variation of the C1 content of three stratigraphic units of the Magela Plain.

The values shown are means ± standard errors for all analyses for each unit at each cross-section (also see Table 3.1). The numbers of the cross-sections are shown on the abscissa along with the distance from the arbitrary datum near the northern end of Mudginberri Billabong. The geographic units defined in Chapter 2 are also shown.

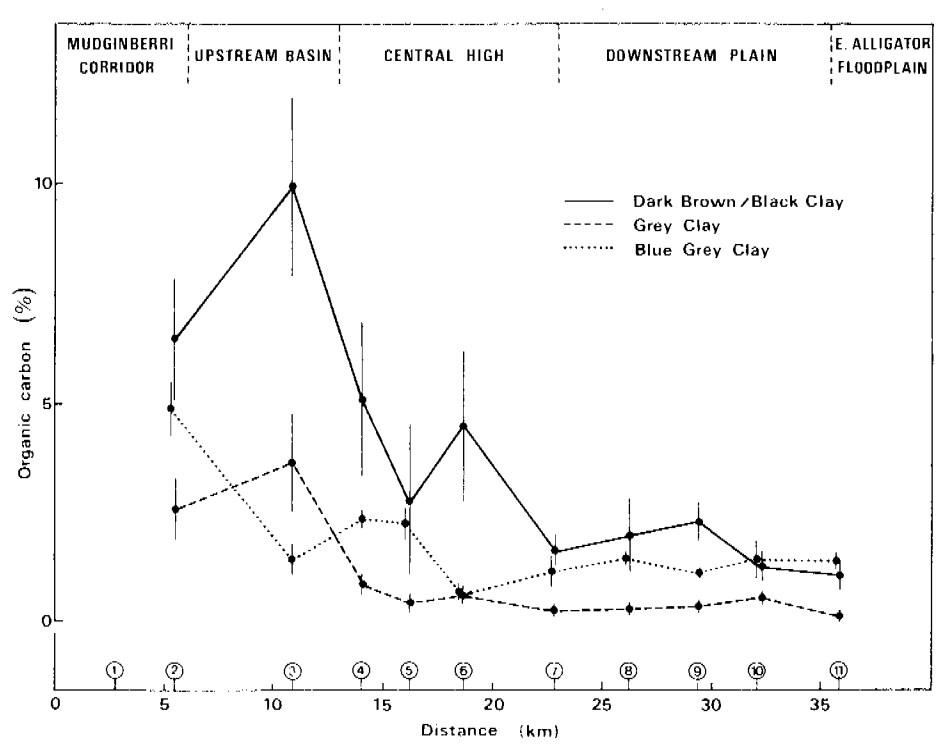


Figure 3.3 Longitudinal pattern of variation of the organic carbon content of three stratigraphic units of the Magela Plain. The values shown are calculated as in Fig. 3.2.

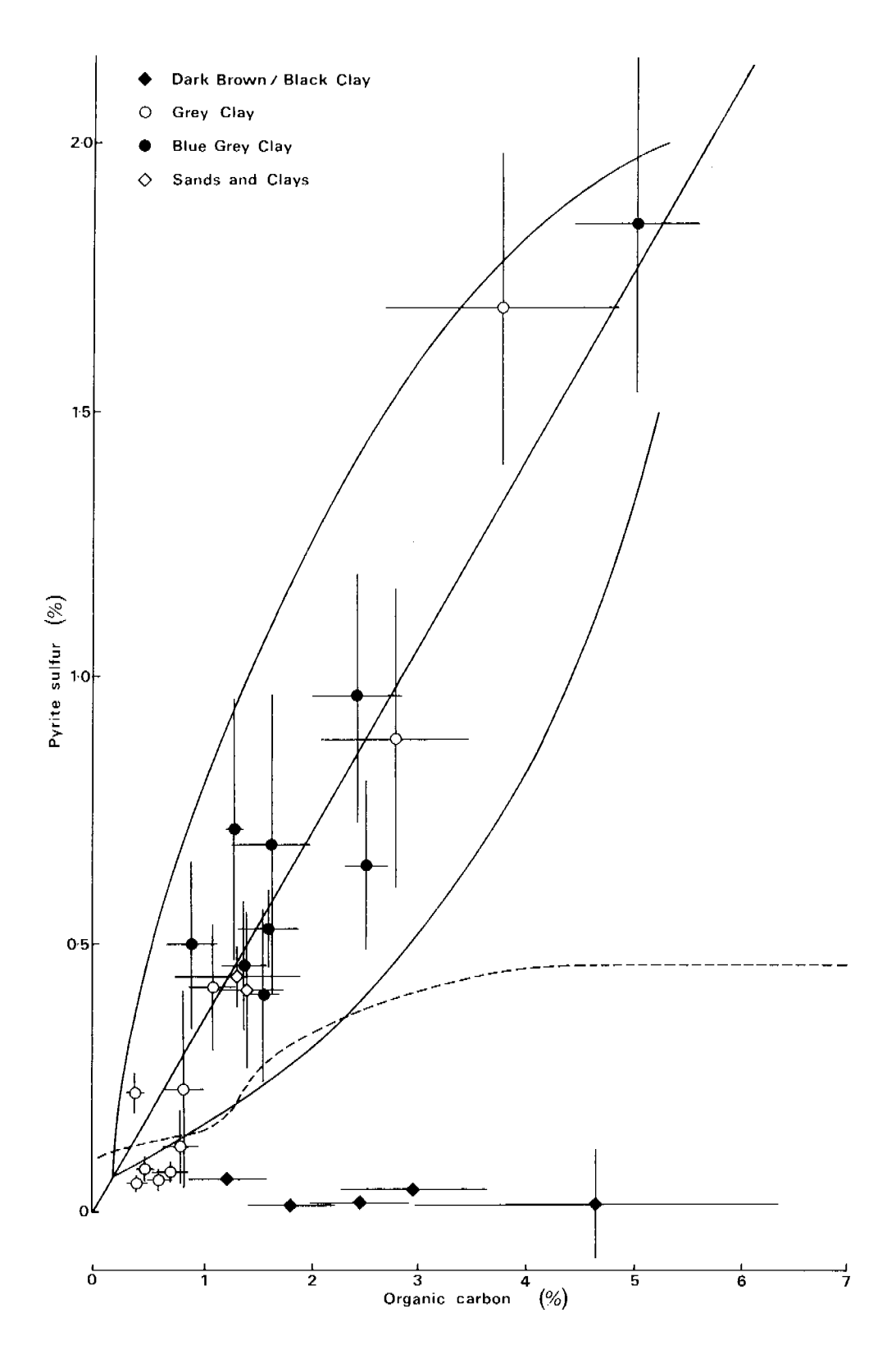


Figure 3.4 Relationship between pyrite sulfur (S_{py}) and organic carbon in four stratigraphic units of the Magela Plain, averaged (\pm standard errors) for each cross-section. The line with a positive slope and the surrounding envelope are for data from normal marine muds (from Berner 1982, 1984). The dashed line encloses data from freshwater lake muds (from Berner 1984).

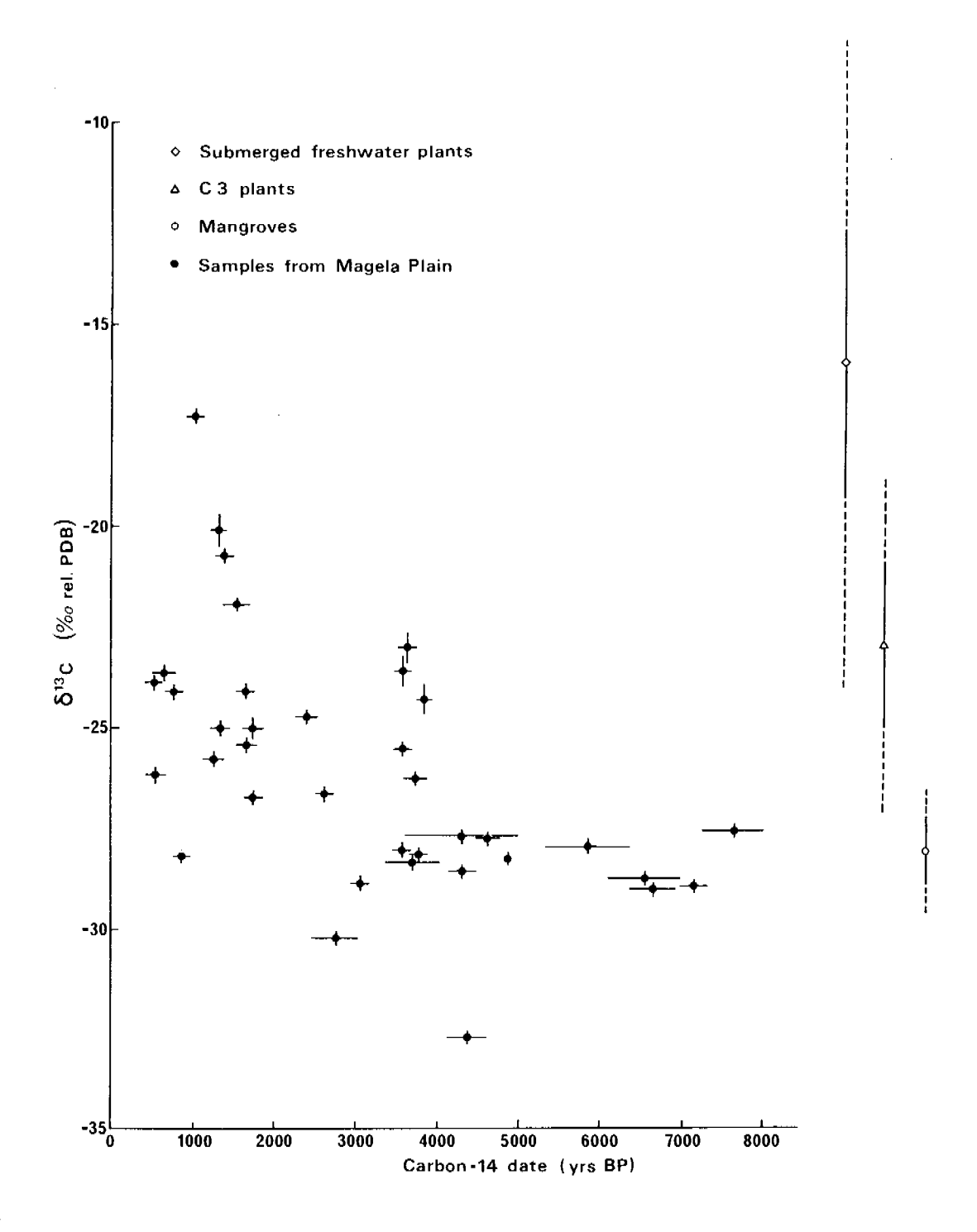


Figure 3.5 Carbon 14 (14 C) ages (years BP) plotted against δ^{13} C for all dated samples from the Magela Plain. Shows a trend from mangrove wood ($^{-28}$ °/.. rel. PDB) to freshwater seasonal swamps, the scatter caused by variable depth/age relationships at different sites. The ranges of δ^{13} C from three different environments, shown at the right side, are from Gupta and Polach (1985).

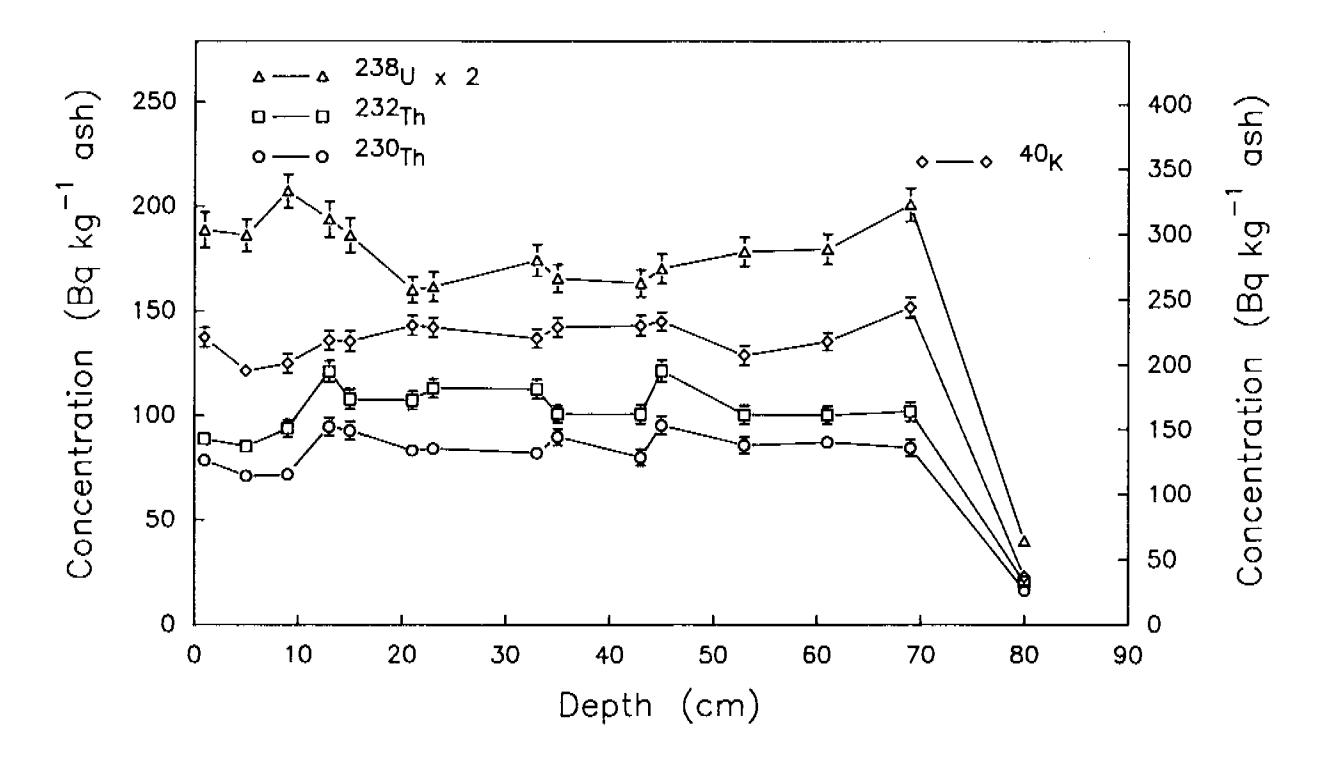


Figure 3.6 Variation with depth of the concentrations of selected long-lived radionuclides in sediment samples at site MX1. The right vertical scale refers to ⁴⁰K concentrations. Note that for clarity all ²³⁸U concentrations have been scaled by x2.

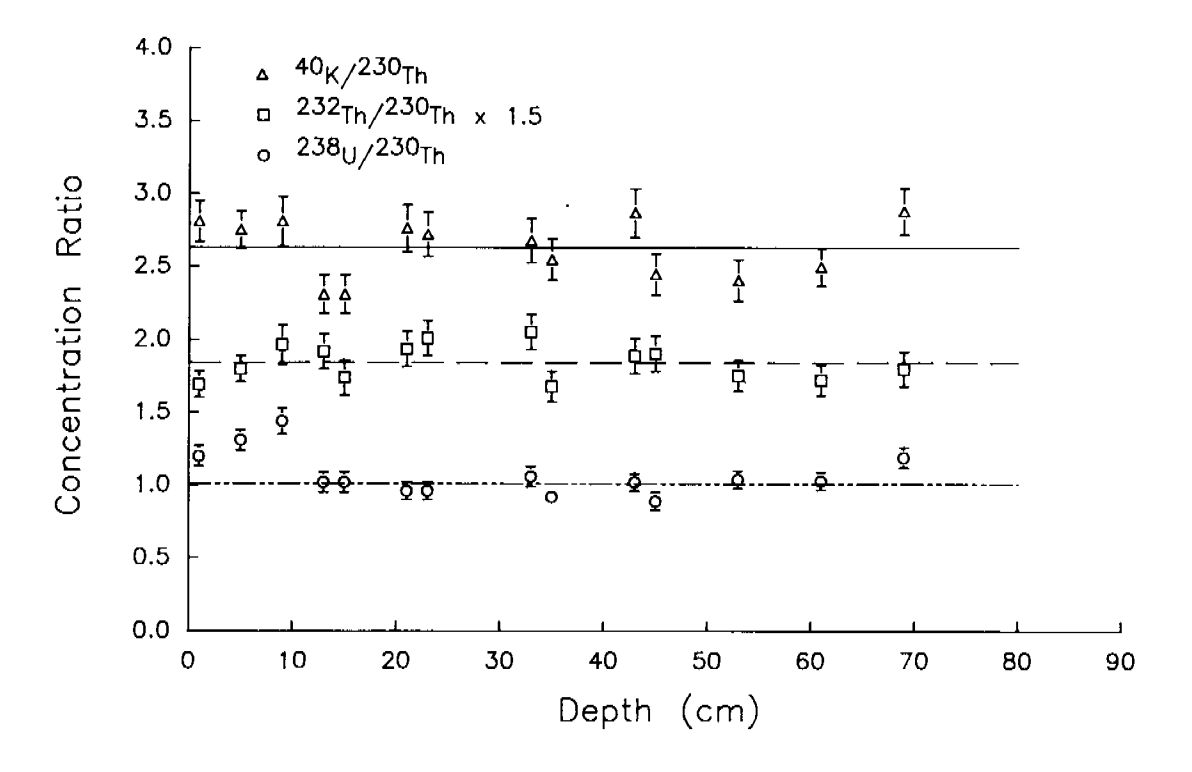


Figure 3.7 Variation with depth of the ratio of the concentrations of selected long-lived radionuclides in sediment samples at site MX1. Note that, for clarity, results for ²³²Th/²³⁰Th have been scaled by x1.5.

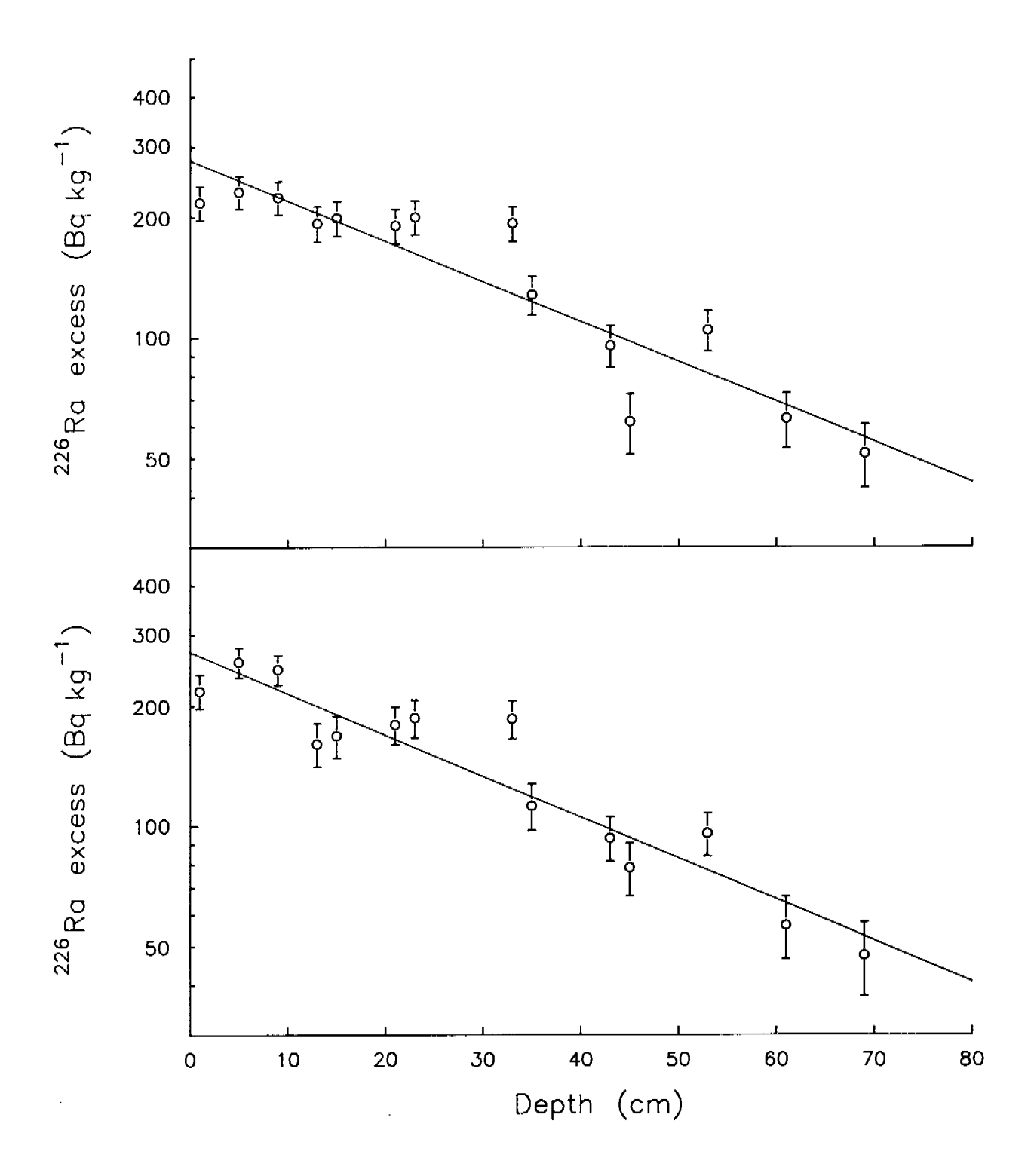


Figure 3.8 Variation with depth of the ²²⁶Ra excess in sediment samples at site MX1. Upper graph shows raw data. In the lower graph results have been corrected as described in the text. The lines result from an exponential unweighted least squares fit.

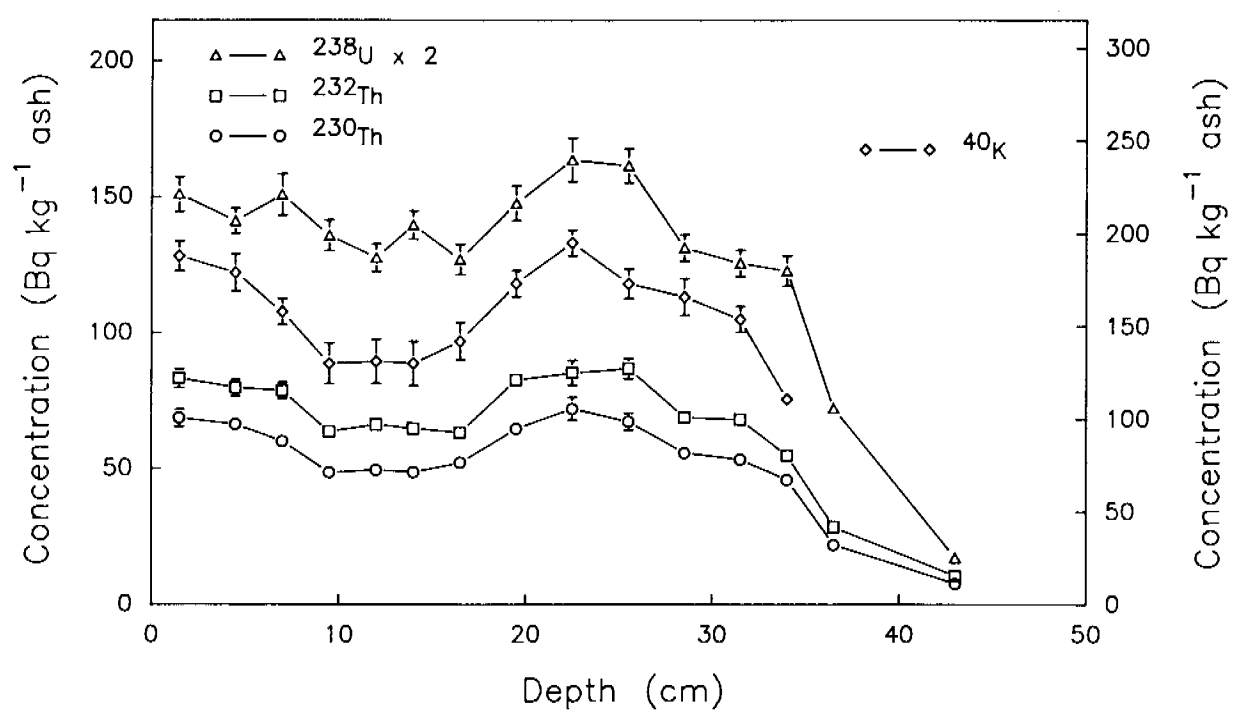


Figure 3.9 Variation with depth of the concentrations of selected long-lived radionuclides in sediment samples at site MX2. The right vertical scale refers to ⁴⁰K concentrations. Note that for clarity all ²³⁸U concentrations have been scaled by x2.

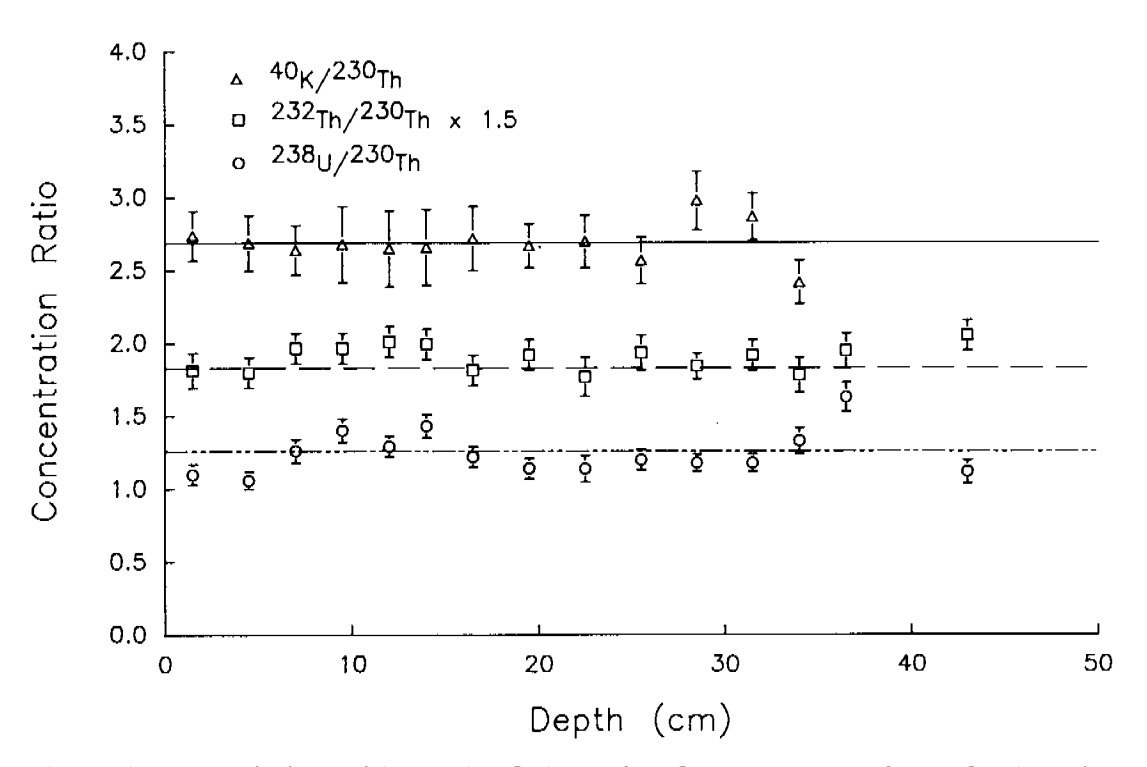


Figure 3.10 Variation with depth of the ratio of the concentrations of selected long-lived radionuclides in sediment samples at site MX2. Note that, for clarity, results for 232 Th/ 230 Th have been scaled by x1.5.

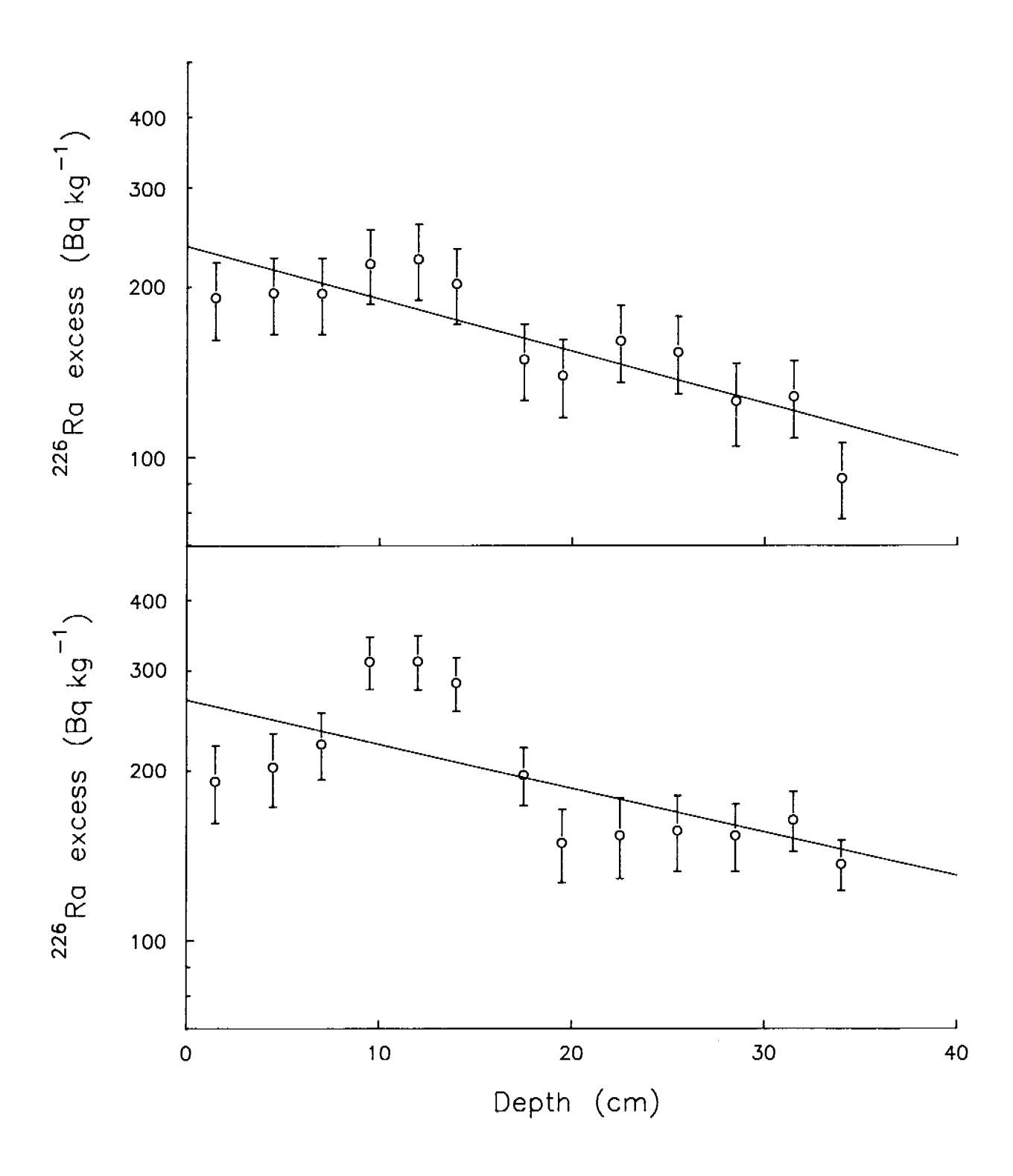


Figure 3.11 Variation with depth of the ²²⁶Ra excess in sediment samples at site MX2. Upper graph shows raw data; in the lower graph results have been corrected as described in the text. The lines result from an exponential unweighted least squares fit.

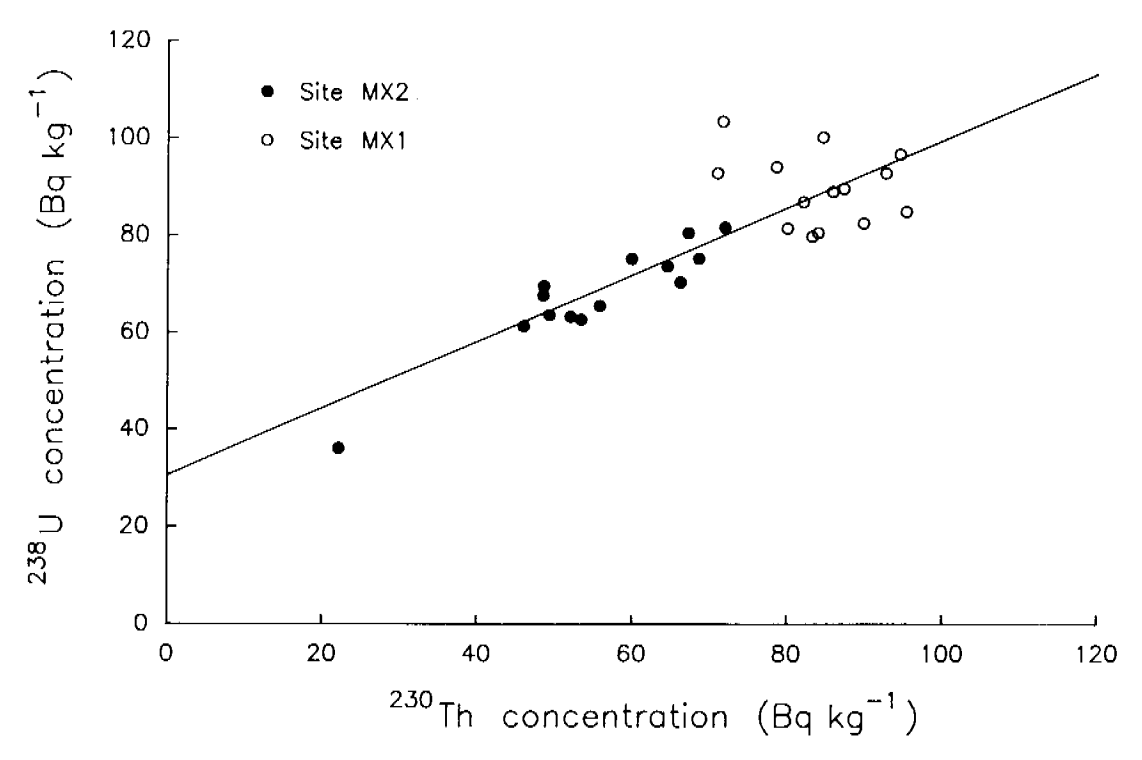


Figure 3.12 Correlation between concentrations of ²³⁸U and ²³⁰Th in sediment samples from sites MX1 and MX2

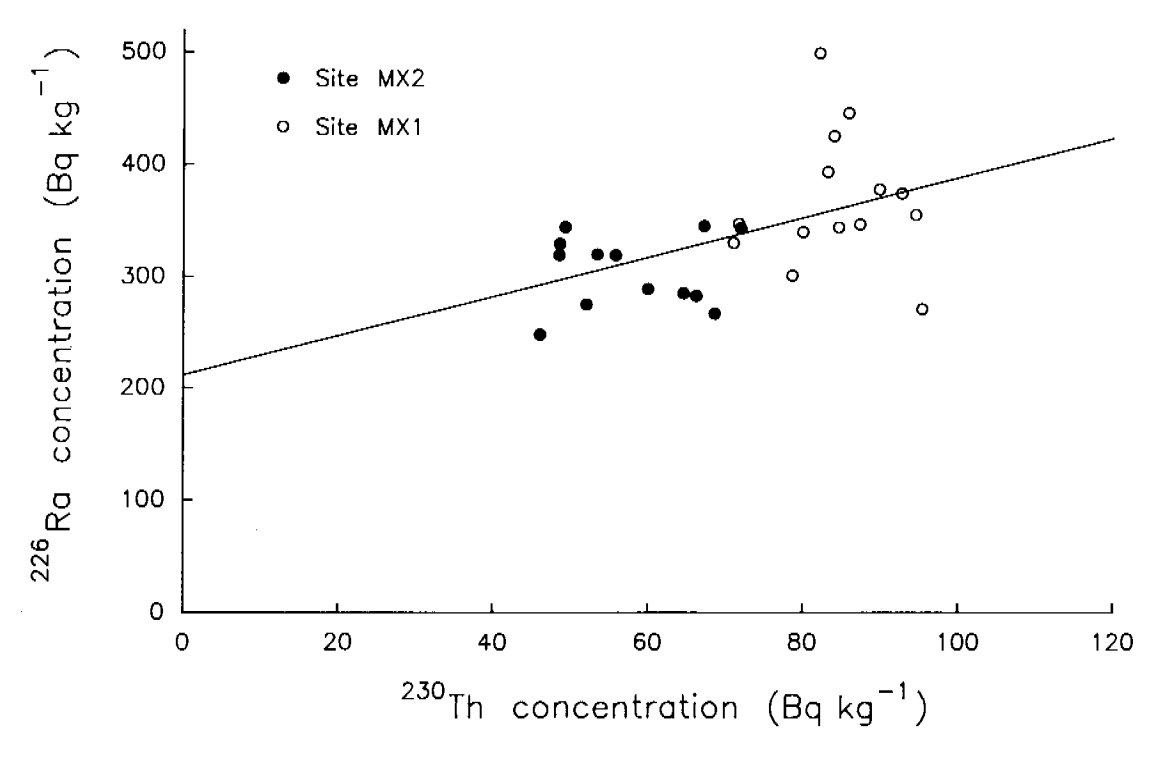


Figure 3.13 Correlation between concentrations of ²³⁰Th and initial concentrations of ²²⁶Ra in sediment samples from both sites

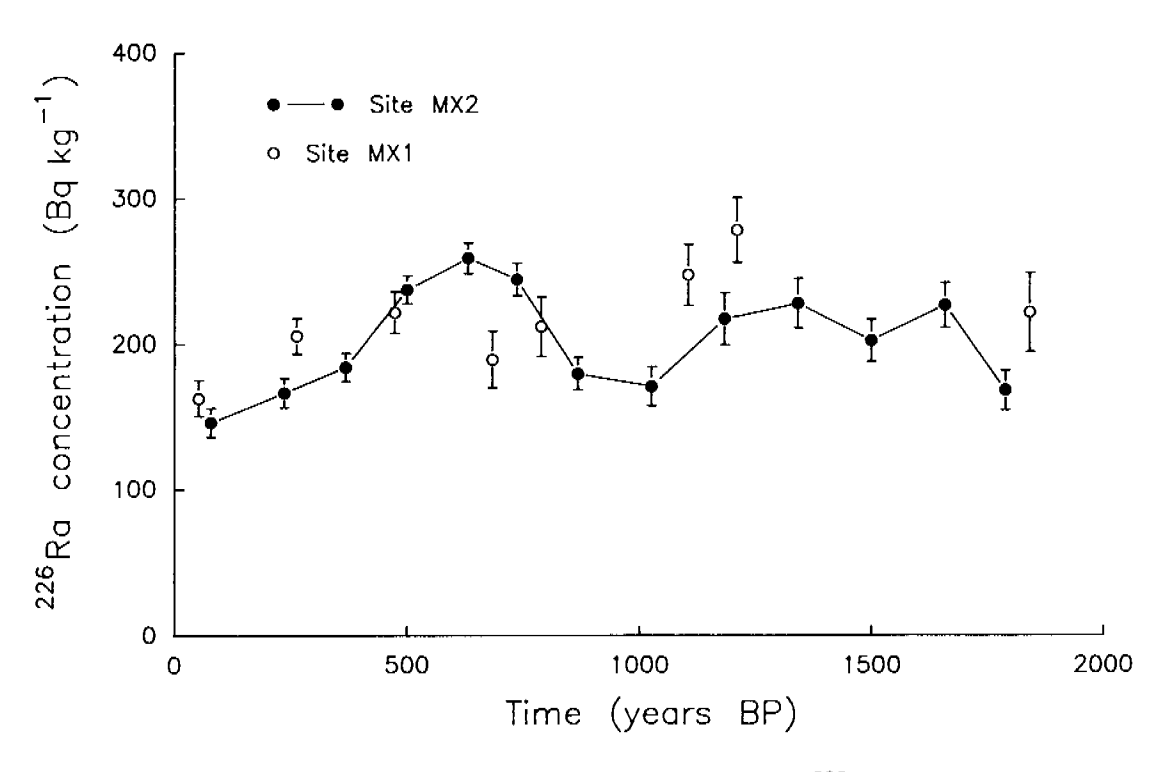


Figure 3.14 Variation with time of the initial concentration of ²²⁶Ra in the second sediment component at sites MX1 and MX2

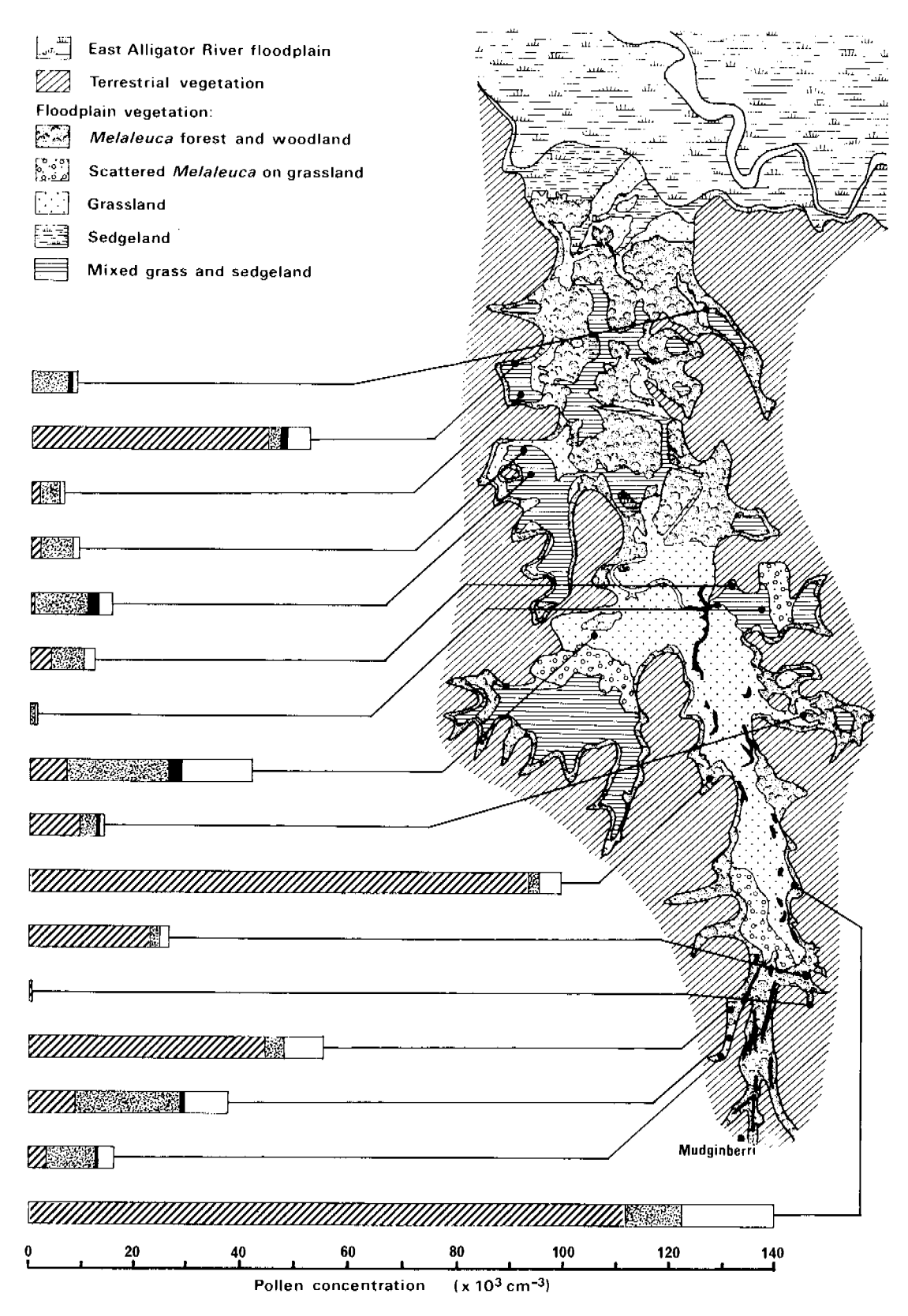


Figure 3.15a The modern vegetation of the Magela Plain (modified from Finlayson *et al.* 1989) with samples from tributary arms that might not be directly affected by Magela water, or that are most affected by local inflows, shown on the left.

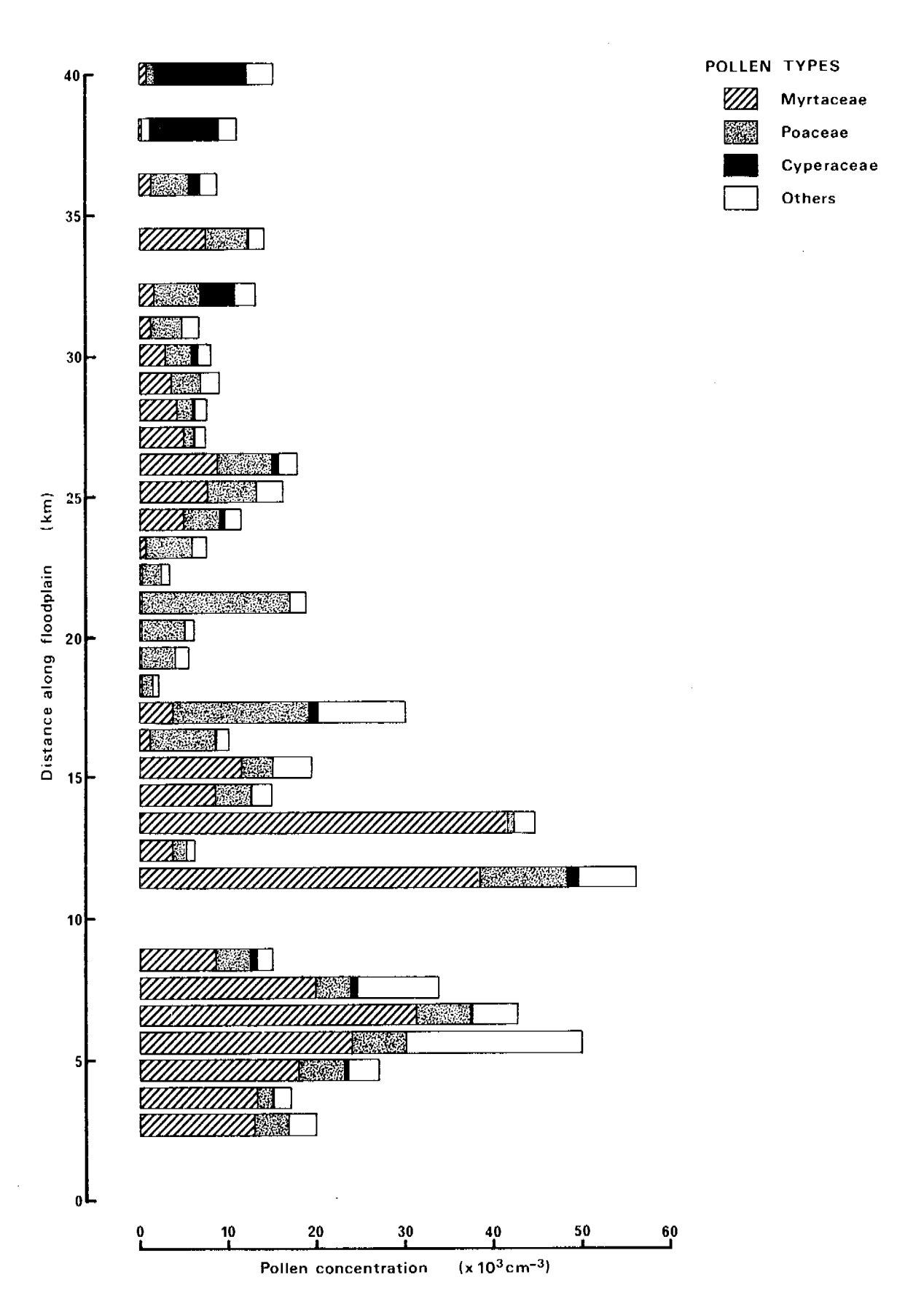


Figure 3.15b Mean concentration of various pollen types in surface samples at 0.5, 1 or 2 km intervals along the Plain

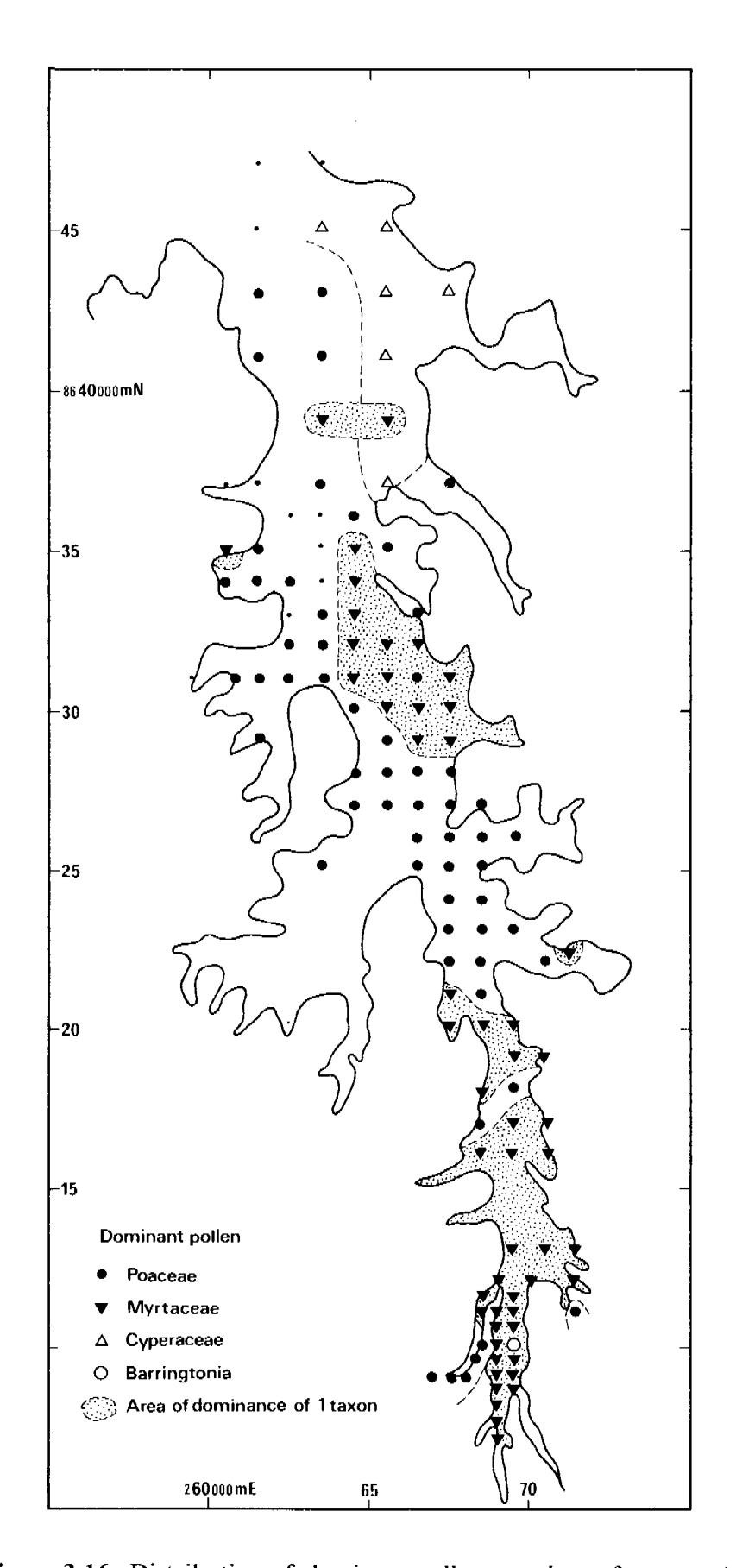


Figure 3.16 Distribution of dominant pollen taxa in surface samples

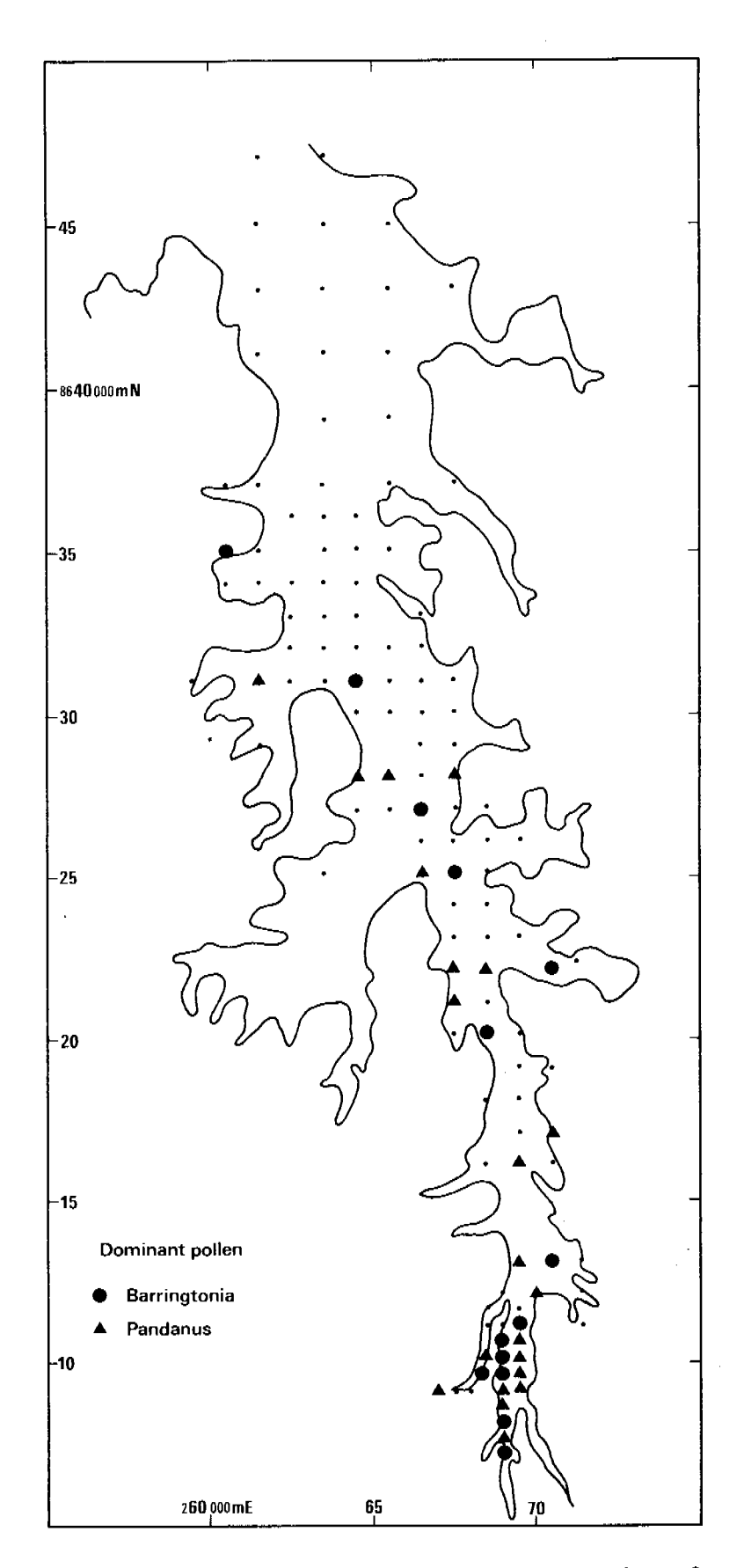


Figure 3.17 Distribution of Barringtonia and Pandanus pollen in surface samples

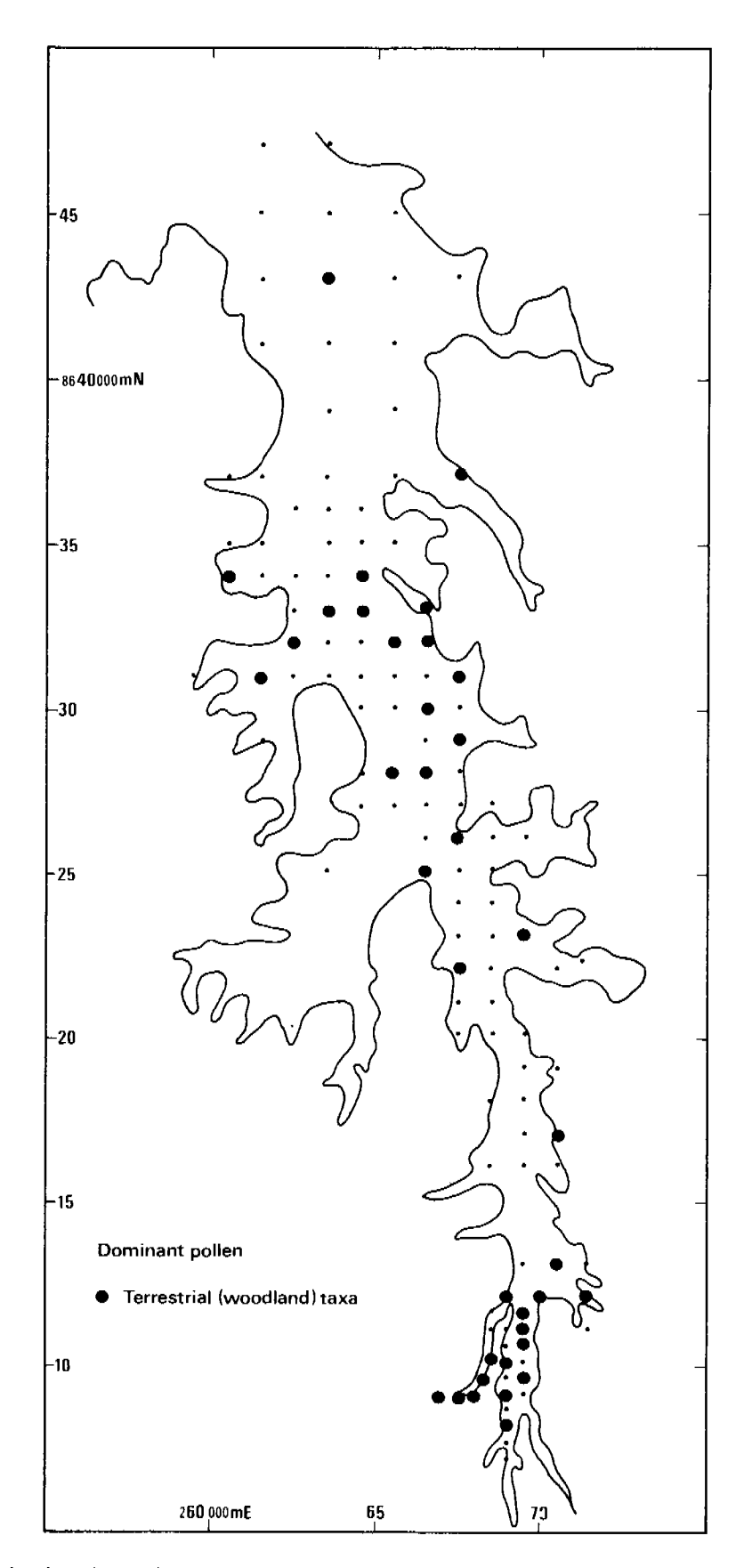


Figure 3.18 Distribution of sites where terrestrial (woodland) taxa dominate surface pollen assemblages

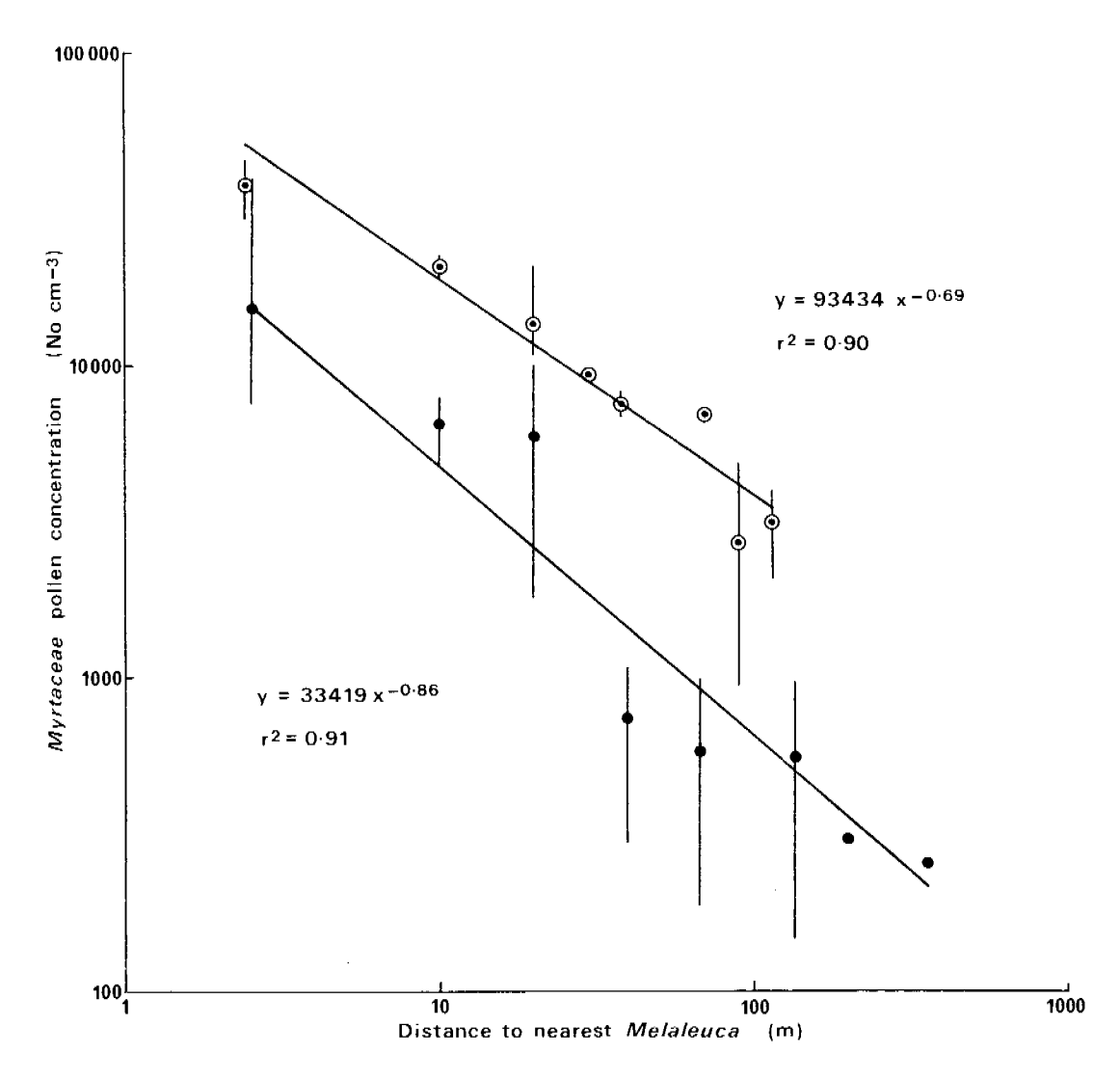


Figure 3.19 Percentage of Myrtaceae pollen (in surface samples) in relation to the distance of sample sites from the nearest tree of Melaleuca spp. The upper curve refers to the Mudginberri Corridor and the Upstream Basin, while the lower curve refers only to the Downstream Plain and East Alligator Flood Plain. Data are shown as mean ± standard error. Where there is only one data point it is shown as a single dot.

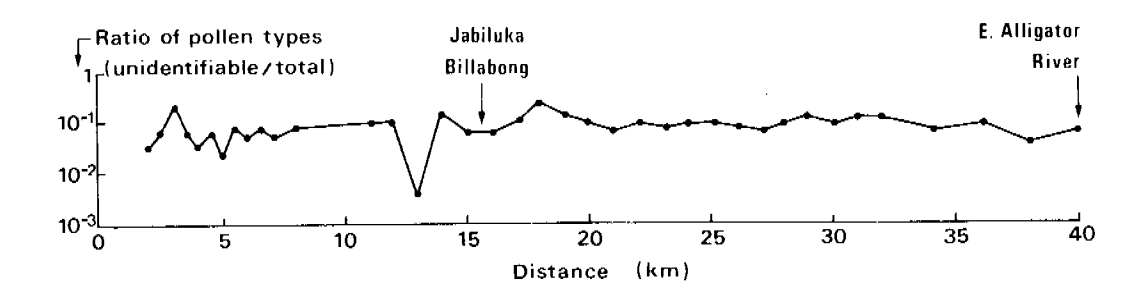


Figure 3.20 Longitudinal distribution of the ratio of unidentifiable total pollen in surface samples

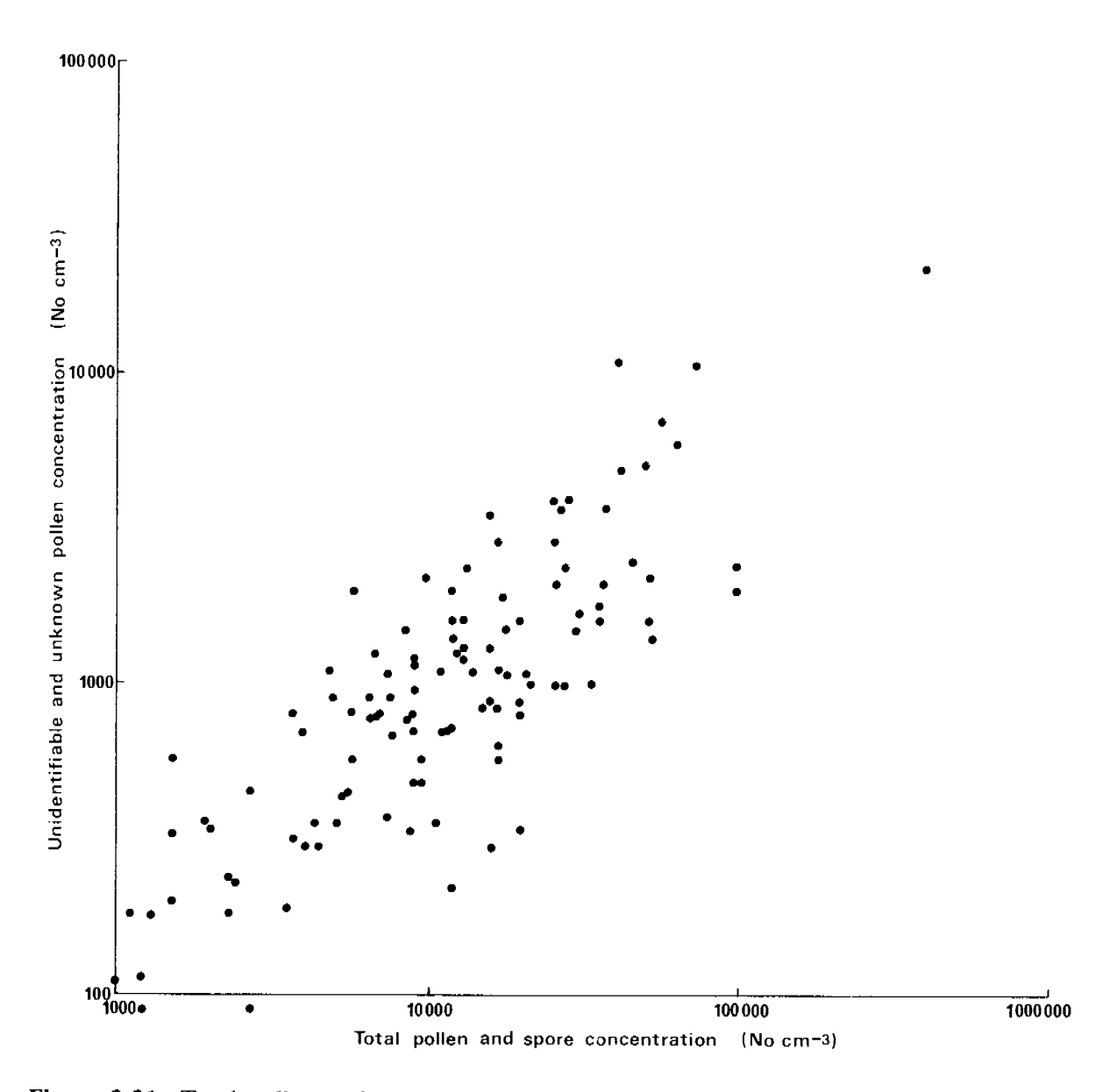


Figure 3.21 Total pollen and spore concentration versus unidentifiable and unknown pollen concentrations

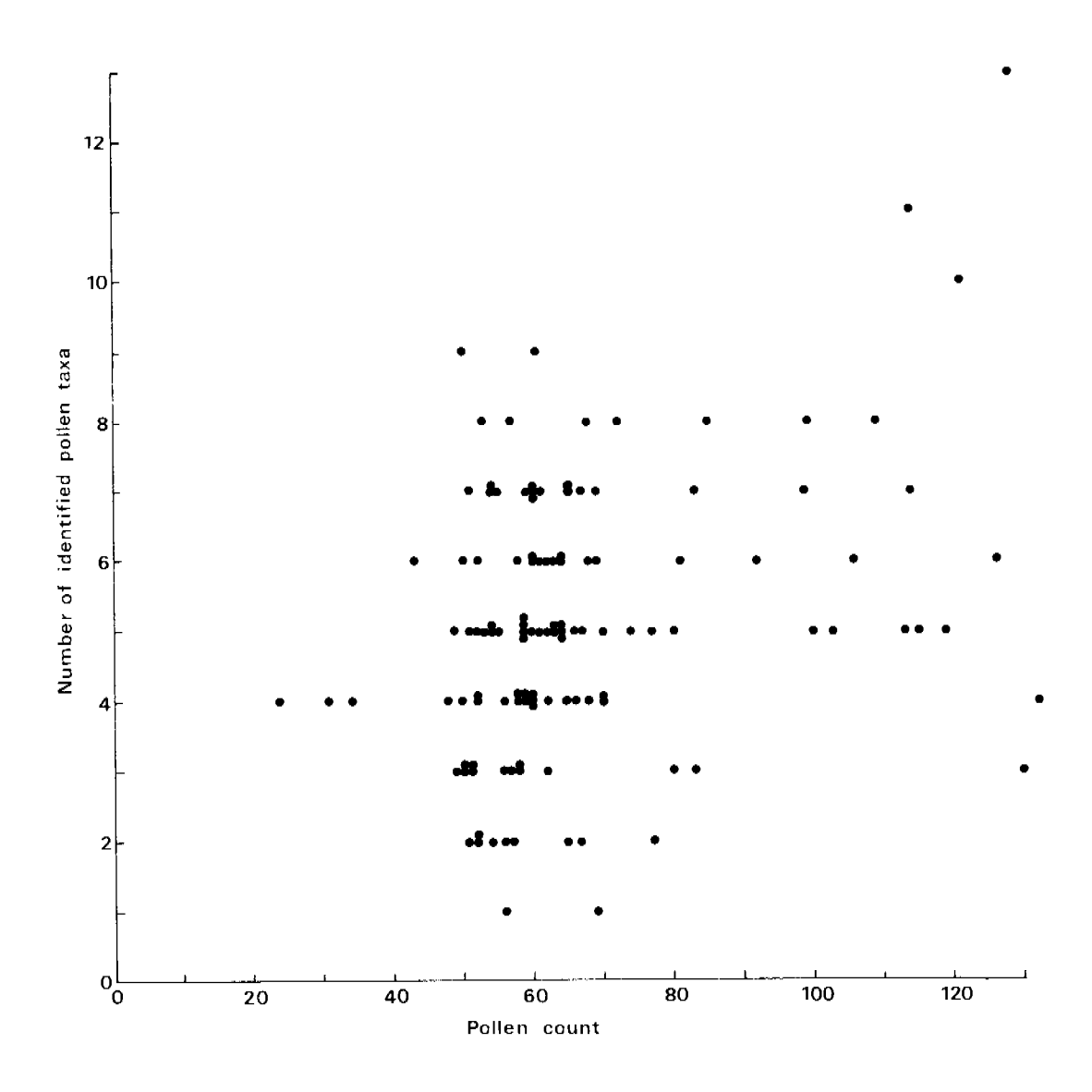
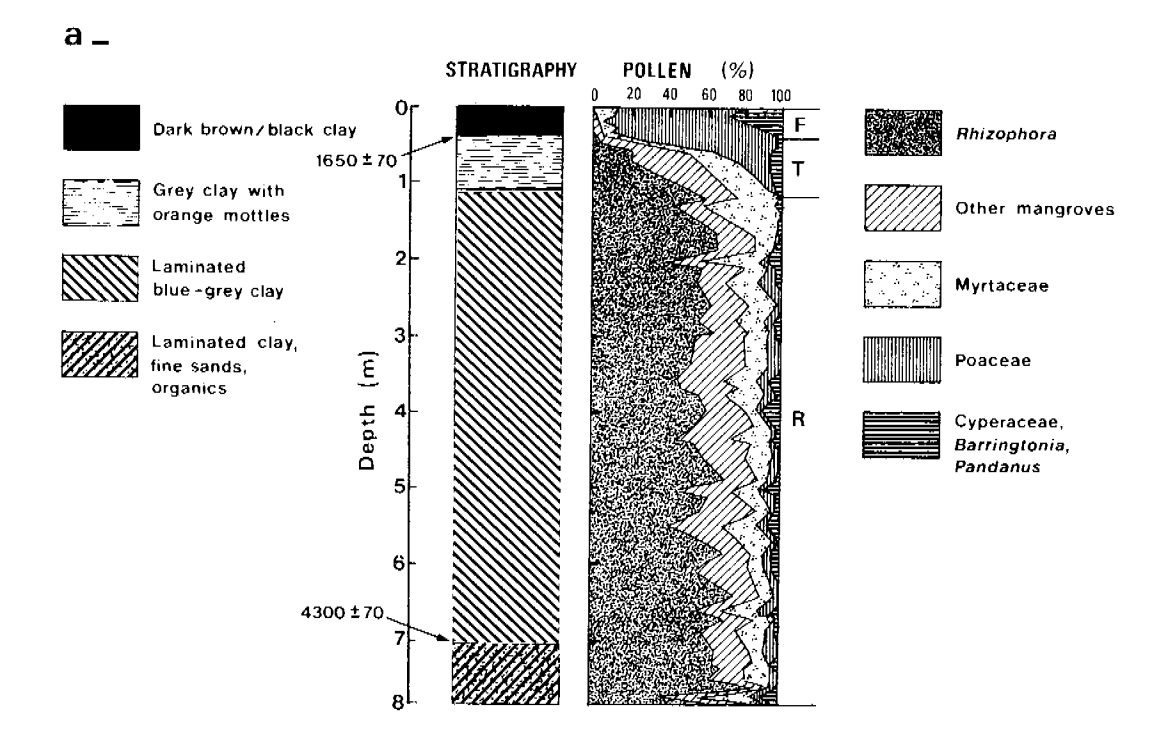


Figure 3.22 Pollen count versus number of identified pollen taxa



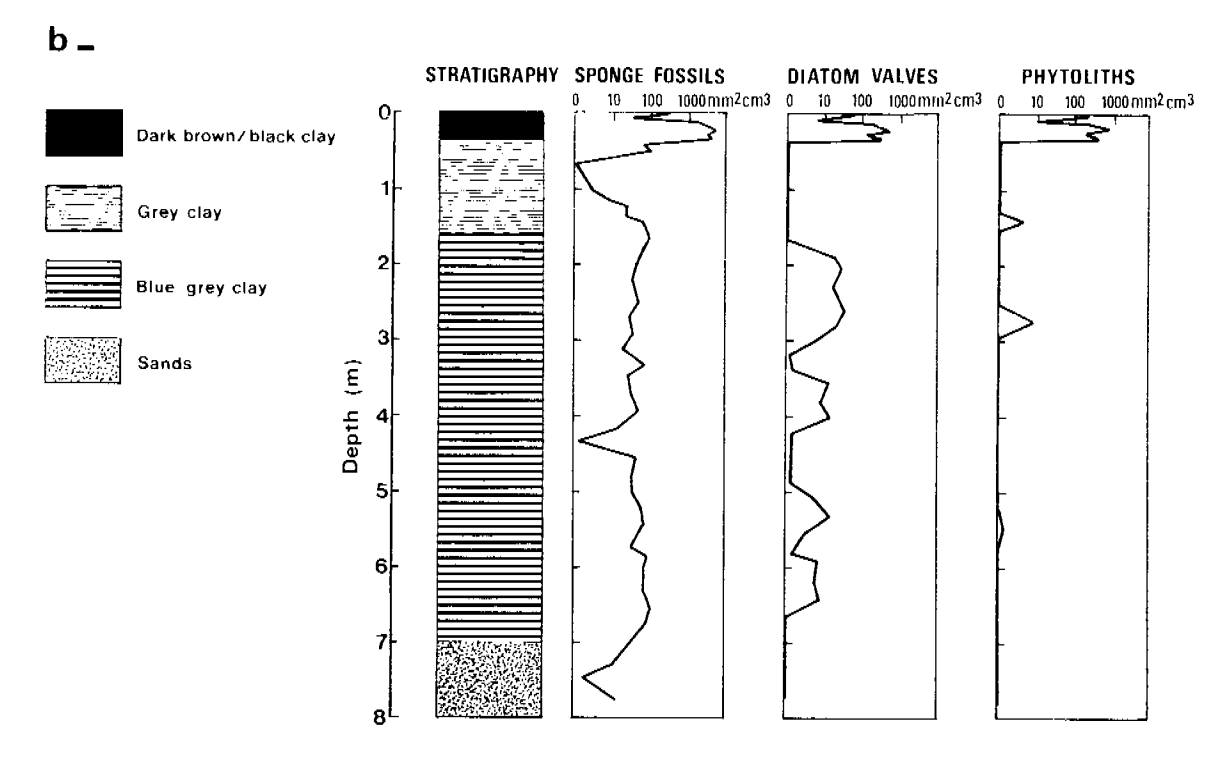


Figure 3.23a Lithology and dominant pollen groups for core M8 from near Jabiluka Billabong. The three principal biostratigraphic units are shown: F, freshwater wetland; T, transition between the units above and below; R, mangrove forest dominated by Rhizophora.

Figure 3.23b Biogenic silica fractions from the M8 core

CHAPTER 4. LATE QUATERNARY EVOLUTION OF THE MAGELA PLAIN

4.1 INTRODUCTION

Stratigraphic data, specifically for this project, have been gathered from 98 sites on the Magela Plain, supplemented by drillhole descriptions from the N.T. Geological Survey, mining companies and the BMR (Bureau of Mineral Resources). Most of the stratigraphic sites have been arranged on cross-sections the locations of which are shown on Fig. 2.3. Lithologic, chemical, pollen and chronometric data, described and discussed in Chapter 3, are drawn together in this Chapter to describe the evolution of the Plain. Each of the cross-sections is discussed in detail in section 4.2. The vegetation history, and so in large measure the history of depositional environments, is discussed in section 4.3. The geomorphic evolution of the Plain is summarised more fully in section 4.4. The most recent phase of the Plain's history, namely the deposition of the Dark Brown/Black Clay (the so-called 'black soil') is considered in detail in section 4.5 and climatic changes during this time are inferred in section 4.6 and section 4.7. In section 4.8 the changes documented on the Magela Plain are placed in the wider context of global climate change. Finally, the origin of the patterned ground in the Upstream Basin is briefly discussed in section 4.9.

The stratigraphic synthesis accomplished in section 4.2 will be developed further in Chapter 5. Here the relationships between primary depositional environments and pedogenic alteration will be explored by relating lithology, pollen and soil chemistry by means of both individual cores/pits and cross-sections.

4.2 THE STRATIGRAPHIC CROSS-SECTIONS

The cross-sections are arranged in Figs 4.1 to 4.11 beginning with the most upstream (southerly) section near where the Oenpelli road crosses Magela Creek (Fig. 2.3). Each diagram has the lithostratigraphy at the top, showing the locations of all cores/pits/auger holes. Each graphic log is projected onto the section, and the amount of projection can be seen in Fig. 2.3. At the bottom of each diagram are the results of pollen analysis, mostly of cores. Radiocarbon dates are shown on both the lithostratigraphic and biostratigraphic diagrams. Those cores that are not on cross-sections, and were analysed for their pollen content, have been combined on Fig. 4.12.

In most cases the pollen results show that a Rhizophora forest grew during much of the time represented by the cores. The percentage of Rhizophora pollen remains roughly constant then declines during the transition period discussed in Chapter 3. The point at which this decline begins is defined as the base of the transition zone (and of course the top of the mangrove forest zone). The Rhizophora pollen declines to zero (or only a few present) as the freshwater zone is entered. The point at which Rhizophora pollen is absent (or nearly so) is defined as the base of the freshwater zone. It is not always possible to define these boundaries in the precise way just described, depending upon sampling interval, pollen preservation and the complexity of pollen variations through time. As a result the boundaries can be specified as occurring within a range of depths. The best estimates of the depths of boundaries are given in Table 4.1 for all analysed sites.

These boundaries have been superimposed on the lithostratigraphy (taking sedimentology into account) to produce cross-sections showing environments of deposition. These sections have been arranged as a pseudo-perspective diagram in Fig. 4.13. Where the pollen data are either inadequate or absent, the boundaries between environments of deposition are based upon correlations between pollen and lithology.

CROSS-SECTION 1

This section lies at the downstream end of an extensive suite of river terraces. Examples of Pleistocene terraces were found on this section, buried by Holocene sediments. The Pleistocene alluvium is clearly different from the Holocene sediments, being more weathered, drier and containing gravel. The upper surfaces of the buried terraces are marked by reddened zones interpreted as palaeosols.

The ancestral valley that was cut into bedrock and flanked by the river terraces is filled by a thick body of sands and clays that, at least in the upper part, were deposited either in or near a mangrove forest. Although pollen evidence is not available from this section, similar sediments on core MC8 on cross-section 2 (Fig. 4.2) show a change from mangrove pollen to freshwater taxa at about -4 m AHD. This is also the maximum elevation at which Rhizophora pollen has been found in cores just upstream of Mudginberri Billabong (Nanson et al. 1989). For these reasons, a boundary between freshwater and mangrove depositional environments has been sketched at -4 m AHD on Fig. 4.13.

The sea reached this location well before 4400 years BP (4.4 ka) (Fig. 4.1), with a persistent channel on the eastern side. The transition zone is a gently undulating body of sediment that is clay rich. The beginning of freshwater conditions was about 4 ka and occurred during the deposition of Grey Clay and Clayey Sands. This body of sediment was replaced about 2.5 ka by organic-rich freshwater sediments of the Dark Brown/Black Clay stratigraphic unit. The major topographic features of the section were established during the deposition of the grey clays and sands. The most recent sediments are a veneer. Both of the young bodies of freshwater sediment accumulated coevally with colluvium derived from the adjacent uplands.

CROSS-SECTION 2

The oldest sands and clays intersected on this section contain freshwater pollen with a change to *Rhizophora* dominance, as noted above (Fig. 4.2). The Blue-Grey Clay stratigraphic unit is well represented here, and is overlain by a transition zone in Grey Clay/Blue Clay clay. The beginnings of the Island Billabong levee (actually a levee prow, as described in Chapter 2) can be seen in the transition zone, at about 3.8 ka. Freshwater grey clay was deposited across this incipient levee and adjacent surfaces, and the axis of the levee shifted westwards.

The sequence just described lies beneath the levee and low plain. The high plain at the eastern end of the section, is underlain by a complex body composed substantially of Pleistocene sediment. The brown sands and clays that underlie the Holocene Grey Clay contain freshwater pollen in the upper parts. *Rhizophora* pollen occurs, in very low concentrations, from at least -0.5 m AHD to 1.0 - 1.5 m AHD in sediments that are dry Blue-Grey Clay equivalents. This is interpreted as a dewatered fragment of estuarine sediments deposited during the last interglacial, about 120 ka.

As on cross-section 1, the end of the *Rhizophora* forest came about 4 ka. The shape of the current landscape then began to form, although the Pleistocene promontory to the east set the shape of the land from a much earlier time. On this section we see evidence for diachronism at the base of the Dark Brown/Black Clay.

CROSS-SECTION 3

This section (Fig. 4.3) lies adjacent to and above the Jabiluka uranium deposit. This is a relatively simple section with estuarine sands and clays underlying Blue-Grey Clay of the mangrove forest period. The transition period here occurs within the Grey Clay. At site

MV2, detailed pollen analysis (see section 4.3) shows that freshwater conditions occur either at or only just below the base of the Dark Brown/Black Clay (Clark & Guppy 1988).

The start of the transition was soon after 3.6 ka and freshwater conditions began at 1.3 ka. A date of 870±60 BP on mangrove wood at this site is anomalous, one possible explanation of which is that a shallow channel was lined with the last vestiges of mangroves and that it was backfilled during the last nine centuries. The dated wood was found in a large pit within which there were no signs of such a channel infill. An adequate explanation for this date cannot be found, so it has been discarded.

Throughout the estuarine phase represented in the holes drilled at this site, there was coeval deposition of sands and clayey sands in a piedmont apron extending from the Arnhem Land Escarpment to the edge of the Plain. This is discussed by Bettenay *et al.* (1981) and Fig. 4.3 includes some of their data.

CROSS-SECTION 4

The basal sands intersected in cores M8 and M9 (Fig. 4.4), and further upstream in M10 (Fig. 4.12), contain what could be a transgressive pollen sequence signalling the replacement of freshwater fluvial conditions by estuarine conditions. Alternatively, the pollen data can be interpreted as showing fluctuations of an environment that was generally dominated by *Rhizophora*. The rather limited data are most conservatively interpreted as reflecting fluctuations rather than transgression.

The dates of 6.5 ka and 4.3 ka at the top of the sand in two cores about 900 m apart suggest that a sedimentologically undetected tidal channel was backfilled starting about 4.3 ka.

Cores from the low plain to the west of the levee on Jabiluka Billabong show the transition beginning below the top of the Blue-Grey Clay. At M9 this occurred at about 2.5 ka. This is the first evidence that at least some of the Blue-Grey Clay was deposited under conditions other than those of a mangrove forest. The transition in JB5 is abrupt and prolonged, with *Rhizophora* pollen in the Dark Brown/Black Clay. This is the only core that shows this pattern and may be the result of erosion and redeposition of mangrove-rich sediment.

Freshwater conditions were established in the Grey Clay on the low plain after 2.8 ka. On the levee there is no transition, unlike at Island Billabong (Fig. 4.2), and the levee was deposited under freshwater conditions. There are high proportions of *Barringtonia* and *Pandanus* pollen in both the Jabiluka and Island Billabong levees. The landscape during the early stages of levee construction at Jabiluka was dominated by a plain in 'transition' with a freshwater channel and levee.

CROSS-SECTION 5

All of the cores here are short and none reaches the base of the mangrove mud (Fig. 4.5). All sediments are oxidised below the surface, as indicated by low pollen concentrations. The transition zone has no consistent relationship with the top of the Blue-Grey Clay. Freshwater conditions were established in the Grey Clay.

CROSS-SECTION 6

The sands at the base of core M11 contain *Rhizophora* pollen as do the near-basal sands and clays in NB3 (Fig. 4.6). These coarse estuarine sediments were replaced by Blue-Grey Clay by at least 6.6 ka, while a tidal channel persisted at NB3 from before 4.3 ka, filling with both sands and the laminated facies of the Blue-Grey Clay. This channel, and one on cross-section 4 (Fig. 4.4), existed at the same time and were probably connected.

There is no consistent relationship between the beginning of the transition and the top of the Blue-Grey Mud, as on section 5. Freshwater conditions were established in the Grey Clay. The levee complex at Nankeen Billabong was established during the transition which is hard to define because of deep oxidation and loss of pollen. Here the levee transition sediments are not rich in pollen of *Barringtonia* and *Pandanus*. The shape of the levees has been substantially modified by deposition of Dark Brown/Black Clay.

CROSS-SECTION 7

The deepest core at this site (Fig. 4.7) did not reach sands, although interpretation of deep drilling (Fig. 3.1) indicates that sandy clays are likely to underlie this cross-section. The Blue-Grey Clay gives way to a transition zone within the Grey Clay which is overlain by the Dark Brown/Black Clay. There are no systematic relationships between the boundaries of these lithologic units and the pollen changes. That is, the mangrove forest zone continues well into the Grey Clay and, in LB23(A), into the Dark Brown/Black Clay. The presence of significant *Rhizophora* in sediments that are elsewhere freshwater is unique to this site and is not repeated in the adjacent core LB23(C). This suggests mixing of deeper pollen and sediment into overlying sediment, probably by erosion and redeposition.

CROSS-SECTION 8

The Blue-Grey Clay on this section is undated but, by comparison with core M12 (Fig. 4.12) some 2 km upstream, the sediments at about -5 m AHD were deposited about 7 ka. This is not the base of the estuarine sediments.

On this cross-section the transition begins in the Grey Clay and there is a freshwater section in both the Grey Clay and the overlying Dark Brown/Black Clay.

CROSS-SECTION 9

The cores here are all short (Fig. 4.9) and the interpretation in Fig. 3.1 shows the region below this section to be transitional between the shelly sandy clays near the East Alligator and the mud basin upstream.

Most samples taken for pollen analysis were oxidised so that pollen was either infrequent or absent. The base of core LBI shows *Rhizophora* dominance and a transitional zone is inferred between mangrove forest and the Dark Brown/Black freshwater sediments. The shallow channel has no reflection in the base of the Dark Brown/Black Clay suggesting that the previous drainage was different from its modern counterpart.

CROSS-SECTION 10

The Blue-Grey Clay is overlain by a transition zone and the freshwater sediments are restricted to the Dark Brown/Black Clay (Fig. 4.10). The base of this latter unit coincides with oxidation of pollen in core LP1 but not in the other cores.

The palaeochannel visible on aerial photographs, and mapped on Fig. 2.3, is traversed by this cross-section and two cores penetrate it. There is no evidence in either core, or in a large pit dug on the side of the modern channel (adjacent to GS019), for laminated channel sediments in the Blue-Grey Clay. It seems that this channel was passively filled then buried by younger sediment, its visibility on aerial photographs being a palimpsest.

The Dark Brown/Black Clay contains a moderate amount of *Ceratopteris* (cf.) pollen. This pollen taxon is common in transition sediments in cross-sections further upstream.

CROSS-SECTION 11

Oxidative destruction of pollen has occurred to considerable depth in the cores examined on this section (Fig. 4.11), making difficult the identification of depositional environments above the Blue-Grey Clay. The transition zone here is inferred and the boundary between it and the Blue-Grey Clay is taken to lie just above the top of the clays coloured blue-grey in fresh cores, as found at most other sites. Palaeochannels are reconstructed from both the presence of laminated muds and aerial photograph interpretation (Fig. 2.3).

Ceratopteris (cf.) pollen is found in surface samples across this area, the East Alligator Flood Plain. The banks of the Magela Creek tidal channel that is traversed by this cross-section have occasional mangroves, mostly Avicennia marina. As will be shown in the next section, the transition is marked by Ceratopteris (cf.) and (declining) Avicennia pollen. The East Alligator Flood Plain is therefore a modern example of a transition landscape. The Dark Brown/Black Clay and underlying Grey Clay are both transitional sedimentary environments on this cross-section and, to some extent, on cross-section 10.

4.3 VEGETATION HISTORY AND IMPLICATIONS FOR GEOMORPHIC DEVELOPMENT OF THE PLAIN

In addition to the pollen analyses reported in the last section, a core was chosen for detailed study of the transition from estuarine to freshwater sediments. Core M8, taken near Jabiluka Billabong (Fig. 4.4) was selected, but after many samples had been processed it was discovered that a section had been lost. A second core, MV2, collected near Mine Valley Billabong (Fig. 4.3), was chosen. Samples were taken at contiguous 1 cm intervals through the top 100 cm of MV2 and of the available transition sediments of M8. Wet density, water content and loss on ignition (for organic matter content) were determined from duplicate samples and a further replicate set was used to extract biogenic silica (remains of sponges, phytoliths and diatoms). Results from core M8 are shown in Fig. 3.23. Estuarine mangrove vegetation persisted through most of the record and was replaced towards the top of the sediment by freshwater conditions, with mainly grasses and sedges. Between these two there is a marked transition zone. This sequence is typical of the whole Plain.

The stratigraphy of, and pollen concentrations in, the upper sections of cores MV2 and M8 are shown in Fig. 4.14. The litho-stratigraphies of the two cores are readily matched, as is the case with almost all samples of floodplain sediments. In MV2, where contiguous samples were taken through the 100 cm section, some samples contained very little or no detectable pollen. Since these samples came from oxidised parts of the core, as indicated by mottling and sediment chemistry (see Chapter 5), it is likely that pollen has been destroyed after deposition. Both cores show high pollen concentrations above and below the sections bereft of pollen, in full estuarine and full freshwater conditions, although freshwater pollen concentrations in MV2 are higher than those in M8. Because of the likely post-depositional destruction of pollen grains, it is not possible to calculate pollen influx rates.

Figure 4.16 also shows the major pollen and spore types as percentages of the total of pollen grains and spores in each sample. The taxa are divided into mangroves and those living in freshwater or terrestrial environments. This habit/habitat distinction is not always valid as *Barringtonia acutangula* can be regarded as a freshwater mangrove. Further, some grasses and sedges are tolerant of saline soils and there is one estuarine Myrtaceous mangrove in the region, *Osbornia octodonta*.

The percentage pollen data are plotted on ternary diagrams in Fig. 4.15 with all pollen and spore taxa divided into three groups: (a) Rhizophora, (b) mangroves other than Rhizophora, and (c) non-mangrove taxa. The pollen record in Figs 4.14 and 4.15 has been divided into three main phases; mangrove forest, transition and freshwater wetland, with the transition

phase further subdivided. The levels at which changes occur, marked on Fig. 4.14, were determined from Fig. 4.15. Each phase includes one or more samples that fall within the range of values of a later phase, but the selected level of change from one phase to the next is that after which the vegetation does not return to its former composition. The mean values within each phase are also shown in Fig. 4.15, with lines connecting the means to show the sequence of changes. In all cases change is neither gradual nor continuous.

One ecosystem, a freshwater wetland, has completely replaced another, an estuarine mangrove forest. As the requisite physical environments are mutually exclusive rather than forming a continuum, the transition cannot be one of gradual replacement of one ecosystem by another. Because of this, we will first consider the age and variability of the present freshwater wetland as indicated by the pollen record, then the past mangrove forest and, finally, the transition between the two.

THE FRESHWATER WETLAND

The character of the wetland has been described in Chapter 1. The most abundant vegetation consists of the aquatic grasses, Hymenachne acutigluma, Pseudoraphis spinescens and Oryza spp., and sedges, particularly Eleocharis species. The annual vegetation at any one point is highly variable from year to year, and Taylor and Dunlop (1985) attribute this to differences in timing, duration and intensity of the Wet season. Extensive areas of paperbarks (Melaleuca spp.) form swamp forests or woodlands, while billabongs are sometimes lined by riverine species, predominantly Barringtonia acutangula and Pandanus spp. Towards the outlet of Magela Creek into the East Alligator River, stream banks have occasional mangroves, mostly Avicennia marina with some Excoecaria agallocha and Lumnitzera racemosa. Eucalyptus woodlands surround the flood plain and, upstream along Magela Creek, where it crosses the lowland from the Arnhem Land Escarpment, Melaleuca species dominate, with an understorey of grasses and shrubs away from the active, sandy stream channel. One plant that is not abundant today appears on the pollen diagrams (Fig. 4.14). It is Ceratopteris thalictroides, a small aquatic fern.

The pollen record of the freshwater wetland extends to 39 cm depth in core MV2 and about the same depth in core M8. At both sites the *Poaceae* predominate, providing over 60% of the pollen in most samples. It is these high grass pollen percentages, and the absence of all but occasional mangrove pollen grains, that distinguish the present freshwater wetland. The mangrove pollen has probably been reworked from older estuarine sediments. *Cyperaceae* pollen has been more abundant through the freshwater phase at M8 than at MV2, while the reverse is true of *Myrtaceae* pollen. This may reflect the locations of the two sites, with MV2 nearer to fringing *Melaleuca* woodlands, although the difference is not evident in the surface samples (0-1 cm) from these sites. The scatter of data in Fig. 3.19 shows that some sites will poorly reflect the close-by *Melaleucas*.

At M8 there have been changes through the freshwater wetland phase in the proportions of grasses and sedges, similar to observed differences from year to year (Taylor & Dunlop 1985; Finlayson et al. 1985). At MV2, where sedges have been less abundant for most of the time, there have been changes in the proportions of grasses and paperbarks, which appear almost cyclic.

Most of the pollen samples contained little or no charcoal, but it is usually present through the *Rhizophora* forest period and occasionally in the transition phase. In the freshwater sediments at MV2, the first charcoal appears at 14 cm depth, it is abundant between 10 and 11 cm, and in significant quantities from there to the surface. At M8, charcoal first appears in the 17-18 cm samples and is abundant above 6 cm. Fires on the flood plain are thus relatively recent (i.e. within the last 700-800 yr) but do not appear to have had any significant effect on the vegetation.

Williams (1984) observed significant tree loss in 38% of the *Melaleuca* forest on the Magela flood plain between 1950 and 1975, and suggested that fire, strong winds and buffaloes may have been responsible. The pollen record indicates that the observed changes are within the limits of former variability and therefore reversible, provided that boundary conditions have not changed significantly. If the cause of the recent decline has been buffaloes, then their removal should allow a return to former vegetation dynamics, but not necessarily to the 1950 forest density.

THE MANGROVE FOREST

Of the identified mangrove pollen types, Rhizophora, Ceriops and Bruguiera are all genera in the Rhizophoraceae. Ceriops and Bruguiera pollen grains are indistinguishable, but are distinguished from Rhizophora pollen grains mainly by size. Reciprocal changes in abundance of the two pollen types in adjacent samples between 73 cm and 78 cm depth of core MV2 suggest that the distinction is not always easy or valid. Other estuarine mangrove genera included in the diagram are Lumnitzera, Sonneratia, Camptostemon and Avicennia. It was not possible, using light microscopy, to identify any of the mangrove pollen to species level.

Many mangroves have limited environmental tolerances, and species may grow in characteristic zonation patterns, largely determined by substrate and water salinity, and tide levels (M. Ball, pers. comm.). Both of the Sonneratia species that grow today in the Alligator Rivers Region colonise accreting shoals or the lowest tidal fringes of rivers, inundated by most high tides (Wells 1982; Davie 1985; Woodroffe et al. 1986). Sonneratia lanceolata grows upstream and S. alba towards the mouth of the rivers. Rhizophora stylosa, Avicennia marina and Camptostemon schultzii tend to form the fringing vegetation along tidal waterways (Wells 1982), although the pattern is by no means fixed (Woodroffe et al. 1986). Lumnitzera racemosa grows at the landward edge of mangroves, or on higher ground with Avicennia marina, as near the Magela outlet today. Avicennia marina grows in a wider range of environments than any other mangrove (see papers in Clough 1982). The other Avicennia growing today in the Alligator Rivers Region, A. officinalis, is confined to lower tidal levels and accreting mud (Wells 1982).

At the base of the core sections illustrated in Fig. 4.14, the pollen spectra are similar to each other and to most other samples taken from the estuarine mangrove sediments of the Plain. Through the estuarine phase, the dominant mangroves were Rhizophora, although other mangrove taxa were always present. The range of variability is shown by the samples plotted in Figs 3.23a and 4.15. The uniformity evident over an area of about 200 km² and a period of several thousand years is possibly due to the mobility of mangrove muds and their contained pollen in an area with a large tidal range, wet season floods and occasional cyclones. But it is more likely that the pollen is accurately reflecting extensive mangrove forests formed almost exclusively of Rhizophora species, such as occur in north Queensland today (Dowling & McDonald 1982). Woodroffe, Thom & Chappell (1985) and Woodroffe et al. (1986), from stratigraphic evidence of widespread mangrove muds, postulated a mid-Holocene 'big mangrove swamp' on the South Alligator Flood Plain, but they had insufficient pollen analyses to determine its species composition. The Rhizophora forest would have been a highly unstable environment on the small scale, but stable on the larger scale, both spatial and temporal. Homogenisation of some of the muds and their pollen content would have been effected by crabs and other agents of bioturbation.

THE DECLINE OF THE MANGROVES

At MV2, Rhizophora decreases in stages through the transition from estuarine to freshwater. At both sites there are increases in *Avicennia* and *Ceriops/Bruguiera* pollen as *Rhizophora* decreases and, at MV2, increases in *Sonneratia* and *Camptostemon* as well. Mangrove taxa disappear, apart from occasional grains, in the same sequence at both sites: *Lumnitzera* does

not last beyond the mangrove forest stage, Sonneratia disappears later, followed by Ceriops/Bruguiera, then Camptostemon and, finally, Avicennia.

Similar increases in Sonneratia and Avicennia as Rhizophora declined were found on the South Alligator River by Russell-Smith (1985), and by Woodroffe et al. (1986) in one of their cores, the other showing an increase only in Avicennia. Woodroffe et al. noted the similarity between the vertical sequence in their core (Sonneratia to Rhizophora to Avicennia) and zonation on present-day stream banks, related to tide level, but they also show in another paper (Chappell & Grindrod 1985) that there is little relationship between present mangrove vegetation and the pollen in surface samples from beneath it. This suggests high mobility and reworking of mangrove muds, both past and present, mixing the contained pollen. In none of the Magela cores is there an unequivocal vertical succession of several mangrove species which could be attributed to accretion of the sediment through a stable tide range.

The first stage of the vegetation transition (a) in core MV2 is marked by an increase in Sonneratia. Whichever species this is, it suggests increased instability with shoaling, accretion or exposure of lower tidal mud to be colonised by these pioneer mangroves. Subsequently, Camptostemon, Avicennia and Ceriops or Bruguiera increase at the expense of Rhizophora, and Sonneratia decreases (transition b). There was a temporary resurgence of Rhizophora and a corresponding decrease in Avicennia in the middle of this period, more marked at M8 than MV2. The decrease in Rhizophora and increases in other mangrove genera probably indicate the existence of a network of stream and tidal channels within the extensive Rhizophora forest. This would have created many more sites for a range of mangroves to grow, reduced the area of tidal inundation and, hence, of Rhizophora, and possibly led to the landward margins becoming hypersaline flats, eliminating the environments suitable for Lumnitzera. If this were the case, an increase in Chenopodiaceae pollen would be expected as there are two or three species that grow, albeit sparsely, on hypersaline flats throughout the region. Chenopod pollen is rare in the Magela sediments, so perhaps it does not survive in a hypersaline environment. Alternatively it may be very dilute in sediments in long-term deposition sites, or in the past there may not have been large areas of hypersaline soils.

In the third stage of the transition (c) at MV2 the remaining mangroves, predominantly Avicennia, decline then disappear. At M8 the abrupt change in pollen composition at 55 cm suggests that some sediment was eroded in the middle of this period. Alternatively, the change might really have been sudden and the steady decline in mangrove pollen at MV2 be due to reworking of older sediments. Isolated mangrove pollen grains in the freshwater sediments above are almost certainly reworked.

ESTABLISHMENT OF THE FRESHWATER WETLAND

Through the *Rhizophora* forest stage in all cores from the Magela Plain, the most abundant freshwater pollen taxon is the *Myrtaceae*. As mentioned above, this is believed to be predominantly *Melaleuca* pollen from the paperbarks that are so abundant today in wetlands and along streams. At M8, there was a significant increase in *Myrtaceae* pollen before the main transition from estuarine to fresh conditions (Fig. 3.23) and, at the same time, grass pollen virtually disappeared. This early increase in *Myrtaceae* pollen has not been found at other sites.

As Rhizophora declined at MV2, so too, but to a lesser extent, did the Myrtaceae. When Avicennia and Ceriops/Bruguiera reached a maximum, there were also significant increases in Poaceae and Cyperaceae. The grasses and sedges growing at that time may have been salt-tolerant species, but we have been unable to identify grass pollen grains to genus level, with the exception of Oryza. It may be possible to determine which genera were present from the phytoliths abundant in the sediments (Rovner 1983; Fujiwara et al. 1985).

The third phase of the transition (c) is marked by a very large increase in abundance of grass pollen, although it was not yet totally dominating. Myrtaceae pollen increased again, but there was less Cyperaceae. At M8, Barringtonia and Pandanus pollen appeared more often, suggesting freshwater channels nearby, of which Jabiluka Billabong may be a remnant. As in the earlier part of the transition, the grasses may have been salt-tolerant species and the vegetation similar to that near the Magela outlet and along upstream parts of the South Alligator and East Alligator Rivers today. These are open woodlands with an overstorey of Avicennia marina and other mangroves, and ground cover of salt-tolerant grasses such as Sporobolis virginicus and Cynodon dactylon.

The evidence against this comes from the abundance through this period at MV2 of the freshwater fern, Ceratopteris thalictroides, and of a legume, probably Aeschynomene indica, a small shrub. The latter is not shown on the pollen diagram (Fig. 4.14), but it makes up from 14% to 40% of the pollen at MV2 between 44 cm and 50 cm, corresponding with a drop in the proportion of grass pollen. Aeschynomene indica grows today in the region on flood plains and river levees and is a seed-bearing annual (Taylor & Dunlop 1985). Ceratopteris thalictroides can grow on mud, submerged, emergent or free-floating. Its spores germinate in water or on mud and, in the axes of fertile fronds, it produces plantlets that break free and float away (Jones & Clemensha 1981; Sainty & Jacobs 1981). These reproductive and survival characteristics suggest a pioneer species, able to spread rapidly as the environment changed, but eventually out-competed, in this case by grasses.

Ceratopteris is abundant in transition phase c at MV2, but in phase b at M8. The alternative explanations of this observation are: (a) changes in the mangroves were synchronous, but Ceratopteris was locally abundant at different times; or (b) Ceratopteris was abundant at both sites at the same time, but mangroves remained longer near M8 than MV2. Without radiocarbon dates on transition sediments from these two sites, it is difficult to decide which alternative is correct. Part of the ternary diagrams of Fig. 4.15 is enlarged in Fig. 4.16 to show only the samples falling within transition phase b. Samples are numbered with their depths in the sediment and adjacent samples are connected to show the direction of change. Through this phase, variability was high, but there is a remarkable parallelism in changes with depths at the two sites. This is strong evidence for the conclusion that changes in the mangroves occurred simultaneously and Ceratopteris was abundant later at MV2 than at M8.

Changes in the freshwater taxa through the transition phase from *Rhizophora* forest to freshwater wetland support the conclusion drawn from the changes in mangrove taxa. It appears that the original large area subject to tidal inundation was dissected by channels that created a range of new environments, including areas that rapidly became fresh. Most of these channels have since filled in or shallowed, but remnants are visible as palaeochannels, networks of deeper water or isolated billabongs.

4.4 GEOMORPHIC EVOLUTION OF THE MAGELA PLAIN

From the data presented in Chapter 3 and the interpretation of this chapter, it is possible to describe the evolution of the Plain. The amount of palaeoenvironmental detail available is greatest in the youngest sediments in the upstream part of the Plain. This bias is deliberate, concentrating on the area most likely to be affected by Mine Site detritus.

The lithologic longitudinal section of Fig. 3.1 has been augmented with other indicators of sedimentary environment in Fig. 4.17. The boundaries between sedimentary environments in the upper 3-4 m of the section were estimated for each cross-section by selecting the depth where most samples (containing indicators of a particular environment) coincided, rather than the mean. These values were then plotted below the mean height of the Plain, taken from Fig. 2.1.

The boundaries between the sandy and non-sandy facies of the Blue-Grey Clay are known moderately well from coring in the upstream part of the Plain, but are poorly known near the East Alligator River. The basal and upstream boundary of the Blue-Grey Clay is known from pollen analysis of cores on cross-sections 1 (Fig. 4.1a) and 2 (Fig. 4.2), from pollen analyses of cores taken upstream of Mudginberri (see Nanson et al. 1989), and from lithologic correlations informed by pollen analysis. The detail of this boundary is schematic.

The critical radiocarbon dates, discussed in Chapter 3 and shown on the cross-sections (Figs 4.1a-4.13), have been projected onto the longitudinal section of Fig. 4.17. Dates from palaeochannel infills have been omitted. Where appropriate, and possible, isochrons have been drawn on this section to show the approximate position of the sediment surface at various times in the past.

SEA LEVEL CHANGE

It is evident from the longitudinal section (Fig. 4.17) that freshwater sediments (the Sands and Clays, and Basal Sands and Gravels) filled a substantial fraction of the Magela palaeovalley. The earliest indication of marine influence is a date of 7.7 ka on organic fragments in sandy and shelly Blue-Grey Clay containing abundant *Rhizophora* pollen. The depositional surface at this time was relatively flat, at least as far upstream as cross-sections 4 and 5. Further upstream, freshwater sediment from the Magela Creek was moving downstream to become interbedded with the estuarine sediments.

In a little over 1000 years about 4 m of sediment accumulated above the initial flat part of the depositional surface. Sand was deposited with Blue-Grey Clay in the upstream reaches, possibly from reworking of the freshwater sediments that both underlay the estuary and flanked it as terraces (cf. Woodroffe et al. 1986). Sand and shells in the Blue-Grey Clay at the downstream end indicate an input of sediment from the East Alligator River.

The marine influence, beginning a little before 7.7 ka, came about as sea level rose from its lowest point about 18 ka when ice was much more extensive on land at high latitudes, that is, at the last glacial maximum. The deglaciation resulted in the sea invading valleys, like the Magela, that had previously been occupied by sand and gravel bed streams.

The radiocarbon dates calculated for either identified mangrove fragments, or from unidentified organic remains embedded in sediments rich in *Rhizophora* pollen, are plotted in Fig. 4.18. Included in this diagram are the 'basal samples' of Woodroffe et al. (1986) that indicate the change of sea level in the palaeoestuary of the South Alligator River during the last 9 ka. The Magela data plot in the envelope defined by the South Alligator data, up to nearly 0 m AHD (i.e. mean sea level). Sea level, relative to the level of the land, has been recorded by mangrove remains (which are almost exclusively intertidal) at both sites in the same way. Sea level rose from about -13 m AHD to near present sea level between 8 ka and 5.5 to 7.0 ka. Mangrove remains first occur within the height range of modern mangroves between 5.5 and 7.0 ka, centred on about 6.2 ka.

Woodroffe et al. (1986) determined the elevational range of various living mangroves along the South Alligator River, in areas connected to tidal flows. The present range is from -1.0 m to 3.7 m AHD (see Fig. 4.18). Rhizophora stylosa grows between 0.2 m and 2.9 m AHD. Sonneratia lanceolata grows between -1 m and 2.8 m AHD. The elevational range in which Avicennia marina and Lumnitzera racemosa are dominant is 2.4 m to 3.7 m AHD.

It is clear that the astronomical tides, with spring ranges to over 6 m on the coast, combined with the effect of tidal channel morphology on tidal range upstream from the coast, allows the growth of mangroves well above 0 m AHD. From pollen analysis, the maximum elevation of *Rhizophora* forest at Magela sites is 2.9±0.2 m AHD, equal to the upper limit of modern *Rhizophora* stylosa in the South Alligator River. The maximum elevation of Magela

mud containing Avicennia pollen is 3.8±0.2 m AHD, compared with the modern value of 3.7 m. The dated mangrove detritus above 0 m AHD in Fig. 4.18 is all less than 5 ka and has accumulated above the sea level that has prevailed for the last 6 ka. Woodroffe et al. (1987) have dated mangrove wood up to 1.4±0.1 m AHD, from the South Alligator River, giving an age of 2200±60 BP.

The remarkable agreement between the modern and ancient upper limit of mangroves shows that the transition from *Rhizophora* forest to freshwater wetland was at least in part a result of sedimentation raising the Magela Plain above tidal inundation. A future rise of sea level could return the Plain to a mangrove forest, as will be seen in Chapter 8.

SEDIMENTATION IN THE PALAEOESTUARY

Sedimentation in the palaeoestuary was in a *Rhizophora* forest, called the 'big swamp' by Woodroffe et al. (1986). Most of the sediment is clay although fine sand and silt were deposited with the clay in some areas, as seen earlier. The sand appears to have come from both upstream and downstream (the East Alligator River). The sand at the downstream end does not have the configuration of a tidal delta because it does not occur in all deep cores (Fig. 4.11) but appears as laminated channel sediment. Given its distribution, the fine sand and silt in this palaeochannel probably moved upstream into the Magela embayment. The ~7.0 ka isochron (Fig. 4.17) is not consistent with the formation of a tidal delta and subsequent filling of a mud basin upstream.

The surface of the muds deposited in the *Rhizophora* forest is domed, in longitudinal section (Fig. 4.17). The 14C dates and isochrons also show that this surface is diachronous, getting younger downstream. The upstream boundary of the *Rhizophora* forest migrated downstream and was replaced by transition vegetation and sediments.

This pattern of change is most clearly shown on the age/distance graph of Fig. 4.19. Here the age of the upper boundary of the *Rhizophora* forest muds is plotted, using the dates on Figs 4.1 to 4.12. Where necessary, the age of the boundary (and other boundaries) is calculated by interpolating between ¹⁴C dates.

The migration between 4.4 ka (cross-section 1) and 2.3 ka (cross-section 4) of the mangrove forest boundary is not truly regressive because it does not reflect the retreat of the sea. This is clear from the approximated age of the boundary downstream of cross-section 4. The presence of mangrove forest on the Central High as recently as 2.3 ka shows that, at that time, seawater spread across the Plain at that point. Both upstream and downstream at 2.3 ka the Plain was in transition.

THE TRANSITION AND FRESHWATER PERIODS

The change from *Rhizophora* forest to transition sediments was probably accompanied by the establishment of a network of channels that allowed a greater diversity of mangroves to grow, reduced the area of tidal inundation, and possibly allowed the creation of hypersaline flats, as seen earlier. Most of the Plain was still lower than the upper limit of modern *Rhizophora stylosa* and so the decrease of *Rhizophora* pollen implies that tidal connections were being progressively severed.

This hydrologic change occurred after the period of infilling of major palaeochannels between about 5 ka and 3.5 ka upstream of cross-section 6 (Fig. 4.19), although it is likely that the modern billabongs of the Plain are remnants of tidal channels that existed until transition time. Coring beneath the billabongs is difficult and so there is little direct evidence of tidal ancestors to these water bodies. The levees that flank the billabongs and, more importantly, seal their downstream ends, formed either during the transition or at its beginning (Fig. 4.19); the exception are the low levees that have formed during the

deposition of the Dark Brown/Black Clay. The channels that were dismembered to form billabongs would have carried large quantities of sea water to the upper reaches of the Plain. Their demise reduced tidal connections significantly.

It should be noted that creation of the billabongs by scour during the transition is highly unlikely given that this was a time of lessening longitudinal gradients on the Plain, by contrast with the gradients defined by the 4.5 to 3.6 ka isochrons on Fig. 4.17. The lessening gradient from about 4.5 to 3.0 ka probably explains the onset of the transition at Island Billabong at least. The levees that were initiated during the transition, namely Mine Valley and Jabiluka, formed in response to the continued lessening of gradients during the transition.

The transition period was brought on by sedimentation changing the Plain's gradient which led to reduced tidal connection, rather than sediment raising the Plain and so removing the mangroves' habitat. Only at the upper limit of *Rhizophora* growth were mangroves denied a habitat by sedimentation, as seen earlier.

The period of restricted tidal access, the transition period, was complex. It probably contained the greatest diversity of vegetation types seen during the last 8 ka, with a mosaic of sedimentary environments ranging from tidal channels to hypersaline flats. Mangroves at cross-section 4, as late as 2.3 ka, implies that a tidal channel extended this far from the East Alligator estuary. But downstream, Fig. 4.19 shows that the Plain had been in transition since about 3.5 to 3.0 ka. This pattern implies that a tidal channel existed up to Jabiluka Billabong and that most of the Plain was only poorly connected to tidal flows.

The final removal of the mangroves and the transition sedimentary environment occurred first at the upstream end of the Plain and was brought about by sediments derived from Magela Creek. These grey clays spread across the transition sediments between cross-sections 1 and 2 at an average (horizontal) rate of 1.7 m yr⁻¹. Between 2 ka and 1.7 ka most of the sediments on the Plain were grey freshwater clays, derived from both upstream and tributaries to the Plain, with the switch to freshwater conditions occurring at about the same time downstream of cross-section 2. The transition environment still exists on the downstream end of the Plain.

The final stage in the evolution of the Plain was the establishment of near-modern conditions, represented by freshwater pollen taxa, and the accumulation of organic matter to form the Dark Brown/Black Clay, or 'black soil'. Between cross-sections 1 and 2 this type of sediment covered the grey freshwater clays by downstream migration at an average (horizontal) rate of 3.1 m yr⁻¹. Once again, the change from cross-section 2 downstream occurred at about the same time, between 1.5 and 1.0 ka.

The major topographic units (Chapter 2) are of course direct reflections of the youngest freshwater sediments. Figure 4.20 shows that the Central High was first established between 3 and 2 ka, and was a prominent feature during the transition period. The maximum relief of the surface of the Plain was greatest at about 2 ka. Sedimentation since that time has maintained the major topographic units established two millennia ago, but the Plain's maximum relief has been lessened.

The metre high mound that formed between cross-sections 7 and 4 between 3 and 2 ka fills that part of the Plain that narrows most. Figure 4.19 shows that the upstream limit of a tidal connection lasted longest in the vicinity of cross-section 4, the upstream side of the mound. It is likely, therefore, that sediment from tributaries moved upstream and piled up in the narrow part of the Plain. Further upstream, where the Plain is even narrower, sediment was probably derived from Magela Creek rather than from the tidal channels and tributaries. As will be shown in Chapter 6, sediments from Magela Creek still fail to get beyond cross-section 4 in detectable quantities.

The palaeogeography of the Plain has been summarised in the various longitudinal sections of Figs 4.17, 4.19 and 4.20. These are convenient ways of showing, at a glance, changes through time but suffer by providing no planimetric views. Palaeogeographic maps of the Plain's major sedimentary environments at 3.5 ka (Fig. 4.21) and 2.5 ka (Fig. 4.22) provide another way of viewing the Plain's evolution. The two time slices presented were chosen because they could be mapped with least ambiguity. These maps show the most dramatic change that the Plain experienced: the demise of the *Rhizophora* forest.

4.5 ACCUMULATION OF THE DARK BROWN/BLACK CLAY

THE PRINCIPAL CONSTITUENTS

The youngest stratigraphic (and morphostratigraphic) unit is distinguished from the underlying Grey Clay by its much darker colour and slippery feel when moist. The boundary between these two units, in the field, is most often very sharp at and upstream of cross-section 6. Downstream of this section the boundary is almost always gradational, like that seen between the organic A and poorly organic B horizons of some soils. At the upstream sites the sharp boundary is like that to be expected in a sedimentary sequence in which different quantities of organic matter have been deposited above and below the boundary.

These differences, expressed in the field, are also seen in measured organic contents and bulk densities (Fig. 4.23). Organic contents of the Dark Brown/Black Clay are much higher upstream of section 6, as also shown in Fig. 3.3.

The highest organic contents occur in the Upstream Basin (represented in Fig. 4.23 by P Pit 1, MV2 and M8). Each of the profiles in Fig. 4.23 shows decreasing organic content with depth, although the trend is not well expressed in MV2. This trend can be explained as the result of either increased deposition of organic matter or as progressive destruction of previously deposited organic matter. These hypotheses will be returned to below.

The bulk density profiles shown in Fig. 4.23 show that upstream of section 6 the Grey Clay is more dense than the overlying organic-rich sediments which, at P Pit 1, have densities as low as 0.35 g/cm³. Downstream of section 6 there is no consistent difference above and below the boundary between the two stratigraphic units.

Apart from organic matter and detrital mineral fragments (i.e. mineral sediment), the remaining major constituent of the Dark Brown/Black Clay is biogenic silica. Density separation of the biogenic silica and light microscopy has shown that the major components are diatom valves, phytoliths from vascular plants, sponge spicules and gemmules, and scales and resting spores from chrysophytes. The spores are in minor quantities. The total mass of biogenic silica in the sediment was determined by weighing after density separation. The mean reproducibility (relative) uncertainty for these estimates is 7.4%.

It is clear from Table 4.2 that detrital mineral sediment dominates the Plain, but substantial quantities of both organic C and biogenic silica occur in the Dark Brown/Black Clay in the Upstream Basin. Once again cross-section 6 is a dividing point, this time between upstream sediments rich in organics and biogenic silica, and downstream sediments poor in these constituents.

There is a positive correlation ($r^2 = 0.94$, n = 11, p = 0.01) between organic C and biogenic silica percentages in the Dark Brown/Black Clay. The bulk of the biogenic silica consists of phytoliths, and most of the diatoms and probably the sponges are epiphytic. On average, a lot of vegetation has promoted high productivity of biogenic silica.

SEDIMENTATION RATES AND THE PLAIN'S RECENT EVOLUTION

The rates of accumulation of detrital mineral sediment can be calculated given the age of the sediment, its bulk density and its content of non-mineral sediment. These data are available for all cross-sections and are summarised in Table 4.3. The average annual flux of biogenic silica and detrital mineral sediment for each cross-section (with uncertainties due to dating and laboratory procedures) are plotted in Fig. 4.24.

Detrital mineral matter flux is highest on cross-section 1 in the Mudginberri Corridor and lowest in the Upstream Basin. The flux rises further downstream reaching a peak in the Downstream Plain. Note that the highest value at cross-section 10 may be an artifact of the sampled location being next to a channel where the sedimentation rate is likely to be high even without clear evidence of a levee.

The mean annual flux of biogenic silica, during the last 1-2 ka, has been highest in the Corridor and Upstream Basin, and lowest downstream. The large uncertainties on these very small numbers make further comment about spatial pattern unwise.

It is not possible to calculate fluxes of organic matter to the Plain because it is not known how much has been destroyed since deposition (see Finlayson et al. 1988). It is noteworthy that the highest organic C contents on the Plain (Table 4.2) occur in the Upstream Basin where, currently, aquatic grasses and sedges dominate. These plants contribute on average 75 t/ha/yr of organic matter (Finlayson, pers. comm.) to the Plain's surface. Lower organic C contents occur in the areas currently supporting Melaleuca forests, namely cross-section 1, 7, 8, 9. These forests deposit 14 t/ha/yr of organic matter on average (Finlayson pers. comm.). The lowest organic C content occurs on cross-section 11, in the modern 'transition zone', for which there are no measurements of organic matter fall. But here the vegetation is most sparse all year round and is least protected, by trees or waterlogging, from oxidation during the Dry season.

The correlation between modern vegetation and the organic C content of the sediments deposited during the last 1-2 ka is only meaningful if the large-scale vegetation patterns have remained roughly constant during the last millennium. Unfortunately pollen has been destroyed in the relevant sediments at many sites at the downstream end of the Plain. Pollen in sites upstream of cross-section 6 confirm that grasses and sedges have dominated in the Upstream Basin while Myrtaceae pollen are very common in sediments of the Mudginberri Corridor. It seems likely that the organic C of the sediments reflects a pattern of vegetation that has been stable at the coarsest scale during the last 1 to 2 ka. This pattern is also reflected in the biogenic silica contents of the freshwater sediments.

It is likely that during the last 1 to 2 ka the gross pattern of grasses, sedges and paperbarks has been constant. The high organic content of the Upstream Basin is the result of high organic matter fall from grasses and sedges, the composition of which appears to be controlled by water depth and the period of inundation during the Wet season (Finlayson et al. 1989). The high organic content of the sediment in the Upstream Basin reduces infiltration and ponds water longer than elsewhere on the Plain, except in the channels and billabongs. As a result, aerobic decomposition of the organic matter is slowed.

The conditions of the modern Plain began to form at the boundary between the Grey Clay and Dark Brown/Black Clay when organic matter was either preserved or was deposited more abundantly. Biogenic silica has been detected in Grey Clay in only 3 out of 15 samples examined. These siliceous fossils are fractured, like all such remains in the Plain's sediments and, again like all samples examined, show no signs of etching that might result from dissolution in such an acid environment.

The abundance and taxa of siliceous fossils therefore accurately reflect their environments of deposition. The small amount of biogenic silica in the Grey Clay consists overwhelmingly of phytoliths, with diatoms and sponge remains being in tiny amounts. Diatom valves appear in significant quantities in the overlying organic-rich sediments. This change can be explained as the result of either: few macrophytes existing during deposition of Grey Clay thereby providing little habitat for periphytic diatoms and sponges; or briefer periods of inundation favouring phytolith production from emergent and terrestrial plants rather than frustules from submerged diatoms. These hypotheses will be considered further, below.

It is now clear that aquatic conditions on the Plain were substantially different between the Grey Clay and Dark Brown/Black Clay. The organic matter of the latter stratigraphic unit reflects an increase in organic productivity on the Plain rather than less preservation of organics during deposition of Grey Clay. Shallow freshwater conditions like those of today had their origin only 1 to 2 ka over most of the Magela Plain.

4.6 ENVIRONMENTAL VARIATIONS DURING DEPOSITION OF THE DARK BROWN/BLACK CLAY

LITHOSTRATIGRAPHY

There are few substantial changes in the character of the sediments in this stratigraphic unit downstream of cross-section 5, and pollen preservation is poor. Very little can therefore be said about changes in this area.

The Dark Brown/Black Clay at and upstream of cross-section 5 contains distinct layers of markedly different colour. The bulk of the organic-rich sediment is black (Munsell dry colour 10YR 2/1) or brownish black (10YR 3/2). Well defined layers of yellowish grey (2.5Y 5/3) and greyish yellow (2.5Y 6/2) occur within the dominantly black material. These pale layers vary between 2 and 11 cm in thickness. They have low densities, are powdery when dry and sometimes contain siliceous nodules up to 2.5 cm in diameter. The field character of the thickest examples of the pale layers is that of a diatomite.

The pale layers visible in the field or in cores occur in various forms: 1, a striking greyish yellow layer which is apparently homogeneous, and has sharp upper and lower boundaries; 2, interbedded black and greyish yellow laminae (up to 0.5 cm thick) like that in number 1; 3, a distinct yellowish grey layer which is homogeneous with moderately sharp upper and lower boundaries; 4, interbedded black and yellowish grey laminae (up to 0.5 cm thick) as in number 3; 5, intermixed black and either greyish yellow or yellowish grey sediment.

Types 1 and 3 are largely undisturbed and are the best developed forms of the pale layers. Types 2 and 4 are responses to alternating conditions at a site, and type 5 is probably the result of bioturbation. The various pale layer types are shown in Fig. 4.25 where they are also correlated between sites. This correlation has been guided by the characteristics of the various layers and by their stratigraphic superposition. That is, types 1 and 2 always appear above types 2 and 3 whenever they occur at the same site.

There were two periods within the last 1 to 2 ka when pale layers formed but both are well represented at only a few sites. Elsewhere the layers are of types 2, 4 or 5, or they may be absent. To explore the nature and origins of these pale layers it seemed necessary to analyse both the sites where both layers are best developed and where they are only weakly developed. Sites P Pit 1 and MC15A, both on cross-section 2, contain excellent examples of the two layers, while site MV2 contains less well developed examples.

Site P Pit 1

This site was excavated in the patterned ground typical of the Upstream Basin on an example of High Plain (Fig. 4.2). It is currently vegetated by a *Pseudoraphis* grassland with scattered Melaleucas (Finlayson *et al.* 1989). The site that was sampled was not disturbed by the formation of micro-relief, in the way described in section 4.9.

The lithostratigraphy of this site is depicted in Fig. 4.26. The bulk density is low throughout the Dark Brown/Black Clay and is higher in the Grey Clay beneath 43 cm. The clay content (relative error of $\pm 2\%$) steadily decreases through the section, but varies according to the stratigraphy. The silt content (relative error of $\pm 3\%$) shows no single pattern but, once again, reflects the stratigraphy. The sand fraction (relative error of $\pm 5\%$ for fine and $\pm 3\%$ for coarse) is mainly fine and varies very little. As will be shown below, the particle size data do not simply reflect detrital mineral sediment.

The organic C content is trivial in the Grey Clay and increases towards the surface. As noted previously, this trend is most likely the result of increasing production of organic matter through time. The alternative explanation, namely progressive destruction of organic matter and loss of the oldest carbon first, appears to be inconsistent with the evidence of biogenic silica. Yet organic matter must be destroyed during the highly oxidative Dry season. A guide to the degree of organic matter destruction is the C/N ratio. A ratio of about 10 suggests organic matter destruction, while a ratio of 20 or more implies that the organics have resisted attack. The mean ratio at this site is 10.34 ± 4.24 , implying substantial destruction of deposited organic matter. Values of C/N are only a rough guide, depending upon the original chemistry of the vegetation and algae as well as the vigour of destruction. Atomic ratios of the principal constituents of organic matter, C, N, H, O, give clues to the nature of the preserved organics. According to Steelink (1985) and Head (pers. comm.) the following rules can be formulated:

- 1. Low H/C, low O/C and high N/C indicates plant degradation products of the polyphenolic (aromatic) kind.
- 2. High H/C, high O/C and low C/N indicates the degradation products predominantly of algae, and are largely allophatic.

Applying these rules to P Pit 1 (Fig. 4.27) we find that most of the organic-rich black clays are dominated by aromatic plant degradation products, especially near the surface. The older black clays contain both allophatic and aromatic compounds. The two pale layers are dominated by allophatic compounds which are tentatively attributed to the breakdown of algal remains.

Breakdown of organic matter is demonstrated. Are the pale layers the results of advanced organic breakdown and the dark layers the result of slower breakdown? The Al content of the black clays in the Upstream Basin is high and appears to occur as alunite $(K(AlO_2H_2)_3(SO_4)_2)$, according to x-ray diffraction analysis. Up to 7% alunite equivalent has been found in the Dark Brown/Black Clay at site MV2 (see Chapter 5). Is it possible that this large amount of Al under acidic conditions is toxic to the bacteria partially responsible for organic matter breakdown, and is related to the failure of this material to reduce despite saturated conditions? (see Chapter 7).

Al is mobilized by the acid sulphate process in the subsurface of the Magela Plain (see Chapter 5) and rises to the surface during the early Wet season. The free Al (Al_D) is measurable as the extract in sodium dithionite and sodium citrate (Holmgren 1967). If this form of Al is complexed by organic matter, and so reducing bacterial breakdown, the organic C and Al_D content of the sediments should be directly related. That they are is evident in Fig. 4.28. But what is also clear from this figure is that the organically complexed

Al (Al_p) , represented here as the sodium pyrophosphate extractable Al (McKeague *et al.* 1971), is almost equal to Al_D .

It is concluded that Al moves under the very acidic conditions from the subsurface into the surface layers where it is complexed with organic matter. But the highest concentration of either form of Al is not in a pale layer where it would be expected if there was a link with toxicity to bacteria. Another explanation for the pale layers must be sought.

The biogenic silica content of the P Pit 1 sediments is generally high. There is between 15 and 48% (by weight) biogenic silica in these sediments (Fig. 4.29). The biogenic silica is in the form of frustules of diatoms, phytoliths from vascular plants, scales and resting spores from chrysophytes, and sponge scleres. The siliceous fossils are commonly broken but show no signs of chemical dissolution. The valves of only a few robust taxa (e.g. Anomoeoneis rhomboides, Eunotia camelus) are intact. Extensive fragmentation of 'lacustrine' diatom fossils is unusual, although Scherer (1988) has reported poor preservation in sediments from other tropical floodplains. The fragmentation may be the result of repeated processing of the sediments by benthic invertebrates. This explanation is consistent with the random orientation of siliceous fragments found in thin sections of Magela sediments.

The number of taxa and concentrations of siliceous fossils in this site are given in Tables 4.4 and 4.5. Figure 4.29 shows that the Grey Clay is very poor in biogenic silica, as seen previously. The weight percentage of biogenic silica increases to the youngest pale layer then declines. The number concentrations of all siliceous microfossils has a broadly similar pattern to the weight percentage data but shows much higher concentrations in the youngest pale layer and in the topmost samples.

The steady rise towards the ground surface of numbers of diatom valves and sponge fossils is evident. The phytolith concentration, with the exception of that in the youngest pale layer and the youngest sample, remained approximately constant through time. The ecology of diatoms on the Magela Plain is well enough known to interpret the fossil record. Unfortunately, little is known about the sponges and phytoliths.

A large proportion of the diatoms in P Pit 1 belong to the genus *Eunotia*, and particularly *Eunotia camelus*. This species grows as ribbons of cells attached end to end and entwined about aquatic macrophytes and other epiphytes. Other species of *Eunotia* have similar habits. The concentration of valves of *Eunotia camelus* in P Pit 1 is shown on Fig. 4.29, and it largely follows the trend of total diatom remains.

The rise towards the present implies an increasing quantity of aquatic macrophytes through time. The pale layers were also times of abundant macrophyte growth, relative to both the concentration gradient through the site and the concentration in samples either side of the pale layers. The oldest pale layer is dominated by *Eunotia* remains (Table 4.5), whereas the change in the top 5 cm is due to both *Eunotia* and *Pinnularia*. The latter is a benthic genus which has obviously thrived during the last 200 years.

Both pale layers show slight increases in epiphytic diatoms but only the upper layer has an abundance of phytoliths. Phytoliths are produced by aquatic macrophytes as well as aquatic grasses. McBride and Brady (unpubl. ms.) showed that digestions of macrophytes yielded only a small number of phytoliths and sponge spicules. The lack of spicules is not surprising, since epiphytic sponges appear to prefer grass (Finlayson pers. comm.). But the paucity of phytoliths implies that aquatic grasses are their principal source on the Plain.

A lack of ecologic information makes a detailed interpretation of Fig. 4.29 a task for the future. It is possible to suggest the following. There has been an increase of aquatic macrophytes through time. The lower pale layer was deposited when macrophytes were important but the upper pale layer was a time of some macrophytes but abundant grass.

During the last ~200 years (0-5 cm) grass has increased dramatically as indicated by the phytoliths and sponge remains, and macrophytes have also increased. The lower weight percentage of biogenic silica in this uppermost sample, by comparison with the number concentration, is probably the result of less compaction near the surface.

A test of these conclusions is to examine pollen in the same sediments. Figure 4.30 and Table 4.8 show that the aquatic macrophytes dominated the Grey Clay. Of the two hypotheses offered in section 4.5 to explain the paucity of diatoms and sponges in the Grey Clay, the presence of nearly 60% macrophyte pollen means that the second is favoured: that is, the periods of inundation during deposition of the freshwater Grey Clay were briefer than subsequently.

Aquatic macrophyte pollen increased from the base of the Dark Brown/Black Clay to a peak in the lower pale layer, consistent with the diatom (Fig. 4.29) and chemical (Fig. 4.23) data. The change at 19 cm depth is also consistent with the diatom concentrations. The high grass pollen content in the top 5 cm is also consistent with the sponge and phytolith data, but the diatom concentration is not consistent with the percentage of aquatic macrophyte pollen. Unfortunately the pollen is too sparse in the upper pale layer to test the inference drawn about its origin under a dominantly grassland vegetation.

In order to condense the interpretations of the P Pit 1 data, a vegetation index (VI) will be used:

$$VI = (P+S)-D$$

where P is number of phytoliths/g, S is number of sponge remains/g and D is number of diatom valves/g. This index should be low where aquatic macrophytes dominate and high in grasslands (? and grass sedgelands). Figure 4.31(a) shows VI for the P Pit I site. Figure 4.31(d) shows that in the lower part of the sediment there is a weak inverse relationship between VI and aquatic macrophyte pollen, and in Fig. 4.31(e) in the same sediments a weak positive relationship was grass pollen. But for the two samples in the upper part of the sediment, a line between the two data points in each case shows the expected relationship. That is, VI is positively related to grass and negatively related to aquatic macrophytes.

The pattern of change of VI in Fig. 4.31(a) is viewed as reflecting vegetation change. The Dark Brown/Black sediments beneath about 23 cm were deposited on a Plain apparently rich in aquatic macrophytes. The Plain has been becoming a grassland (or grass-sedgeland) from a depth of 23 cm, with larger amplitude changes of vegetation and hydrology superimposed on this trend. The lower pale layer was deposited on a Plain rich in aquatic macrophytes while the upper pale layer occurred in a grassland. But why are these layers pale?

Figure 4.31(b) shows the ratio between total number of siliceous remains (Table 4.5) and organic C. The trend in the value of this ratio (not including the pale layer values) has been removed by linear regression and the residuals plotted as Fig. 4.31(c). The upper pale layer has the largest quantity of biogenic silica fragments per unit of organic C, and the lower layer has the second largest ratio. The value at 41 cm is probably an artifact of the very low organic C at this depth whereas the value at 2.5 cm probably reflects a trend towards the formation of another pale layer.

Site MC15A

This site is in *Pseudoraphis* grassland with scattered paperbarks on Low Plain on cross-section 2 on the east edge of Hades Flat, Wirrnmuyurr Swamp, a tributary to the Magela Plain. The pale layers here are visibly more complex than at P Pit 1, the lower of the two containing various shades of yellow orange and yellow brown (Fig. 4.32). The upper pale layer is much less distinct than the deeper example. An adjacent core, MC15, shows the

same litho-stratigraphic features as MC15A yet the lower pale layer is of type 4; that is, interbedded black and yellowish grey laminae. Here is clear evidence of rapid spatial variations in the character of the pale layers.

Organic content (Fig. 4.32) is steady through most of MC15A but rises steeply near the groundsurface, differing from the pattern in P Pit 1. The biogenic silica and detrital mineral sediment weight percentage shows a remarkable pattern of variation. The palest part of the lower pale layer consists only of biogenic silica, within the relative measurement uncertainty of about 8%. The very high biogenic silica content of the upper pale layer is evident and contributes to the layer's colour. Once again the pale layers are where the ratio of siliceous microfossils to organic content is at a maximum.

The fine sampling of MC15A shows a pseudo-cyclic pattern of change in the proportions of biogenic silica and detrital mineral particles. This pattern is not as clear in the coarsely sampled P Pit 1 site, but has been inferred to produce the smooth curve in Fig. 4.31(c).

Site MV2 and MV1

These sites are only a few metres apart in the *Pseudoraphis* grassland of the Upstream Basin. The lithostratigraphy is generally like that elsewhere but the pale layers are not as well developed as in P Pit 1 and MC15A (Fig. 4.33). The lower pale layer is distinct but the upper layer is only faintly visible. These cores were contiguously sampled for pollen analysis and then, unfortunately, allowed to dry. Consequently, re-sampling for analysis of biogenic silica was only partially successful. The biogenic silica data for MV2 are sparse and are supplemented with data from MV1.

Both cores reveal increasing biogenic silica content towards the present but then a decrease to the groundsurface. Organic matter content increases rapidly in MV2 along with biogenic silica, as at other sites.

Phytoliths then phytoliths and sponges dominate the Grey Clay in MV1, although the quantity of biogenic silica in this unit is lower than in most of the overlying sediments. Diatoms only become significant in the lower pale layer, then increase upwards reaching a peak in the upper layer. Recall that the upper pale layer in P Pit I is dominated by phytoliths. The sponge fossils and phytoliths in MV1 peak between the two pale layers, implying that grass was at this time abundant. The mixture of siliceous remains in the upper pale layer reflects a complex of fluctuating mixed vegetation dominated by grass but containing aquatic macrophytes and sedges. The increase of Cyperaceae pollen in MV2 occurs as the Poaceae pollen content settles to a mean of about 75%.

The diatom flora identified in the 8 samples from MV1 (Tables 4.6 and 4.7) within the Dark Brown/Black Clay is similar to that of the present day. No taxa were observed which have not been found in the modern flora, and the most abundant taxa (Anomoeoneis rhomboides, Anomoeone exilis, Cymbella minuta, Eunotia camelus, Eunotia lineolata, Eunotia lunaris, Eunotia monodon. Eunotia pseudoindica var. gracilis, Eunotia trinacria, Frustulia rhomboides, Navicula radiosa) are common or widely distributed in the present flora (Thomas 1983). The two most abundant fossil taxa, Eunotia camelus and Frustulia rhomboides, are also the most common living Eunotia and naviculoid taxa respectively in the modern taxa. These taxa are restricted to acid freshwater and they are not found in estuarine or alkaline conditions, a conclusion consistent with all other evidence from this morphostratigraphic unit.

Eunotia camelus, an epiphytic diatom that grows on aquatic macrophytes, increases and decreases sympathetically with total numbers of diatom valves (Fig. 4.33). Its peak in the upper pale layer denotes a peak of aquatic macrophytes at this time.

At first glance the MV2/MV1 data appear to differ from those from P Pit 1. Comparison of these two sites is difficult because sampling has been different. Within this limitation it is possible to reach the following conclusions after comparison of the two sites. The Grey Clay at both sites contains the same siliceous fossil assemblage and was deposited under conditions of briefer inundation than occurred subsequently. From VI in Fig. 4.34, the oldest pale layer was deposited under a mixed vegetation of grass and aquatic macrophytes. The youngest pale layer was deposited at a time when aquatic macrophytes were important, as reflected in both the value of VI and the highest values for the remains of *Eunotia camelus* (Fig. 4.33). But here VI must be carefully interpreted because the high and almost equal quantities of sponge and phytolith remains have almost reduced VI to zero.

Figure 4.32 shows that the upper pale layer was deposited in a mixed vegetation of grass, sedge and aquatic macrophytes. The difference between this layer at MV1/MV2 and P Pit 1 may reflect the topographic and hydrologic differences between the sites. Aquatic macrophytes have always occurred at MV1/MV2 but phytoliths, as a proportion of the total siliceous microfossils, are increasing with time as sponges and diatoms decrease. Therefore, grass (and sedges to judge from the pollen) are gradually becoming more significant at both sites.

The comparison of MV1/MV2 and P Pit 1 is made most difficult by the differences of the ratios of total siliceous microfossils/organic C (Fig. 4.31, 4.34). The ratio is at a maximum in the upper pale layer and marginally so in the lower pale layer in the de-trended data of P Pit 1. The equivalent upper layer in MV1 has the highest ratio but this is not the case for the lower layer. To confidently accept that biotic differences really did exist at these two sites during the deposition of the same pale layer, the major defining features of the layers should correlate. But an explanation for the colour of the pale layers appears not to be the same at the two sites. The reason for this may be evident in Fig. 4.34 where a dashed line shows the interpolated ratio (for samples that have not been analysed) necessary to be consistent with P Pit 1. This curve is not inconsistent with the existing data from MV1. In the face of this uncertainty we must rely upon data from P Pit 1 as the best available description of environmental change during the deposition of the Dark Brown/Black Clay.

4.7 PALAEOCLIMATE AND CHANGE ON THE MAGELA PLAIN

LONG-PERIOD CHANGES

It has already been concluded that the freshwater part of the Grey Clay was deposited at a time when the length of the Wet season inundation was shorter than subsequently. This implies a generally drier climate in which open water for the growth of aquatic macrophytes was uncommon. The change to the Dark Brown/Black Clay occurred as the length of the period of inundation increased, presumably under a generally wetter climate. Finding a palaeoclimate signal in earlier sediments is difficult in the face of changes caused by and following sea level stabilisation.

The freshwater part of the Grey Clay was deposited between 1.9±0.2 ka and 1.4±0.3 ka. This was also towards the end of a period of enhanced chenier ridge formation in northern Australia which began at ~2.8 ka. Lees and Clements (1987) argue that chenier formation occurs when storm waves can quarry from the seabed a rich quantity of shells. Chappell and Grindrod (1985) argue that muddy sedimentation reduces shell production in the lower intertidal and subtidal source areas. Cheniers are therefore built when the amount of mud exported from coastal rivers is at a minimum. The Late Holocene period of chenier ridge construction is therefore regarded as a time of relative aridity.

This period of reduced streamflow and briefer floodplain inundation ended at 1.8 ka and 1.4±0.3 ka respectively. To further understand this period, correlates have been sought in other palaeoclimate sequences. The site closest to the Magela Plain is on the Atherton

Tableland where, using pollen analysis, Kershaw and Nix (1989) have shown that mean annual precipitation was between 200 and 1000 mm higher and mean annual temperature was 2-3°C above present values between 5 and 3.6 ka (Fig. 4.35). Since 3.6 ka the Atherton sites have not recorded a climate distinguishable from that of today.

Further south at Lake Frome, in northeastern South Australia, Singh (1981) has shown using pollen that the lake was full before 4 ka for several millennia. This is supported by Wasson (unpubl. data) who dated beaches at this lake to 5.6 ka. Subsequently, the lake dried to become a playa and shoreline dunes were built around 2.5±0.9 ka. This lake is a good hydrologic indicator of summer rainfall in northern Queensland, receiving flow from Cooper Creek via Strzelecki Creek.

The relatively arid period that set in after 3 ka at Lake Frome is paralleled by frequent cold episodes in the Southern Hemisphere (Fig. 4.35) during which glaciers advanced. This cooling trend is also recorded by δ^{18} O values in a speleothem in a cave in Tasmania at 41°34'S, from ~9 ka, and continuing from 6 ka to 3 ka. A speleothem in a cave near Nelson at ~40°S in New Zealand shows much warmer conditions by 800 BP (Hendy & Wilson 1968).

The cooling and drying just described occurred as desert dunes in central and southeastern Australia became more active (Wasson 1989). Figure 4.35(f) shows a histogram of scores which reflect dune building activity. The histogram has been compiled by giving a score of 1 to one or more radiocarbon or thermoluminescence dates from materials within a dune, and a score of 1 to each occurrence of an age estimated by stratigraphic correlation with a dated sequence of alluvium or lake sediments (Wasson 1986). The histogram shows that dune building was most intense at 2-3 ka.

In the Northern Hemisphere, Lamb (1966, 1977) has provided the data for Fig. 4.35(e). This curve is generally applicable to Europe and North America and shows a warm period up to 5 ka (the post-glacial warm epoch) and a much cooler period between 3.5 and 2.4 ka. There is a general warming to a peak (or secondary optimum) between 0.8 and 0.6 ka. The temperature record compiled by Lamb for central England is shown in Fig. 4.35(e) and is astonishingly similar to that of the New Zealand speleothem.

The palaeotemperature records of Fig. 4.35 are broadly paralleled by lake levels in southeastern and central Australia (CLIMANZ 1983), as previously discussed in the case of Lake Frome. Lakes were deep prior to 5-6 ka and were low during the dry and cooler period that began about 3.5 ka. Water depth mostly increased within the last 1-2 ka. The apparent phase difference between the period of highest temperatures in the Northern Hemisphere and Atherton Tableland (Fig. 4.35(e) and (b), respectively) may be the result of poor dating. But it may be the result of out-of-phase solar forcing. Kutzbach and Guetter (1986) have used a Global Circulation Model to retrodict the earth's climate at 3 ka intervals for the past 18 ka. The model uses: prescribed changes of orbital parameters (date of perihelion, axial tilt, eccentricity) that influence the amount of solar radiation reaching the top of the earth's atmosphere; and the boundary conditions of ice sheet distribution, land albedo, sea ice distribution and sea surface temperature, all derived from the palaeoenvironmental record. The high tropospheric loadings of land and marine aerosols of glacial times were not included, and atmospheric CO₂ changes were only partially included.

Monsoon circulations and tropical precipitation in the model responded almost directly to orbitally produced solar radiation changes. Summer monsoon precipitation in North Africa-South Asia was 10-20% higher than present at 12-16 ka as a result of orbital variations. Southern Hemisphere monsoons were weaker at this time, with precipitation 20% lower than present as a result of weaker summer radiation. The major rainfall source on the Atherton Tableland is the monsoon circulation, particularly the monsoon trough. The increase of summer temperature and precipitation between 6 and 3 ka in the model, as solar radiation

increased to the present value, appears to broadly agree with the palaeoclimate record (both temperature and rainfall) from Atherton.

The temporal resolution of the modelling by Kutzbach and Guetter (1986) is not fine enough to define the cool/dry period that followed the past-glacial optimum just described. This was a time of chenier ridge construction in northern Australia, deposition of the freshwater part of the Grey Clay, desert dune building, and generally low lake levels in Australia.

Numerous hypotheses have been advanced to explain the palaeoclimate and environmental changes of the last 6 millennia (e.g. Lamb 1977; Bartlein 1988). These involve variations of solar radiation, volcanic dust, atmospheric composition, autovariation of the kind that occurs in non-linear (so-called chaotic) systems, and a damped oscillation following the major change that occurred as the last glacial maximum gave way to the Holocene interglacial. Kutzbach and Guetter (1986) have come closest to modelling the many combinations of changing climate variables and their likely controls.

The model of Kutzbach and Guetter (1986) is a description of the past, resolved at 3 ka intervals. Variations on time-scales <3 ka are therefore lost and the model only has predictive ability for slowly changing variations. These long-period variations, apparently brought about by solar radiation changes, have been modelled by Berger (1980) to 'explain' the variations of δ^{18} O in foraminifera in deep-sea sediment during the last 400 ka. The auto-regressive model suggests that, if the Greenhouse Effect does not intervene, a major cooling is likely to begin soon with reduction of the mean annual global temperature by 2 to 3°C by 5 ka in the future. This change, if constant, would reduce global temperature by 0.4 to 0.6°C within the next 1 ka. Prediction is not readily available for a specific site on the earth using either the techniques of Berger or Kutzbach and Guetter.

SHORT-PERIOD CHANGES

Some of the shorter period variations appear to be more predictable. The palaeotemperature records from New Zealand (Fig. 4.35(d)) and central England (Fig. 4.35(e)) depict a global pattern of change, showing a temperature high at about 0.75 ka (~1200 AD) and a low centred on 0.3 ka (~1750 AD). The latter is known as the Little Ice Age and, in addition to Europe and New Zealand, has been recorded in China (Shen 1974), in North America (Lamb 1977), in an ice cap at 13° 56'S in Peru (Thompson et al. 1986), in the ice of Antarctica (Morgan 1985; Etheridge and Morgan, in press), and in corals of the Galapagos Islands (Enfield 1988). This period has been thoroughly considered by Grove (1988).

The Little Ice Age was coincident with an anomalous scarcity of sunspots (the Maunder minimum). Eddy (1976) conjectured a link between solar activity and terrestrial climate from this correlation. This connection might be by means of a modulation of the solar output radiation, associated with a change of the solar diameter as suggested by Ribes et al. (1987). Libby (1987) has used Fourier transforms of D/H and ¹⁸O/¹⁶O in tree rings, organic C and uranium in rapidly deposited marine sediments, ¹⁸O/¹⁶O in Greenland ice, and ¹⁴C in bristlecone pine from California to demonstrate a persuasive link between solar activity and global temperatures. Her argument is that variations of the sun cause variations in the temperature of the sea surface, thus causing the isotopic composition of water vapour leaving the sea to vary. This water is then 'stored' in trees and ice. In addition, the solar wind reduces both the cosmic ray flux to the earth's atmosphere and the production of cosmogenic nuclides like 14C. There is recorded in tree rings an inverse relationship between ¹⁴C content and the activity of the sun. Support for this hypothesis is found in evidence for lowered sea surface temperatures in the areas of El Ni o during the Little Ice Age (Enfield 1988). Libby treated U and C in Californian marine sediments as surrogates for sea surface temperature, and also found correlations with her tree-ring data.

Stuiver (1980) tested the solar-terrestrial climate link by using the ¹⁴C content of tree rings and ten climatic records covering the last 1 ka. He found no convincing relationship, although he did not explore a link with the central England temperature record shown in Fig. 4.35(e). In a later paper, Stuiver and Braziunas (1989) have used much longer records of climate (including that of Röthberger 1986; Fig. 4.37(e)) and ¹⁴C content of tree rings. An auto-regressive technique shows that there is an association between spectral peaks in the climatic, ¹⁴C and solar records. Table 4.9 shows the peaks recorded by Libby (1987) (to the left) and by Stuvier and Braziunas (1989) (to the right). There is impressive agreement although a formal non-parametric test of concordance is not possible because all of the peaks are not recorded in each medium.

Landscheidt (1987) aimed to find a set of predictable time series relating long-term solar variation and climatic change, thereby making dependable the forecast of solar activity and so climate. Impulses of the torque that drive the sun's rotation around the centre of mass of the solar system seem likely to relate to secular and supersecular cycles of solar activity. Extremely strong impulses of the torque occur at grand minima of solar activity, like the Maunder minimum.

For convenience, Landscheidt used a continuous function of the time rate of change of the torque. Maxima and minima of this function coincide with positive and negative impulses of the torque and are proportional to their strengths. A Fourier analysis of the function covering the last millennium yielded a period of 83 yr which compares favourably with a period found commonly in various climatic and solar activity records (Table 4.9). When all extrema of impulses of the torque are treated as a smoothed time series for the last 7.6 ka, a mean length of 166 yr for the resulting wave is found. Each extremum (A₈) of this wave is related to a maximum in the secular sunspot cycle.

The supersecular cycle of sunspots, that is, the envelope of yearly sunspot numbers, is related to features like the Little Ice Age (the Maunder minimum) and the so-called Medieval maximum peaking at ~1100 AD. These features are in turn related to the variations of the secular wave proportional to A_s^2 . A smoother plot of A_s^2 is shown with the central England and New Zealand curves, and tree ring ¹⁴C content, in Fig. 4.36. The ¹⁴C and A_s^2 data are highly significantly correlated, as are the temperature and A_s^2 curves. It can be concluded that during the last millennium the world's climate has undergone changes that correspond closely in date, phase and amplitude with the sun's variations. To this Landscheidt has added the wave pattern of the impulses of the torque.

Figure 4.36(b) shows a prediction by Landschiedt of A_s^2 to 2000 AD, implying a new supersecular maximum. The following secular minimum that is predicted from the course of the secular wave is likely to lead to global cooling (also suggested by Wigley 1988). Libby (1987) has used Fourier analysis to predict future cooling, at least in California. These predictions take no account of increasing atmospheric CO_2 .

The ratio BS/C (Fig. 4.31(c)) is also plotted in Fig. 4.36 where it is compared with other records. The BS/C peaks in Fig. 4.31 have estimated ages of 740±180 BP and 1340±80 BP in P Pit 1. The youngest peak has an obvious equivalent at 630±120 years in the ²²⁶Ra concentration curve of Fig. 3.14 which is thought to reflect the biogenic silica content of the sediments. The older BS/C peak lies at the summit of a broad peak centred on 1350±260 years. Another peak at about 1650±315 years in the ²²⁶Ra curve may be the equivalent of the partially defined (and unexplained) high in the BS/C curve at 1843±110 BP. The poor definition of the older BS/C peaks is reflected in the shape of the ²²⁶Ra curve.

The chronologies from P Pit 1 and the MX sites are in good agreement. There is remarkable concordance between BS/C and the other records in Fig. 4.36. The grass peak occurs at the time of the Medieval maximum and the return to aquatic macrophytes occurred as the earth cooled. The complete record of BS/C in the Dark Brown/Black Clay is shown in Fig. 4.37

with temperature records from the northern and southern hemispheres, the solar activity envelope of Eddy (1978), and Röthlisberger's (1986) record of glacial advances and retreats in New Zealand. The grass peak (740±180 yr BP) can now be seen to have occurred when global conditions were warm. At this time glaciers retreated in New Zealand and, according to Röthlisberger, worldwide. The low points in the BS/C curve occur at cool times when solar activity is low and when glaciers were on the advance. Glaciers respond both to temperature and precipitation but Grove (1988) has shown that temperature is the key variable.

The chronology for P Pit 1 is not adequate to resolve a correlation between the lower pale layer (expressed as a low bump on the VI curve) and the other indicators. But it is possible that it relates to a coeval increase of temperature in the Antarctic (Fig. 4.37) and on Devon Island in Greenland (Morgan 1985).

The pale layers are distinguishable as times of high VI and also high BS/C in P Pit 1. High biogenic silica implies high plant biomass and so low values of organic C need to be explained. Organic matter must have been destroyed during the periods of pale layer deposition. If the Magela Plain had been a warmer place at such times, as implied by Fig. 4.37, then organic matter could have been destroyed more readily than at other times. But is there a plausible mechanism to link BS/C to climatic change?

Observation of the Plain since 1979 by C.M. Finlayson (OSS), P. McBride (OSS) and R. Hall (Pancontinental) indicate that major changes in vegetation are controlled by the timing and amount of rainfall. As pointed out by Taylor and Tulloch (1985), moisture is the primary limiting factor for the biota in the seasonally wet-dry tropics. Finlayson *et al.* (1989) conclude that the duration and period of inundation is a major determinant of the vegetation composition on the Magela Plain. Related factors are flow velocity and water depth. Away from the billabongs and channels, variation of velocity is likely to be unimportant.

Grass germinates on the Plain if rainfall occurs early, that is, in the pre-Wet season months of September and October. If rainfall then persists, even intermittently, grass will dominate the Plain and so VI should be high. Aquatic macrophytes, by comparison, are favoured by an abrupt start to the wet season followed by persistent and usually abundant rainfall. Under these circumstances VI should be low.

The key to a link between these characteristics of the vegetation's response to rainfall and the major controls on rainfall is the pre-Wet season rainfall. This (spring) rainfall is correlated with the Southern Oscillation Index (SOI). The Southern Oscillation is a planetary scale atmospheric pressure pattern manifested in a negative correlation between pressure over Indonesia and the southeast Pacific. The SOI is the difference in mean sea level pressure between Papeete and Darwin, normalised for each calendar month (Troup 1967). The SOI is related to climatic events all over the earth, and an extreme negative value of the index usually coincides with an anomalous warming of the east equatorial Pacific Ocean, known as El Niño (Rasmusson & Carpenter 1982). This is a time when rain is heavy over western coastal South America, and eastern and northern Australia is drier than average. The most recent, catastrophic, example of this pattern occurred in 1982/83. Rainfall at either end of the pressure see-saw varies inversely with pressure. A strong positive SOI is therefore related to high rainfall over eastern and northern Australia (Pittock 1975; Allan 1985). The combined phenomena of the Southern Oscillation and El Niño is referred to as ENSO. The main correlations are caricatured in Table 4.10.

The pressure at Darwin in the winter months of June to August is correlated with the date by which 250 mm of rain has accumulated at Darwin (Nicholls et al. 1982). The total amount of spring rainfall (September to November) is strongly related to the June to August SOI. That is, rainfall in spring is high if the winter SOI is positive.

There is a large fall in correlations between rainfall and the SOI from pre-monsoon (spring) to monsoon (summer) (McBride & Nicholls 1983). A statistical analysis of these relationships by these authors showed that the SOI is the dominant large-scale influence on the interannual rainfall variability in both the pre-monsoon and monsoon. The smaller correlations between the SOI and rain during the monsoon months is explained as the result of other controls operating on smaller spatial-scales, like organised convection.

Grass is favoured when spring rain occurs and when the SOI is positive. This is, on average, a time when El Niños are rare, or an anti-El Niño occurs. From Fig. 4.37 anti-El Niños and positive SOIs should be favoured when the earth is warm. When the earth is cool, the SOI should be on average negative (or at least less positive) and El Niños should be relatively common. A high value of BS/C should be related to spring wet and warm conditions over northern Australia and a low value of BS/C should be related to drier and cooler conditions.

Tropical cyclones are strongly related to the SOI. Nicholls (1985a-d) showed that Darwin pressure is strongly related to cyclone numbers and number of cyclone days in a cyclone season. In northern Australia, there should have been more cyclones during the peak of BS/C than during the cooler and drier times. That is, tropical cyclones should have formed closer to the northern Australian coast at times when sea-surface temperatures were higher (cf. Libby 1987) and the monsoon trough more commonly over the Australian landmass (cf. Allan 1985).

In a search for corroborative evidence of the relationships that have just been conjectured, we must turn to the few long-term records of ENSO. Enfield (1988) has summarised the most promising records. Quinn et al. (1987) have used historical records to reconstruct El Niño events from the arrival of Francisco Pizarro in Peru in 1525 AD. The evidence consists largely of records of floods on coastal rivers. Enfield concluded that El Niño is not perfectly periodic, that is, there is not a uniform interval between onsets. There is a quasi-centennial cycle between times when El Niño is more intense and frequent and those when the opposite applies. Michaelson (1989) found the same amplitude/frequency modulation from tree ring data in arid southwestern North America, an area affected by ENSO by means of a long-distance atmospheric teleconnection.

The data for strong and very strong El Niños from Quinn et al. (1987) are plotted as a cumulative frequency graph in Fig. 4.38. The quasi-centennial cycles are visible, and the departures from the perfectly periodic case (the straight line), centred on 1720 AD and 1870 AD, are significant at p = 0.05 using a Kolmogorov-Smirnov two-sample test. The New Zealand palaeotemperature curve (Fig. 4.37), as a global temperature surrogate, is included in Fig. 4.38. The steep segments of the cumulative number of El Niño events, that is the periods of most frequent El Niños, occur as the temperature warms. The mean number of years between events is shown on the cumulative curves. The warming periods have an El Niño event every 7 years whereas the intervening periods have an event every 10-15 years.

Variations in the frequency of El Niños is presumably prima facie evidence of variations in the frequency of anti-El Niños. That is, during the warming periods the number of severe floods in coastal Peru was high and so too were the number of severe droughts in Australia. A link between ENSO and droughts in Australia has been established for the last two centuries (Nicholls 1988). The link inferred from Fig. 4.38 for the previous two centuries is untested.

The conclusion drawn from Fig. 4.37, namely that when the earth is cool the SOI is on average negative and when the earth is warm the SOI tends to be positive, can now be modified in the light of Fig. 4.28. During warming episodes during the last 450 years the frequency of ENSO cycles has been much higher than at other times, either during stable periods (1740 to 1856 AD) or cooling periods (1523 to 1696 AD). The frequency of ENSO cycles therefore appears to be a complex function of atmospheric/ocean couplings which

change through time. The transfer of the insights gained for the last 450 years to the previous 1500 years is uncertain.

Other palaeoenvironmental records of El Niño are less convincing than that of Quinn et al. (1987). Shen et al. (cited by Enfield 1988) have used the oceanic nutrient and therefore upwelling surrogate Cd/Ca in coral cores from the Galapagos Islands. Their record extends to 1600 AD and there appears to be evidence of cooler waters surrounding the islands during the Little Ice Age. They infer that El Niño was relatively uncommon during this period of cool conditions, because upwelling dominated under the influence of the southeast trade winds.

Enfield (1988) points out that the conclusions from the coral cores are contrary to those of Michaelson's (1989) tree-ring data and his own analysis of the data assembled by Quinn et al. (1987). The amplitude and frequency statistics for El Niño events are very similar to those of this century. But the analysis in Fig. 4.38 shows that a factor of 1.4 to 2.1 separates the mean annual frequencies of El Niños. On average, there were less El Niño events prior to 1850 AD, the often quoted end of the Little Ice Age (Grove 1988), than subsequently.

Although by no means secure, it is possible that ENSO frequency was very much higher when BS/C was high and vice versa. The peak of BS/C (Fig. 4.37) may have been a time of remarkably variable climate, which may explain why some examples of this layer are of type 2 (see section 4.6). The power spectrum of the SOI for the 115 year period between 1860 and 1975 AD has a peak between 3 and 4 years (Allan 1985). This peak may have occurred at lower periodicity when BS/C was high. If the periodicity was very low, each Wet season would have been the same. That is, the SOI was permanently positive and the Walker Circulation had only one mode.

4.8 PREDICTION OF FUTURE CLIMATE IN THE MAGELA CATCHMENT

The investigation of environmental and climatic change during the period of deposition of the Dark Brown/Black Clay was motivated by the need to determine the natural variability, and its causes, of the Magela Plain over the last 1 ka to provide a basis for prediction; if strictly periodic climatic changes have occurred in the past which would facilitate prediction. There is no need to labour the natural variability of the Plain's vegetation and sedimentation patterns. This is illustrated in the diagrams of this chapter, although there is clearly more that needs to be done to properly define the changes. The predictability of climate, however, needs further discussion.

The most likely forcing variables of climate at various time scales have been identified as: solar radiation variation, produced by orbital geometry at time scales of millennia and impulses of the torque at centennial time scales; and CO₂ variations, at time scales from centuries to millennia, amplifying variations of solar radiation to produce temperature change on the earth's surface. Volcanic dust may induce change on annual and possibly decadal time scales (Grove 1988), and change of vegetation cover may sufficiently alter albedo to make small adjustments to climate.

The slowly changing forcings are modelled best by Kutzbach and Guetter (1986) and for the last 6 ka they have included most (but not all) of the important factors. Yet their simulations of climate at 9 ka (COHMAP Members 1988) for Australia are poor. This need not worry us unduly because the slowly changing forcings are unlikely to have a significant effect over the next 1 ka.

The more rapidly changing forcings, principally the solar radiation changes driven it seems by impulses of the torque, are not adequately modelled. Schneider and Mass (1975) have simulated the observed global temperature history since 1600 AD by combining a relationship between sunspot number and variation of the solar 'constant', and a dust veil

index to take account of volcanic eruptions. Gribbin (1978) shows how the addition of a CO_2 increase to the Schneider and Mass model leads to increased warming of about 0.5°K over that due to solar activity by 1989. But the model is based upon empirical solar cycle variations and has little predictive power.

While deterministic predictions are not available, statistical predictions have been made by Libby and Landscheidt. Neither of these takes account of CO_2 increase. Estimates of the statistical properties of ENSO are available, based upon the instrumental record starting in 1861 (Allan 1985). Most of this period has deviated little from the strictly periodic curve of Fig. 4.38 and so is not useful for prediction of the behaviour of ENSO during a rapidly warming period of the kind suggested for the coming century. Apart from the effects of CO_2 , the prediction of the properties of ENSO would appear to depend upon prediction of solar activity which we have seen is not possible for more than a few decades.

The non-periodic nature of climate change and ENSO behaviour over the last 2 ka means that the series is both deterministically unpredictable and statistically non-stationary. The engineer designing long-lasting structures at Ranger will have to use the statistics of the instrumental period with considerable caution. But there is an additional course of action. Evidence should be sought of the return period of intense rainstorms, or their surrogates. Beach ridges on islands off Darwin are currently being investigated as a record of tropical cyclone frequency. One hypothesis to be tested against this record is that cyclones were most frequent when BS/C was at a maximum.

Any model that can accurately simulate the past may be effectively mute about the future under increasing CO_2 . Global circulation models (GCMs) are the basis of most predictions of climate under elevated atmospheric CO_2 , and can be used to estimate the equilibrium climate at a particular multiple of current CO_2 concentrations. But most modelling of future climate takes no account of solar activity and so is not a good predictor of transient states. In addition, Wigley (1989) suggests that SO_2 from industrial sources may increase cloud condensation nuclei, and hence global albedo, sufficiently to offset the temperature changes wrought by CO_2 alone.

The uncertainties about future climate are large. In the final chapter of this report the impact of future climate will be assessed not by using predictions but by the use of 'futures'.

4.9 THE PATTERNED GROUND IN THE UPSTREAM BASIN

The ridge and trough topography, principally upstream of Ja Ja, provides evidence of another change on the Plain within the period of deposition of the Dark Brown/Black Clay. Figure 4.39 shows lines drawn parallel to the ridges and troughs, and orthogonals to these lines. The orthogonals describe the expected flow paths of water on the Plain. The ridges and troughs have been caused by flow, or at least have aligned themselves with the flow.

A series of trenches dug parallel to an orthogonal across cross-section 2 has exposed the structure of the patterned ground. Figure 4.40 shows that the pale layers have been disrupted in a pattern reminiscent of shear structures in ductile rocks. This pattern is seen again in a second trench dug through the upstream side of a ridge (Fig. 4.41), but in trench 3 the pale layers dip the other way.

The Grey Clay is sub-horizontal beneath the deformed Dark Brown/Black Clay, but in a few cases has been intruded into the overlying low density material diaper-like. It appears, then, that the very low density surface layer has been deformed by water flows into a series of shallow thrust sheets, the tops of which have probably been eroded. This deformation has occurred since deposition of the youngest pale layer, that is, within the last part of the last

seven centuries. These features offer resistance to flow and may eventually become sites of preferred clastic deposition.

4.10 SUMMARY

The techniques detailed in Chapter 3 were used in this Chapter to produce a stratigraphic synthesis for the Late Quaternary sediments of the Magela Plain. Depositional environments have been described and mapped on each of the eleven cross-sections. The general history of these environments is: a large mangrove forest (the Big Swamp) occupied the estuary as sea level stabilised ~6 ka after the postglacial rise of sea level; the demise of the mangroves in the 'transition zone' as other taxa became dominant in an environment of hypersaline mudflats, possibly salt tolerant grasses, and decreasing tidal connections; establishment of the freshwater wetland as sedimentation raised the Plain above tidal inundation and the tidal connection was severed as channels linked to the sea were dismembered.

The conclusion that at least part of the major vegetation changes on the Plain were the result of decreasing tidal connection, on surfaces at altitudes still below the tidal range, is very important for predictions of the impact of sea level rise as a result of the Greenhouse Effect. A rise in sea level of say 1 m cannot be simply translated into an area of salt water inundation using topographic data. The area of salt water incursion will be largely determined by the locations and shapes of tidal channels. Predictions must therefore combine the best estimates of sea level rise, a detailed contour map, and insights into the likely locations of future tidal channels.

The end of transition conditions and the beginning of freshwater dominance occurred between 1.7 and 2 ka over most of the Plain, although the transition still exists on the downstream end of the Plain. This change occurred when, it is inferred from both the biogenic silica content of the sediments and from indicators of climate at other sites, the climate was drier than at present. The final major change in the Plain's history occurred between 1.5 and 1 ka as the climate became wetter, increasing the biomass of the Plain and the production of biogenic silica. This reconstruction is once again useful for predictions of the impact on the Plain of the Greenhouse Effect. The sequence from mangrove forest to transition conditions to freshwater conditions first with the deposition of Grey Clay then Dark Brown/Black Clay, is not the inevitable sequence that is to be expected in reverse if sea level rises. The sequence recorded in the sediments is the result of the combination of a sea level rise and climatic change. We must therefore be selective in choosing the palaeoenvironment analogues of future conditions.

The history of the deposition of the Dark Brown/Black Clay is complex, and its interpretation depends upon identifying the conditions under which layers of various colours were deposited. Biogenic silica, pollen and chemistry has allowed the conclusion that major changes of vegetation have occurred on the Plain over the last 1 to 2 ka, superimposed on a trend of increasing dominance of grass. These changes have been driven by climate which, it is argued, have been forced by solar variation on time scales of centuries. It is further argued that the atmosphere has responded to the variations in the amount of insolation it receives by varying the frequency (and intensity) of the ENSO phenomenon. During warming periods the Plain becomes a grassland as the SOI becomes strongly positive, the monsoon trough is more southerly on average, and the Wet season is longer and wetter. For most of the Plain's history, it has experienced conditions more like those of today when the SOI is more negative and the monsoon is relatively weak.

These reconstructions provide insights into predicting future climates on the Plain and at Ranger. The current atmospheric models that purport to predict the effects of the Greenhouse Effect do not take account of variations of solar radiation. They are therefore likely to be inadequate. That significant climatic changes have occurred in the Magela

region on time scales of centuries during the last 2 ka is now clear. These changes are not perfectly periodic (or even nearly so) and so are not predictable deterministically.

The climatic series of the last 2 ka is not stationary and so the use of rainfall intensities from the instrumental record of the last few decades as a basis for designing structures to last 1 ka is hazardous. Evidence should now be sought of the return period of intense variations, or their surrogates. Cyclone constructed beach ridges seem to offer this opportunity.

The dated Dark Brown/Black sediments have yielded estimates of mean long-term fluxes of detrital mineral material and biogenic silica. The former is highest in the Mudginberri Corridor and drops to its lowest figure in the Upstream Basin. The flux rises further downstream reaching a peak on the Downstream Plain. The Plain has been shown to be morphologically disjunct at the upstream boundary of the Downstream Plain (Chapter 2). This disjunction is also reflected in the vegetation and in surface pollen concentrations (Chapter 3).

The pattern of detrital sedimentation just described cannot be the result of sediment from Magela Creek dominating the Plain. The disjunction must result, in part, from different sources of sediment. The most likely pattern is for the rapid decline of detrital sediment flux downstream of the Mudginberri Corridor to be the result of input from Magela Creek, and the higher fluxes downstream resulting from tributary inputs. This hypothesis is tested further in Chapter 6. The tentative implication of these results is that sediment derived from the Mine Site should go no further than Jabiluka Billabong.

The Upstream Basin is also the area of greatest organic matter accumulation on the Plain, at the feather edge of detrital input from Magela Creek. Downstream, organic matter tends to be less well preserved and apparently to behave differently in the sediments.

This disjunction, effectively upstream and downstream of the Central High, appears to have originated between 3 and 2 ka. The Central High was a prominent feature during the transition period. Sedimentation since this time has maintained the major topographic units established two millennia ago, but the Plain's maximum relief has been reduced. The sediment source dominance inferred above to explain the fluxes of detritus in the Dark Brown/Black Clay may have been established at 2 ka, thereby accounting for the topographic pattern just described for that time.

The final part of this Chapter is a brief account of the patterned ground of the Upstream Basin. Although morphologically like some forms of gilgai, these ridges and troughs seem to be the result of flow-induced deformation of the low density, plastic surface sediments.

The results compiled in this Chapter have demonstrated that the past not only can inform us about how the present state of a landscape came to be, but is also a guide to the future. Inferences about tidal connection, climatic change, and reasons for climatic change all bear on whether the current predictions of the Greenhouse Effect are robust and, if they are, whether or not they can be translated into concrete predictions for the Magela Plain and Ranger Mine.

Table 4.1. Heights (AHD) of major stratigraphic boundaries based on pollen.

	Cross- section no.	Distance along grid (km)	Core/ auger/ pit code	Height AHD (m)	Top of Rhizophora forest AHD	Base of** freshwater wetland AHD
			<u> </u>		(cm)	(cm)
Mudginberri	1	4	M1	3.6	25-35	150-115
corridor			M2	3.6	No po	llen
			MC4	4.6	277-186	369-277
			MC5	4.3	247	156
			MC6	5.5	390	500
Downstream	2	7.5	MC11	4.8	-	450-297
end of			MC10	5.6	286-194	530-377
Mudginberri			MC8	5.3	317-256	439-347
corridor			M4	5.0	410-350	500*-410
			MC12A	3.4	-26 to -117	+66 to -26
			MC12	4.0		eshwater
			MC13	4.1	No po	
			MC3	4.0	No po	
			MC15	3.7	152-131	360-334
Mine Valley	3	13	M7	3.6		310
Billabong			M6	3.2	278-240	286-279
Ü			MV2	3.0	212	261
Jabiluka	4	16	M9	3.9	302-250	338-303
Billabong			M8	4.4	330	393
			JB4	4.7	287-257	
			JB3	5.0	226-134	
			JB2	5.1	Below 231	361-326
			JB5	4.4	318-288	140-318
			JB1	5.0	No po	
Nankeen	5	18	NB8	3.9	294-277	322-305
Billabong			NB7	3.9	288-260	323-289
South			NB6	3.8	285-270	354-332
			NB5	4.2	328-310	351-329
Nankeen	6	20.5	NB1	3.8	179-159	330-300
Billabong			MII	3.8	232-168	372-260
North			NB2	4.2	304-281	333-305
			NB3	5.1	236-144	510*-236
			NB4	4.4	325-265	- -

Table 4.1. Page 2.

	Cross- section no.	Distance along grid (km)	Core/ auger/ pit code	Height AHD (m)	Top of Rhizophora forest AHD (cm)	Base of** freshwater wetland AHD (cm)
Downstream Plain	7	25	LB23 (core) LB23 (auger) LB20	4.0 4.0 4.1	292-264 309-217 225-200	400* 370-309 389-226
Downstream Plain	8	25.5	LB5	3.2	131-110	313-295
Downstream Plain	9	31.5	LB4 LB2 LB1	3.8 3.7 3.0		330 275 275
Downstream Plain	10	34.5	LP3 LP2 LP1	3.6 3.3 3.2	216-147 144-120 206-166	360*-228 285-190 307-279
East Alligator Flood Plain	11	38	M13 LP4 LP21	3.6 3.3		340 300 300
Not on cross-sections		11 15 26 ?	M5 M10 M12 MC7	3.6 3.8 3.7 ?	261-201 175-70 185-165 No po	335-316 339-300 370*-250

^{**}Top of mangroves
*Surface

[&]quot;No pollen" usually means none below the topmost sample.

Table 4.2. Proportion of major components in the Dark Brown/Black Clay and Grey Clay.

Cross- section	Orgar %	nic C	Mineral se	diment	Biogenic sil	ica
no.	Black	Grey	Black	Grey	Black	Grey
1	2.2±2.0		89.50±7.07		10.3±7.14	
2	6.65±1.45	2.8±0.7	80.75±1.08		19.25±1.08	
3	10.1±2.0	3.8 ± 1.1	64.36±8.22	100	35.64±8.22	0
4	5.25±1.75	10.5±0.25	85.08±3.70	100	14.92±3.70	0
5	2.95±1.6	0.65±0.25	91.69±5.56		8.31±5.56	•
6	4.65±1.75	0.8 ± 0.2	90.06±4.14	99.86	9.94±4.14	0.14
7	1.8±0.4	0.4 ± 0.1	98.57±0.65	100	1.43±0.65	0
8	2.15±0.8	0.5±0.1	98.38±0.32	100	1.62±0.32	0
9	2.4±0.5	0.5±0.15	97.87±0.97	100.0±0.38	3.06±1.45	0±0.4
10	1.4 ± 0.4	0.7±0.15	98.54±0.75	100	1.46±0.75	0
11	1.25±0.35	0.3±0.1	99.26±1.26	100	0.98±1.45	0

Table 4.3. Fluxes to the Plain of major sedimentary components.

Cross-section no.	Midpoint of dated depth interval (cm below surface)	Age (ka)	Mineral sedimention rate (cm yr ⁻¹)	Mineral sedimention flux (g cm ² yr ⁻¹)	Biogenic silica flux (g cm ² yr ⁻¹)
1	71	2.4±0.17	0.03±0.003	0.05±0.005	0.005±0.003
	95	3.6±0.08	0.03±0.009	0.04±0.01	0.004±0.003
2	41	1.7±0.1	0.02±0.001	0.01±0.0006	0.002±0.0002
	22	0.5±0.14	0.04±0.01	0.01±0.0003	0.002±0.0002
3	22	1.3±0.07	0.02±0.003	0.01±0.001	0.004±0.001
4	27	1.7±0.08	0.02±0.006	0.02±0.002	0.003±0.0008
	35	1.7±0.07	0.02±0.006	0.03±0.003	0.005±0.0009
6	32	1.3±0.12	0.03±0.004	0.03±0.004	0.003±0.001
	17	0.7±0.06	0.02±0.002	0.03±0.003	0.003±0.001
8	34	1.2±0.12	0.03±0.004	0.05±0.006	0.0008±0.0002
9	55	1.5±0.17	0.04±0.005	0.06±0.008	0.002±0.001
	28	1.7±0.09	0.02±0.02	0.03±0.003	0.0009±0.0004
10	20	0.5±0.09	0.04±0.008	0.07±0.01	0.001±0.0005
11	12	1.0±0.11	0.01±0.001	0.02±0.003	0.002±0.003

Table 4.4. Number of microfossils observed in Magela PP1 samples

Taxon	0-5 cm	5-10 cm	10-12 cm	12-16 cm	16-19 cm	19-23 cm	23-27 cm	27-31 cm	31-37 cm	37-43 cm	43-48 cm
Anomoeoneis rhomboidea	1	2	1		1	1	1	3	1	2	
Anomoeoneis exilis			1								
Anomoeoneis styriaca	1										
Cymbella large spp		2			2						
Cymbella minuta	1										
Cymbella spicula										2	
Eunotia camelus	7	12	14	5	5	3	2	6			
Eunotia curvata								ī			
Eunotia diodon			1	1							
Eunotia flexuosa	2				1	1					
Eunotia formica	$\bar{1}$		1			_		1		1	
Eunotia lineolata	2		_					ī		-	
Eunotia lunaris	_		. 3	1	3	2		Ī		I	
Eunotia monodon	1	1	2	i	ĺ	_		-		-	
Eunotia monodon var. scandica	_	-	_	_	-			1			
Eunotia parallela		1			1		1	î			
Eunotia pectinalis	2	_			-		_	-			
Eunotia trinacria	_	1									
Frustulia rhomboides		3	2	3				1			
Gomphonema gracile	2	1	2 2	1		2		-	1		
Gomphonema parvulum	_	-	_	ī		_			-		
Melosira granulata				ī							
Navicula bremensis		2		-							
Navicula radiosa	1	_	1	1							
Neidium sp.	2		•	•							
Pinnularia braunii	2	1	2		3						
Pinnularia large spp	5	4	3		3	2		7	1		
Stauroneis sp.	,	•	,		5	-		i	•		
Stenopterobia intermedia			3					•			
Sponge megascleres (pointed)	5	7	8	2	3	2	4	11	4	5	
Sponge megascleres (rounded)	12	16	13	11	16	24	17	28	24	19	
Sponge gemmoscleres (small)	20	33	17	10	29	43	30	60	22	24	•
S. gemmoscleres (rough-ended)	1	2	ì	10	2)	2	1	1	2	27	
Phytoliths (smooth-edged)	32	2	43	77	45	56	46	79	74	78	113
Phytoliths (dumbbell-shaped)	2	6	1	5	1	6	1	4	1	ī	113
Phytoliths (opaque rods)	1	J	3	4	5	6	6	7	4	5	

Table 4.4. Page 2

Taxon	0-5	5-10	10-12	12-16	16-19	19-23	23-27	27-31	31-37	37-43	43-48
	cm	cm	cm	cm	cm	cm	cm	cm	cm	cm	cm
Phytoliths (wavy-edged) Charcoal	1	63	1	1	1				1		
No. of fields examined No. of diatom taxa No. of diatom valves No. of sponge fossils No. of phytoliths	30	43	67	43	27	31	44	44	31	34	41
	14	11	13	9	9	6	3	11	3	4	0
	30	30	36	15	20	11	4	24	3	6	0
	38	58	39	24	48	71	52	100	52	48	0
	36	69	47	87	52	68	53	83	79	84	113
Total no. of microfossils	104	157	123	126	121	150	109	207	135	138	113

Table 4.5. Concentration of microfossils observed in Magela PP1 samples

	0-5 cm 10 000s fossils /g	5-10 cm 10 000s fossils /g	10-12 c 10 000s fossils /g	10 000s fossils	10 000s fossils	10 00 fossi	00s	10 000s fossils	10 000s fossils	10 000s fossils	m37-43 cm 10 000s fossils	10 000s fossils
	/8	/ g	/ B	/g	/g	/g		/g	/g	/g	/g	/g
Anomoeoneis rhomboidea	409	180	111	0	124	110	83	3 145	62	135	0	
Anomoeoneis exilis	0	0	111	0	0	0	0		0	0	Ö	
Anomoeoneis styriaca	409	0	0	0	0	0	0) 0	0	0	Ö	
Cymbella large spp	0	180	0	0	248	0	0	0	0	Ō	Ō	
Cymbella minuta	409	0	0	0	0	0	0		0	Ö	Ö	
Cymbella spicula	0	0	0	0	0	0	0		Õ	135	Ö	
Eunotia camelus	2866	1083	1559	1470		329	166	_	Ŏ	0	ő	
Eunotia curvata	0	0	0	0	0	0	0		Ŏ	ŏ	Õ	
Eunotia diodon	0	0	111	294	0	0	0		0	Ŏ	Ö	
Eunotia flexuosa	819	0	0 .	0	124	110	ō	_	Ŏ	Ŏ	ő	
Eunotia formica	409	0	111	Ō	0	0	Ŏ	_	Ŏ	68	ő	
Eunotia lineolata	819	0	0	0	0	ō	Ŏ	_	Õ	0	Õ	
Eunotia lunaris	0	0	334	294	_	219	Õ		Õ	68	ñ	
Eunotia monodon	409	90	223	294	124	0	0	_	Õ	0	ň	
Eunotia monodon var. scandi		0	0	0	0	Ŏ	Õ	•	Õ	Õ	ŏ	
Eunotia parallela	0	90	0	0	124	ō	83	_	Õ	Õ	ň	
Eunotia pectinalis	819	0	0	0	0	Ō	0		Ŏ	ŏ	ŏ	
Eunotia trinacria	0	90	0	0	Ō	Ō	0	•	Õ	Õ	ň	
Frustulia rhomboides	0	271	223	882	Ö	Ô	0	_	Õ	Õ	ň	
Gomphonema gracile	819	90	223	294		219	Ö		62	ő	ŏ	
Gomphonema parvulum	•			294	Ö	0	0	_	0	Õ	ŏ	
Melosira granulata				294	Ŏ	Ŏ	ő	-	Ô	Õ	ő	
Navicula bremensis	0	180	0	0	Ŏ	Ŏ	ő	•	0	0	0	
Navicula radiosa	409	0	111	294	Ŏ	Ŏ	ŏ	•	ő	Ô	0	
Neidium sp.	819	Ö	0	0	0	Õ	ő	=	0	Ô	ñ	
Pinnularia braunii	819	90	223	Ö	372	Õ	Õ	_	0	n	Ô	
Pinnularia large spp	2047	361	334	Ŏ	_	219	ő	•	62	0	n	
Stauroneis sp.				Õ	0	0	ő		0	0	0	
Stenopterobia intermedia	0	0	334	Õ	Õ	Ô	0		0	0	0	

Table 4.5. Page 2.

Taxon	0-5 cm 10 000s fossils	5-10 cr 10 000s fossils	10 000 fossils	Os 10 000 s fossils	Os 100 s foss	00s ils	10 000s fossils	n 43-48 cm 10 000s fossils				
	/g	/g	/g	/g	/g		/g	/g	/g	/g	/g	/g
Sponge megascleres (pointed	d) 2047	632	891	588	372	219	333	533	247	338	0	
Sponge megascleres (rounde		1444	1448	3233	1982	2631	1414	1357	1479	1283	0	
Sponge gemmoscleres (smal		2978	1893	2939	3592	4714	2490	5 2908	1356	1620	0	
S. gemmoscleres (rough-end	•	180	111	294	0	219	83	48	123	0	0	
Phytoliths (smooth-edged)	13104	0	4789	22633	5574	6139	382	7 3829	4561	5266	9 193	
Phytoliths (dumbbell-shape		541	111	1 470	124	658	83	194	62	68	0	
Phytoliths (opaque rods)	409	0	334	1 176	619	658	499	0	247	338	0	
Phytoliths (wavy-edged)	409	5 685	0	294	124	0	0	0	0	0	0	
Charcoal	0	0	111	0	124	0	C	0	62	0	0	
Total diatom valves	12285	2707	4009	4409	2477	1206	5 33:	3 1163	185	405	0	
Total sponge fossils	15560	5234	4343	7054	5946	7784	432	5 4846	3205	3241	0	
Total phytoliths	14471	6227	5234	25572	6441	7455	440	9 4022	4869	5672	9193	
Total microfossils	42 587	14 168	13 698	37 035	14 988	16 44	5 9 06	8 10 032	8 321	9 318	9193	
Prop'n diatoms in												
microfossils	0.29	0.19	0.29	0.12	0.17	0.0	7 0.0	4 0.12	0.02	0.04	0.00	
Prop'n sponges in microfossils	0.37	0.37	0.32	0.19	0.40	0.4	7 0.4	8 0.48	0.39	0.35	0.00	
Prop'n phytoliths in microfossils	0.35	0.44	0.38	0.69	0.43	0.4	5 0.4	9 0.40	0.59	0.61	1.00	

Table 4.6. Number of microfossils observed in Magela MV1 samples.

Species	0-1 cm	5 cm	1-12 cm 1	6-17 cm	20 cm	25 cm	30 cm	35 cm
Sample weight (g)	1.664	1.492	1.284	1.235	3.773	2.972	3.034	3.186
Anomoeoneis rhomboides	2	3	7	7	1	1	0	0
Anomoeoneis exilis	5	13	7	2	0	1	0	Ō
Anomoeoneis styriaca	0	1	2	0	0	0	0	0
Cymbella minuta	3	12	3	0	0	0	0	0
Cymbella spicula	0	2	0	0	0	0	0	0
Eunotia camelus	25	58	12	8	2	1	0	0
Eunotia curvata	4	7	1	1	0	2	0	0
Eunotia flexuosa	1	0	2	2	0	0	0	0
Eunotia formica	2	0	0	0	0	0	0	0
Eunotia lineolata	13	7	0	3	0	0	0	0
Eunotia lunaris	15	12	3	4	1	0	0	0
Eunotia monodon	10	20	3	I	0	1	0	0
Eunotia monodon var. scandica	0	3	3	I	0	0	0	0
Eunotia parallela	4	11	10	6	2	0	0	0
Eunotia pectinalis	1	0	0	0	0	0	0	0
Eunotia rhomboidea	4	6	0	3	0	0	0	0
Eunotia pseudoindica var. gracilis	11	9	2	2	0	0	0	0
Eunotia trinacria	4	30	3	1	0	0	0	0
Eunotia zygodon	1	0	0	0	0	0	0	0
Frustulia rhomboides	36	49	12	3	i	3	2	0
Gomphonema gracile	5	14	10	11	1	2	0	0
Navicula bremensis	1	2	0	0	0	0	0	0
Navicula radiosa	11	19	1	1	0	0	0	0
Nitzschia gandersheimiensis	0	5	0	0	0	0	Ö	Ŏ
Nitzschia palea	5	12	0	1	0	0	Ö	Ŏ
Nitzschia pseudoamphioxys	1	1	1	0	0	Ö	Ö	Ŏ
Pinnularia braunii	6	3	5	0	0	1	0	Ô
Pinnularia gibba	0	1	0	0	0	0	Ö	Ŏ
Pinnularia legumen	10	6	1	2	Ō	Ŏ	Ö	ő
Pinnularia microstauron	4	8	3	4	Ō	Õ	Õ	ő
Pinnularia stauroptera	0	3	0	0	Õ	0	Õ	ŏ

Table 4.6. Page 2

Species	0-1 cm	5 cm	11-12 cm 1	6-17 cm	20 cm	25 cm	30 cm	35 cm
Stenopterobia sp.	4	2	1	1	0	0	0	0
Sponge megascleres (pointed)	15	15	17	12	27	7	0	0
Sponge megascleres (rounded)	46	80	97	92	53	51	0	0
Sponge gemmoscleres (small)	81	97	209	144	107	116	2	0
S. gemmoscleres (rough-ended)	2	7	6	7	9	4	1	0
Phytoliths (smooth-edged)	223	157	160	70	100	101	351	281
Phytoliths (dumbbell-shaped)	23	0	28	19	1	1	0	0
Phytoliths (opaque rods)	8	22	18	14	14	19	0	0
Phytoliths (wavy-edged)	3	0	5	9	0		0	0
Charcoal	12	31	6	8	7	7	6	8
No. of fields examined	176	235	285	317	230	37 5	169	225
No. of diatom taxa	26	28	21	19	6	8	1	0
No. of diatom valves	188	319	92	64	8	12	2	0
No. of sponge fossils	144	199	329	255	196	178	3	0
No. of phytoliths	257	179	211	112	115	121	351	281
Total no. of microfossils	601	728	638	439	326	318	362	289

Table 4.7. Concentration of microfossils observed in MV1 samples

Species	0-1 cm 10 000s fossils /g	5 cm 10 000s fossils /g	11-12 cm 10 000s fossils /g	16-17 cm 10 000s fossils /g	20 cm 10 000s fossils /g	25 cm 10 000s fossils /g	30 cm 10 000s fossils /g	35 cm 10 000s fossils /g
Anomoeoneis rhomboides	172	690	1925	1799	116	90	0	0
Anomoeoneis exilis	430	2990	1925	514	0	90	0	Ŏ
Anomoeoneis styriaca	0	230	550	0	0	0	0	Ö
Cymbella minuta	258	2 760	825	0	0	0	Ö	Ö
Cymbella spicula	0	460	0	0	0	Ö	0	Ô
Eunotia camelus	2150	13340	3300	2056	232	90	Ö	ŏ
Eunotia curvata	344	1610	275	257	0	180	Õ	ŏ
Eunotia flexuosa	86	0	550	514	Ō	0	ŏ	Õ
Eunotia formica	172	0	0	0	Ō	Ö	Õ	ñ
Eunotia lineolata	1118	1610	0	771	Ö	Ö	ŏ	ň
Eunotia lunaris	1290	2760	825	1028	116	ŏ	ň	ñ
Eunotia monodon	860	4600	825	257	0	90	ñ	ñ
Eunotia monodon var. scandica	0	690	825	257	Ô	0	ň	Ô
Eunotia parallela	344	2530	2750	1542	232	Ô	Ô	0
Eunotia pectinalis	86	0	0	0	0	ő	ň	Ô
Eunotia rhomboidea	344	1380	Ö	771	ő	ő	ñ	0
Eunotia pseudoindica var. gracilis	946	2070	550	514	Ö	ő	ň	0
Eunotia trinacria	344	6900	825	257	Õ	ő	ň	0
Eunotia zygodon	86	0	0	0	ŏ	Ô	0	0
Frustulia rhomboides	3096	11270	3300	771	116	270	392	0
Gomphonema gracile	430	3220	2750	2827	116	180	0	0
Navicula bremensis	86	460	0	0	0	0	0	0
Navicula radiosa	946	4370	275	257	ŏ	ő	0	0
Nitzschia gandersheimiensis	0	1150	0	0	0	0	0	0
Nitzschia palea	430	2760	ŏ	257	0	0	0	0
Nitzschia pseudoamphioxys	86	230	275	0	0	0	0	0
Pinnularia braunii	516	690	1375	0	0	90	0	0
Pinnularia gibba	0	230	0	0	0	0	0	0
Pinnularia legumen	860	1380	275	514	0	0	0	0
Pinnularia microstauron	344	1840	825	1028	0	0	0	•
Pinnularia stauroptera	0	690	023	0	0	0	0	0

Table 4.7. Page 2.

Species	0-1 cm 10 000s fossils /g	5 cm 10 000s fossils /g	11-12 cm 10 000s fossils /g	16-17 cm 10 000s fossils /g	20 cm 10 000s fossils /g	25 cm 10 000s fossils /g	30 cm 10 000s fossils /g	35 cm 10 000s fossils /g
Stenopterobia sp.	344	460	275	257	0	0	0	0
Sponge megascleres (pointed)	1290	3450	4675	3084	3132	630	0	0
Sponge megascleres (rounded)	3956	18400	26675	23644	6148	4590	0	0
Sponge gemmoscleres (small)	6966	22310	57475	37008	12412	10440	392	0
S. gemmoscleres (rough-ended)	172	1610	1650	1799	1044	360	196	0
Phytoliths (smooth-edged)	19178	36110	44000	17990	11600	9090	68796	39621
Phytoliths (dumbbell-shaped)	1978	0	7700	4883	116	90	0	0
Phytoliths (opaque rods)	688	5060	4950	3598	1624	1710	0	0
Phytoliths (wavy-edged)	258	0	1375	2313	0	0	0	0
Charcoal	1032	7130	1650	2056	812	630	1176	1128
Total diatom valves	16168	73370	25300	16448	928	1080	392	0
Total sponge fossils	12384	45770	90475	65535	22736	16020	588	0
Total phytoliths	22102	41170	58025	28784	13340	10890	68796	39621
Total microfossils	51686	167440	175450	112823	37816	28620	70952	40749
Prop'n diatoms in microfossils	0.31	0.44	0.14	0.15	0.02	0.04	0.01	0.00
Prop'n sponges in microfossils	0.24	0.27	0.52	0.58	0.60	0.56	10.0	0.00
Prop'n phytoliths in microfossils		0.25	0.33	0.26	0.35	0.38	0.97	0.97

Table 4.8. Major pollen taxa, including aquatic macrophytes, in P Pit 1

Depth	0-5 cm	5-10 cn	n 10-12 cm	12-16 cr	m 16-19 c	cm 19-23 cm	23-27 cm	27-31	cm 31-37	cm 37-43	cm 43-48 cm
Avicennia	4	7	2	1		13	8				7
Barringtonia	1	24	1	3		1	1	1	1		
Myrtacea	64	50	37	4	1	59	137	3	55	147	12
Poaceae	26	6	1	1		16	22	3	15	11	12
'Aquatics' + Blyxa	1					13	6	11	25	4	43
Ceratophyllum						4	4	5			
Aponogeton	2							_	15		6
Other	6	1				9	1	1	5	2	3
Damaged	5	9		2		•	5	_	5	_	_
Total	109	97	40	11	1	115	184	24	121	164	85

Note: 'Aquatic' pollen is very thin walled, roughly spherical, with visible ornamentation. While identifiable as aquatic they cannot be identified to a particular taxon.

Table 4.9. Spectral peaks recorded in a variety of phenomena

Crypto- meria Japonica	Sar Bar mar cor	bara ine	Bristle- cone pine	Green- land ice core	x±1σ	Sun- spots	Aurorae	Tree rings	Climate records	x±lσ
D/H ¹⁸ O/ ¹⁶ O	Org. C	U	¹⁴ C	¹⁸ O/ ¹⁶ O		No.	No./104	14C	Yrs	Yrs
156 156	161	156	162	179	162±9	-	_	140	143	142±2
110 124	121	118	108	_	116±7	_	130	127	123	127±4
97 97	95	95	-	100	97±2	_	_	_	102-104	98±4
86 88	82	81	-	78	83±4	90	88	85-87	88	88±2
65 70	71	70	-	68	69±2	_	-	_	-	64±3
58 55	55	53	-	58	55±2	_	-	_	_	56±3
						22	_	-	_	22

Table 4.10. Major correlations of the ENSO phenomenon

SOI	El Niño	Atmospher Darwin	ic pressure Papeete	Rainfal N. Australia	l W. South Am.	Trade winds	Tropical cyclones
Strongly negative	Strong	High	Low	Low	High	Weak	Few
Strongly positive	Anti	Low	High	High	Low	Strong	Common

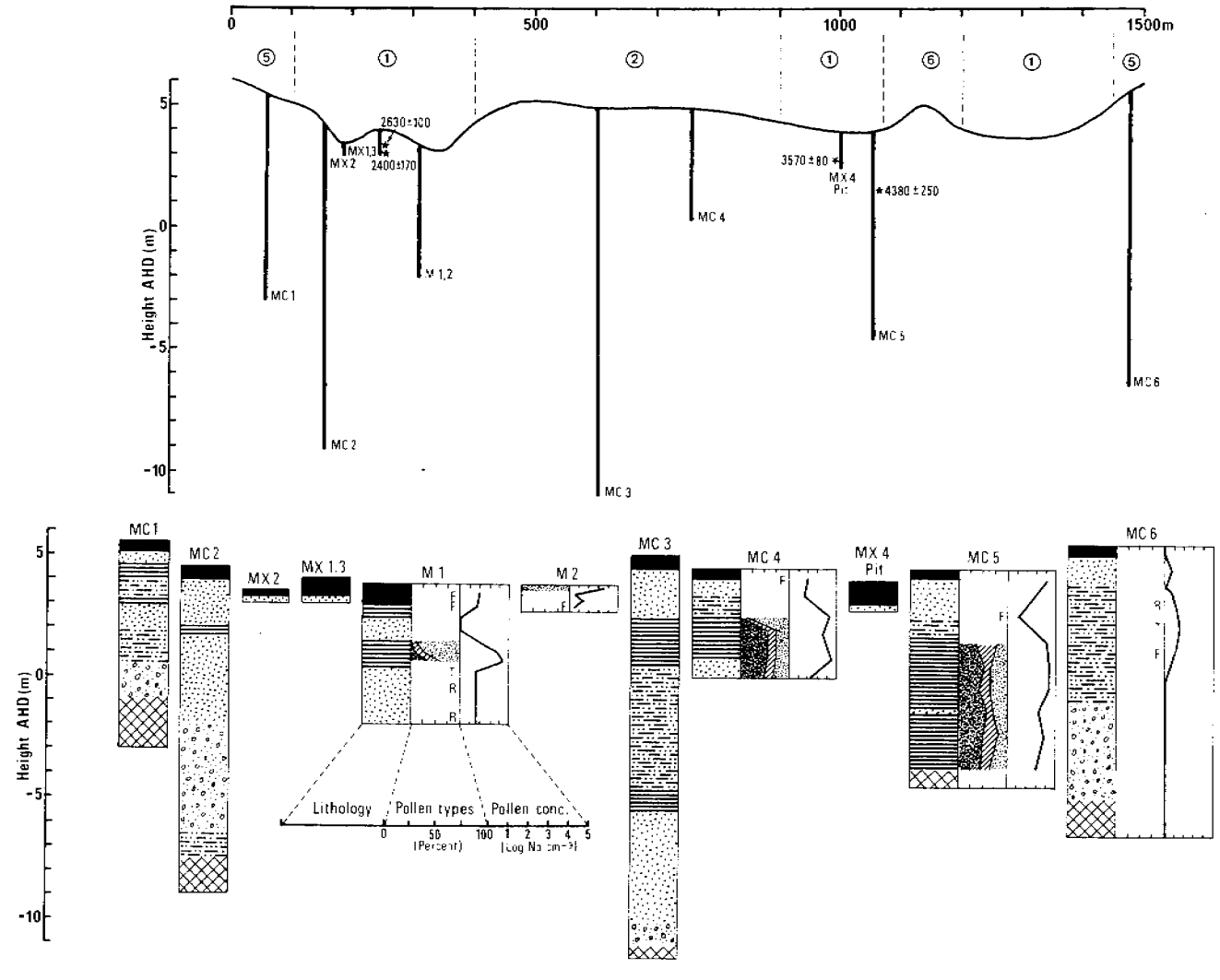


Figure 4.1a Lithostratigraphy (top) and biostratigraphy (bottom) of cross-section 1 (see Fig. 2.3 for location). The reference numbers for the cores, pits and auger holes are given, and reference to Table 3.1 should be made for further details. The radiocarbon dates on the graphic and pollen logs are those believed to be the most reliable, given the tests discussed in Chapter 3. No radiumthorium dates are shown.

KEY TO	STRATIGRAPHIC CROS	SS-SECTION	ONS								
MC3	Core No	630 ± 140	Radiocarbon date								
1	Low plain	2	High plain	3	Backslope						
4	Marginal depression	5	Upland margin	6	Levee						
LITHOLO	OGY										
	Dark Brown/Black Clay organic rich; some sedi		y, clay loam and loamy l structures.	ight clay;							
	Grey Clay light grey, brown and sometimes dark brown clay with minor sand; no visible sedimentary structures.										
	Blue Grey Clay — grey, mauve grey and blue grey clay, often with large fragments of wood and leaf remains. For details of facies, see Chapter 3.										
	Sands and Clays $\underline{\ }$ sandy clay and clayey sand; the brown or grey brown facies is of Pleistocene age.										
	Sands and Clays — sands (fine to coarse) free of gravel; a muddy sand facies is laterally equivalent to Blue Grey Clay.										
0 0 0 0			fine to coarse) and grave setter sorted towards the								
	Bedrock		No data								
POLLEN	TYPES										
	Rhizophora		Freshwater and terrestrial		Other mangroves						
	Pandanus		Barringtonia	- - - - - - - - - - - - - - -	<i>Pandanus</i> and <i>Barringtonia</i>						
	Cf. Ceratopteris		No data								
R	Rhizophora forest	Т	Transition	F	Freshwater						

Figure 4.1b Key to the symbols used in Figure 4.1a and 4.2 to 4.11

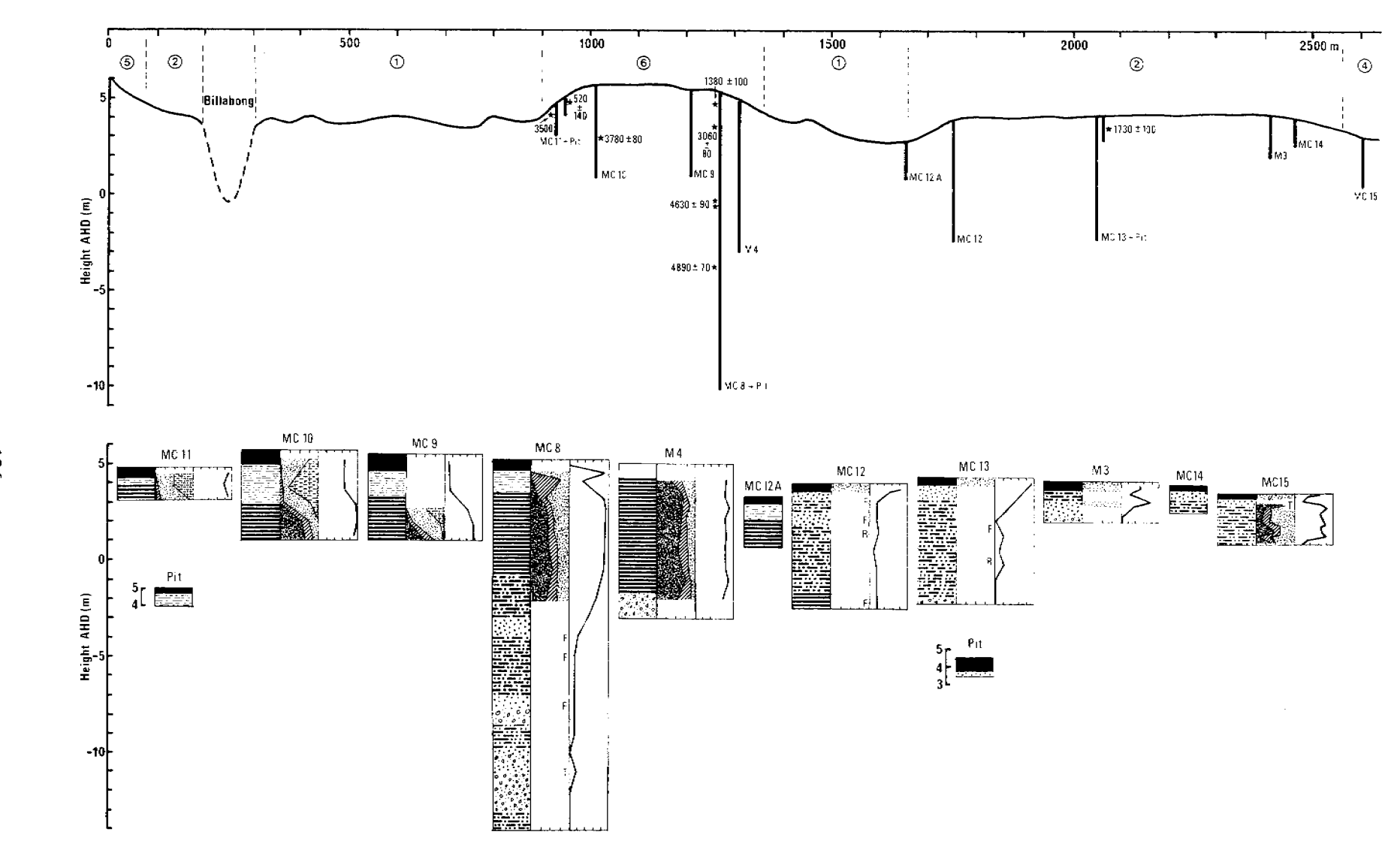


Figure 4.2 Lithostratigraphy and biostratigraphy of cross-section 2

Cross-section 2. See caption to Fig. 4.1(a) for details and Fig. 4.1(b) for a key to the symbols.

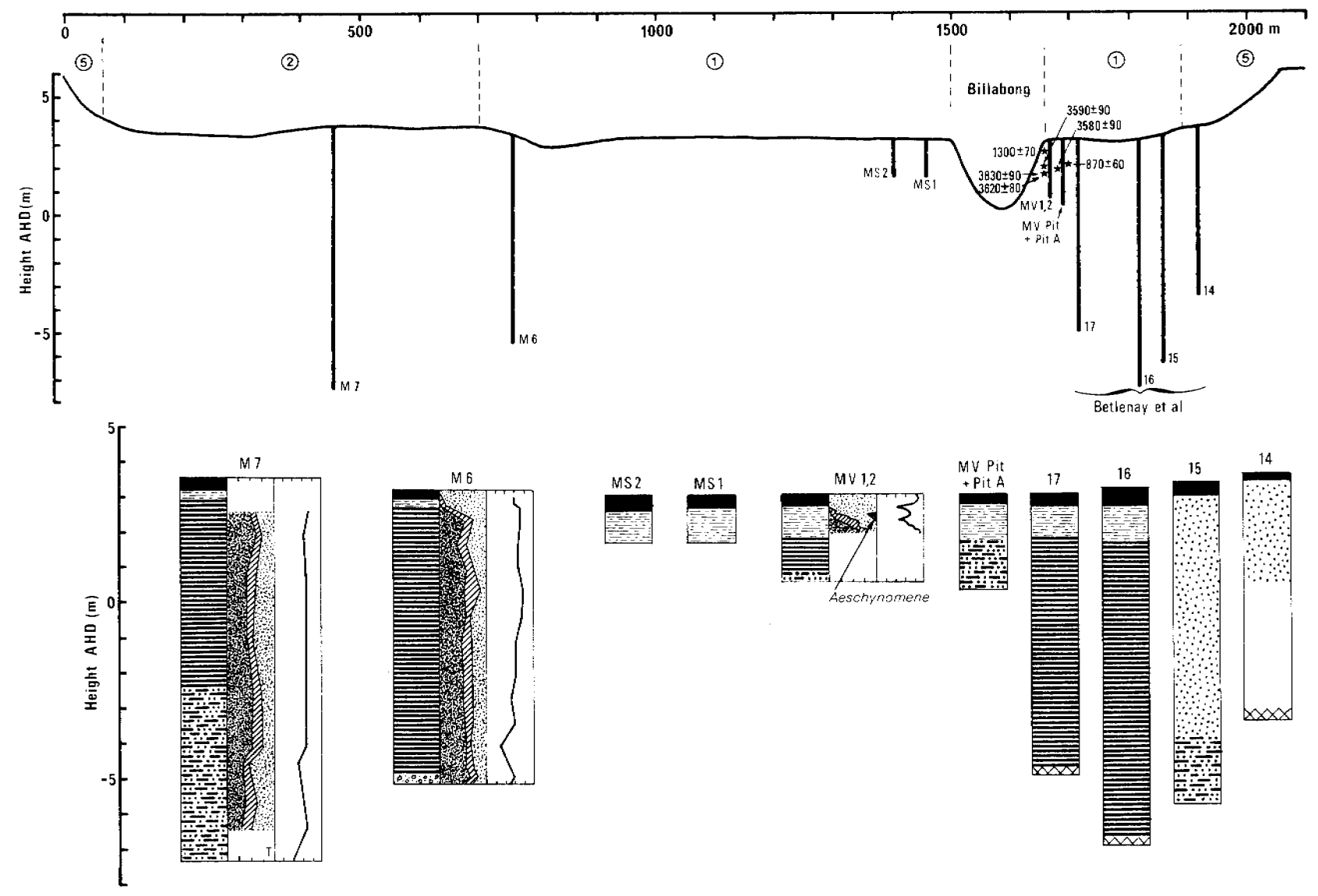


Figure 4.3 Lithostratigraphy and biostratigraphy of cross-section 3 Cross-section 3. See caption to Fig. 4.1(a) for details and Fig. 4.1(b) for a key to the symbols.

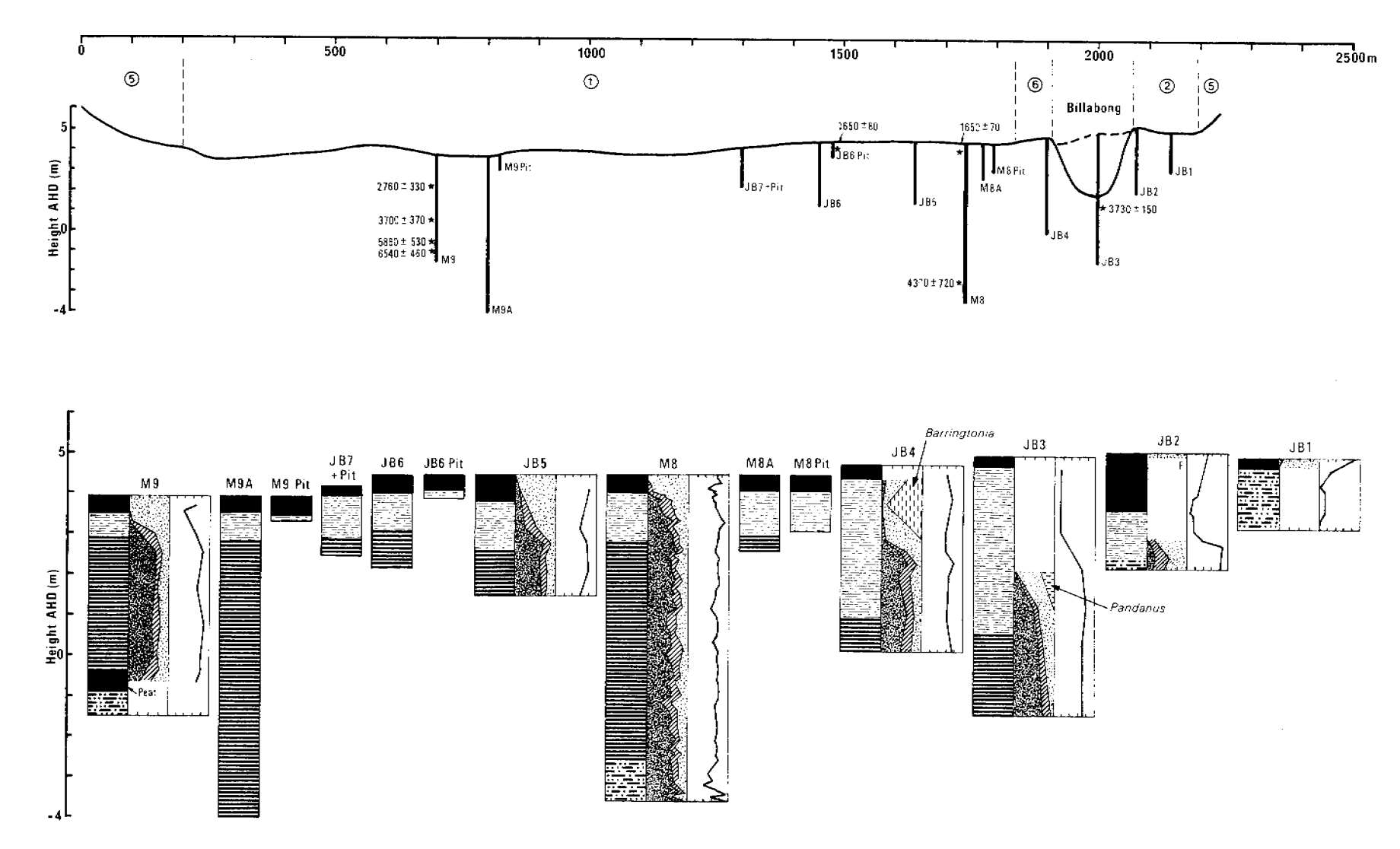


Figure 4.4 Lithostratigraphy and biostratigraphy of cross-section 4 Cross-section 4. See caption to Fig. 4.1(a) for details and Fig. 4.1(b) for a key to the symbols.

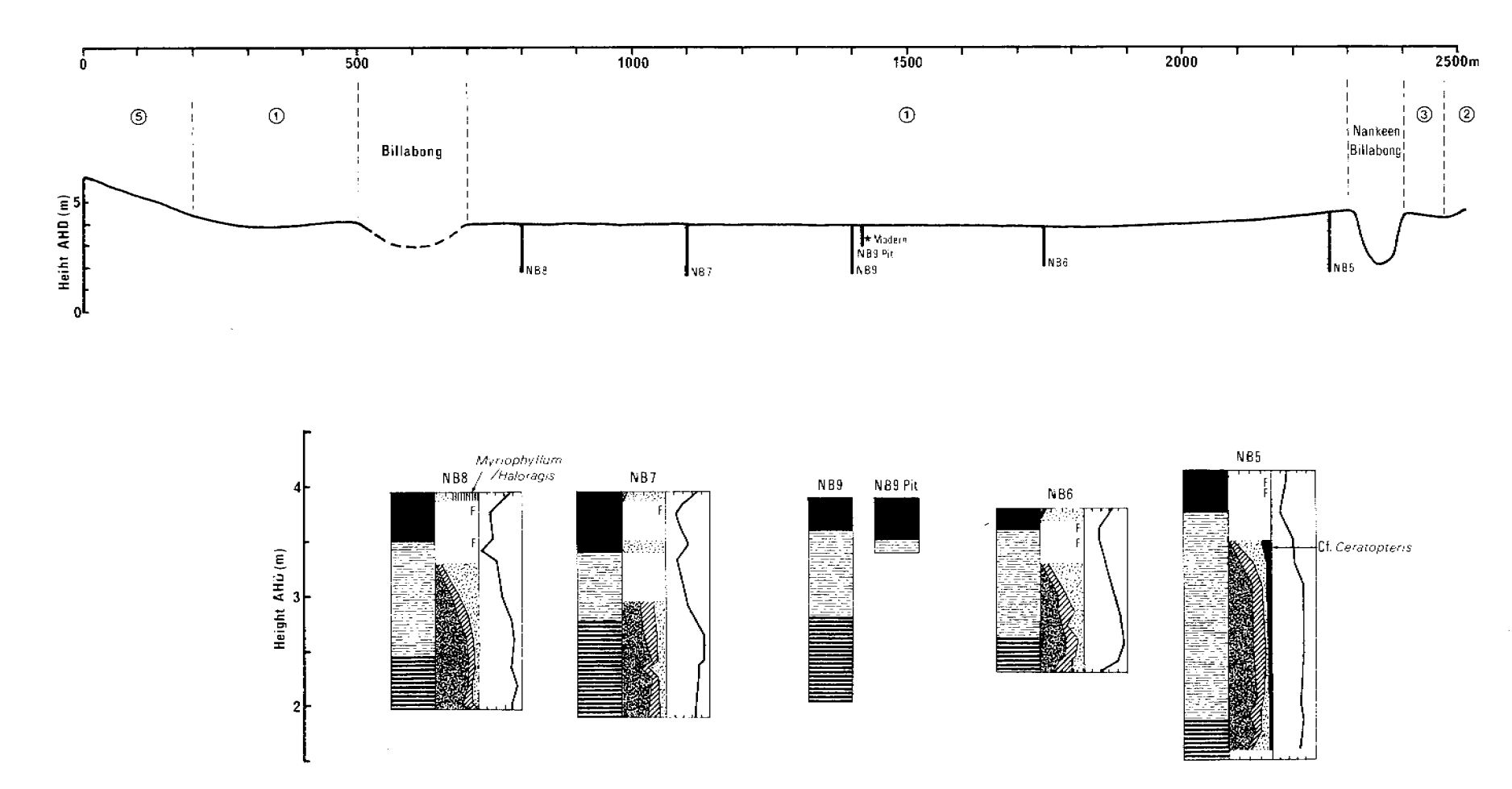


Figure 4.5 Lithostratigraphy and biostratigraphy of cross-section 5 Cross-section 5. See caption to Fig. 4.1(a) for details and Fig. 4.1(b) for a key to the symbols.

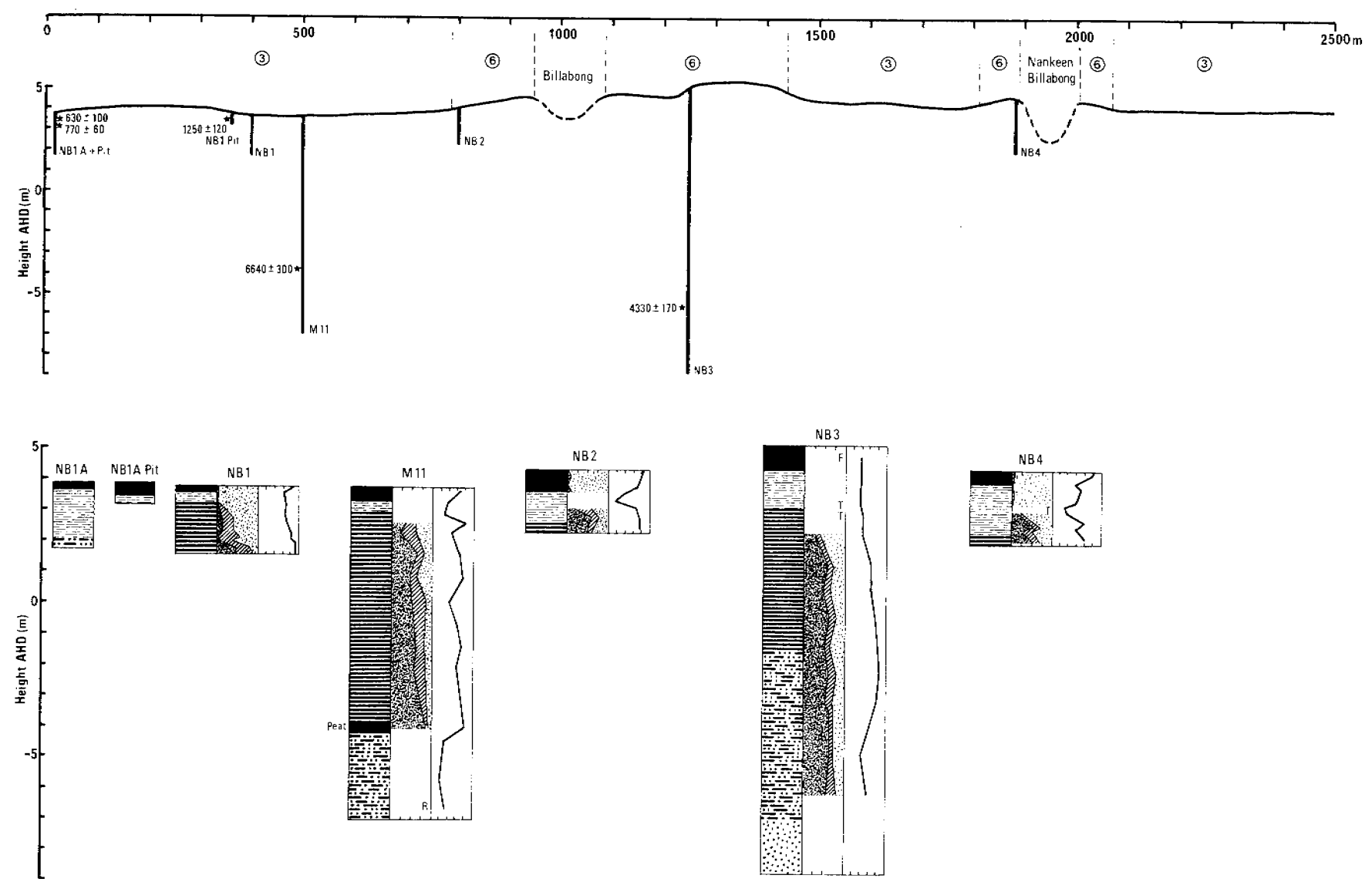


Figure 4.6 Lithostratigraphy and biostratigraphy of cross-section 6 Cross-section 6. See caption to Fig. 4.1(a) for details and Fig. 4.1(b) for a key to the symbols.

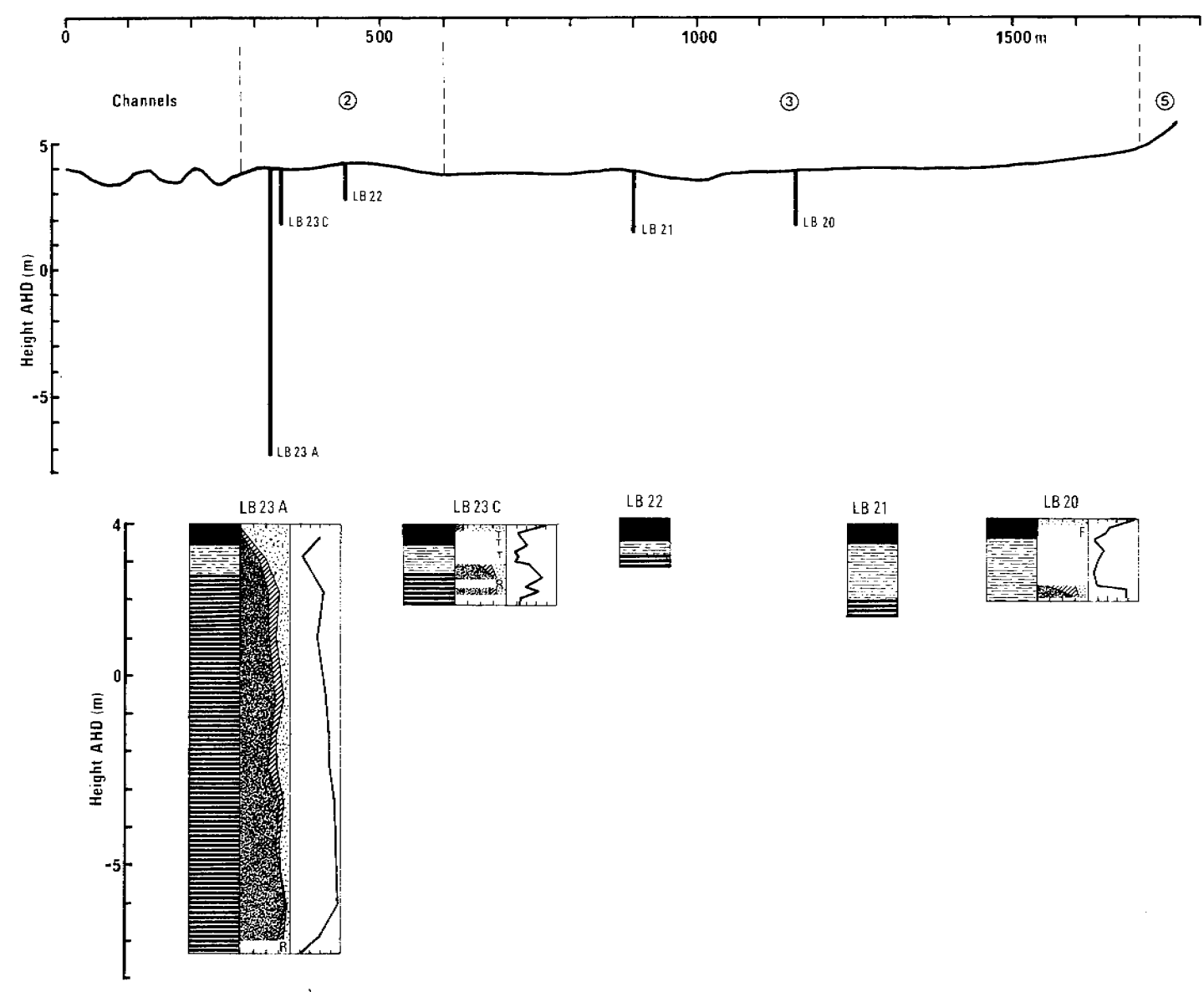


Figure 4.7 Lithostratigraphy and biostratigraphy of cross-section 7 Cross-section 7. See caption to Fig. 4.1(a) for details and Fig. 4.1(b) for a key to the symbols.

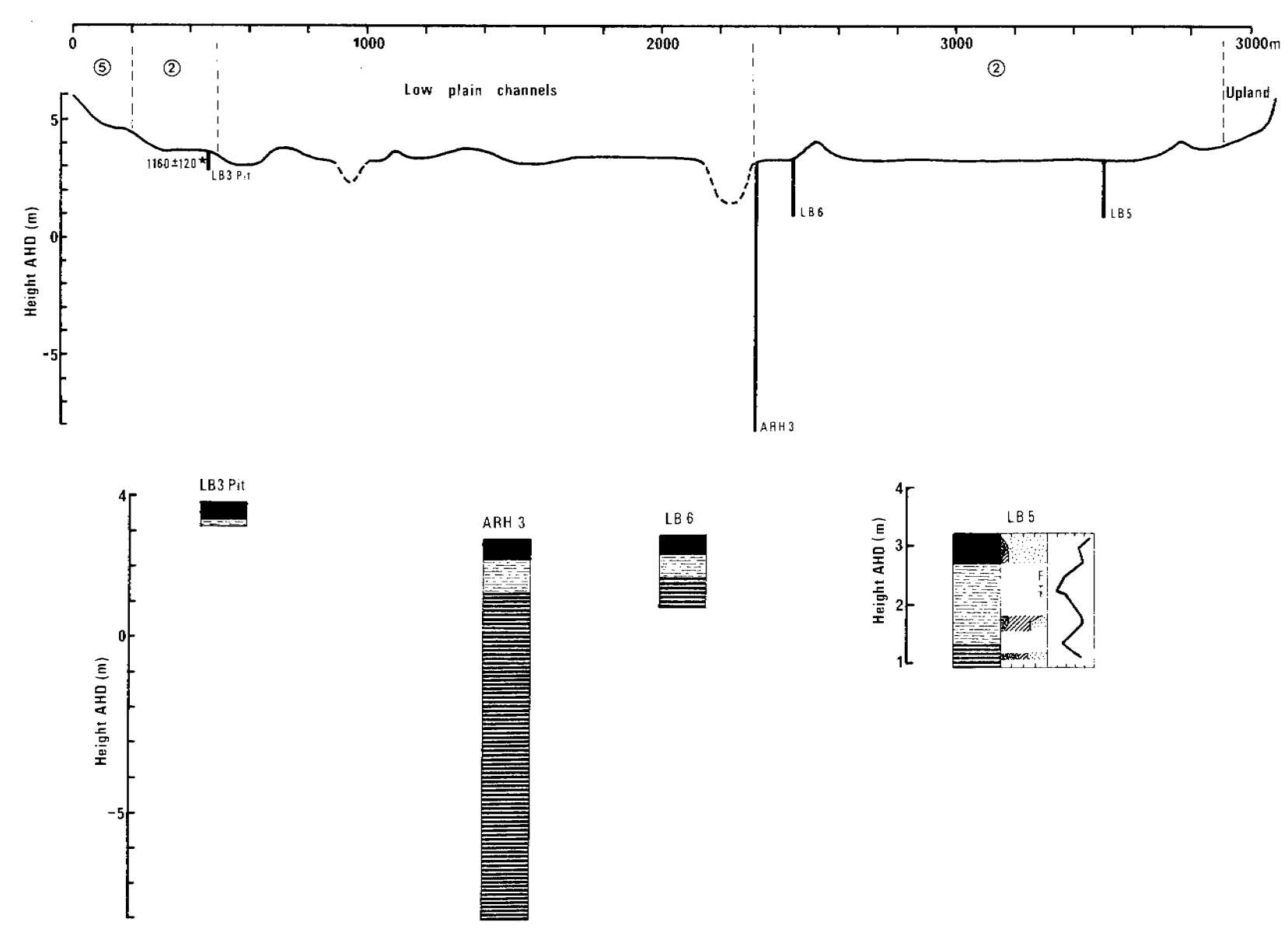


Figure 4.8 Lithostratigraphy and biostratigraphy of cross-section 8 Cross-section 8. See caption to Fig. 4.1(a) for details and Fig. 4.1(b) for a key to the symbols.

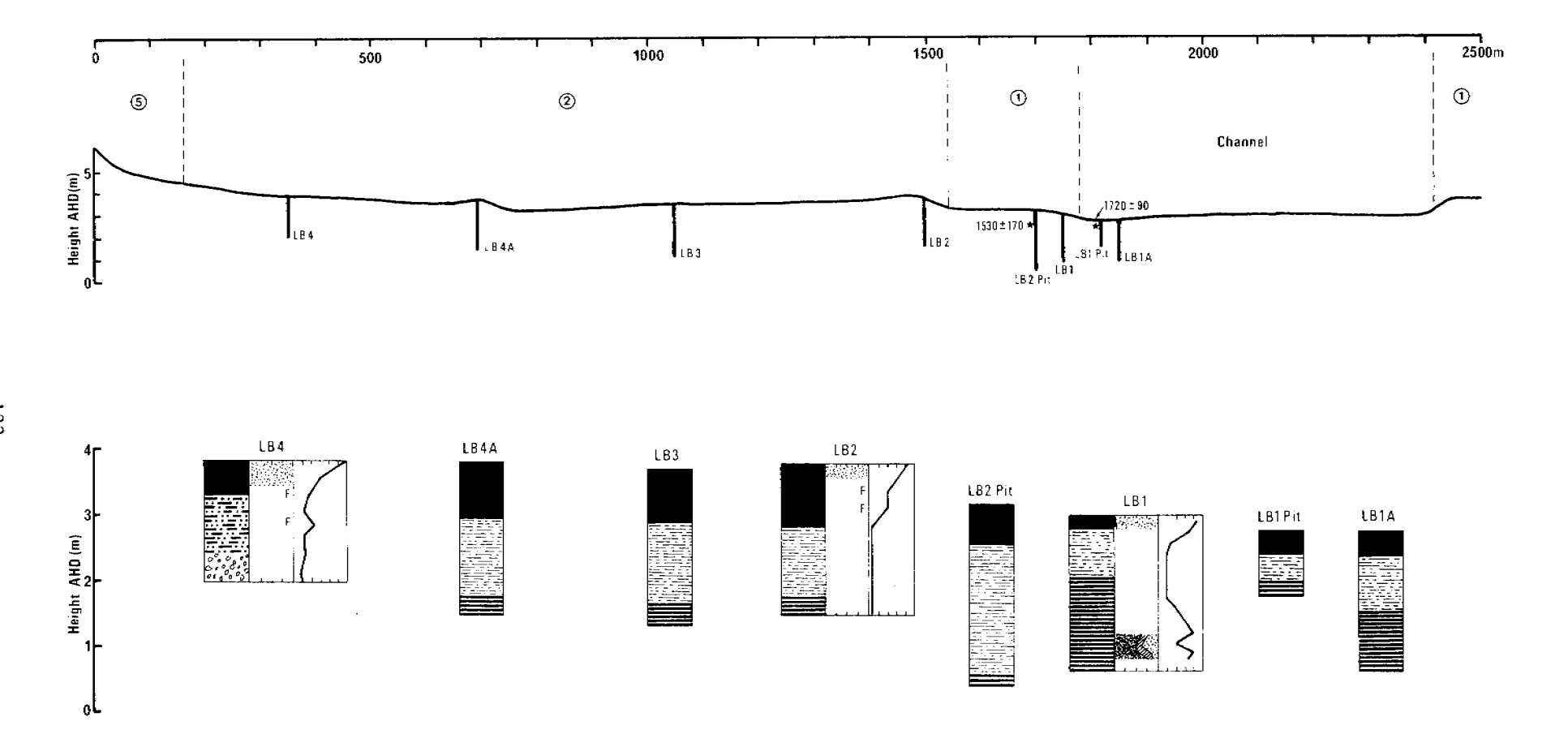


Figure 4.9 Lithostratigraphy and biostratigraphy of cross-section 9

Cross-section 9. See caption to Fig. 4.1(a) for details and Fig. 4.1(b) for a key to the symbols.

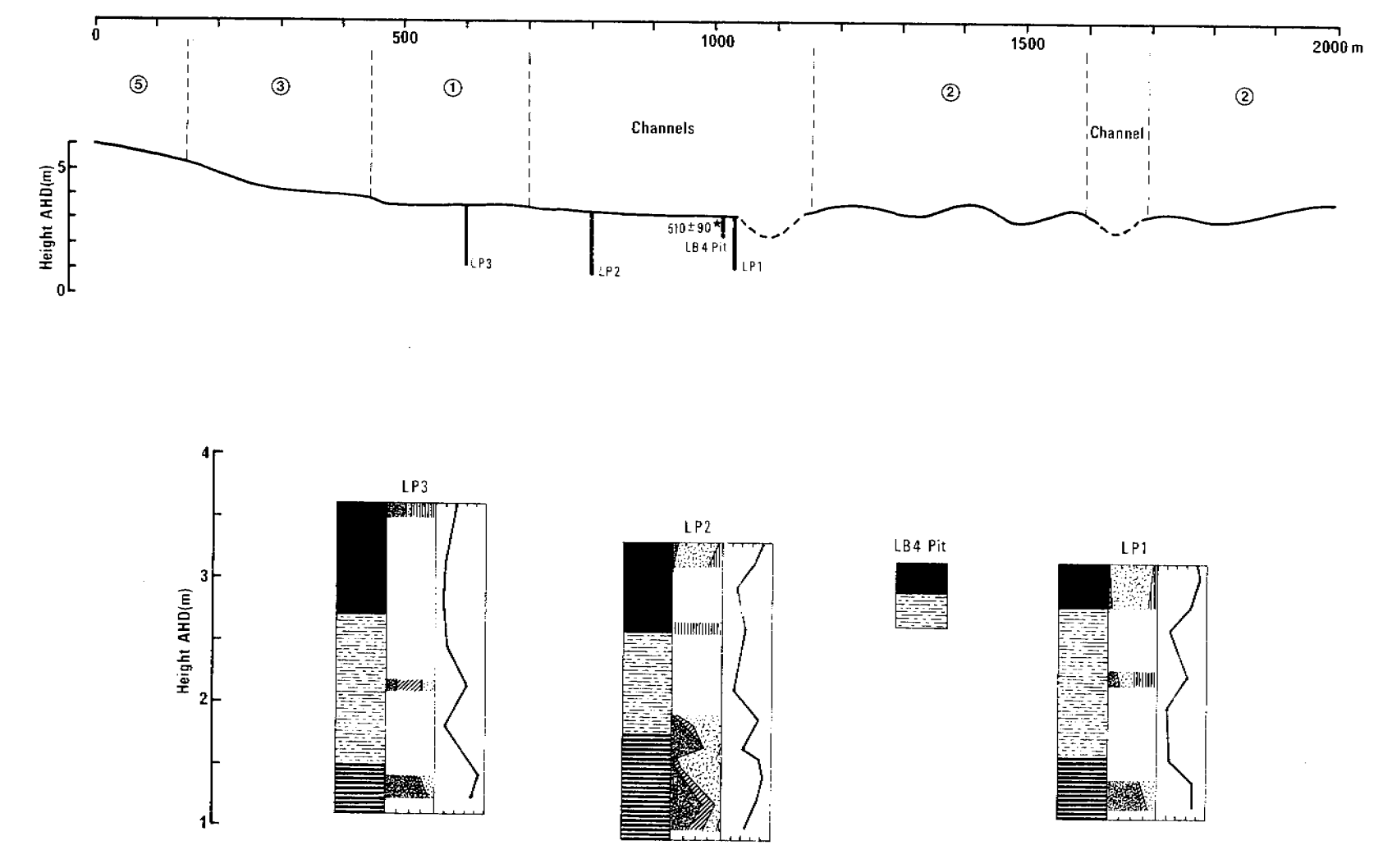


Figure 4.10 Lithostratigraphy and biostratigraphy of cross-section 10 Cross-section 10. See caption to Fig. 4.1(a) for details and Fig. 4.1(b) for a key to the symbols.

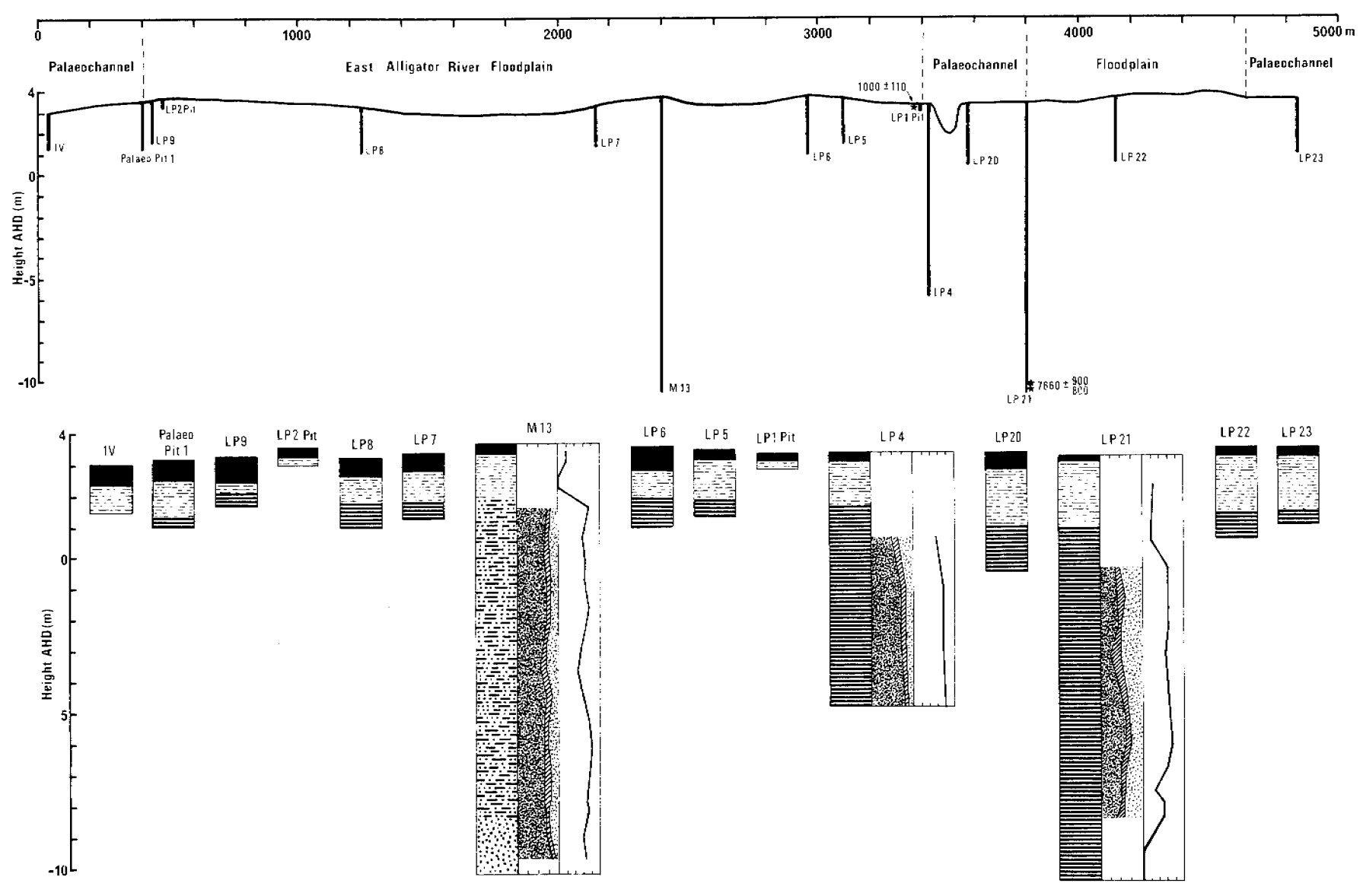


Figure 4.11 Lithostratigraphy and biostratigraphy of cross-section 11 Cross-section 11. See caption to Fig. 4.1(a) for details and Fig. 4.1(b) for a key to the symbols.

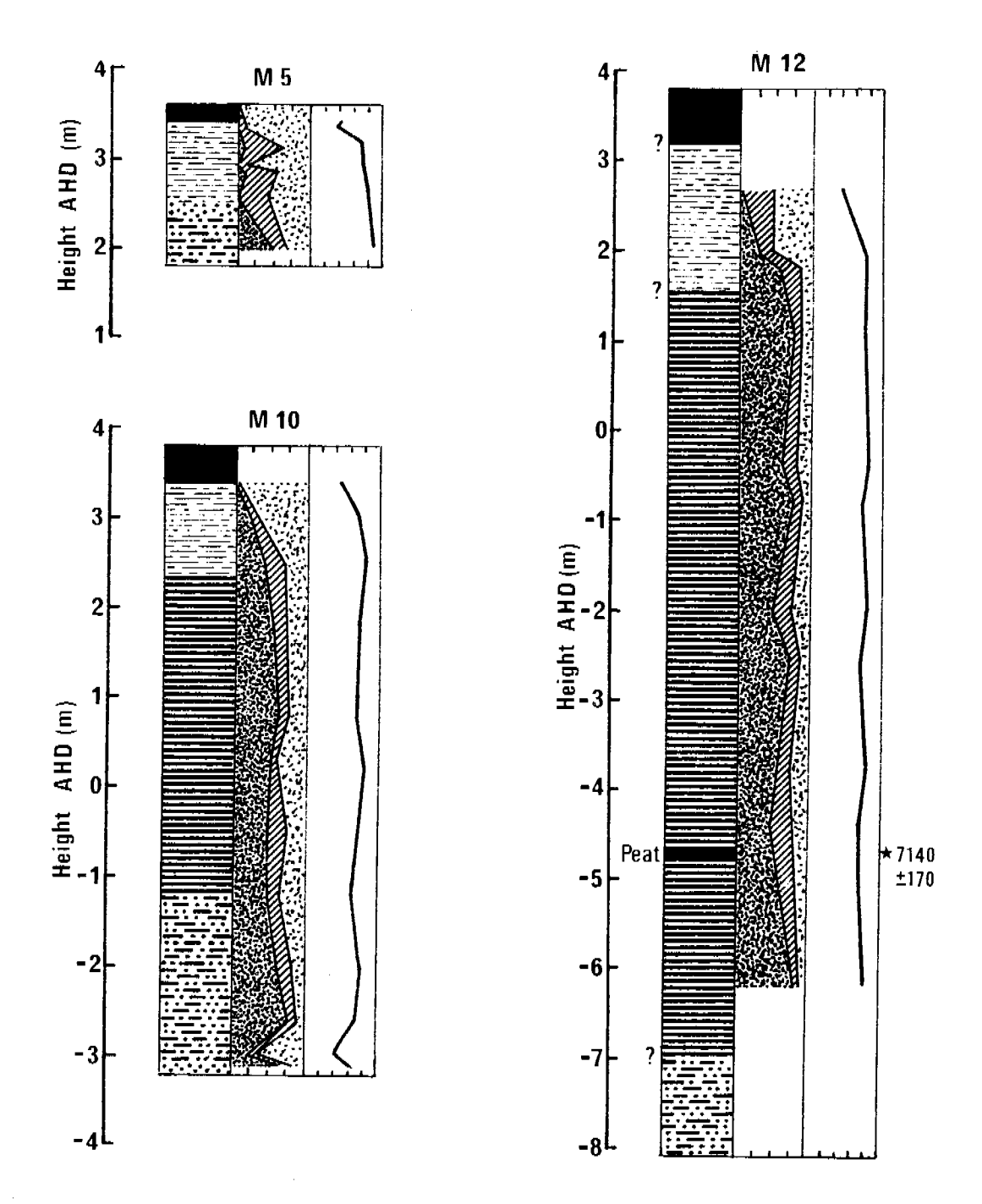


Figure 4.12 Lithostratigraphy and biostratigraphy for sites M5, M10 and M12 Lithostratigraphy and biostratigraphy for sites M5 (between cross-sections 2 and 3; see Fig. 2.3 for location), M10 (between cross-section 3 and 4) and M12 (between cross-sections 7 and 8). See Fig. 4.1 (b) for a key to the symbols used.

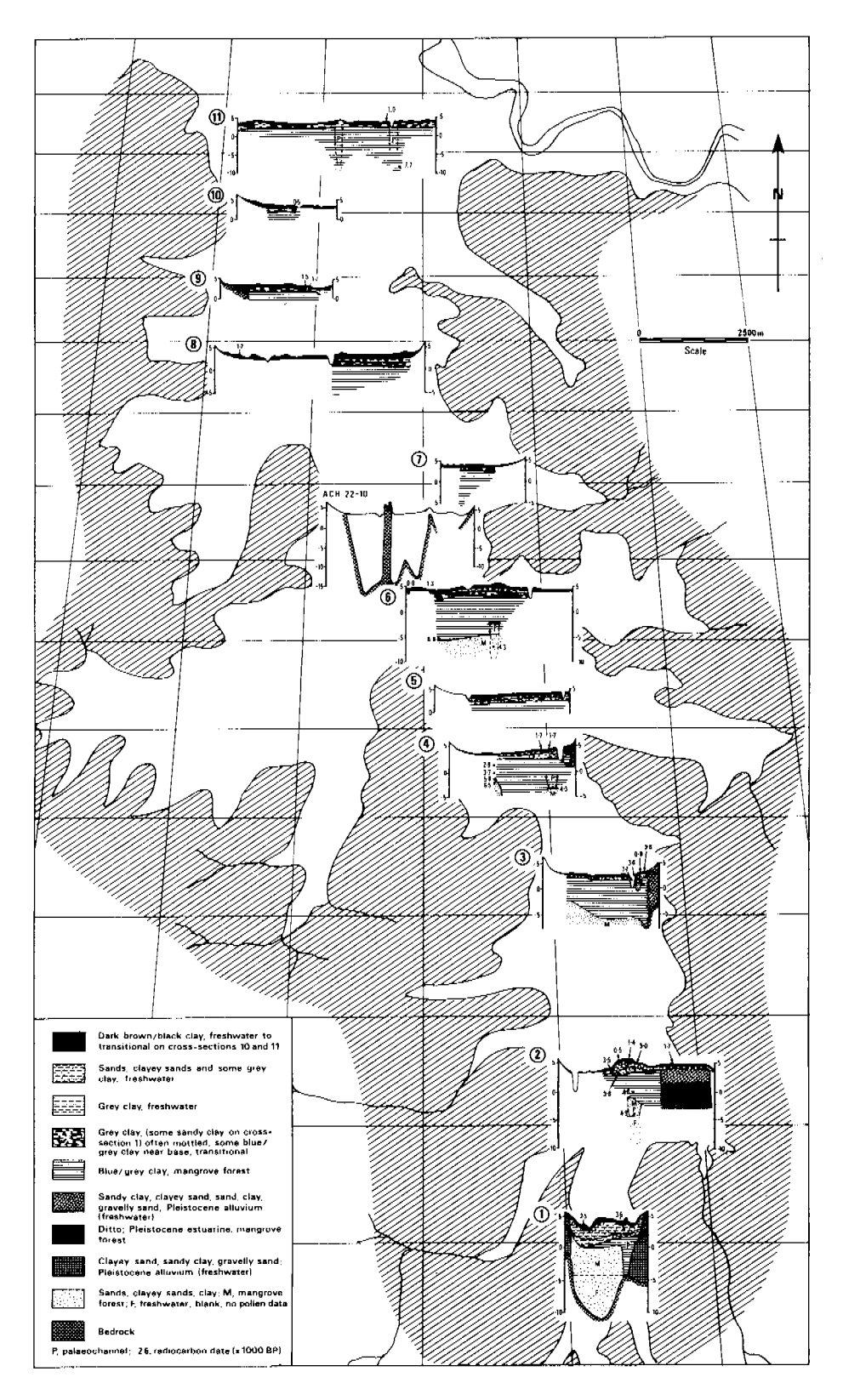


Figure 4.13 Isometric, pseudo-perspective, diagrams showing cross-sections 1 to 11 arranged with respect to elevation (AHD) and distance from Mudginberri. The cross-sections are summaries of both lithologic and pollen data presented in Figs 4.1 to 4.12 and show environments of deposition.

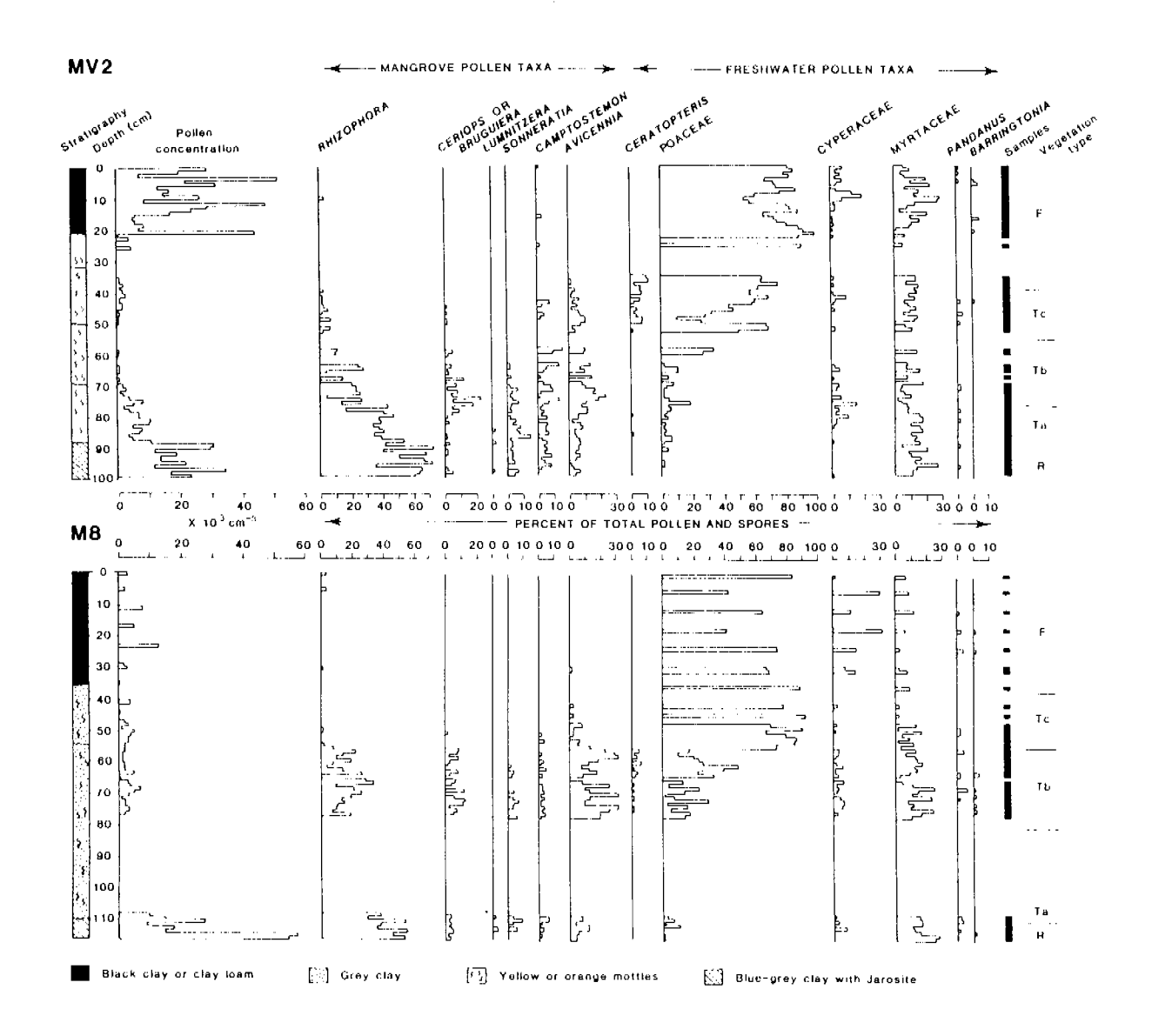


Figure 4.14 Stratigraphy, pollen concentration and relative pollen content of the top sections of cores MV2 and M8, with sample depths and the major vegetation/depositional environments indicated (R, Rhizophora forest; T, transition, subdivided into a, b, c; F, freshwater wetland). Only the dominant or indicator non-mangrove pollen taxa are included and their abundance is expressed as a percentage of all pollen and spores counted at each level. Contiguous 1 cm samples were taken from core MV2; where no results are given there were fewer than 20 pollen grains counted. In none of these oxidised samples was the pollen assemblage significantly different from well-preserved samples immediately above or below. Where there are no result from core M8, no samples were taken; all parts of the core samples had adequate pollen for counting.

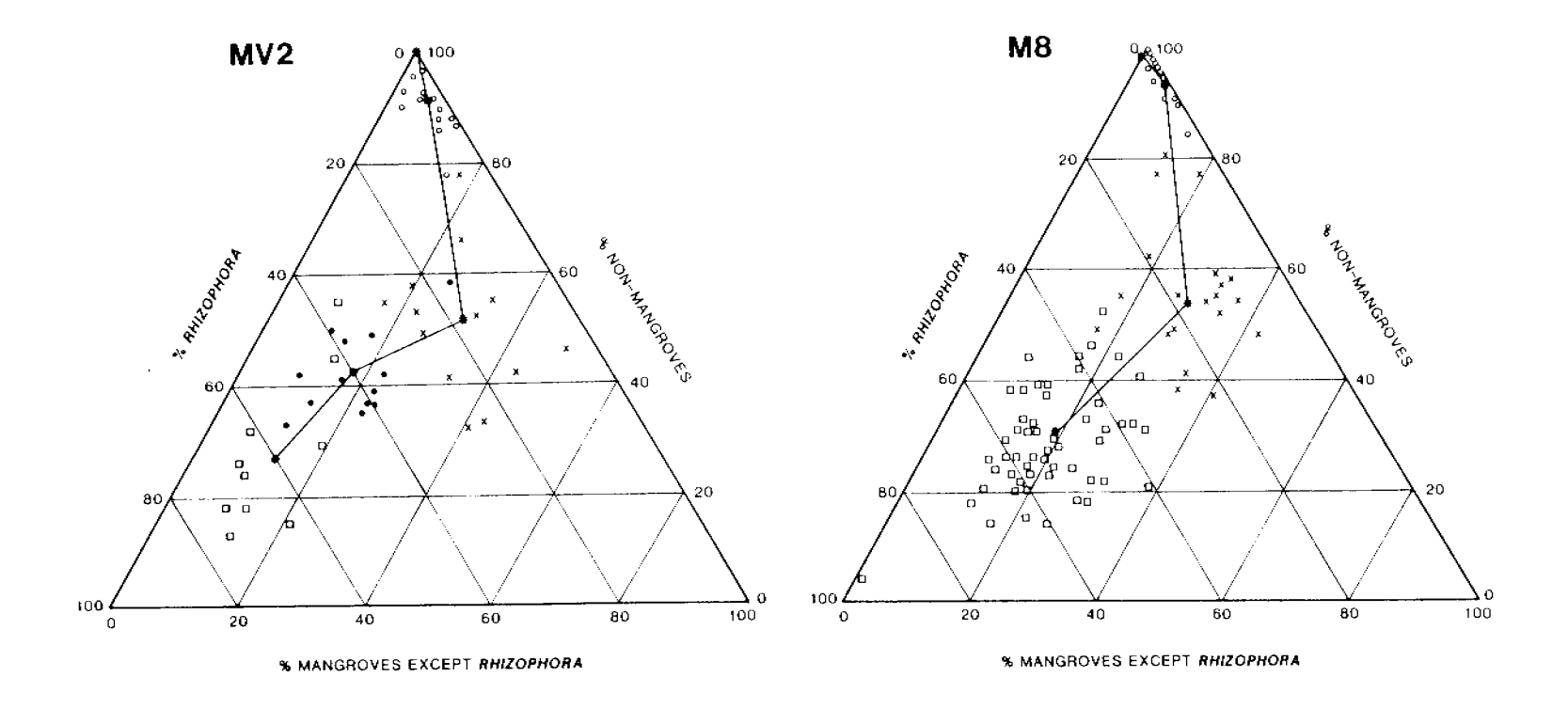


Figure 4.15 Ternary diagrams presenting changes in percentages of three groups of pollen taxa and all non-mangrove taxa:

Rhizophora, other mangroves, and all non-mangrove taxa (freshwater and terrestrial). Different symbols are given for samples within each vegetation type: squares are Rhizophora forest (MV2, 99-89 cm; M8, 781-110 cm); closed circles are Transition a (MV2, 89-76 cm; for M8, the two samples from this period, 108-110 cm, have been included with those from the Rhizophora forest); crosses are Transition b (MV2, 76-58 cm; M8, 77-75 cm); open circles are Transition c (MV2, 58-39 cm; M8, 55-c. 39 cm). Samples from the freshwater period are not shown as almost all fall on the 100% non-mangrove vegetation point. Means for each vegetation type are shown by asterisks and the lines connecting them indicate the direction of change from Rhizophora forest to freshwater wetland.

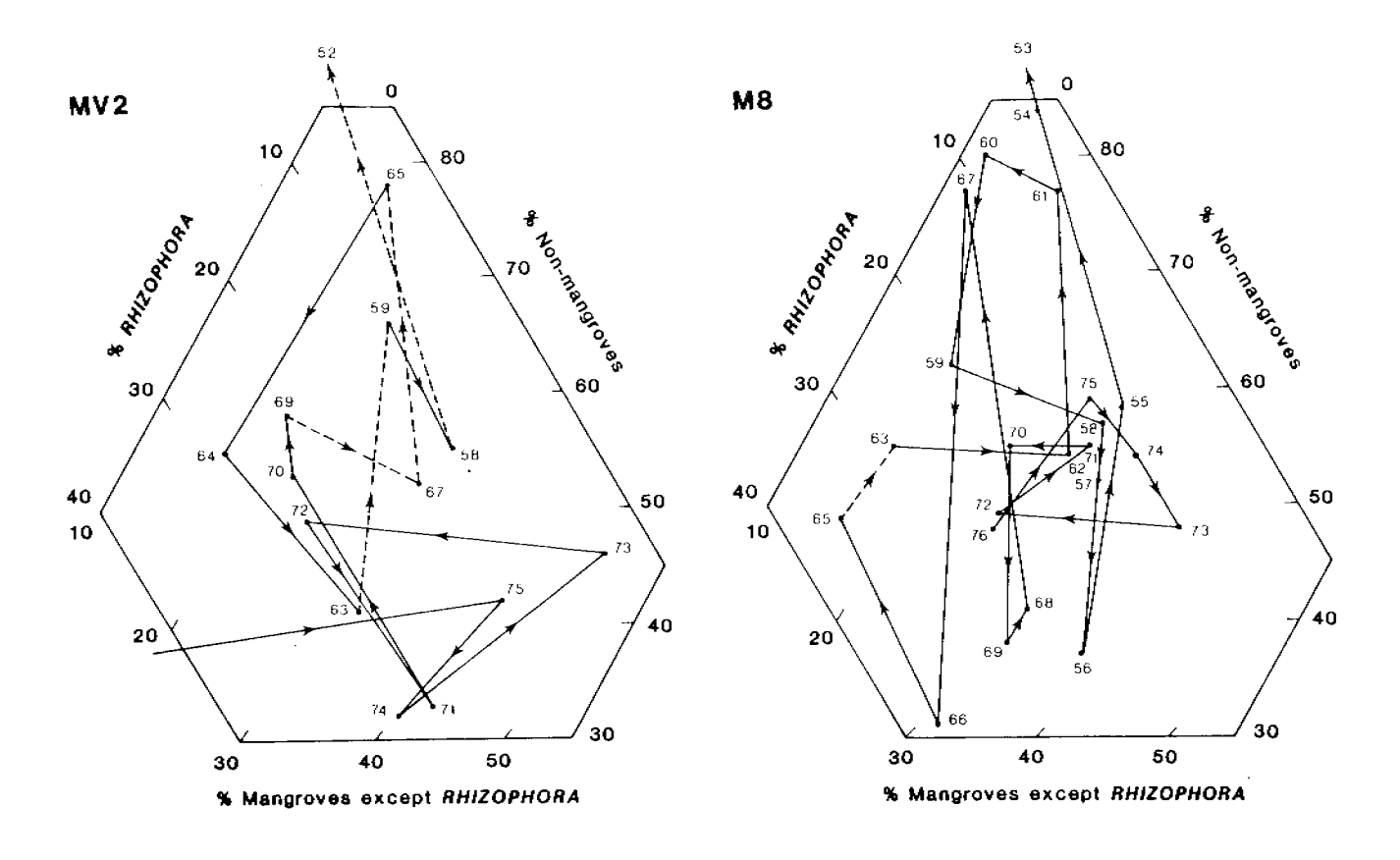


Figure 4.16 Enlargement of part of the ternary diagrams in Figure 4.15, showing samples in transition phase b (Fig. 4.14) labelled with their depths in centimetres in cores MV2 and M8. Lines connect adjacent samples and arrows indicate the direction of change; dashed lines connect sequential samples where intermediate samples were missing or contained insufficient pollen.

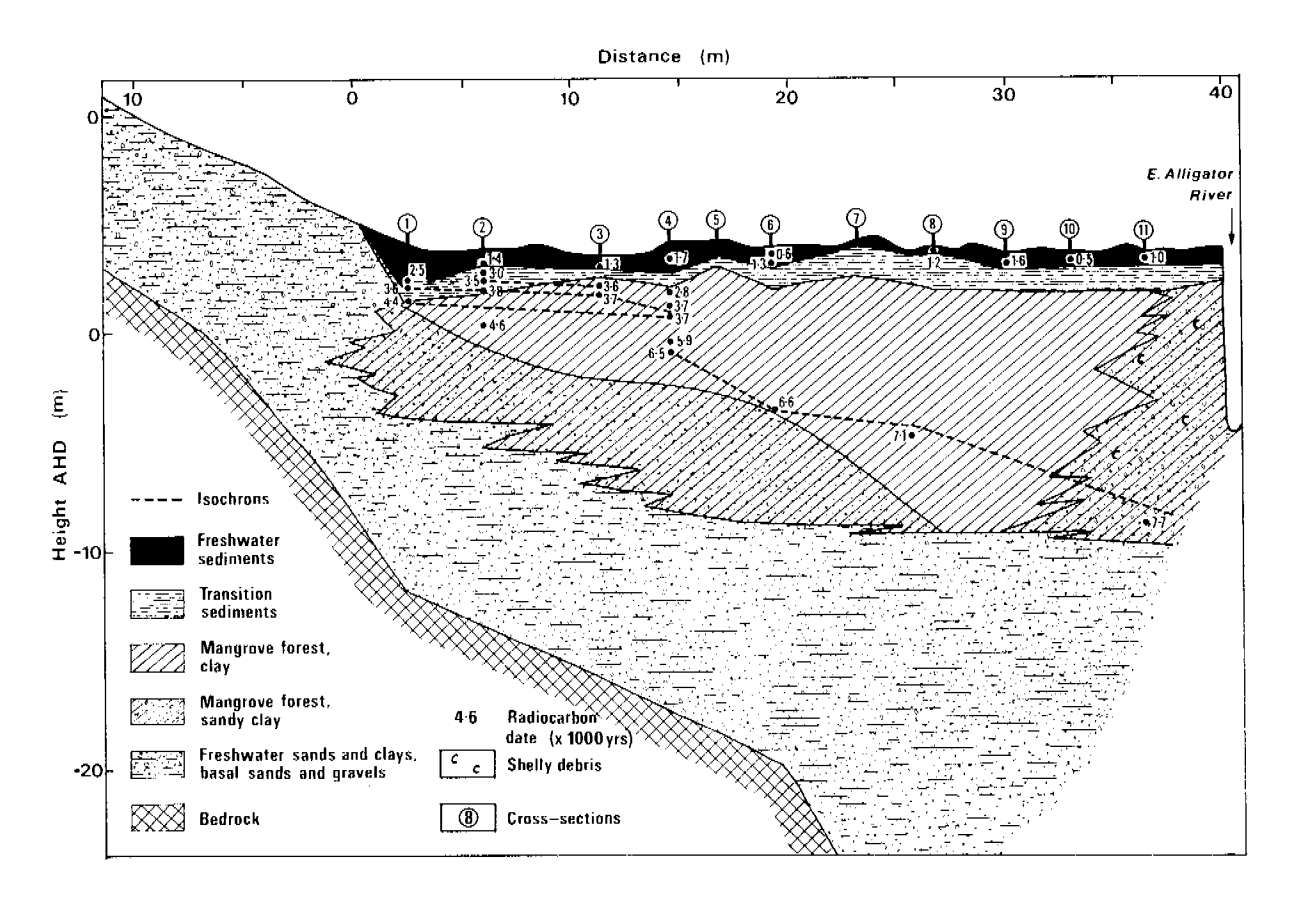


Figure 4.17 A longitudinal section of the Magela Plain showing the major sedimentary environments

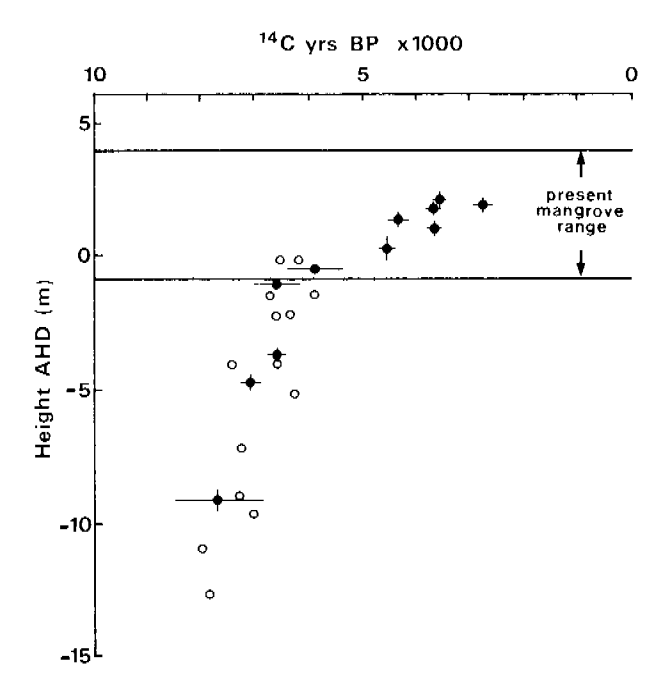


Figure 4.18 Depth-age plots showing dates from the Blue-Grey Clay mangrove forest sediments and the 'basal samples' of Woodroffe et al. (1986). These data chart the course of sea level rise in the two palaeoestuaries of the Magela and South Alligator respectively.

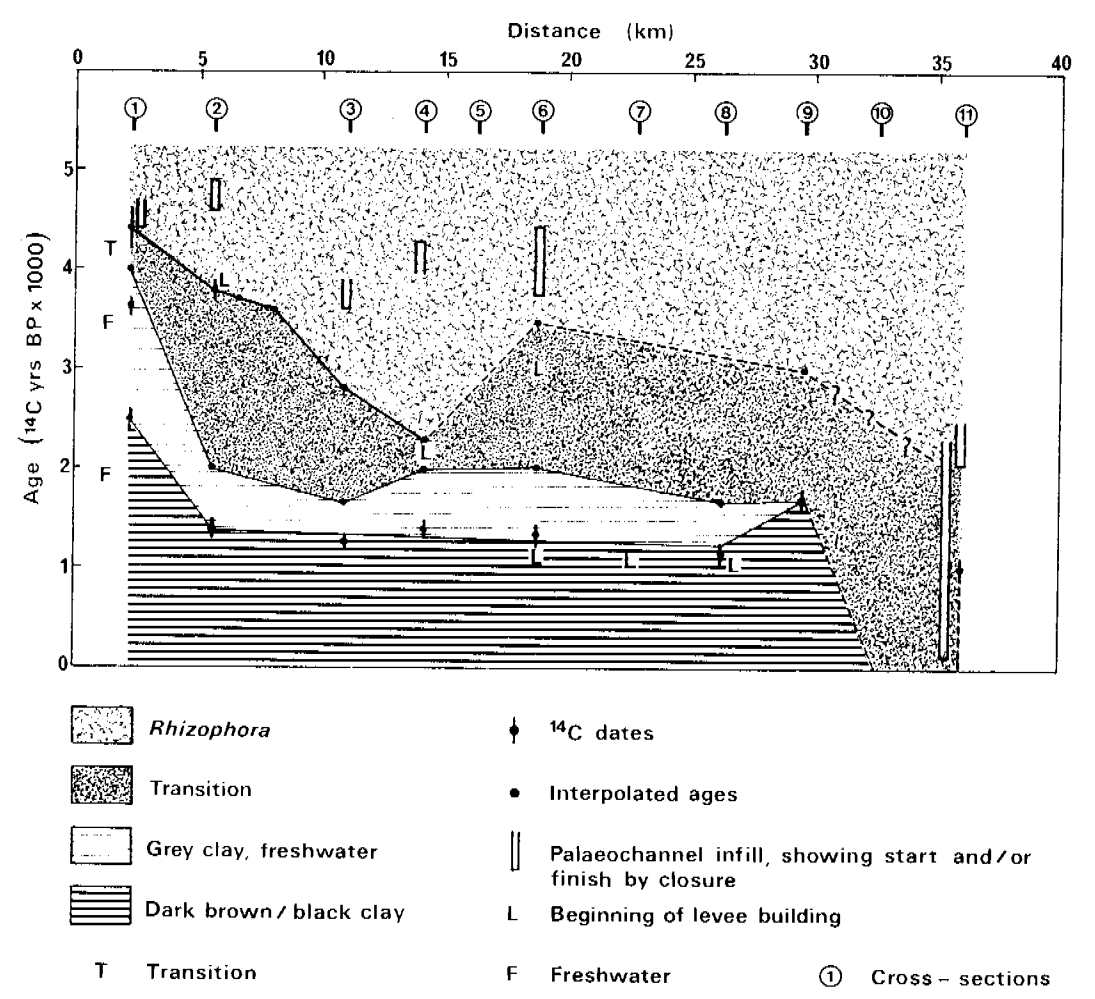


Figure 4.19 Age-distance plot of the sedimentary environments of the Magela Plain, projected onto a longitudinal section. The sedimentary environment shown at a particular distance and time is the dominant. At 2.5 ka there must have been a tidal channel (with flanking mangroves) extending from the E. Alligator River to cross-section 4, but only the dominant (transitional) sediments are shown downstream of this cross-section.

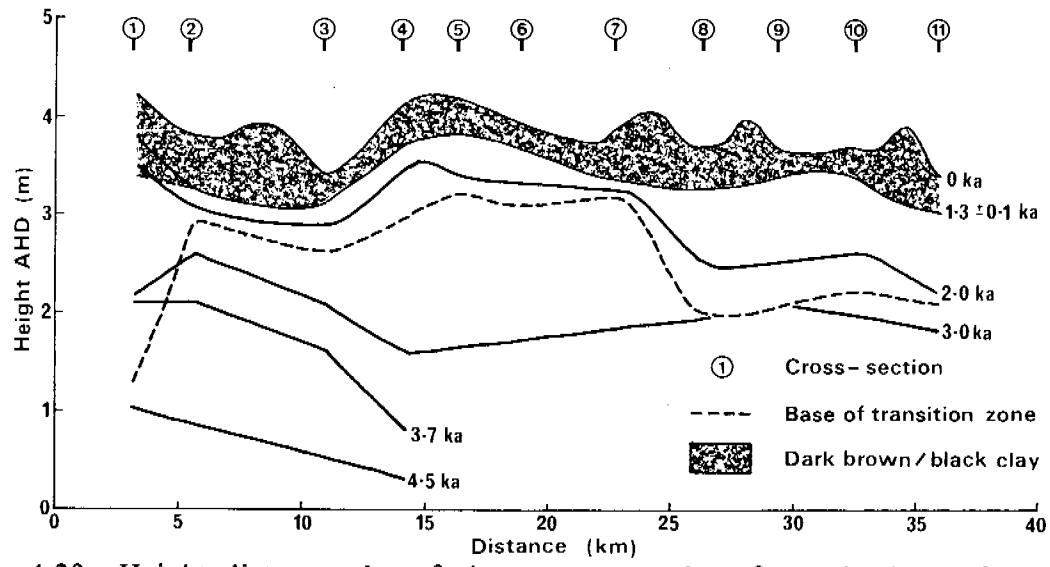


Figure 4.20 Height-distance plot of the mean ground surface, the base of the Dark Brown/Black Clay, the base of the transition zone and various isochrons. The dashed lines are plots of height and distance and are not isochronous.

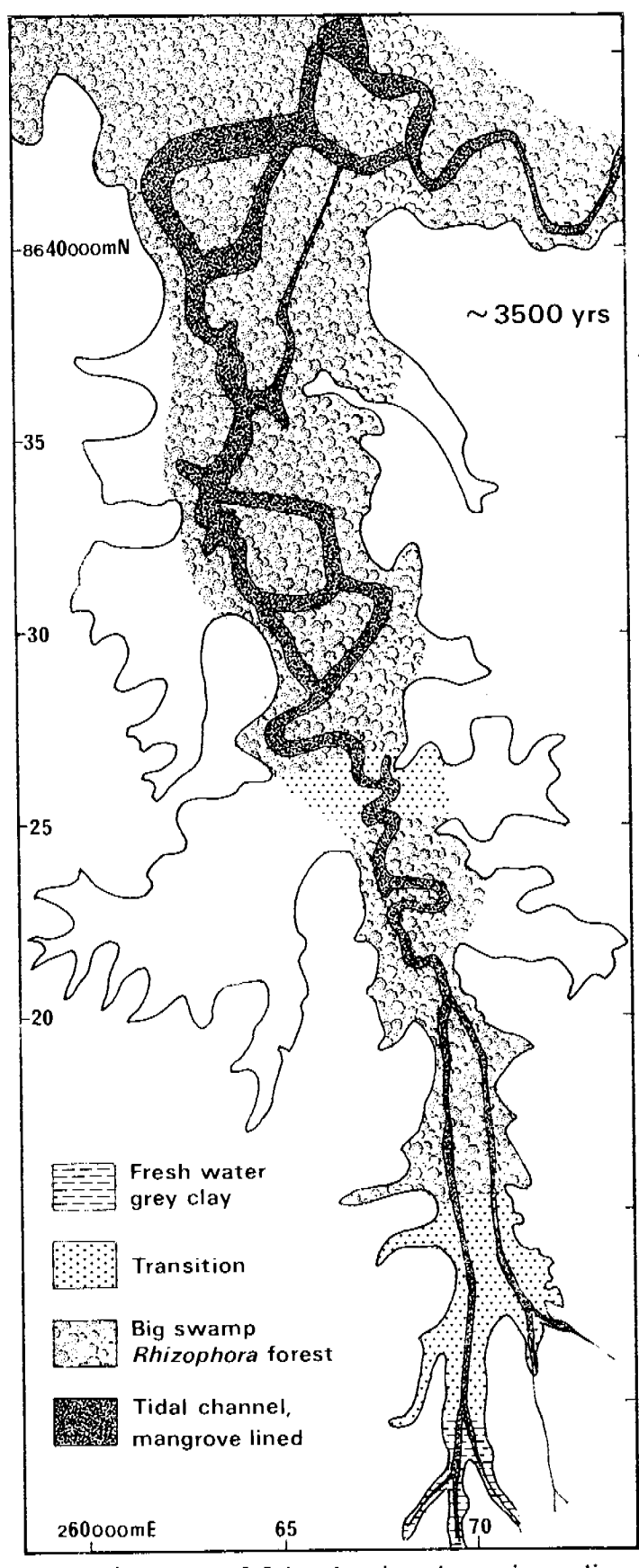


Figure 4.21 Palaeogeographic map at 3.5 ka showing the major sedimentary environments then in existence

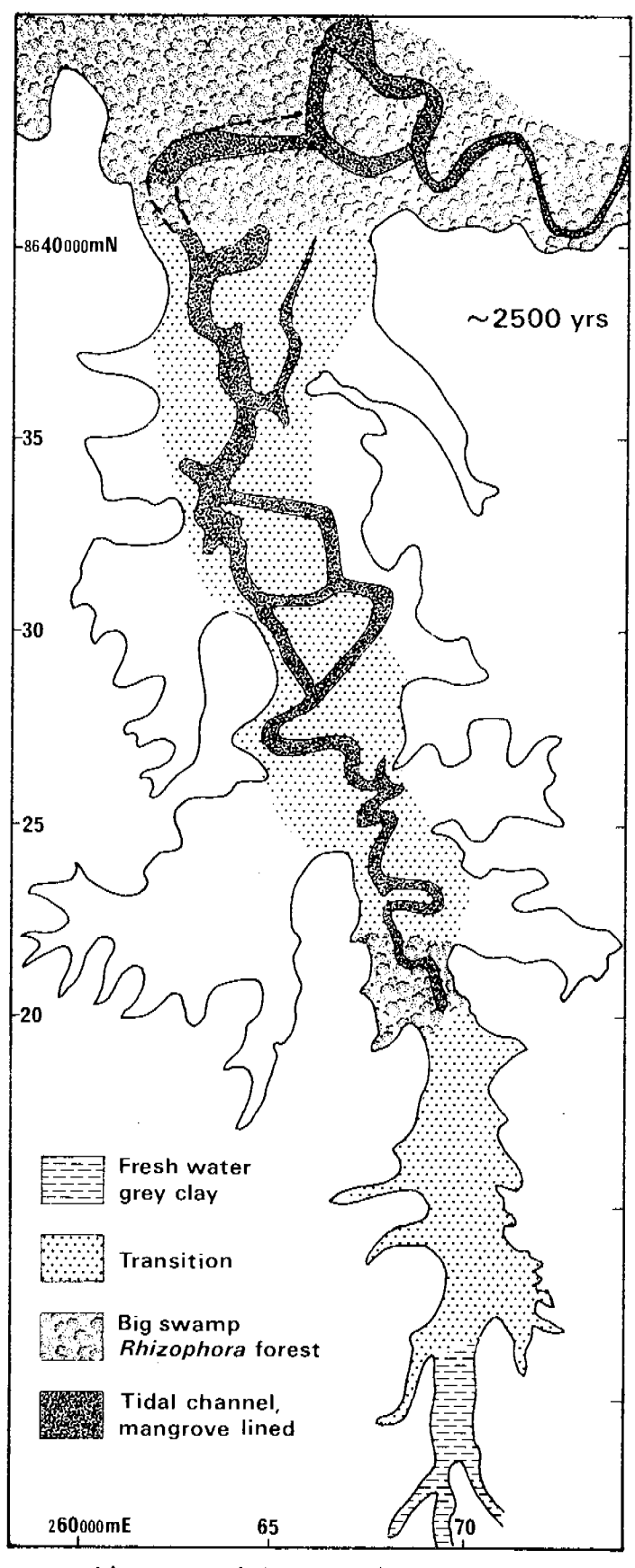


Figure 4.22 Palaeogeographic map at 2.5 ka showing the major sedimentary environments then in existence

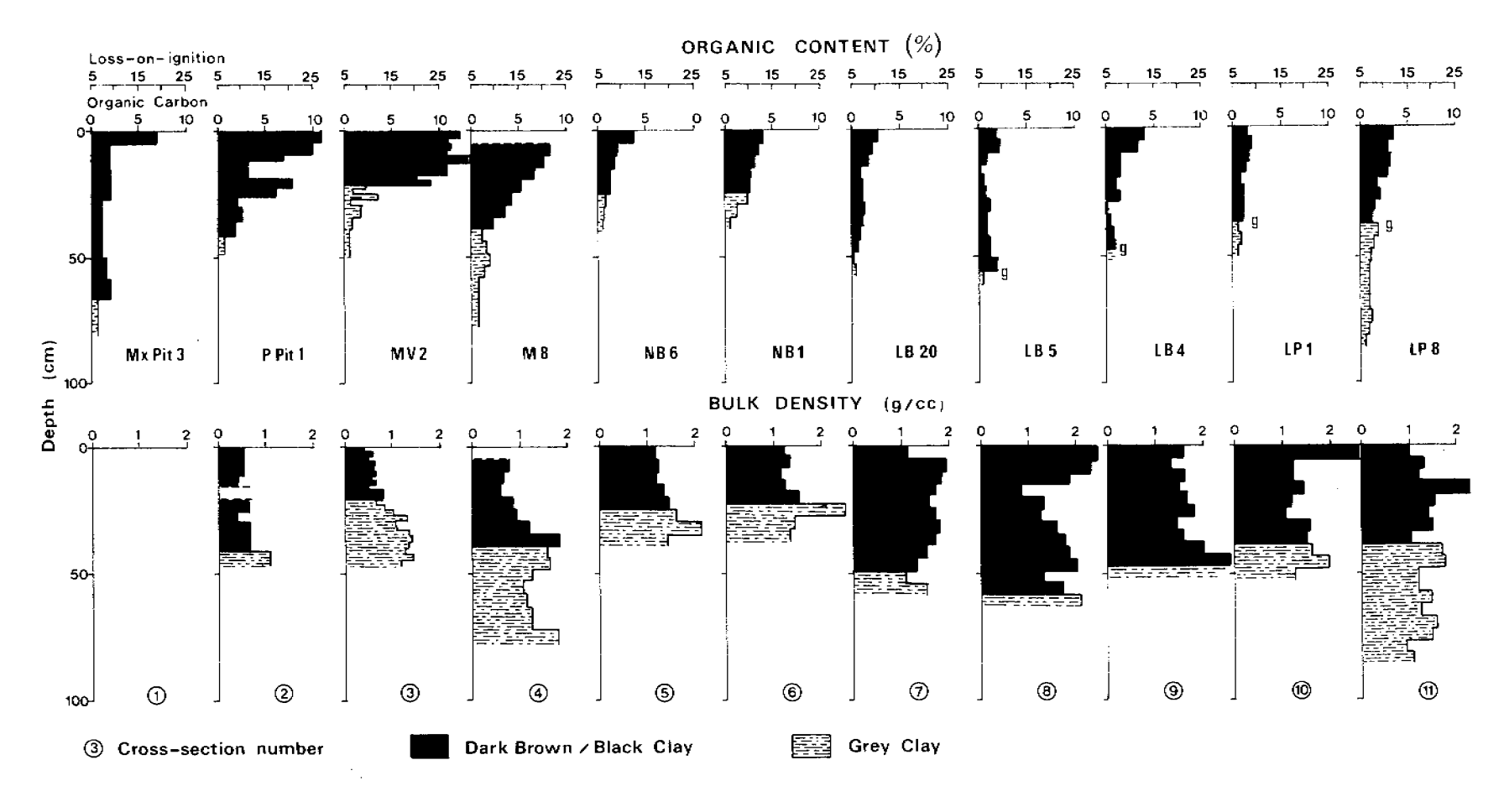


Figure 4.23 Depth profiles of sites on the Magela Plain showing organic content (top) and bulk density (bottom). The organic content in each case was measured as loss-on-ignition (LOI) and these measurements were converted to organic C by means of a regression between LOI and Walkley-Black organic C determined for a set of samples from the Magela Plain.

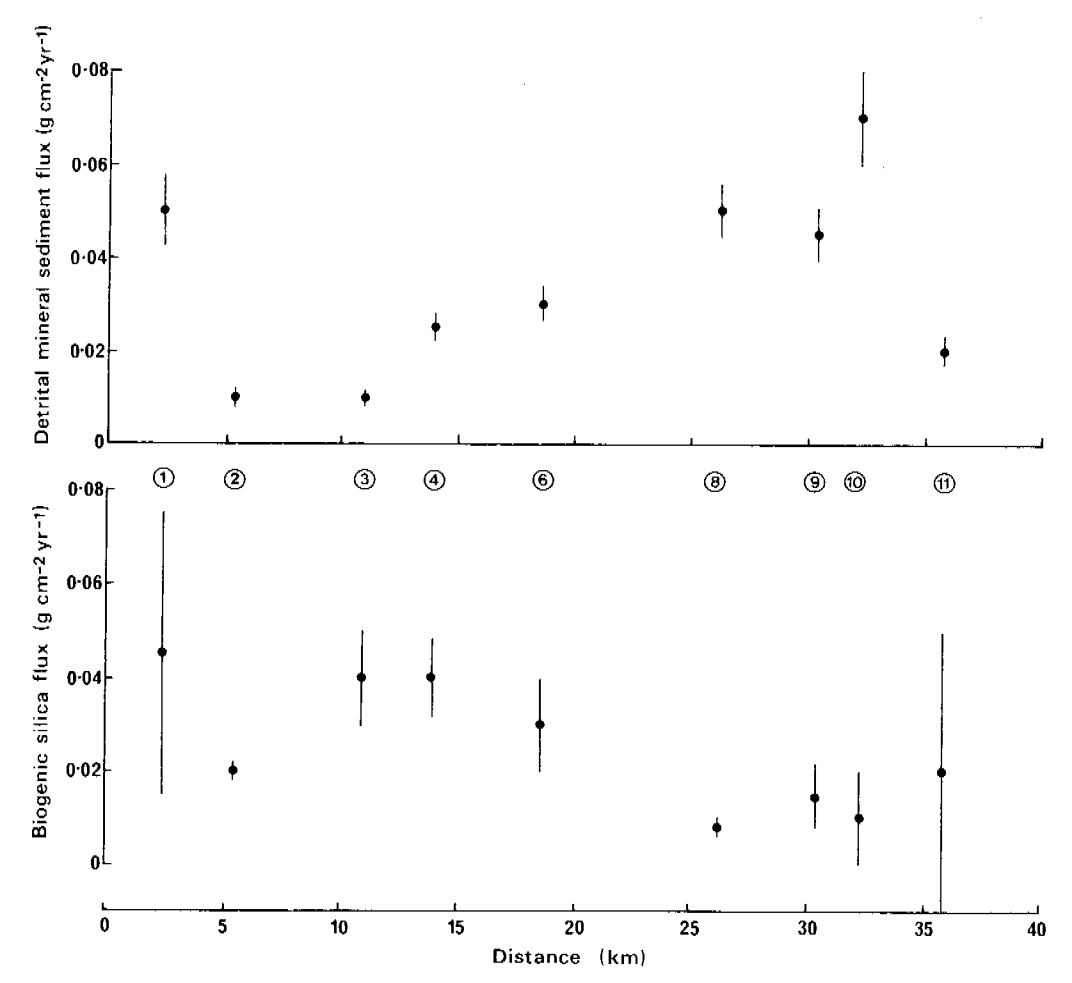


Figure 4.24 Flux to the Magela Plain of detrital mineral sediment and biogenic silica. The values are average $(\pm 1\sigma)$ at numbered cross-sections for the entire depth of the Dark Brown/Black Clay. Distance along the sampling grid is shown.

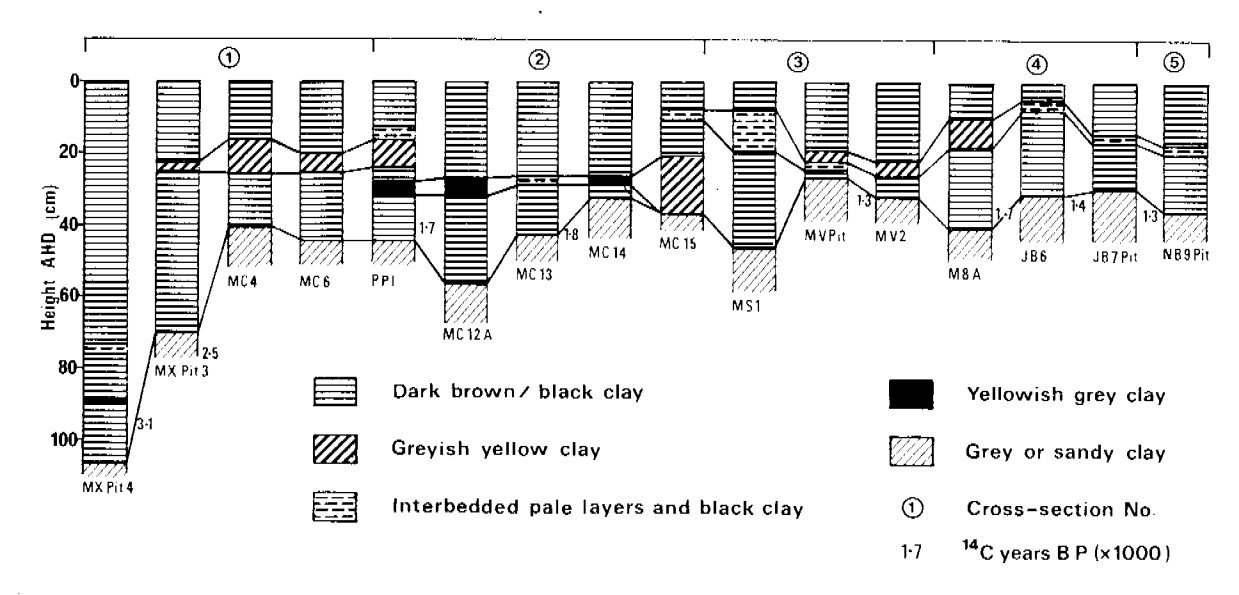


Figure 4.25 Lithostratigraphic diagrams of selected sites on the Magela Plain showing the various kinds of pale layers and their most likely correlations

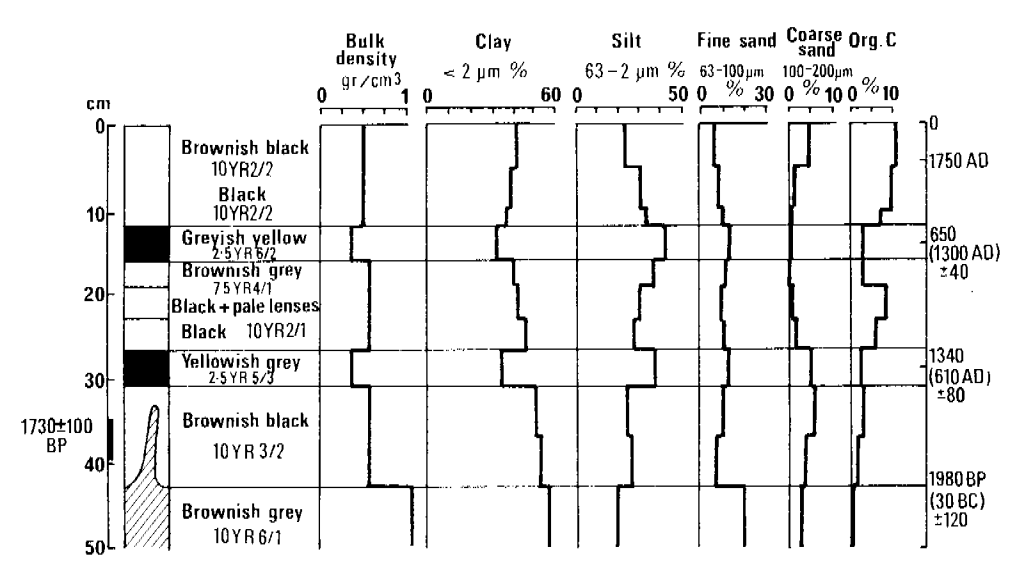


Figure 4.26 Site P Pit 1 on cross-section 2, showing lithostratigraphic subdivisions, colours determined on dry samples, bulk density, particle size and organic C determined by the Walkley-Black method. A radiocarbon date is shown on the left, and on the right, ages of important stratigraphic features estimated by using the ¹⁴C date and by assuming a constant rate of sedimentation of 1 cm in 46 years. The age datum (0 years) is not at the groundsurface because 1950 is the zero for ¹⁴C dates. The pale layers are highlighted.

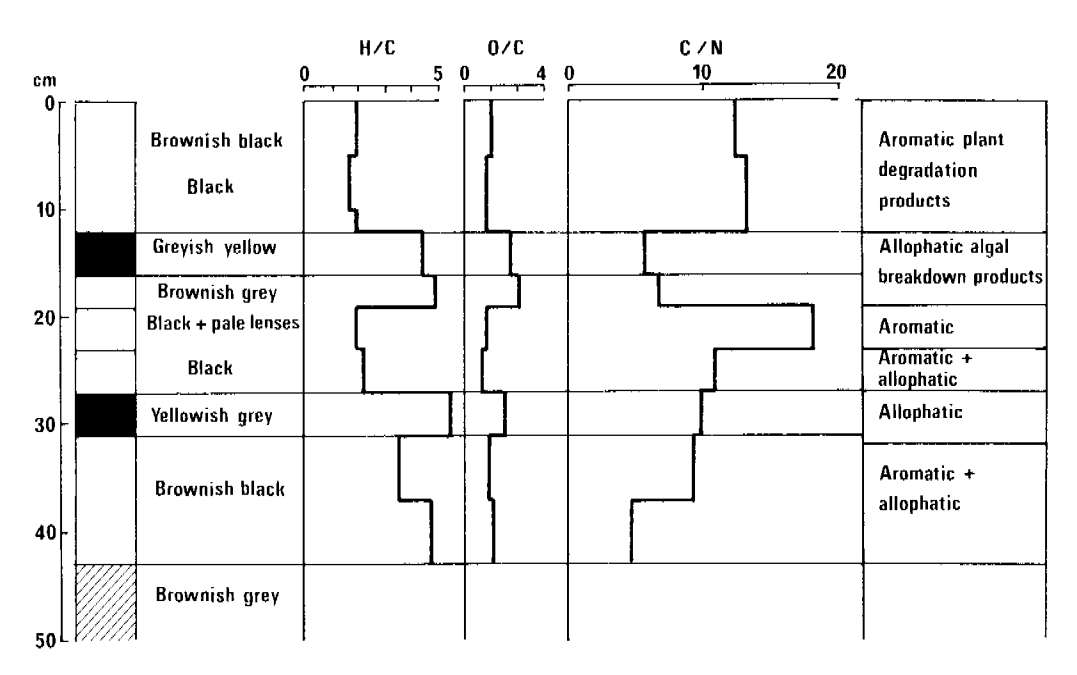


Figure 4.27 Atomic ratios of the major constituents of the organic matter in site P Pit 1, calculated to remove the effect of variations in the amount of organic matter in each sample. The pale layers are highlighted.

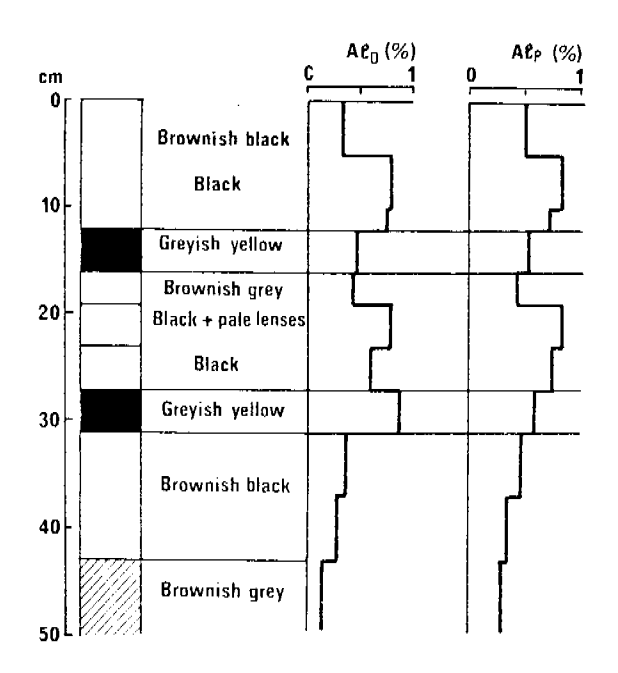


Figure 4.28 Site P Pit 1 showing dithionite-citrate and pyrophosphate extractable A1, $A1_D$ and $A1_p$ respectively

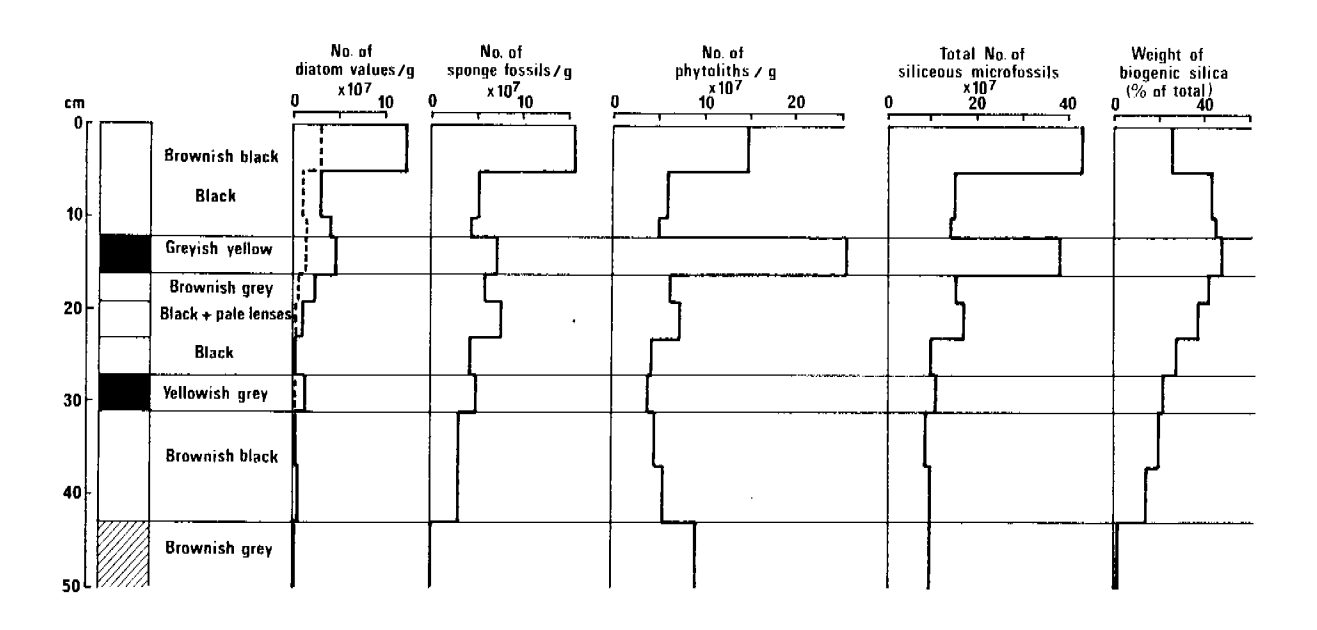


Figure 4.29 Site P Pit 1 showing siliceous microfossil mass % and concentrations, calculated on an organic matter free basis. The dashed line in the diatom valve column depicts *Eunotia camelus*.

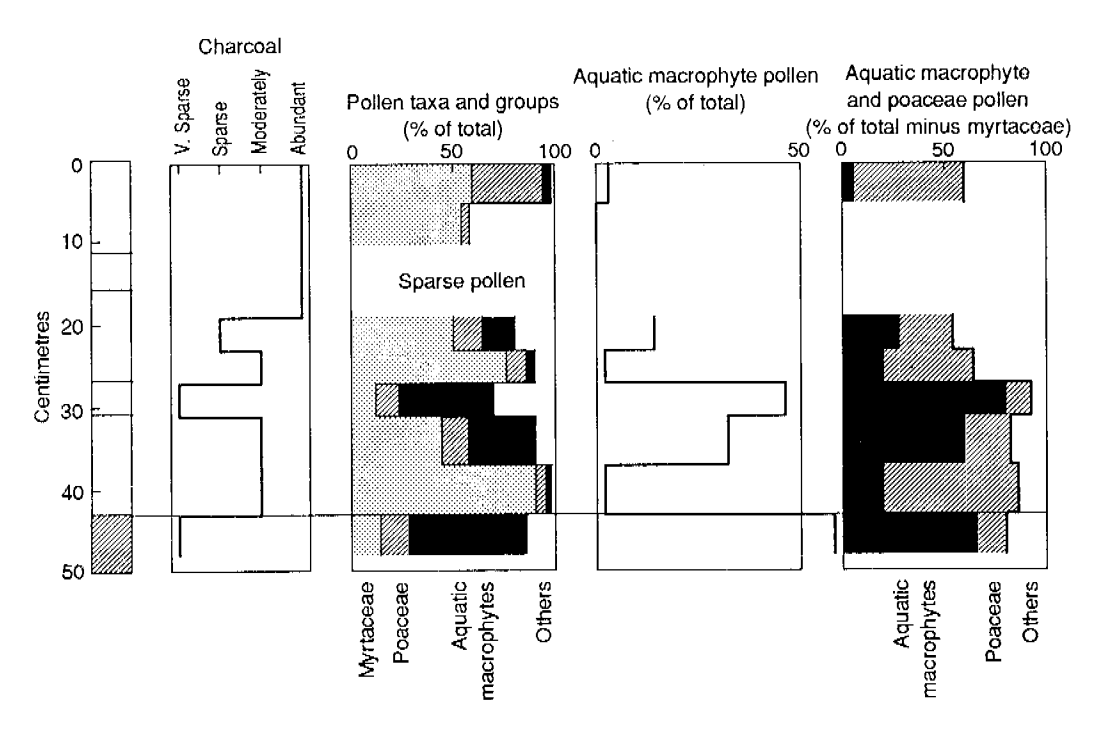


Figure 4.30 Site P Pit I showing the major pollen taxa and groups plotted in different ways and an indication of the amount of charcoal in the sediments

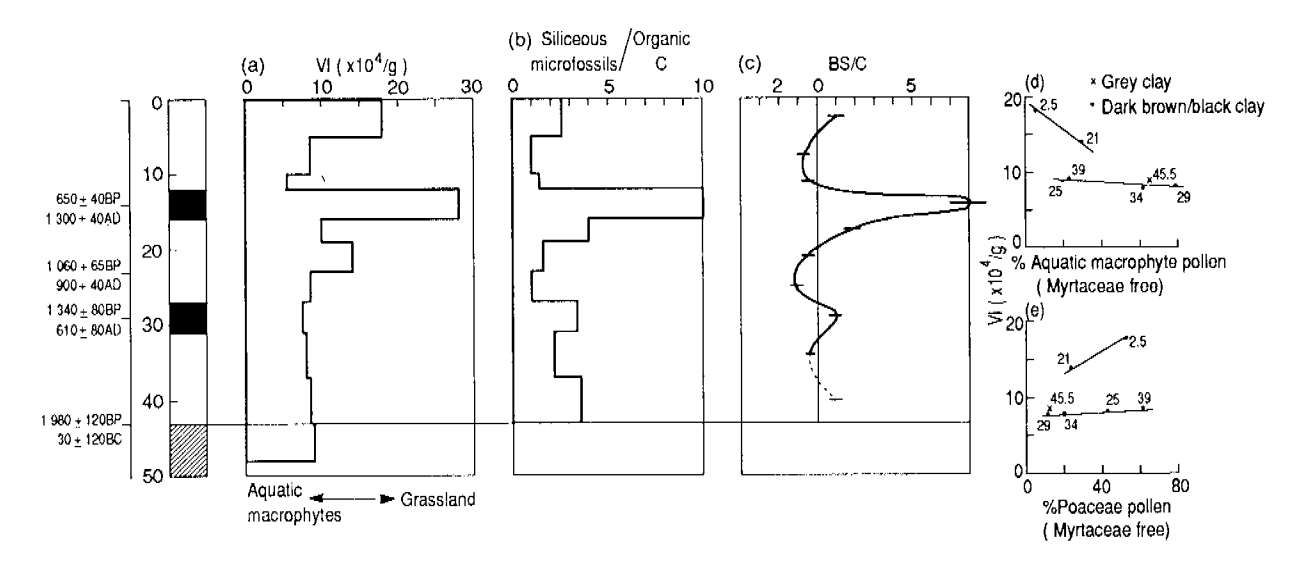


Figure 4.31 Site P Pit I showing: (a) the index VI; (b) the ratio of numbers of siliceous microfossils per gram and organic C content, reduced to an arbitrary scale of 0 - 10; (c) the residuals of the ratio from the linear least squares curve in b, with associated uncertainties; (d) VI plotted against per cent aquatic macrophyte pollen calculated on a Myrtaceae pollen free basis to remove the effect of long-lived plants; (e) VI plotted against per cent Poaceae pollen, also calculated to exclude Myrtaceae pollen

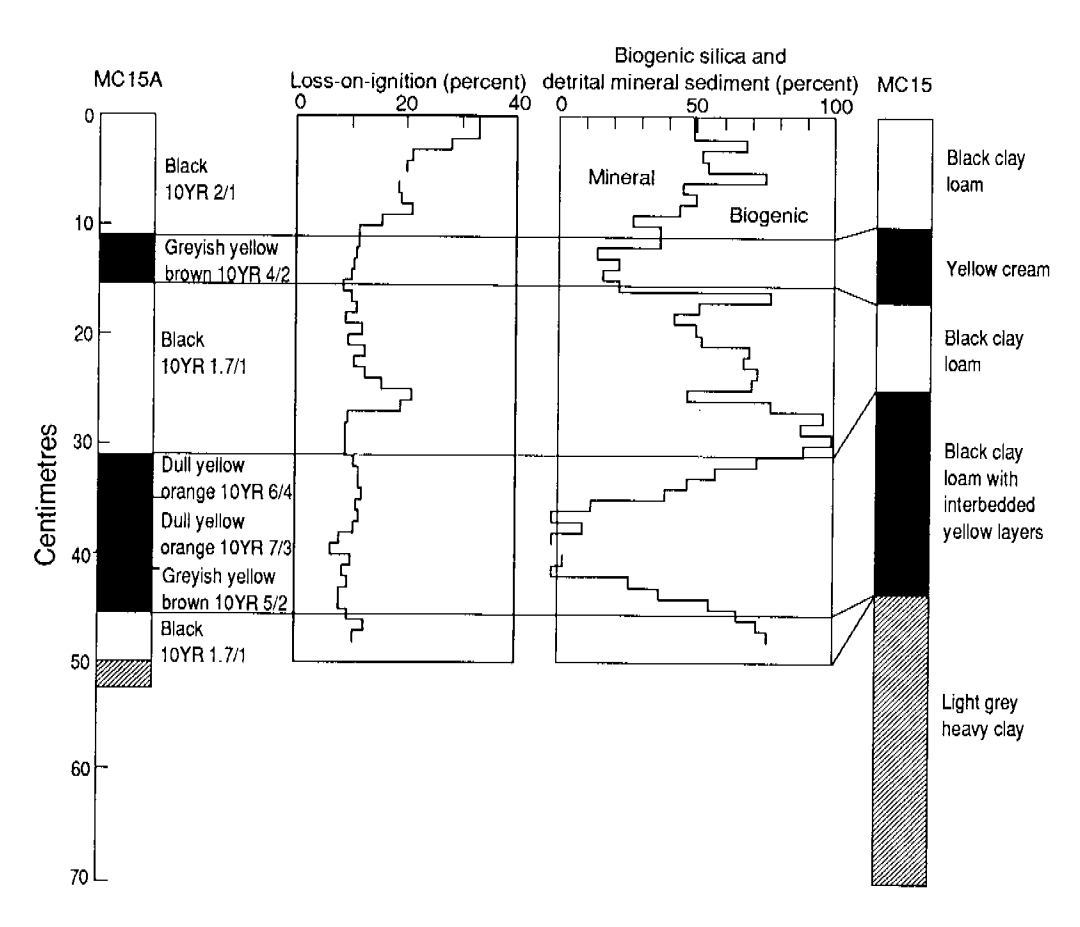


Figure 4.32 Site MC15A showing: a log of colour variations, loss-on-ignition and the proportion of biogenic silica and detrital mineral sediment. The major features of an adjacent core, MC15, are shown and correlated with MC15A.

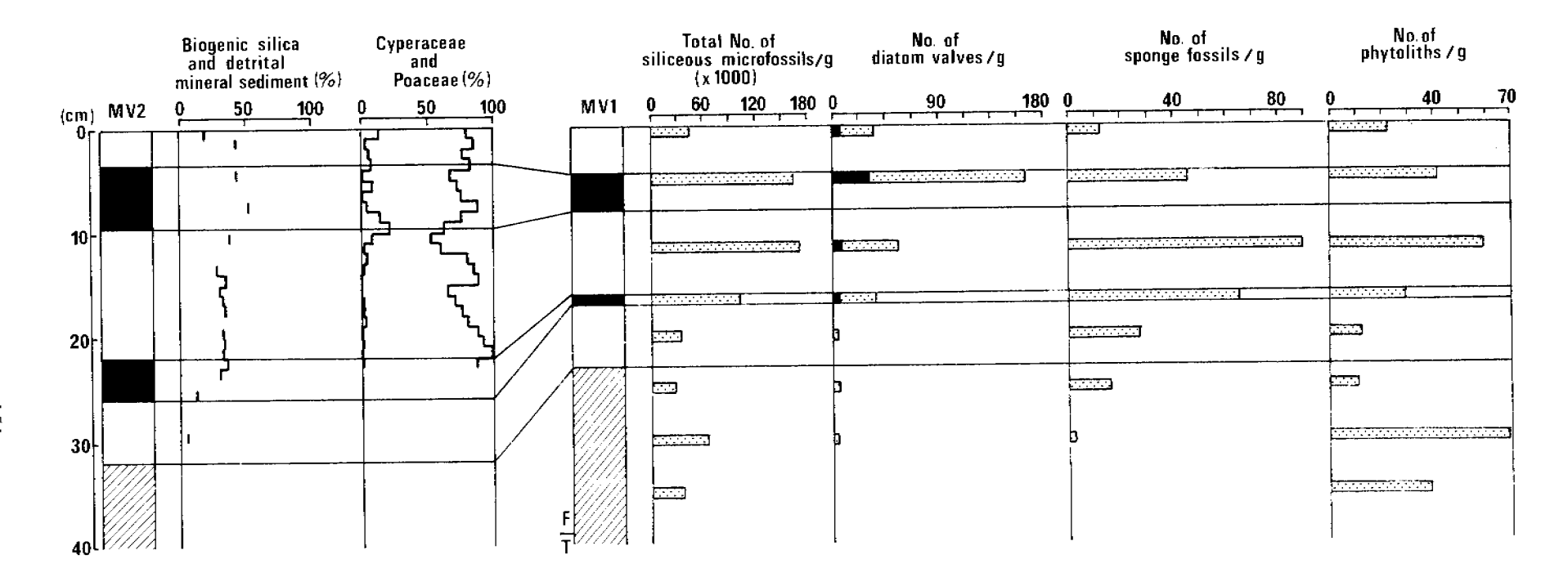


Figure 4.33 Site MV2/MV1, adjacent cores on cross-section 3. Correlation of the cores allows the joint use of measurements made on both cores. The measurements of siliceous microfossils are also provided in Table 4.5. The hatched part of the column showing 'number of diatom valves/g' depicts variations in *Eunotia camelus*. T is transition and F is freshwater.

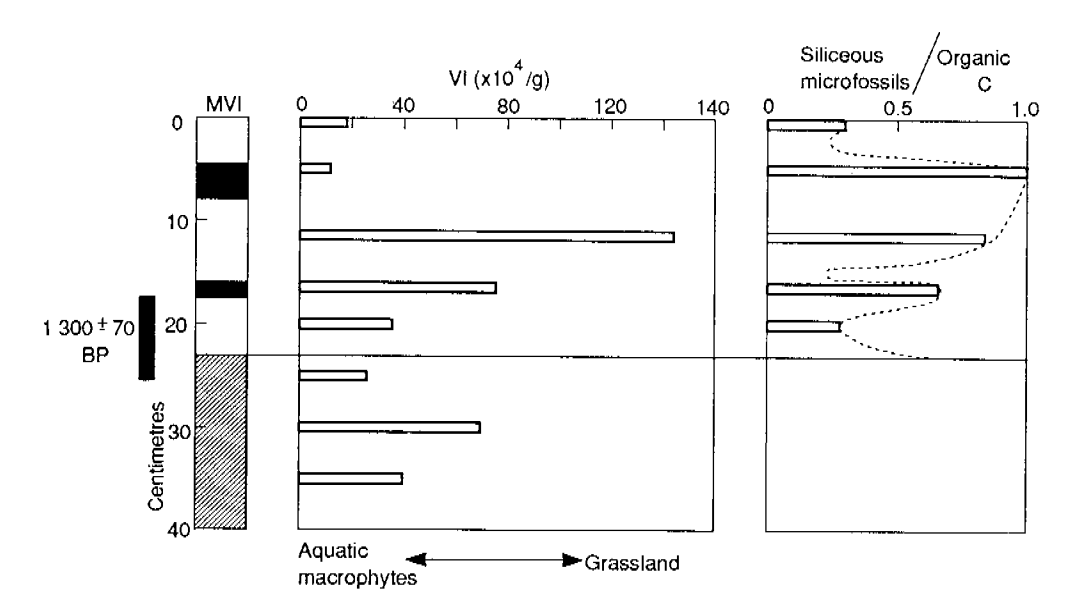


Figure 4.34 Site MVI showing the index VI and the quantity of total siliceous microfossils/organic C. The date is actually derived from MS Pit (Table 3.6) at the site of MSI on Fig. 4.3. The date is shown in its equivalent position.

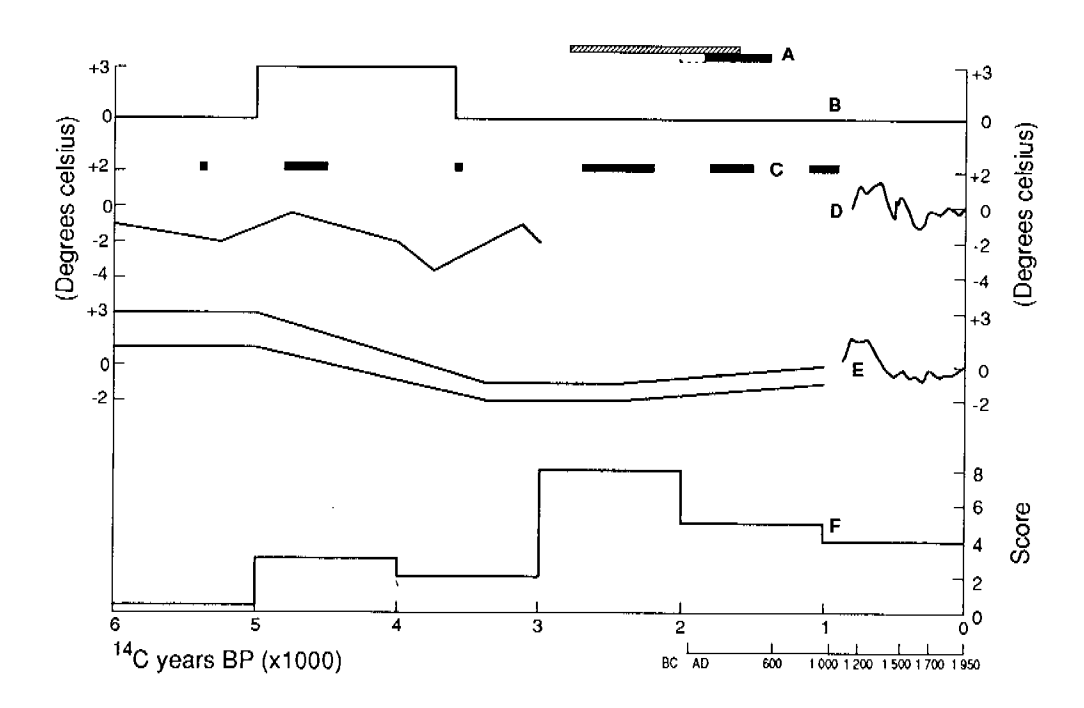


Figure 4.35 Palaeoenvironment records for the last 6 ka. A: Cross-hatched box shows the period of chenier formation that Lees and Clements (1987) argue occurred during a dry period; the filled and dashed boxes show the definite and likely period of deposition of the freshwater Grey Clay. B: palaeotemperature derived by Kershaw and Nix (1989) from the Atherton Tableland. C: Cool episodes in the Southern Hemisphere, from Burrows (1979). D: Palaeotemperature derived from δ¹8O in a speleothem in a Tasmanian cave (left) (Goede & Hitchman 1984) and from a speleothem in a New Zealand cave (Lamb 1977; Hendy & Wilson 1968). E: Palaeotemperature for Europe and North America, after Lamb (1966, 1977). F: Dune age scores from central and southeastern Australia, after Wasson (1986, 1989).

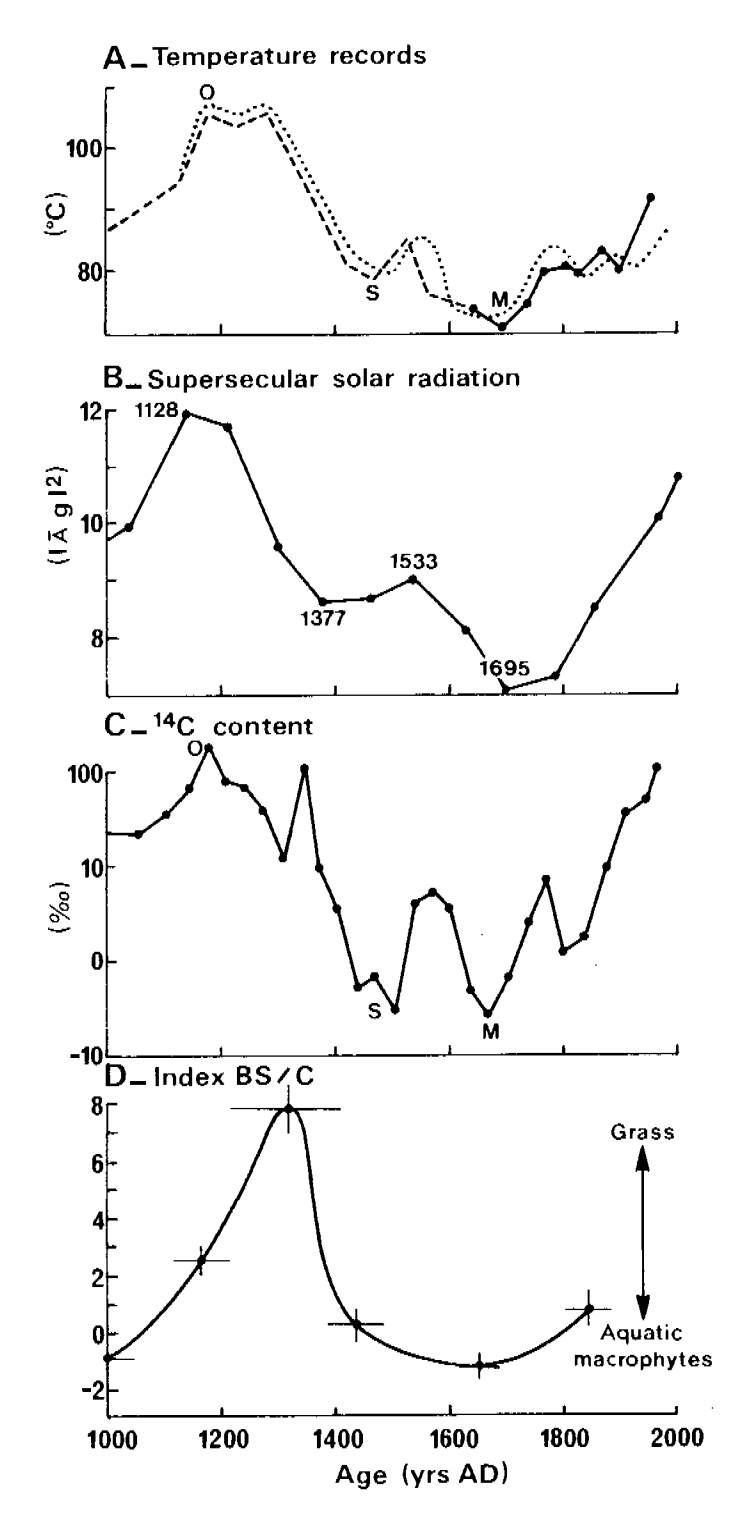


Figure 4.36 A: Temperature records from central England (solid line) after Lamb (1966, 1977) and New Zealand (dotted line) after Hendy & Wilson (1968). B: Supersecular variation in the energy of the secular wave, from Landscheidt (1987). C: ¹⁴C content of tree rings, after Damon (1977). D: The index BS/C for site P Pit 1 on the Magela Plain. O is the Medieval maximum, S the Spörer minimum, and M the Maunder minimum.

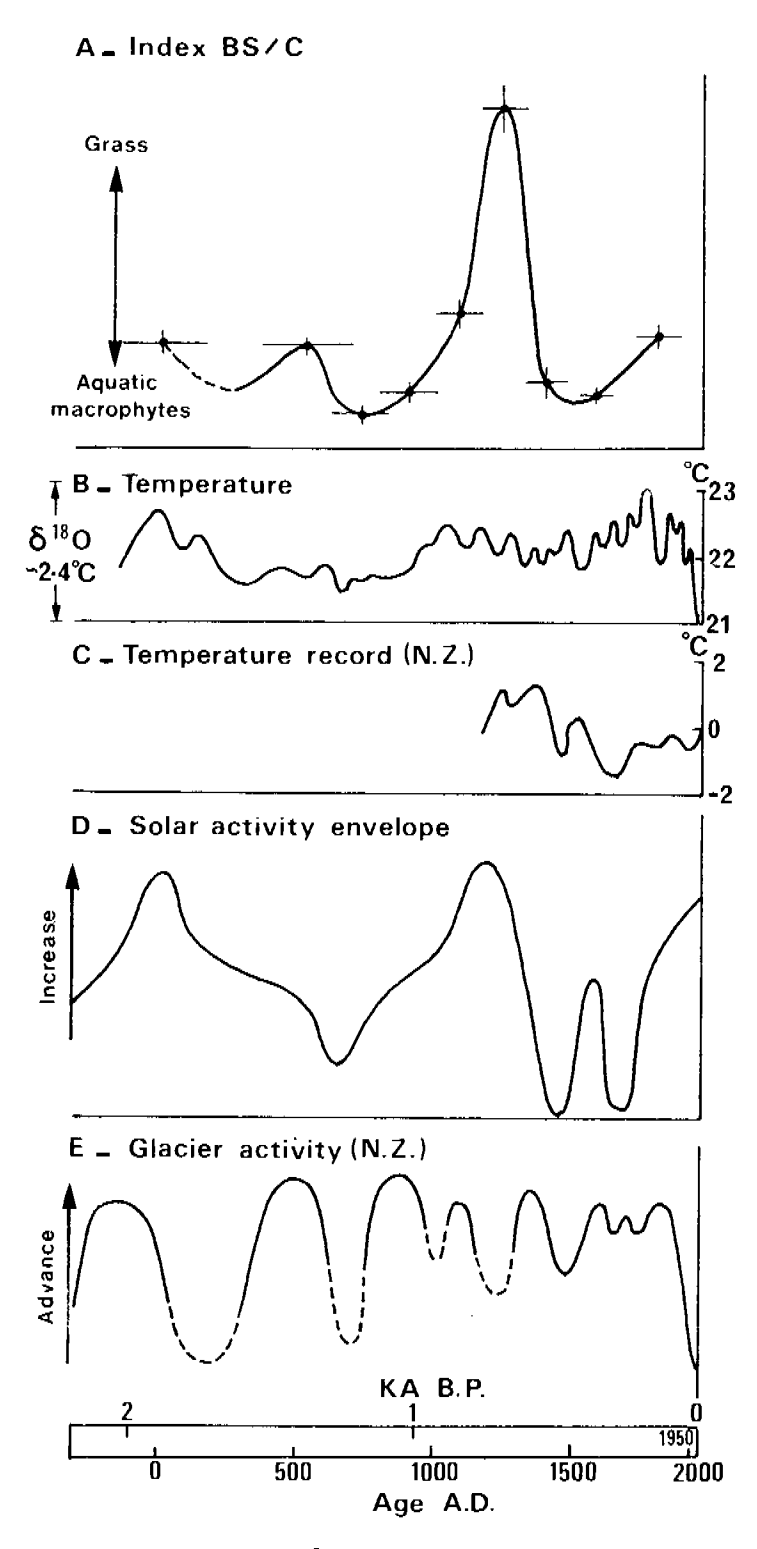


Figure 4.37 A: BS/C in P Pit 1. B: δ18O and an approximate temperature scale obtained from an ice core from Law Dome in East Antarctica (Etheridge & Morgan 1989). C: New Zealand temperature record (from Hendy & Wilson 1968). D: Solar activity envelope (from Eddy 1977). E: Glacier advances and retreats in New Zealand (from Röthlisberger 1986).

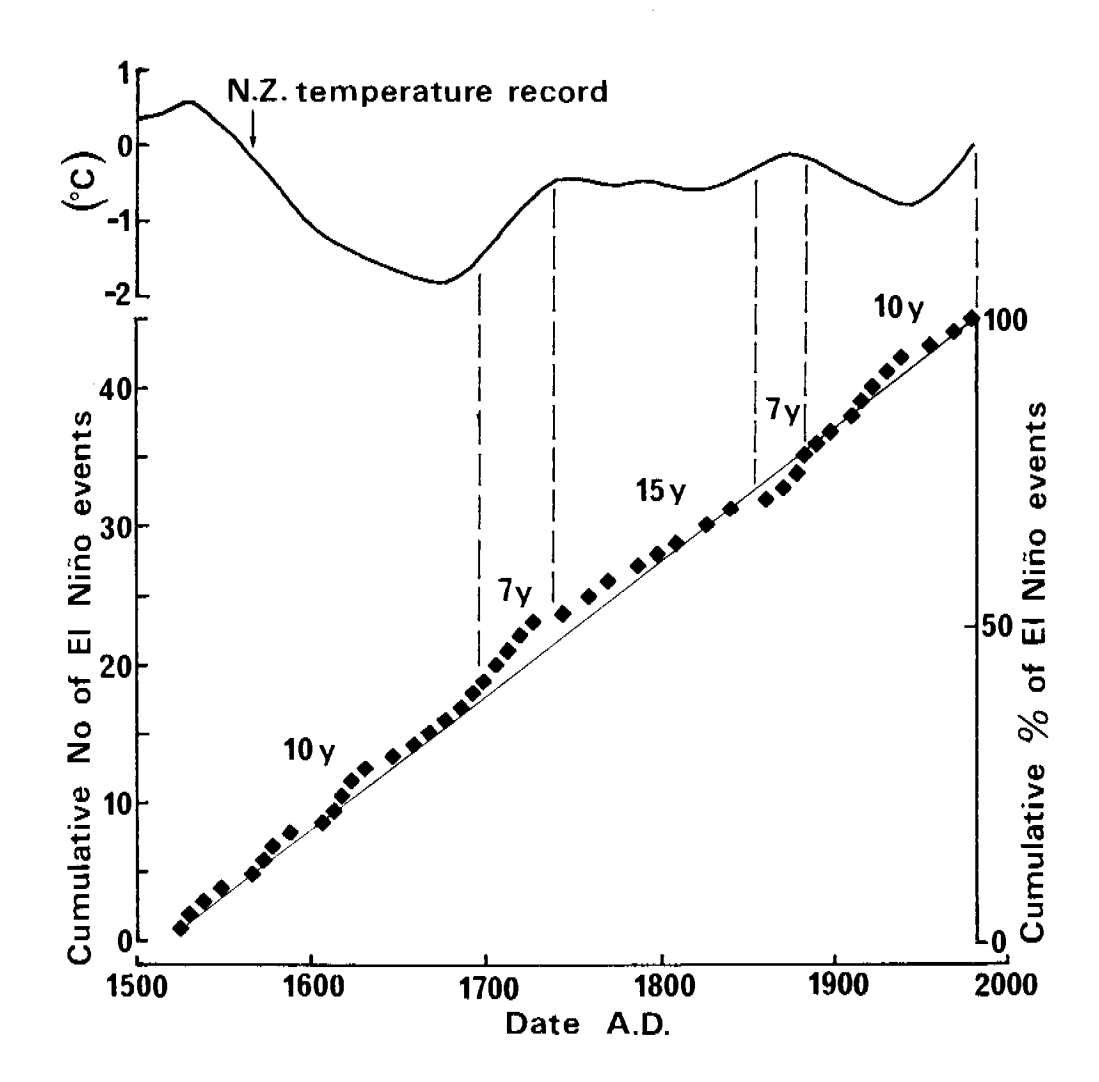


Figure 4.38 Top: New Zealand temperature record (from Hendy & Wilson 1968). Bottom: Cumulative number of El Niño events since 1523 AD (from Quinn et al.1987). The mean number of years between events is shown for various segments of the cumulative curve.

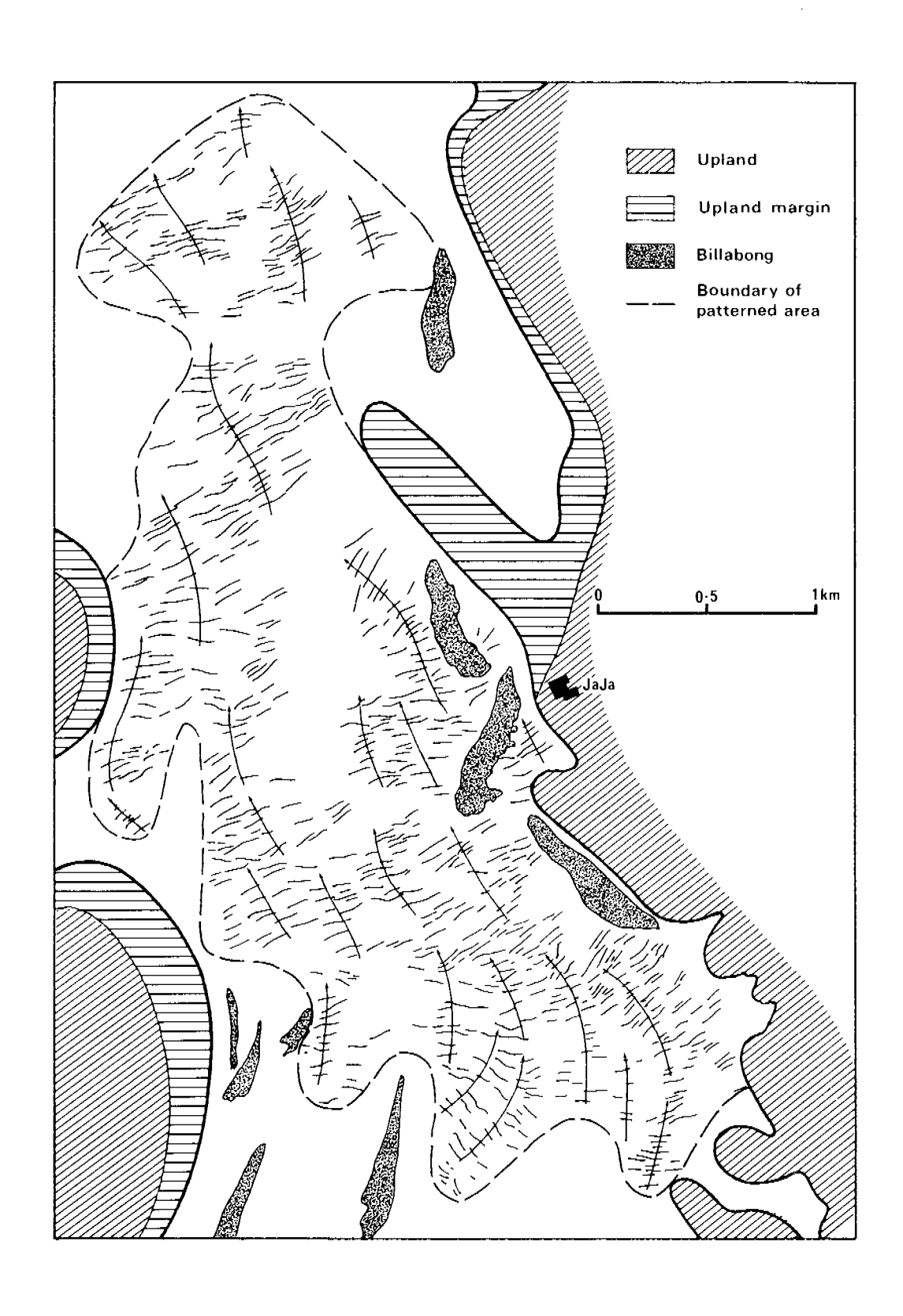


Figure 4.39 Map of the Upstream Basin showing the pattern of ridges and troughs and orthogonals to this pattern which are flow lines

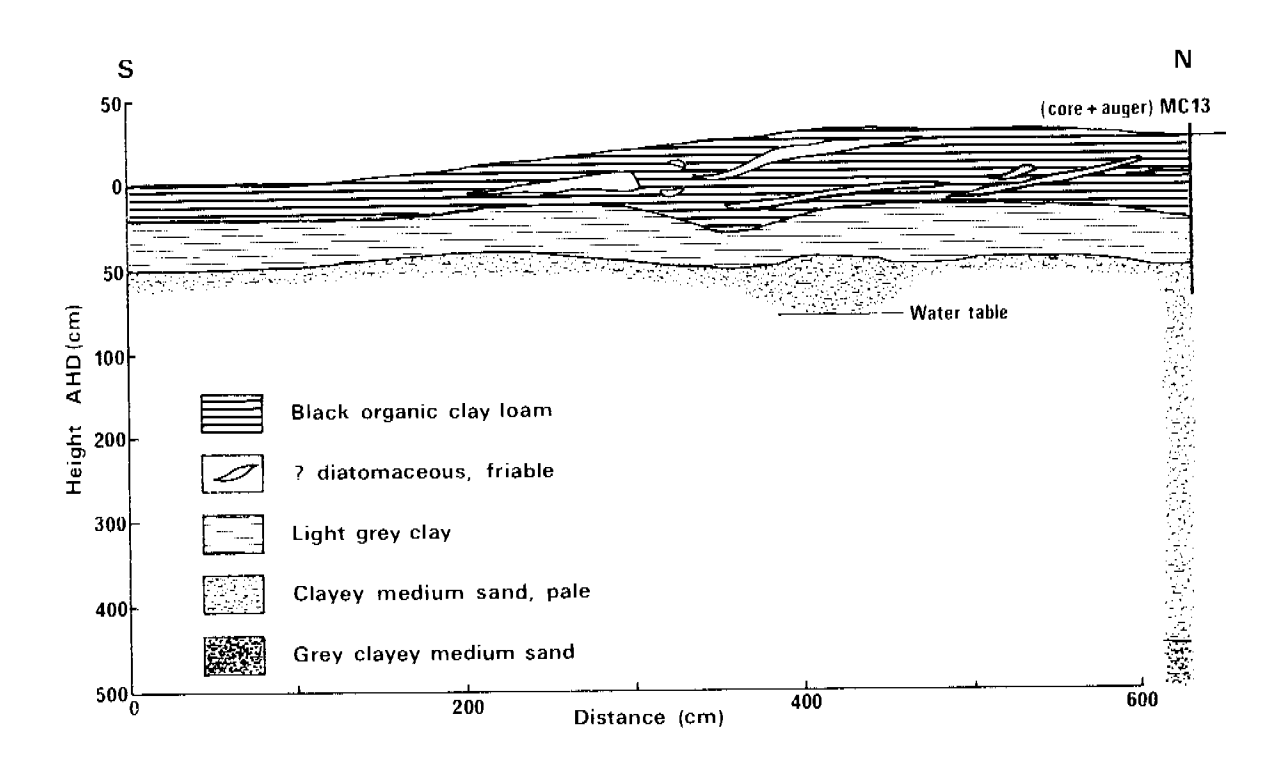


Figure 4.40 Trench 1 through a trough (left) and a ridge (right) in the Upstream Basin on cross-section 2. The diagram shows the deformation of the Dark Brown/Black Clay, made visible by shearing of the pale layers.

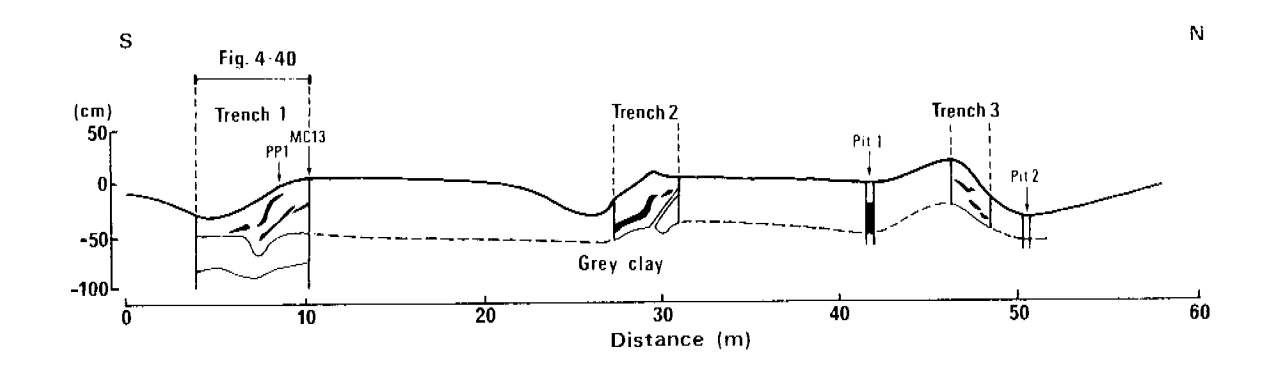


Figure 4.41 Trenches 1, 2, 3 and pits dug into ridges and troughs across cross-section 2. Details of trench 1 are shown in Fig. 4.40

CHAPTER 5. SOIL MATERIALS AND THEIR FORMATION ON THE MAGELA PLAIN

5.1 INTRODUCTION

The environments of deposition that produced the various bodies of sediment that constitute the surface and subsurface of the Magela Plain were defined in the last chapter. Syndepositional alteration of these sediments by bioturbation almost certainly occurred during the period of the Big Swamp. Once sediment began to accumulate above the level of high tide, oxidation and chemical alteration were added to bioturbation to alter the primary sedimentary features. The post-depositional diagenesis of pyrite and clay minerals was possible after major tidal connections were severed, about 2500 yr BP. This was the beginning of soil formation on the Plain, a set of processes that has gone on simultaneously with sedimentation.

The research reported in this chapter was designed to describe and explain the types and distribution of the soils of the Plain, in particular the acid sulfate soils, as a further step towards understanding how the Plain has evolved to its current state. This understanding will allow at least a qualitative prediction of future pedogenic states on the Plain, and provides a context for the experiments in which tailings have been reacted with various soil materials from the Plain.

Previous work (Hooper 1969; Wells 1979) showed the soils were uniform and fine-textured with seasonal cracking. The soils are almost exclusively Ug 5 when classified according to Northcote (1975). In terms of Great Soil Groups (Stace et al. 1968), Ug 5.4 profiles correspond with the grey clays, not to be confused with the stratigraphic unit of the same name. Hooper (1969) recognised six soil families which included four grey clays, acid swamp soils and solonchaks (Table 5.1). 'Acid swamp soils' refers to Stephens's (1961) term for acid peats overlying clays. Walker (1963) recognised some acid swamp soils of New South Wales as acid sulfate soils. Solonchaks were described by Stace et al. (1968) as highly saline soils with pedogenesis confined to the surface 30 cm, below which sedimentary layers occurred.

Hooper's (1969) report was a broad reconnaissance from the Adelaide River to the East Alligator River, and Wells's (1979) larger scale study of the Magela Plain grouped all the Ug 5.4 soils into one mapping unit. Bettenay et al. (1981) identified jarosite in soils near Mine Valley Billabong and noted pyrite and a sulfurous smell in the substrata. These surveys indicated strong similarities between the soils of the Magela Plain and the coastal soils of the Macleay and Shoalhaven flood plains in which the presence of estuarine, pyritic strata strongly influenced soil formation (Walker 1972; Willett & Walker 1982).

While similarities can be seen between the poorly described Magela Plain soils, and better described soils of coastal plains in eastern Australia, it was necessary to sample in detail the Magela soils. A robust classification was also considered necessary to overcome the confusion of soils names that had already been applied to soils of the type found on the Magela Plain.

Fifty-two soil profiles were selected from the sites sampled on the eleven cross-sections described in Chapter 4. The auger holes and cores were briefly described during drilling using colour, texture, mottling and inclusions. The cores were taken to the laboratory, split lengthwise, re-described and one half of each core sampled. Sampling was carried out on the basis of morphology using either soil horizons or sedimentary layers. For the soil studies almost all cores were sampled down to the unoxidised pyritic Blue-Grey Clay. The samples

were oven dried at 80°C as soon as possible, either on the day of sampling or within two days, to minimise oxidation. The samples were then finely ground for analysis. A total of 405 samples from 52 profiles were analysed for pH, EC, Cl, organic C, and extractable Fe, Al, and Mn and S fractions. The organic C results were corrected for pyrite as described in Willett and Beech (1987).

5.2 MAJOR SOIL FEATURES AND TYPES

During the description of the cores, nine horizon types were recognised. These are, from the surface-down:

- 1. Ao brown to black organic surface mat, usually < 5 cm.
- 2. Al dark, organic surface, sometimes rich in biogenic silica.
- 3. B B horizon with uniform colour, light to dark grey, light to heavy clay.
- 4. Mr Grey clay with abundant orange and/or red mottles.
- 5. Myl Grey clay with occasional yellow (oxide) mottles.
- 6. My2— Grey clay with abundant yellow (oxide) mottles.
- 7. J Grey clay with abundant jarositic mottles, or jarosite on ped surfaces, root channels or closely associated with organic fragments.
- 8. S Slightly oxidised pyritic clay. Occasional jarosite in channels.
- 9. G Unoxidised pyritic clay, usually blue-grey (the Blue-Grey Clay).

All 52 profiles could be described in terms of combinations of the nine horizons (Figs 5.1 to 5.11). Horizon G consists of the unaltered Blue-Grey Clay. Horizons J and S are also derived from estuarine clays but have been altered by pyrite oxidation. Air has penetrated to the depths of the J and S horizons and indicates the lowest limit of the water table. The mottled horizons overlying J and S undergo cycles of saturation and drying and could have been affected by the translocation of pyrite oxidation products. The horizons overlying J and S represent alluvial sediments. The Ao, Al and B horizons are derived from alluvium and have minimal soil development.

The results for four soil profiles are presented in detail to illustrate the predominant soil types of the Magela Plain. Thereafter, the results of a factor analysis will be used to: summarise the chemical properties of each soil type and horizon; describe the distribution of soils in relation to the topographic and landform units; and identify the dominant soil forming processes, particularly the processes leading to the formation of acid sulfate soils.

A. Acid clay soils on deep alluvium.

These soils occur in the Mudginberri Corridor and on the levees of billabongs throughout the Magela Plain, where the alluvium is deepest. Profile JB3 (Fig. 5.4) on the levee-prow of Jabiluka Billabong represents this soil type. The surface 250 cm of soil is very acid but the pH values do not fall below 4.0 to indicate pyrite oxidation (Fig. 5.12). EDTA-extractable S (water soluble and adsorbed sulfate, and gypsum if present) levels are low throughout the profile, and no jarosite was detected. Extractable Fe and Al increase toward the surface and are relatively uniform in the sulfidic (G) stratum. This profile strongly reflects the properties of the materials at the time of deposition (see Chapter 4) and shows a marked contrast in chemical properties between the estuarine and alluvial deposits. There has been no pyrite oxidation in this profile.

B. Acidic clay soils on shallow alluvium (unoxidised).

These soils occur between the Upstream Basin and the Downstream Plain (Fig. 5.6). The sulfidic estuarine stratum occurs within 150 cm of the surface but there is no evidence of pyrite oxidation since the pH is above 4.0 and EDTA-extractable S is low throughout the profile (Fig. 5.13).

C. Acid clay soils on shallow alluvium (oxidised).

These soils and those of B occur in similar landforms. Oxidation of the sulfidic stratum is shown by pH values of 4.0 or lower, and the presence of jarosite (Fig. 5.14). Another characteristic of soils that have been affected by oxidising pyrite is that EC does not simply mirror the concentration of Cl because of the presence of soluble sulfate. These soils show an accumulation of CDB-extractable Fe in the mottled horizons overlying the jarositic horizon (Fig. 5.14).

D. Alkaline and saline soils overlying unoxidised pyritic clay.

These soils predominate on the East Alligator flood plain (Fig. 5.10). The sulfidic stratum has not been oxidised and the pH is usually greater than 7.0 except at the surface (Fig. 5.15). The salinity is dominated by chloride rather than sulfate. The extractable Mn concentrations are highly variable in the alluvium, and probably reflect wide variation in the Mn content of the deposited alluvium rather than translocation during soil development.

Soil type C is an acid sulfate soil, whereas the others are potentially acid sulfate soils. Soil B may correspond with the Cairncurry family and soil D with the Carpentaria family of Hooper (1969) (Table 5.1).

5.3 FACTOR ANALYSIS

A varimax-rotated principal factor analysis was applied to the (405×13) matrix of soil chemical properties in order to reduce the large matrix to a smaller number of variables or factors. The factors are associated with a specific set of chemical properties which reflect pedogenic processes. The identity of the processes associated with the factors was established from: the varimax-rotated factor pattern (or the factor-soil property relations); the soil profile depth functions of the soil chemical properties and factors; and the relations between the factors and the morphology of the soil profiles expressed in the soil (Table 5.2). The nature of the processes was then further explored by examining the relations between the processes, as expressed in the factors, and the Plain's landforms and stratigraphy. The spatial pattern of the processes was described in relation to the Plain's geographical units. Data for samples of Pleistocene pre-estuarine substrata were excluded from the data set following a preliminary factor analysis.

Soil data have been logarithmically (base 10) transformed before undertaking principal factor analysis. The variables are: pH, conductivity (EC), chloride (Cl), dithionite extractable manganese (MnD), oxalate extractable manganese (MnOx), dithionite extractable iron (FeD), oxalate extractable iron (FeOX), organic carbon (C), water soluble sulfur (SWSABS), jarositic sulfur (SJAR), pyritic sulfur (SPYR), dithionite extractable aluminium (AlD), and oxalate extractable aluminium. The principal factor analysis was carried out using the procedure FACTOR of the SAS statistical package (SAS 1985). Principal factor analysis assumes that the unique factors are uncorrelated both with each other and with the common factors. Each common factor is assumed to contribute to at least two variables, otherwise it would be a unique factor (SAS 1985).

Factors were rotated by the varimax method in order to make them as close as possible to the 'extreme soil types'. A varimax rotation shifts the factor axes until they coincide with the most divergent factors in the multidimensional space, subject to the constraint that the factors retain their orthogonality. As the varimax method yielded an acceptable model, it was not necessary to resort to oblique rotation. The varimax-rotated factor score pattern is shown in Table 5.3.

FACTOR-PROCESS ASSOCIATIONS

The factor analysis was used to reduce the soil data set to five factors. The varimax-rotated factor pattern (Table 5.3) shows that each factor is associated with a distinct set of factor scores on each of the 13 chemical properties. The factor scores reveal which soil chemical properties are most significant in characterising the individual factors.

The five factors can be envisaged as representing five distinct soil types, each of which is associated with a particular formative process. These processes, which in this application are either pedologic or sedimentologic, are inferred from the chemical properties of the horizons, the mean factor loadings for the horizons (Table 5.2), and the varimax-rotated factor pattern (Table 5.3).

Factor 1 shows a strong association with Mn and Fe. The rotated factor score for MnD is 0.83, for MnOX 0.82, FeOX 0.65, and FeD 0.59 (Table 5.3). The unmottled, and the mottled B horizons (Mr, Myl, and particularly My2), show the highest concentrations of both forms of extractable Mn and Fe (Table 5.2). The generally high Factor 1 loadings soils characterised by B horizons are displayed in bivariate plots of B horizon samples in terms of their loadings on selected pairs of the five factors (Fig. 5.16). Fe-CDB, MnOX and MnCDB concentrations are lower in the lower (S, G) horizons than in the overlying horizons (Table 5.2). In the S and G horizons a large fraction of Fe-CDB was also extracted by oxalate indicating that the Fe occurs as poorly ordered Fe(III) oxides (ferrihydrite) or Fe(II) compounds (excluding pyrite, FeS₂). In constrast, Fe-OX in the Mr, Myl and My2 horizons is only a small fraction of Fe-CBD, suggesting that the Fe occurs as better ordered Fe(III) oxides such as goethite. The higher CDB-Fe and MnCDB levels in the mottled B horizons may be caused by the translocation of Fe²⁺ and Mn²⁺ from the oxidising substrata and their deposition on oxidation in the B horizon, as noted in acid sulfate soils by Van Breemen (1982).

The differences between the B horizons and the underlying horizons are greater for Mn than for Fe, although the total concentrations of Fe are higher throughout. FeOX and FeCDB have low final communality estimates (Table 5.4) indicating that Mn transport and accumulation may be more marked than is the case for Fe.

Factor 1, therefore, is interpreted as representing the accumulation of secondary forms of Mn, and to a lesser extent Fe, in B horizons. The associated processes are the redox reactions and transport of Fe and Mn. During the oxidation of the pyritic substratum, Fe²⁺ and Mn²⁺ appear to form and are then translocated upward into the overlying sediment. Factor 1 explains the highest proportion of variance in the data (Table 5.3), emphasising the dominance of Mn and Fe accumulation and redox processes in the sampled profiles.

Factor 2 gives high positive rotated factor scores for AlOX (0.86), Al-CDB (0.81), and a lower positive score (0.48) for organic C (Table 5.3). The means of Factor 2 loadings are highest in the Ao and Al horizons. Levels of extractable Al and organic C are correspondingly highest for these horizons (Table 5.2). The generally high and positive Factor 2 loadings for samples from the Al horizon are depicted in plots of A horizon samples in terms of their loadings on Factors 1 and 2 (Fig. 5.17). The A horizons have developed exclusively in the Dark Brown/Black Clay. The A horizon and the G horizons, (the latter also high in organic C), were distinguished by the low concentrations of extractable Al in the G horizons. Although the Factor 2 score on organic C is lower than for the extractable Al, a high communality means that organic C possesses good discriminating power. Consequently, soils from the stratigraphically lower layers (J, S, G horizons) all display low loadings on Factor 2.

Factor 2 is interpreted as representing the recent deposition of fine grained organic freshwater sediments.

Factor 3 is characterised by high positive scores on SWABS (0.63) and SJAR (0.60), and a high negative loading on pH (-0.64) (Table 5.3). Factor 3 also shows a strong association with the J and S horizons (the oxidised Blue-Grey Clay and jarositic layers), the means of Factor 3 loadings being highest for samples from these horizons (Table 5.2). The generally high Factor 3 loadings for samples from the J and S horizons are depicted in plots of samples from these horizons in terms of their loadings on selected pairs of the five factors (Figs 5.18 and 5.19). The relatively high concentrations of jarosite and water soluble sulfate combined with low (acid) pH values result from the oxidation of pyrite and the formation of acid sulphate horizons. High concentrations of SWABS and SJAR in the lower parts of profiles, in the J and S horizons, is consistent with the characteristics of acid sulfate horizons. Low levels of pyrite in the jarositic (J) horizon indicates depletion of the pyrite by oxidation. High levels of SJAR and SWABS in the S horizon together with high concentrations of pyrite suggest ongoing and active oxidation in this layer. In the underlying G (Blue-Grey Clay) horizon, fewer than half the samples displayed positive loadings on Factor 3 (Fig. 5.20). A small number of samples have high Factor 3 loadings indicating some localised oxidation of this stratum. This oxidation is not evident morphologically and hence did not influence the field classification of these soil horizons or profiles. The low final communality estimate for SJAR (0.38) implies that less weight must be given to jarosite in the interpretation of this factor (Table 5.4).

Factor 3 is interpreted as representing the oxidation of pyrite in the Blue-Grey Clay and the concomitant formation of jarosite and sulfate in acid sulfate horizons.

Factor 4 is characterised by high positive factor scores on C1 (0.833) and EC (0.792) (Table 5.3). The mean factor 4 loadings are mainly positive for the J and G horizons, and high and negative for the surface horizons (Ao, A1, B horizons) (Table 5.2). Similarly, mean CI concentrations and mean electrical conductivities are higher in the lower strata than in the surface (Table 5.2). The EC and CI levels are highest in the G horizons and lowest in the surface alluvium (Ao, A1 horizons). The generally high Factor 4 loadings for samples from the J, S and G horizons are displayed in plots of factor loadings for samples from these horizons (Figs 5.18, 5.19, 5.20). In the J and S horizons sulfate resulting from the oxidation of pyrite also contributes to the electrical conductivities (Table 5.2). The high ECs and CI concentrations are indicative of an estuarine origin for these layers, as shown in Chapters 3 and 4. Factor 4 is therefore interpreted as being associated with the deposition of estuarine clays.

The rotated factor score pattern (Table 5.3) shows that Factor 5 is characterised by high scores on pyritic sulfur (SPYR, 0.643) and organic carbon (C, 0.595). The mean Factor 5 loadings are highest for the S (0.88) and G (0.85) horizons (Table 5.2). The generally high Factor 5 loadings for the S and G horizons are displayed in plots of Factors 1 and 5 loadings on the samples from these horizons (Figs 5.21, 5.22). Pyrite concentrations are highest in the S and G horizons and decrease markedly in the overlying horizons. Abundant saltwater mangrove detritus has provided large quantities of organic carbon in the pyritic clay layers. Levels of organic carbon were also high in the surface Ao horizon although the absence of pyrite in the alluvium gives rise to lower Factor 5 loadings than in the case of the pyrite estuarine clays (Table 5.2). The mean of Factor 5 loadings on samples from the Ao horizon is 0.33, reflecting the high organic carbon for this layer. Factor 5 also clearly distinguishes the unoxidised and partially oxidised (G and S) horizons from the overlying oxidised (J) horizon (Table 5.2). The description of this factor was improved by the varimax rotation of the factor matrix.

Factor 5 represents unoxidised estuarine clays rich in mangrove detritus. The Ao horizons also give positive although generally lower loadings on this factor. Stratigraphic position and morphological properties (colour, texture) clearly differentiate these two sediment types.

5.4 DOWN PROFILE VARIATION IN FACTORS AND CHEMICAL PROPERTIES

Each of the five principal factors was shown above to be associated with a distinctive set of chemical properties, which in turn are associated with particular horizons. Each factor was ascribed a tentative process label, either pedologic or sedimentologic, on the basis of these relations. In this section, the profile variation in the five factors and associated processes for the four predominant soil types are examined in order to define more precisely the factor interpretations, and to aid in an explanation of the genesis of the profiles.

Profile JB3 (Fig. 5.12) shows that the surface alluvium (A1, B horizons) has a strong association with Factor 2, and is characterised by high levels of extractable A1 (see Chapter 3) and Fe. Organic carbon is elevated but to a lesser extent. Below the layer dominated by Factor 2, there is an abrupt change to a layer of estuarine clay. Factor 5 is uniformly high and positive throughout this layer. The marine origin of this layer is evidenced by increasing pyrite, EC and C1 with depth. The apparently abrupt change from samples dominated by Factor 2 to those dominated by Factor 5 shows the depth at which marine deposition changed to freshwater conditions. The profile at site JB3 consists of freshwater alluvium overlying unoxidised estuarine clays.

Profile NB2 (Fig. 5.13) shows that the estuarine clays are associated with positive loadings on Factors 1 and 4, and with Factor 5 at depth. Negative loadings on Factor 3 are also characteristic. High Factor 1 loadings, particularly in the upper My horizon, are associated with high levels of Fe and especially Mn. Increasing Factor 4 loadings with depth are associated with corresponding increases in C1 and EC. The high positive loadings on Factor 5 in the G layer are associated with the presence of pyrite. The negative loadings on Factor 3 relate to low levels of (EDTA) water soluble sulfate and an absence of jarosite which, combined with the high pyrite, indicates an absence of oxidation. Alkaline pH values are consistent with this explanation. Site NB1 is indicative of profiles in pyritic estuarine sediments which have not been oxidised.

The more important factor associations for the profile at site NBI (Fig. 5.14) are a thin (A1) layer of acid alluvium dominated by Factor 2, and a Factor 3 dominant oxidised clay (J) substratum characterised by decreasing pH values and a deficiency of pyrite. Jarosite and the water soluble sulfate (SWABS), the products of the oxidation of the pyrite, are present. Additional features of this profile are the development of a Factor 1 dominant mottled B (My) horizon which is high in FeCDB, and positive Factor 4 loadings on the substratum, associated with relatively high values for EC and Cl. This profile shows a thin layer of acidic clayey alluvium overlying an oxidised marine clay.

Profile LP3 (Fig. 5.15) shows the B horizon to be associated with high positive loadings on Factor 1. This layer is strongly alkaline with relatively high concentrations of extractable Mn. The B horizon is underlain by a red-mottled (Mr) Factor 4 dominant layer, in which Cl and EC increase with depth. At the base of the sampled profile this layer changes abruptly to a Factor 5 dominant, unoxidised estuarine clay. This sediment is typically saline and high in pyrite. This profile therefore shows the formation of alkaline horizons overlying an unoxidised, saline (marine), pyritic clay. The process explanations for the five factors are consistent with the properties and stratigraphy of the four main soil types.

5.5 SPATIAL DISTRIBUTION OF FACTORS IN SOILS OF THE PLAIN

DISTRIBUTION OF FACTORS IN RELATION TO TOPOGRAPHIC UNITS

In this section, the spatial variability of the 5 factors (or processes) over the Plain is examined. Firstly, the distribution of the five factors in relation to the Topographic Units is examined in order to establish the spatial distribution of soil profile types and processes. Secondly, the distribution of the five factors is examined in relation to the Plain's Landform Units.

The main relationships between the Topographic Units, the five factors, and their related processes are determined from: bivariate plots of samples identified by Topographic Unit in terms of the five Factors (Figs 5.23 to 5.28); and topographic cross-sections along soil sampling traverses with zones of dominant factor loading (Figs 5.29 to 5.39).

Factor 1.

In excess of seventy-five of the East Alligator Flood Plain and Downstream Plain samples had positive factor loadings on Factor 1 (Figs 5.23 & 5.24, respectively). The cross-sections of dominant factors for the soil sampling traverses (Figs 5.35 to 5.39) show that a Factor 1 layer dominates all sampled profiles for the East Alligator Flood Plain and the Downstream Plain. This layer extends from the ground surface to a depth of about 1 m on all profiles. In the Central High, a Factor 1 layer is also present as a generally discontinuous layer of between 1 and 2 m thickness (Figs 5.32, 5.33, 5.34), the surface of which occurs at a depth of about 1 m. A Factor 1 layer was not recorded in either the Upstream Basin or the Mudginberri Corridor (Figs 5.29, 5.30, 5.31). Thus the process associated with Factor 1, the accumulation of Fe and Mn, in B horizons and surface sediments is not common at the downstream end of the Plain, less well developed in the middle of the Plain, and absent from the upstream part of the Plain. Once again, the disjunction at the Central high is found.

Factor 2.

The highest positive loadings on Factor 2 were recorded for the Upstream Basin and the Central High. Slightly more than half these samples had positive loadings on this factor (Figs 5.40 & 5.41). The cross-sections of the soil sampling traverses with zones of dominant factors (Figs 5.30, 5.31, 5.32, 5.33 & 5.34) show the presence of a Factor 2 dominant surface layer extending to a depth of about 1 m. This layer extends the full length of these traverses. In contrast, less than half of the samples from the Downstream Plain and the East Alligator Flood Plain had positive loadings on Factor 2 but they were not as high as for the upstream Units (Figs 5.23 & 5.24). Similarly, the cross-sections for the Downstream Plain and the East Alligator Flood Plain show only a limited development of a Factor 2 dominant surface zone (Figs 5.35 & 5.36). Therefore Factor 2, the (freshwater) deposition of alluvium, tends to be more dominant in the central and upstream parts of the Plain.

Factor 3.

In excess of seventy-five percent of samples from the Upstream Basin (Fig. 5.27) had high positive loadings on Factor 3. This Factor 3 dominant layer is generally about 2 m thick and occurs directly below the surface Factor 2 layer. In all cases it has formed in close proximity to either channels or billabongs (Figs 5.31, 5.32, 5.33). Fewer than half the Central High and Downstream Plain samples showed positive loadings on this factor. In the case of the East Alligator River samples, fewer than twenty percent of samples had positive loadings (Fig. 5.28). Therefore, Factor 3, associated with the formation of acid sulfate materials by pyrite oxidation, has been most active in the upstream part of the Plain and

decreases in a downstream direction, being almost undetectable on the East Alligator River Flood Plain.

Factor 4.

Fewer than half of the samples from the Mudginberri Corridor and the Upstream Basin (Fig. 5.27) display positive loadings on Factor 4. In the Central High and Downstream Plain approximately half the samples analysed load positively on this factor. On the East Alligator Flood Plain, the majority of samples have high positive loadings (Fig. 5.28). This downstream increase in the importance of Factor 4 is displayed more precisely in the cross-sections (Figs 5.29 to 5.39) in which a Factor 4 dominant layer is seen to become better developed towards the East Alligator River. This layer is typically about 1 m thick and has formed directly beneath the Factor 1 (Mn and Fe enriched layer). Thus the Factor 4 process, associated with high concentrations of Cl and high ECs in the mottled, J, S and G horizons, increases in a downstream direction, to reach a maximum on the East Alligator River Flood Plain.

Factor 5.

Approximately 50% of samples from the Mudginberri Corridor, Upstream Basin (Fig. 5.42) and the Central High display high positive loadings on Factor 5. Fewer samples from the Downstream Plain (Fig. 5.26) and the East Alligator River Flood Plain (Fig. 5.25) load positively on this factor although these loadings are generally high. The cross-sections (Figs 5.29 to 5.39) show that a subsurface Factor 5 dominant layer occurs at variable depths under the entire Plain. These also show a systematic downstream increase in the depth that this layer occurs. The increasing thickness of the top stratum downstream biased the sample numbers towards this layer, and consequently the fewer samples from the downstream reaches do not indicate a diminution in the occurrence of this layer or the associated process(es).

DISTRIBUTION OF FACTORS IN RELATION TO LANDFORM UNITS

The factor analysis was also used to summarise the chemical properties in relation to their Landform Unit. Because the classification of Landform Units is based on both topographic and geomorphologic process criteria, an examination of the Landform Unit-Factor relations may allow a more rigorous definition of the factors and associated processes.

As in the case of the Topographic Units, the relations between the Landform Units, the five factors and their related processes are determined from: plots of samples identified by Landform Unit in terms of pairs of the 5 factors (Figs 5.43 to 5.49); cross-sections showing zones of dominant factor loading.

Factor 1.

In excess of 80% of Channel and East Alligator Flood Plain (Fig. 5.44) samples have positive loadings on Factor I. These landforms are characterised by marked fluctuations in seasonal water table levels, conditions which would cause cycles of oxidation and favour the translocation of Mn and Fe. By contrast, almost all samples from the Marginal Depressions (Fig. 5.43) show negative loadings on this factor. This is consistent with the definition of Factor I and accumulation of Mn and Fe in that the high water tables and extended periods of inundation would be expected to inhibit oxidation and prevent the formation of Mn²⁺ and Fe²⁺. The most elevated of the Plain's landforms are the Backslopes, Levees and the High Plain. As with the East Alligator Flood Plain, they are subjected to marked seasonal water table fluctuations. However, because of their relatively high elevations, the large fluctuations in the water table produce a zone of Mn and Fe oxidation and accumulation to a depth of about 1 m. This process is best developed in the Central High — the most

elevated area of the Plain consisting of Backslopes, High Plain and Levees (Figs 5.32, 5.33, 5.34). Thus the process associated with Factor 1 is represented mostly at the lower end of the Plain, and in the subsurface in the more elevated middle part.

Factor 2.

Approximately half the samples from Marginal Depressions (Fig. 5.29), Backslopes (Fig. 5.35), Low Plain and Levees have positive loadings on Factor 2. Fewer than half the samples from Channels and the East Alligator River Flood Plain (Fig. 5.44) show positive loadings. Factor 2 was shown above to be associated with recent freshwater deposition which, from stratigraphic evidence, currently operates over most of the surface of the Plain. The near ubiquitousness of this process is not revealed by the cross-sections of dominant factors, as post-depositional translocation of Mn and Fe into this stratum masks the original primary depositional properties (Al and C), especially downstream of the Central High. High Factor 2 loadings were obtained on samples from the elevated landforms, such as High Plain, Levees and Backslopes (see for example, Fig. 5.35), parts of which were above the upper limit of oxidation. The low lying areas of the Plain, such as the Low Plain and patterned ground in the Mudginberri Corridor and the Upstream Basin, are below the level of the water table for most of the year and do not undergo oxidation. At these sites the original (Factor 2) character of the sediment prevails.

Factor 2 occurs over the entire Plain, but appears to be dominant only where the landsurface is either too elevated or depressed to enable oxidation of the pyritic substrata and the upward translocation of Mn and Fe.

Factor 3.

About 80% of the Low Plain samples have very high positive loadings on Factor 3 (Fig. 5.46), the factor associated with the oxidation of pyrite in the estuarine muds and the formation of acid sulfate materials. Areas of Low Plain, which include areas of patterned ground, are located mainly in the Upstream Basin (Figs 5.45, 5.46). Low Plain occurs also to a more limited extent along the margins of the Central High and in the Downstream Plain (Fig. 5.37). Low Plain consists of low lying areas with average elevations intermediate between Marginal Depressions and Backslopes. Areas of Low Plain dry out later in the Dry season than more elevated areas, while the patterned ground may, in wet years, be inundated all year. In contrast to the Factor 3 dominant Low Plain in the Upstream Basin, areas of Low Plain in the Mudginberri Corridor (Figs 5.29, 5.30) and the East Alligator Flood Plain (Figs 5.45, 5.39) have few Factor 3 dominant samples. In both these parts of the Plain, relatively deep surface alluvium inhibits oxidation of pyrite muds. In the case of the Backslopes and Levees, fewer than 50% of samples have positive loadings on Factor 3 (Fig. 5.47). These landforms are generally more elevated and have a greater thickness of the surface alluvial layer (especially in the case of the Levees, see Fig. 5.32) than the Low Plain. The thicker alluvial layer tends to reduce the availability of oxygen to sub-surface strata, thereby inhibiting oxidation in these layers.

In summary, the oxidation of pyrite (Factor 3) in the sub-surface extuarine Blue-Grey Clay is most pronounced in the low-lying wetter areas of the plain, in Low Plain areas of the Upstream Basin and to a lesser extent the Central High and Downstream Plain. Only during very dry (or short) Wet seasons will oxygen be able to penetrate into this pyritic layer.

Factor 4.

In excess of 80% of soil samples from the East Alligator River Flood Plain (Figs 5.45, 5.28, 5.39) have positive loadings on Factor 4, compared with approximately half of all samples in the case of Levees and Backslopes (Fig. 5.47). In contrast, the marginal depressions and low plain areas generally have the lowest Factor 4 loadings. These landforms occur mainly along

the Plain's periphery and in the Upstream Basin and Mudginberri Corridor respectively. There are no Factor 4 dominant strata in either of these topographic units (Figs 5.29, 5.30, 5.31). The estuarine muds in the downstream part of the Plain have the highest EC and Cl levels, while the marginal and upstream areas are relatively deficient in these properties. These patterns are consistent with the presence of a Holocene estuary and saltwater mangrove swamps in what is now the Magela Plain. Salinity levels in the estuarine muds would have been highest at the mouth of the estuary (in the vicinity of the East Alligator Flood Plain), and would decrease in the direction of the upper end of the estuary (the Mudginberri Corridor and Upstream Basin) and in embayments in the estuary margins (the present day Marginal Depressions), as shown in Chapter 4. The lower salinity levels result from dilution of the saline muds by terrestrial sediment and runoff from Magela Creek and its tributaries.

In summary, the Blue-Grey Clay which underlies the entire Magela Plain shows spatially variable salinity levels, being highest in the lower (coastal) end of the palaeo-estuary and lowest in the upper, inland extremity beneath the Mudginberri Corridor. Significant positive loadings on Factor 4 for the Plain's substratum is a more precise indicator of the presence of the estuarine Blue-Grey Clay than Factor 5 (pyrite and carbon) which is associated only with the relatively high levels of organic C and pyrite-S in the unoxidised clay.

Factor 5.

Inspection of bivariate plots of factor pairs with samples identified by landform unit shows little evidence of a relationship between Factor 5 and present day landforms. Rather, a Factor 5 dominant substratum underlies the entire plain (Figs 5.29, 5.39). The association of Factor 5 with high pyrite and organic carbon indicates that this layer is unoxidised. The upper surface of this layer shows little relation to the topography of the present day surface as shown in Chapter 4. It does, however, arch up beneath some localised topographic rises, such as Levees and High Plain areas, where oxidation of the pyrite mud has been inhibited by the thicker alluvial cover (Figs 5.30, 5.32). The Factor 5 dominant stratum, which is present at a depth of 1 to 3 m throughout the Plain, tends to increase in depth downstream towards the East Alligator River (Figs 5.29, 5.30, 5.34 & 5.39). This downstream increase in depth is a consequence of the development of a Factor 3 dominant layer in alluvium in the Upstream Basin and Central High (Fig. 5.31, 5.32), and the formation of Factor 1 (Fe and Mn) and Factor 4 (saline) dominant layers which increase in importance downstream from the Central High to the East Alligator Flood Plain (Fig. 5.33 to 5.39).

In summary, unoxidised pyritic (Factor 5) Blue-Grey Clay underlies the entire Plain. The depth to this layer tends to increase in a downstream direction as oxidation of the pyrite becomes locally important and, further downstream, as alluvium enriched in Mn and Fe thickens. At the extreme downstream end of the Plain, increasing salinity replaces pyrite as the predominant characteristic of this layer.

5.6 SUMMARY

A varimax-rotated principal factor analysis was applied to selected chemical properties of the soils of the Magela Plain to establish the origin of the soil material. The processes associated with the factors and their spatial distribution were then explained more fully by examining them in relation to the Plain's history and contemporary landforms.

The factor analysis of the matrix of soil chemical properties yielded five principal factors. Each of these five factors is associated with a small number of specific soil properties:

Factor 1 — oxalate and dithionite extractable Fe and Mn.

Factor 2 — oxalate and dithionite extractable Al, and organic carbon.

Factor 3 — jarosite, water soluble sulfate and pH.

Factor 4 — chloride and electrical conductivity.

Factor 5 - pyrite and organic carbon.

The five factors are interpreted as representing distinct processes, either primary sedimentary or post-depositional pedogenic. The kinds of processes was identified from the soil properties associated with the factor scores, and the factor-soil horizon relations:

Factor 1 — Mn and Fe oxidation and translocation.

Factor 2 — Deposition of freshwater sediments.

Factor 3 — Oxidation of pyritic estuarine sediments with the formation of acid sulfate horizons.

Factor 4 — Deposition of saline estuarine sediments.

Factor 5 — Deposition of pyritic, estuarine sediments.

The loadings on the five factors for individual samples give the relative contributions, to the genesis of that sample, of the five processes. The spatial pattern of the five processes on the Plain has been defined in relation to Topographic Units.

Starting at the upstream (southern) end of the Plain, the main Topographic Unit-Dominant Factor relations are:

Mudginberri Corridor — freshwater sediment deposition (Factor 2) over unoxidised pyritic estuarine muds (F.5).

Upstream Basin — freshwater deposition (F.2) over oxidised (F.3) and unoxidised (F.5) estuarine muds.

Central High — freshwater deposition (F.2) over mottled (F.1) and occasionally oxidised (F.3) saline (F.4) pyritic (F.5) estuarine clay.

Downstream Plain — mottled horizons (F.1) overlying predominantly unoxidised (F.5) and saline (F.4) estuarine muds.

East Alligator Flood Plain — mottled horizons (F.1) overlying highly saline (F.4) unoxidised pyritic (F.5) muds.

These relationships are shown more objectively in Table 5.5 where the depositional environments are shown against matching soil chemistry factors, the latter listed (from left to right) in order of dominance.

The entire surface of the Plain is mantled with organic-rich alluvium, which becomes more intensively mottled by secondary Fe and Mn downstream. Estuarine clay sediments underlie the entire Plain. The upper pyritic layers of these muds are extensively oxidised to form acid sulfate materials in the upstream area of the plain (with the exception of the Mudginberri Corridor) and become less oxidised in a downstream direction. The muds are generally more saline towards the East Alligator River.

The relations between the factors and the Plain's contemporary landforms and associated processes enable a more comprehensive definition of the soil forming processes and assist in explaining their spatial and down profile operation:

Channels — although there were few samples from the channels, there was some evidence of increased oxidation (F.3) in the vicinity of contemporary channels and palaeochannels.

Marginal Depressions — these form embayments in the Plain's margins and are the topographically lowest and therefore wettest landforms. Alluvium (F.2) overlies largely unoxidised (F.5) estuarine muds of low salinity (F.4).

High Plain — flat and relatively elevated areas of shortest inundation, in which a thick surface alluvial stratum (F.2) overlies unoxidised (F.5) estuarine mud, with mottled B horizon development (F.1) in downstream areas of the plain.

Levees — elevated, localised linear or curvi-linear banks often flanking permanent billabongs in which thick alluvium (F.2) overlies unoxidised (F.5) estuarine muds.

Backslopes — gentle slopes of intermediate elevation and inundation on which alluvium (F.2) overlies mottled (F.1) and occasionally oxidised (jarositic F.3) and saline (F.4) estuarine muds (F.5).

Low Plain — topographically low areas of the Plain (mainly upstream), characterised by long periods of Wet season inundation; alluvium (F.2) overlies oxidised (jarositic or F.3) estuarine muds.

East Alligator River Flood Plain — contemporary flood plain of the East Alligator River in which alluvium (F.2) overlies highly saline (F.4) unoxidised (F.5) estuarine muds.

The above relations show that the present day landforms are associated with specific soil profiles and soil-forming processes. Areas of Low Plain are characterised by well developed acid sulfate soil profiles in pyritic mud, in areas of low topography with a relatively thin alluvial cover. At Levee and High Plain sites, the generally thicker surface alluvial layers reduce air entry into the pyritic substratum, thereby inhibiting oxidation and the formation of acid sulfate horizons. Despite the fact that these High Plains experience the shortest period of inundation, their substrata have not been oxidised. The Backslopes are intermediate in elevation between the Levees/High Plain, and Low Plain, and are characterised by only localised oxidation and formation of jarositic horizons. The East Alligator River Flood Plain soil profiles are characterised by well developed mottled, and to a lesser extent, unmottled materials, and few oxidised jarositic horizons. The relatively high concentrations of Mn and Fe in the materials of the East Alligator Flood Plain appears to be due to the deposition of sediment enriched in the oxides of Fe and Mn, rather than their vertical translocation.

Figure 5.50 summarizes the spatial distribution of the main pedologic and sedimentary processes represented by the factors, and the main relations between individual soil horizons, processes, and landforms. This diagram and the following summary represents the final synthesis of Topographic, Landform, sedimentary and pedologic phenomena.

The Mudginberri Corridor is characterised by a surface layer of alluvium which directly overlies unoxidised estuarine sandy clay sediments. The dominant landform type is Low Plain which, because of its low lying topography, is generally covered by surface water until well into the Dry season. The surface alluvium is thickest in this part of the Plain and has prevented oxidation of the underlying estuarine sediments.

In the Upstream Basin, A and B horizons developed in freshwater sediments overlie both oxidised and slightly oxidised estuarine sediments. Jarosite, formed through the oxidation of pyrite, coats ped faces and rootlet channels and is characteristic of these oxidised (acid sulfate) horizons. Low Plain is the dominant landform throughout the Upstream Basin with the topographically lower, upstream area being covered by a patterned ridge and trough topography. Acid sulfate profiles have developed in the Upstream Basin, presumably because of the combination of highly pyritic material with relatively thin veneers of alluvium, and fluctuations in the water table below the surface of the pyritic substratum.

The Central High consists largely of High Plain and Backslope landforms, with small areas of Low Plain. The higher ground flanks a continuous shallow channel within which is Nankeen Billabong. This part of the Plain is the first to emerge at the end of the Wet season. Acid sulfate horizons have formed locally in the Low Plain sites where the surface alluvium is relatively thin. At more elevated sites, the thicker surface alluvium has inhibited oxidation of the pyritic muds. The estuarine clays in this middle part of the Plain are characterised by higher salinities than the estuarine clays further upstream.

Chloride concentrations and electrical conductivies are sufficiently high to be diagnostic of the majority of these horizons. The lower salinities of the estuarine sediments upstream of the Central High, and of those sediments in the marginal depressions, are attributed to the dilution of the estuarine sediments at the time of deposition with freshwater runoff and terrigenous sediments derived from upstream. The presence of mottled B horizons characterised all sampled profiles in the Central High. Upstream, mottles were either absent or only weakly formed. Mn and Fe accumulations give rise to mottled B horizons in areas of more elevated terrain, and result from the operation of a seasonally fluctuating water table within the upper two metres of soil profiles.

Immediately downstream of the Central High, the Plain again becomes relatively low lying. The medial part of the Downstream Plain is dominated by Low Plain and Backslopes, which are flanked by Marginal Depressions. The upper parts of all profiles are typically thin A horizons underlain by thick B horizons with well developed red mottles in which Mn and Fe accumulation dominates. These mottled horizons grade into strongly saline and generally unoxidised estuarine muds. Acid sulfate horizons have formed locally but are generally much less extensive than in the Central High and Upper Basin further upstream.

On the East Alligator River Flood Plain, A and unmottled B horizons overlie a thick yellow, mottled B horizon. The factor analysis of the soil chemical properties shows that the upper parts of the sampled soil profiles (A, unmottled B and upper mottled B) are high in Mn and Fe. At depth the high salinity of the unoxidised estuarine muds is the distinguishing characteristic. This part of the Plain coincides with the mouth of the mid-to-late Holocene estuary and would have been the site of the deposition of the most saline sediments, as already concluded in Chapter 3.

There are some unresolved problems in the soil development of the Plain, largely to do with the fate of Mn and Fe released by oxidation of pyrite. On cross-section 6 (Fig. 5.34) for example, unoxidised pyritic clay is overlain by saline and slightly oxidised pyritic clay and a small lens of acid sulfate development. The thick layer of Fe and Mn accumulation appears not to have a source if it is argued that these elements move vertically upwards. Cross-section 5 (Fig. 5.33) however, contains one substantial zone of acid sulfate development and little accumulation of Fe and Mn. Cross-section 5, or at least the area upstream of cross-section 6, may be the source of the Fe and Mn deposited on cross-section 6.

This invocation of lateral rather than solely vertical movement of extractable Fe and Mn may also explain the absence of a factor 1 layer over a factor 3 layer on cross-section 3, and the occurrence of a factor 1 layer beneath a factor 3 layer on cross-section 4 (Fig. 5.32). Finally, the change from factor 2 (organic C and extractable Al) dominance to factor 1 dominance in the Dark Brown/Black Clay between cross-sections 6 and 7 (Fig. 5.35), that is, between the Central High and Downstream Plain, may also be the result of lateral transport. Here the explanation lies in the transport of suspended solids from different sources, combined with lower concentrations of organic carbon. The sources and pattern of deposition of relatively recent sediment is the subject of the next chapter.

Table 5.1. Summary description of Grey Clay soils of floodplains of the Alligator Rivers Region (Hooper 1969).

Soil family	Summary description	Northcote	Stace et al.
Adelaide	Black self-mulching clays with CaCO ₃ nodules	Ug 5.28	Grey Clay
Wildman	Black massive clays over alkaline, saline estuarine mud	Ug 5.4	Grey Clay
Carmor	Black massive, or weakly self-mulching clays with CaCO ₃ over alkaline estuarine mud	Ug 5.4/ Ug 5.28	Grey Clay
Counmoul	Black massive clays, acid over buried acid riverine, dune, or lateritic sands or mottled sandy clays	Ug 5.4	Grey Clay
Cairncurry	Black massive mottled clays over acid gypsic swamp clays	Ug 5.4	Acid swamp soil
Carpentaria	Grey gleyed saline clays	Ug 5.4/ 5.2/5.1	Solonchak

172

Table 5.2. Means for horizons of factor loadings and chemical properties.

					Horizo	ns				
		1 Ao	2 Al	3 B	4 MR	5 My1	6 My2	7 J	8 S	9 G
No. of samples		5	53	59	17	108	25	21	46	71
Mean factor	1	-0.37	0.25	-0.37	0.24	0.14	0.16	-0.52	-0.06	0.01
loading	2	1.95	0.86	0.32	-0.12	-0.30	-0.10	0.18	-0.26	-0.44
-	3	-0.07	-0.24	-0.39	-0.59	-0.36	-0.02	1.42	0.97	0.16
	4	-0.50	-0.96	-0.54	-0.47	0.37	0.20	0.44	0.05	0.51
	5	0.33	0.06	-0.23	-0.24	-0.62	-0.47	-0.47	0.88	0.85
Mn-CBD mg kg-1	x	13	120	145	220	215	206	27	90	135
	S	4.4	19	21	43	18	35	4.6	15	13
Mn-OX mg kg-1	x	11	92	115	184	159	144	22	83	103
	S	32	15	19	36	14	26	3.7	15	11
Fe-CDB %	x	0.45	0.97	0.71	0.85	0.80	0.95	0.85	0.60	0.49
	S	0.095	0.094	0.075	0.086	0.035	0.025	0.13	0.073	0.02
Fe-OX %	x	0.39	0.45	0.20	0.17	0.26	0.19	0.16	0.41	0.25
	S	0.071	0.059	0.015	0.025	0.01	0.024	0.019	0.080	0.021
Al-CDB mg kg-1	x	4720	2771	2225	1591	1194	1386	1876	1527	1136
	S	1107	264	256	186	68	95	114	153	89
Al-OX mg kg ⁻¹	x	3420	2153	1646	1005	857	952	1275	1139	274
	S	672	229	231	93	40	69	126	101	37
Organic C %	х	7.17	3.3	1.41	0.73	0.36	0.62	1.33	2.64	1.89
	S	1.51	0.54	0.25	0.10	0.03	0.09	0.23	0.37	0.19

Table 5.2. Page 2

	Horizons					ns				
		1	2	3	4	5	6	7	8	9
		Ao	Al	В	MR	My1	My2	J	S	G
EDTA extr-S	x	1151	821	751	377	533	1392	3870	7128	2250
mg kg-1	S	171	124	128	80	68	374	522	1491	334
Jarosite-S	x	20	20	51	20	28	23	3868	1240	256
mg kg-1	S	0.5	0.5	22	0.5	8.1	3.2	956	396	124
					- 0	~ 0			4.5	
pН	x	4.7	5.6	6.3	6.9	7.8	6.8	4.1	4.7	6.8
	S	0.09	0.17	0.23	0.25	0.13	0.27	0.13	0.29	0.23
EC mS cm ⁻¹	x	0.43	0.50	0.87	0.80	2.26	2.01	2.59	3.57	3.30
	S	0.08	0.07	0.13	0.14	0.14	0.23	0.19	0.42	0.20
1									1510	2400
Cl mg kg ⁻¹	X	182	274	714	614	2783	1339	1191	1749	3190
	S	63	66	142	113	240	279	200	307	348
S-pyrite %	x	0.02	0.03	0.03	0.05	0.04	0.04	0.16	0.69	0.62
- IA	s	0.001	0.002	0.009	0.02	0.003		0.086	0.09	0.08

Table 5.3. Varimax-rotated factor score pattern.

	Factor 1	Factor 2	Factor 3	Factor 4	Factor 5
MND	0.826	-0.250	-0.266	0.265	0.030
MNOX	0.816	-0.217	-0.287	0.278	0.078
FEOX	0.646	0.116	0.115	0.004	0.063
FED	0.594	0.083	0.144	0.035	-0.400
ALOX	0.012	0.859	0.164	-0.224	0.036
ALD	-0.091	0.809	0.224	-0.267	-0.080
SWSABS	-0.052	0.221	0.632	0.103	0.228
SJAR	0.036	0.085	0.604	0.029	0.050
рH	0.275	-0.333	-0.688	0.357	-0.210
CL	0.200	-0.303	-0.183	0.833	-0.052
EC	0.180	-0.246	0.300	0.792	0.159
SPYR	0.035	-0.171	0.382	0.229	0.643
C	0.027	0.477	0.322	-0.176	0.595
Variance ex	plained by each	factor			
	2.282	2.100	1.876	1.798	1.076
Final comm	unality estimate	s: total = 9.130			
Squared mu	ltiple correlation	is of the variable	les with each fa	ctor	
•	0.890	0.815	0.773	0.821	0.690

Table 5.4. Squared multiple correlation coefficients (SMCs) and Kaiser's measure of sampling adequacy (MSAs) (unrotated matrix).

Variable	Prior communality estimates (SMC)	Final Communality estimates (SMC)	Residual correla- tions	Kaiser's MSA
рН	0.78	0.83	0.02	0.80
EC	0.79	0.84	0.02	0.58
C1	0.81	0.85	0.02	0.68
C	0.66	0.72	0.03	0.69
FeOX	0.49	0.45	0.06	0.56
MnOX	0.90	0.88	0.03	0.72
AlOX	0.76	0.82	0.02	0.72
FeD	0.50	0.54	0.04	0.53
MnD	0.91	0.89	0.03	0.72
AlD	0.75	0.79	0.02	0.78
SPYR	0.60	0.65	0.03	0.60
SJAR	0.36	0.38	0.03	0.79
SWSABS	0.49	0.51	0.02	0.86

Table 5.5. Summary of soil chemistry factors and sedimentary environments occurring at each cross section of the plain.

Cross-section No.	Sedimentary environment	Soil chemistry factor
l Mudginberri Corridor	Blue-Grey Clay Transition Freshwater Grey Clay Dark Brown/Black Clay	5 5, 2 2, 5 2
2 Mudginberri Corridor	Blue-Grey Clay Transition Freshwater Grey Clay Dark Brown/Black Clay	5 5, 2 2, 5 2
3 Upstream Basin	Blue-Grey Clay Transition Dark Brown/Black Clay	3, 2 2, 3 2
4 Central High	Blue-Grey Clay Transition Freshwater Grey Clay Dark Brown/Black Clay	1, 3, 5, 4 3, 1 2 2
5 Central High	Blue-Grey Clay Transition Freshwater Grey Clay Dark Brown/Black Clay	5, 3, 4, 1 3, 1, 4 2, 1, 3 2, 5
6 Central High	Blue-Grey Clay Transition Freshwater Grey Clay Dark Brown/Black Clay	5, 4, 1, 3 1, 2 2, 1 2, 1
7 Downstream Plain	Blue-Grey Clay Transition Dark Brown/Black Clay	5, 4, 3, 1 1, 4 1, 2
8 Downstream Plain	Blue-Grey Clay Transition Freshwater Grey Clay Dark Brown/Black Clay	4 4 1 1
9 Downstream Plain	Blue-Grey Clay Transition Dark Brown/Black Clay	5, 4, 3, 1
10 Downstream Plain	Blue-Grey Clay Transition Dark Brown/Black Clay	5, 4 3, 1 1
II E. Alligator Flood Plain	Blue-Grey Clay Transition Dark Brown/Black Clay	5, 4 1, 4 1, 2



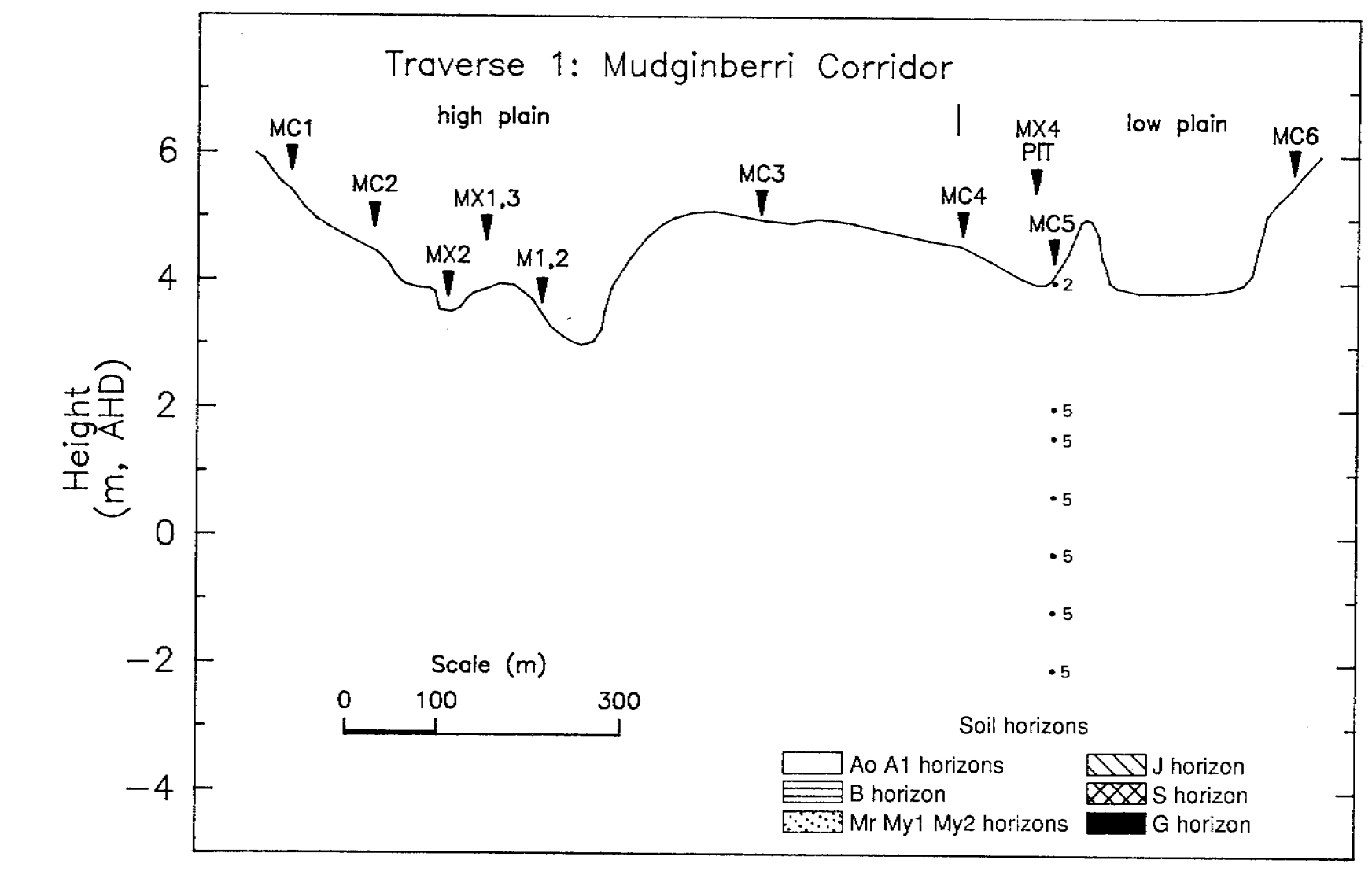


Figure 5.1 Cross-section of traverse 1 showing soil horizons

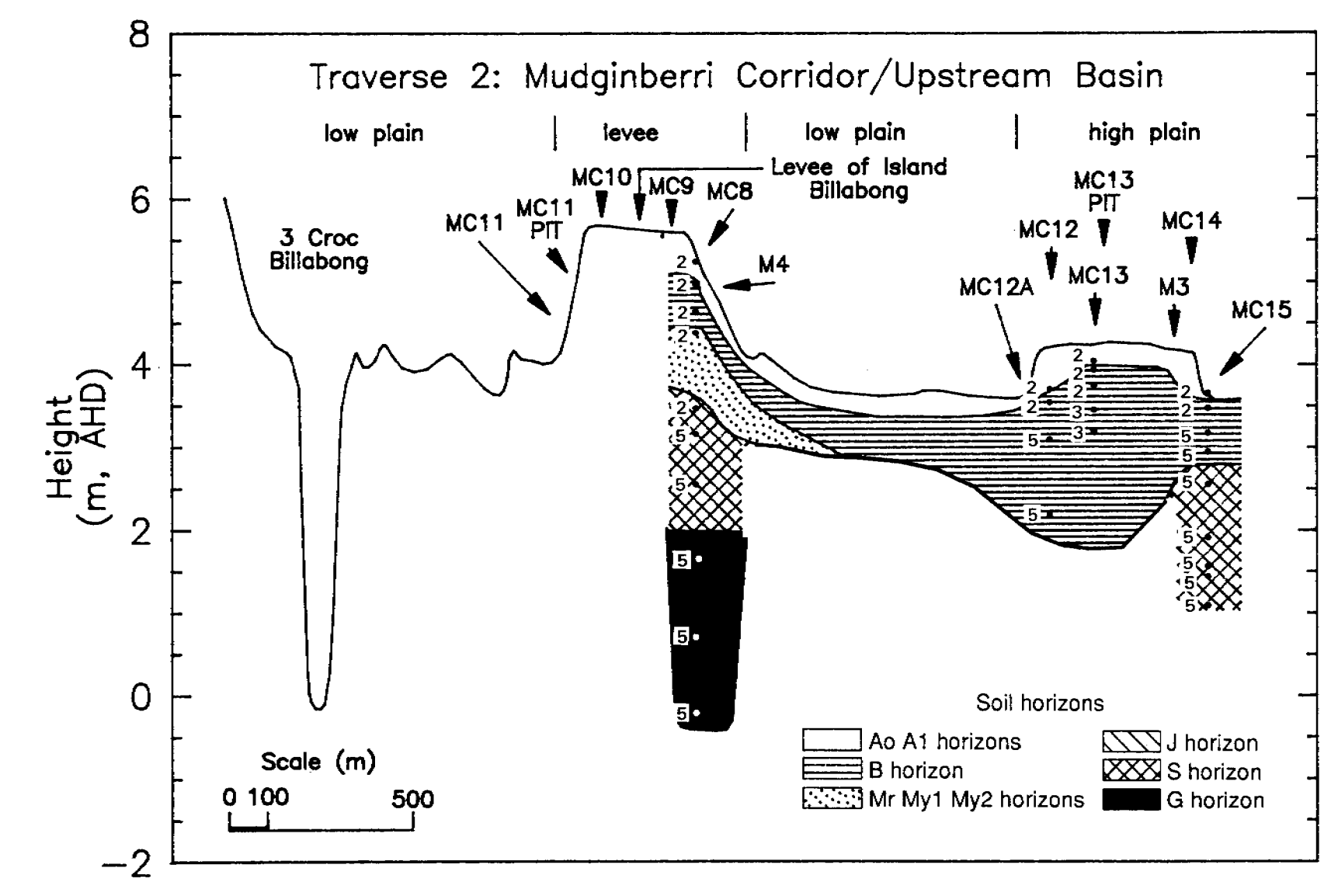


Figure 5.2 Cross-section of traverse 2 showing soil horizons

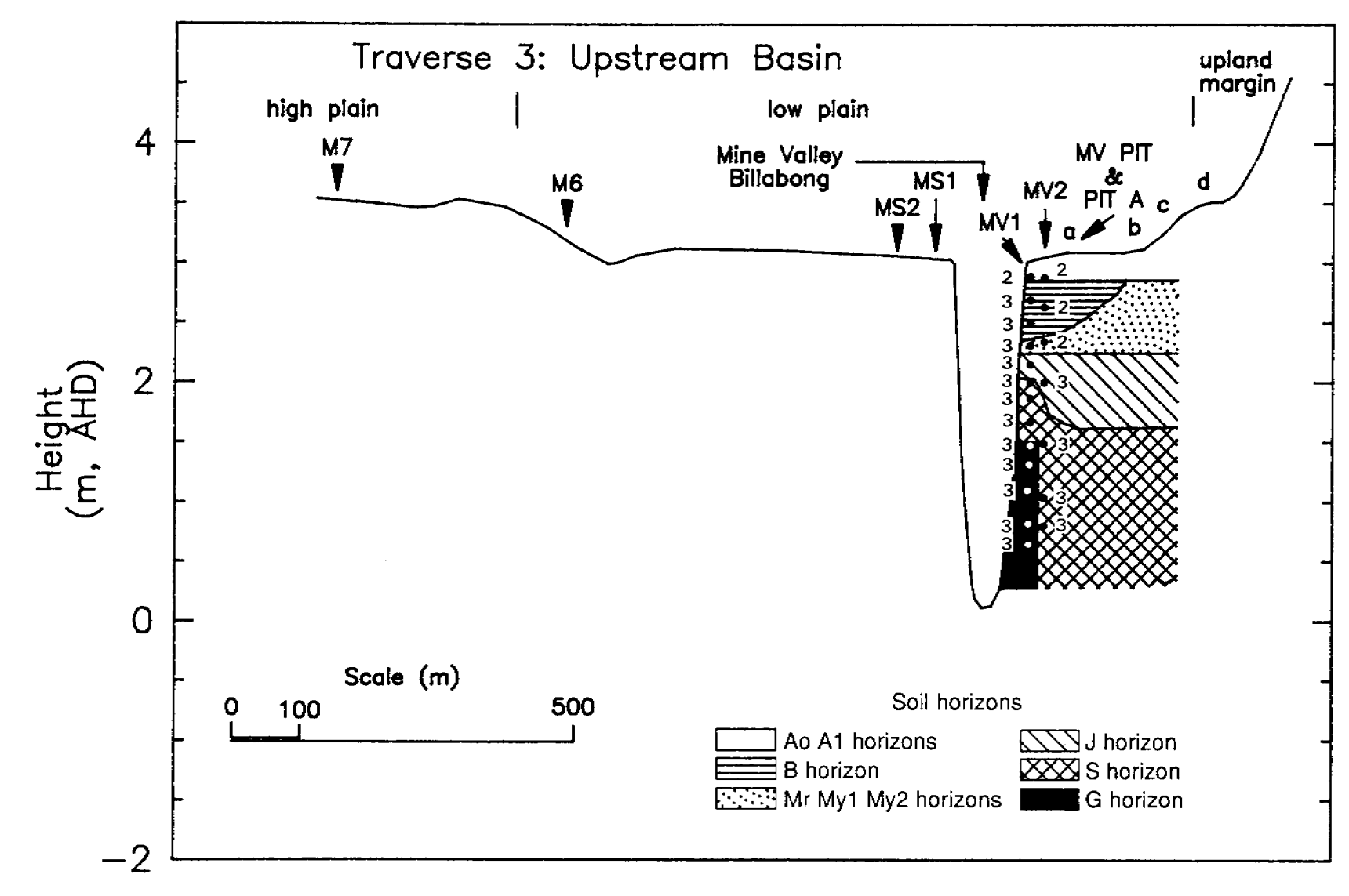


Figure 5.3 Cross-section of traverse 3 showing soil horizons

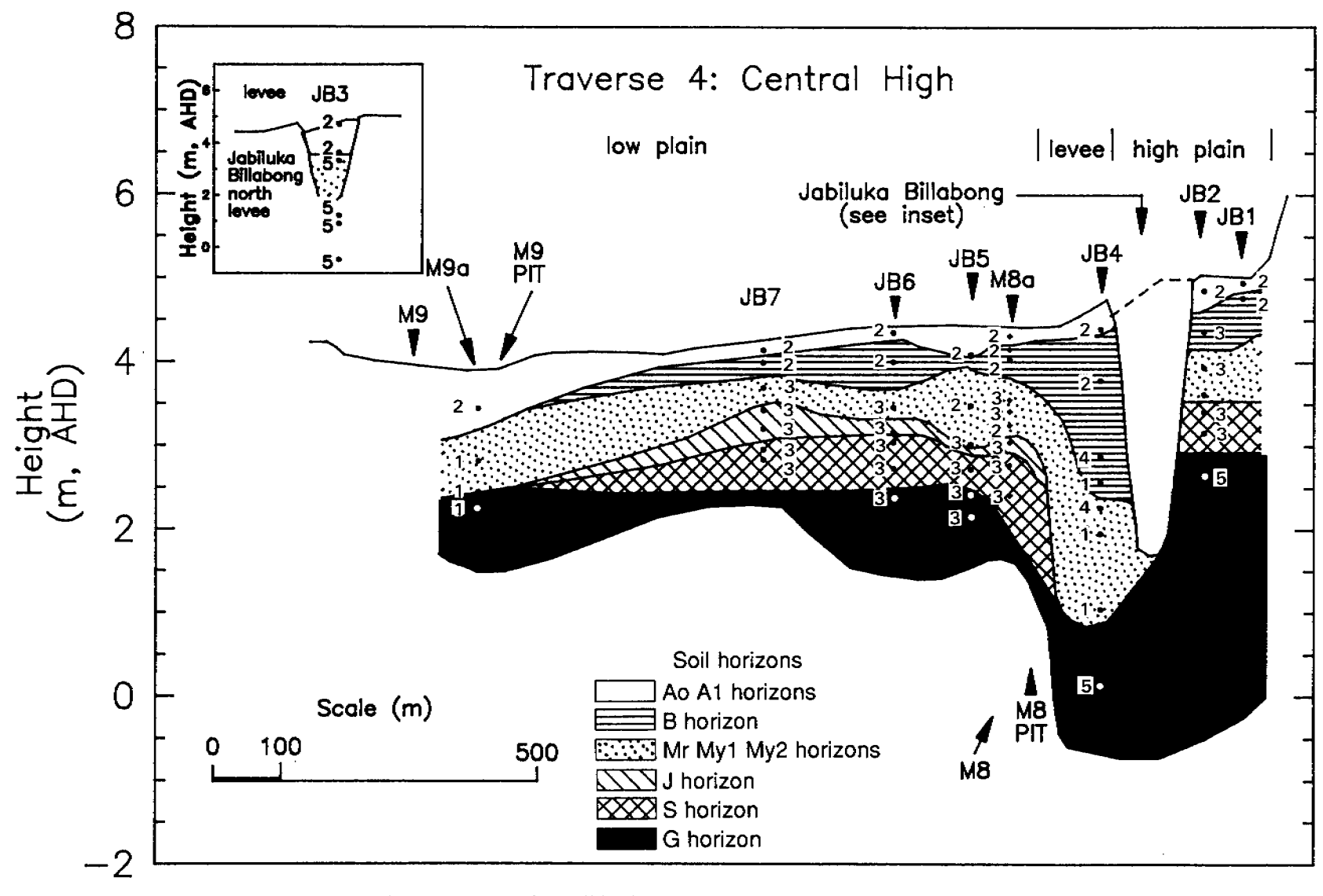


Figure 5.4 Cross-section of traverse 4 showing soil horizons

Figure 5.5 Cross-section of traverse 5 showing soil horizons

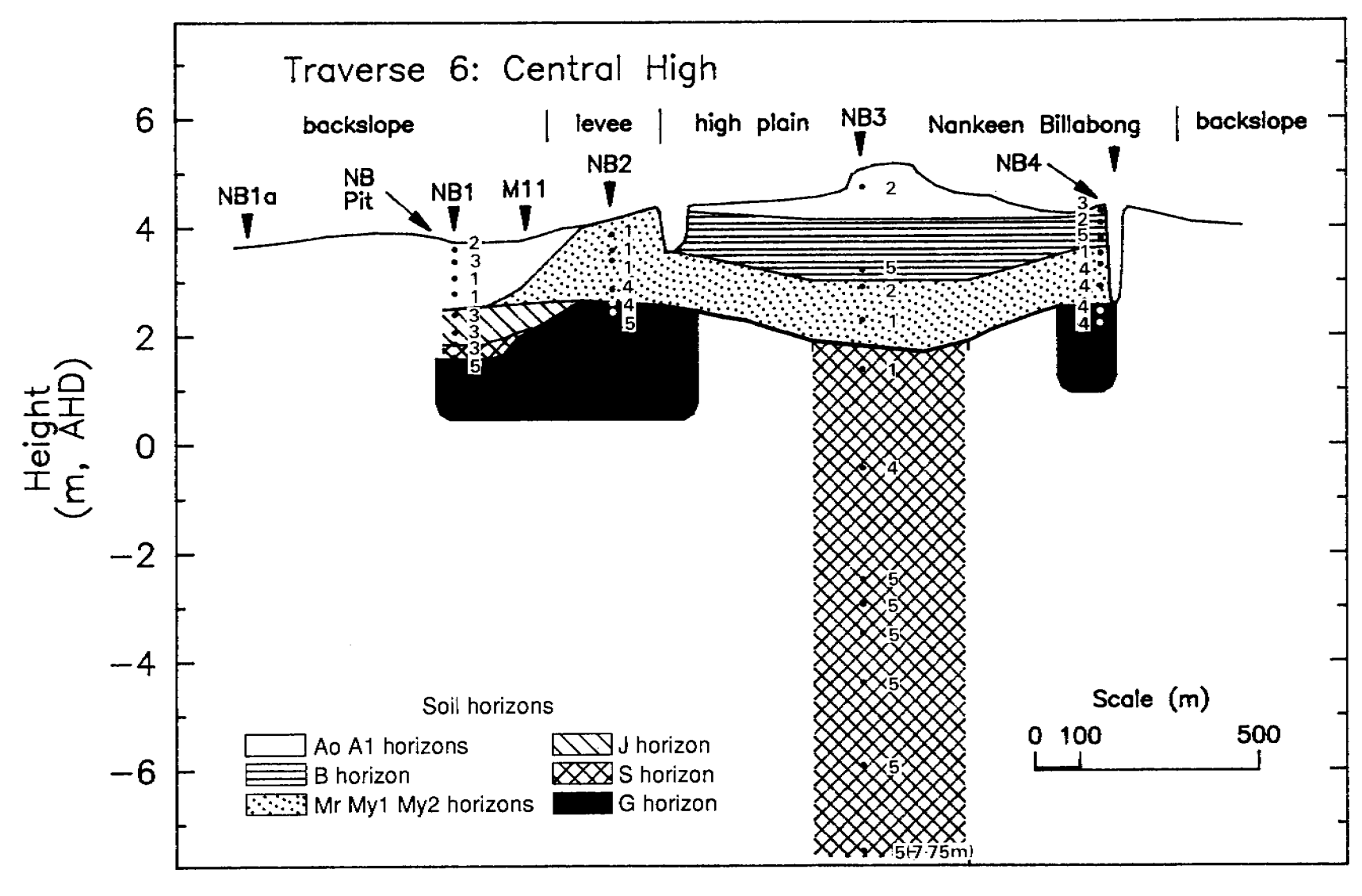


Figure 5.6 Cross-section of traverse 6 showing soil horizons

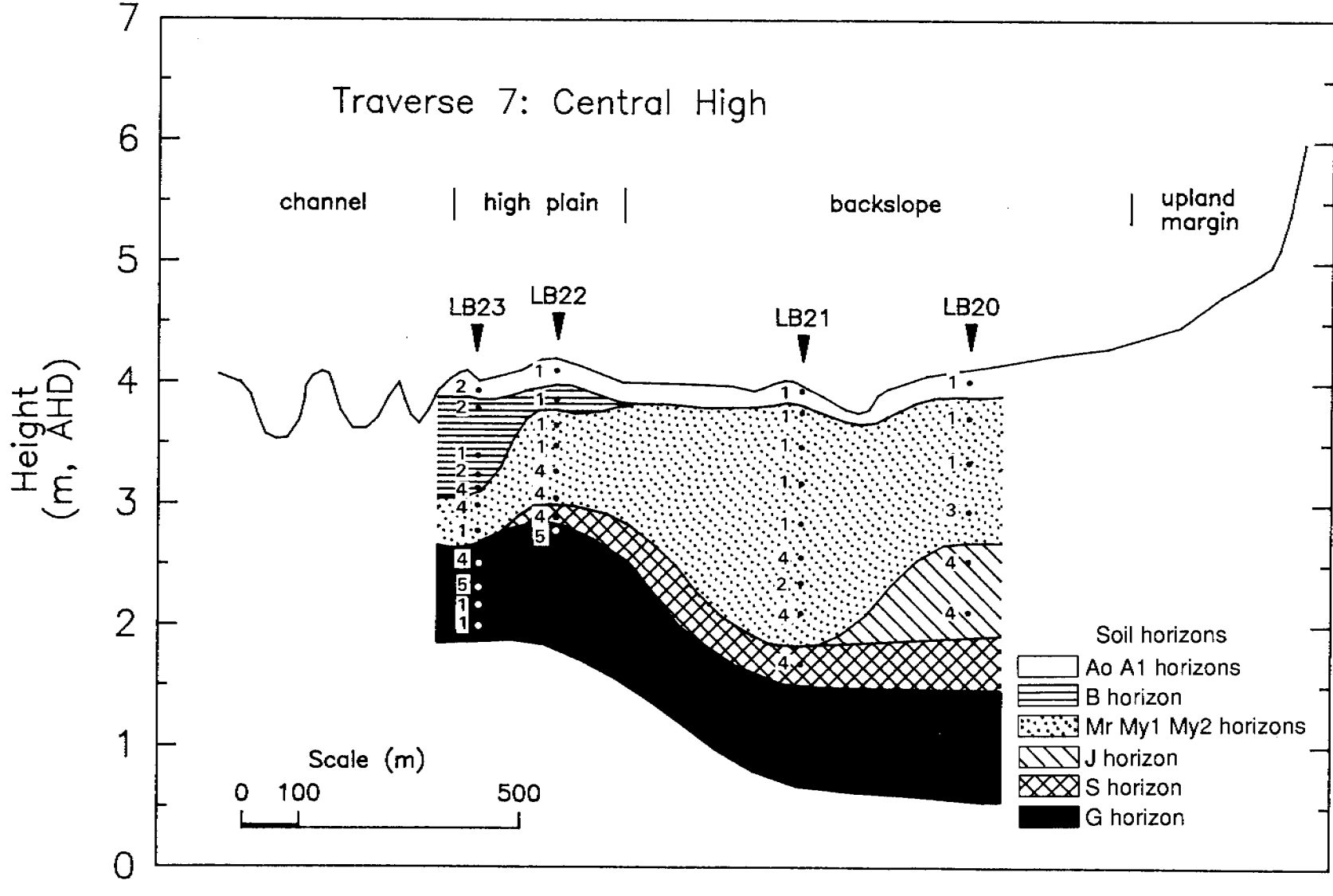


Figure 5.7 Cross-section of traverse 7 showing soil horizons



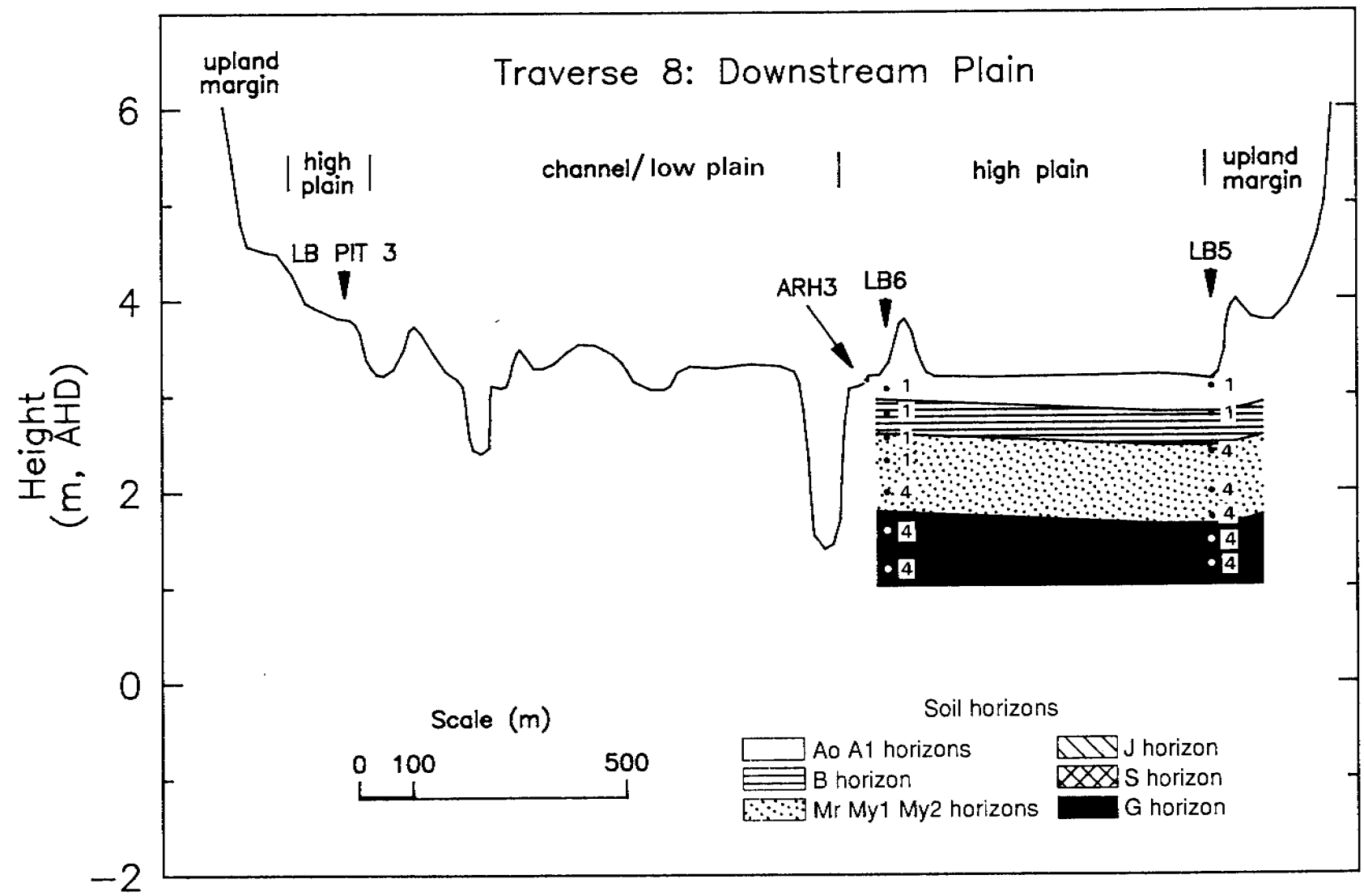


Figure 5.8 Cross-section of traverse 8 showing soil horizons

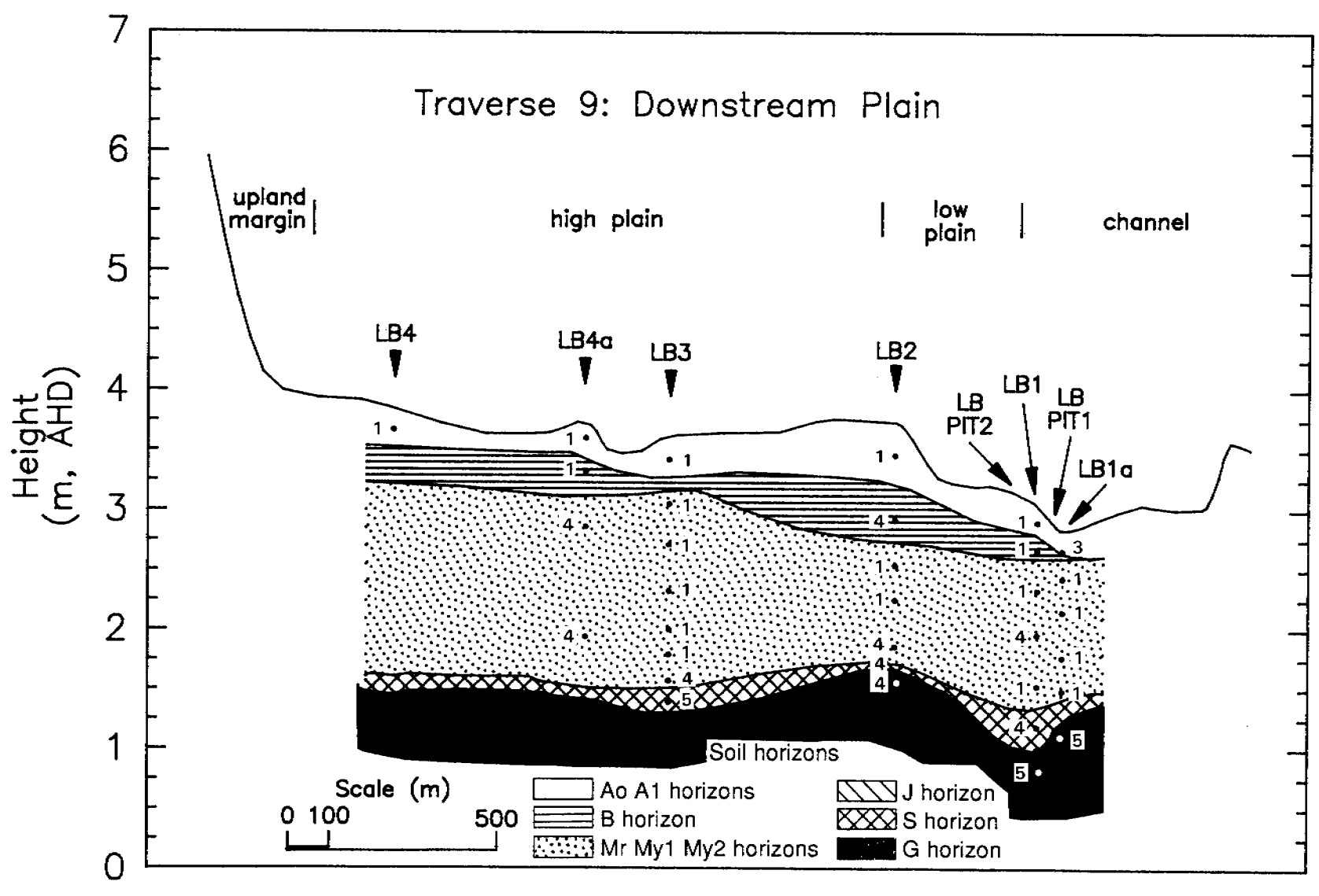


Figure 5.9 Cross-section of traverse 9 showing soil horizons

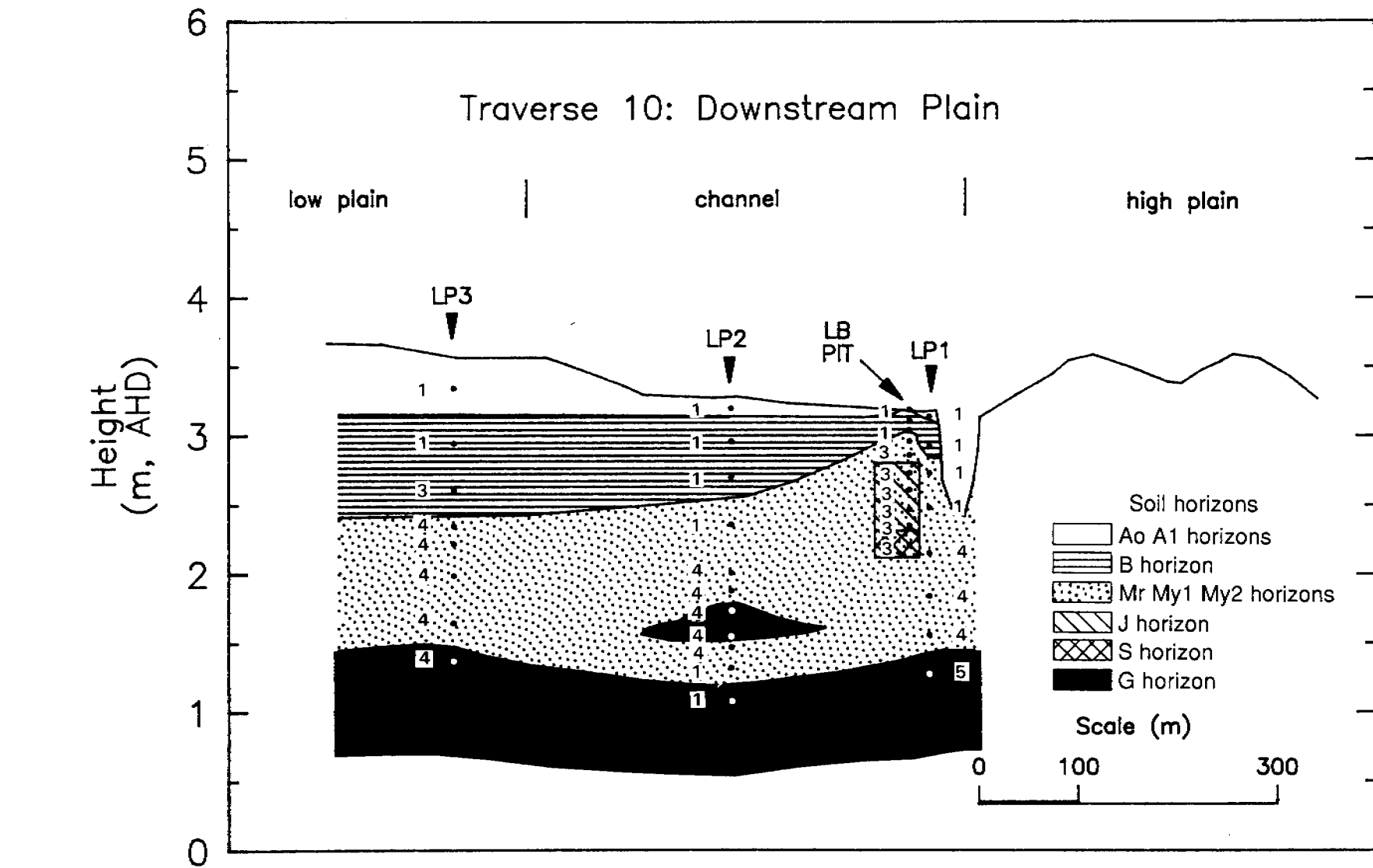


Figure 5.10 Cross-section of traverse 10 showing soil horizons

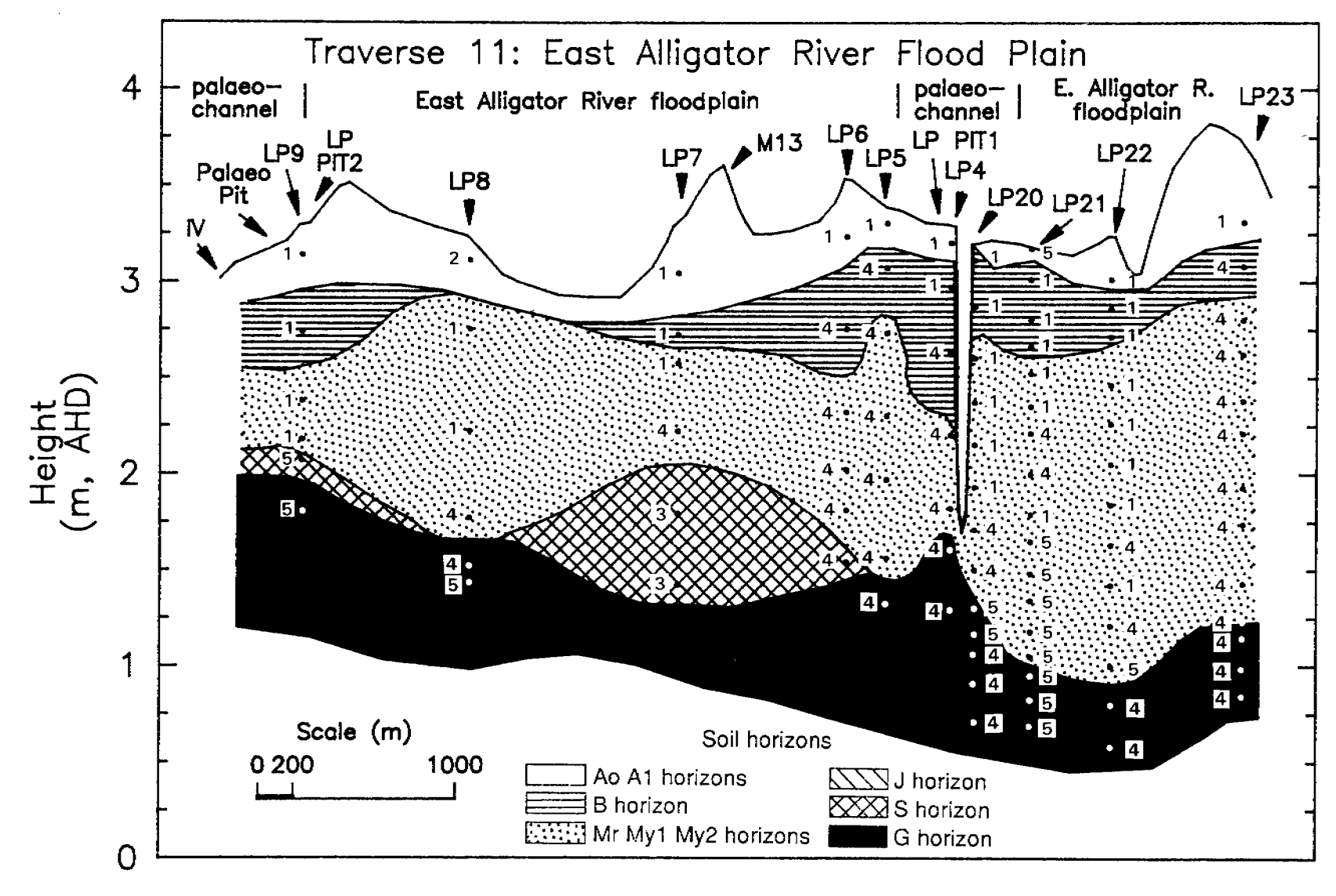


Figure 5.11 Cross-section of traverse 11 showing soil horizons

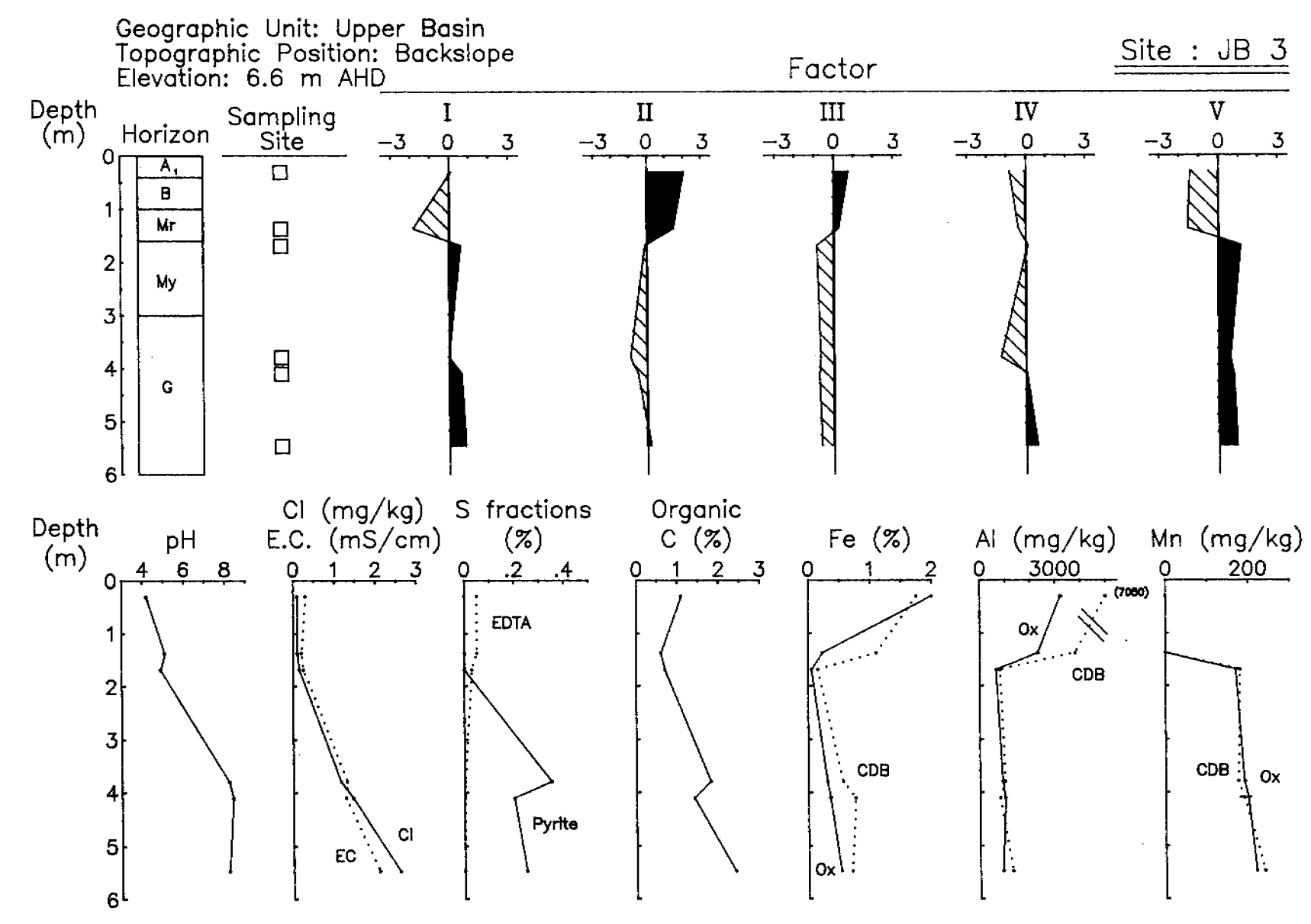


Figure 5.12 Relationships between factor loadings and soil chemical properties with depth for profile JB3

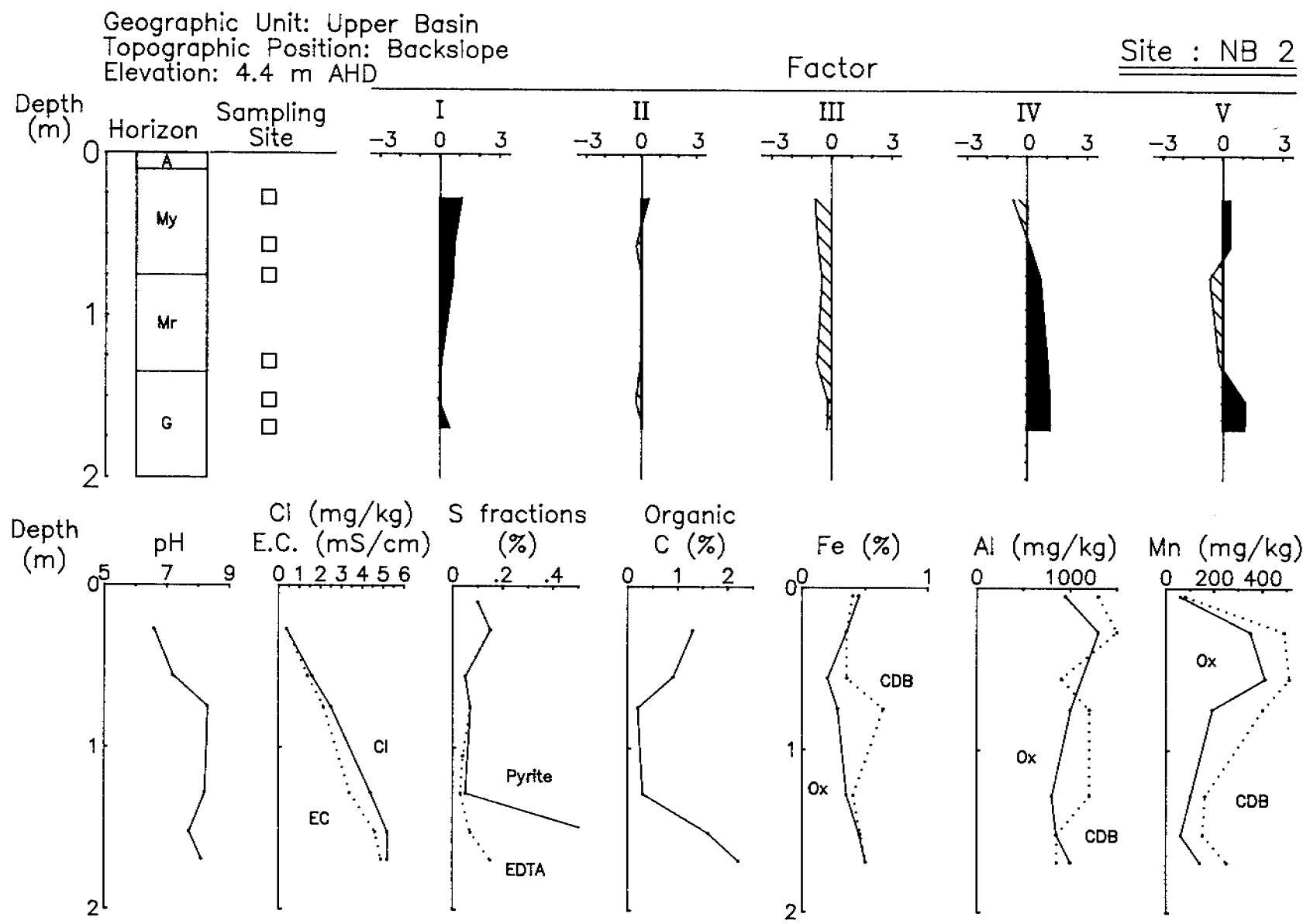


Figure 5.13 Relationships between factor loadings and soil chemical properties with depth for profile NB2

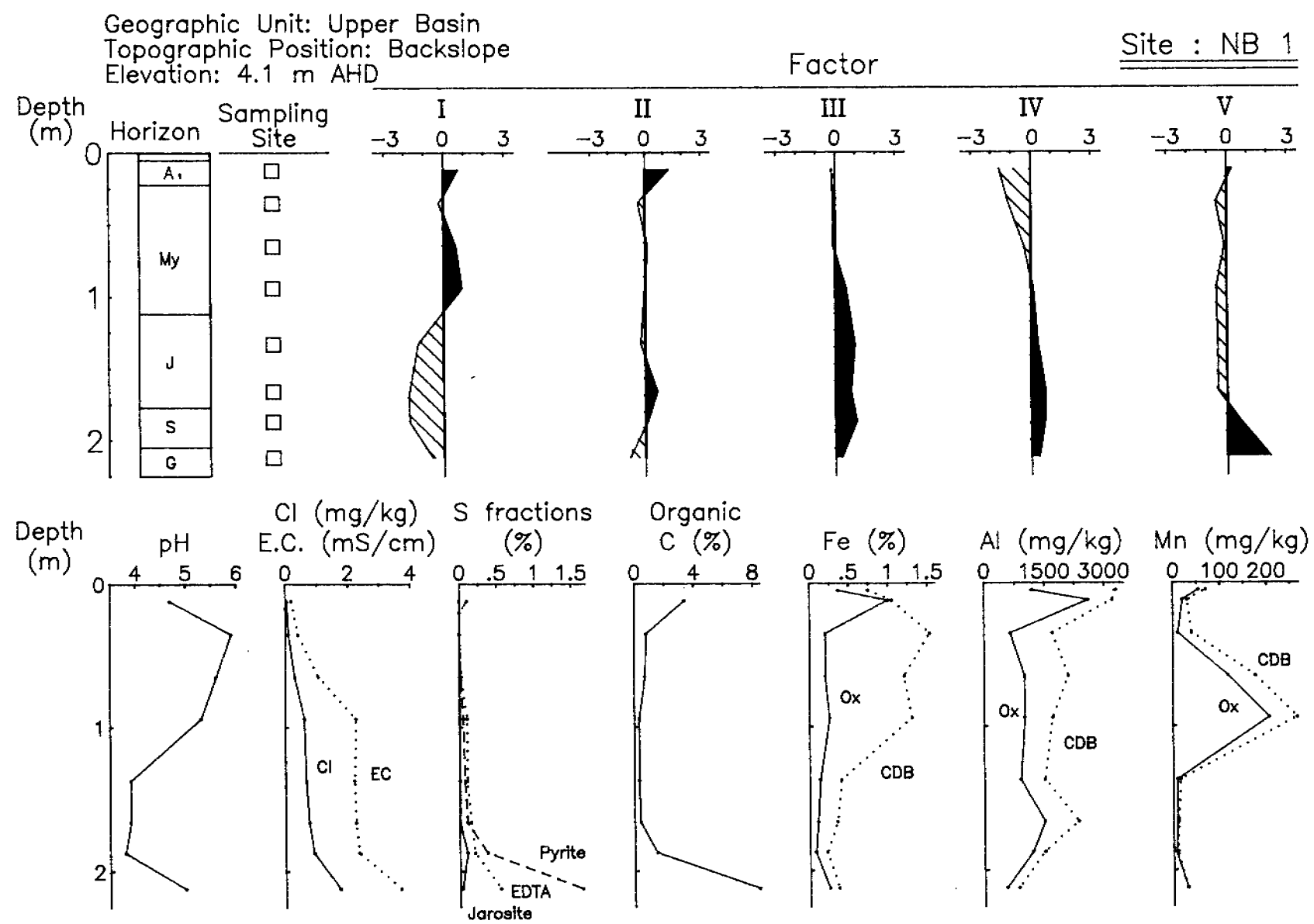


Figure 5.14 Relationships between factor loadings and soil chemical properties with depth for profile NB1

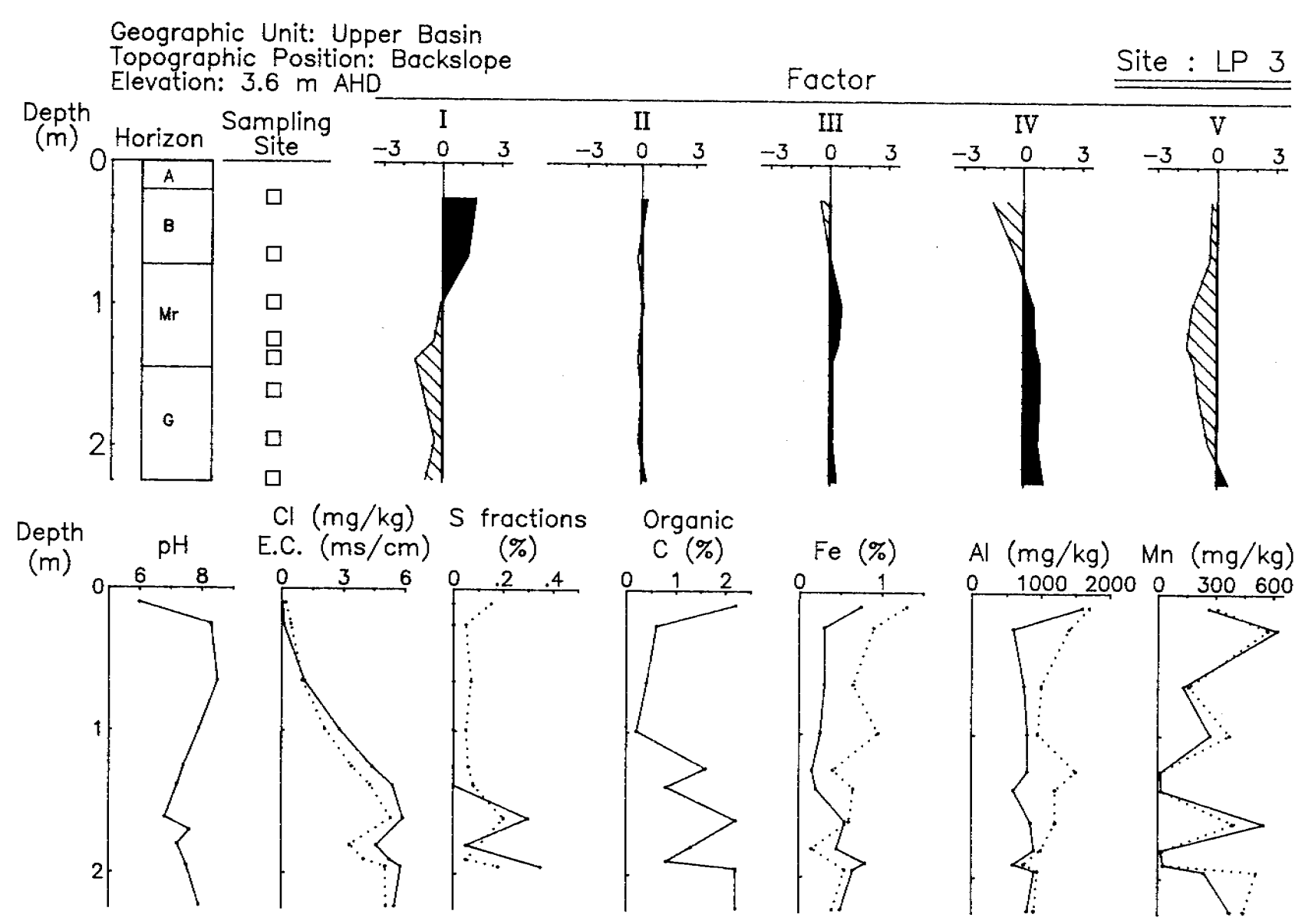


Figure 5.15 Relationships between factor loadings and soil chemical properties with depth for profile LP3



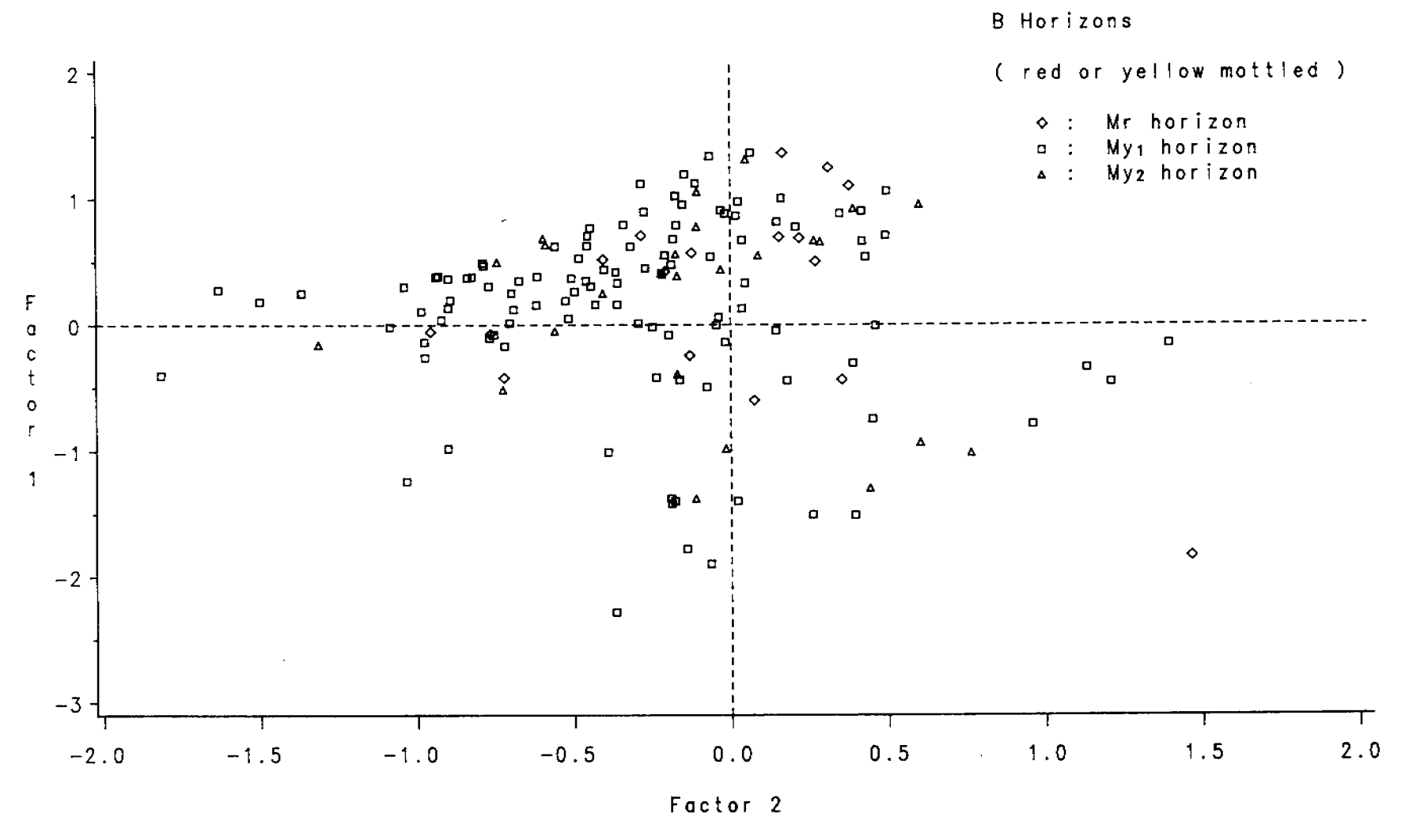


Figure 5.16 Loadings of factors 1 and 2 for the B horizons of soils of the Magela Plain

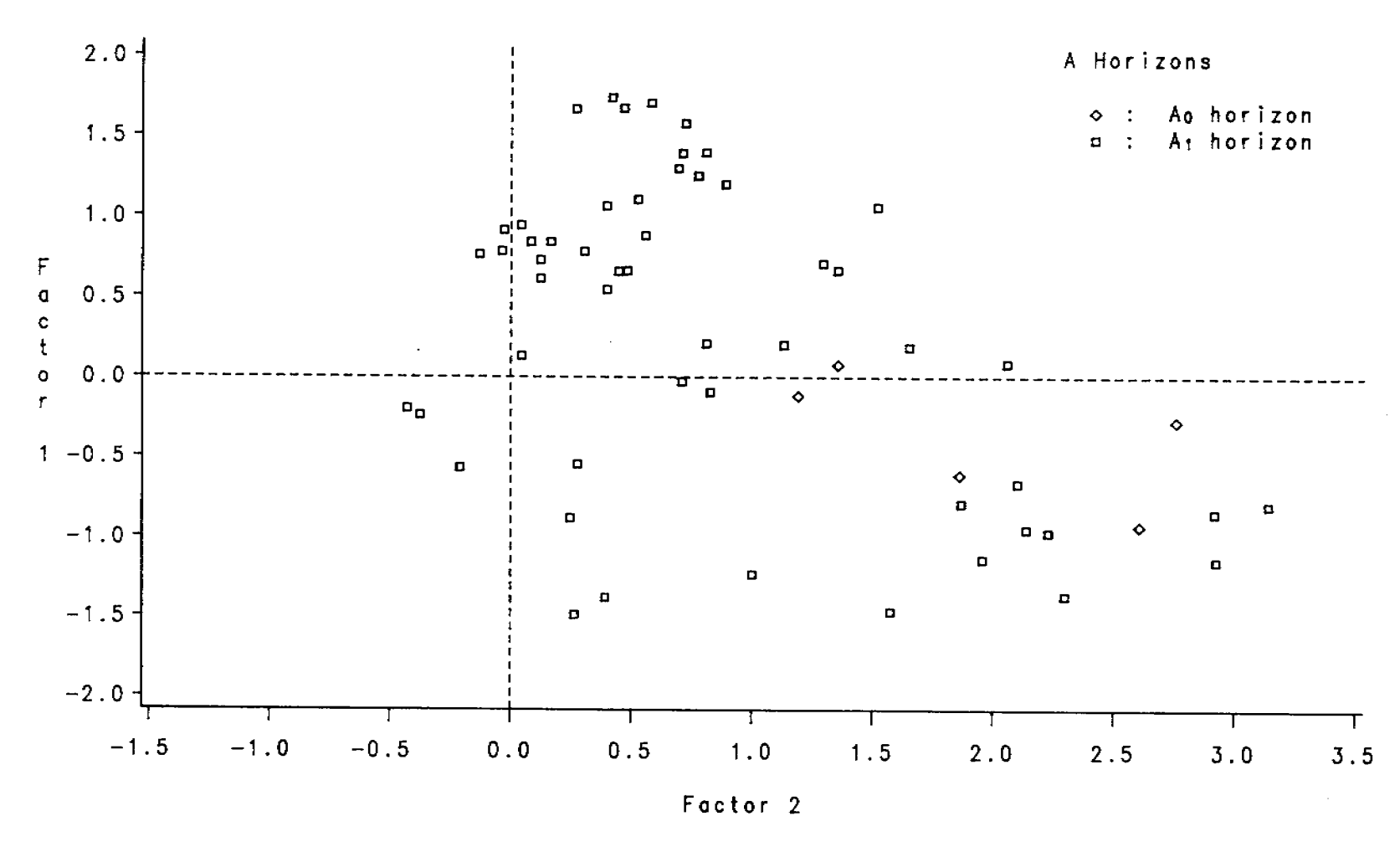


Figure 5.17 Loadings of factors 1 and 2 for the A horizons of soils of the Magela Plain



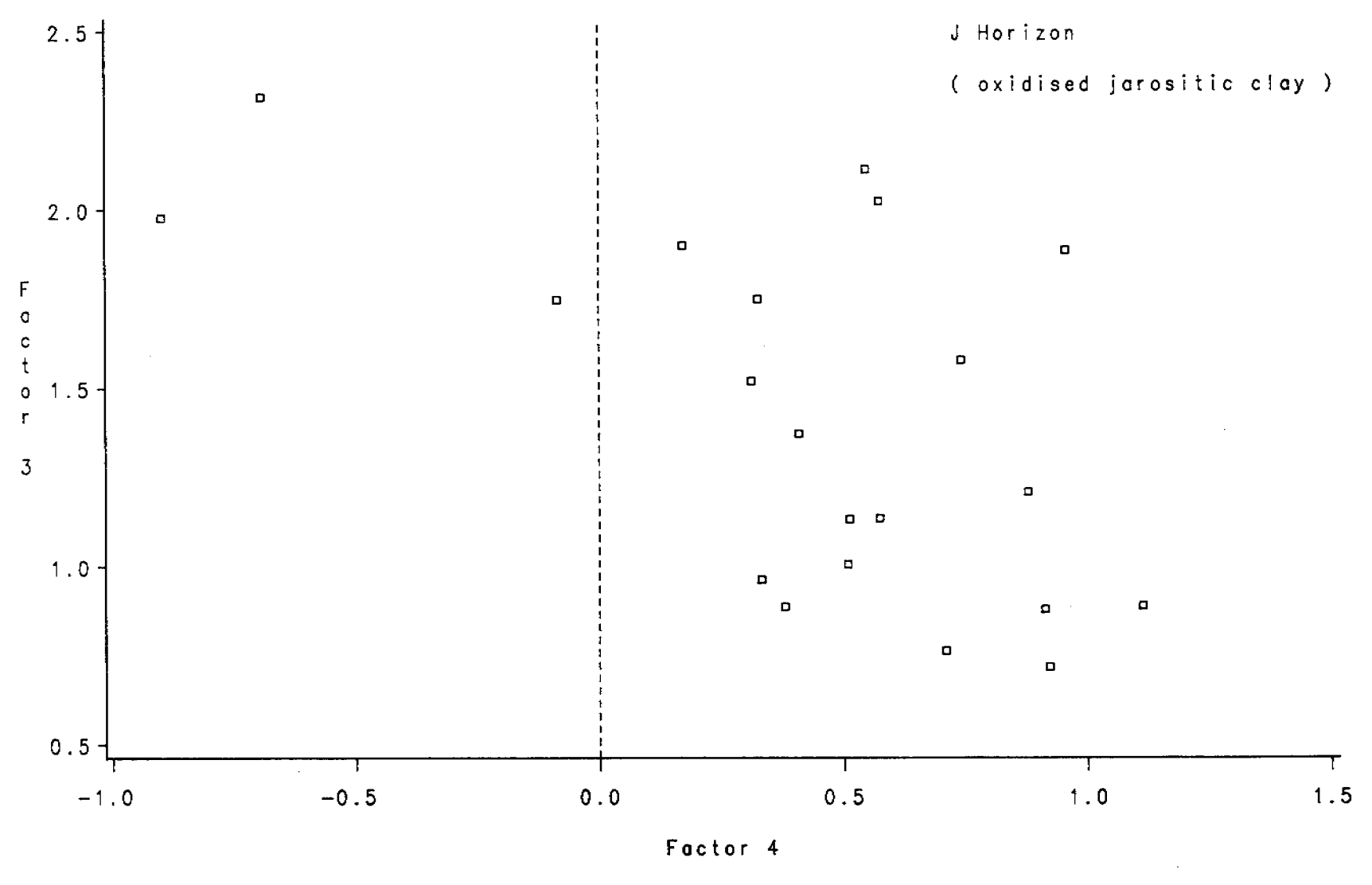


Figure 5.18 Loadings of factors 3 and 4 for the jarositic horizons of soils of the Magela Plain

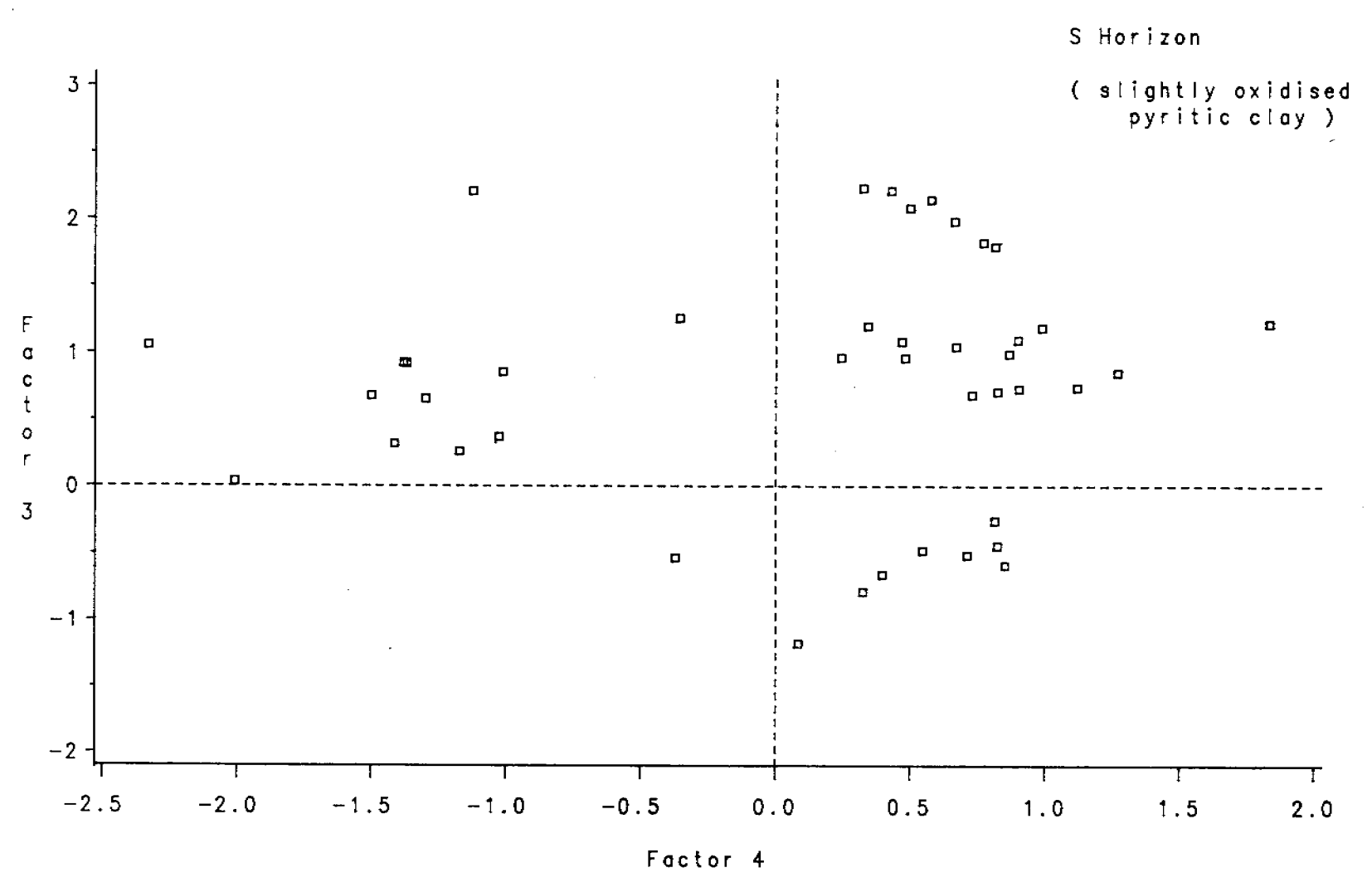


Figure 5.19 Loadings of factors 3 and 4 for the slightly oxidised pyritic clays of the Magela Plain

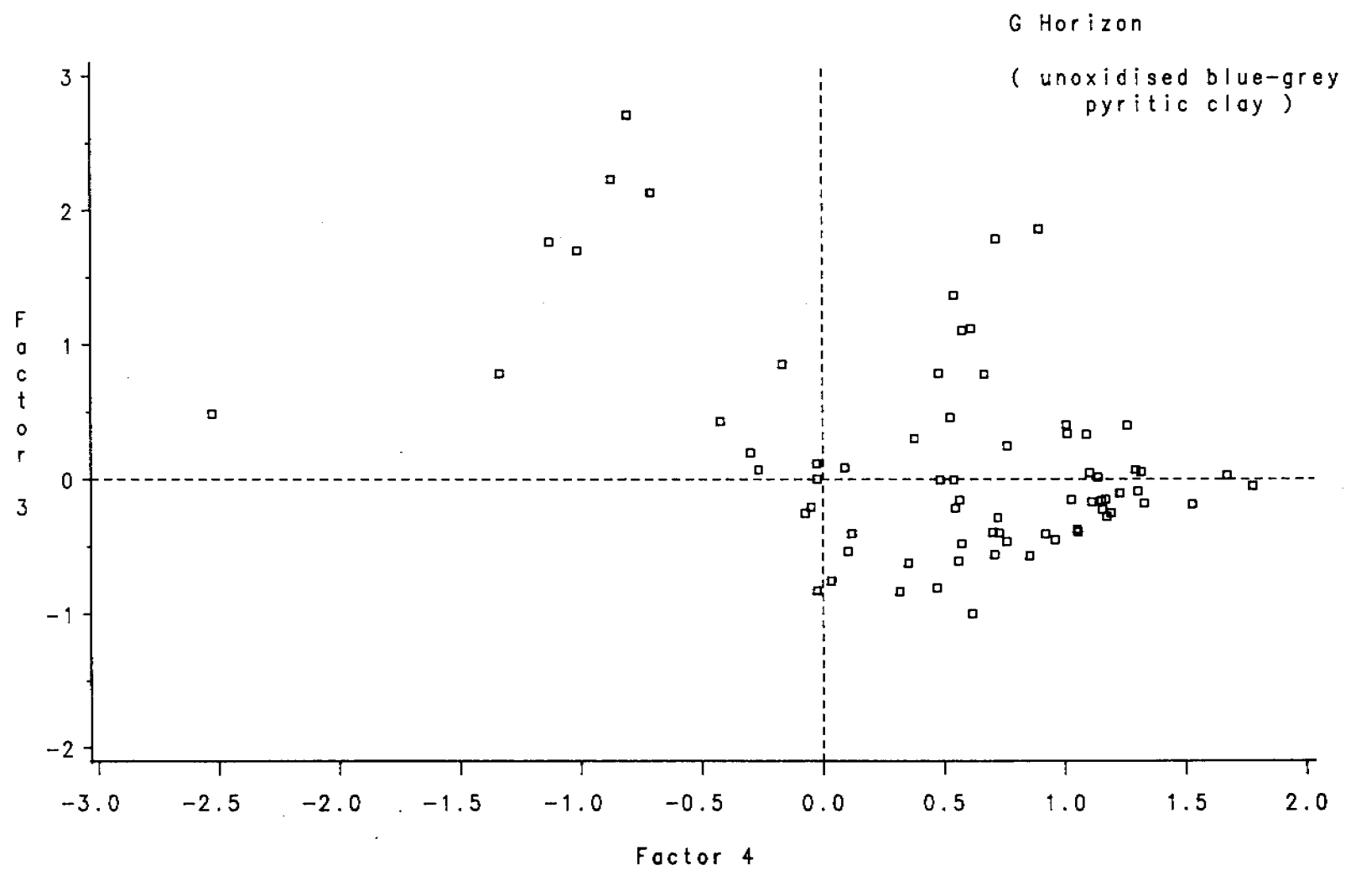


Figure 5.20 Loadings of factors 3 and 4 for the unoxidised pyritic clays of the Magela Plain

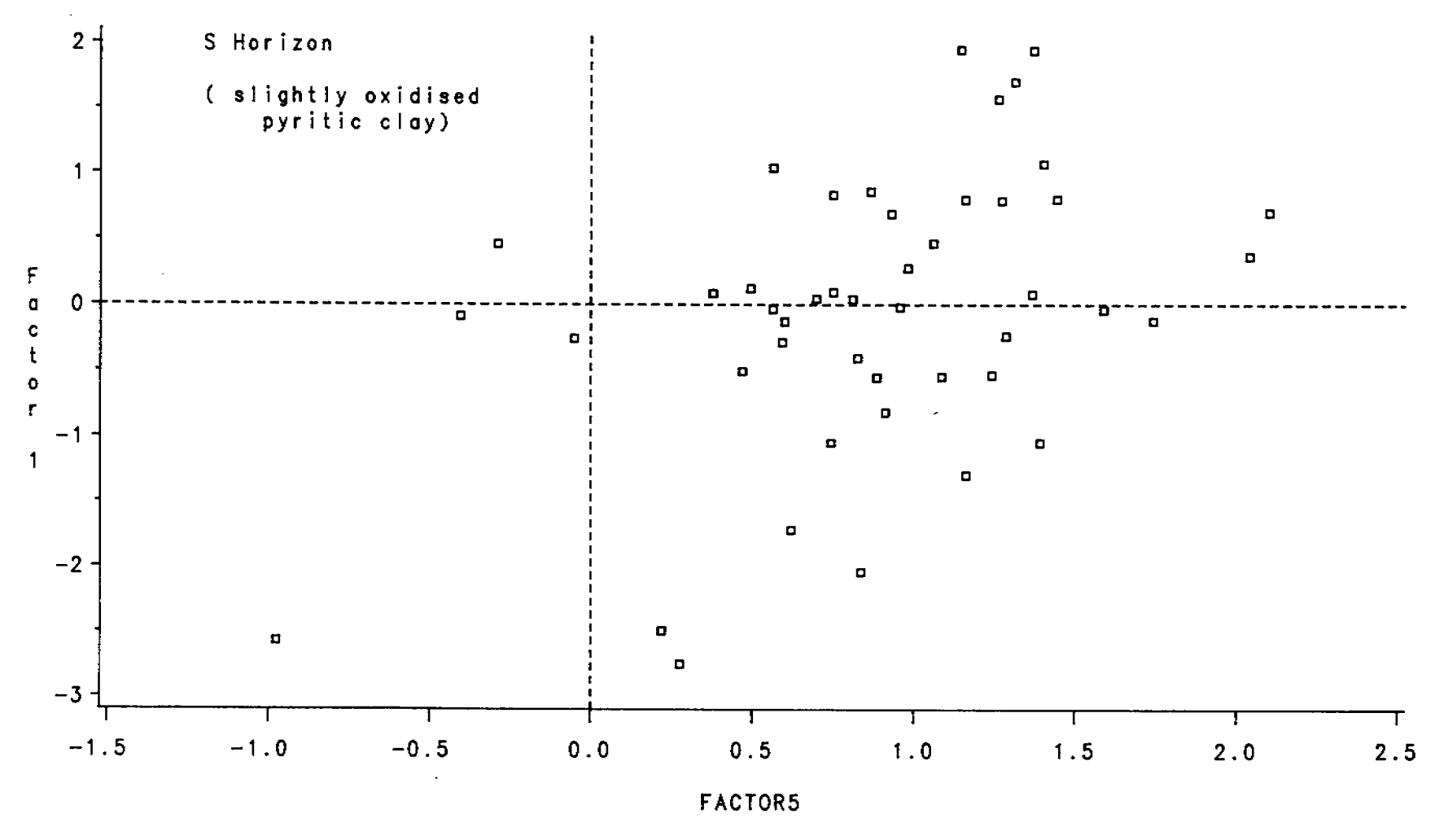


Figure 5.21 Loadings of factors 1 and 5 for the slightly oxidised pyritic clays of the Magela Plain

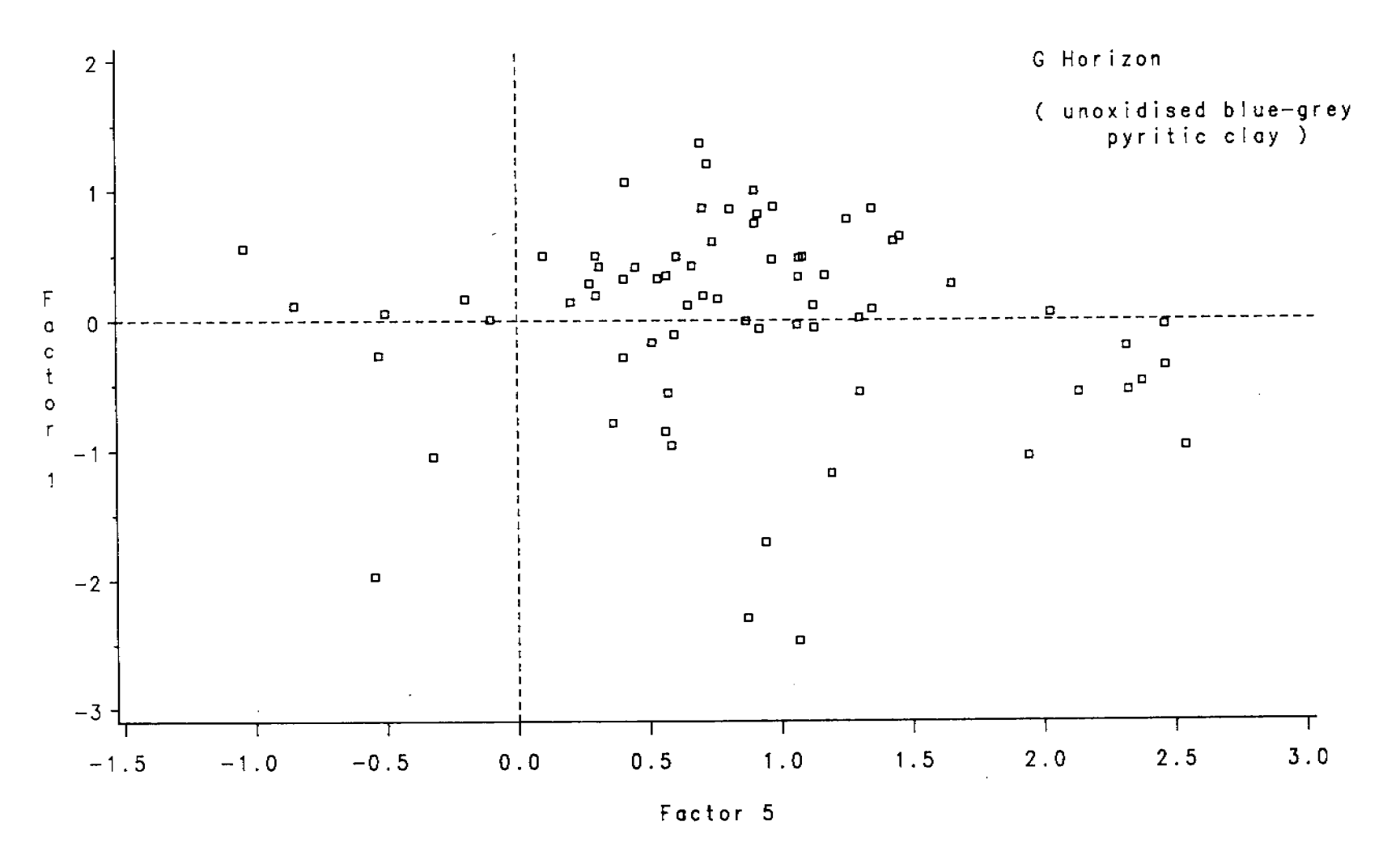


Figure 5.22 Loadings of factors 1 and 5 for the unoxidised blue-grey pyritic clays of the Magela Plain

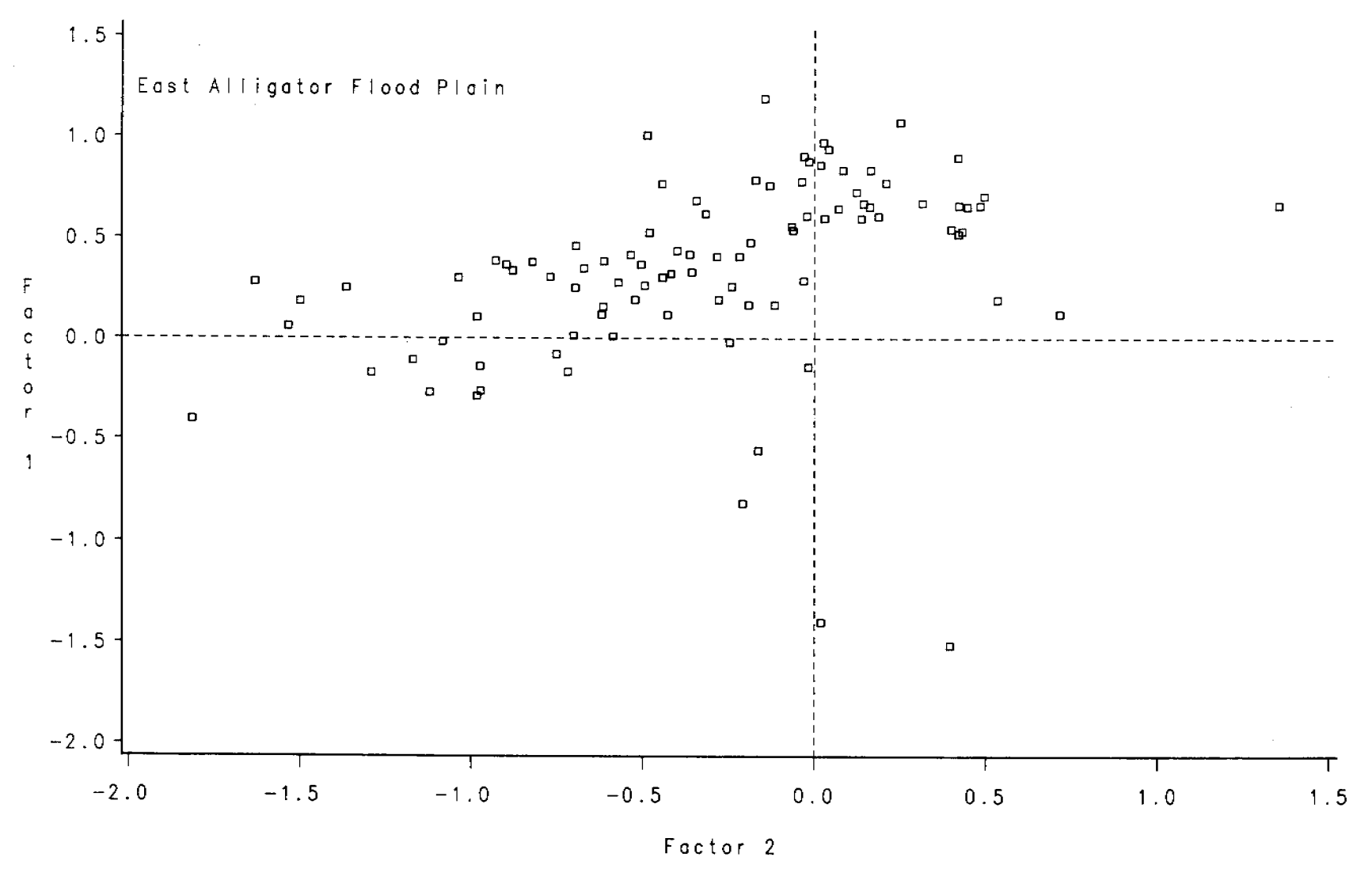


Figure 5.23 Loadings of factors 1 and 2 for soils of the East Alligator Flood Plain

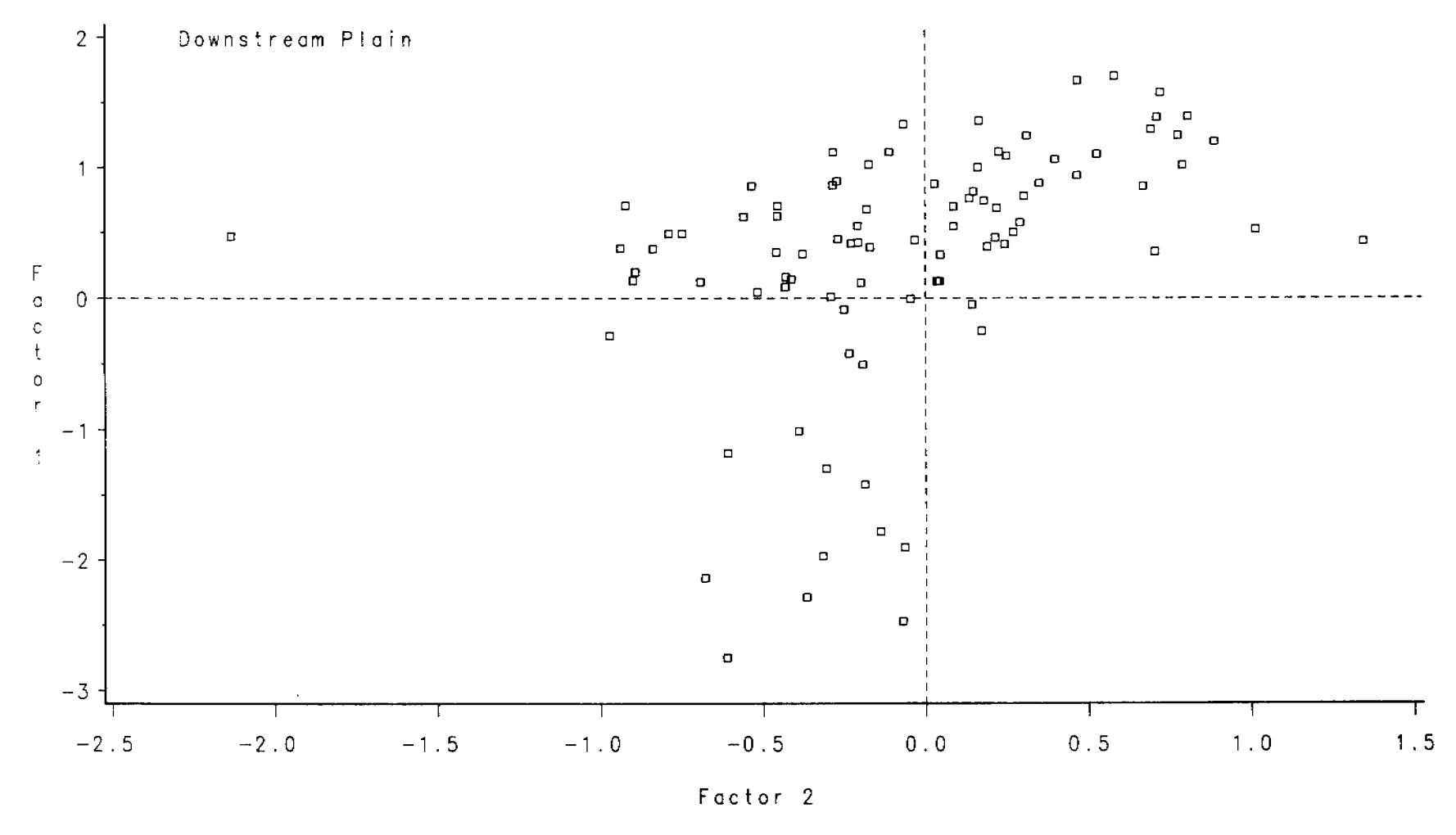


Figure 5.24 Loadings of factors 1 and 2 for soils of the Downstream Plain

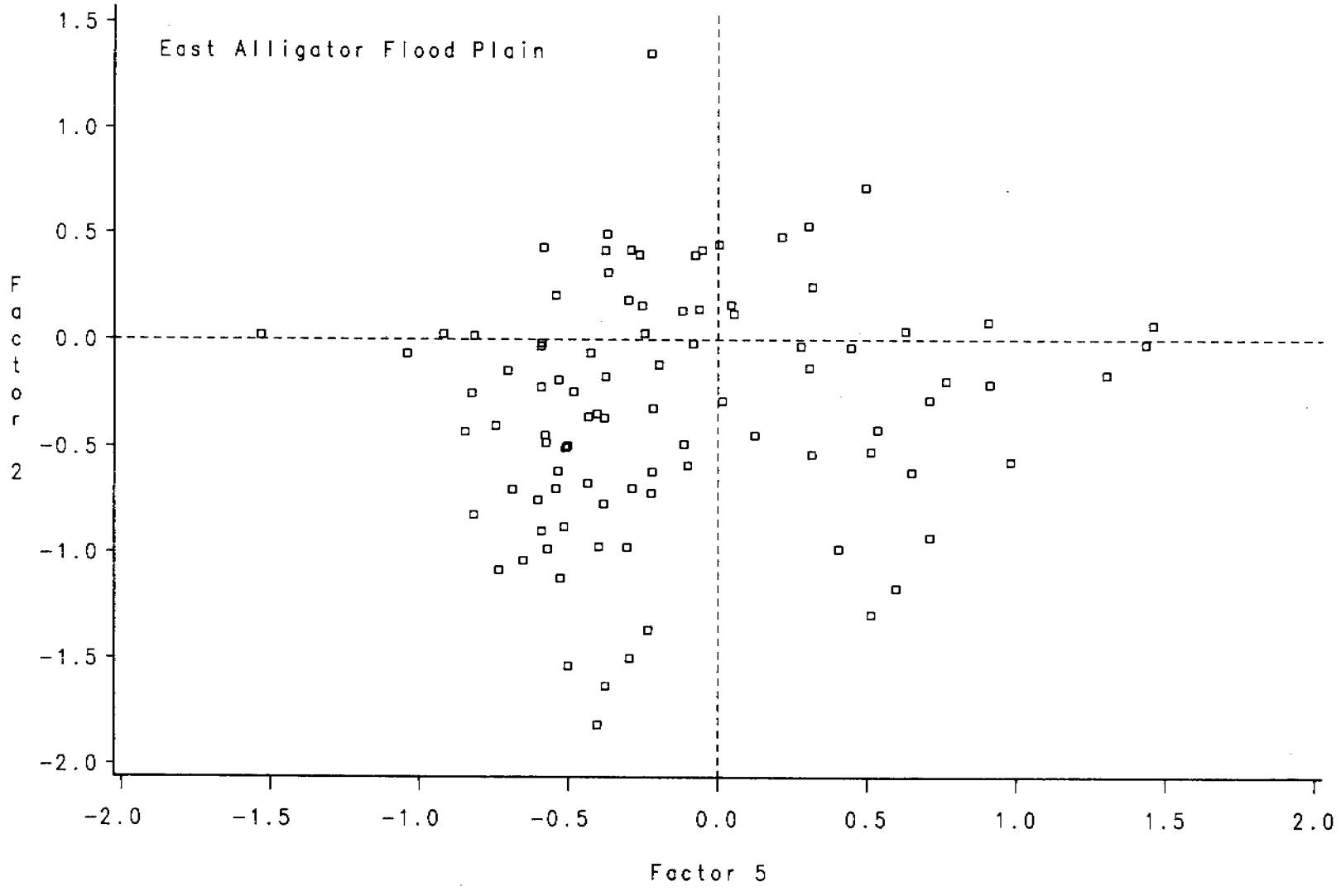


Figure 5.25 Loadings of factors 2 and 5 for soils of the East Alligator Flood Plain

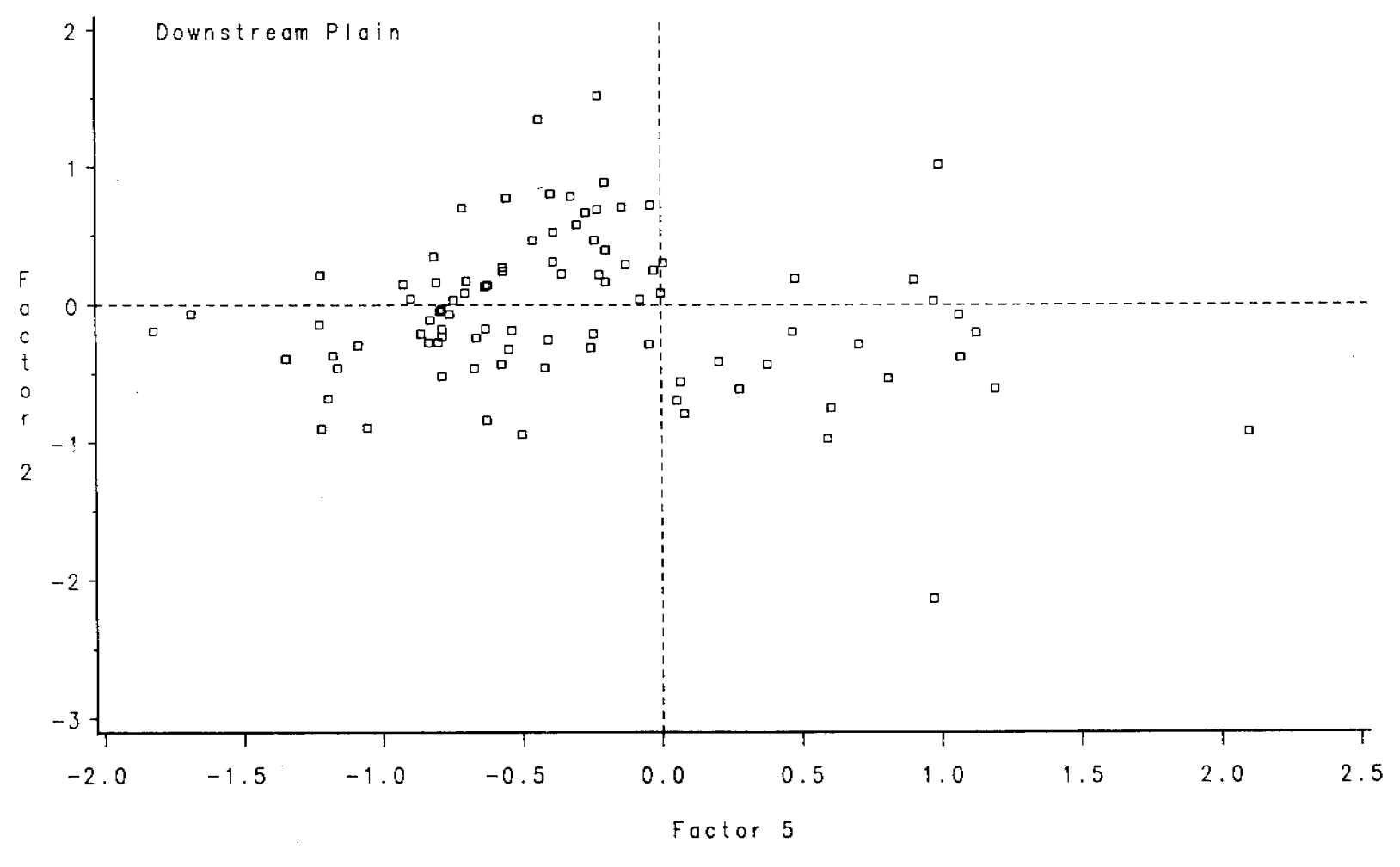


Figure 5.26 Loadings of factors 2 and 5 for soils of the Downstream Plain

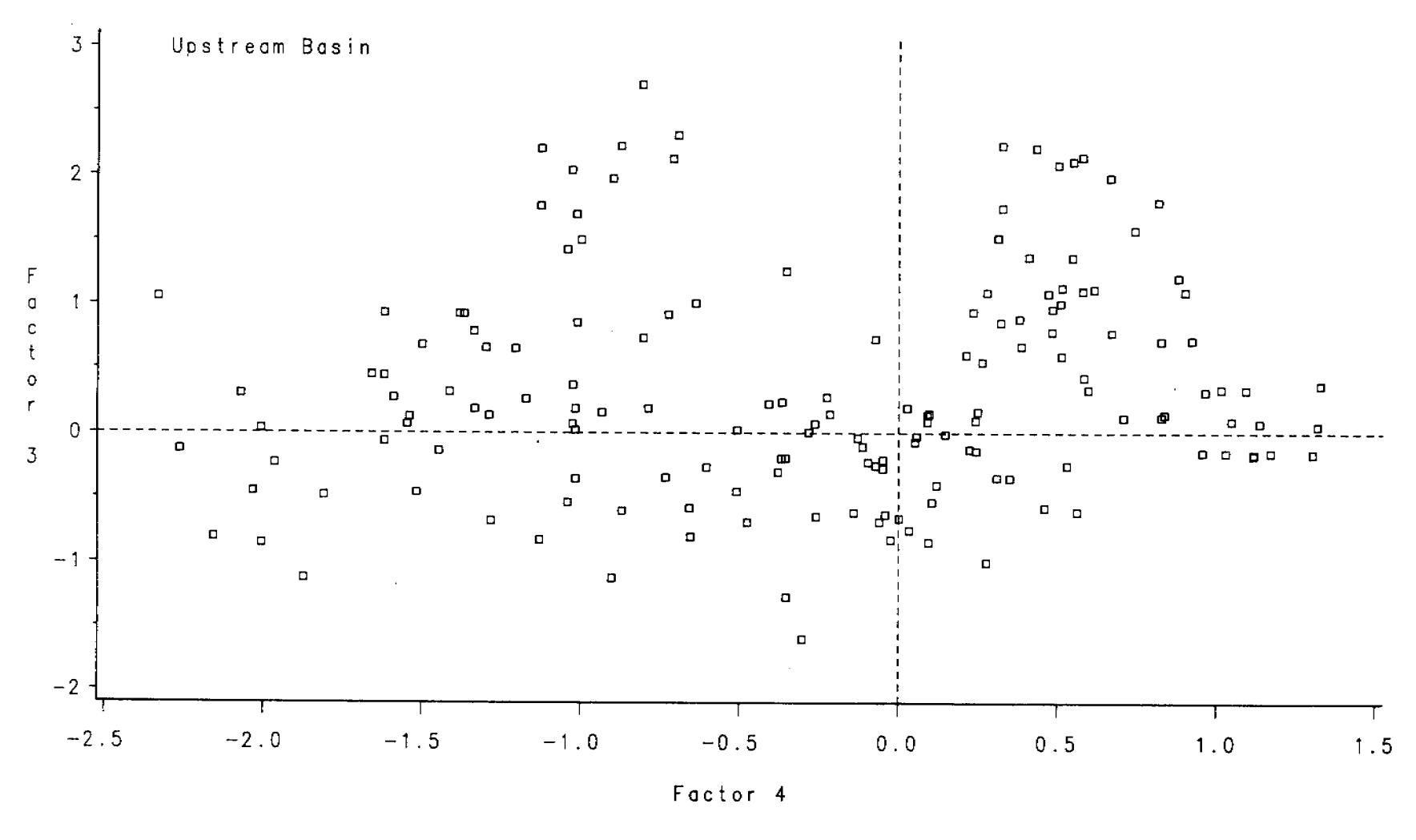


Figure 5.27 Loadings of factors 3 and 4 for soils of the Upstream Basin

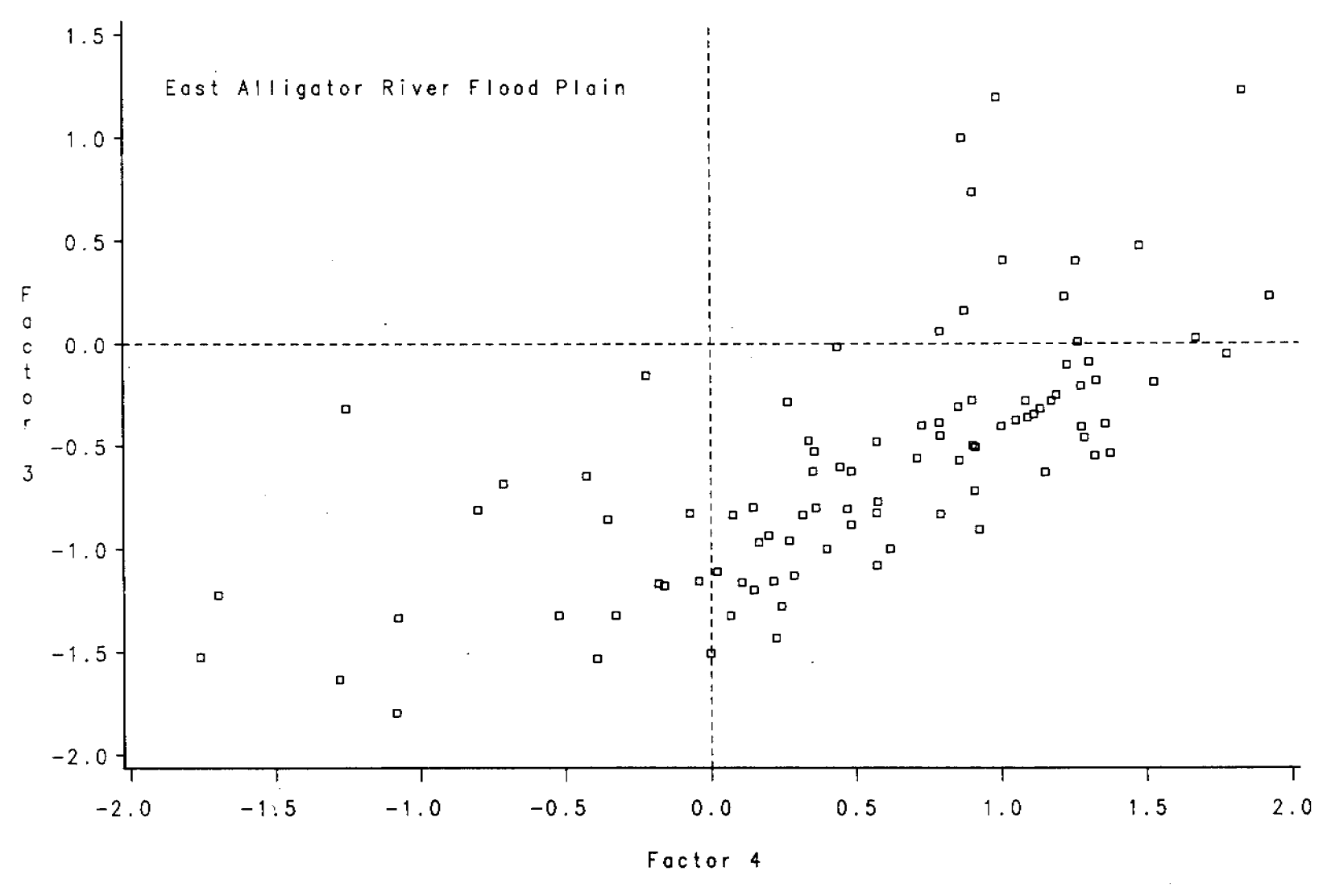


Figure 5.28 Loadings of factors 3 and 4 for soils of the East Alligator River Flood Plain

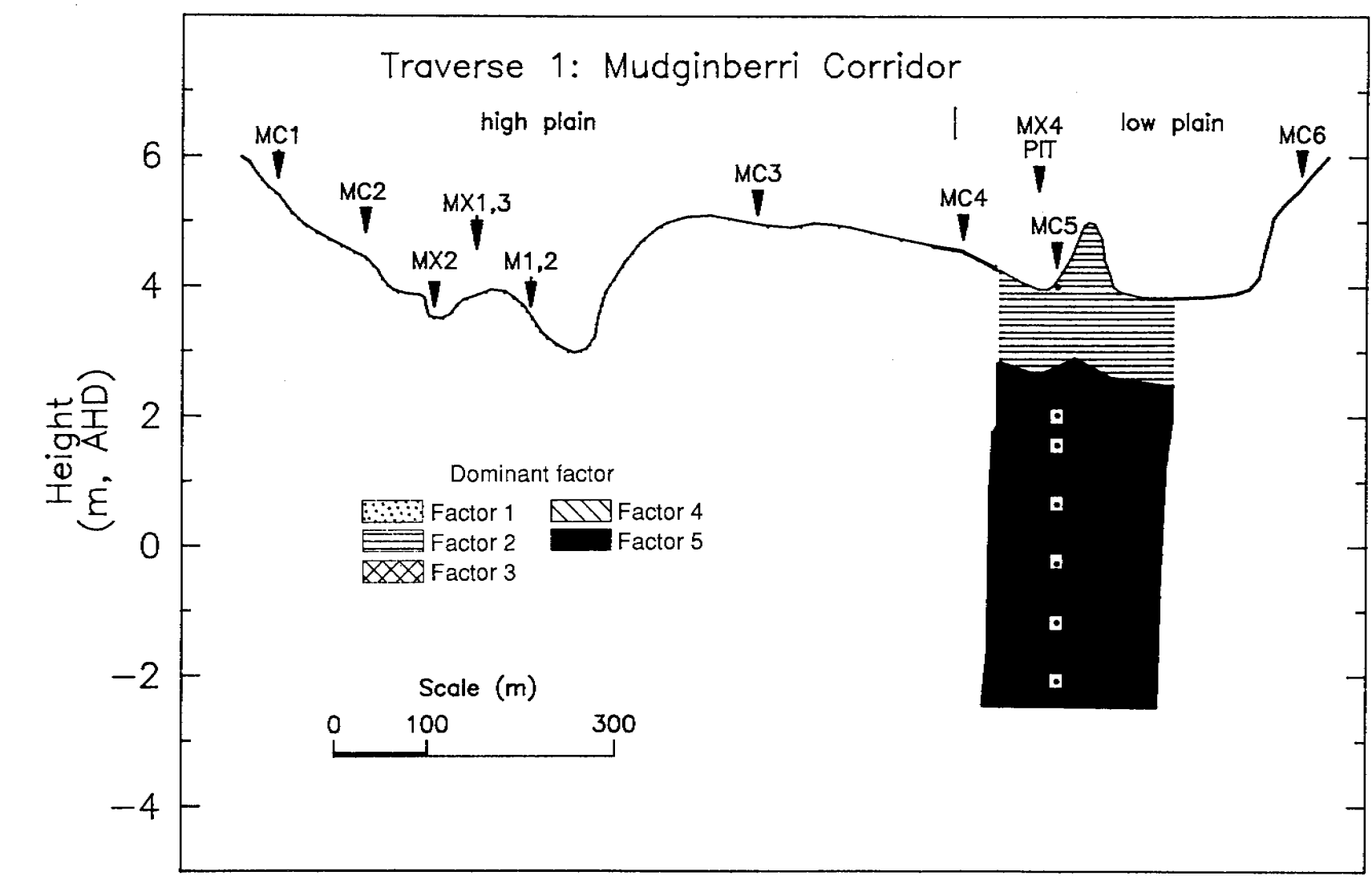


Figure 5.29 Factor loadings in relation to cross-section 1

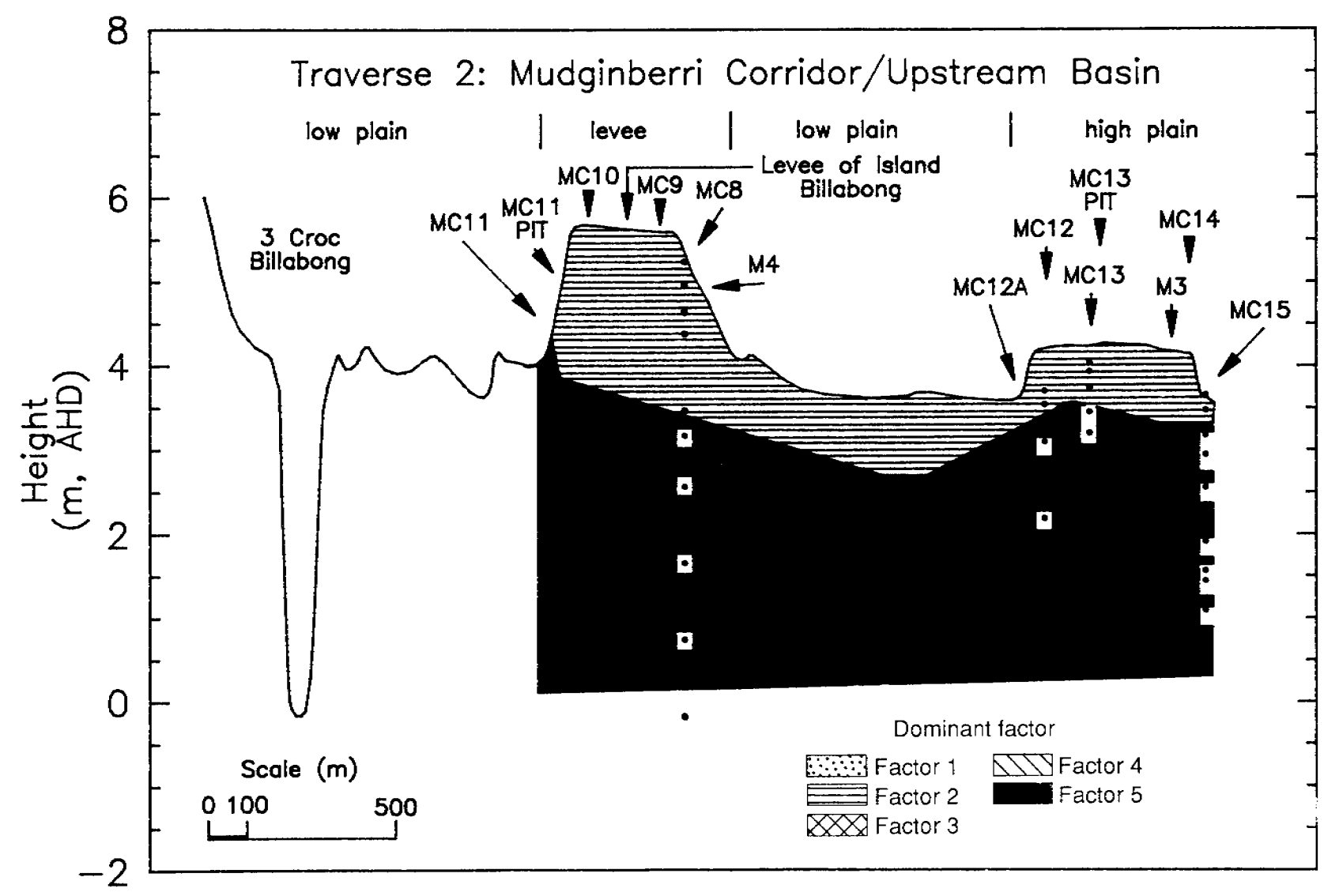


Figure 5.30 Factor loadings in relation to cross-section 2

Figure 5.31 Factor loadings in relation to cross-section 3

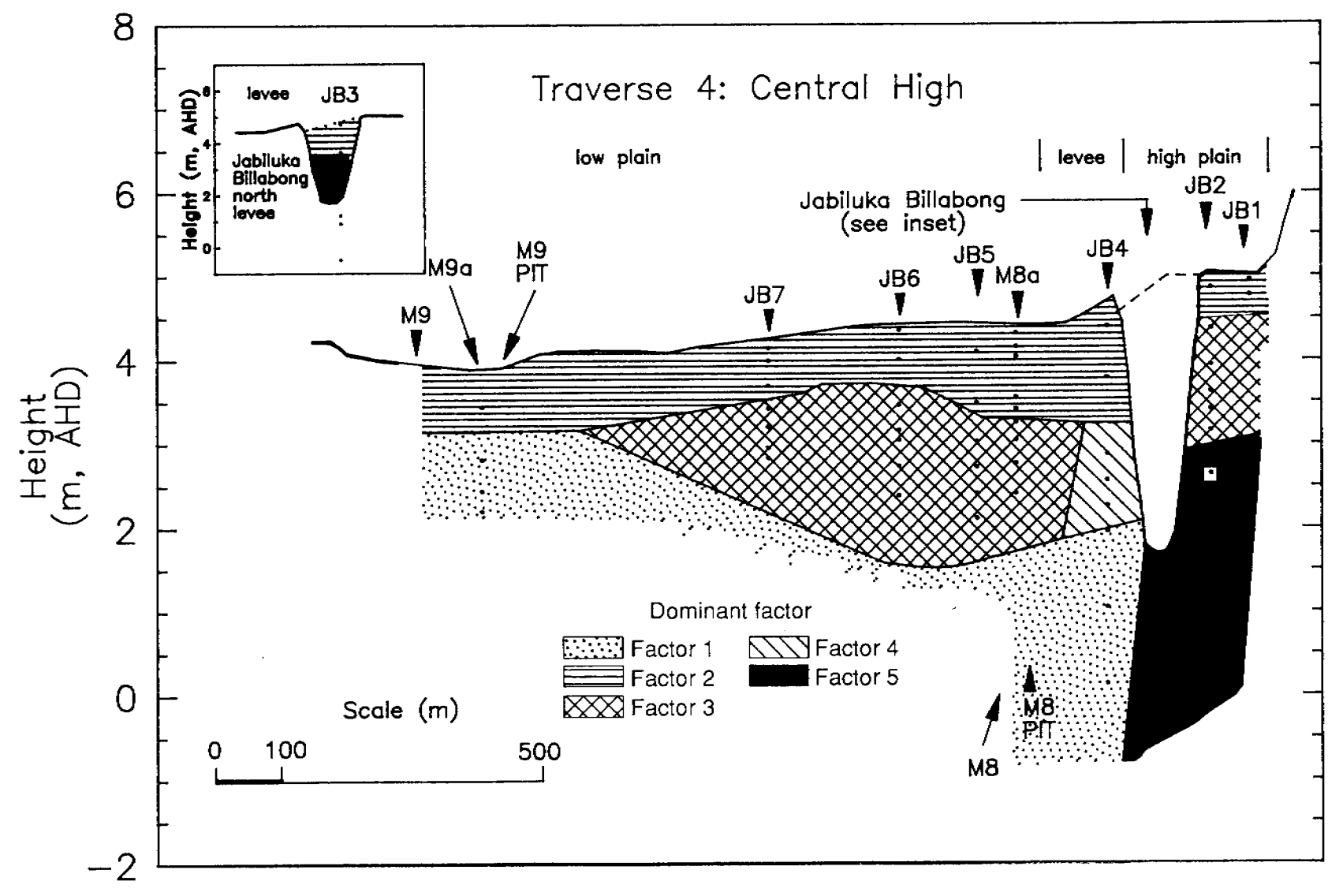


Figure 5.32 Factor loadings in relation to cross-section 4

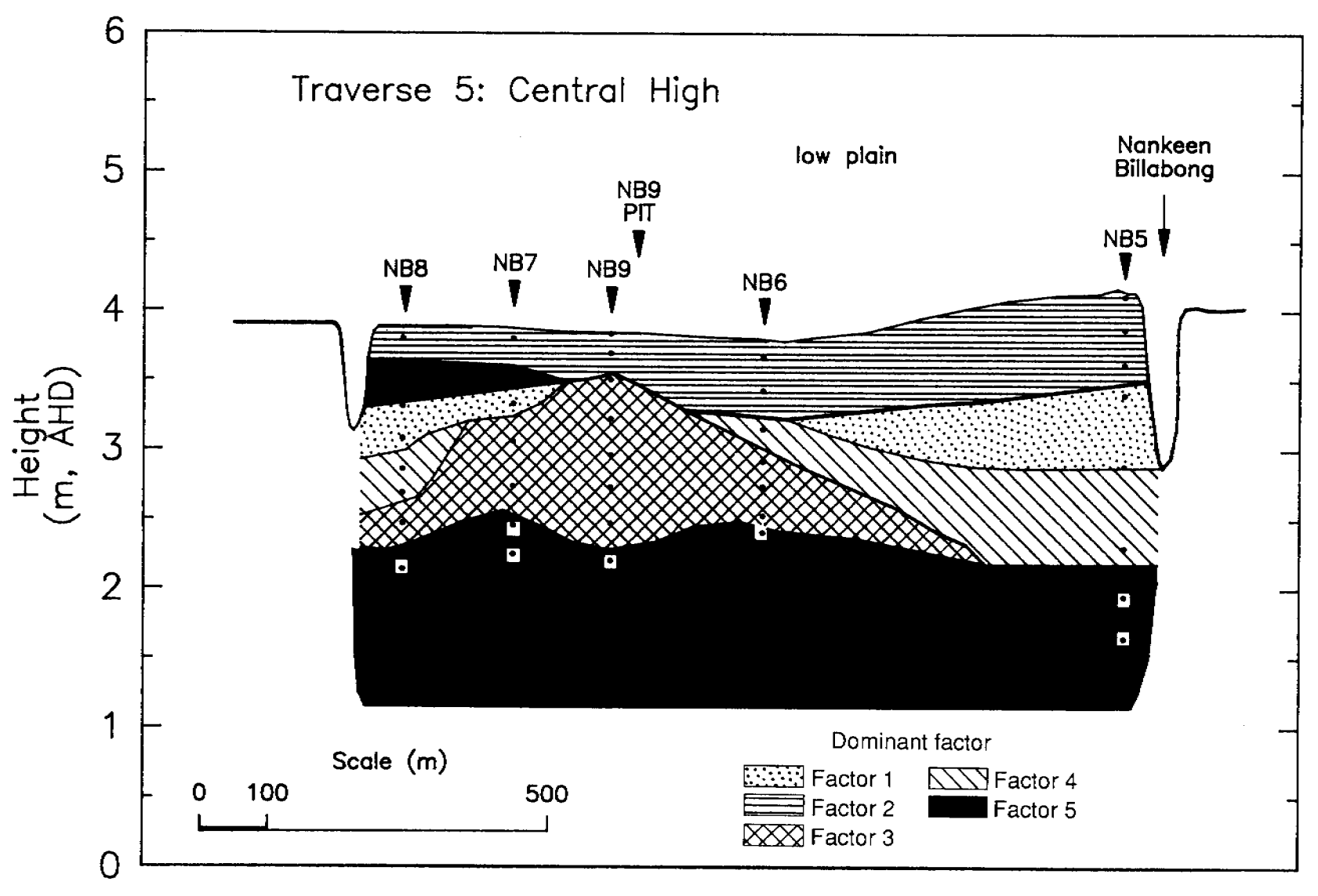


Figure 5.33 Factor loadings in relation to cross-section 5

Figure 5.34 Factor loadings in relation to cross-section 6

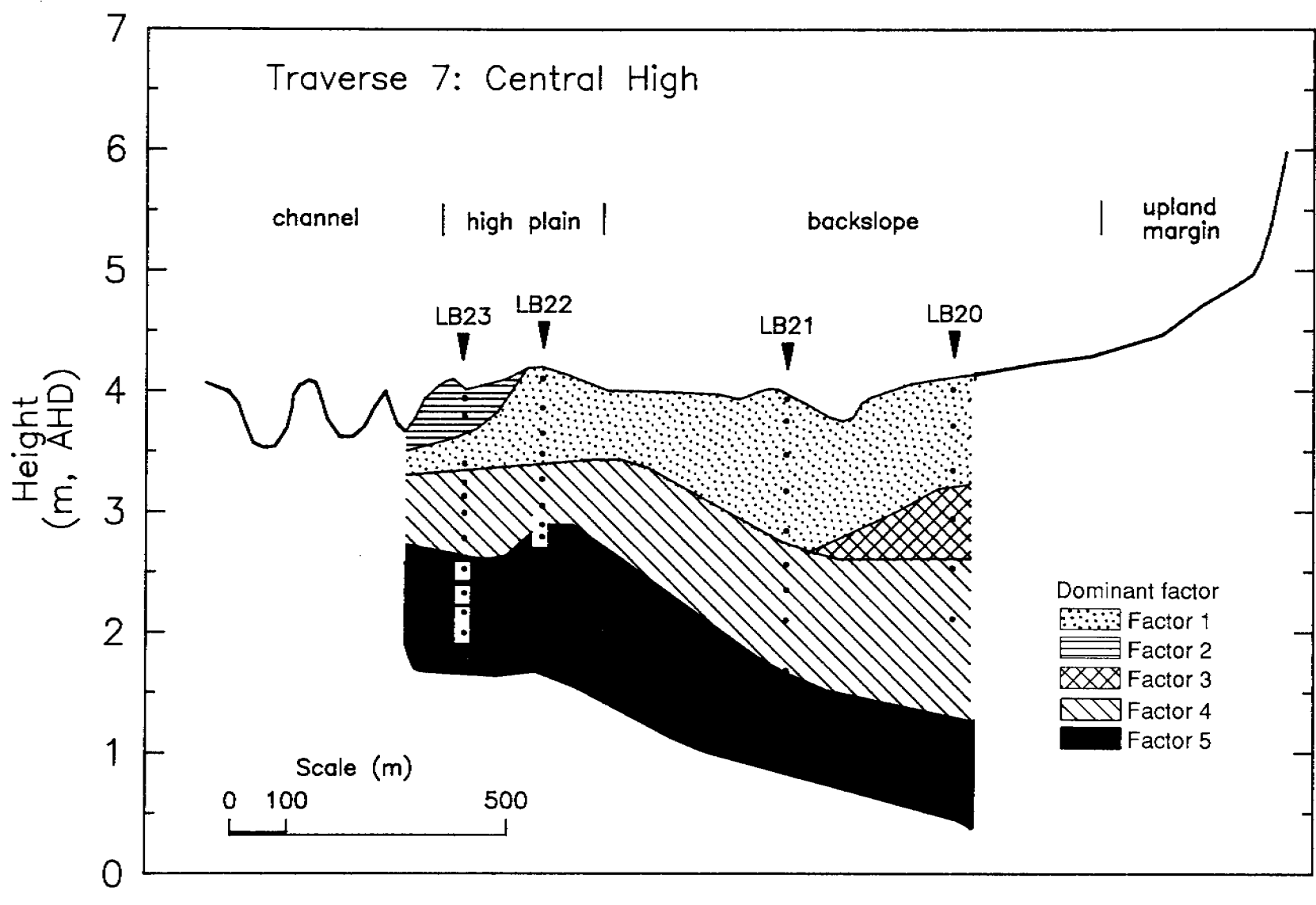


Figure 5.35 Factor loadings in relation to cross-section 7

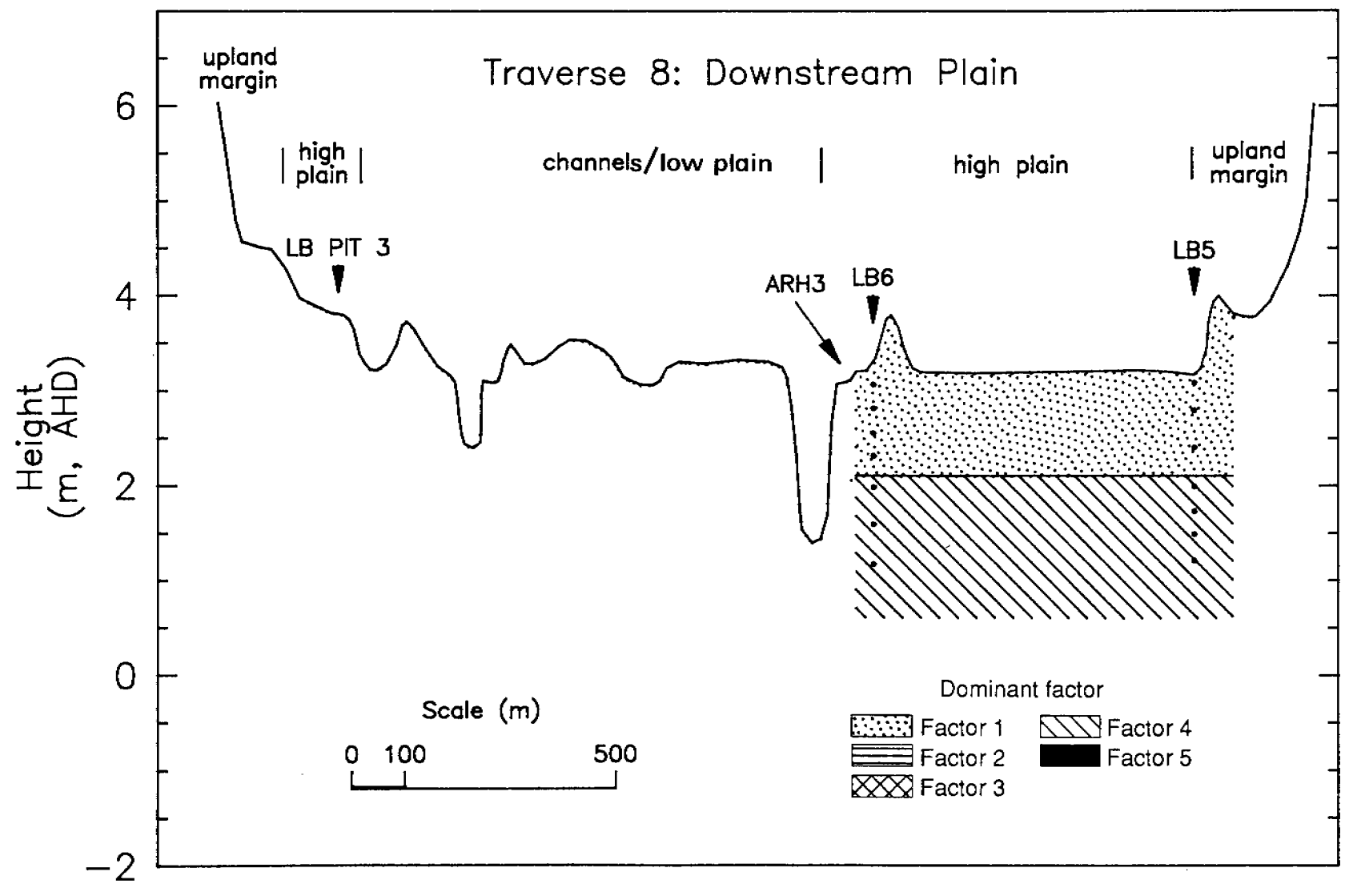


Figure 5.36 Factor loadings in relation to cross-section 8

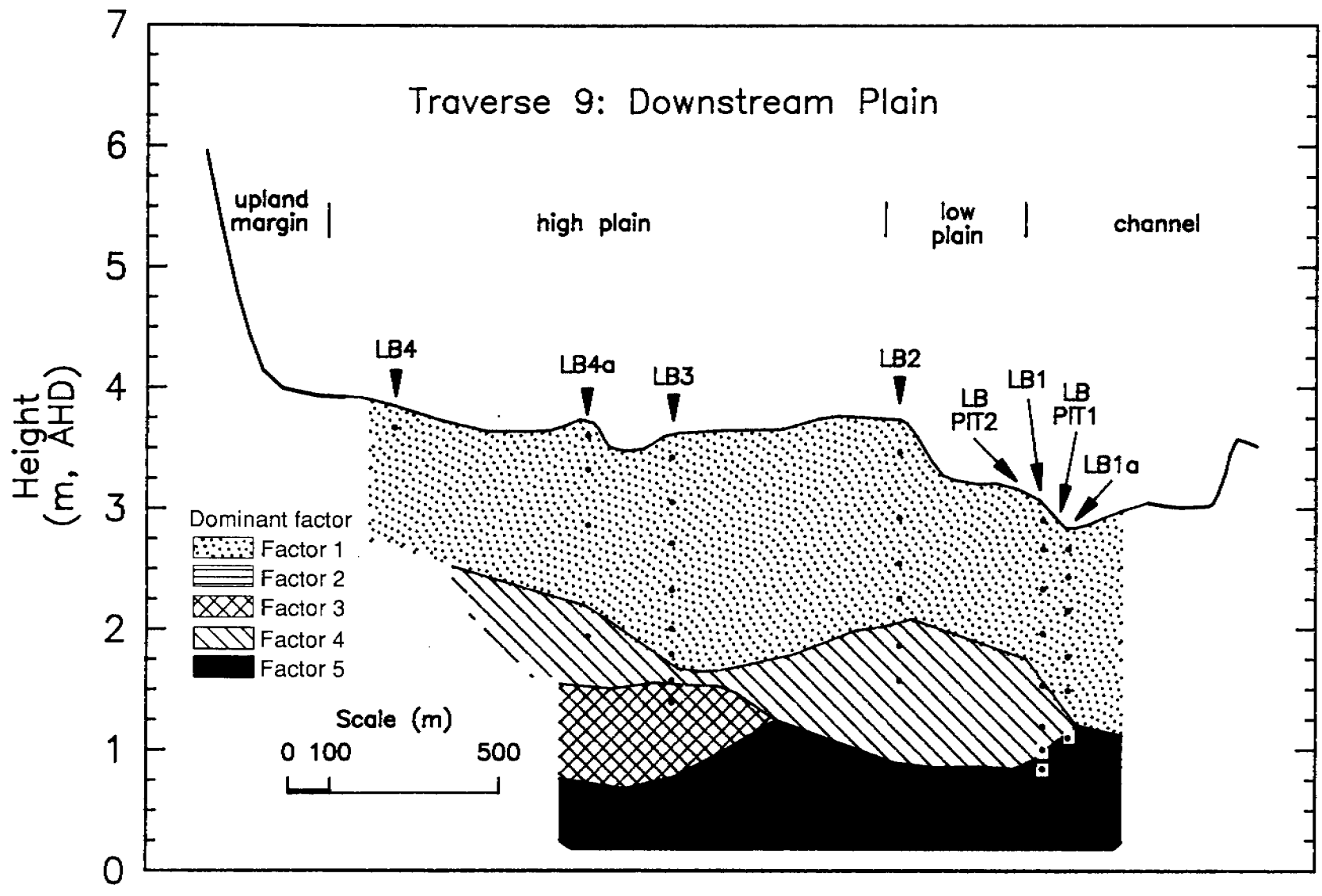


Figure 5.37 Factor loadings in relation to cross-section 9

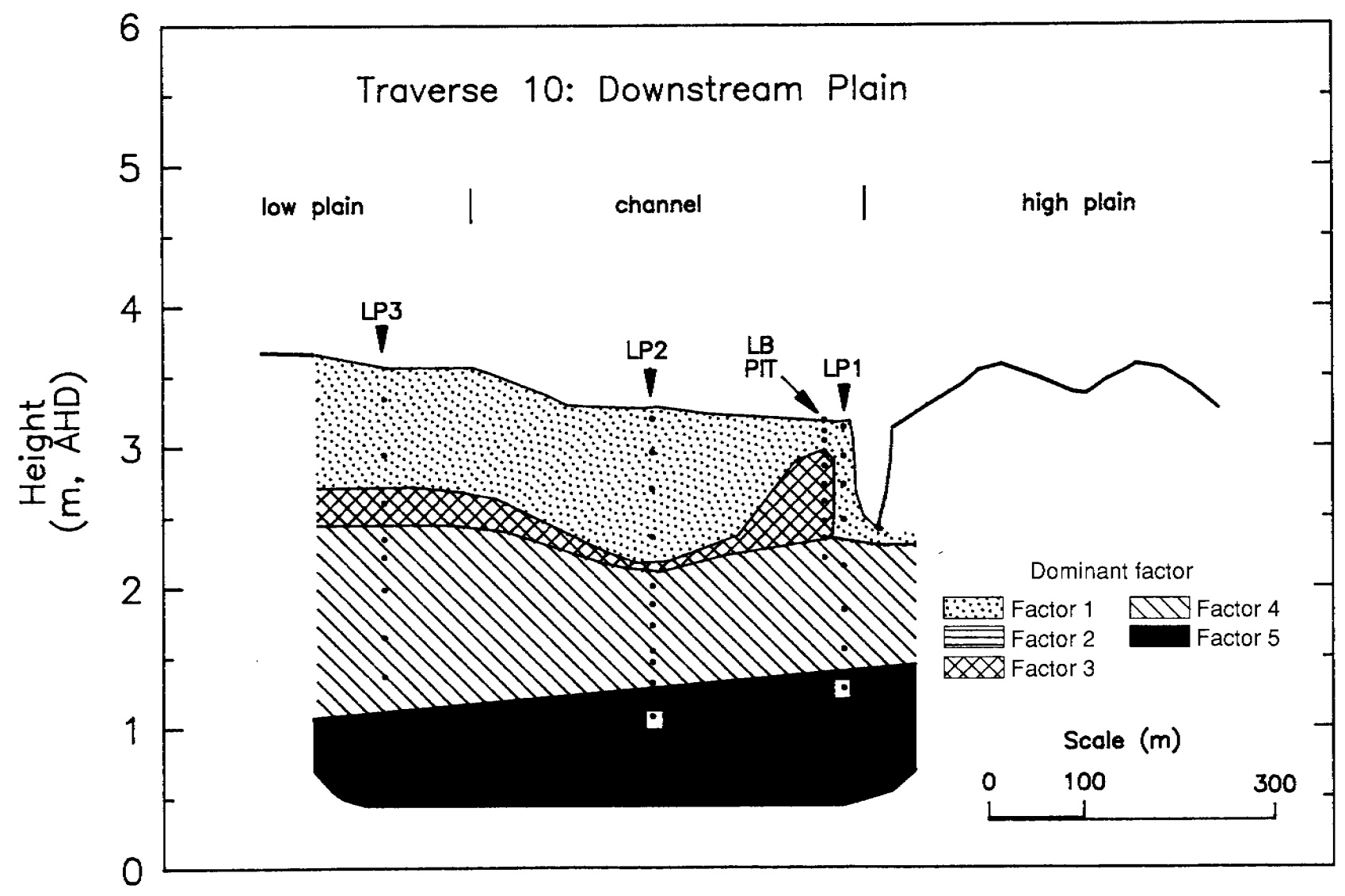


Figure 5.38 Factor loadings in relation to cross-section 10

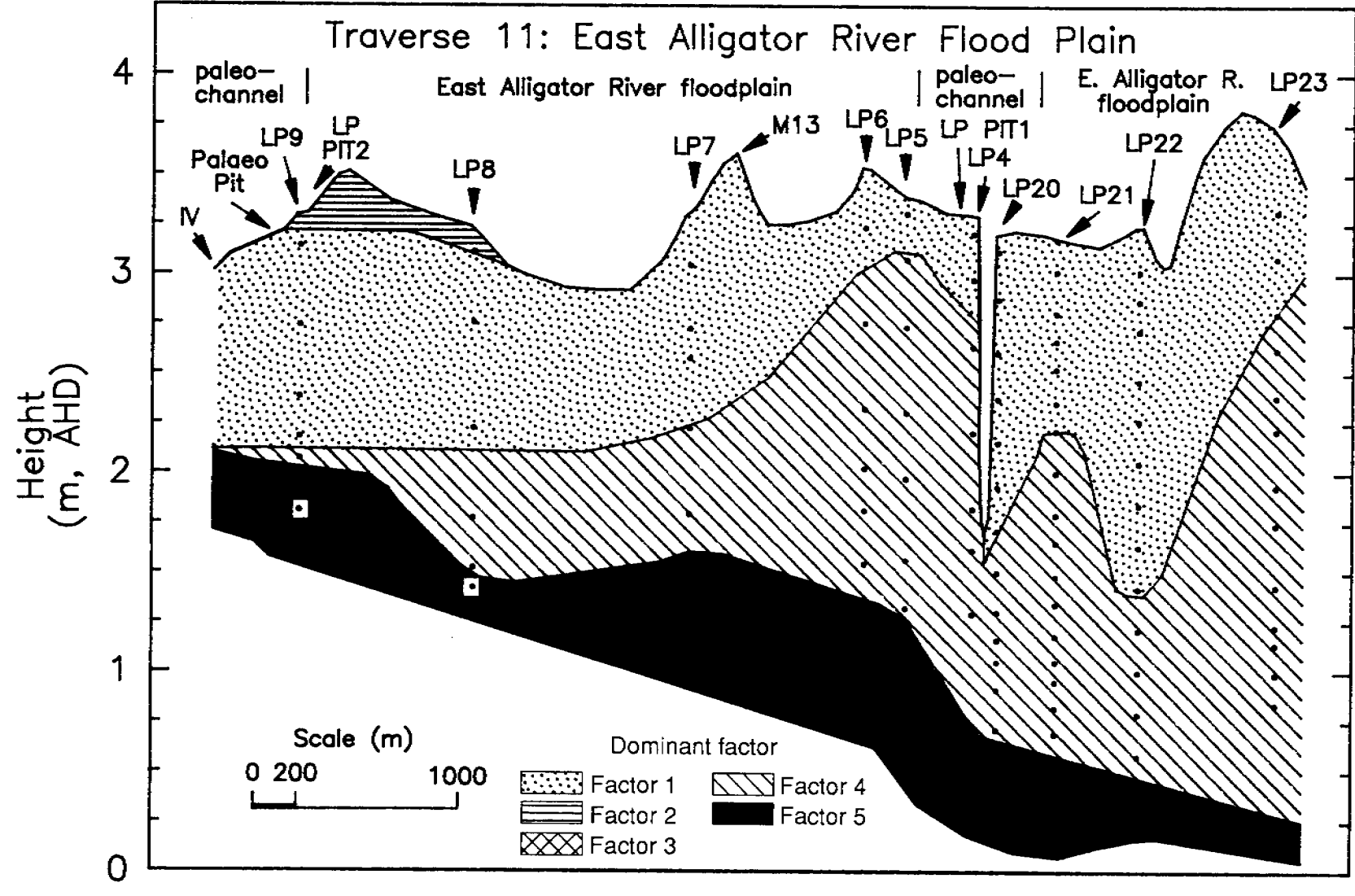


Figure 5.39 Factor loadings in relation to cross-section 11

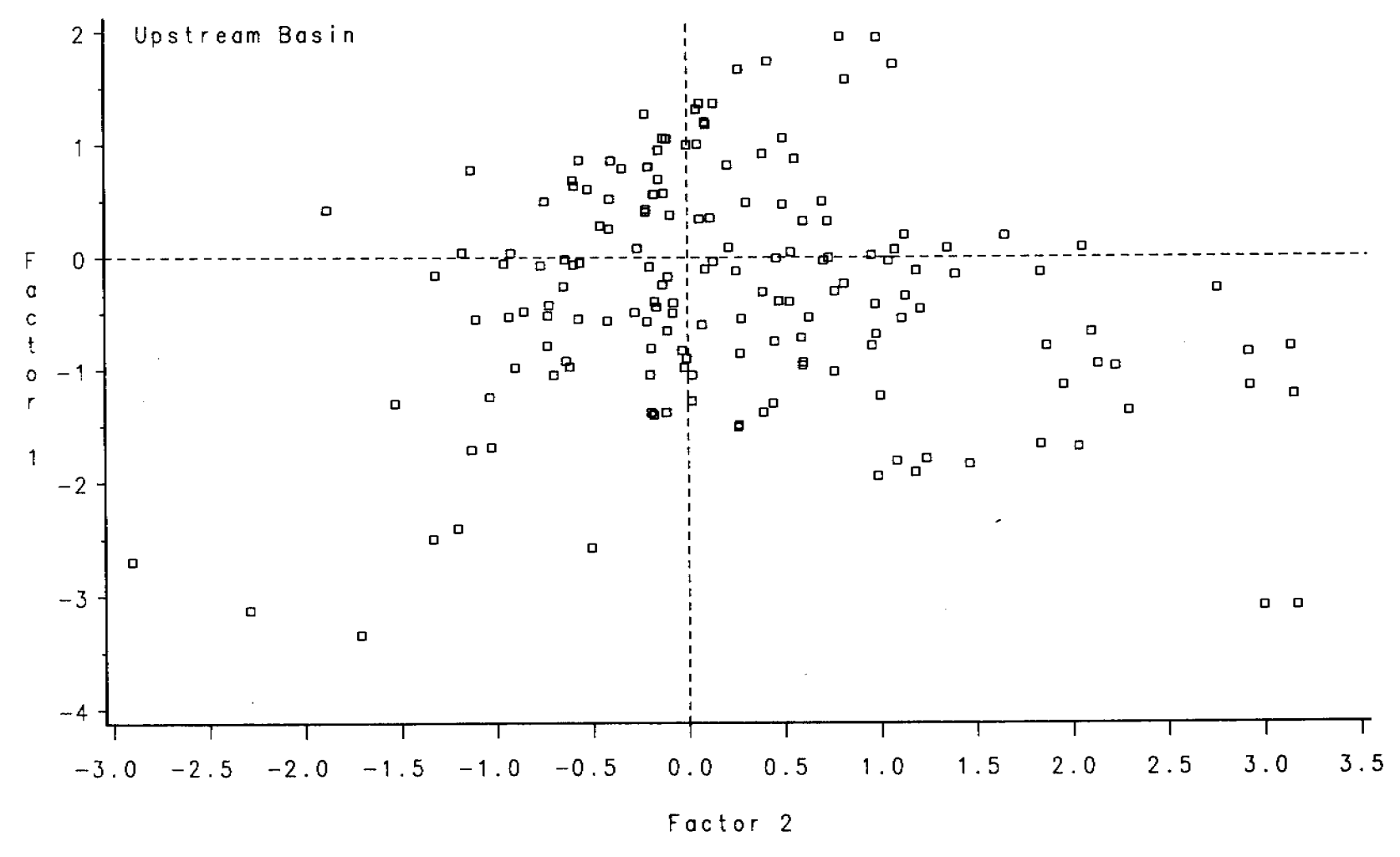


Figure 5.40 Loadings of factors 1 and 2 for soils of the Upstream Basin

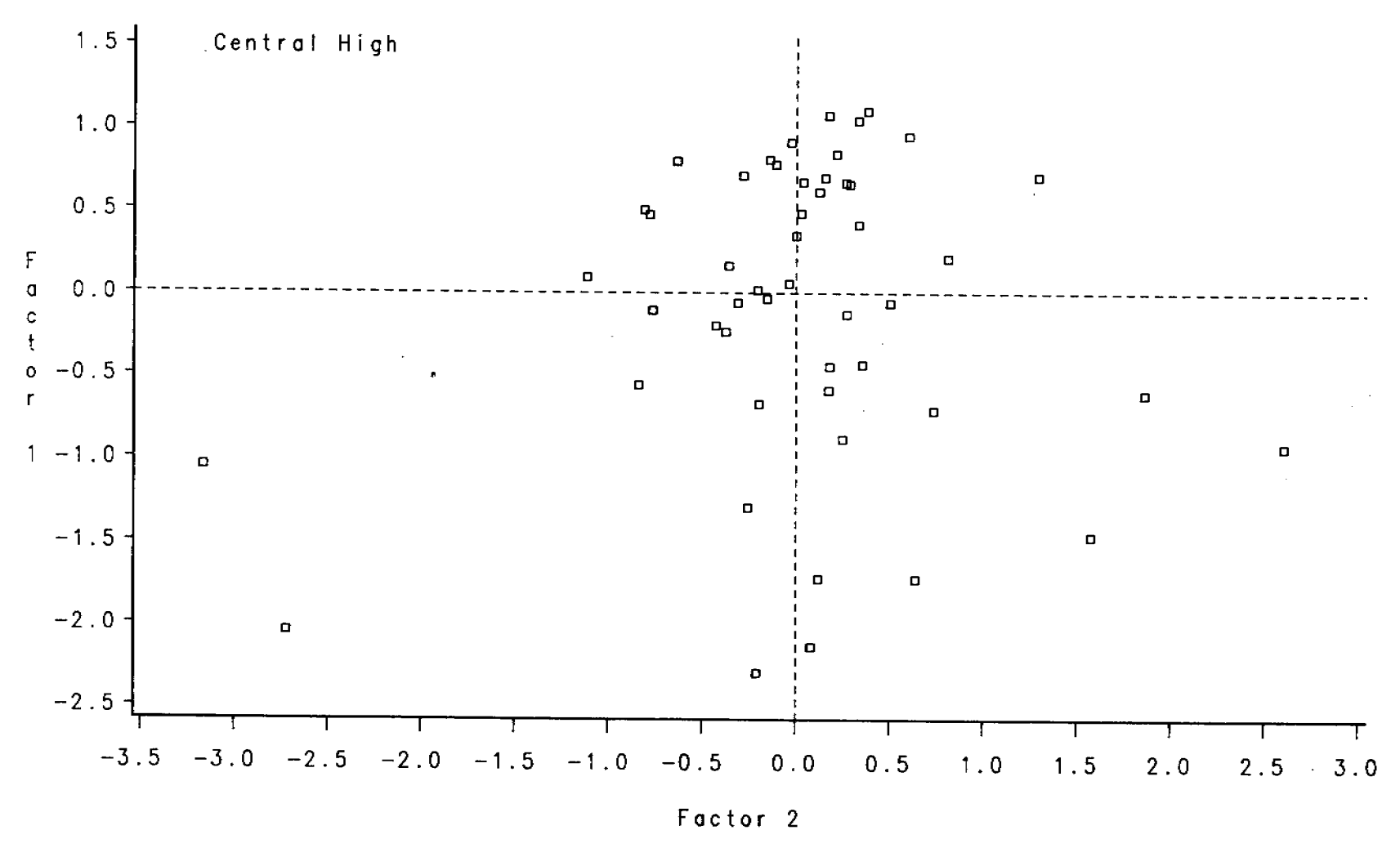


Figure 5.41 Loadings of factors 1 and 2 for soils of the Central High

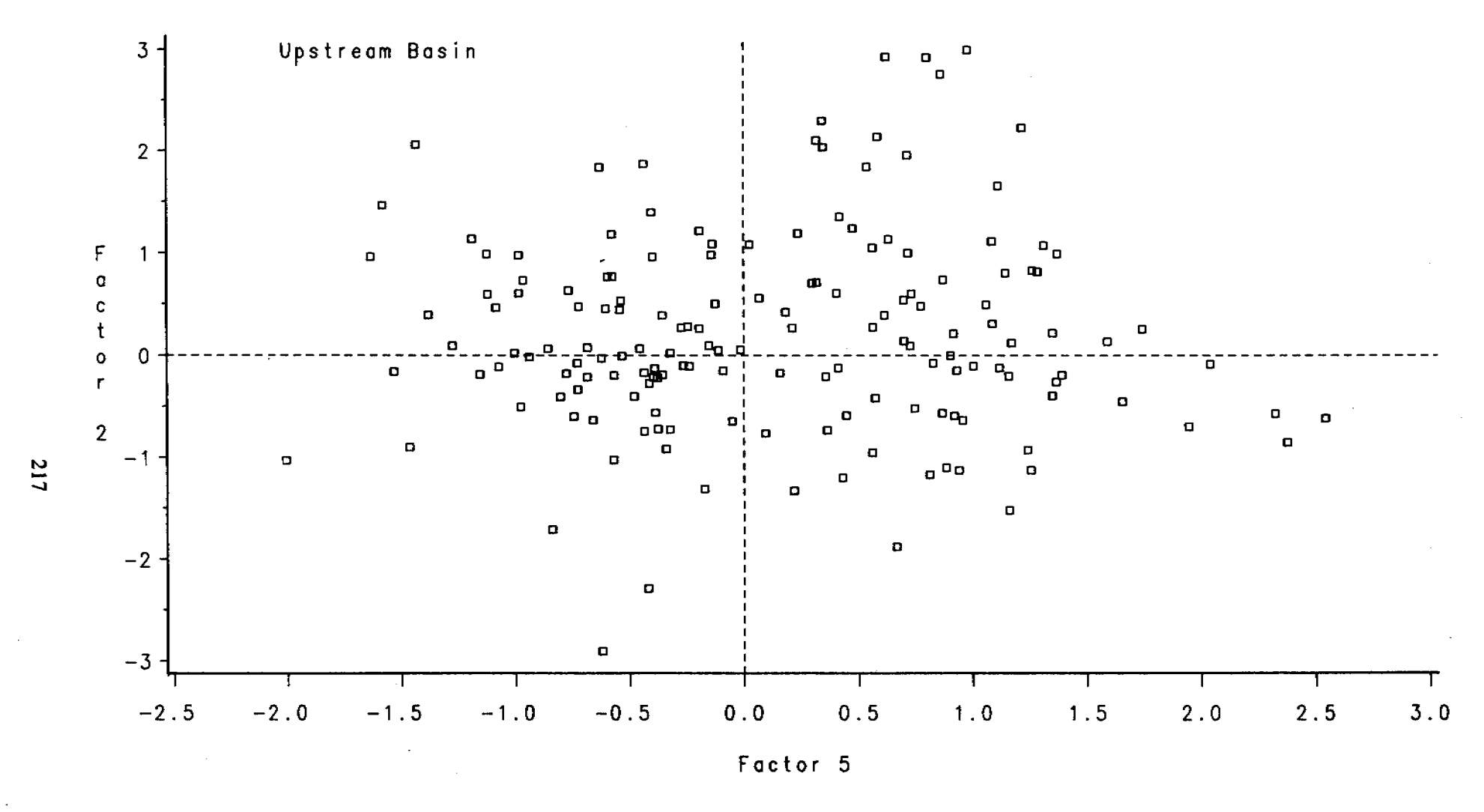


Figure 5.42 Loadings of factors 2 and 5 for soils of the Upstream Basin

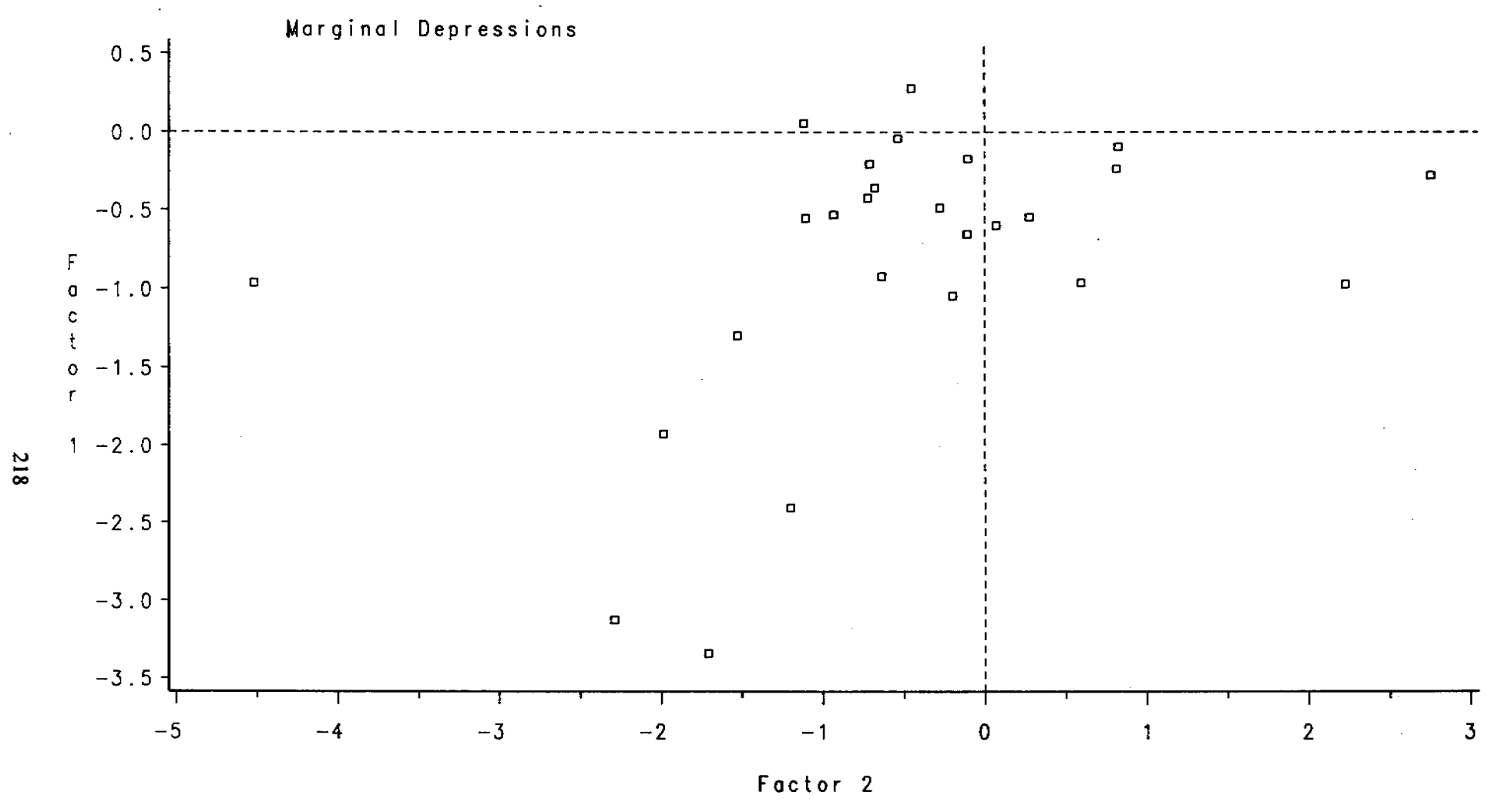


Figure 5.43 Loadings of factors 1 and 2 in soils of the Marginal Depressions

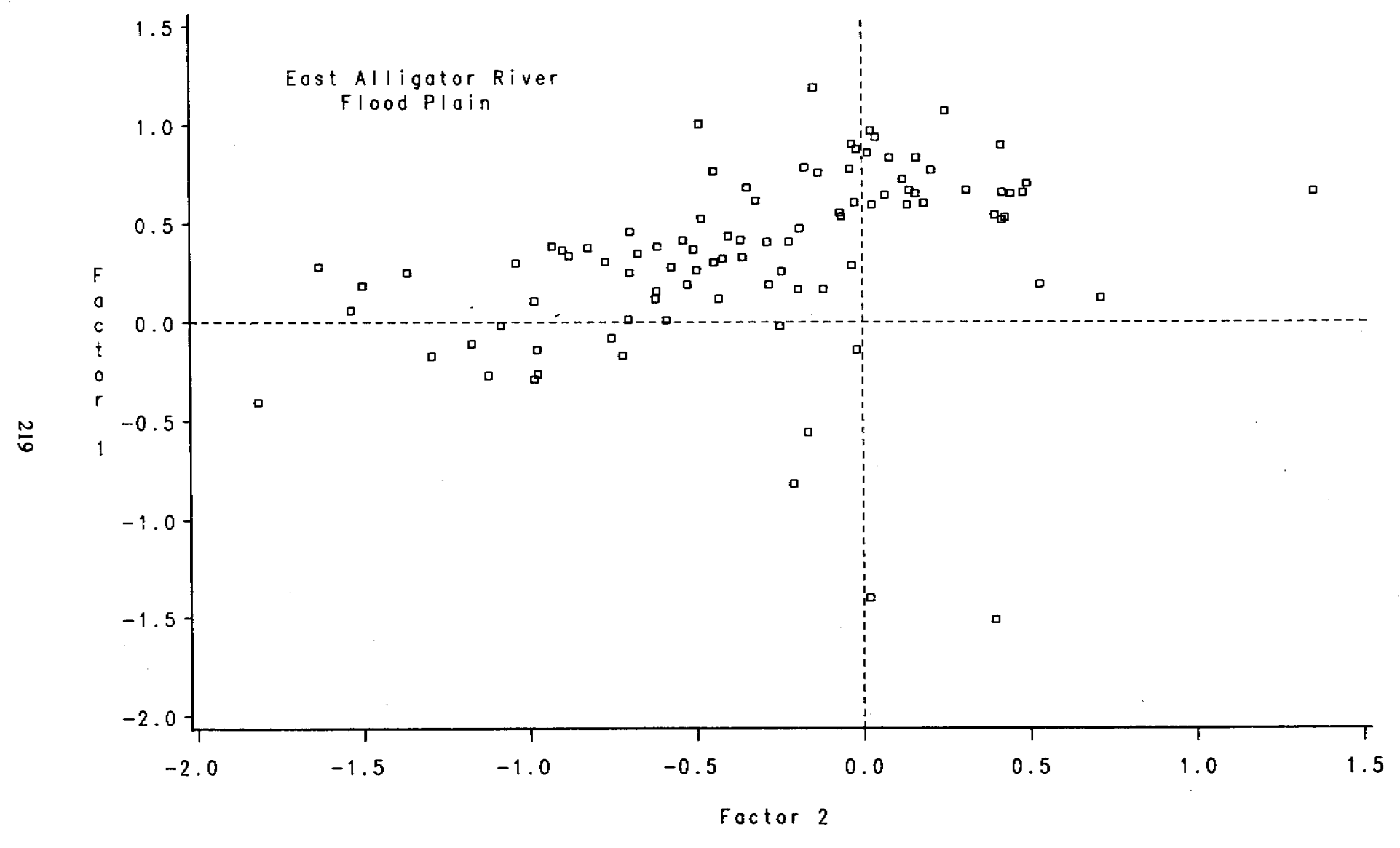


Figure 5.44 Loadings of factors 1 and 2 in soils of the East Alligator River Flood Plain

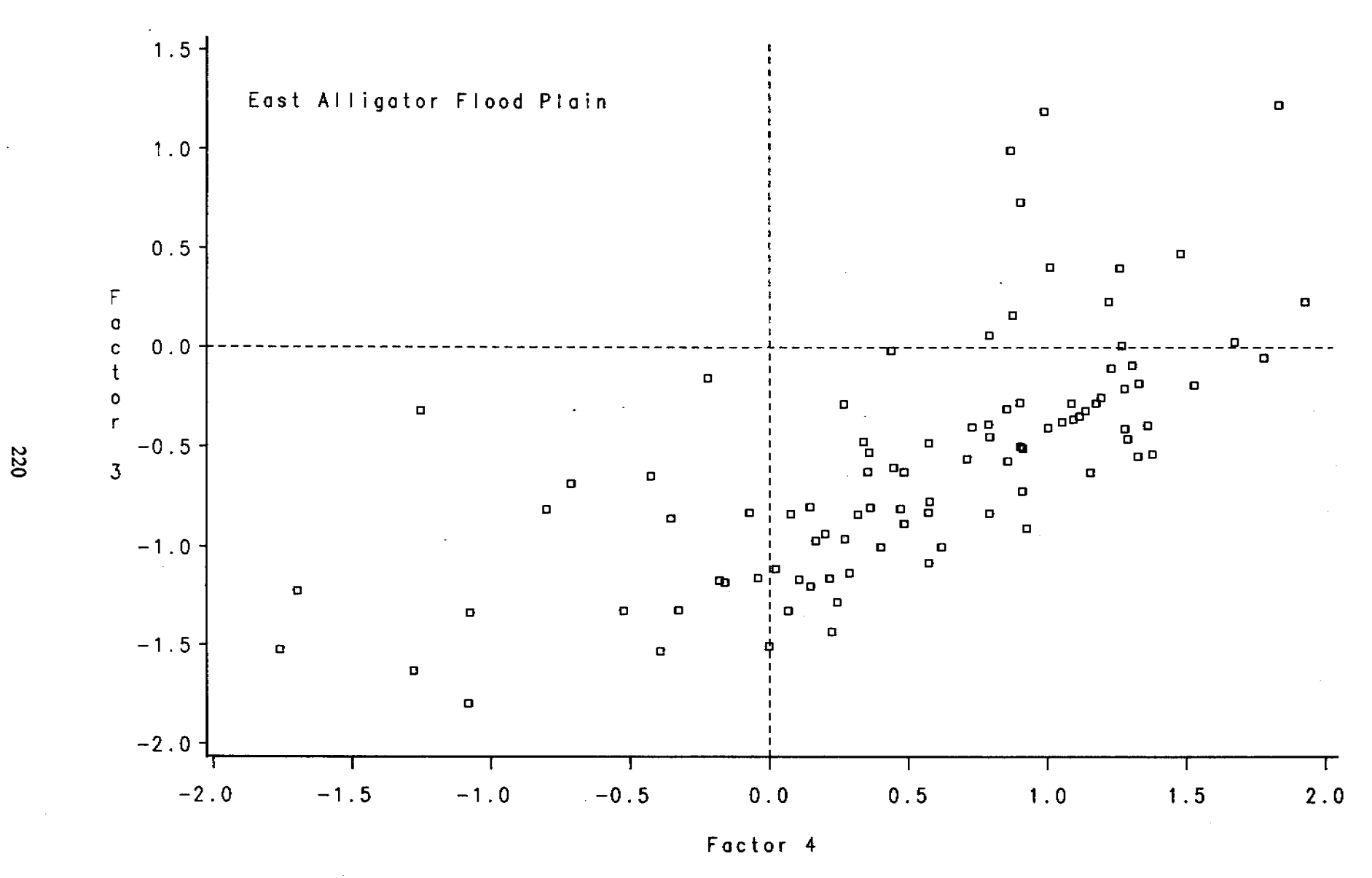


Figure 5.45 Loadings of factors 3 and 4 in soils of the East Alligator Flood Plain

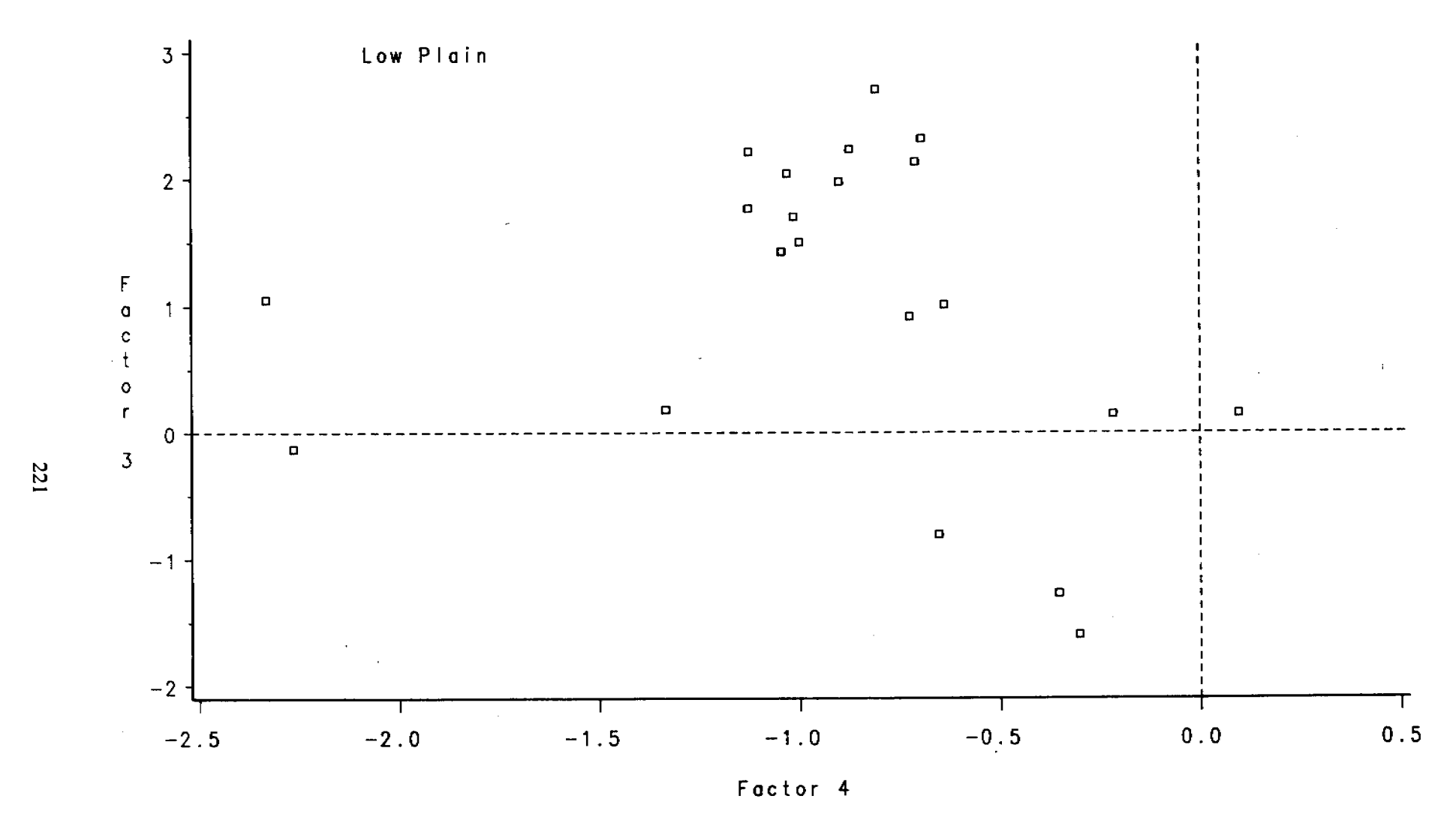


Figure 5.46 Loadings of factors 3 and 4 in soils of the Low Plain

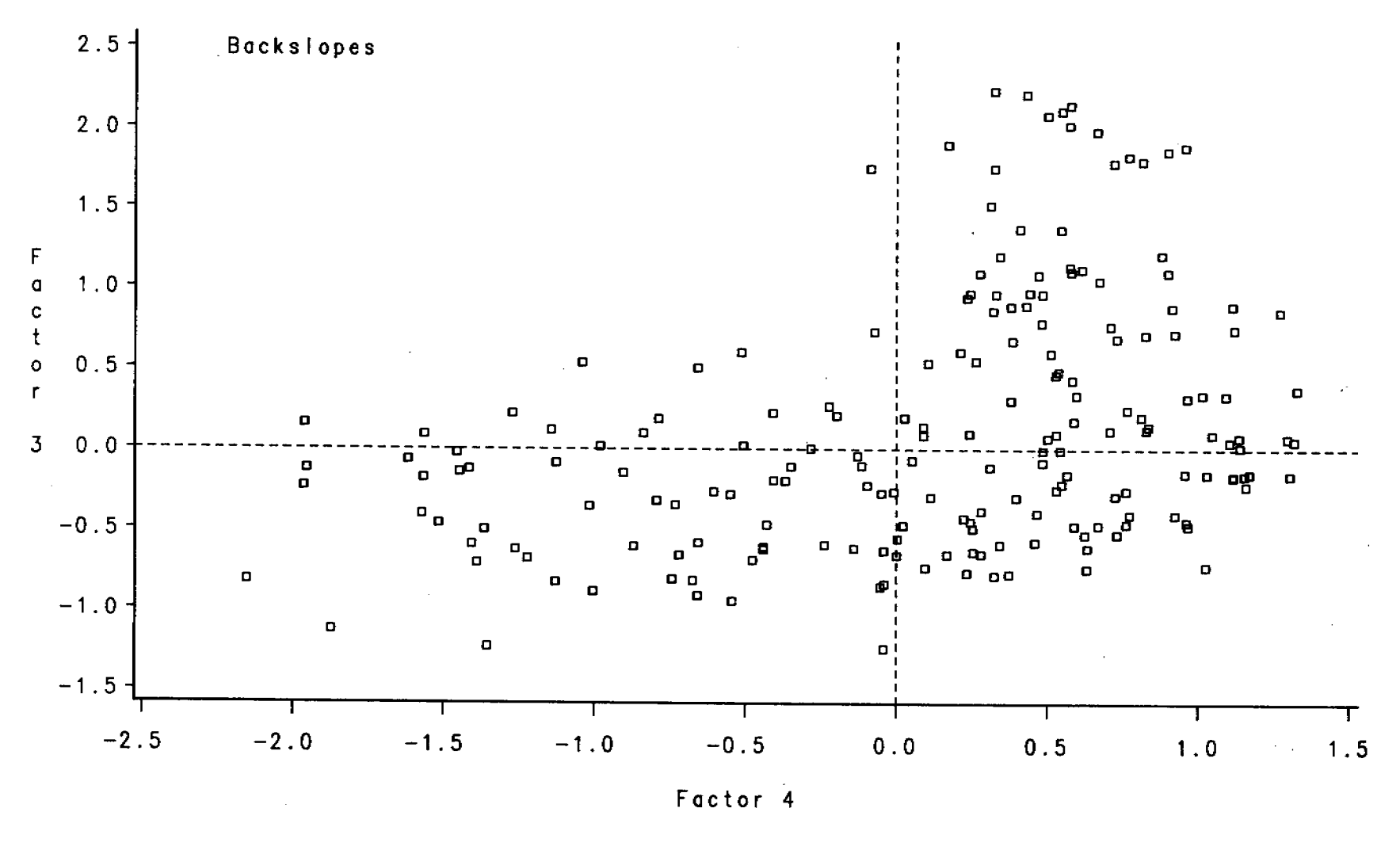


Figure 5.47 Loadings of factors 3 and 4 in soils of the Backslopes



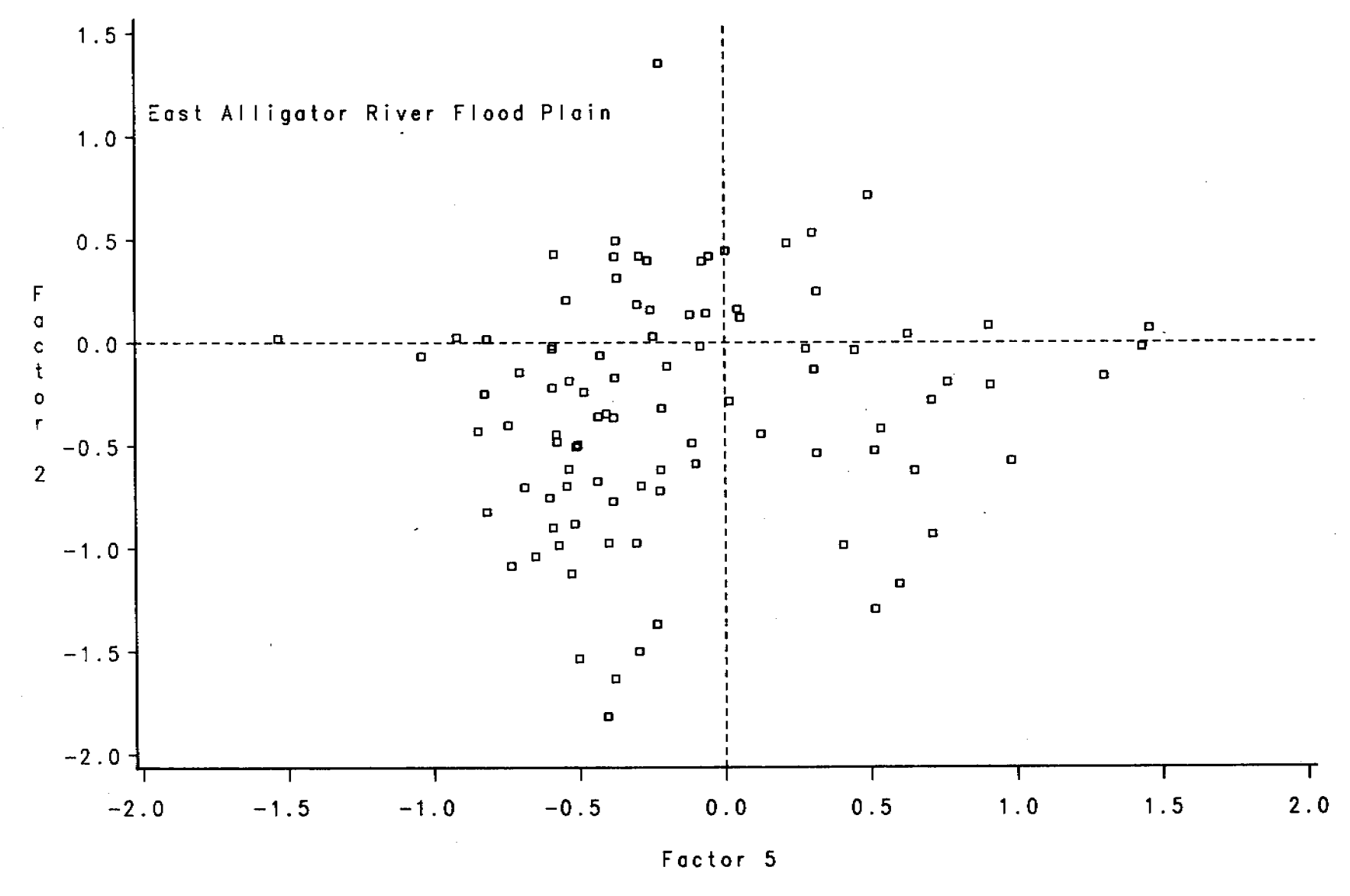


Figure 5.48 Loadings of factors 2 and 5 in soils of the East Alligator River Flood Plain

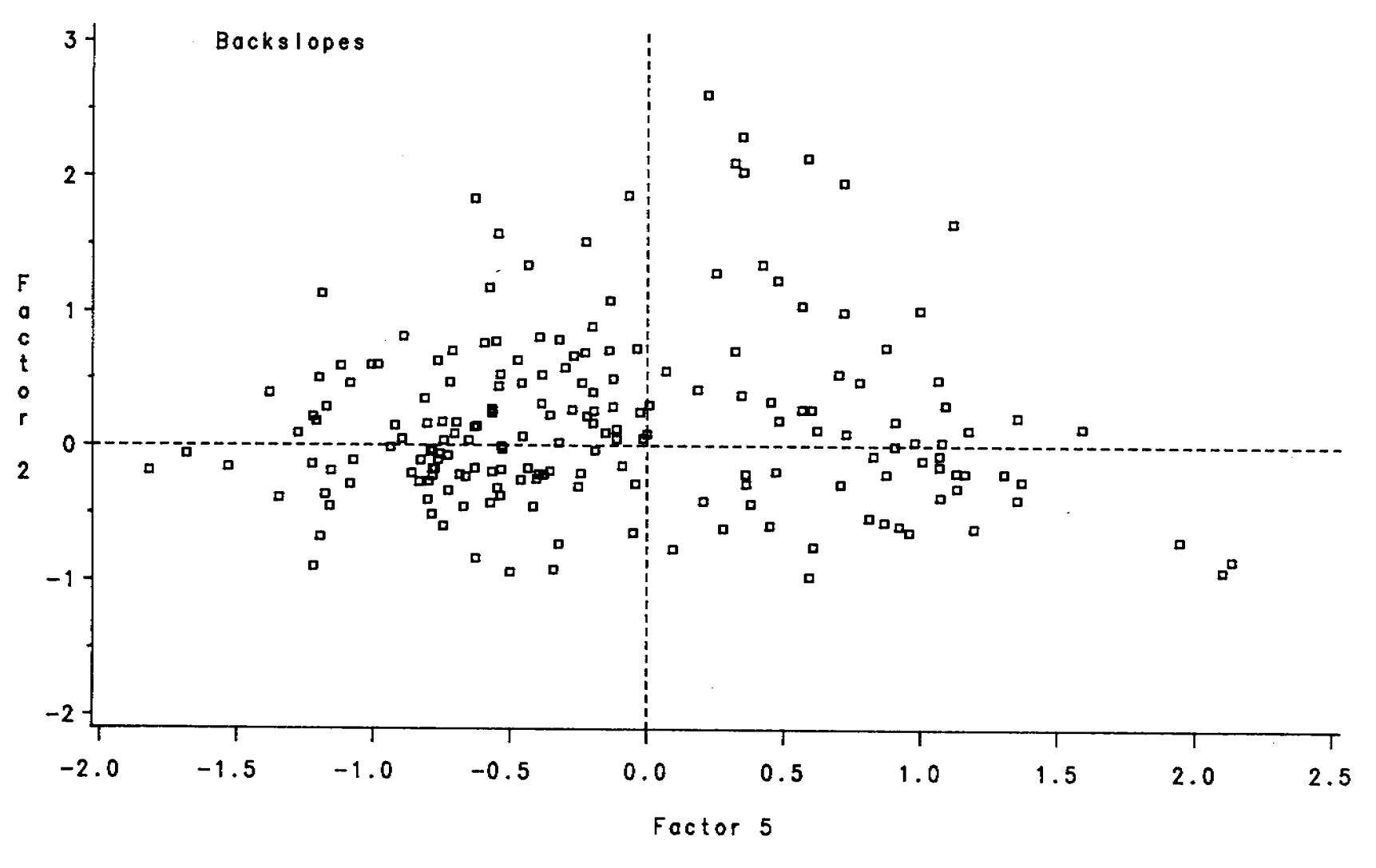


Figure 5.49 Loadings of factors 2 and 5 in soils of the Backslopes

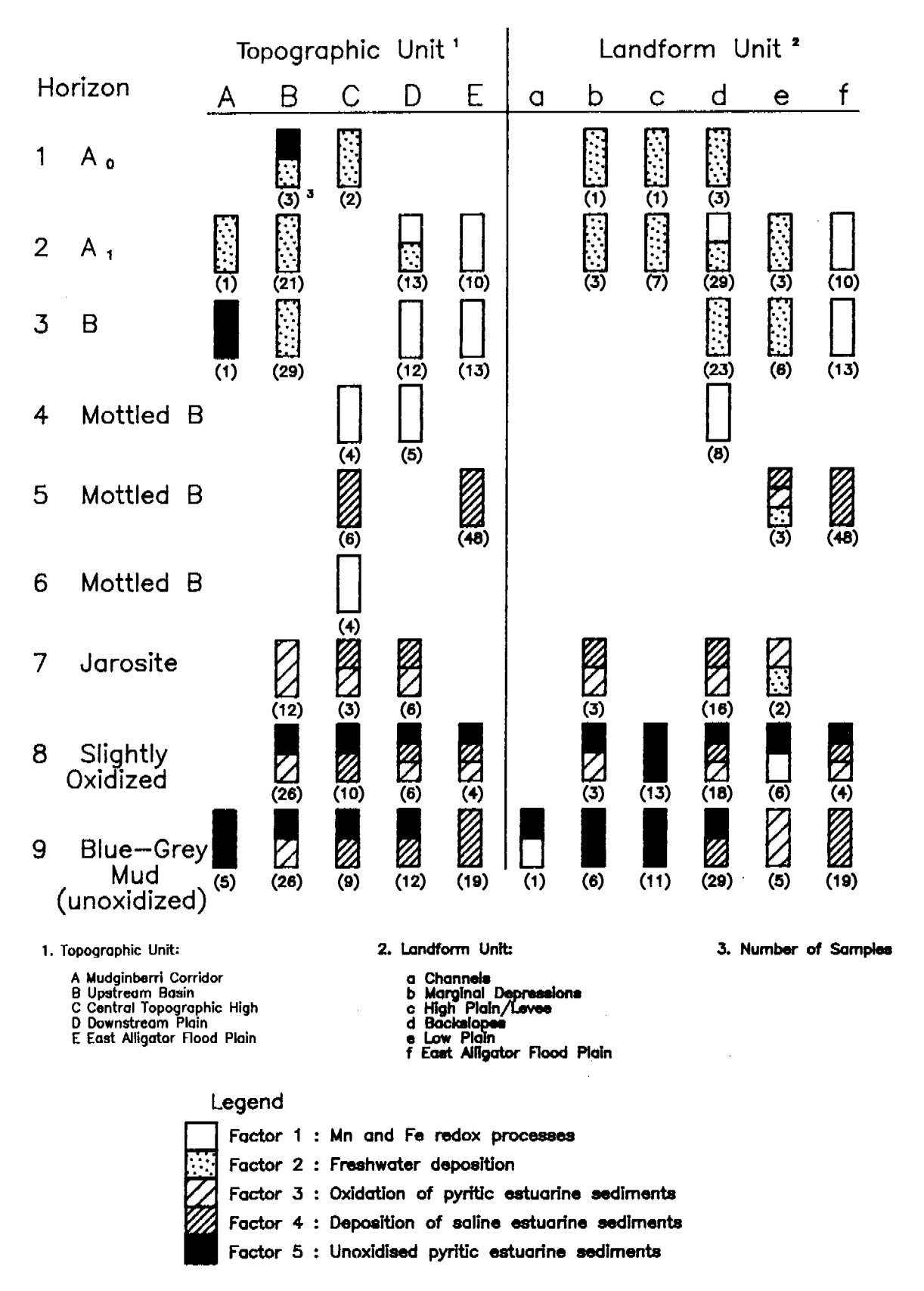


Figure 5.50 Summary of mean factor loadings according to factor and classified by Geographic unit, Landform unit and Horizon

CHAPTER 6. PAST, PRESENT AND FUTURE SEDIMENTATION ON THE MAGELA PLAIN AND IN ITS CATCHMENT

6.1. INTRODUCTION

Long-term average sediment fluxes to the Plain were determined in Chapter 4 using stratigraphic and chronometric techniques. The history of the Dark Brown/Black Clay indicates that changes of sedimentation rates have occurred through time, although the assumption of a constant rate for the thorium-radium dating gave estimates of basal age in good agreement with those based on radiocarbon dating. While time-dependent variations occurred, they were not large. We might expect, therefore, that estimates of short-term sediment flux will be similar to the long-term estimates. Here is the first aim of this Chapter, to see if sedimentation rates have been approximately constant over various time periods during the last 2 ka. If the boundary conditions of the Plain during the future 1 ka are within the range of the last 2 ka, then extrapolation of sediment fluxes is legitimate.

The second aim of this Chapter is to determine the pattern of contemporary sedimentation as a guide to where Mine Site sediment might be deposited. Once again the use of the nearpast as a guide to the future is dependent upon the assumption that the sediment delivery system is not likely to change dramatically in the next 1 ka as a result of climate change or sea level variations, or by being overwhelmed by sediment eroded from the Mine Site.

6.2 SUSPENDED SEDIMENT LOADS

The procedure used here to determine the mass of sediment passing through a cross-section of known shape in a particular period of time is called the sediment rating curve method. It relies upon a well established water stage-discharge curve, a discharge duration relationship, and a statistically significant relationship between discharge and sediment concentration. This last relationship is determined by depth integrated sampling randomly in time at the cross-section. If a large number of sediment samples is taken then the range of flow conditions, from baseflow to major floods, will be adequately sampled. If only a few samples are taken then, usually, big floods are inadequately represented. This leads to serious underestimates of mean annual loads based upon an inadequate sediment rating curve (Rieger & Olive 1988).

The suspended sediment load (L) at a point in a channel is given by

$$L = k \int_{0}^{t} CQ dt$$
 6.1.1

where C is sediment concentration (mg l⁻¹), Q is discharge (m³ sec⁻¹) and k is a conversion factor. Load is calculated from a discrete form of this expression or as a function of discharge. As pointed out in Rieger and Olive (1988), the relationship between concentration and discharge places discharge on both sides of the rating curve. This is an unsound procedure and a better way of estimating loads is by continuous or near-continuous monitoring of concentration through storm events.

The sediment rating curve is not the only source of error in calculating loads. The hydrologic data and relationships may also be in error. On the Magela Creek and Plain the major problems are as follows (data in NT Water Div. 1979, 1980, 1982).

Stage-discharge ratings upstream of Mudginberri in the shifting sand bed channels appear to have been reliable, but for lagoons, on the Plain, at the Plain outflow, and on the tidal reach of Magela Creek these ratings have been difficult to accomplish. At Jabiluka Billabong (Gauging Station 017), a key site between the Upstream Basin and the Central High, four stage-discharge curves existed between January and May 1979 when gauging was almost daily. With rising stages, discharge increased and then decreased with falling stages, in an expected fashion. When rises to high stages were rapid, discharge increased faster than stage as flood waves passed through the water body. Falling stages normally indicate decreases of discharge but, when accompanied by increased velocities set up by head variations as flood waves drained from the Plain, there were small increases of discharge. It follows that fluctuations could also occur with no change of stage.

Velocities on the Plain are generally low and have to be measured by floats which are hard to use in wind. Velocity measurements are therefore subject to more error than is usual. More importantly, the floats can often only be used on the Plain when vegetation has been cleared, thereby creating artificial conditions in which to measure discharge. Annual variations in vegetation change stage-discharge relationships both through a Wet season and between Wet seasons (Vardavas 1988). Annual rating may be necessary, as at the Outflow gauge (019).

In summary, the measurements of discharge and probably sediment concentration are subject to considerable errors. The rating curve method for determining loads is far from adequate but is the only method applicable in the case of the Magela Creek data. Consequently, loads have been calculated and the quantifiable uncertainties determined.

SUSPENDED SEDIMENT LOADS FROM NT WATER DIVISION DATA

Data from three sites have been used: Jabiru gauging station (009) in the sand tract, with a catchment of 600 km²; Jabiluka gauging station (017) on stratigraphic cross-section 4, between the Upstream Basin and Central High with a catchment of 1115 km², including 1085 km² of upland; Outflow gauging station (019), on stratigraphic cross-section 10, near the downstream end of the Downstream Plain, with a catchment of 1570 km² including nearly 1385 km² of uplands. Ideally, other gauges should have been used (e.g. Mudginberri 018, Island Billabong 023, Mine Valley 042, Pelican Camp 022 and the tidal outflow 041) but ratings are limited and discharge data not adequate at these sites.

Only one good year of discharge data exists for the Jabiluka gauge (017). The water year 1978/79 was relatively dry, especially by comparison with the following two years (NT Water Division 1979, 1980, 1982). Two approaches have been used to obtain discharges at Jabiluka for 1979/80 and 1980/81. The first relies upon ratings from 1978/79 to predict daily runoff from stages recorded in the two subsequent years. The second employed relations between discharge and catchment areas to predict the total discharge at 017.

The first method underestimated discharge because big storms of the kind that occurred in 1979/80 and 1980/81 were not represented in the rating curve of 1978/79. The second method may also underestimate discharge but total yield could still be used to estimate load because the exponent in the sediment rating curve derived from 017 is close to unity.

The least squares power curves for estimating total annual (water year) suspended sediment loads are given in Table 6.1, using all data considered adequate. The annual loads at each gauge are given in Table 6.2 (along with data from other sources, to be discussed below) where the standard errors of Table 6.1 and the standard error of the interannual load variability have been used to estimate the uncertainties for each load by quadratic addition.

These estimates, based upon the NT Water Division data, are placed beside estimates made by Hart et al. (1987) in Table 6.3. Unfortunately a comparison can be made for only one

year, 1978/79, where the estimates give the same result, within the errors. Hart et al. (1987) took their own samples and used two methods to calculate the load. Their storm loading technique gave the results in Table 6.3, a technique most like the continuous sampling preferred by Rieger and Olive (1988).

OTHER SOURCES OF DATA AND RELATIONSHIPS WITH CATCHMENT AREA

In Table 6.2, the data for the South Alligator River come from Woodroffe et al. (1986), the Adelaide River data from Williams (1976), the Kawudjulah Creek data from Duggan (pers. comm.), the data from Gulungul and Georgetown Creeks from Duggan (1988), and from Williams (1973) in the case of the erosion plots at Brocks Creek. The uncertainties in all cases other than those of the Magela Creek gauging sites (009, 079 & 019) are standard deviations of interannual variations of sediment loads. These uncertainties are therefore underestimated because they take no account of sampling errors and statistical variance in the sediment rating curves. Unfortunately, it is not possible to obtain the necessary data to carry out a full analysis of uncertainties. These estimates of sediment yield contain varying proportions of bedload, depending upon the sampling methods used. But the uncertainties are so large that the bedload is believed to be well within these uncertainties.

The mean annual specific sediment yields are plotted against catchment areas in Fig. 6.1. All of those listed in Table 6.2 have been determined from measurements of sediment concentrations, or by direct trapping of the products of sheet erosion in the case of Brocks Creek. Although suffering from the inadequacies already discussed, these estimates of sediment yield are at least comparable.

The inverse relationship between specific sediment yield and catchment area shown in Fig. 6.1 is usual for data collected over years to decades (Schumm 1977). For a landscape such as that of the Magela Creek catchment, the relationship is explained as the combined result of: increased deposition, with distance downstream, of sediment derived from uplands; and decreasing erosion rates on slopes adjacent to valley floors as slope gradients decline with increasing catchment area. Over short periods of time only a small fraction of eroded sediment reaches the outlet of the catchment. The ratio of the total erosion to the catchment output is called the sediment delivery ratio. Duggan (1983) has shown that this ratio is less than unity for small catchments in the vicinity of Ranger. This ratio has obvious implications for sediments leaving the Mine Site, namely, that in a period of a few years by no means all would get much beyond the immediate vicinity of the Mine — at least under conditions not substantially affected by a tropical cyclone.

The argument that the curve in Fig. 6.1 is partially the result of decreasing efficiency of sediment delivery as catchment area increases, implies that surface erosion rather than channel erosion supplies some of the sediment carried by streams. There are few incised channels in the Magela catchment. The sand bed channels often have sloping, uneroded banks. The exception is Gulungul Creek which not only is incised over long distances but has deep, vertical-sided gullies tributary to it in the vicinity of the tailings dam. This difference in stream morphology, and presumably a large sediment source, is reflected in Fig. 6.1 where the specific sediment yield for Gulungul Creek plots higher than the rest of the data. The Gulungul sediment yield has therefore been excluded from the calculation of the least squares equation of the curve because it belongs to a different sediment 'regime'.

There is additional evidence that slopes are a source of sediment reaching the Magela Creek under current conditions. The sediment loads carried by successive floods during Wet seasons show a weak tendency to get smaller, both in the data of Hart et al. (1987) and in the Water Division data. Williams (1976) showed the same pattern in the Adelaide River data. As the Wet season progresses, grass covers the slopes and sediment movement declines, as discussed in Chapter 2. Furthermore, a lag of pisolithic gravel seals disturbed surfaces

within a short period of time, keeping sediment yields from slopes very low (Duggan 1983). While slopes yield some of the sediment, this yield is low.

GEOLOGIC DENUDATION RATES

The inverse relationship in Fig. 6.1 cannot be sustained over 'geologic' time, that is, over millions of years, even in a tectonically stable landscape. If specific sediment yield remains high in very small catchments (principally near drainage divides) for millions of years then the lowlands will be gradually buried in detritus if there is no mechanism to flush the detritus. In the Magela catchment, base level has changed substantially as the level of the ocean has risen and fallen in step with interglacials and glacials with a major period of ~100 000 years. As sea level rises, sediment is trapped onshore, but then is eroded as base level falls and streams incise. This is evident in the stratigraphy of the Magela Plain (Fig. 4.19). There can be no continued burial of the lowlands in detritus from the uplands because of base level changes implying, yet the curve of Fig. 6.1 must be near-horizontal on time scales of millions of years.

Some idea of the medium-term denudation rate, that is, the rate at which the land is lowered, can be had from the work of Airey et al. (1982-83). They have used an open system model to describe the behaviour of weathering zones, arranged vertically, in the metamorphic rocks that host uranium mineralisation at Nabarlek, Ranger One and Jabiluka One. The zones are thought to move downwards with denudation. The rate of advance of the weathering front is assumed to balance approximately both the rate of denudation and the time-averaged position of the water table. The data of Tables 2 to 6 in Airey et al. (1982-83) for the weathering zone above the present water table provides estimates of mean medium-term denudation rates as follows:

Jabiluka One	$0.05\pm0.04 \text{ mm/y}, 31\pm25 \text{ t/km}^2/\text{y}$
Nabarlek	$0.05\pm0.02 \text{ mm/y}, 31\pm13 \text{ t/km}^2/\text{y}$
Ranger One	$0.37\pm0.52 \text{ mm/y},230\pm330 \text{ t/km}^2/\text{y}$

These estimates are likely to be the most precise but include only 16 calculated denudation rates from various cores. The grand mean of all 45 estimated denudation rates is $25\pm19 \text{ t/km}^2/\text{yr}$ or $0.04\pm0.03 \text{ mm/y}$, the value plotted as data point 9 on Fig. 6.1.

This mean is representative of the denudation rate that has prevailed over the last 59 000±6700 years, estimated from the model devised by Airey et al. and dependent in this case upon the decay constants of various radionuclides in the weathering zone. Therefore, over a period of about half a glacial-interglacial cycle, the lateritic upland surfaces are likely to be lowered at 0.04±0.03 mm/y.

The sandy earths that cover the laterite in places are also likely to be lowered at the same rate. In this case the curve of Fig. 6.1 will be flatter but only horizontal over much longer time periods.

6.3 A SEDIMENT BUDGET FOR THE MAGELA PLAIN

The equation of the curve in Fig. 6.1 is

$$y = 17.05 - 1.70 \ln x$$
 6.3.1

where y is specific sediment yield $(t/km^2/yr)$ and x is catchment area (km^2) , and $r^2 = 0.98$, and enables a sediment budget to be constructed for the Plain when combined with the measured loads at 019, 107 and 009. The sediment budget is viewed as a series of boxes or compartments (see Chapter 2) in Fig. 6.2. The number and location of the gauging stations determines the maximum number of compartments, although the upstream compartment is

defined as all of the Magela Creek catchment upstream of the Mudginberri Corridor because 009 lies in the sand tract.

The upstream compartment has an area of 845 km². The average annual flux of suspended solids past its lower boundary is calculated from equation 6.3.1. The mean relative error at 009 of 89% has been applied to the flux at the upstream edge of the Mudginberri Corridor. Between this point and 017, tributary streams contribute sediment to the Plain. Each tributary catchment has been mapped and their areas used to calculate mean annual sediment yields, once again using equation 6.3.1. The same approach has been used for the tributaries joining the Plain in the area between 017 and 019. The use of equation 6.3.1 neglects the known minor areas of channel incision as sediment sources.

The major elements of the sediment budget are assembled in Table 6.4. Here the uncertainties have been standardised to make them comparable, by averaging the asymmetric uncertainties of Table 6.1 and by using a standard error estimate for equation 6.3.1. Summation in quadrature then gives the uncertainties for the deposition rates, the best estimates for which are simply the differences between mean inputs and outputs. The mineral sediment fluxes are estimated by assuming a bulk density of 1.2 g cm⁻³. Note that all calculated digits have been carried through but only significant figures will be considered in the subsequent discussions. All of the sediment loads have been reduced by $28\pm11\%$ to take account of their likely organic content, based on the results of Hart and Beckett (1986).

The contemporary mineral sediment flux to the Upstream Basin and Mudginberri Corridor is, on average, $0.008\pm0.02~g/cm^2/yr$ (Table 6.4, upper panel) compared with the average for cross-sections 1-4 of $0.02\pm0.0001~g/cm^2/yr$ (Table 6.4, bottom panel) based on ¹⁴C dating. For the Central High and Downstream Plain the fluxes are $0.003\pm0.004~g/cm^2/yr$ and $0.05\pm0.0002~g/cm^2/yr$, respectively. At one significant figure the difference for the best estimates is a factor of 2.5 in the upstream compartment where the data for both estimates are best. Downstream, where the data are poorer, the difference is nearly seventeen fold. However, both flux estimates for both compartments overlap within the (large) uncertainties. Within the vagaries of the data and methods, it is concluded that sediment fluxes (and so deposition rates of the mineral sediment) have remained constant over time periods of both 2000 and about 10 years in the Upstream Basin and Mudginberri Corridor.

From the measured loads of suspended sediments it has been possible to construct a sediment budget for the Plain and to estimate sediment fluxes to the depositional sinks. The large uncertainties attached to each flux estimate make it very difficult to resolve the budget so that firm statements can be made about the distribution on the Plain of sediment derived from Magela Creek. Radionuclides can act as tracers of sediment sources and sinks, and also provide realistic analogues of the behaviour of particle-related radionuclides that might one day leave the Ranger Mine Site. The next sections allow significant refinement of the conclusions drawn from the sediment budget.

6.4 DETERMINATION OF SEDIMENT SOURCES AND SINKS USING 137Cs

The radionuclide ¹³⁷Cs (half life 30.0 years) is entirely anthropogenic. Almost all of the ¹³⁷Cs activity present in the southern hemisphere is derived from atmospheric nuclear weapons testing, primarily in the northern hemisphere, and of significance only since 1954. Radioactive material from these tests has been deposited on the earth's surface by rain washout and turbulent dry precipitation (see Fig. 6.3). When ¹³⁷Cs reaches the ground, it is rapidly sorbed by soil particles, particularly clays, and so in undisturbed soils the majority remains close to the surface, often within a few centimetres (see, for example, Longmore 1982). Brisbin *et al.* (1974) have shown that when such ¹³⁷Cs is transported by water, it remains attached to sedimentary particles, and so can be used as a tracer of surface soil movement.

In this study it was proposed to investigate the ¹³⁷Cs deposition pattern on the Magela Plain and, if possible, use this information to determine sediment sinks and sources. It was also intended to determine a mean ¹³⁷Cs load on the Plain and, by comparison with integrated atmospheric fallout, calculate the fraction of the catchment inventory of ¹³⁷Cs that has been transported to the Plain.

SAMPLING

Samples were collected at the grid points shown in Fig. 6.4. At each point, cores were taken at two depths, 0-25 and 25-35 cm, using 10 cm diameter high pressure PVC tube. One end was chamfered, and the 30 cm length of tube was driven into the ground using a steel dolly and a sledge hammer. On return to the laboratory, the samples were extruded, oven dried at 60°C, and the total dry weight recorded. The dry material was then homogenised by grinding to approximately < 200 μ m in a ring grinder, and a portion of about 20 g ashed at 450°C. The weight loss was recorded. The remaining material was then cast in polyester resin and counted on a low background gamma spectrometer, based on a high resolution intrinsic 'p' type germanium detector. Typical sample weights were about 650 g, and samples were counted for 24 hours, giving analytical uncertainties of typically ±0.15 Bq kg⁻¹. A full description of the analytical technique is given in Murray et al. (1987).

ATMOSPHERIC INPUT

An estimate of the integrated atmospheric input of ¹³⁷Cs since 1954 has been determined by taking core samples from three well separated hilltops near the Magela Plain. Deposition or erosion at these sites is extremely unlikely. The sites are

- (i) adjacent to the Magela Crossing, but well above the level of floods
- (ii) adjacent to the Oenpelli Road, about 2 km from the Arnhem Highway junction, and
- (iii) adjacent to the Arnhem Highway, about 4 km west from the junction with the Oenpelli Road.

Table 6.5 gives the observed areal concentrations of ¹³⁷Cs in these samples, at various depths. It is apparent that all the activity is retained within the top 25 cm, and only these values are used to derive the mean of 350±40 Bq m⁻². Longmore et al. (1983) present fallout data for Brisbane (latitude 25° south) for 1954 to 1978, by which time the fallout rate had decreased to a negligible level. Using a set of samples taken from topographic high points at a similar latitude, they obtained good agreement with the integral of their fallout curve. This curve has been replotted in Fig. 6.3, after correcting for decay to the end of 1985 (when the cores were analysed), and the integrated fallout at that time was 700 Bq m⁻². This figure can be corrected for latitude to the Magela Plain, by using the latitude dependence curve derived by Lal and Peters (1967). This indicates a ratio of 0.62 for 12°/25°S, implying a fallout of 430 Bq m⁻². It is thought that any difference between this and the directly observed data primarily reflect the uncertainties in the latitude dependence, a function derived for the northern hemisphere in which hemispheric symmetry has been assumed.

Using the total catchment area and the hilltop results, the total ¹³⁷Cs inventory of the Magela Plain catchment is 370±40 g Bq, with the uncertainty based only on the uncertainty in the areal concentration of the hilltop samples. This figure represents the total activity that has fallen on the catchment, not including the Plain itself, corrected for decay to 1985. The actual inventory will be less than this, depending on how much ¹³⁷Cs-labelled surface soil has left the catchment past 019.

RESULTS FROM THE PLAIN

At the time the sampling procedure was designed, it had been expected that deposition on the Plain would vary only slightly with location, and because ¹³⁷Cs should be tightly bound to particulates, the deposited 137Cs areal concentration would behave similarly. Unfortunately, as analysis progressed, the apparent randomness in the data called this assumption into question. An explicit test was arranged by sampling at two locations, about 5 m apart, one on top of a ridge about 0.3 m above the adjacent sample in a runnel, both on cross-section 2 in the patterned ground referred to in Chapter 4. At each location, three samples were taken to a depth of 25 cm on a triangle of 1 m sides. It was expected that while the two locations might differ in 137Cs areal concentration, the results should be less variable within each group of three. A negligible fraction of ¹³⁷Cs will have been lost by not sampling below 25 cm, as it is known that in this region of the Plain the 25-35 cm depth increment contains on average 0.05±0.06% of the total activity. Unfortunately the bulk densities of these samples are not available. It is also known from the general sampling results that these do not vary markedly with location or with depth in the upper 25 cm. For constant depth, direct proportionality between mass concentration and areal concentration can be safely assumed.

The concentrations observed for ¹³⁷Cs and ²¹⁰Pb excess (over its parent ²²⁶Ra) are given in Table 6.6, along with those for some other natural radionuclides. ²¹⁰Pb excess is of interest because it is derived from atmospheric fallout like ¹³⁷Cs, but from the decay of naturally occurring radon gas (222Rn) rather than bomb fallout. Thus 210Pb and 137Cs should behave similarly. Although the mean values for 137Cs and 210Pb concentrations are probably different for the two groups of samples, the scatter in these nuclides is large, and much greater than that in those nuclides of only sedimentary origin (238U, 226Ra, 232Th). The overall variability for 137 Cs ($\sigma = 150\%$ and 90%) and 210 Pb ($\sigma = 170\%$ and 90%) is considerable when compared with mean analytical uncertainties of 4% and 50% respectively. although the variability in the non-atmospherically derived nuclides only ranges between 5 and 20%. On the other hand, there is correlation between the concentration results for 210Pb and ¹³⁷Cs, confirming their common atmospheric source. This also suggests that most of the variability in the data derives from deposition rather than from post deposition mobilisation, because the chemistry of caesium and lead is very different, and similar mobilisation would be very unlikely. This may indicate a variability of either the pattern of deposition of sediment or in the direct atmospheric component. This will be discussed further below.

MASS CONCENTRATION RESULTS

The variability discussed above has serious implications for the interpretation of the data from the rest of the Plain. Given that only one sample was taken at each grid sampling point, ranging from 500 m spacing in the Mudginberri Corridor to 2 km on the Downstream Plain, it is unlikely that each point measurement is very representative, and some averaging of the data is necessary. This was confirmed by attempting to produce a contour map of ¹³⁷Cs deposition, which showed an almost random pattern, with little correlation with known depositional features.

To cope with some of this variability, the data were first averaged on each northing. Data which might be affected by sediment arriving from side channels were not included in this averaging. This process gave averages based on between one and five data points. The transverse averaged data were then smoothed longitudinally, by a three point average, to give the longitudinal concentration profile shown in Fig. 6.5. Error bars represent a three point average of the standard deviations derived from either the transverse averaging or, in the case of a single data point, the analytical uncertainties.

There is a clear peak in the ¹³⁷Cs concentrations in the Mudginberri Corridor, with another less clearly defined on the southern end of the Central High. The proportion of activity found below 25 cm depth varies with distance down the Plain, with a minimum in the Corridor, and a maximum in the Downstream Plain. Various mechanisms can give rise to such variations in the vertical distribution:

- (a) Sedimentation at the northern end of the Plain at least 25 cm of material may have been deposited since about 1958 (by which time enough ¹³⁷Cs had been precipitated from the atmosphere to be detectable in sediment samples almost one half life later in 1985), giving a deposition rate of 1.1 cm y⁻¹. This is contradicted by overwhelming evidence from ¹⁴C and radium thorium dating (see Chapters 3 and 4) and this explanation is rejected. It is noteworthy that ¹³⁷Cs has penetrated into sediment confidently dated to about 1000 yr BP.
- (b) Bioturbation buffalo, pigs and magpie geese all cause severe disturbance to the surface layers of the Plain, and can easily account for vertical mixing of tens of centimetres. However such disturbance is, if anything, less likely at the northern end of the flood plain, where the open grassland areas, and thus the grazing quality, are much reduced, with the predominant cover being melaleuca open forest and woodland. Moreover, lamination is preserved at most sites examined, implying that bioturbation is not significant at sites used for stratigraphic purposes. However, the ¹³⁷Cs samples were not taken with stratigraphy in mind and so were not vetted for stratigraphic integrity.
- (c) Drying/wetting cycle deep cracks develop annually during the Dry season in the 'black soil' of the Plain, with a horizontal separation of only tens of centimetres. Animal movement can cause the edges of these cracks to crumble, with surface material penetrating to depth.
- (d) Presence of competing ions the sorption of ¹³⁷Cs to clay particles decreases in the presence of competing ions such as Na⁺ or K⁺ (see, for example, Aston & Duursma 1973). The potassium concentration of surface sediments increases down the Plain, with a minimum in the region of the Upstream Basin. The ¹³⁷Cs is found nearest the surface where the potassium concentration in the sediment is at a minimum, but penetrates further into the sediment where the potassium concentration is highest.
- (e) Presence of organic matter it is known that ¹³⁷Cs is bound by organic matter (e.g. Ritchie et al. 1972). The concentration of organic matter is at maximum in the Upstream Basin, and low at the northern end. To produce the observed depth profile, the ¹³⁷Cs would have migrated down the sediment profile after deposition. This is more likely to be consistent with the observed organic contents if the organic matter was distributed by migration, rather than by sedimentation. The argument for a sedimentary origin was provided in Chapter 4.

AREAL CONCENTRATION RESULTS

Figure 6.6 shows the variation in bulk density at the two depths, 0-25 cm and 25-35 cm, with distance down the Plain. There is a marked minimum in the Upstream Basin resulting from a large content of biogenic silica, with a steady rise downstream to the outfall. The areal concentration data are derived for each depth by multiplying the mass concentration data by the appropriate bulk density, and by the sampling depth interval. To derive the total ¹³⁷Cs deposition, the results from 25-35 cm are then added to those from 0-25 cm. The former do not form a complete data set, and so the data were considered in each of the topographic units. For each area a mean activity ratio between the 0-25 cm and the 25-35 cm layers was derived and this mean value used to correct those points for which no 25-35 cm data were available. This total areal concentration is shown in Fig. 6.7, with the mean atmospheric deposition. The Mudginberri Corridor peak remains clearly defined, and there is also a peak at the upstream (southern) end of the Downstream Plain. There may also be a

peak at the upstream end of the Central High, as in Fig. 6.5. The intermediate low concentrations all have similar value, consistent with no deposition other than from the atmosphere. However it would be unwise to assume that there is therefore no sedimentation occurring in these areas. For reasons discussed below, it may be that the atmospheric component varies with location, especially in the Downstream Plain.

A direct comparison of these data with the catchment inventory is not possible, because data from the edges of the Plain have been omitted from Fig. 6.7. The omitted data may be influenced by side channels and so obscure the overall longitudinal trends. To permit a comparison with the catchment inventory all data have been combined and the mean areal concentration in each topographic unit calculated, with the associated standard error. When these figures are compared with the atmospheric input, and its standard error, the upstream end of the Plain again has a higher total deposition of ¹³⁷Cs than the downstream end. This pattern can have several explanations:

(a) Variation in sedimentation rate.

The total deposition of ¹³⁷Cs labelled sediment is greater at the upstream end of the Plain than further downstream. Given that the results from the Downstream Plain are indistinguishable from atmospheric deposition, this implies no nett deposition of previously labelled material in this area.

(b) Interception of atmospheric fallout.

The comments in (a) assume that the atmospheric fallout is constant over the Plain. However it is known that vegetation cover can intercept a significant fraction of atmospherically derived radionuclides, at least in the short term. Usually this component of fallout reaches the ground on leaf litter, or other decaying organic matter, and the fallout integrated over a few years is essentially unaffected, although local redistribution can occur. In this case the majority of the Downstream Plain is covered with melaleuca open forest and woodland, with a canopy cover of between 10 and 70% (Finlayson 1988). A large fraction of the atmospheric deposition will be trapped on this canopy, reaching the ground during leaf fall, which occurs predominantly early in the Wet season, and in the middle of the Dry season. Finlayson (pers. comm.) has observed that the majority of such litter is transported out of forested areas by water flow, and in this case it is likely that transport will be to the East Alligator River. It is similarly concluded that Myrtaceae pollen is flushed from the Downstream Plain (Chapter 3). Thus a substantial fraction of the atmospheric deposition in the Downstream Plain will not remain on the Plain. It is less likely that this type of argument can be applied to the upstream grassland areas of the Upstream Basin and the Central High, although local transport and redistribution of decaying organic matter may account for the areal concentration peaks of the Central High and the Downstream Basin, which are visible in Fig. 6.7. In any case, the dominance of the atmospheric component limits the usefulness of the technique as a tracer of sedimentation in this environment.

(c) Competition and organic content.

Both the above explanations are in terms of variations in the deposition of ¹³⁷Cs. The two variables identified earlier, potassium concentration and organic content, could also have an effect on the ¹³⁷Cs areal concentration. High potassium and/or low organic content could increase the mobility of ¹³⁷Cs after deposition, allowing some fraction to be resuspended, and flushed out to the East Alligator River, again giving reduced concentrations at the northern end of the Plain.

Given the small difference between total and atmospheric deposition, and the uncertainties in the atmospheric component, any attempt to derive a ¹³⁷Cs budget for the Plain is suspect. It is possible to put reasonable limits on the figure for activity imported to the Plain from

the catchment. The total deposition in those topographic units for which there are data, an area of 177 km², is 68±4 GBq. Assuming this applies to the whole of the Plain, the total deposition is 77±5 GBq.

If the atmospheric input is assumed to be zero in the wooded Downstream Plain, but at its full value elsewhere, then it is likely that the overall atmospheric deposition to the Plain is underestimated. Under this assumption, the atmospheric component is 35±4 GBq, 45% of the total, giving an upper limit to the sedimentary component of 42±6 GBq. This represents about 11±2% of the ¹³⁷Cs inventory on the Plain's catchment.

On the other hand, if atmospheric deposition is assumed to be constant, and at its full value throughout the Plain, then the sedimentary component is only 8±10 GBq over the whole Plain, that is, 2±2 % of the catchment inventory.

Assuming that, say 90% of the 137 Cs in the catchment is to be found in the top 10 cm, and that it is exponentially distributed with depth, then 10% will be contained in the top 5 mm. This suggests a surface lowering of < 0.2 mm y⁻¹, assuming no particle size effects, or a sedimentation rate on the Plain of < 0.9 mm y⁻¹.

This attempt to use ¹³⁷Cs as a tracer of sedimentation has been confounded by an unexpected spatial variability in the data, and by gross uncertainties in the atmospherically derived component of the ¹³⁷Cs areal concentration caused by variable tree cover and unknown rates of export of organic matter. Local redistribution of atmospheric fallout on decaying organic matter may also have further complicated the distribution. Such effects are of great significance because atmospheric fallout comprises more than 45% of the total deposition on the Plain. Nevertheless, it has proved possible to calculate an upper limit to the overall sedimentation rate, of < 0.9 mm y⁻¹.

6.5 DETERMINATION OF SEDIMENT SOURCES AND SINKS USING U AND TH SERIES RADIONUCLIDES

The use of radionuclides as tracers of sediment sources and sinks will now be extended to include the natural U and Th series. The extent to which radioactive disequilibrium occurs among the natural series nuclides in the particulate matter carried by the flood waters of Magela Creek, and other tributaries to the Plain, has been used to identify sediment sources. The modern state of disequilibrium has been investigated in two floods and these results used to interpret the radionuclide content of the surface 3 cm (~ 100 years) of the Plain.

RADIOACTIVE DISEQUILIBRIUM IN SURFACE WATERS

Two floods were studied in detail: 19-21 February 1985 when a maximum instantaneous flow rate of 250 m³ sec⁻¹ was recorded, and 10 April 1986 when the maximum flow rate was 60 m³ sec⁻¹. Water samples were collected every 2 hours throughout the floods and both filtered and unfiltered (< 0.45 μ m) samples were analysed by alpha-particle spectroscopy (Martin & Hancock 1987).

The variation of total concentrations with time through the 1985 flood is shown in Fig. 6.8 for the isotopes ²³⁸U, ²³⁰Th, ²²⁶Ra, ²¹⁰Pb and ²¹⁰Po. A pronounced peak is observed in the concentrations of ²²⁶Ra, ²¹⁰Pb and ²¹⁰Po about 10 hours after the start of sampling. This peak was in advance of the hydrograph which reached its maximum about 7 hours later. No such peak is observed for ²³⁸U, and for ²³⁰Th and ²³⁴U (omitted for clarity) there was only a slight enhancement of concentrations. The concentrations of all nuclides in the filtrate remained essentially constant throughout the flood.

Hart et al. (1982) observed a similar peak of total concentrations in advance of the peak of the hydrograph for suspended solids and the metals Mn, Zn and Cu in their study of flood

events in Magela Creek during the 1978-79 Wet season. The main significance of the current data, however, is the demonstration of a substantial disequilibrium in the uranium series radionuclides between ²³⁰Th and ²²⁶Ra in the suspended matter carried by Magela Creek.

The concentrations of ²²⁶Ra in the particulate matter of samples collected during the flood of 10 April 1986 were obtained both with respect to water volume and with respect to the mass of suspended matter. The former data again show a peak in the radionuclide concentrations in advance of the hydrograph but the latter remain approximately constant throughout the flood. The mean value and standard deviation were 220 Bq kg⁻¹ and 40 Bq kg⁻¹ respectively. Thus the peak in radionuclide concentrations during floods is attributed solely to the increased concentrations of suspended solids and not to any significant variation in the concentration of radium in the suspended material. Analysis of similar material collected outside the flood periods shows similar constancy of radium concentrations at about 210 Bq kg⁻¹ and concentrations of ²³⁰Th of about 50 Bq kg⁻¹ deduced from thorium systematics.

RADIONUCLIDE CONCENTRATIONS IN SEDIMENTS

Average values of radionuclide concentrations were obtained on 19 transects of the Creek and Plain by combining two measurement techniques. A rapid quantitative assessment of the distribution of natural radionuclides (primarily ²²⁶Ra, ²²⁸Ra and ⁴⁰K) was provided by gamma-ray dose rate measurements. These dose rate data were used to select a typical site on each transect from which sediment cores were obtained and subdivided into 3 cm sections. These sections were analysed by gamma-ray spectroscopy (Murray et al. 1987) to obtain concentrations of ²³⁸U, ²²⁶Ra, ²¹⁰Pb, ²²⁸Ra, ²²⁸Th and ⁴⁰K. The standard error in the dose rate data for each transect was then used as an estimate of the variability of individual concentrations. The reliability of this technique was confirmed by detailed study on one complete transect.

Concentrations of 238 U and 226 Ra in the top 3 cm of sediment are plotted in Fig. 6.9 as a function of distance from the zero datum at the head of the Plain. In the sand tract (x < 0) concentrations are, as expected, low. The absolute concentrations and the extent of radioactive disequilibrium observed at the southern end of the Plain (0 < x < 5 km) agree very well with observations on the suspended matter carried by Magela Creek. However, disequilibrium is not observed on the northern part of the floodplain (x > 20 km). Therefore, since sedimentation rates are approximately independent of location (Chapter 4), sedimentation in the northern region (which accounts for about 80% of the Plain) must have arisen from inputs other than Magela Creek, even though this creek provides about half the volume of water entering the Plain.

These data have been interpreted using a two-component model of sedimentation. The two components are: input of particulate matter from Magela Creek with a concentration of radium C_m ; and input from the remainder of the catchment with concentration C_r . The average concentration of radium in surface (0-3 cm) sediments at distance x, C(x), is then given by

$$C(x) = (C_m - C_r)f(x) + C_r$$
 6.5.1

where f(x) is the fraction of sediment at x that results from deposition of particulate matter from Magela Creek. The areal rate of deposition of radium, R(x), is related to both the concentration C(x) and to the rate of change of the radium load, L(x), in the water column, that is:

$$R(x) = \rho r(x) C(x)$$
 6.5.2

where ρ is the density of sediment, w is the floodplain width, and r(x) is the total sedimentation rate at x.

The form of f(x) and the values of the variables C_m and C_r have been determined from the radium data in Fig. 6.9. f(x) is given by $\exp(-x/\lambda)$ where the attenuation length λ is 8.5 km, $C_m = 190$ Bq/kg and $C_r = 50$ Bq/kg. Thus C_m is in good agreement with the observed value of radium concentrations in particulate matter of Magela Creek, namely about 220 Bq/kg. Assuming r(x) does not vary substantially over the region 0 < x < 3 km, equations 6.5.2 and 6.5.3 can be solved to determine the current sedimentation rate, r, near the southern end of the Plain. Thus $r = L_s/(w\lambda\rho)$ where L_s is the annual average load of suspended solids carried by Magela Creek. Using known values of r0 and r1 km and 4000 tonnes/r1 km and 4000 tonnes/r2 (Fig. 6.2) respectively, and the value of r3 deduced above gives r4 mm/r5. This value is in good agreement with independent estimates using thorium-radium dating of floodplain sediments from the same location (see Chapter 3).

The principal conclusion of this section is that particulate matter from Magela Creek appears to contribute to sedimentation on only a small fraction of the Plain. Using the value of λ determined above, about 90% is deposited in the first 18 km of Plain with an area of about 30 km² (Fig. 6.10).

6.6 RADIONUCLIDE CONCENTRATIONS IN TOTAL AND FILTERABLE SAMPLES FROM FLOOD WATER — EVIDENCE OF SEDIMENT SOURCES, SINKS AND RESIDENCE TIMES

Murray et al. (1989) made 185 sample collections between February and June 1984, and during the 1985 Wet season from sites downstream of Ranger. Each sample consisted of two 20 litre aliquots, one of which was filtered to 0.45 μ m using a flow through cartridge filter system, and the filtrate retained. Both filtered and unfiltered samples were analysed by alpha spectrometry. The total alpha activity, in mBq/l, was also determined from observed alpha count rates for both the total and filterable samples.

Samples were taken in Magela Creek at Ranger, at gauging station 009, in Mudginberri Billabong, in the Upstream Basin at Ja Ja, and at the gauging station 019 at the northern end of the Downstream Plain. By comparing alpha activity at these sites it has been possible for Murray et al. (1989) to reach conclusions about the distribution of suspended sediment deposition. During the 1985 Wet season the filterable alpha activity concentrations show a 30% decrease between the sand tract at Mudginberri Billabong and Ja Ja, and then remain constant to 019. The total concentrations also show a 30% decline between Mudginberri Billabong and Ja Ja, but then decline by a further 50% between Ja Ja and 019. This latter decline is thought to be the result of sediment deposition as water is dispersed and resistance from vegetation increases on the Downstream Plain. The filterable to total ratio increases down the Plain as a result of these processes. Water leaving the Plain at 019 carried essentially no particulate related alpha activity during the 1985 Wet season.

Murray et al. (1989) also calculated alpha activity loads. In 1985, 10.0±0.3 GBq of particulate related alpha activity passed Mudginberri and entered the Plain. This load was all deposited on the Plain because, as seen above, very little or no particulate related activity passed 019 in this Wet season. All of the additional particulate activity entering the Plain from small catchments adjacent to the Plain must also have been trapped. The conclusion that all of the particulate related activity from Magela Creek stays on the Plain was reached in section 6.5 using the radionuclide signature ²²⁶Ra/²³⁰Th. An activity ratio of 4 was deduced for the upper 3 cm of sediment in the Mudginberri Corridor. The calculated mean ratio for particulate related activity in 1984 is also about 4.

These results suggest that the 1984 and 1985 Wet season may be typical of the ~100 year period represented by the upper 3 cm of the Plain's sediments, although in 1986 alpha activity was found in samples taken at 019 (Murray et al. 1989). The radionuclide results for 1985 and 1986 therefore imply that during the last 100 years or so there has been little (but not zero) loss of suspended sediment from the Plain. The estimated mean annual flux past 019 of 3600±3400 tonnes/year (Fig. 6.2, Table 6.4) is consistent with this conclusion, the presence of measurable quantities of sediment in the water at 019 implying that not all particulates are trapped. The mean annual flux past 019 is 37±57% of the mean annual total flux of suspended sediment to the Plain. The most likely conclusion is that a small (and variable inter-annually) proportion of the particulates delivered to the Plain passes 019 but this proportion cannot be accurately quantified with currently available data. It was shown earlier that organic matter, including pollen, does leave the Plain.

In contrast to the particulate load, there is essentially no difference in the alpha activity of the colloidal/soluble (i.e. < $0.45~\mu m$) load passing Mudginberri Billabong and 019. Murray et al. (1989) argue that this observation, combined with the increase in total flow between these two sites, implies that some resuspension of the finest sediments must occur. Further, if the alpha activity concentrations in the filterable fractions delivered by the side catchments are similar to those at Mudginberri Billabong, then, despite resuspension, all the colloidal and soluble activity transported by Magela Creek must be retained on the Plain.

Further information can be gained by examining the ratio of radium nuclides along the length of the Plain. Murray et al. (1989) showed that the Magela Creek values for 226 Ra/ 228 Ra are 3.7 (total) and 2.2 (filterable) times that at 019. At the outfall the mean values of 226 Ra/ 228 Ra in both total and filterable fractions are within experimental uncertainty of each other. The absolute difference in ratio value between the two sites probably reflects the likely difference in source, that is, Magela Creek and the smaller side tributaries to the Plain.

It is likely that the fine particles have a longer residence time in the large catchment before being entrained by the creek. That is, the delivery ratio is low giving enhanced irreversibly bound ²²⁶Ra concentrations on particles, relative to ²²⁸Ra. This process would be less likely in the smaller side catchments where, as observed at 019, the total and filterable values of ²²⁶Ra/²²⁸Ra would be similar. This argument can be inverted to give an estimate of the average transport time in catchments of various sizes. For the hypothesised mechanism to hold, the transport time for fine particles from the sites at which they obtain their final radium ratios to the Creek must be significant compared with the 1600 year half-life of ²²⁶Ra, that is, greater than hundreds of years. For the smaller catchments it must be months to years. Once again, there is evidence for a significant lag between the release of any suspended solids from the Ranger Mine Site and their deposition on the Plain.

6.7 PARTICLE SIZE OF MODERN ALLUVIA

UPSTREAM OF MUDGINBERRI BILLABONG

Limited sampling of surface sediments along Gulungul Creek and the lower reaches of the sand tract of Magela Creek provides some insight into the locations where fine sediment is stored, some only temporally, on its way to the Plain. These locations are likely to be preferred by suspended solids transported from the Mine Site.

Those reaches of Gulungul Creek that are channeled have cross-sections like that in Fig. 6.11. The channel is flanked by levees that give way to shallow flood basins to either side, between the channel and the valley sides. The particle size distributions across this typical cross-section show that the levees and channel are most sandy, although sand (> 63 μ m) dominates at most sampled sites. The silt (2-63 μ m) and clay (< 2 μ m) constitute the minor fraction at all sites but are at their highest concentrations on the floodplain. The

channels store less than 2% fine sediment and so can be thought of as rapid transit zones for this fraction. This conclusion cannot be drawn for the unchanneled valley floors in the vicinity of the Mine Site, where the surface sediments contain up to about 20% silt and clay.

Fine sediment leaving a slope in the vicinity of the Mine Site may be stored in an unchanneled valley floor but, once in a channel, will be transported rapidly to Magela Creek. Fines that go overbank in the channeled reaches will also be stored. Once in Magela Creek there are few opportunities for storage.

Fig. 6.11 shows a cross-section at Sandy Crossing on Magela Creek. The three samples taken from the active multi-channel area contain < 6% silt and clay. One sample, in a channel-side basin, contains 24% silt and clay in a veneer only 2 cm thick. At depth, such veneers are interbedded with channel sands. Storage of fines does occur but in small quantities that are rapidly buried.

A cross-section across Magela Creek at the upstream end of Mudginberri Billabong was sampled and the results are shown in Table 6.7. Sand dominates in the areas of highest stream velocity, and fines are stored in the levee (50% silt and clay) and in a channel-side depression (58% silt and clay) like that sampled at Sandy Crossing (Fig. 6.11). Although the amounts of fine sediment stored at these locations are significant, the total volume of fines stored in the sand tract of Magela Creek is $\leq 10\%$ when the total area of storage of fines is considered.

The tailings consist of 32±9% sand, 52±8% silt and 16±11% clay (Pickup et al. 1987). They are more silty than the sediments outside the channel on the Gulungul Creek cross-section (Fig. 6.11) but are sufficiently similar to allow storage in the fluvial system. Only the sandy fraction of the tailings is likely to be stored, for a short period, in the channel. If tailings were to get to Magela Creek then, once again, only the sand fraction would accumulate. The clay and much of the silt would be transported to the Plain.

The above argument, which indicates where particular sediment size fractions would lodge, is reasonable only if the transport capacity of the flow is greater than the supplied load of either tailings or other sediment from the Mine Site (Higgins et al. 1987). Much finer fractions may accumulate in Gulungul Creek, for example, if the stream's transport capacity were overwhelmed. But this would only be temporary and subsequent flows, occurring when there was less Mine Site sediment available, would move the finest sediment downstream.

DOWNSTREAM OF MUDGINBERRI BILLABONG

At 107 of the sample points shown on Fig. 6.4, particle size was determined for the Plain's sediments between 0 and 2 cm. All data for a particular fraction on each northing have been combined, and a mean and standard deviation calculated. Where there is only one sample on a northing, the uncertainty attached to the value at that point has been estimated from replicate particle size determinations from the same sample. The mean replication uncertainty for all fractions is 10%.

The means, standard deviations and/or replication uncertainties for all sampled northings for the size fractions < 1 μ m, < 2 μ m, 1-2 μ m, 63-125 μ m and > 125 μ m are shown in Fig. 6.12 to 6.14. If sediment transported by Magela Creek dominated the Plain's surface texture, then simple patterns of particle size should emerge, analogous to those on an alluvial fan (e.g. Lustig 1965). The majority of the coarse particles should be deposited near the upstream (proximal) end of the Plain while the proportion of the finest particles should steadily increase downstream (distally). The coarsest fractions, namely sands between 63 and 125 μ m and > 125 μ m (Fig. 6.14) are largely restricted to the Mudginberri Corridor with some in the proximal part of the Upstream Basin. Fine sand occurs in a few percent along the full

length of the Plain while coarse sand is effectively absent downstream of the Upstream Basin.

For the conclusion to be drawn that the Magela Creek dominates sedimentation on the Plain it must be shown that the clay ($< 2 \mu m$) fraction shows the reverse pattern to that of the sand. Fig. 6.12 shows that the bulk of the surface sediments are clay, and mostly $< 1 \mu m$. The $< 1 \mu m$ and $< 2 \mu m$ plots parallel each other, separated by about 10%. This arrangement implies that the 1-2 μm fraction will be nearly constant at about 10%, as shown in Fig. 6.13.

The $< 2~\mu m$ fraction shows a complex pattern of longitudinal variation. There is a peak of about 65% in the middle of the Mudginberri Corridor and a decline into the Upstream Basin. The proportion $< 2~\mu m$ rises at the upstream edge of the Central High and steadily rises to the distal end of the Plain. This longitudinal pattern is not a reflection of one dominant sediment source.

There is an additional factor to be taken into account, biogenic silica. Microscopic examination of samples prepared for identification of biogenic silica remains (Chapter 4) showed that most are of silt size, that is, 2-63 μ m. The longitudinal pattern of this size fraction is shown in Fig. 6.13 and reflects the pattern of variation of biogenic silica mass flux shown in Fig. 4.26. That is, the biogenic silica content of the Plain's sediments is at a maximum in the Upstream Basin and lower elsewhere. The only important difference is at the proximal end of the Mudginberri Corridor where the silt content reaches about 50%, where it is almost certainly minerogenic rather than biogenic.

From the longitudinal patterns it can be concluded that the non-biogenic fractions (clay and sand) do not reflect simple dominance by Magela Creek of the Plain's surface texture. The sand in the Mudginberri Corridor is obviously attributable to Magela Creek while that in the Upstream Basin could have partially come from Kawudjulah Creek. The clay fraction rises in the thick *Melaleuca* forests near the Oenpelli Road crossing, then falls downstream as both the vegetation resistance to flow declines and, more importantly, the proportion of silt (much of which is biogenic) increases. The silt content peaks at the upstream edge of the Central High then declines to the distal end of the Plain. This pattern is the mirror-image of the clay pattern, reflecting both the decline of biogenic silica on the Downstream Plain and, more importantly, the integrated result of fine clays derived presumably from the side tributaries being transported furthest. This interpretation is consistent with the interpretation of radionuclides which show that the influence of sediment from Magela Creek does not extend beyond the Central High.

6.8 A PRELIMINARY SEDIMENT BUDGET FOR THE CATCHMENTS OF THE MINE SITE TRIBUTARIES

Pickup et al. (1987) recommended that a proper evaluation of the potential transport, deposition and storage of tailings (and other sediments derived from the Mine Site), in the small catchments that extend from the Mine Site to Magela Creek, should involve both sediment transport models and an account of alluvial history as well as sediment budgeting. Modelling has not been done and the alluvial history of the small catchments is not well known. Any attempt to assess the potential pattern of sediments derived from the Mine Site must, at the moment, depend upon a rudimentary sediment budget. Some understanding of these catchments is required before, in the next chapter, the impact of tailings on the Plain is considered.

On the basis of the length of the tailings dam wall facing each of the Mine Site catchments (Fig. 6.15), about 42% of the tailings would drain into the Gulungul catchment. The Coonjimba catchment would receive 24%, the Georgetown catchment some 18%, and 15% for the Djalkmarra catchment. Gulungul Creek catchment could play a major role in containing a spill of tailings (Pickup et al. 1987).

ROUTING OF TAILINGS THROUGH THE MINE SITE CATCHMENTS

The tailings dam faces a small subcatchment of 1.6 km² on the right bank of Gulungul Creek at a point where the main channel has a catchment of 42 km² (Fig. 6.15). Downstream the main channel is joined by five other subcatchments totalling another 48 km², giving the catchment an area of 90 km² at its junction with Magela Creek.

Equation 6.3.1 permits the calculation of the natural sediment yield from ungullied catchments (I). The inverse relationship in this equation has been explained in section 6.2 as the result of: increased deposition in valley bottoms, with distance downstream, of sediment derived from adjacent slopes; and/or decreasing erosion rates on slopes adjacent to valley floors as slope gradients decline with increasing catchment area. In the Gulungul Creek catchment a good approximation is that erosion rates outside channels are approximately constant in each unit area of the catchment and that the inverse relationship in equation 6.3.1. is solely the result of increased sediment storage as catchment area increases.

Using this assumption, and a unit area of 1 km², it is possible to calculate the curve of storage (S) versus catchment area (Fig. 6.16). A unit area of 1 km² has an average erosion rate (and, by definition, sediment yield) of 17 t/y. In a 10 km² catchment the total erosion rate is 170 t/y and the yield is 130 t/y (from equation 6.3.1). The sediment delivery ratio (SDR) is therefore 1.0 in the 1 km² catchment, by definition, and 0.76 in the 10 km² catchment. The curve of SDR versus catchment area in Fig. 6.16 is calculated in this way, and the storage curve is the difference between total erosion and yield. The SDR versus catchment area curve is obviously sensitive to the unit area chosen for the calculation of total erosion. The dashed line in Fig. 6.16 has been calculated using a unit area of 0.1 km². The greatest sensitivity is in the smallest catchments.

These calculations are obviously idealised. But it is important to note that the storage component will be underestimated in this approach if the unit area erosion rate is substantially lower in valley bottom slopes because of decreasing slope gradients from interfluves to channels.

The upper 62 km² of the Gulungul Creek catchment does not fall on the line defined by equation 6.3.1 (Fig. 6.1) because, it is thought, of a high sediment contribution from gullying and channel incision. The dashed line in Fig. 6.1 is taken to represent the appropriate curve for that part of Gulungul catchment that is incised. This dashed curve must return to the line of equation 6.3.1 for small catchment areas, but there are no data to allow its definition.

The sediment yield of incised catchments (I) is plotted in Fig. 6.17 along with the total (unincised) erosion (using a unit area of 1 km²) (E) and storage derived from this total erosion (S). The channel erosion (C) component of I can be calculated from the mass balance

$$C = I - (E-S)$$
 6.8.1

From this equation a curve of C versus catchment area is plotted in Fig. 6.17, predicting a mean yield of 1600 t/y from the erosion of the incised channels at the gauging station where Gulungul Creek has a catchment of 62 km². The channel sources represent 70% of the total yield of the catchment, according to this calculation. But this formulation neglects storage of sediment derived from channel erosion. There is no way of estimating this component with currently available data, but it is likely that the proportionate contribution of channel erosion to total catchment yield is less than 70%. It is still likely to be the major source, however.

The subcatchments, erosion rates and fluxes in the entire Gulungul Creek catchment are shown as a sediment budget in Fig. 6.18, based on extrapolation of the curves in Fig. 6.17

and use of equation 6.3.1 for the unincised subcatchments. The tailings dam will feed sediment to the unnamed 1.6 km² subcatchment on the right bank of Gulungul Creek shown in this diagram, should erosion of the structure occur.

With this sediment budget it is now possible to route tailings through the Gulungul catchment to simulate mixing of tailings with natural sediment as it passes into the sand tract of Magela Creek. To illustrate this we begin by eroding tailings at the same natural rate of 17 t/y adopted for the unit area of 1 km². Note that the value of E in the 1.6 km² catchment in Fig. 6.18 has been rounded from 27.2 to 30 t/y. Of this 30 t, only 20 t will leave the catchment each year. This is then joined by 1500 t/y from upstream, and passes along the channel to be joined by a further 1400 t/y before discharging to Magela Creek. In these calculations, once the tailings enter the incised creek it is not known where the storage of 300 t/y (Fig. 6.18) occurs. It is either overbank or within the channel. If it is overbank then it is largely unavailable for further transport for a period much longer than if it is stored in the channel. It is now possible to estimate the amount of dilution of the tailings that would occur through the Gulungul Creek catchment. This dilution is shown in Fig. 6.19 where 30 t/y of tailings produces only 0.2% of the annual load of sediment leaving Gulungul Creek.

If 42% of the tailings were to be transported into the Gulungul catchment, representing 4.2×10^6 t of the expected total 10×10^6 t (C. Unger, pers. comm.), at the natural total erosion rate of 30 t/y, the tailings would take 1.4×10^5 years to be eroded. This rate of erosion is equivalent to 24 t/km²/yr, indistinguishable from the mean 2.5 ± 1.9 t/km²/y for a period of about 0.6×10^5 years calculated by Airey et al. (1982-83) (section 6.2).

Routing the remainder of the tailings, over various time periods, through the Coonjimba, Djalkmarra and Georgetown catchments using the same method as described for the Gulungul Creek catchment, results in the curves of Fig. 6.19. In this diagram it is clear that tailings would dominate the Mine Site catchments if all of the tailings were to be eroded in a period less than 100 years. Coonjimba and Djalkmarra catchments would be dominated by tailings if the total erosion time was less than 1000 years.

The calculations just presented have some severe limitations. Firstly, if all of the tailings were to be eroded in less than 10 years then the modern sediment delivery ratio (SDR) would almost certainly not apply. The transport capacity of the slopes and streams would be overwhelmed and massive deposition would occur. Further, the model that has been constructed to produce Fig. 6.19 assumes a constant value for the SDR. Over a period of years to decades, this is a reasonable assumption for the mean SDR. But it is highly unlikely for periods of thousands of years or more, given that in Chapter 4 climate has been shown to vary substantially over these periods of time. In addition, the local and regional base level of the Mine Site catchments will change within the next 10 000 years, as sea level begins to fall in response to the slow onset of the next global glaciation (Pickup et al. 1987). Within the next 140 000 years, the maximum period considered in Fig. 6.19, sea level will almost certainly have fallen to about 100 m below its present level during a full glacial. Although the effects of sea level change on fluvial sedimentation/erosion appear to decrease exponentially from the coast, the Mine Site catchments would be affected as Magela Creek incised some 8-10 m to re-occupy its pre-Holocene trench. The current aggradational regime will store tailings until base level falls and much of the alluvium currently stored is flushed out of its present location. This conclusion also applies to the Magela Plain.

The other limitations of the calculations are that they take no explicit account of either the Mine Site retention ponds or billabongs, both of which could store sediment.

It is clear that if these various limitations and assumptions could be removed or bettered, then the calculations would be much more accurate and conclusions drawn from them more reliable. But the simple box model used here cannot cope with, for example, changes to the

SDR if very large amounts of tailings are eroded. A more deterministic model is required but the data required for any such model are not available.

6.9 QUANTITIES OF TAILINGS REACHING THE MAGELA PLAIN

The steady state sediment budget and routing of tailings and natural erosion products through the Mine Site catchments provides estimates of the quantity of tailings that might reach the Magela Plain. If all of the tailings were eroded in 1 year, that is, by a catastrophic cyclone in one or two Wet seasons, then 8.53×10^6 t of tailings would pass Mudginberri in a year (Fig. 6.20). Therefore, 1.47×10^6 t of tailings would remain in the catchment, stored in channels and overbank to be eroded in subsequent years.

If the tailings were to be totally eroded at the natural long-term rate, then during each subsequent year tailings would be delivered to the Plain at the average rate of about 70 t/y. It is likely, however, that as tailings moved downstream in each year their rate of remobilisation would decrease, following the decline of SDR with increasing catchment area.

The masses of material moved in years subsequent to the onset of tailings erosion (Fig. 6.20) can only be accepted as guides, for the reasons given above. The model upon which these estimates are based is crude and the data base for the calculated values of the SDR have large uncertainties. Further, the current SDR may not apply if catastrophic erosion occurred, although, the kind of meteorological and hydrological conditions that would apply at the time of such erosion may increase the SDR substantially above the value derived from the relatively benign Wet seasons of the last few years.

Despite all of these reservations, the curve in Fig. 6.20 shows that catastrophic erosion would deliver a higher proportion of tailings to the Plain than erosion at a slower rate. The proportion of tailings in sediment reaching the Plain, if the tailings impoundment were to erode at about the natural long-term rate, is about 1% of the current annual load of about 5000 t. If erosion were to occur within 1 year then tailings would represent 1.7×10^3 times the current load and would dominate the Plain. More tailings than natural sediment would reach the Plain for time periods of total erosion of the tailings of less than about 1800 years.

6.10 PATTERN OF DEPOSITION OF TAILINGS ON THE PLAIN

It is assumed that Fig. 6.20 is a useful guide to the mass of tailings likely to arrive on the Magela Plain, and that the current mean annual load of 5000 t of suspended sediment that passes Mudginberri remains constant. The pattern of deposition of tailings on the Plain can be predicted from equation 6.5.1 (see Fig. 6.10). The estimates of the sediment loads (~ 1500 t/y) entering the Upstream Basin and Mudginberri Corridor from streams other than the Magela will also be taken into account.

The 5000 t/y derived from Magela Creek is deposited in the way shown by curve A in Fig. 6.21, expressed as tonnes per strip of Plain 2 km long (that is, in a downstream direction). Recall that f(x) is solved with a constant Plain width of 1 km, so that curve A in Fig. 6.21 is a smoothed version of the real pattern. This curve has been converted to a flux in curve C and can be compared with curve B, the minerogenic sediment flux estimated from radiocarbon dating (Fig. 4.26).

The areas beneath curves B and C between 0 and 20 km distance from the arbitrary origin, and so the total flux of sediment to the Plain estimated by the two methods, are approximately the same, as seen using other methods earlier in this chapter. But curve C is smoothed, as seen above, whereas curve B is not. If the two curves were strictly comparable, then the differences between them could be viewed as the result of sediments arriving from catchments other than the Magela. Unfortunately, the curves cannot be compared in detail

and so we must treat the input from the side catchments as if it were uniformly distributed on the Plain.

The proportion of tailings in sediments of the Plain (including minerogenic, biogenic silica and organic matter), under various assumptions of the period for total erosion of the tailings, is shown in Fig. 6.22. The curves can be approximated by the exponential function

$$T = a e^{(b D)}$$
 6.10.1

where T is the percentage of tailings in sediment on the Plain at various distances D from the arbitrary origin. The constant is a and the exponent is b. The exponent varies with YR, the time taken for total erosion of the tailings

$$b = 1.43 \ln YR + \ln 6.1189 \times 10^{-6} (1-160 \text{ years})$$
 6.10.2

$$b = 0.17 \ln YR + \ln 0.008 (160-140 000 \text{ years})$$
 6.10.3

The constant at D = 0-2 km also varies with YR

$$a = 99.04 \text{ YR}^{-0.04} (1-160 \text{ years})$$
 6.10.4

$$a = 1184 \text{ YR}^{-0.45} (160-140\ 000\ \text{years})$$
 6.10.5

These equations allow the estimation of the proportion of tailings that will be in the Plain's sediments under any adopted value of YR and for any of the 2 km long segments of the Plain. But such estimates are only realistic for a period of future time during which sea level is close to its present height, as seen in section 6.8.

Following Berger (1980), predictable variations of the orbital geometry of the Solar System will cause a decrease in the flux of solar radiation to the Earth's atmosphere (see Chapter 4) so that the first major cooling of the next glacial cycle will begin within the next 5000 years. This cooling will probably be delayed by the warming that is likely from increased CO₂ in the atmosphere (Mitchell 1989). A super-interglacial during the next few centuries is likely to be followed by a cooling. This statement does not have the support of modelling results because models that can cope with variations in both solar radiation and CO₂ have not been run into the distant future.

The idea of a super-interglacial followed by cooling is based upon the assumptions that: solar forcing dominates the glacial-interglacial cycle; and that all of the fossil fuels and terrestrial vegetation will be burned within the next 1000 years and that the ocean will be a major sink for this CO₂. So the anthropogenic Greenhouse Effect will appear in the geologic record as a spike of substantially enhanced CO₂, temperature and rainfall (Pearman 1988, and references therein).

If all of the tailings at the Mine Site were eroded within the super-interglacial, the curves of Fig. 6.22 are useful for approximate predictions over the next few centuries to 1000 years or so, assuming a stable sea level. If the sea rises, a likely result of the Greenhouse Effect (Pearman 1988), then the re-establishment of tidal connections on the Magela Plain may result in the flushing of sediment rather than its retention.

If substantial erosion of the tailings were to continue into the distant future, that is, past the first predicted substantial cooling when sea level has already fallen, then the curves of Fig. 6.22 are not helpful. A fall in sea level would lead to incision of the Plain, sand tract and possibly the Mine Site tributaries, and sediment flux will probably be increased on the resulting steeper gradients.

It is therefore concluded that the predicted dispersal of tailings (in Fig. 6.22, and equations 6.10.1 to 6.10.5) is most useful for future conditions like those of today. If sea level rises or falls then sediment dispersal patterns will be different, although under conditions of a slightly higher sea level the curves of Figs 6.19 and 6.20 which predict the amount of tailing reaching the Plain will still be useful. Here we assume that the sediment delivery system will not greatly change as global warming occurs.

The discussion of sediment dispersal has concentrated on tailings rather than other sources of Mine Site sediment. There is insufficient information available to consider erosion of roads etc. in the way that the tailings can be treated. Obviously any erosion additional to the natural sediment and tailings will add to the load reaching streams and the Plain. But the tailings will almost certainly dominate the sediment delivery system of the future if they erode at a rate substantially above the natural erosion rate.

6.11 SUMMARY

SEDIMENTATION RATES

The various estimates of sedimentation rates on the Magela Plain are assembled in Table 6.8. Those based on radiometric methods (¹⁴C, Ra/Th) include minerogenic, biogenic and organic components, and integrate the effects of, on average, 1.9 ka of sedimentation and organic degradation. The estimate based on ¹³⁷Cs also includes all of the components, but over about 30 years. The estimate based on observed loads upstream of Jabiluka Billabong is calculated from the minerogenic component, then adjusted to include the mean biogenic and organic component for this part of the Plain.

The estimates based on radiometric methods are very similar and give a grand mean of 0.23 ± 0.13 mm yr⁻¹. This grand mean rate is 2.4 times the best estimate based upon suspended sediment loads measured over 3 years, although the uncertainties attached to each best estimate make them indistinguishable. Within the relatively large uncertainties, the modern sedimentation rate is the same as the long-term rate estimated over periods up to 3.3 ka. The ¹³⁷Cs based rate is an upper limit that is consistent with the other rates, and the estimate of 0.4 mm yr⁻¹ based on radium deposition may be too high.

The rate of sedimentation within the Dark Brown/Black Clay, of about 0.2 mm yr⁻¹, has been nearly constant in the Mudginberri Corridor for up to 3.3 ka, in the Upstream Basin for about 1.6 ka, and in the Central High and Downstream Plain for about 1.2 ka. If sea level and climate remain for the next 1-2 ka approximately as they have been for the last 2-3 ka, then the mean rate of 0.2 mm yr⁻¹ can be extrapolated. In the Upstream Basin and Mudginberri Corridor about 20±13 cm will be deposited during the next 1 ka, on average. This result is probably not very sensitive to a Greenhouse warmed earth.

PATTERN OF SEDIMENTATION ON THE PLAIN

The state of disequilibrium between nuclides in the natural U and Th series in sediments carried by modern floods has been used as a tracer of sediment source (section 6.5). The disequilibrium between ²³⁸U and ²²⁶Ra in the surface 3 cm (~ 140 years), in the part of the Plain extending 5 km downstream from the arbitrary datum, agree well with that in the suspended matter carried by Magela Creek. This disequilibrium is not observed beyond 20 km downstream from the datum. Particulate matter from Magela Creek contributes to 90% of the sediment deposited on the first 18 km of the Plain. That is, 90% of Magela Creek sediment is deposited on only 15% of the Plain. The rest of the sediment comes from other, and generally smaller, catchments that flank the Plain. This result is consistent with the sediment budget of Fig. 6.2 derived from measured loads passing gauging stations.

An attempt to use ¹³⁷Cs as an indicator of patterns of deposition was confounded by large spatial variability in concentration of the nuclide, and by gross uncertainties in the atmospherically derived component. The major, but tentative, conclusion to emerge is that ¹³⁷Cs attached to organic matter is lost from the Downstream Plain. This process reduces the inventory of ¹³⁷Cs in this part of the Plain so that it is indistinguishable from the atmospheric component. The loss of organic matter is consistent with the conclusions drawn from the distribution of pollen in surface sediments (Chapter 3).

The particle size of the non-organic part of the upper 2 cm of the Plain was measured as a further indicator of sedimentation pattern. Although made difficult by silt-size biogenic silica fragments, the pattern of sand and clay is consistent with more than one major source. Further, the particle size and radionuclide data show that Magela Creek contributes no more than a few percent of the sediments deposited on or downstream of the Central High.

There are no explicit data to demonstrate that the influence of Magela Creek on the Plain's sediments has been as it is now for more than ~ 140 years. However, the near constant sedimentation rates in the Dark Brown/Black Clay and a plausible interpretation of the longitudinal disposition of the major sedimentary environments (Fig. 4.21), suggest that the Creek has had no significant influence beyond Jabiluka Billabong for the last 3-4 ka. Accepting this interpretation, and assuming that sea level and climate will remain for the next 1-2 ka approximately as they have been for the last 2-3 ka, then equation 6.5.1 can be used to estimate the Magela Creek derived fraction of sediment deposited at any northing.

PATTERN OF SEDIMENTATION IN THE MINE SITE CATCHMENTS

Many fewer data have been collected in this area than on the Plain because this was not originally thought to be one of the tasks of this study. The pattern of deposition of various particle sizes has been explored as a possible analogue of the future distribution of sediments (including tailings) eroded from the Mine Site. The range of particle sizes is similar in the Mine Site soils, alluvial sediments of the Mine Site catchments, and the tailings. Therefore, the Mine Site valley floors and small parts of the hillslopes could store some of the sediment eroded from the Mine Site. Storage in overbank sites could be for long periods of time.

ROUTING OF TAILINGS TO THE MAGELA PLAIN

A sediment budget has been constructed for the Mine Site catchments, and using this in conjunction with a sediment delivery ratio (SDR), it has been possible to route tailings through transit zones and temporary storages to the Plain.

The proportion of tailings reaching the Plain is, in this analysis with a constant SDR, a function of the time taken for total erosion of the tailings. At about the natural long-term rate of denudation ($25\pm19 \text{ t/km}^2/\text{y}$) the tailings would take 1.4×10^5 years to erode and would represent about 1% of the current annual load of 5000 t that reaches the Plain from Magela Creek. For a time of total erosion of the tailings ≤ 1800 years, more tailings than natural sediments will reach the Plain on average. That is, tailings will represent 50% or more of the load reaching the Plain for a total erosion time of ≤ 1800 years.

The pattern of deposition of tailings on the Plain is calculated using equation 6.5.1, and equations 6.10.1 to 6.10.5 can be used to calculate the proportion of tailings at any northing for a wide range of total erosion times. These results are summarised in Fig. 6.22 for a few total erosion times.

Predictions of the pattern of dispersal of tailings, or other sediment derived from the Mine Site, using these equations are only reliable if the assumptions underlying the sediment routing model are valid and if future boundary conditions do not vary too far from those of

the present and the last 2-3 ka. With currently available data the model cannot be improved. Therefore, we can only judge the reliability of the predictions on the basis of likely future boundary conditions.

The future may hold a higher sea level, caused by Greenhouse warming, followed by a fall of sea level as the mechanics of the solar system once again begins the onset of a glacial. The predictions of tailings dispersal are strictly valid only for a non-saline and unincised Plain. A large rise of sea level would lead to salinisation with tidal connections, and to incision if sea level were to fall substantially. It is likely that the equations developed in this chapter are useful for the next 50-100 years, assuming that sea level rises very slowly as Greenhouse warming proceeds, and then will be useful again as sea level returns to its present level sometime within the next 5000 years. It may be the case that a sea level rise will not re-establish tidal connections to the Upstream Basin (see Chapter 7 for further discussion) and so the equations are useful for the time preceding a fall of sea level, that is a future time period between 1 and 5 ka. As the climate begins to cool within the next 5000 years, incision of the Plain as sea level falls will be a far more important factor in tailings dispersal than climate.

It is clear that for total erosion times approaching the limit set by the natural denudation rate, prediction of dispersal patterns of tailings is not possible. The Magela Plain will have been largely eroded. The small remnant of last interglacial estuarine sediments on cross-section 2 (Chapter 2) shows that, as sea level fell subsequent to 120 ka, Magela Creek eroded almost all of the sediment that had formed an ancestral Plain during that interglacial. The same pattern of erosion can be expected as sea level falls in the future, with tailings being dispersed into the terrestrial equivalent of the East Alligator River and possibly out onto what is now the continental shelf.

The very small proportion of tailings that would occur in the Plain's sediments if the tailings were to erode at about the natural denudation rate is a strong argument for designing the tailings impoundment using geomorphic criteria. Impoundment slopes that are concave and include natural grading of particle sizes appear to most closely mimic natural slopes in the ARR.

Table 6.1. Least squares equations relating sediment loads to discharges.

Gauge	Equation	R ²	n	SE%	
009 Jabiru 017 Jabiluka 019 Outflow	$\begin{array}{c} L = 0.32 Q^{1.33} \\ L = 0.56 Q^{0.99} \\ L = 1.11 Q^{0.84} \end{array}$	0.91 0.85 0.86	45 28 25	+123,-55 +130,-57 +130,-57	

L is load in tonnes/day, Q is discharge in $m^3\ sec^{-1}$, SE is standard error of the estimate.

Table 6.2. Best estimates of average annual suspended sediments loads in the ARR.

Gauge or site	Catchment area (km²)	Specific sediment yield (t/km²/y)	No. of years of data	
009	600	9.15+ ^{11.99} - 6.50	4	
017	1115	3.35+ ^{4.36} _1.91	2	
019	1570	2.30+ ^{3.08} _{-1.52}	3	
S. Alligator River	9000	3.33±1.1	2	
Adelaide River	7640	1.19±0.19	4	
Kawudjulah Creek	63	19.0	1	
Gulungul Creek	62	34.77±23.47	3	
Georgetown Creek	7.8	13.23±16.45	3	
Brocks Creek	0.00004	34.38±5.0	3	

Table 6.3. Comparison of suspended sediment loads (in tonnes/y) calculated by different methods.

Gauge	Year	Hart <i>et al</i> . (1987)	NT Water Division data
009	1978/79	2940	3590+4416 _1975
	1979/80		7810 ⁺⁹⁶⁰⁶ _4296
	1980/81		10770 ⁺¹³²⁴⁷ _5923
	1982/83	2330±2300	
019	1978/79		3280 ⁺⁴²⁶⁴ _1870
	1979/80		5780 ⁺⁷⁵¹⁴ _3295
	1982/83	1720±540	

Table 6.4. Major elements of the sediment budget for the Magela Plain.

Topographic unit(s)	Inputs	Outputs (tonnes/yr)	Deposition	Mineral sediment flux (g/cm²/yr)	Mineral deposition rate (cm/yr)
Mudginberri Corridor and Upstream Basin	6000± 4500	3700± 3500	2400± 5700	0.001± 0.02	0.01± 0.02
Central High and Downstream Plain	7500± 4900	3600± 3400	3900± 6000	0.003± 0.004	0.003± 0.005
East Alligator Floodplain	3600± 3400				
1-4				0.02± 0.0001	0.03± 0.0002
4-10				0.05± 0.0002	0.03± 0.0005

Table 6.5. Concentrations of ¹³⁷Cs on topographic high points to estimate the atmospheric input.

	Mass conc. Bq kg ⁻¹	Bulk density kg m ⁻³	Areal o Bq m ⁻²	
Magela Crossing	0-25 cm	0.77±0.14	1471	280±50
	25-48 cm	0.15±0.12	1417	50±40
	48-73 cm	0.00±0.07	1474	0±30
Oenpelli Road	0-25 cm	0.96±0.16	1857	450±70
	25-37 cm	0.0±0.02	1405	0±70
Arnhem Highway	0-25 cm	0.79±0.16	1594	320±60
	25-45 cm	0.0±0.01	1354	0±30
Average of 0-25 cm	layers			350±40

Note: Uncertainties are given in the least significant figures, and are one standard deviation except for the average, where it is one standard error.

Table 6.6. Radionuclide concentrations at sites chosen for variability tests.

	U-238 Bq kg ⁻¹	Ra-226 Bq kg ⁻¹	Th-232 Bq kg ⁻¹	Pb-210exc. Bq kg ⁻¹	¹³⁷ Cs Bq kg ⁻¹
Lower site					
Α	82±5	109.1±1.4	55.9±0.7	14±25	0.4±0.1
В	93±5	115,4±1,4	63.3±0.8	27±25	3.3±0.1
C	99±4	102.5±1.3	55.3±0.7	-9±19	0.0±0.1
Average	91	109	58	11	1.2
Standard Dev.	10%	6%	8%	170%	150%
Upper site					
Α	81±5	99.2±1.3	67.5±0.8	44±25	2.7±0.1
В	65±5	110.1±1.4	47.1±0.7	190±40	9.2±0.3
C	84±5	99.8±1.3	71.9±0.9	50±30	1.9±0.1
Average	76	103	62	95	4.6
Standard Dev.	14%	6%	21%	90%	90%

Note: Uncertainties given as subscripts are in the least significant figures, and are one standard deviation.

Table 6.7. Particle size distribution of landforms on a cross-section of Magela Creek at the upstream end of Mudginberri Billabong.

Landform	Levee	Levee base	Channel	Inter- channel bar	Channel- side depression	
C. Sand (> 125 μ m)	2	5	95	80	11	
F. Sand (125-63 μ m)	30	50	4	16	17	
Silt (2-63 μ m)	17	11	1	2	18	
Clay (< 2 μ m)	33	24	0.5	2	40	

Table 6.8. Sedimentation rates (mm yr -1) estimated for various parts of the Magela Plain.

Site	MX3	MX1	MX2	MV1	PP1	Cross- Sections 1 - 4	Upstream of Jabiluka	0-3 km	Cross- sections 5 - 9	Whole Plain
Method	¹⁴ C	Ra/Th	Ra/Th	¹⁴ C	¹⁴ C	14C	Rating curve	Ls/ (wλρ)	14C	¹³⁷ Cs
Rate (mm y ⁻¹)	0.26 ±0.04	0.19 ±0.02	0.20 ±0.04	0.15 ±0.01	0.22 ±0.01	0.24 ±0.12	0.10 ±0.25	0.4	0.33 ±0.25	<0.9
Time Period (ka)	3.3±0.1	1.7±0.2	1.6±0.3	1.3±0.08	1.7±0.1	~1.6	0.003	~0.14	~1.2	0.03

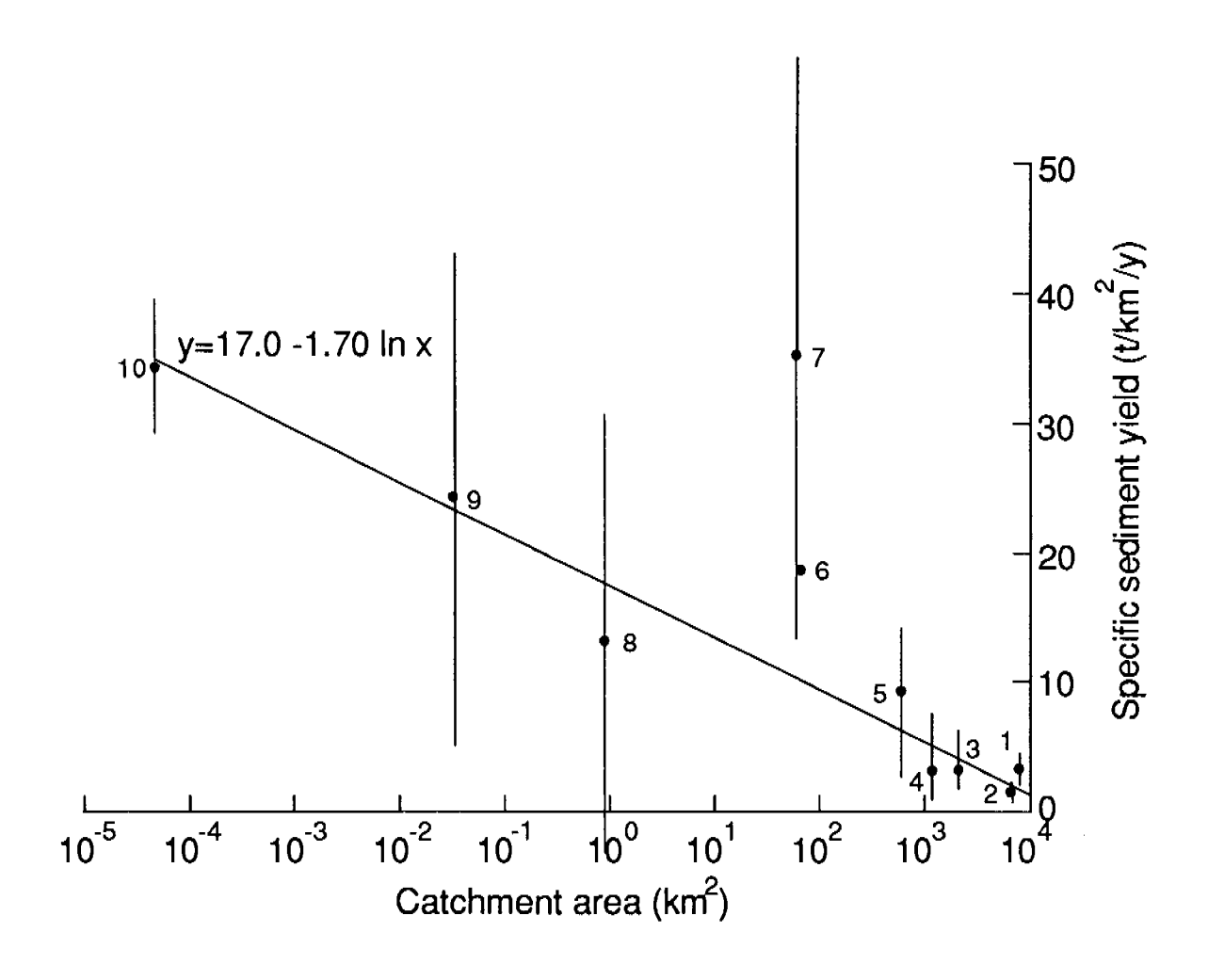


Figure 6.1 Specific sediment yield versus catchment area for sites in the Alligator Rivers Region. 1: South Alligator River; 2: Adelaide River; 3: 019; 4: 017; 5: 009; 6: Kawudjulah Creek; 7: Gulungul Creek; 8: Georgetown Creek; 9: Ranger, Jabiluka and Nabarlek; 10: Brooks Creek erosion plots. With the exception of number 9, all of these data are listed in Table 6.2

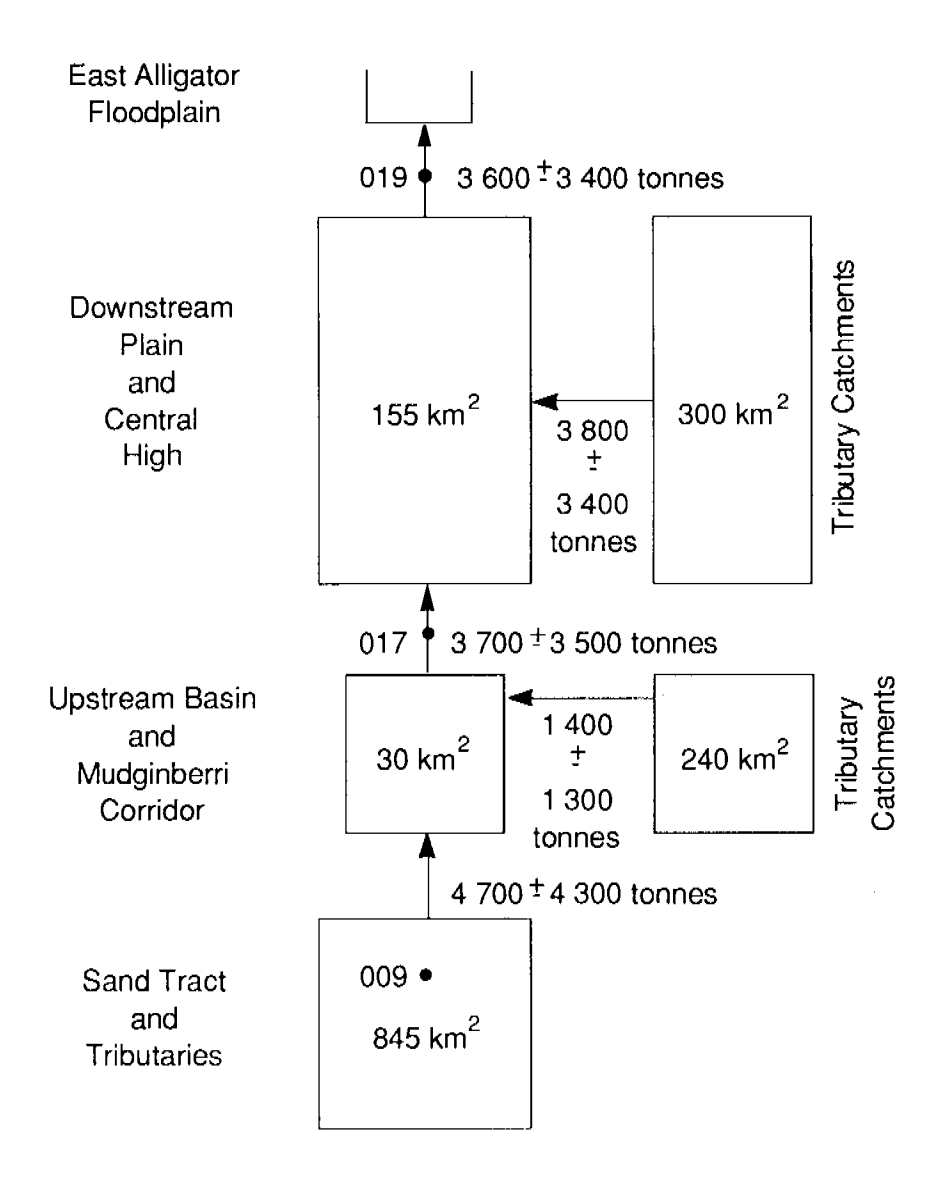


Figure 6.2 Compartment model of the Magela Plain and Catchment showing mean annual fluxes of suspended sediment

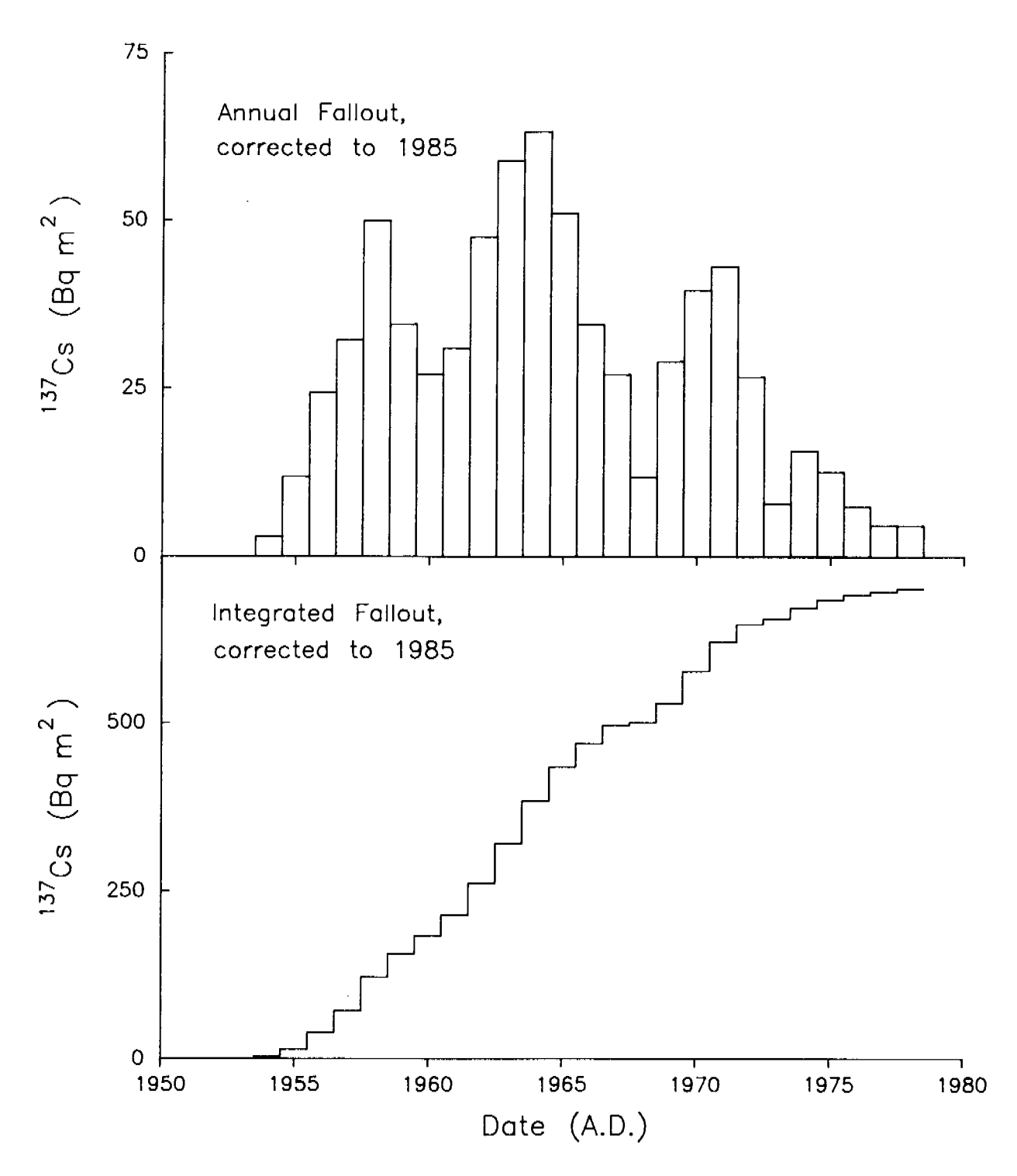


Figure 6.3 137Cs fallout at Brisbane, shown as both cumulative and annual fallout, corrected to 1985 for radioactive decay

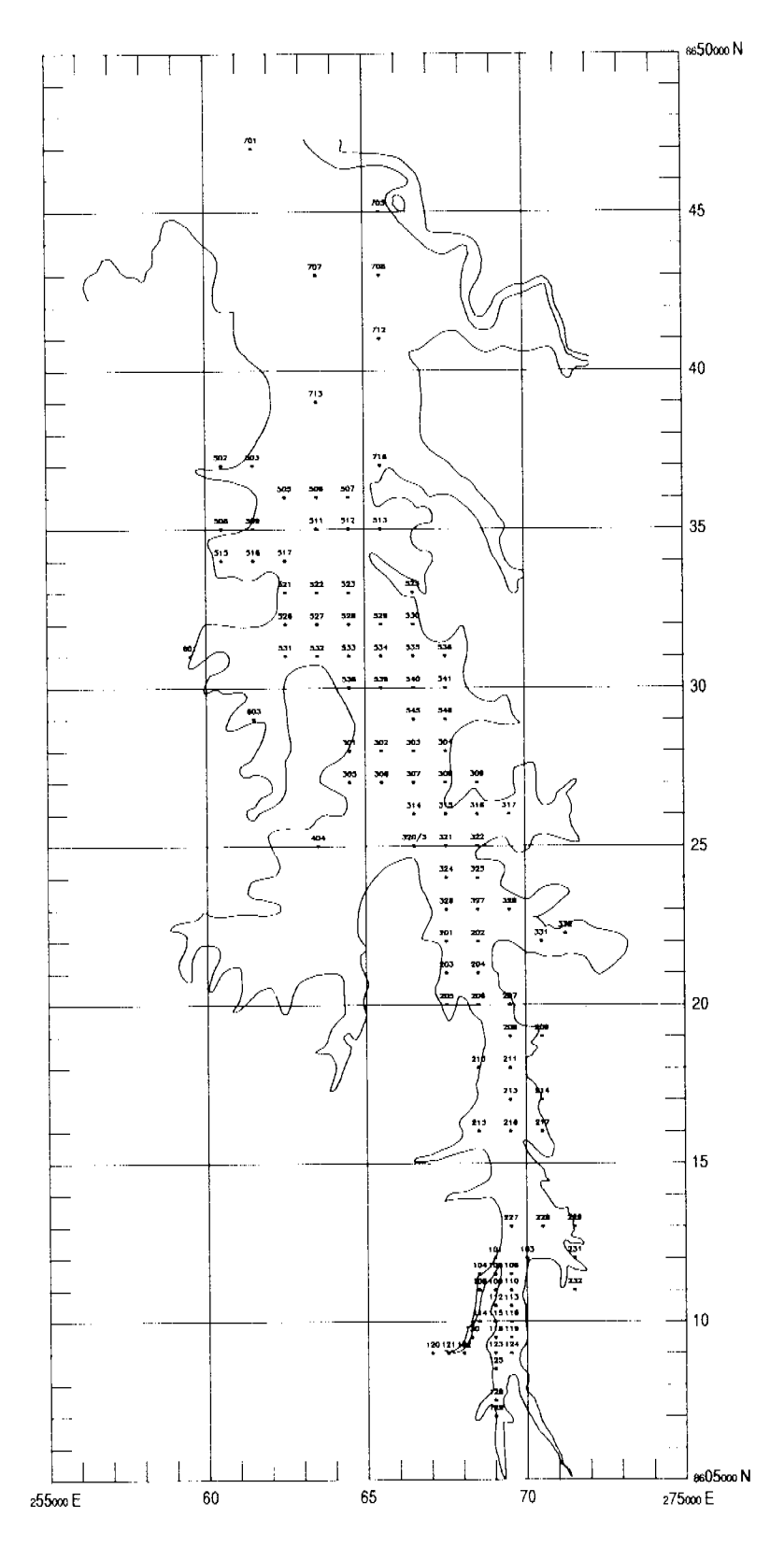


Figure 6.4 Australian Geographic Grid and outline of the Magela Plain showing the points sampled for ¹³⁷Cs measurements. The surface 2 cm was sampled at each of three points for the surface pollen analyses reported in Chapter 3. The appearance of sample points beyond the boundary of the Plain indicates that defining the edge of the Plain is not unambiguous.

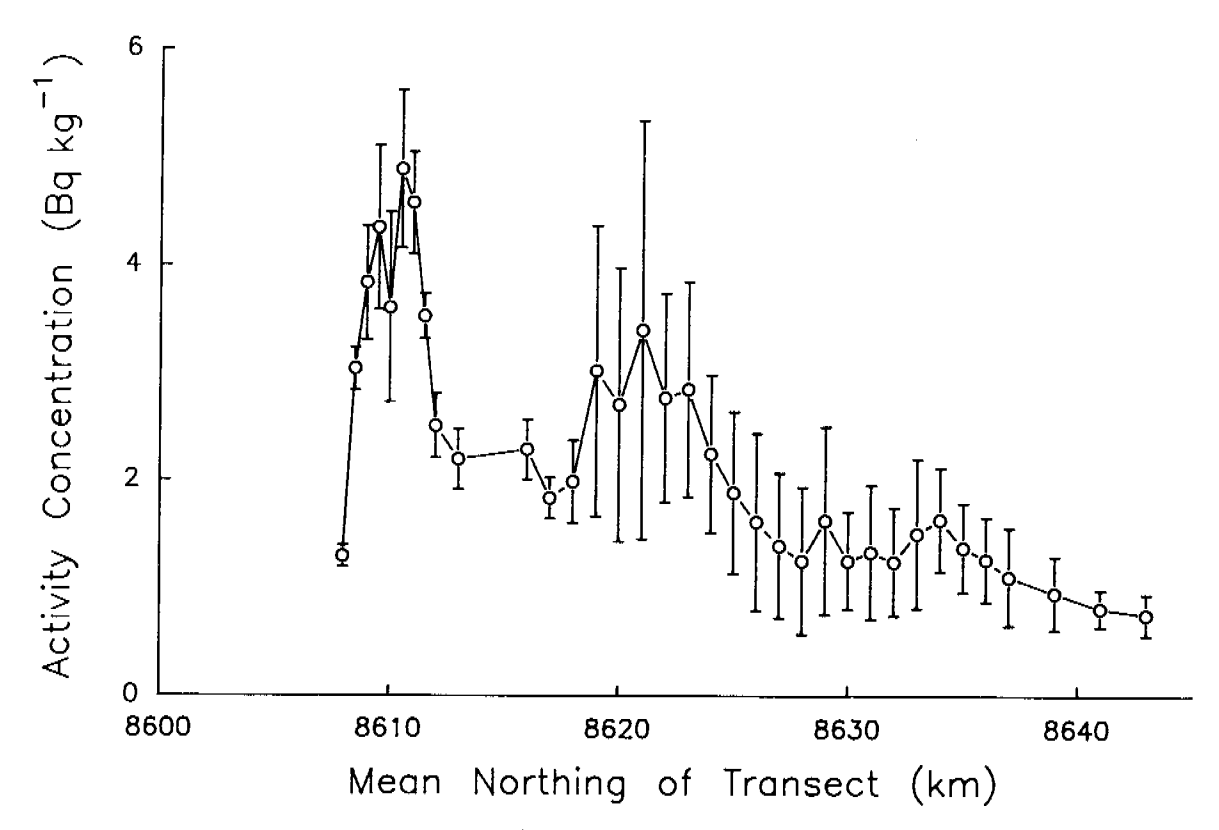


Figure 6.5a Longitudinal profiles of ¹³⁷Cs activity concentration at 0-25 cm

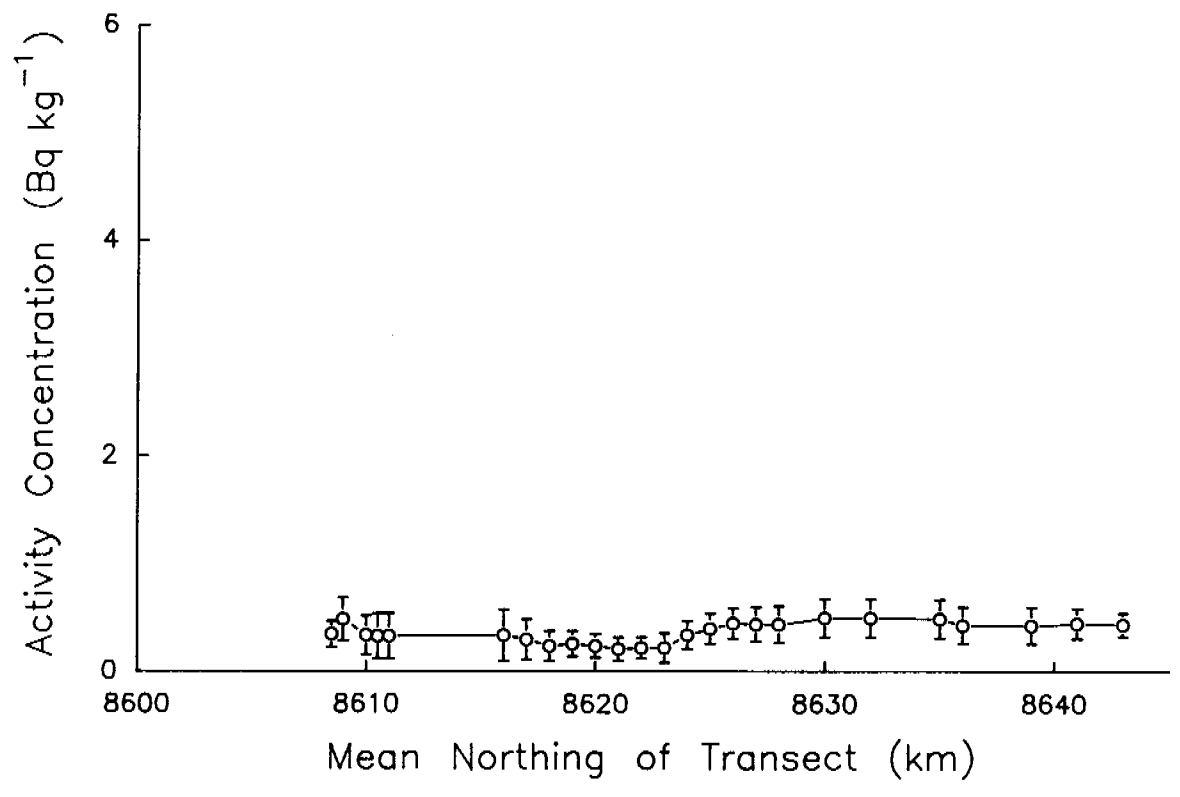


Figure 6.5b Longitudinal profiles of ¹³⁷Cs activity concentration at 25-35 cm. Data from northings have been averaged and these means have been smoothed using a 3 point average.

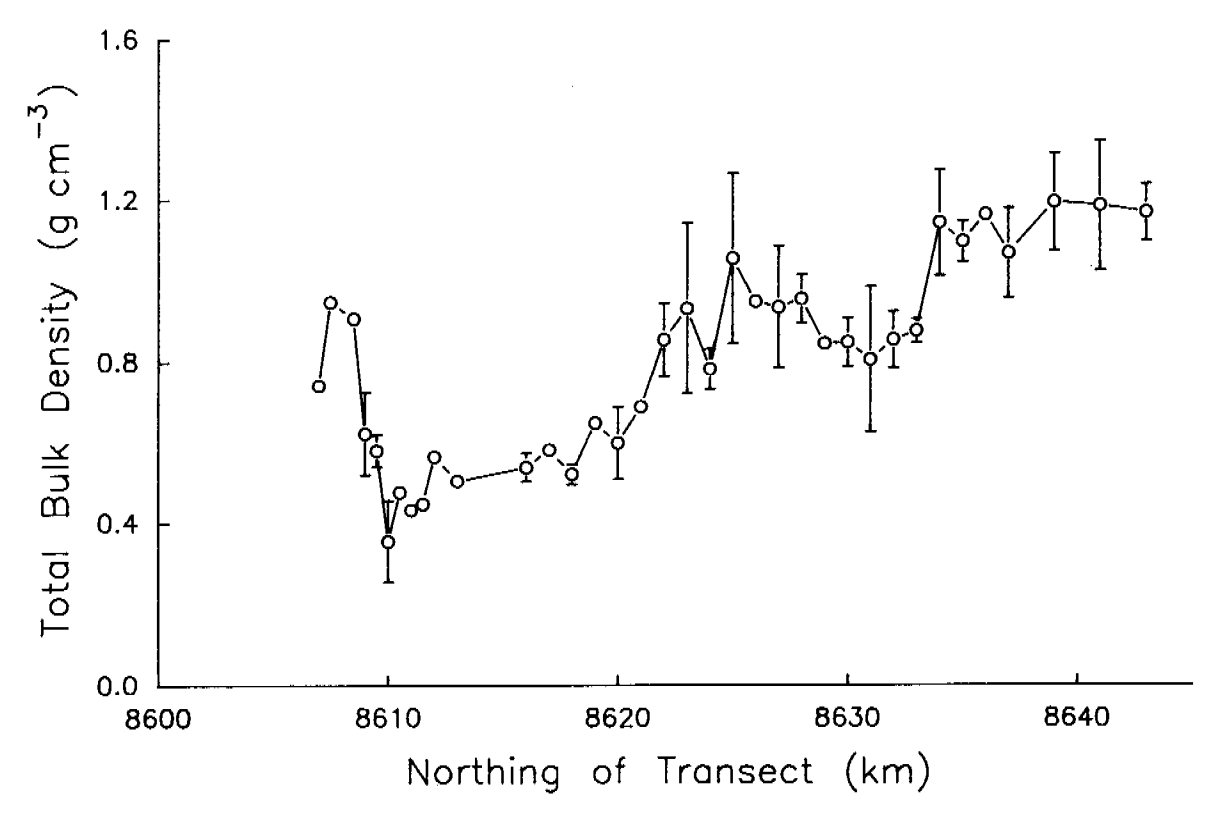


Figure 6.6a Longitudinal profiles of total bulk density between 0 and 25 cm

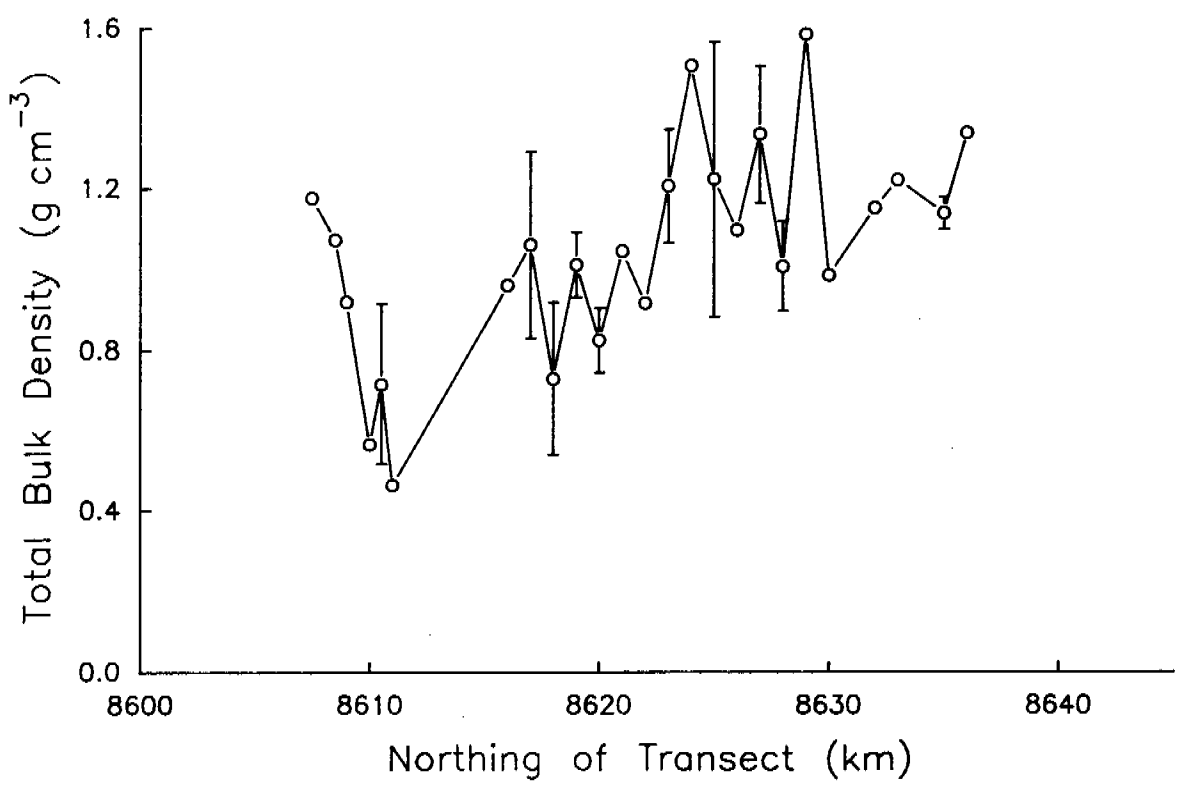


Figure 6.6b Longitudinal profiles of total bulk density between 25-35 cm

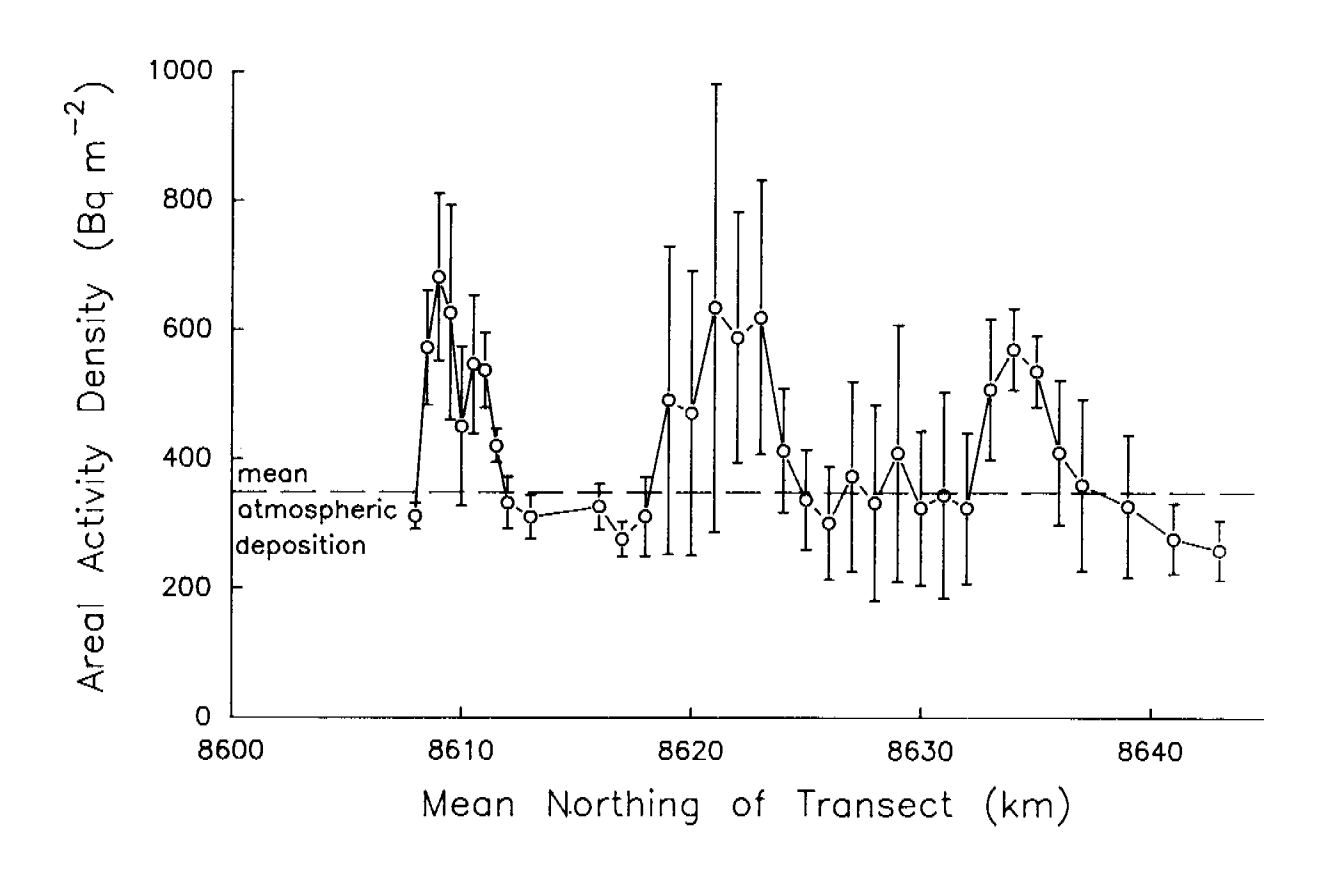


Figure 6.7 Longitudinal profile of 137 Cs areal activity density (Bq/m²) between 0 and 35 cm, averaged as in Fig 6.5. The mean atmospheric deposition figure is also shown.

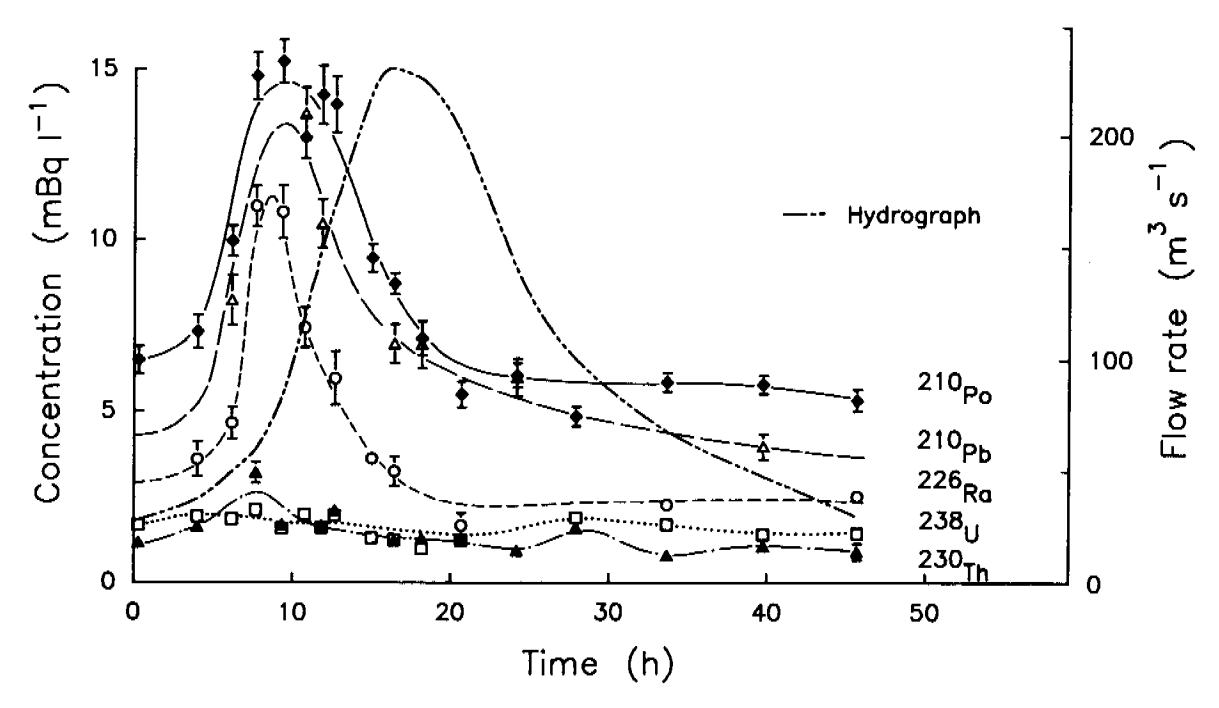


Figure 6.8 Variation of the concentrations of uranium series radionuclides in unfiltered water from Magela Creek at 019 during the flood of 19-21/2/85

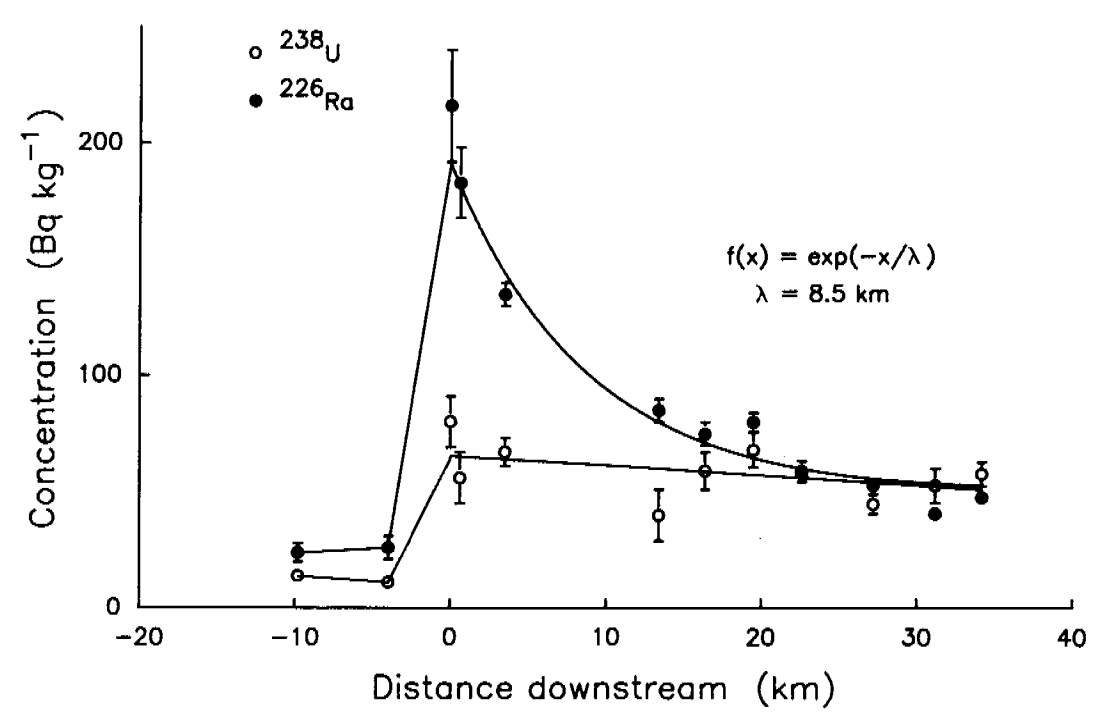


Figure 6.9 Radionuclide concentrations in the sediments of the Magela Creek and Plain as a function of distance downstream and upstream from the arbitrary datum of the sampling grid

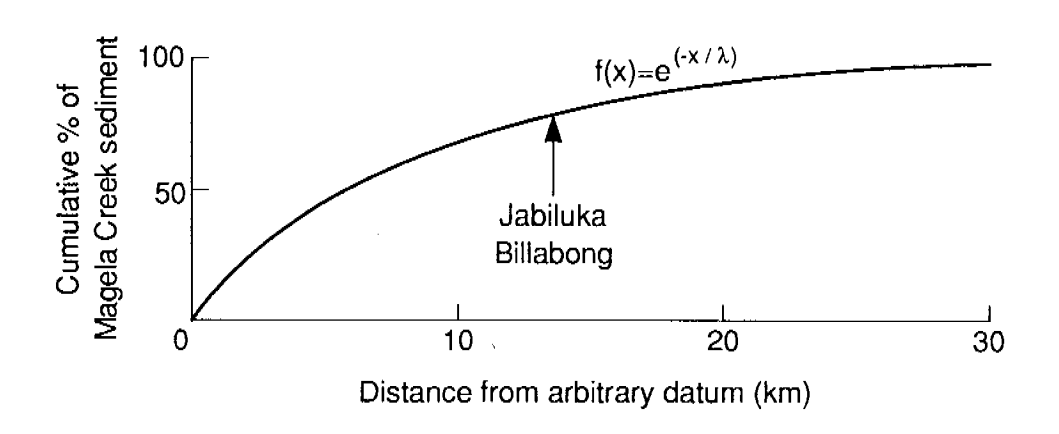


Figure 6.10 Fraction of sediment, derived from Magela Creek, deposited at various distances from the arbitrary datum, derived from f(x) in Figure 6.9

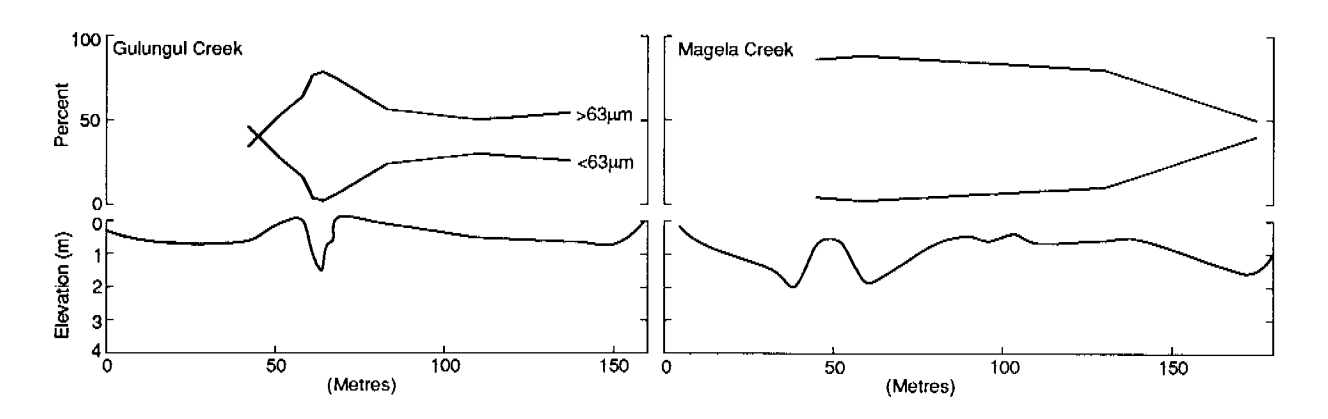


Figure 6.11 Particle size fractions in surface sediments for a cross-section of Gulungul Creek and Magela Creek at Sandy Crossing

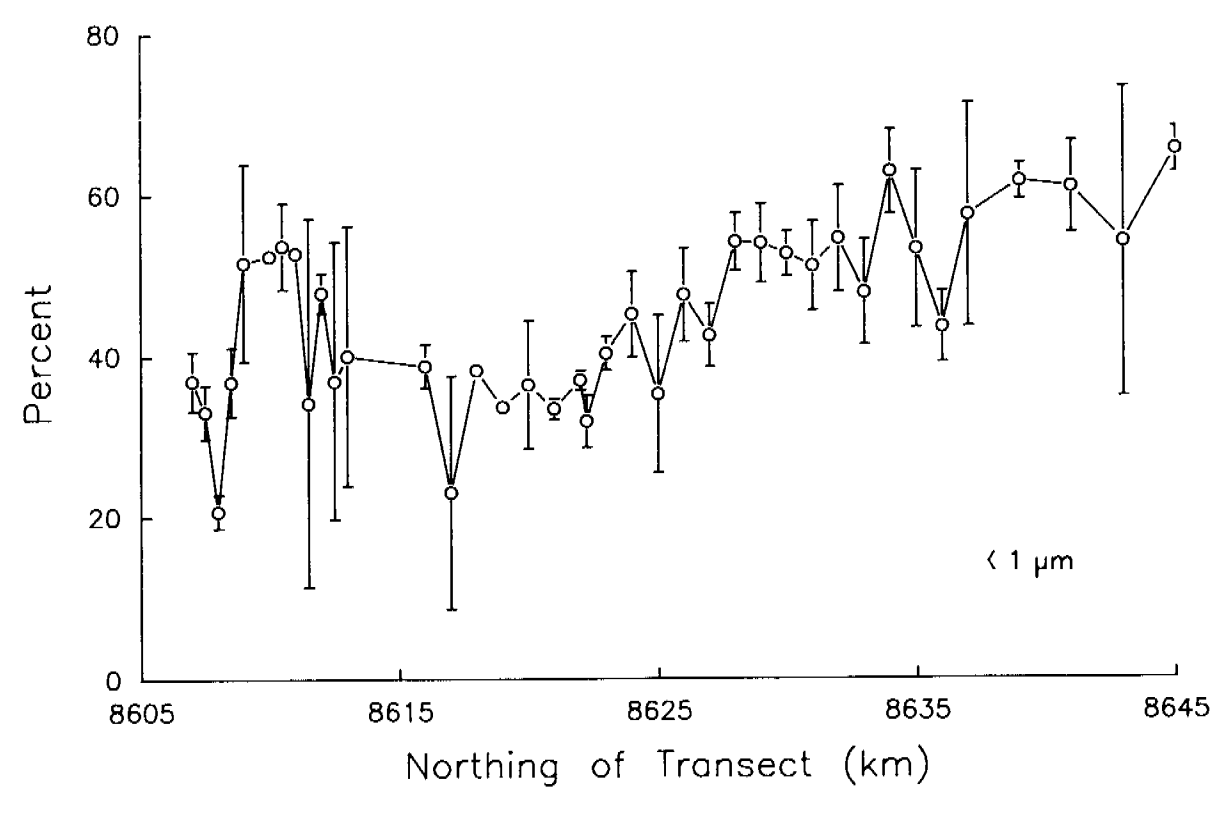


Figure 6.12a The <1 μ m particle size fractions for 0-2 cm averaged for northings on the Plain

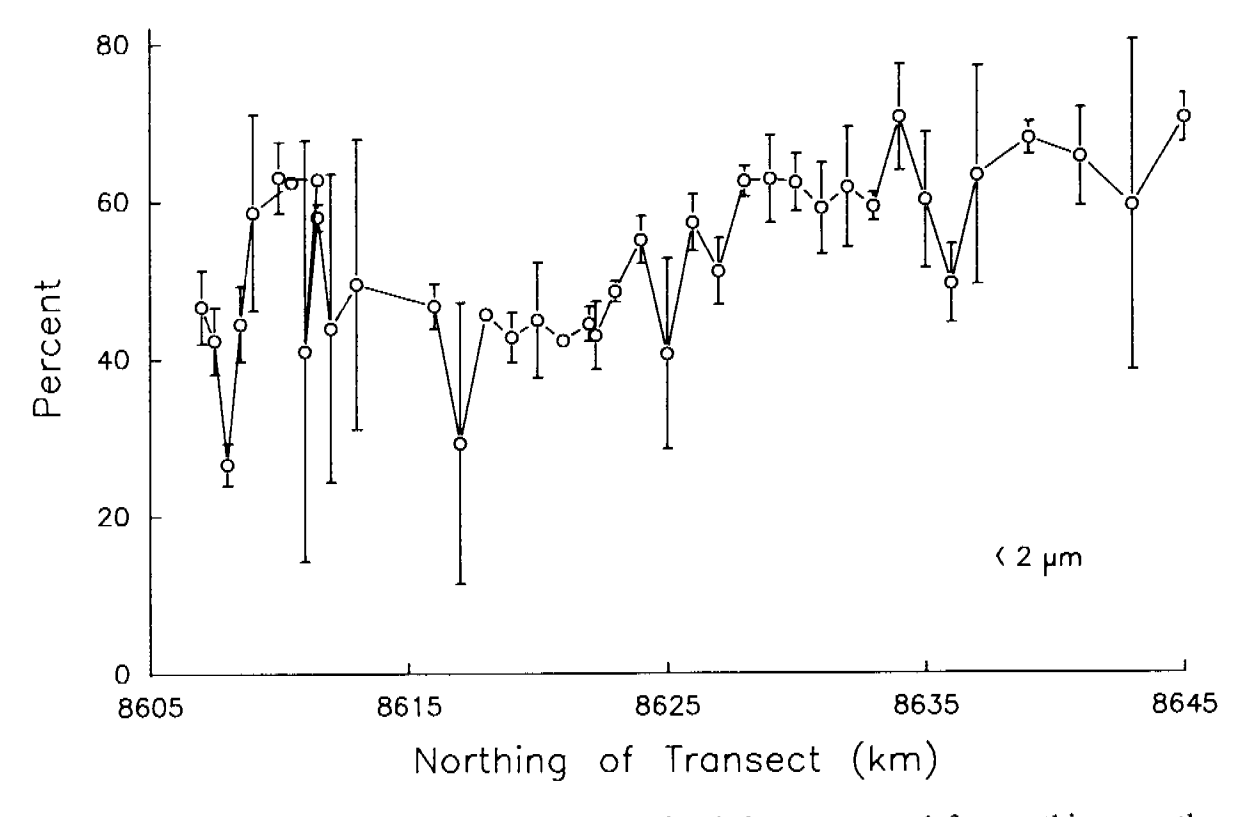


Figure 6.12b The <2 μ m particle size fractions for 0-2 cm averaged for northings on the Plain

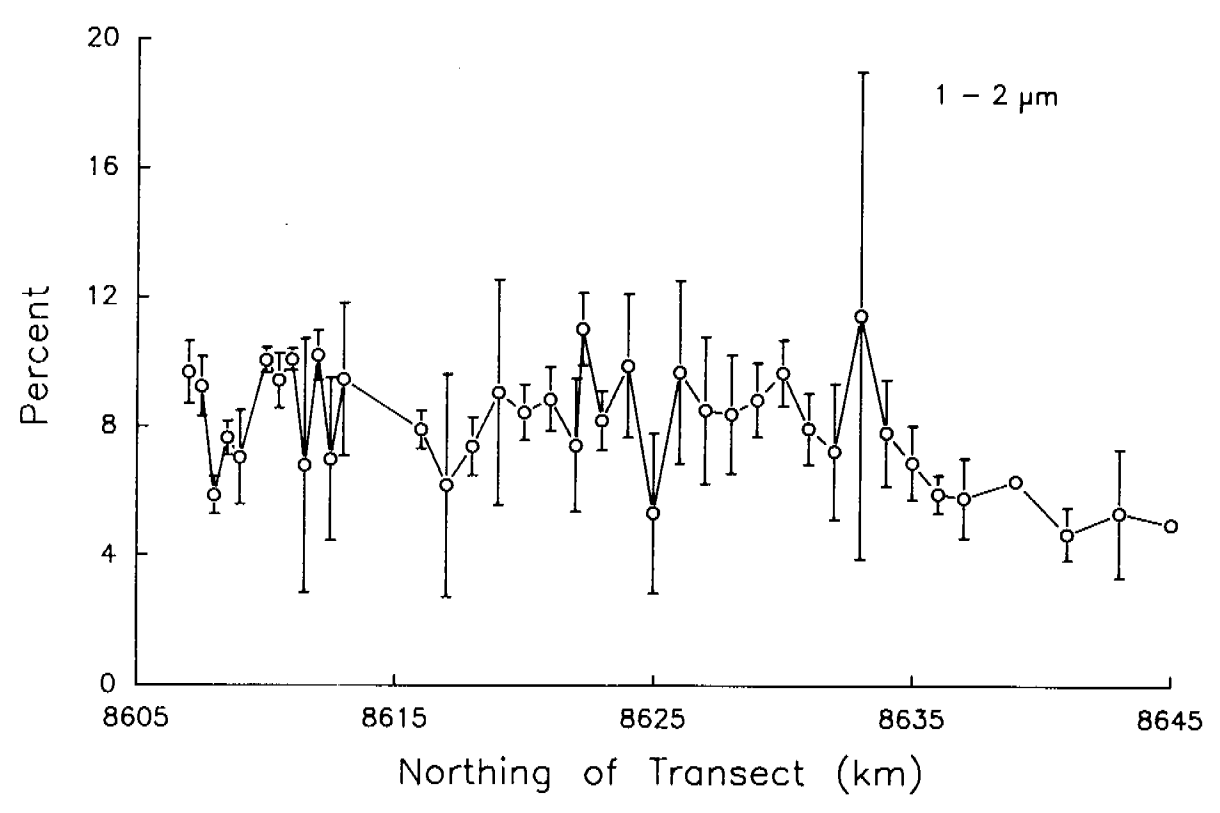


Figure 6.13a The 1-2 μ m particle size fractions for 0-2 cm averaged for northings on the Plain

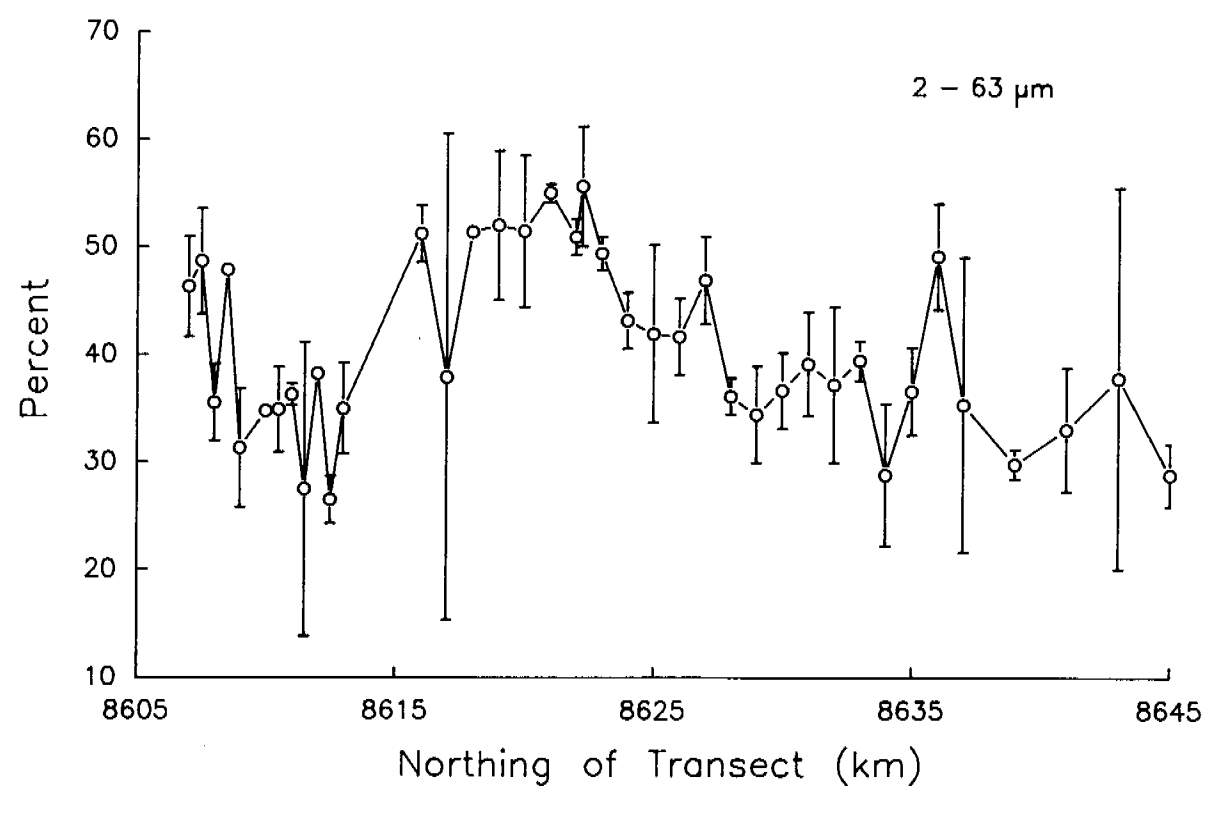


Figure 6.13b The 2-63 μm particle size fractions for 0-2 cm averaged for northings on the Plain

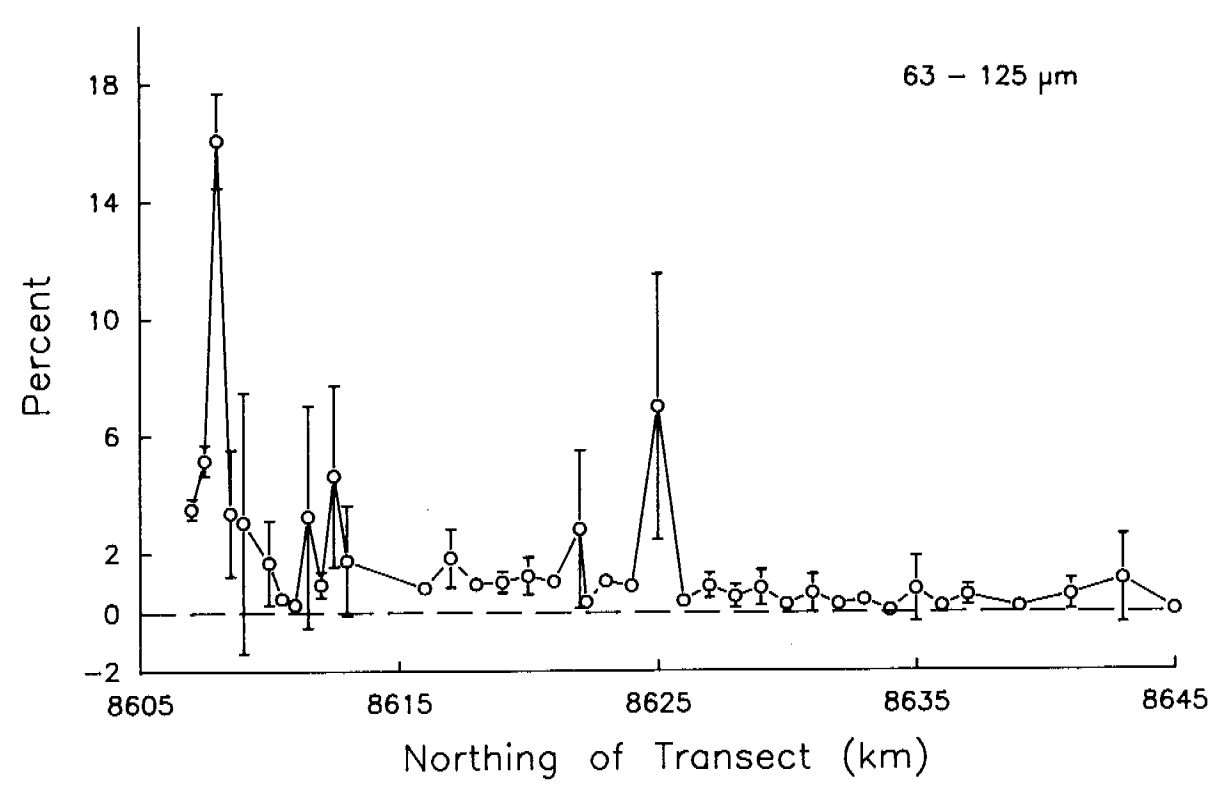


Figure 6.14a The 63-125 μm particle size fractions for 0-2 cm averaged for northings on the Plain

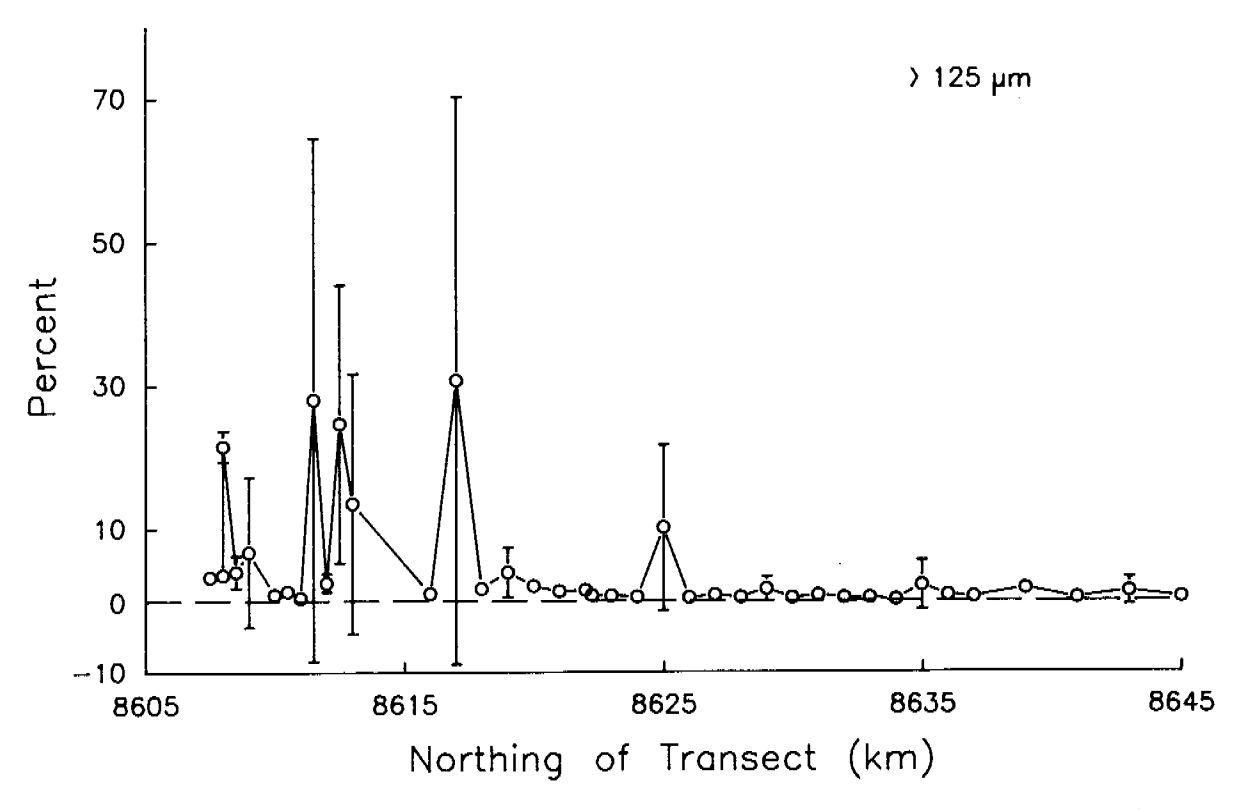


Figure 6.14b The >125 μ m (b) particle size fractions for 0-2 cm averaged for northings on the Plain

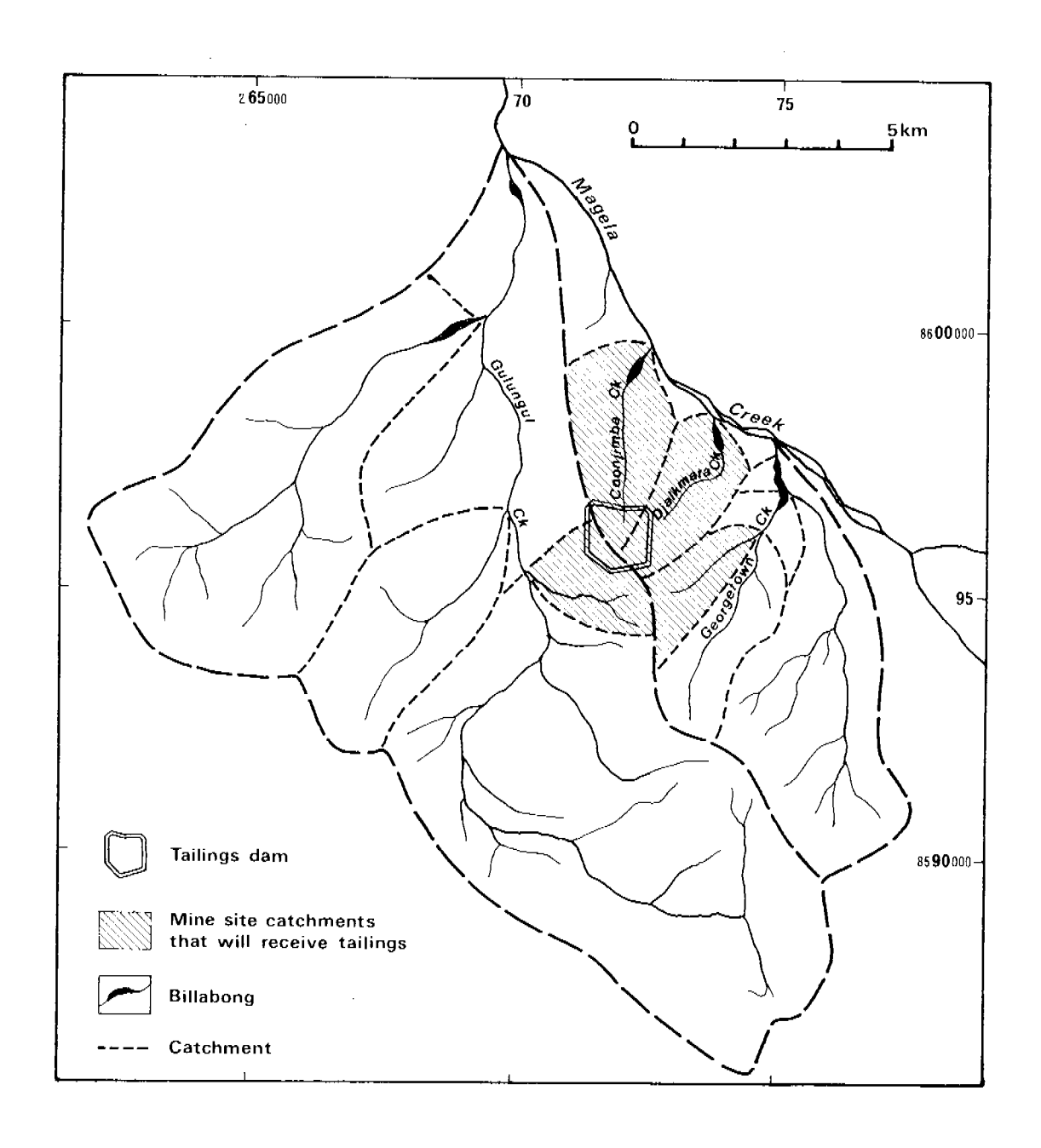


Figure 6.15 Map of the Mine Site tributaries and catchments showing the subcatchments most likely to first receive tailings

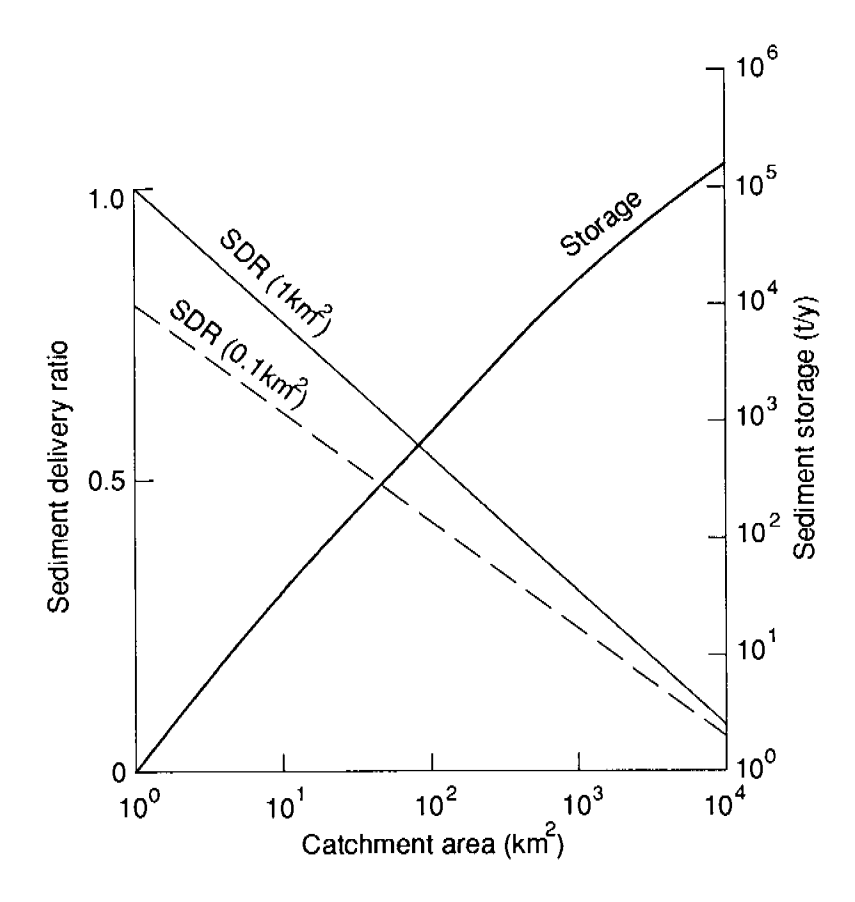


Figure 6.16 Relationships, calculated using simplifying assumptions, showing the dependence upon catchment area of the sediment delivery ratio and sediment storage within catchments

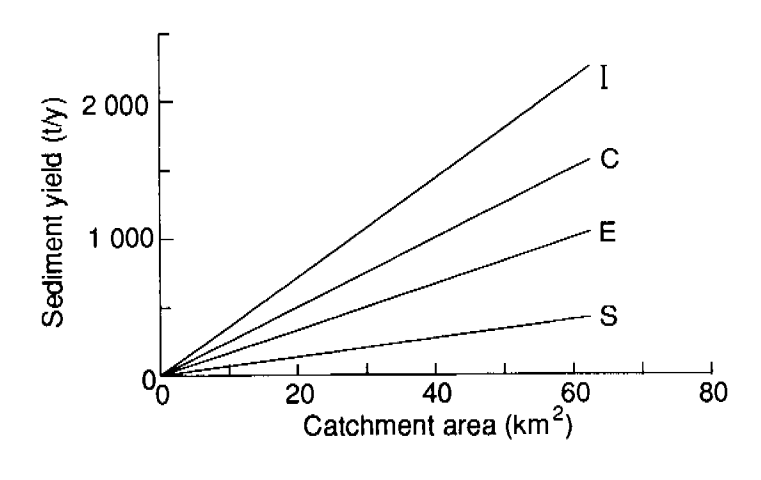


Figure 6.17 Calculated relationships between catchment area and sediment yield (I), channel erosion (C), total slope erosion (E) and slope storage (S) for the Mine Site catchments

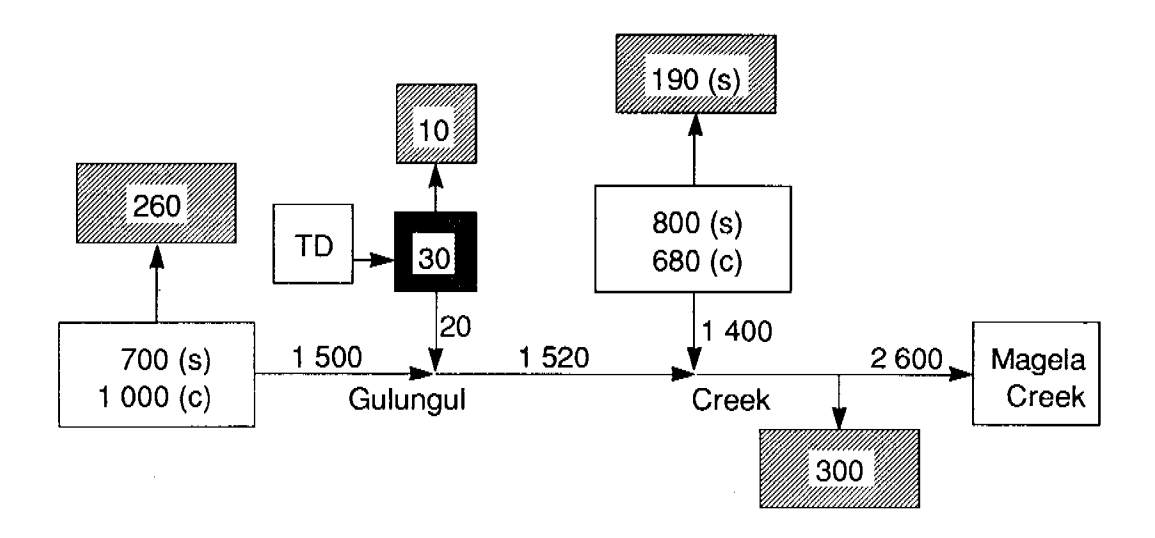


Figure 6.18 Sediment budget, depicted as a box model for the Gulungul Creek Catchment. Figures in the boxes refer to total erosion, (t y⁻¹) of slopes (S) and channels (C), and figures on the arrowed lines are fluxes (t y⁻¹) of sediment. The cross-hatched boxes are storages. The darkest box is the 1.6 km² catchment that will first receive tailings. TD is the tailings dam. The 20 t y⁻¹ from TD is a flux to Gulungul Creek via the unnamed 1.6 km² subcatchment.

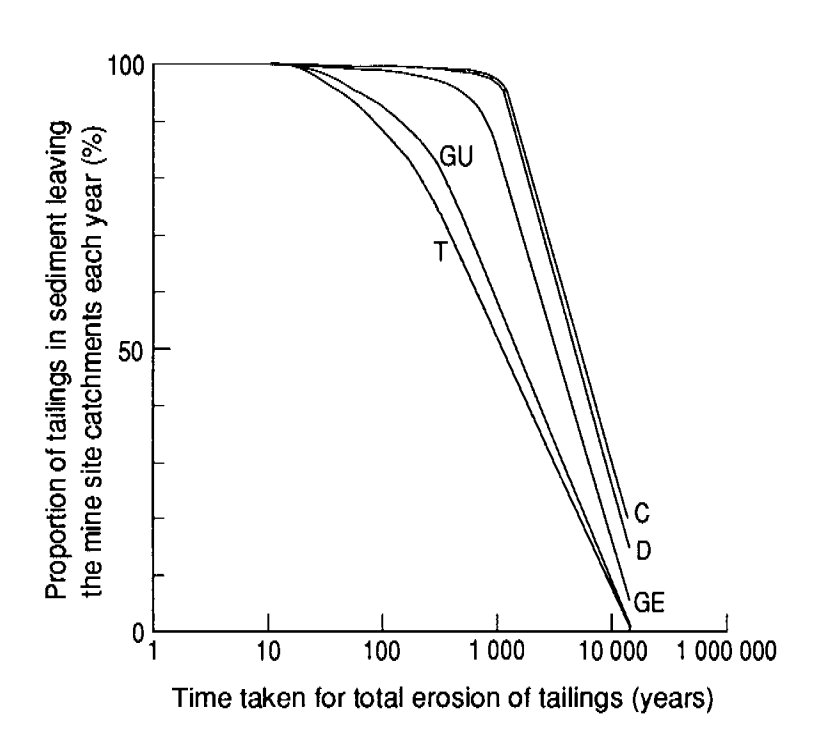


Figure 6.19 Calculated curves for Coonjimba Creek (C), Djalkmarra Creek (D), Georgetown Creek (GE), Gulungul Creek (GU) and the total Mine Site tributaries (T), showing the relationship between the time taken for total erosion of the tailings and the proportion of tailings that will occur in sediment leaving the Mine Site streams

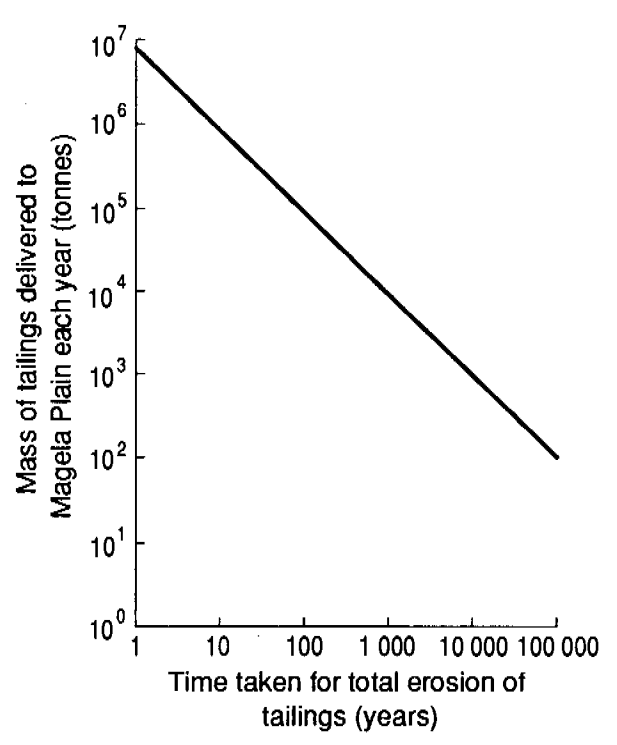


Figure 6.20 Calculated curve showing the variation of the mass of tailings delivered to the Magela Plain each year as the total erosion time increases

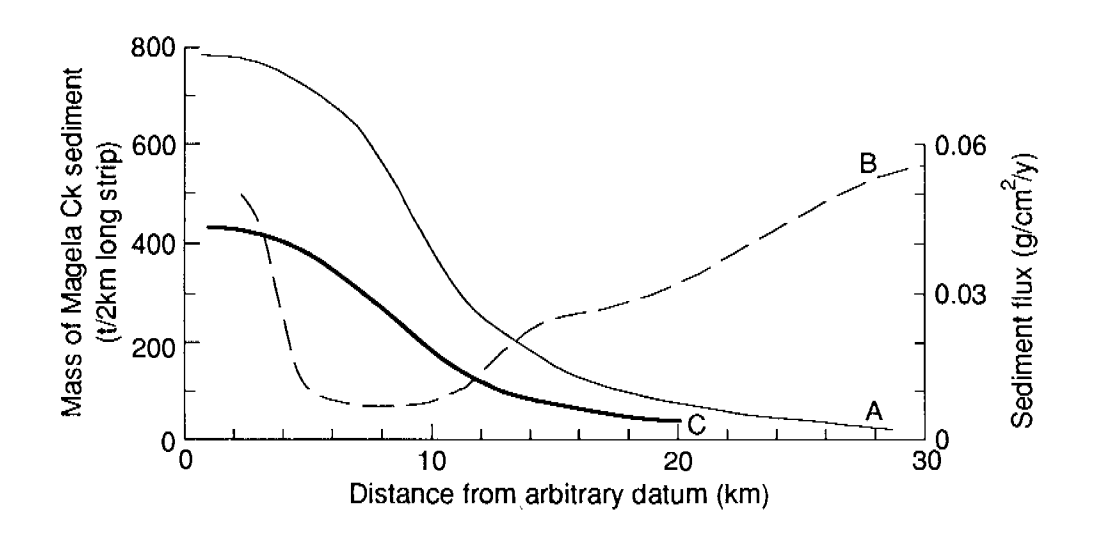


Figure 6.21 Mass (t/2 km long strip of Plain) of Magela Creek sediment (A), the minerogenic sediment flux (g/cm²/y) on the Plain (B), and flux of Magela Creek sediment to the Plain (g/cm²/y) (C), at various distances from the arbitrary datum at Mudginberri Billabong

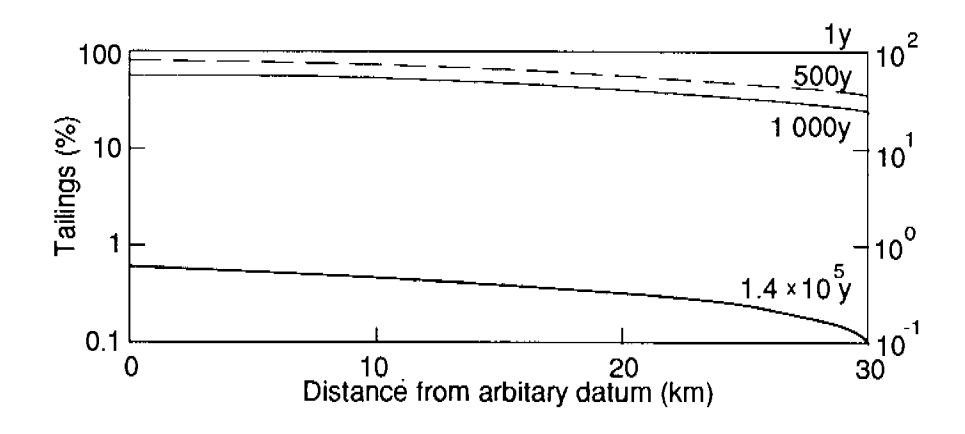


Figure 6.22 Calculated curves showing the proportion of tailings in surface Plain sediments at various distances along the Plain for a range of total erosion times

CHAPTER 7. CHEMICAL TRANSFORMATIONS OF METALS IN MIXTURES OF TAILINGS AND SOIL MATERIALS FROM THE MAGELA PLAIN

7.1 INTRODUCTION

In the last chapter methods were developed to predict the patterns of tailings (and other sediment) dispersal on the Plain, drawing attention to the conditions under which the results are likely to be valid. If the tailings impoundment has erosion rates similar to those of the natural slopes of the ARR, there would be about 1% of tailings in the surface sediments of the Magela Plain during the next few thousand years when the landscape is much as it is today. More precisely, the tailings would constitute, on average over the Upstream Basin and Mudginberri Corridor, 0.4% of the surface sediments.

This proportion and one ten times greater have been chosen as plausible conditions under which to investigate the reactions of tailings when mixed with the various soil/sediment materials of the Magela Plain. A series of experiments is reported in this chapter, designed to document the mobility of the heavy metals (Cu, Fe, Mn, Pb, U and Zn) and ²²⁶Ra in the tailings under conditions that they will encounter on the Plain.

7.2 CHEMICAL PROPERTIES OF RANGER URANIUM MINE TAILINGS

The aim of this section is to characterise the chemistry of the tailings. A 20 kg sample of tailings was collected in 1986 from the Ranger Uranium Mine tailings dam. The sample was air-dried and thoroughly mixed. A subsample of about 1 kg was separated by repeated quartering of the large sample and then gently crushed to break down aggregates. The subsample was thoroughly mixed before analysis or use in experiments. At this time the mine used pyrolusite as an oxidant during U extraction and the tailings were neutralised with lime before discharge.

Two samples of tailings were analysed for total Cu, Fe, Mn, Pb, U and Zn by X-ray fluorescence (Norrish & Chappell 1977). A sequential extraction procedure was also applied to five replicate subsamples of the tailings to obtain exchangeable, reducible and oxidisable fractions of the metals. The differences between the sums of the fractions and total concentrations are referred to as 'residual' forms, that is, metals in crystal lattices of clays and more resistant minerals that are not extracted by the reagents of the selective extraction method. The tailings were also analysed for total ²²⁶Ra.

In addition, the tailings were examined by scanning electron microscopy-electron dispersive X-ray analysis (SEM-EDX). About 25 mg of tailings were set in epoxy resin and polished to expose sections through tailings particles. The polished surfaces were then sputter-coated with gold and examined in a Cambridge Instruments Geoscan Mk IV SEM equipped with a Link Systems EDX analyser. Initial inspections showed that some particles, or parts of particles, were more electron-dense than the majority of particles. The distinction between low and high electron density was clearest in back scattered electron mode, which accentuates the contrast between minerals with high average atomic number (base metal oxides and sulfides) and those of low average atomic number (aluminosilicates and quartz). X-ray diffraction (XRD) results for this sample, and other samples, of Ranger tailings showed that the low electron-dense particles consist of quartz, chlorite, muscovite and gypsum (A.R. Milnes, pers. comm.).

All electron-dense areas in each of four 204 \times 157 μm fields of view were examined because they were likely to be enriched in the elements of interest to the study.

SEM-EDX RESULTS

An example of an SEM micrograph of the tailings is shown in Fig. 7.1. Most of the particles are angular, low electron-dense fragments of ore rocks. Many of the larger particles (> 20 μ m) appear uniform, although some are aggregates of smaller particles with low-electron density. Such particles consist of quartz, chlorite and muscovite.

The electron-dense particles occur as inclusions in lower density fragments as well as individual grains. A summary of the observations and the X-ray analytical data for 65 electron-dense regions from the four fields of view examined in detail is presented in Table 7.1. The particles are grouped into classes corresponding with Pb minerals, other sulfides, U minerals, sulfates, iron oxides, and resistates (rutile and zircon).

Galena is readily identified in 3 particles by the dominance of Pb and S in 1:1 ratio in the EDX spectra. It occurs as inclusions in larger rock fragments. Another two particles rich in Pb also contain U and Cu suggesting carnotite. However, U is disproportionately low in relation to Pb in the X-ray analysis. This could be caused by the extraction of U during milling. A single particle is rich in Pb and P, with an approximate formula of $Pb_{2.7} P_{0.7} S_{0.2} Cl_{0.2} Ca_{0.3}$. It is possibly kampylite if the spectrum is affected by an observed adjacent gypsum particle.

Two particles of primary pyrite are readily identified by their spectra. Three particles of chalcopyrite also occur. Chalcopyrite occurs as one aggregated particle and as angular inclusions in mica. Four particles rich in U are observed in the form of fine inclusions. Two of the particles also contain Pb and Nd, but no anion can be identified. These are probably uranitites derived from unweathered ore rocks which survived the milling process. Two inclusions appear to be uranium phosphates which occur in the weathered zones of the ore bodies of the Alligator Rivers Region (Snelling 1980).

Two small (< $2 \mu m$) particles of gypsum were identified. In addition, a Pb, Sr, Ba sulfate occurs as three particles. There appears to be no mixing of Pb, Sr or Ba sulfates with gypsum. This suggests that gypsum was formed in the absence of dissolved Pb, Sr and Ba during the neutralisation of the tailings, whereas the latter elements were derived from weathered ore rocks.

A total of 21 of the electron-dense particles consists of iron oxides as inclusions and angular particles. Some of the iron oxides contain Mn, Cu, U, P and Pb. These iron oxides are most probably derived from the ore rocks since any formed during processing, particularly during neutralisation, would not occur as inclusions or angular particles. Iron oxides may have formed during processing but would be too small to identify by the SEM-EDX technique.

Twenty-one of the electron dense particles are rich in Ti and are probably rutile. They consist of angular particles and inclusions and are derived from the ore rocks. Three zircon inclusions were also observed.

CHEMICAL ANALYSES

The total concentrations of heavy metals in the tailings sample are shown in Table 7.2. The values obtained are similar to those in tailings samples from several parts of the tailings dam (A.R. Milnes, unpublished data) which suggests that the sample used for this study was not atypical.

The distribution of the heavy metals according to the sequential extraction procedure is also shown in Table 7.2. Exchangeable and water soluble fractions (M Mg(NO)₃-extractable) are only small proportions of the totals, except for Mn which had 21.3% of the total in this fraction. Cu occurred in both the reducible and oxidisable fractions. The former may

indicate that Cu was associated with oxides of iron and manganese, whereas the latter corresponds with the presence of chalcopyrite and other readily oxidisable Cu-bearing minerals. The organic matter content of the tailings is negligible so that the oxidisable fraction can be entirely ascribed to inorganic sources such as sulfides. Iron occurs predominantly as non-extractable (residual) forms, probably as primary minerals derived from the ore rocks. However, 9.4% of total Fe is reducible suggesting the presence of Fe oxides and hydroxyoxides. The former may be derived from the ore rocks, or weathered ore rocks, whereas the latter may have formed during processing. In any case it would be expected that the Fe (hyroxy)oxides would contain heavy metals within their structures, and would be liberated on reductive dissolution. Similarly, the reducible fraction of Mn represents Mn (III,IV) oxides which form on neutralisation of the tailings during processing, and they may also contain other heavy metals. The predominant fraction of Pb is the reducible fraction suggesting that Pb was incorporated with Fe and Mn oxides during processing. The residual fraction of Pb would include Pb SO₄ which would be expected to form during processing and was identified by SEM-EDX.

The residual fraction represents 77% of total U, a result of the milling procedure removing U from more readily extractable forms. Zn was predominantly in the oxidisable fraction. In contrast to Cu and Fe, there was no indication from the SEM-EDX analyses to identify the mineralogic forms of Zn.

Duplicate analyses of tailings for total ²²⁶Ra gave 33.8 and 34.8 Bq g⁻¹ and the mean of 6 replicate analyses of exchangeable ²²⁶Ra gave a mean of 3.9 Bq g⁻¹ with a standard deviation of 0.58 Bq g⁻¹. Therefore 11% of the total radium is in the exchangeable form and can be considered readily bioavailable. This result provides a reference value by which changes in ²²⁶Ra extractability can be compared after the tailings have been reacted with soils.

7.3 CHEMICAL TRANSFORMATIONS OF METALS APPLIED AS TAILINGS UNDER UNSATURATED CONDITIONS

This experiment was designed to determine the mobility of metals in tailings mixed with very acidic soils and sediments of the Magela Plain. Tailings were applied to four soil and sediment types, and incubated for up to four months under moist, aerobic conditions. The distribution of metals in the exchangeable, reducible, oxidisable and residual forms determined.

Four materials were selected. Three samples were taken from the three major horizons (defined in Chapter 5) of MV Pit A (Fig. 4.3) near Mine Valley Billabong: the surface (0-25 cm) horizon (KS), the jarositic (85-97 cm) horizon (Jaro), and the unoxidised pyritic substratum (150-180 cm, MVPA). These samples represent the horizons found in soils of the Magela Plain: respectively, the aluminous, organic and diatomaceous surface; the extremely acidified jarositic horizon; and pyritic layer which underlies most of the Plain. The fourth sample came from the surface 0-10 cm layer taken from site MC8 on traverse 2 in the Mudginberri Corridor (Fig. 4.2), a site likely to receive mine wastes. Samples KS and MC8 are both from the Dark Brown/Black Clay. Bulk samples were collected in 1986. Soils KS, Jaro and MC8 were air-dried and crushed to pass a 2 mm sieve. The pyritic soil, MVPA, was oven-dried at 80°C on the day of sampling to minimise oxidation. After oven-drying it was also crushed to pass a 2 mm sieve.

Some properties of the soils are shown in Table 7.3. All the soils are extremely acid. Only soils Jaro and MVPA have been directly affected by pyrite oxidation but the other soils also contain water soluble and adsorbed sulfate (EDTA-extractable). The low pH and the presence of sulfate and jarosite indicate that some pyrite has been oxidised in soil MVPA during sample preparation. The clay minerals of Jaro and MVPA are similar. The jarositic horizon developed from the pyritic substratum, but has been altered by pyrite oxidation.

The clay minerals in the surface soils (KS and MC8) are dominated by kaolinite to a greater degree than soils Jaro and MVPA. Alunite $[KAl_3(SO_4)_2(OH)_6]$, the Al analogue of jarosite, is present in soil KS and, since a high proportion of the total free Al (citrate-dithionite-bicarbonate extractable) was also extracted by alkaline pyrophosphate, a major part of the free Al occurs in combination with organic matter.

Duplicate sets of the treatments of the full factorial of four soils, 5 times of reaction (0, 1, 2, 3) and 4 months), 3 tailings proportions (0, 0.4) and 4%) were prepared. The tailings-soil mixtures were prepared by vigorously shaking the weight of air-dry soil equivalent to 400 g on an oven-dry basis with air-dry tailings in large polythene bags. The tailings application rate of 0.4% was calculated from the results of Chapter 6, as seen earlier. The proportion of 4% was included to simulate a more rapid total erosion rate of 5×10^4 years. In choosing these two conservative proportions, it was assumed that catastrophic releases of tailings are of very low probability.

The air-dry weights equivalent to 50 g of oven-dry material were placed in glass jars and distilled water added until the water contents were raised to the equivalent of -200 cm water tension. The jars were loosely capped and placed in a cupboard in a constant temperature room operated at 25°C. After 0, 1, 2, 3 and 4 months of reaction the soils were removed from the jars, dried at 40°C, re-mixed, and extracted for the metal fractions. The total metal concentrations and total ²²⁶Ra were determined for the first sampling time only. Because of analytical constraints, exchangeable ²²⁶Ra was determined in the 4% tailings treatment at the final sampling time only, and the fractionation of U was done on all samples of the first and last sampling times only.

The effects of adding tailings on the total metal concentrations of the soils are shown in Table 7.4. As may be expected, the effect of tailings on total concentrations depends on the differences in concentrations between the tailings and the soils (Table 7.5). Cu concentrations are 9.2 to 24 times greater in the tailings than in the soils. The addition of 4% tailings increases total Cu concentrations significantly (p> 0.001) and the effects are similar in each soil. The addition of 0.4% tailings has no detectable effect on total Cu in any soil. Similar results were obtained with U which had up to 50 fold greater concentrations in the tailings than in the soils. The concentrations of Pb were increased (p> 0.001) by both tailings proportions. Total Mn was increased by the addition of 4% tailings, whereas total Fe was increased by both tailings rates.

Even with the addition of 4% tailings, the levels of total Cu, Zn, Mn and U do not exceed the ranges in concentrations of these elements in soils of the Magela area reported by Findlater and White (1984). The concentrations of total Pb in soils amended with 4% tailings are four fold the average of Findlater and White's for 182 soils of the Magela Plain. Pb shows the largest relative increase in concentration as may be expected from the relative concentration of Pb in the tailings and soils (Table 7.5). Of these elements, Pb is most likely to increase in concentration should tailings be deposited on the Plain. However, much greater percentage increases in total concentrations would occur for the radioactive daughter products of uranium.

Marked increases in total concentrations are often considered to indicate significant metal pollution. However, increases in water soluble or exchangeable fractions of metals, which are readily bioavailable and exchangeable with major cations, have greater environmental importance, and can occur with no changes in the total concentration (Calmano & Forstner 1983). The following results for the exchangeable, reducible and oxidisable fractions of metals should permit a more sensitive evaluation of the pollution potential of tailings in these soils.

The main effects of tailings additions to the soils on the fractions of each metal are shown in Table 7.6, and the main effects of time of reaction are shown in Table 7.7.

COPPER

The addition of 4% tailings increases each fraction of Cu, whereas 0.4% has no significant effects. The exchangeable and oxidisable fractions of Cu increase with time of reaction but there is no corresponding decrease in the reducible fraction. Cu was mobilised from residual forms to more readily extractable forms. Figure 7.2 summarises the changes in Cu fractions for each soil and at each reaction time. It shows that before reaction (time 0) the addition of 4% tailings increased the proportion of Cu in the oxidisable form. This result reflects the high proportion of Cu in this form in the tailings, some of which was shown to be in the form of chalcopyrite. There was no detectable exchangeable Cu and little change in the Cu fractions with time in soils KS and MC8. The results for soils Jaro and MVPA show some exchangeable Cu, and in soil MVPA, exchangeable Cu increased with time of reaction. The increases in exchangeable Cu with time in soil MVPA occurred irrespective of tailings additions, and are related to the oxidation of pyrite in this soil, as discussed below.

IRON

The addition of 4% tailings decreased exchangeable Fe and increased the reducible fraction (Table 7.6). Decreases in exchangeable Fe are probably caused by the slight neutralising capacity of the tailings since 4% tailings slightly increased the pH of the most acidic soils (Jaro and MVPA, Fig. 7.3).

Marked increases in exchangeable Fe and corresponding decreases in oxidisable Fe occurred with time of reaction (Table 7.7). The main effects were due to changes in soil MVPA and there were no changes in the other soils (Fig. 7.4). In soil MVPA, marked decreases in oxidisable Fe corresponded with the oxidation of pyrite, and the production of Fe²⁺ during the aerobic incubation (Fig. 7.5). The Fe²⁺ remained in water soluble and exchangeable forms and did not oxidise further to Fe(III) oxides which have contributed to the reducible fraction. The results for Fe were dominated by pyrite oxidation and there was no evidence for any effects of tailings on the transformation of Fe.

MANGANESE

The addition of 0.4 and 4% tailings significantly increased exchangeable Mn, and 4% tailings increases reducible Mn (Table 7.6). Exchangeable and reducible Mn increases with time of reaction whereas oxidisable Mn decreases (Table 7.7). The significant effects of reaction time were due to large increases in soil MVPA (Fig. 7.6); there was little change to the fractions of Mn in the other soils. Marked increases in exchangeable Mn at the expense of oxidisable Mn in soil MVPA occurred irrespective of tailings additions and were probably caused by the oxidation of pyrite. The source of the Mn could be inclusions of Mn in the pyrite, or the dissolution of Mn oxides, or other Mn bearing minerals under the extremely acid conditions. SEM-EDX analyses of individual framboids of pyrite showed no detectable Mn, and it is most likely that Mn was liberated indirectly by acidic dissolution. The similar results for all the tailings proportions suggest that the mobilisation of Mn was similar from the tailings and the soil.

LEAD

The addition of 4% tailings significantly increases the concentrations of exchangeable, oxidisable and reducible Pb (Table 7.6). The concentrations of exchangeable and reducible fractions decreases with time (Table 7.7), and there are overall increases in the residual fraction after 4 months of reaction (Fig. 7.7). This result indicates that Pb added as tailings is immobilised from the exchangeable and residual forms to the less bioavailable residual forms. In view of the abundance of water soluble sulfate in these soils, this could be due to the formation of PbSO₄.

URANIUM

The addition of 4% tailings increases the concentration of all the extractable forms of U (Table 7.6), but concentrations decrease during 4 months of reaction (Table 7.7). In the non-pyritic soils there are large increases in the residual fraction. In soil MVPA, there are large increases in the proportion of exchangeable U as well as in the residual fraction, and marked decreases in the oxidisable fraction (Fig. 7.8). For all the soils it was shown that U was converted from oxidisable to residual forms and this occurred irrespective of tailings additions. In the non-pyritic soils, this may be related to the oxidation of organic matter. In soil MVPA the oxidation of pyrite may also have mobilised U from inorganic sources and resulted in a large proportion (30%) of the U remaining in an exchangeable form.

ZINC

The addition of tailings has no significant effects on any Zn fraction (Table 7.6). There are decreases in exchangeable Zn and decreases in reducible and oxidisable Zn with time of reaction (Table 7.7). The increases in exchangeable Zn with time differed markedly between the soils (interaction significant, p> 0.001), with no changes in soils KS and MC8, small decreases in soil Jaro and increases in soil MVPA (Fig. 7.9). The sources of the increases in exchangeable Zn in soil MVPA were from both the reducible and oxidisable fractions, and were probably caused by acidic dissolution during pyrite oxidation.

RADIUM-226

Total and exchangeable ²²⁶Ra were determined in the 0 and 4% tailings treatments at 0 and 4 months of reaction. The addition of tailings to the soils increased total ²²⁶Ra in approximate proportion to the dilution expected from the values in the tailings (mean 34 Bq g⁻¹) and the unamended soils (Table 7.8). There was no detectable (<0.02 Bq g⁻¹) exchangeable ²²⁶Ra in the unamended soils. The addition of 4% tailings resulted in some detectable exchangeable ²²⁶Ra in the soils, and the levels were considerably greater in soil MC8 than in the other soils. In the tailings sample, exchangeable ²²⁶Ra accounted for 11% of the total. After reaction with soil MC8 the exchangeable ²²⁶Ra attributable to the tailings was 44% of the total. The corresponding value for the other soils ranged from 2 to 7% of the total. ²²⁶Ra was therefore mobilised to the exchangeable form in soil MC8 but was immobilised in the other soils.

7.4 CHEMICAL TRANSFORMATIONS OF METALS APPLIED AS TAILINGS TO SOILS UNDERGOING SATURATION AND DRYING

The previous section examined the transformations of metals applied as tailings to soils under moist, aerobic conditions. Most of the Plain's surface soils undergo annual cycles of reduction during flooding and oxidation during drying. This section presents an experiment aimed to determine the effects of adding tailings on the transformations of metals in soils undergoing a cycle of flooding and drying.

Three soils were selected for this experiment: KS, Jaro and MC8. The air-dry soil equivalent to 500 g on an air-dry basis was thoroughly mixed with tailings at a rate of 4%. The oven-dry equivalents of 100 g of unamended and tailings-amended soil were placed in plastic containers. Two replicates of the factorial combinations of 3 soils and 2 water regimes (saturated, distilled water added to give 1 cm of flood water, and unsaturated, -200 cm water tension) were prepared. The containers were covered with a polythene sheet and incubated for 2 months at 25°C. At the end of the reaction period the free water was gently poured off the saturated soils and Eh and pH measurements made immediately. The Eh was measured by insertion of a Pt electrode to the bottom of the soil and a calomel electrode in the surface. The e.m.f. (Pt-calomel) was measured with a pH meter and the readings converted to Eh by the addition of 245 mV. The pH was measured by inserting a combined

electrode to a depth of 3 cm. The soils were then dried at 40°C and analysed for the total element concentrations, and their fractions as described in the previous section.

SOIL Eh AND pH

The effects of saturation on soil Eh are shown in Fig. 7.10. Tailings have no significant effects on the Eh but there are marked differences between the soils and between water regimes. The soil x water regime interaction is significant (p> 0.001) and is caused almost solely by marked decreases in soil MC8. Only soil MC8 shows reduction in response to saturation. There was no significant reduction in soils Jaro and KS. The lack of reduction of soils during saturation is usually caused by inadequate oxidisable organic matter for microbial activity, but all the soils have organic carbon contents greater than soils which reduce to Eh values around 100 mV (Willett 1989). The lack of reduction in soils KS and Jaro is probably caused by other conditions highly unfavourable for anaerobic microbial activity. For soil KS this may be due to the stabilisation of organic matter against oxidation by complexation with Al (also see section 4.6), whereas for soil Jaro it may be caused by the extremely low pH.

The addition of tailings increases the pH of soil Jaro, as was shown in the previous experiment. Soil pH was greater in soil MC8 under saturated than unsaturated conditions as would be expected because of proton consumption during the reduction of Fe(III) to Fe(II) (Willett 1983).

The Eh and pH measurement showed that only soil MC8 underwent reduction during saturation.

TOTAL METAL CONCENTRATIONS

The effects of the tailings on total metal concentrations (Table 7.9) correspond with those of the first experiment and were described in section 7.2. These data were required again to allow calculation of the residual fractions for this experiment. Effects of saturation and drying on metal fractions will now be examined.

COPPER

The addition of tailings increases total Cu (Table 7.9). The increases correspond with increases in the oxidisable fraction and there are no significant increases in the exchangeable or reducible fractions (Fig. 7.11). This reflects the high proportion of Cu (36.5%) in the oxidisable fraction (Table 7.2) and that readily oxidisable chalcopyrite occurs in the tailings. There are no significant effects of saturated conditions on any fraction of Cu (Table 7.10). Although 15.5% of the Cu in the tailings is in the reducible fraction, and soil MC8 underwent reduction during saturation, there is no apparent mobilisation from the reducible to other fractions. This may be caused by the incorporation of any Cu that may be mobilised into Fe(III) oxides that would form upon drying of the sample.

IRON

The addition of tailings decreases exchangeable Fe, slightly (p> 0.05) increases the reducible fraction, and has no effect on the oxidisable fraction (Fig. 7.12). As proposed for the first experiment, the transformation from exchangeable to reducible forms is probably caused by the neutralising effect of the tailings on the extremely acid soil (Jaro, Fig. 7.10).

The cycle of saturation and drying increases exchangeable and reducible Fe (Table 7.10), and is entirely due to changes in soil MC8, which underwent reduction. There are no effects of saturation on Fe in the other soils, and no effects of tailings on the distribution of Fe (Fig. 7.12).

MANGANESE

Tailings increase total and all the individual fractions of Mn (Fig. 7.13). However, there are no effects of saturation on any fraction of Mn (Table 7.10). Mn reduction would be expected in soil MC8 but, in contrast to Fe, there are no detectable changes after drying.

LEAD

The addition of tailings substantially increases total Pb (Table 7.9) which corresponds with increases in oxidisable and reducible Pb, but not exchangeable Pb (Fig. 7.14). However, there are no effects of the water regime on the distribution of Pb between the fractions.

URANIUM

The addition of tailings increases total U and all its fractions (Table 7.9, Fig. 7.15). However, there are no effects of the water regime on the distribution of U between the fractions. For Pb and U it appears that if there was any effect of reduction in soil MC8 on the distribution of these elements between the fractions then they were completely reversed on oxidation during drying.

ZINC

There are no effects of tailings or water regime on Zn fractions (Table 7.9, Fig. 7.16).

RADIUM-226

The results for exchangeable ²²⁶Ra are shown in Table 7.11. There are no significant differences between the soils that were incubated under saturated or unsaturated conditions, even in soil MC8 which underwent reduction. It appears that ²²⁶Ra is not associated with Fe or Mn oxides as they go through a cycle of reductive dissolution and precipitation by oxidation.

7.5 SUMMARY

The tailings consist of angular fragments recognisable as ground ore rocks. The heavy metals are located as inclusions of minerals in silicate fragments and as minerals expected in the weathered and unweathered zones of the ore. These have survived the acid and oxidising extraction processes of the mill and appear in the tailings largely unaltered. Their preservation indicates that they are in relatively stable forms and unlikely to be readily mobilised if added to soils. Sulfides of Pb, Cu and Fe were identified and are susceptible to extraction in the oxidisable fraction. In the longer term, the metals present as sulfides may be mobilised in oxidising environments. The reducing agent extracted some Mn, Cu and Pb, probably by the dissolution of iron oxides that contain these elements, suggesting that these elements would be mobilised if added to reduced (saturated) soils.

A comparison of the total concentrations of the metals in the tailings with those of four soils of the Plain shows that the tailings are considerably higher in Mn, Pb, U and ²²⁶Ra than the soils. These metals are therefore those which would be expected to be most markedly increased if tailings are added to these soils. However, at rates of addition of 0.4% (which assumes erosion of the tailings at about the natural long-term denudation rate), only increases in total Pb and ²²⁶Ra were detectable by the methods used. Increases were readily detected at the 4% addition rate for all metals except Zn. The pollution potential of the tailings is highest for Pb and ²²⁶Ra and might be expected to increase as the total time for tailings erosion decreases. The pollution potential is lowest for Zn.

In the non-pyritic soils, the extractability of the heavy metals in the tailings does not markedly change after 4 months of aerobic incubation. In accordance with the SEM-EDX analyses, which showed that the metals occurred as stable minerals that had survived the strongly acidic and oxidative milling processes, increases in readily exchangeable and bioavailable forms of the metals that could be ascribed to the tailings are small, except for Mn. In contrast there are significant changes in metal extractability, and therefore their chemical form, in the soil undergoing pyrite oxidation. In the cases of Mn and Fe, large increases in exchangeable forms occur irrespective of tailings additions and are a direct result of pyrite oxidation. Tailings contributed to these fractions, and Mn and Fe in the tailings are mobilised in a way similar to those in the soil. Cu and U are mobilised to the exchangeable form during pyrite oxidation, and this occurred in the unamended soil as well as after the addition of tailings, and appears to be due to acidic dissolution of oxides and other minerals containing these elements. Pb is immobilised, probably by the formation of PbSO₄, and was not mobilised even under very acidic conditions.

The effects of adding tailings to the soils on the forms of the metals were generally small, and smaller than those found during pyrite oxidation. There appears to be greater potential for metal mobilisation from native sources of the metals within soil MVPA than from those added as tailings.

 226 Ra is immobilised in soils KS, Jaro and MVPA, possibly by formation of RaSO₄, but is mobilised in soil MC8. As a large proportion of the 226 Ra in soil MC8 remains in an exchangeable form it would be readily bioavailable and exchangeable with other cations.

A cycle of saturation and drying has little effect on the distribution of metals. In soils KS, Jaro and MVPA this is caused by their failure to reduce. In soil MC8 any effects on metal distribution during reduction were not studied but they appeared to be reversible on oxidation during drying.

These results apply to tailings additions of 4%. Larger additions rates would increase the effects. However, the neutralising influence of the tailings on the soils may result in lower bioavailability of the metals than may be expected from the results obtained with 4%.

Table 7.1. Summary of SEM-EDX analyses of tailings particles.

Clas	ss	Dominant elements	Sub dominant elements	Habit	Mineral	Number (out of 65)
1	a	Pb, S		Inclusions	Galena	3
1 1	b c	Pb, Cu, U Pb, S, P	P, Fe, S, V Ca, Cl	Inclusions Inclusions	Carnotite Kampylite/	2
		, -,	,		pyromorphite?	1
2		Fe, S		Particles	Pyrite	2
3		Fe, Cu, S		Inclusions and angular particles	Chalcopyrite	3
4	a	U, Th, Pb	Nd	Inclusions	Uranitite	1
4	b	U, Pb	Cu, Nd	Inclusions	Uranitite	1
4	c	U, Th	Р	Inclusions	Renardite- dewindtite	2
5		Ca, S		Small particles	Gypsum	2
6		Pb, S, Sr, Ba		Small particles	(Sulfates)	3
7	a	Fe	Mn	Small	Iron oxides	13
7	b	Fe	Mn, Cu	angular	Iron oxides	5
7	c	Fe	U, P	particles,	Iron oxides	2
7	d	Fe	Pb	a few included	Iron oxides	1
8		Ti		Small, angular particles and inclusions	Rutile	21
9		Zr		Inclusions	Zircon	3

Table 7.2. Chemical properties of Ranger Uranium Mine Tailings.

	Cu	Fe	Mn	Pb	U	Zn
Total, mg kg ⁻¹	312	36 200	3070	1144	176	55
		Means of 5	analyses (s.d.	where availa	able)	
Exchangeable, mg kg ⁻¹ % of total	<0.4 <0.1	<1 <0.003	654 (9.3) 21.3	13 (0.8) 1.1	<0.01 <0.01	<0.5 <11
Reducible, mg kg ⁻¹ % of total	47.8 (6.1) 15.3	3396 (169) 9.4	1084 (30) 35.3	802 (23.3) 70.1	18 (0.8) 10	6.1 (0.61) 11.1
Oxidisable, mg kg ⁻¹ % of total	114 (15.0) 36.5	471 (62) 1.3	13.6 (0.96) 0.4	29 (2.2) 2.5	23 (1.4)	36.6 (3.7) 66.6
Residual* mg kg-1 % of total	150 48.1	32 333 89.3	1318 42.9	300 26.2	135 77	12.3 22.4

^{*}By difference.

Table 7.3. Properties of the soils of the Magela Plain used in experiments 1 and 2.

	KS	Jaro	MVPA	MC8
pH	3.8	2.8	3.3	3.5
E.C. mS cm ⁻¹	1.6	2.7	1.6	0.44
Cl mg kg ⁻¹	138	25	29	40
EDTA-extra. S, mg kg ⁻¹	3984	5 877	3850	1394
Organic C, %	9.78	2.09	3.81	6.24
Pyrite-S, %	0	0	3.95	0
Clay %	36	64	41	49
Silt %	30	19	14	17
Fine sand %	13	10	10	14
Coarse sand %	1	4	28	2
Illite %	13 (±3)	18 (±4)	19 (±4)	6 (±1)
Kaolinite %	67 (±13)	39 (±4)	40 (±8)	68 (±1)
Smectite %	14 (±5)	37 (±9)	35 (±9)	25 (±6)
Vermiculite %	trace	0	0	0
Quartz %	1 (±1)	2 (±1)	2 (±1)	l (±1)
Alunite %	7 (±1)	0	0	< l
Jarosite %	0	4 (±1)	$3(\pm 1)$	0
CDB-Fe %	0.17	1.19	0.35	0.92
CDB-A1 %	1.03	0.35	0.06	0.25
CDB-Mn mg kg ⁻¹	33	20	35	14

Table 7.4. Effects of tailings additions on total metal concentrations (experiment 1): means of duplicates (mg kg⁻¹).

Soil	Tailings %	Cu	Fe	Mn	Pb	S	U	Zn
KS	0	33	10 400	95	12	18 300	5.0	25
KS	0.4	32	10 400	100	18	18 200	5.0	20
KS	4.0	49	11 100	160	54	18 300	11.6	29
Jaro	0	17	35 400	70	34	11 300	6.6	29
Jaro	0.4	17	35 500	70	38	10 800	6.1	29
Jaro	4.0	30	36 000	155	80	10 200	12.5	33
MVPA	0	13	43 300	230	24	15 800	4.5	39
MVPA	0.4	15	46 500	240	29	17 100	5.5	40
MVPA	4.0	19	45 700	270	58	16 800	10.5	38
MC8	0	34	22 300	65	22	2 200	3.5	23
MC8	0.4	38	23 100	70	26	2 400	4.5	24
MC8	4.0	43	23 400	140	61	2 800	10.5	24
Soil x tailings								
Significance, p<		NS	0.001	0.05	0.001	0.01	NS	NS
s.e.d.			321	9.8	1.5	3 014	-	-
								-
Soils means	0	25	28 100	115	23	11 900	4.9	29
	0.4	25	28 900	120	28	12 100	5.3	28
	4.0	35	29 100	181	63	12 000	11.3	31
Tailings main eff	ects							
Significance, p<	****	0.001	0.001	0.001	0.001	NS	0.001	NS
s.e.d.		1.9	160	5	0.8	-	0.35	-

Table 7.5. Total element concentrations in tailings in comparison with four Magela soils. Ratio (tailings:soil).

		•					
Soil	Cu	Fe	Mn	Pb	U	Zn	
KS	9.5	3.5	32.3	95.3	35.2	2.2	
Jaro	18.4	1.0	43.9	33.6	26.7	1.9	
MVPA	24.0	1.6	13.3	47.7	39.1	1.4	
MC8	9.2	0.8	47.2	52.0	50.3	2.4	

Table 7.6. Main effects of tailings on metal fractions; means of duplicates (mg kg⁻¹).

Fraction	Tailings (%)	Cu	Fe	Mn	Pb	U*	Zn
	0	1.1	1714	46	4.9	0.77	5.5
	0.4	1.2	1852	54	5.3	0.74	5.5
Exchangeable	4	1.9	1478	99	7.6	1.11	5.3
	Significance	>0.001	>0.001	>0.001	>0.001	>0.001	NS
	s.e.d.	0.09	24	0.5	0.21	0.060	
	0	0.3	2870	5.3	1.6	1.39	2.4
	0.4	0.4	2850	5.9	1.4	1.51	2.4
Reducible	4	0.6	2987	13.4	3.8	2.61	2.6
	Significance	>0.001	>0.001	>0.001	>0.001	>0.001	ns
	s.e.d.	0.07	34	0.20	0.36	0.120	-
	0	6.1	4081	10.2	9.8	2.00	5.4
	0.4	6.1	4012	10.7	11.0	2.55	5.2
Oxidisable	4	9.8	3936	11.5	13.4	5.13	5.3
	Significance	>0.001	ns	ns	ns	>0.001	ns
	s.e.d.	0.99	-	-	0.40	0.625	-

^{*}Averaged over 2 times of incubation (0 and 4 months)

Table 7.7. Main effects of time of incubation on metal fractions; means of duplicates (mg kg⁻¹).

Fraction	Time	Cu	Fe	Mn	Pb	U	Zn
	0	1.1	788	53	8.7	1.09	4.6
	1	1.3	1588	68	5.8		5.8
Exchangeable	2	1.4	1866	70	4.7		5.9
	3	1.6	2071	72	6.1		5.4
	4	1.6	2093	69	4.2	0.66	5.4
	Significance	>0.001	>0.001	>0.001	>0.001	>0.001	>0.001
	s.e.d.	0.11	31	0.7	0.26	0.049	0.17
	0	0.5	2764	7.9	4.5	2.73	3.2
	1	0.2	3026	7.6	3.5		2.7
Reducible	2	0.5	3204	6.6	2.5		2.5
	3	0.4	2552	10.7	0.5		2.0
	4	0.5	2965	8.3	0.2	0.94	1.9
	Significance	>0.001	>0.001	>0.001	>0.001	>0.001	>0.001
-	s.e.d.	0.10	43	0.26	0.46	0.010	0.17
	0	5.6	5327	22.9	10.6	4.59	5.6
	1	6.3	4316	11.9	11.5		9.8
Oxidisable	2	6.8	3603	8.2	17.1		6.4
	3	10.0	3582	5.9	7.7		2.4
	4	8.1	3219	5.0	9.9	1.86	2.2
	Significance	>0.001	>0.001	>0.001	>0.001	>0.001	>0.001
	s.e.d.	1.27	145	0.73	0.52	0.510	0.21

Table 7.8. Total and exchangeable ²²⁶Ra in tailings amended soils after 4 months of reaction; means of 2 duplicates.

Soil	No taili	²²⁶ Ra (Be	sq g ⁻¹) 4% tailin g s		
	Total	Exchangeable	Total	Exchangeable	
KS	0.09	<0.02	1.2	0.02	
Jaro	0.07	<0.02	1.9	0.13	
MVPA	0.12	< 0.02	1.6	0.06	
MC8	0.12	<0.02	1.9	0.75	

Table 7.9. Effects of tailings on total metal concentrations, experiment 2; means of duplicates (mg kg^{-1}).

	Tailings %	Cu	Fe	Mn	Pb	S	U	Zn
KS	0	34	10 400	100	13	18 200	5.8	27
KS	4	42	11 200	155	51	17 900	11.0	22
Jaro	0	20	35 800	73	36	11 100	5.5	33
Jaro	4	30	35 400	138	76	10 900	13.2	30
MC8	0	35	22 800	70	17	2 900	4.1	26
MC8	4	45	24 100	148	58	3 400	11.0	30
Soil means	0	29	23 000	81	22	10 700	5.1	28
	4	39	23 600	147	62	10 700	11.7	27
	Significance	0.001	0.001	0.001	0.001	NS	0.001	NS
	s.e.d.	1.4	120	6	0.6		0.52	-

Table 7.10. Main effects of soil saturation on metal fractions, experiment 2 (mg kg⁻¹).

		Cu	Fe	Mn	Pb	U	Zn
Exchangeable	Unsaturated	0.6	129	48	3.1	0.12	2.9
	Saturated	0.6	150	47	3.5	0.12	2.7
	Significance	NS	>0.05	NS	NS	NS	NS
Reducible	Unsaturated	0.5	2344	6.4	2.0	0.21	2.2
	Saturated	0.6	2567	6.1	1.8	0.21	2.2
	Significance	NS	>0.01	NS	NS	NS	NS
Oxidisable	Unsaturated	7.0	1816	2.2	11.6	0.77	2.1
	Saturated	7.4	1761	2.3	12.0	0.80	2.1
	Significance	NS	NS	NS	NS	NS	NS

Table 7.11. Effects on exchangeable ²²⁶Ra of saturated and unsaturated incubation of soils amended with 4% tailings; experiment 2.

Mg $(NO_3)_2$ extractable ²²⁶ Ra, (Bq g ⁻¹)								
Soil	Incubation:	Unsaturated	Saturated					
KS		0.002	0.004					
Jaro		0.19	0.23					
MC8		0.75	0.70					

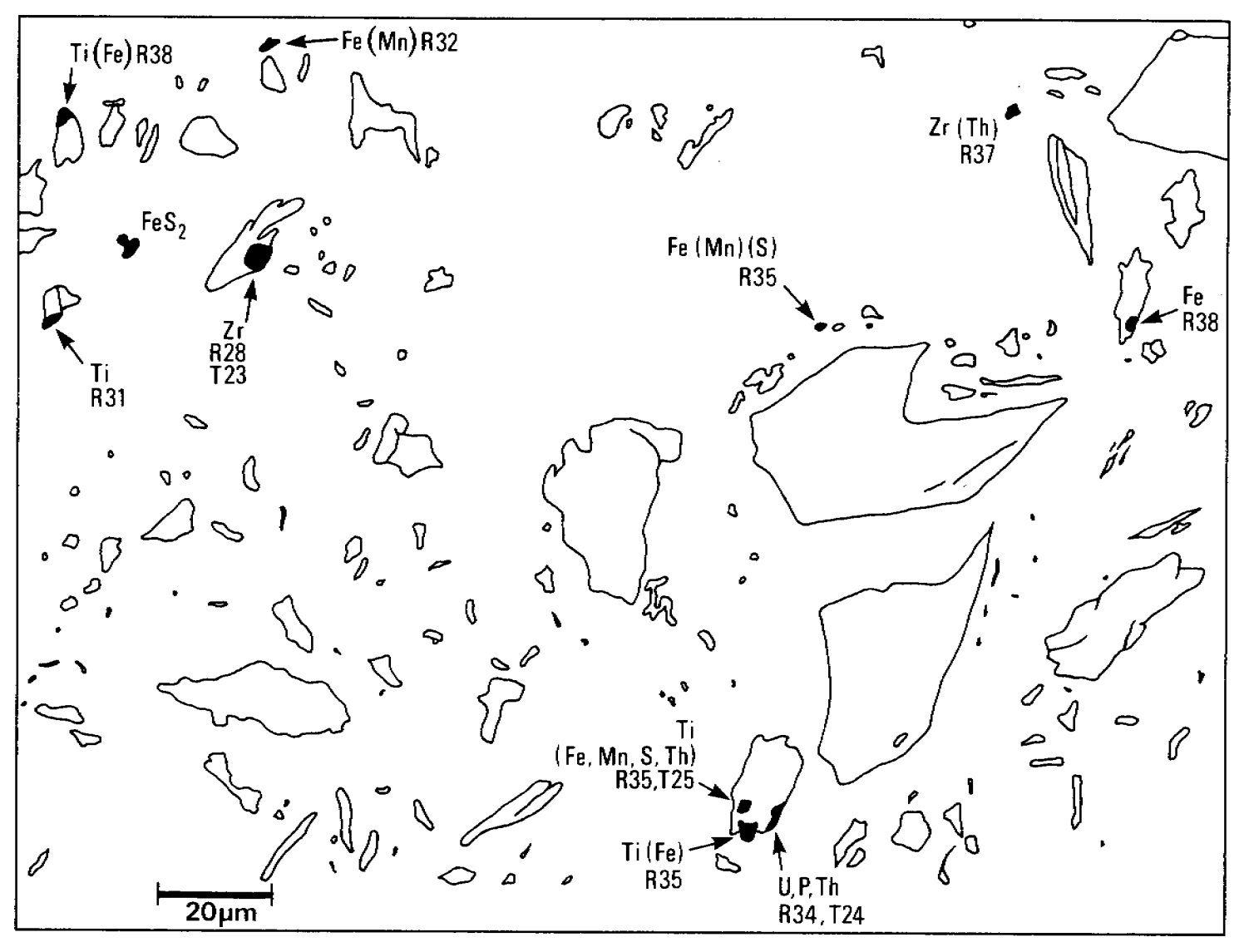


Figure 7.1 Examples of a SEM micrograph of tailings and diagram to show the distribution of dominant heavy metals determined by EDX

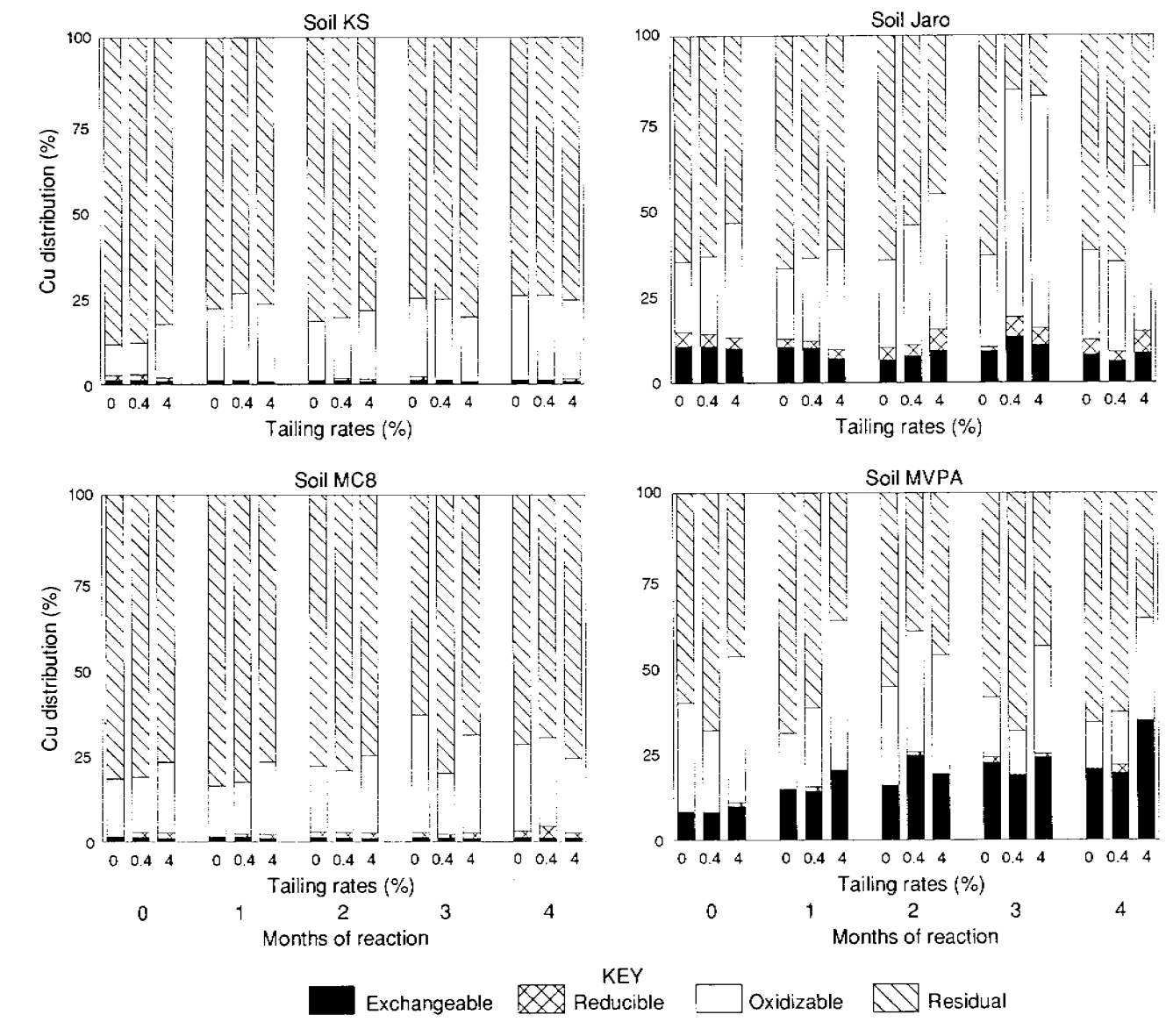


Figure 7.2 Changes in the distribution of copper fractions with time of reaction

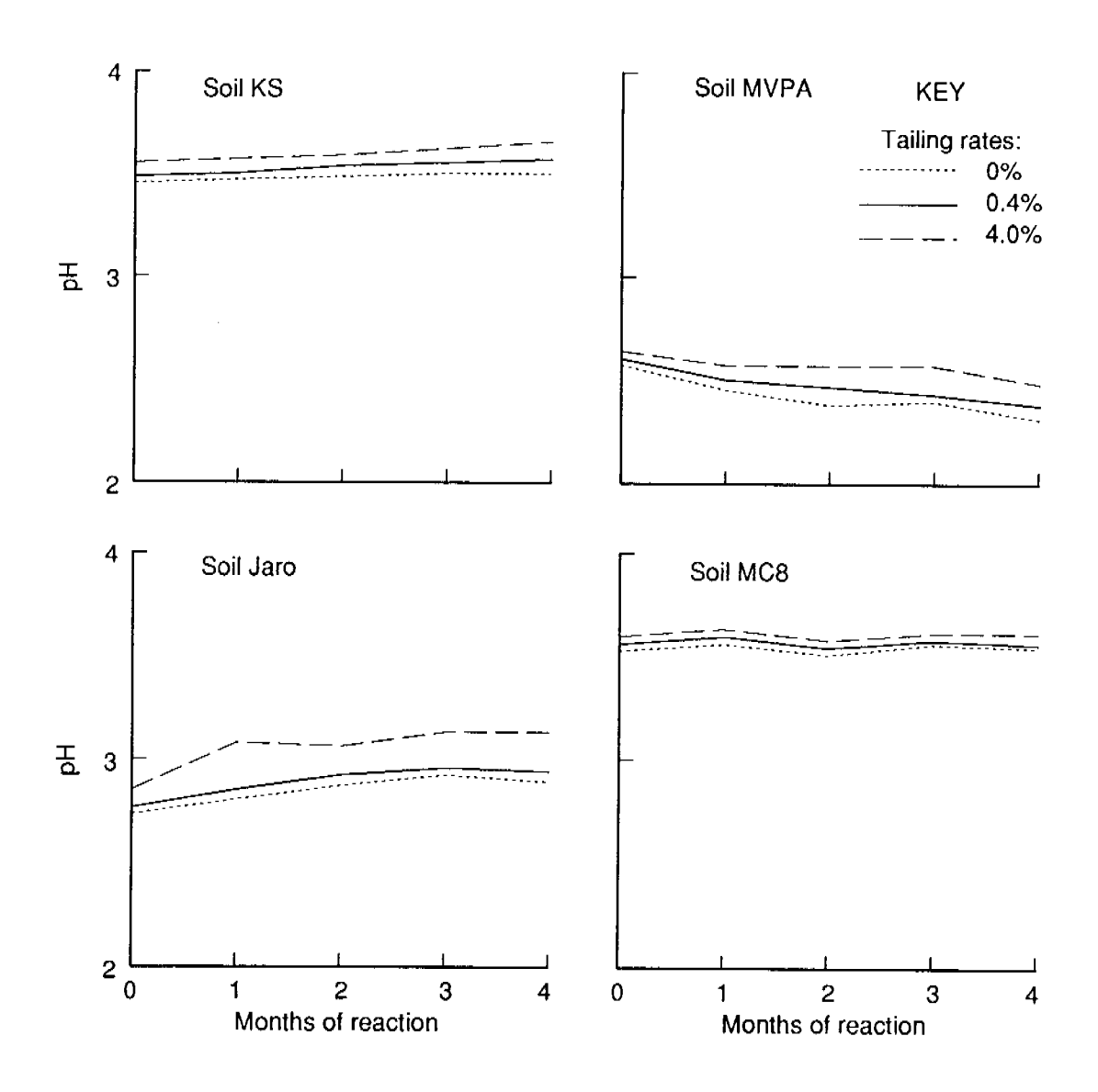


Figure 7.3 Effects of tailings on soil pH (experiment 1)

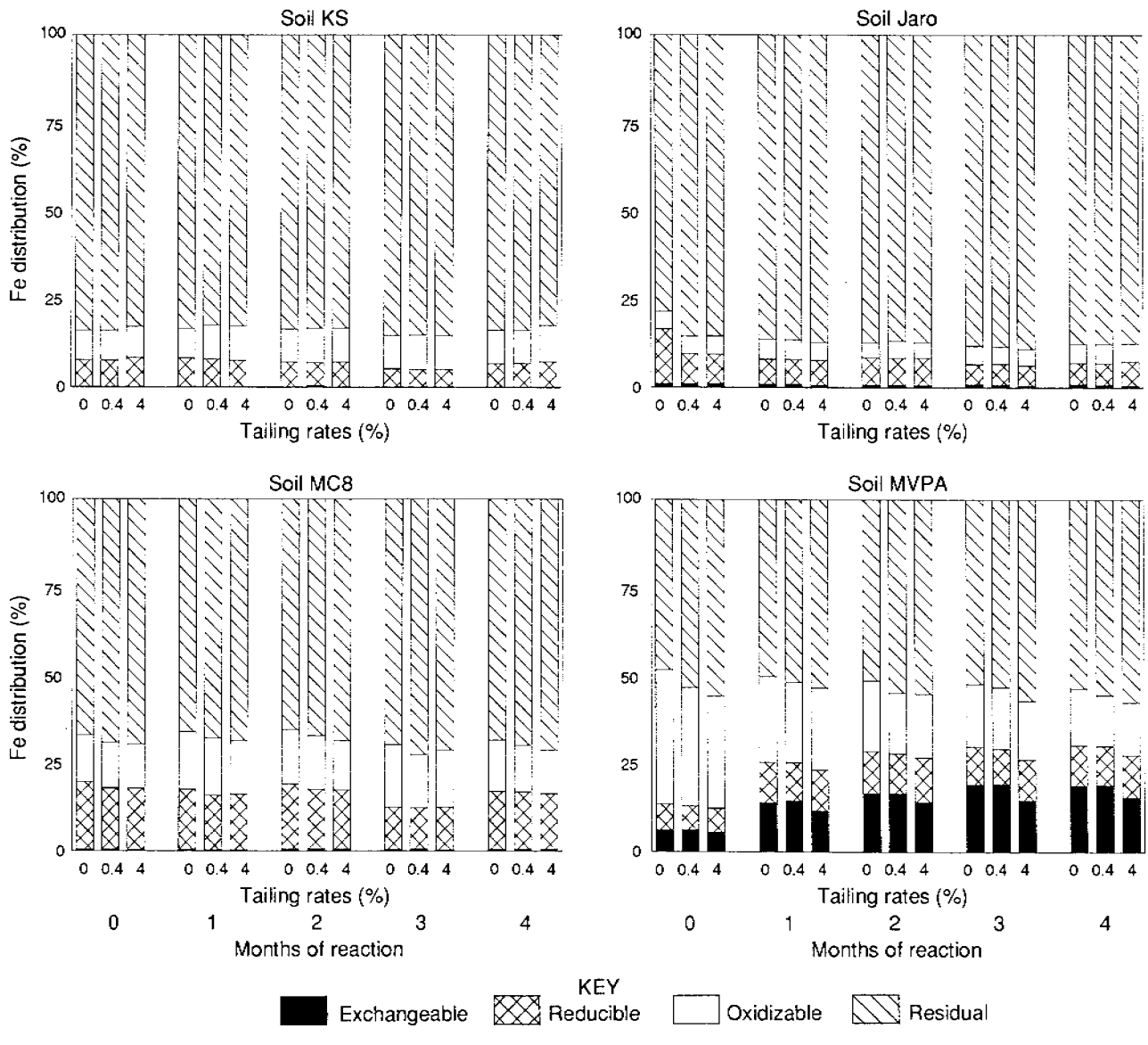


Figure 7.4 Changes in the distribution of iron fractions with time of reaction

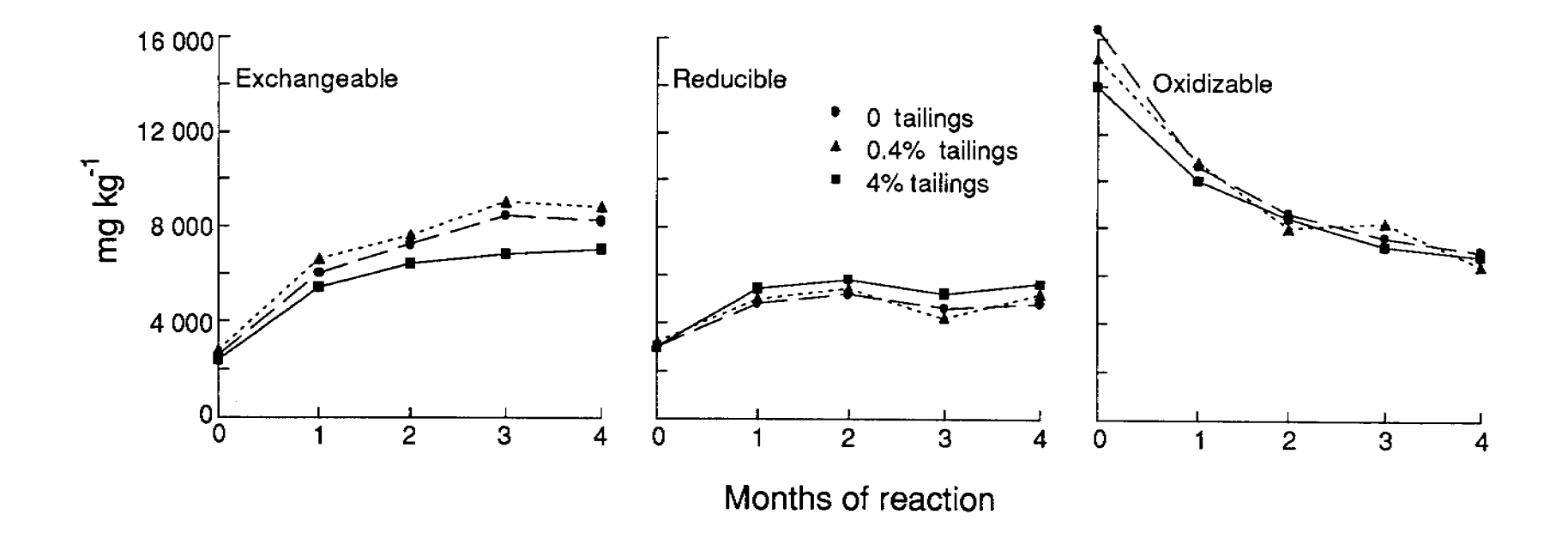


Figure 7.5 Changes in iron fractions in soil MVPA during incubation

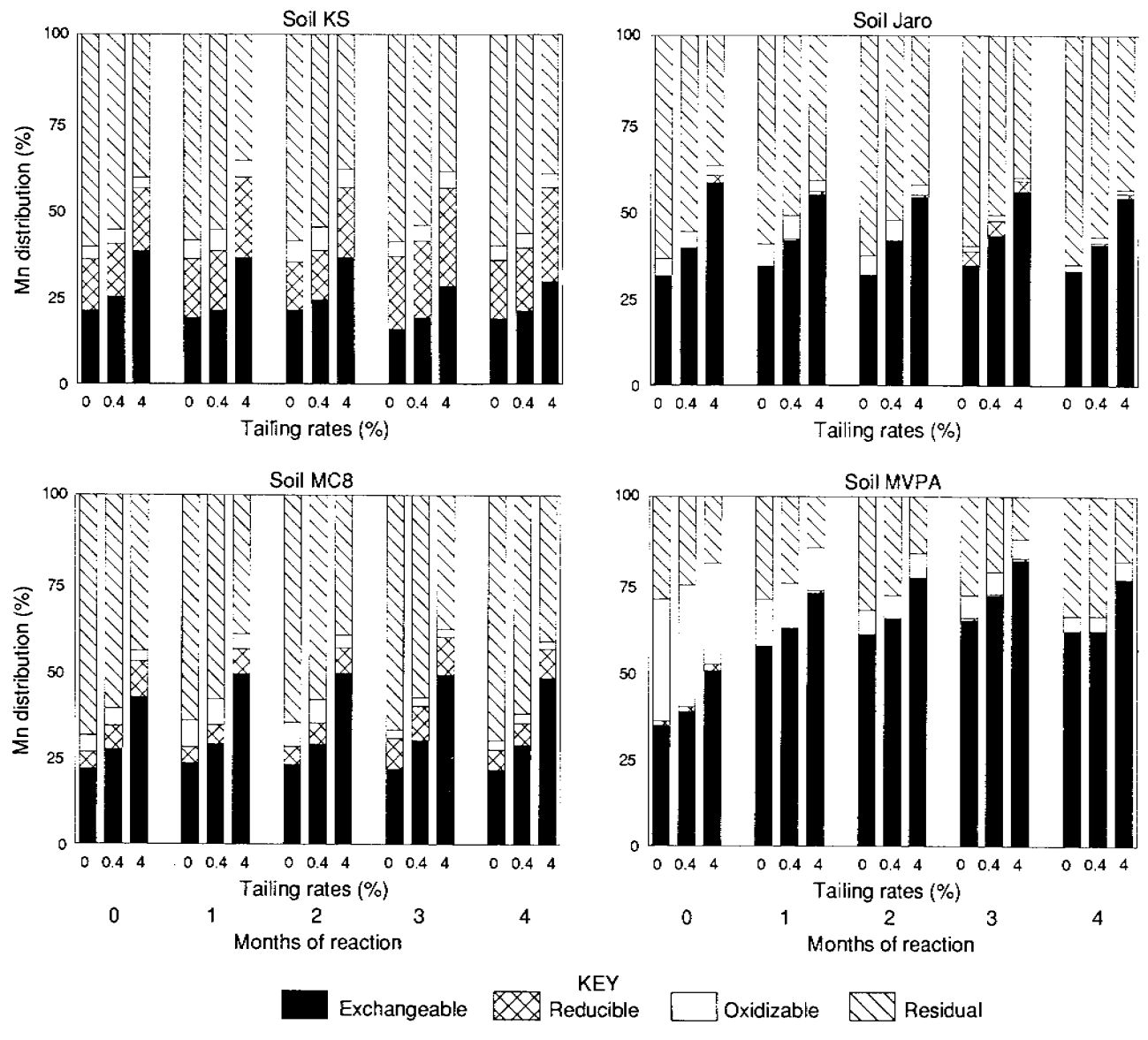


Figure 7.6 Changes in manganese fractions with time of reaction

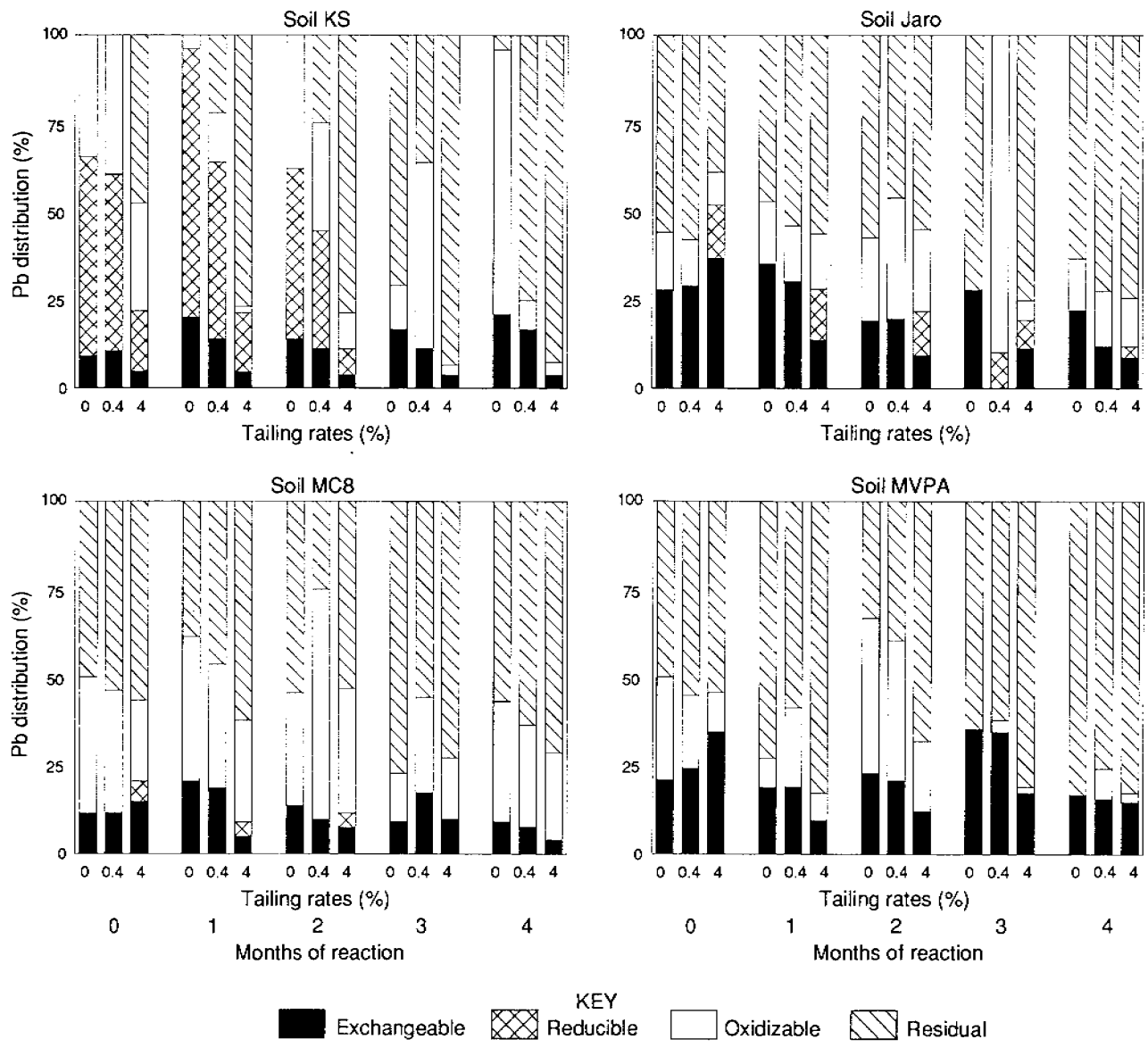


Figure 7.7 Changes in lead fractions with time of reaction

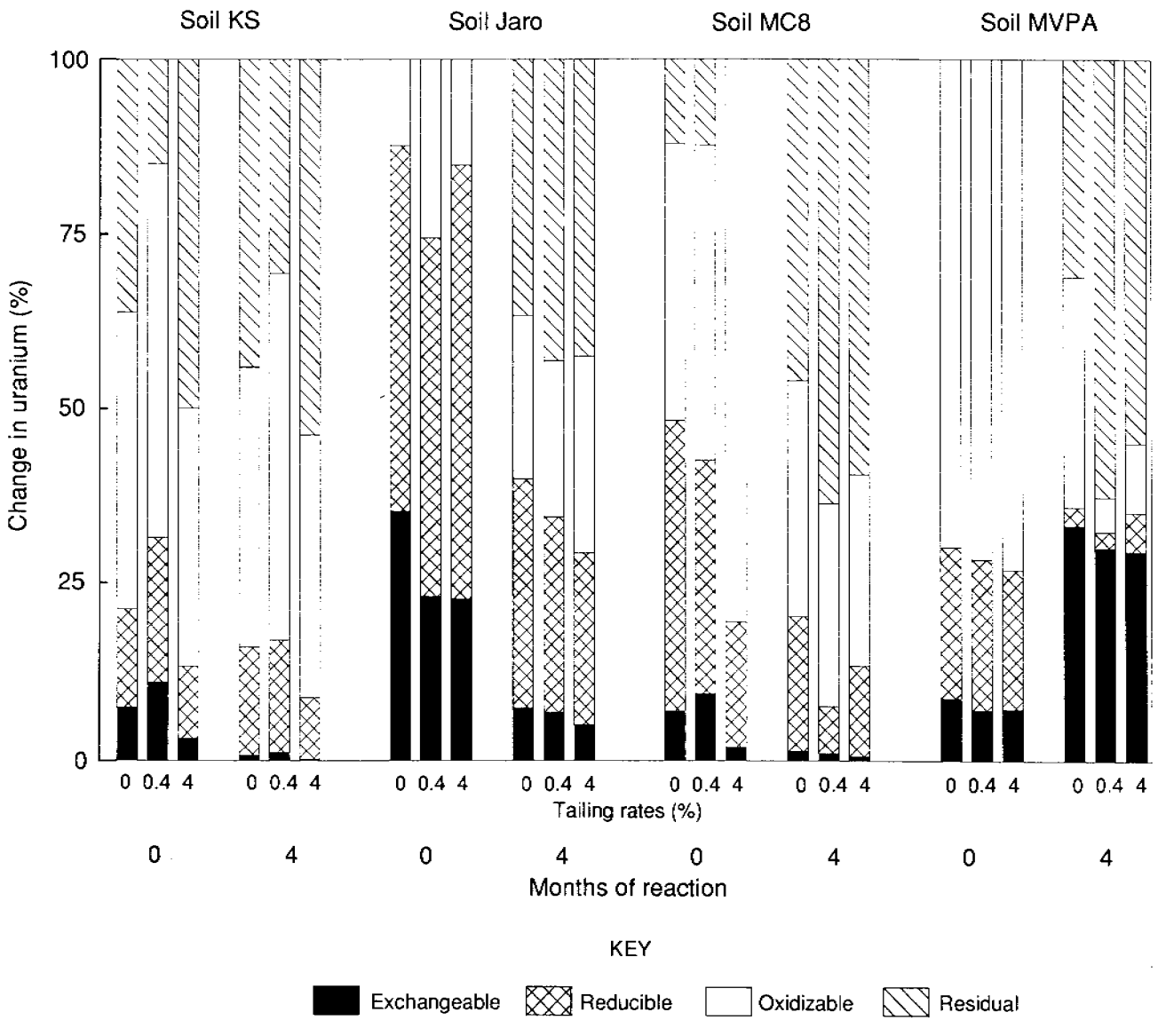


Figure 7.8 Changes in uranium fractions with time of reaction

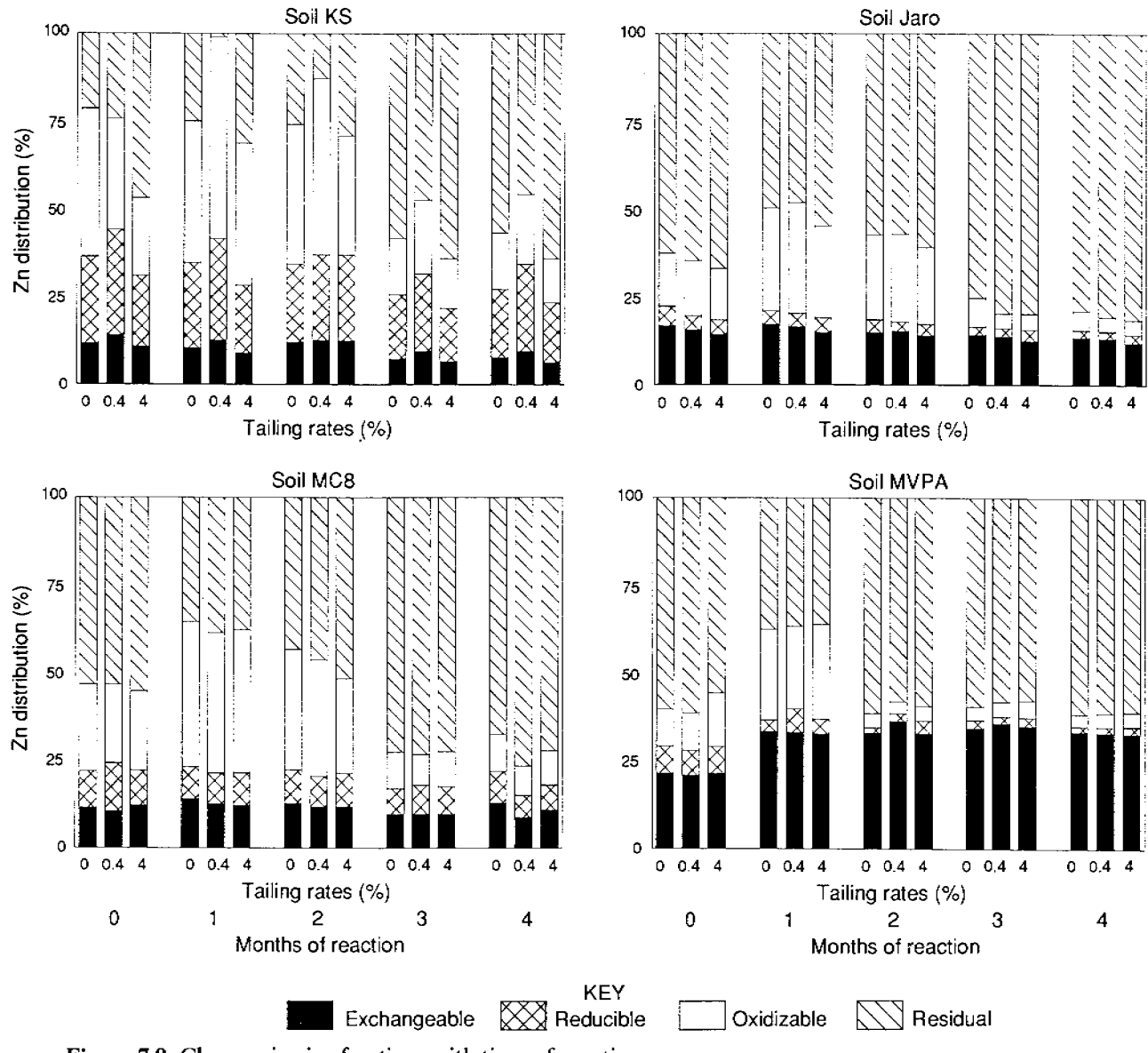


Figure 7.9 Changes in zinc fractions with time of reaction

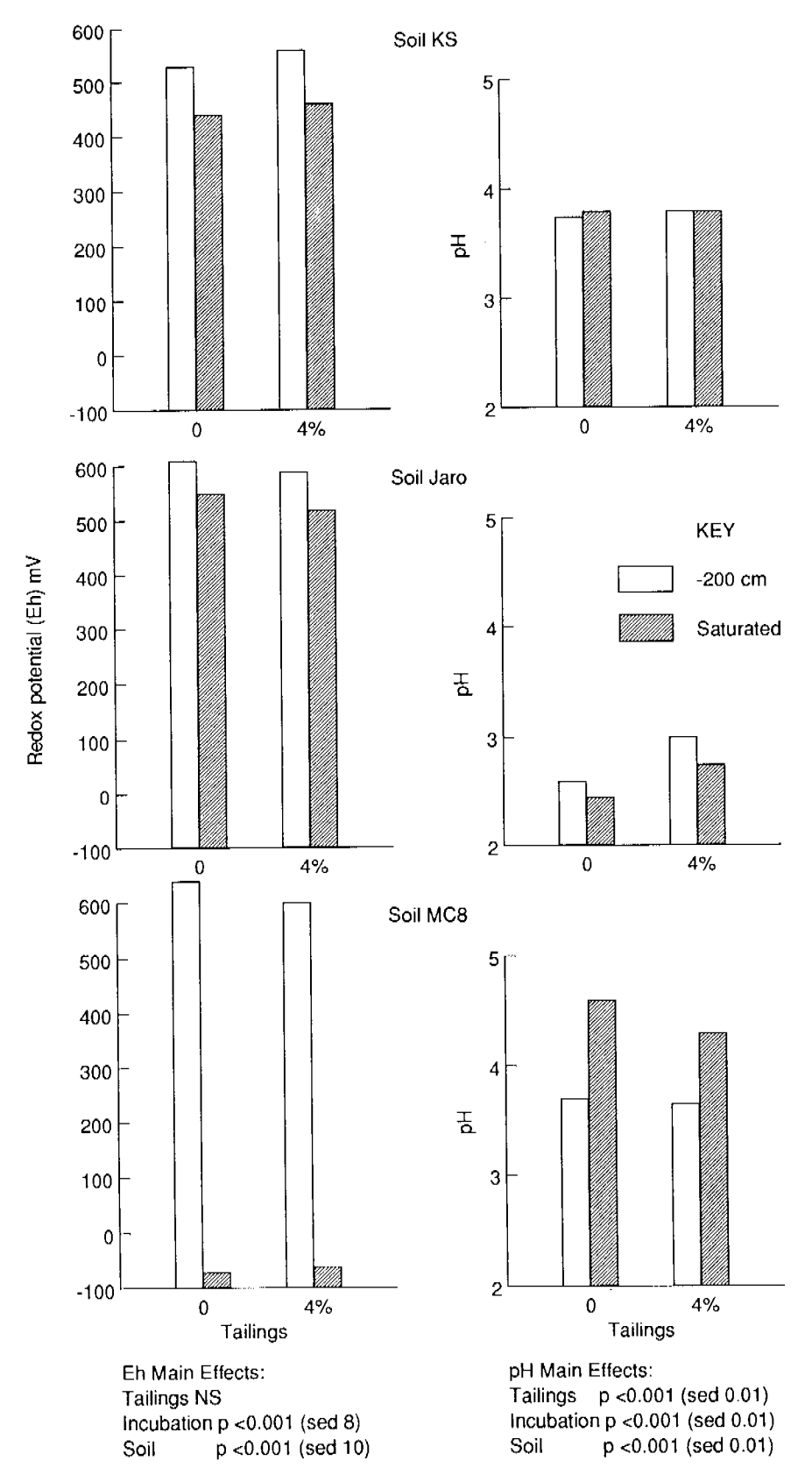


Figure 7.10 Soil redox potential and pH after 60 days of either unsaturated or saturated conditions

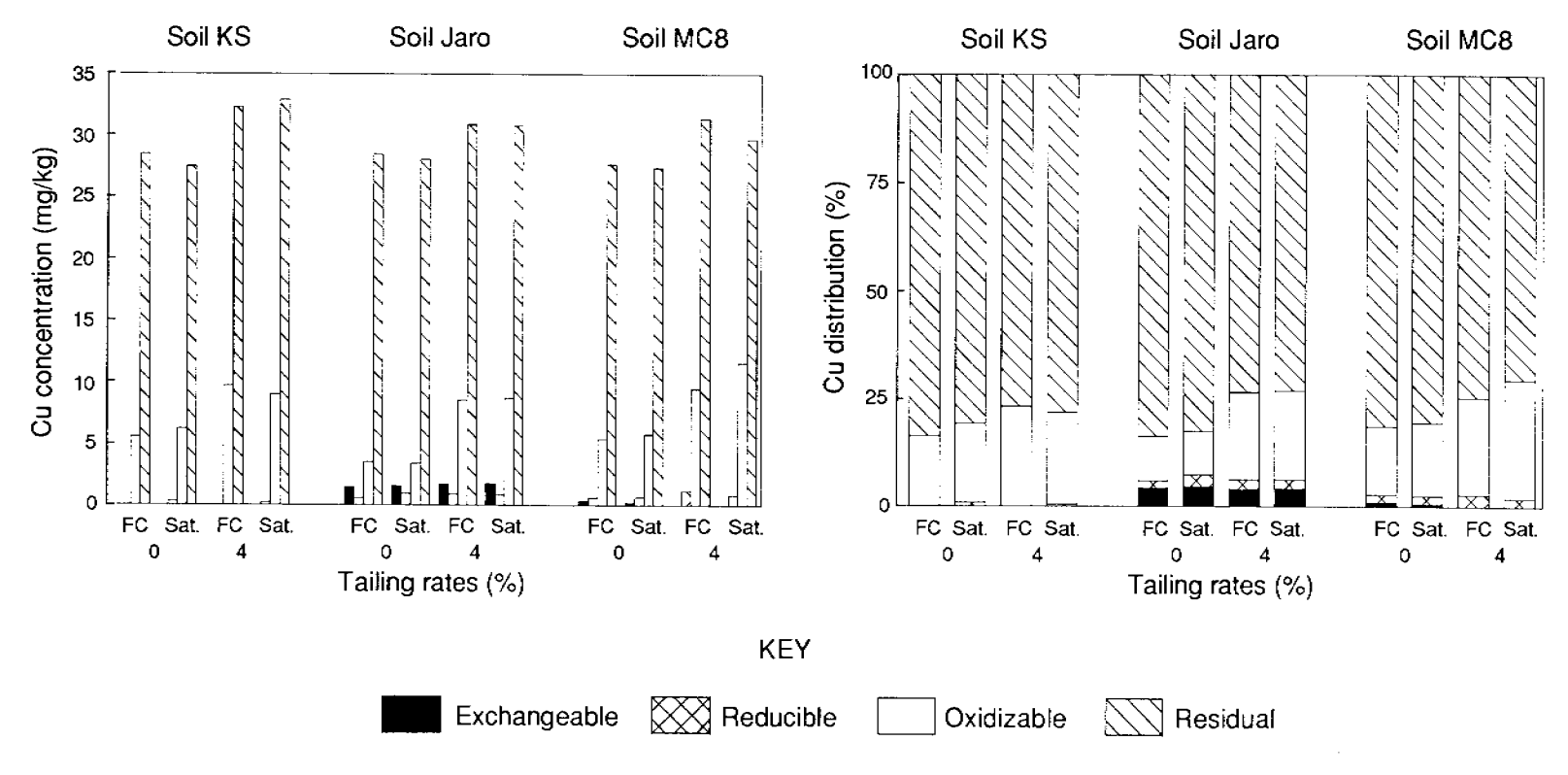


Figure 7.11 Effects of saturation on copper fractions and their distribution

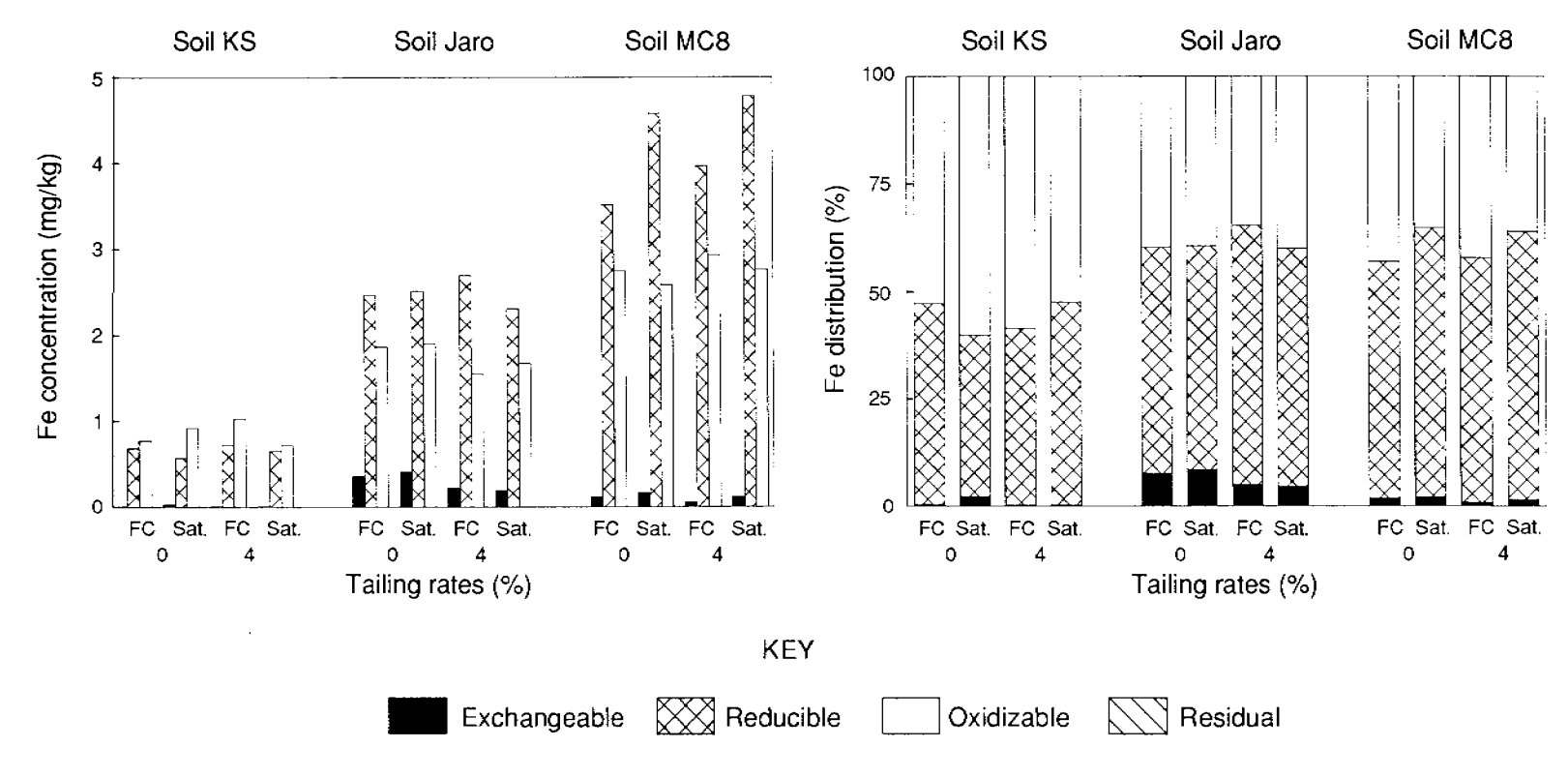


Figure 7.12 Effects of saturation on iron fractions and their distribution

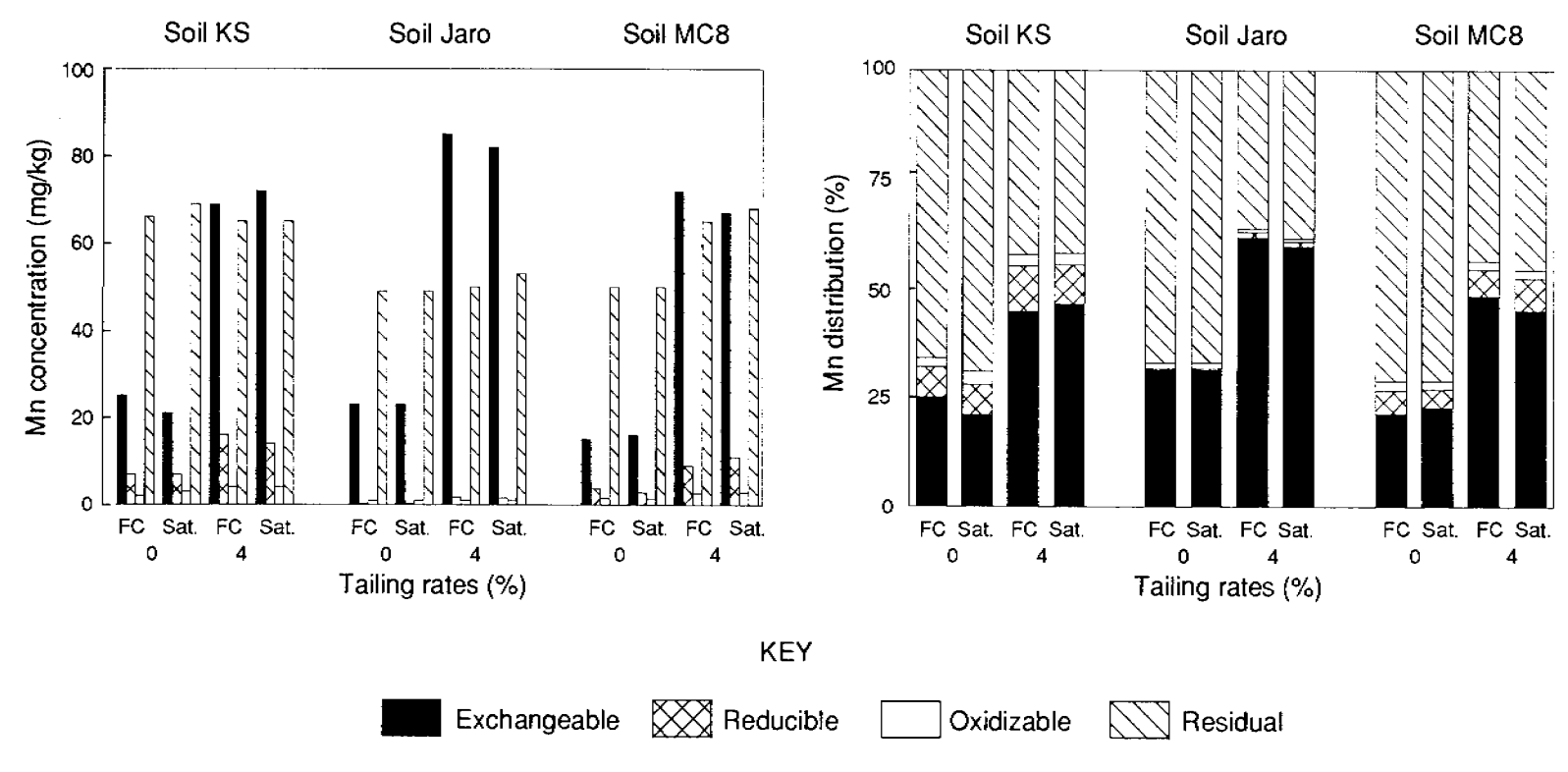


Figure 7.13 Effects of saturation on manganese fractions and their distribution

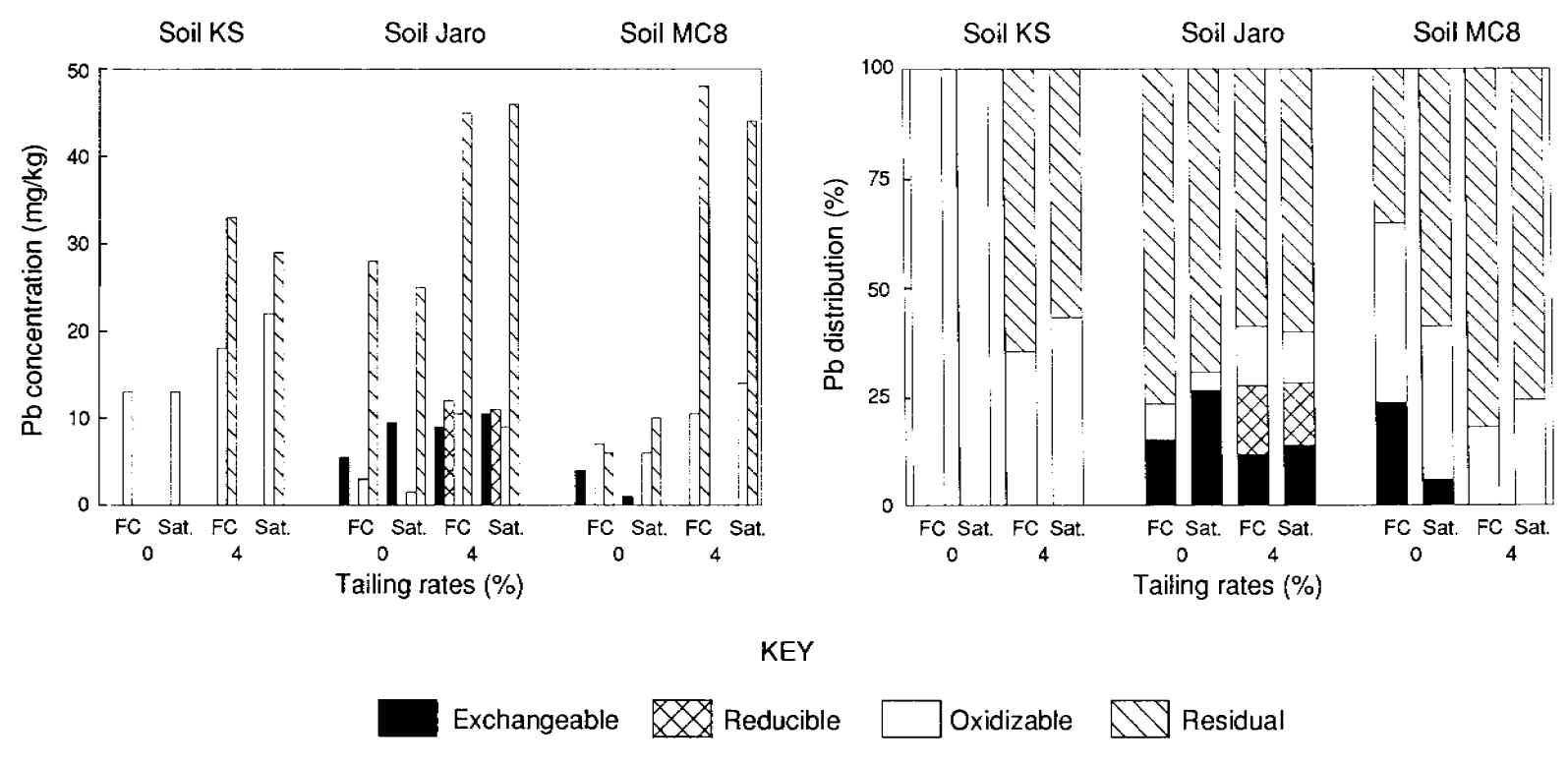


Figure 7.14 Effects of saturation on lead fractions and their distribution

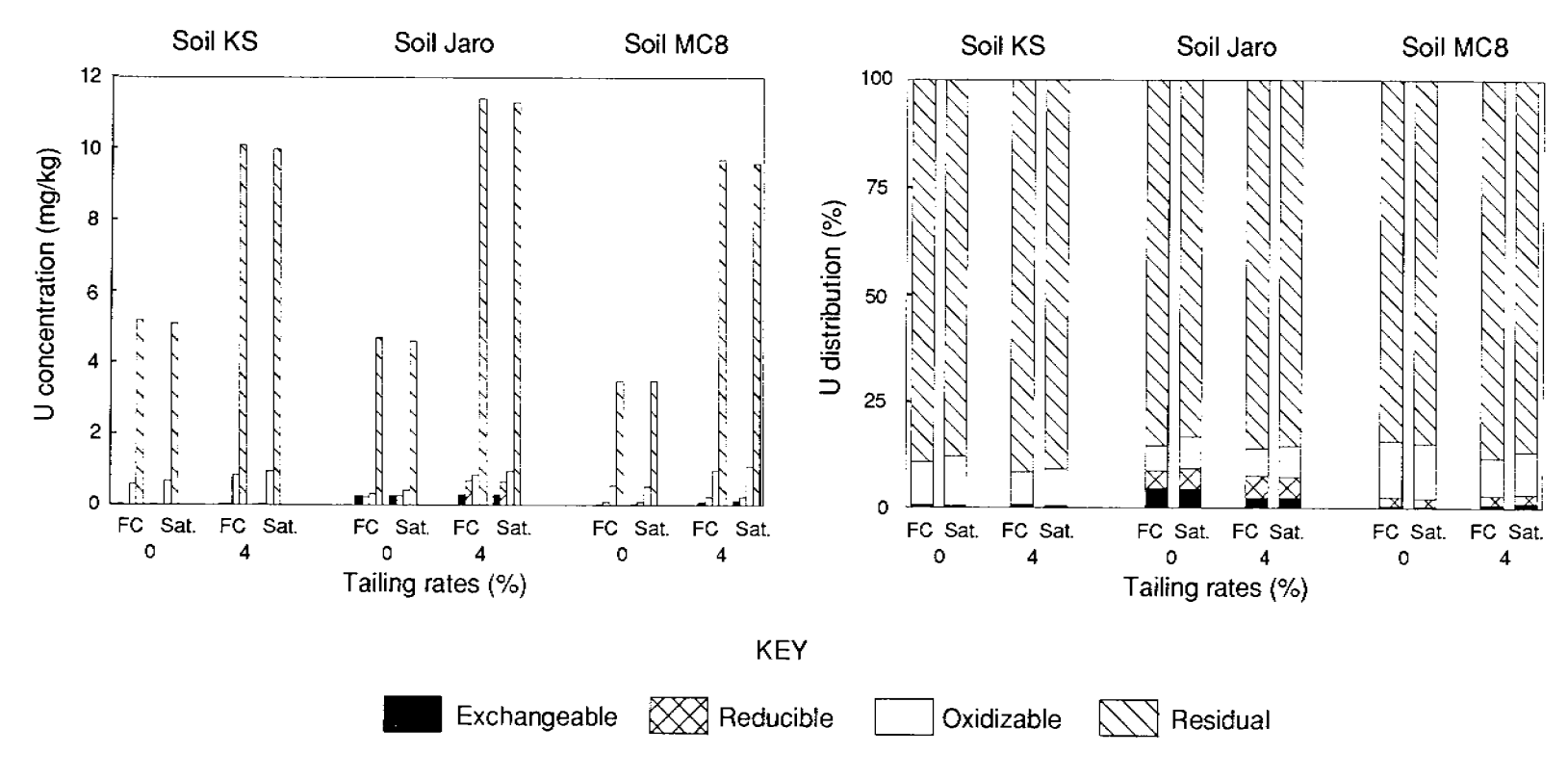


Figure 7.15 Effects of saturation on uranium fractions and their distribution

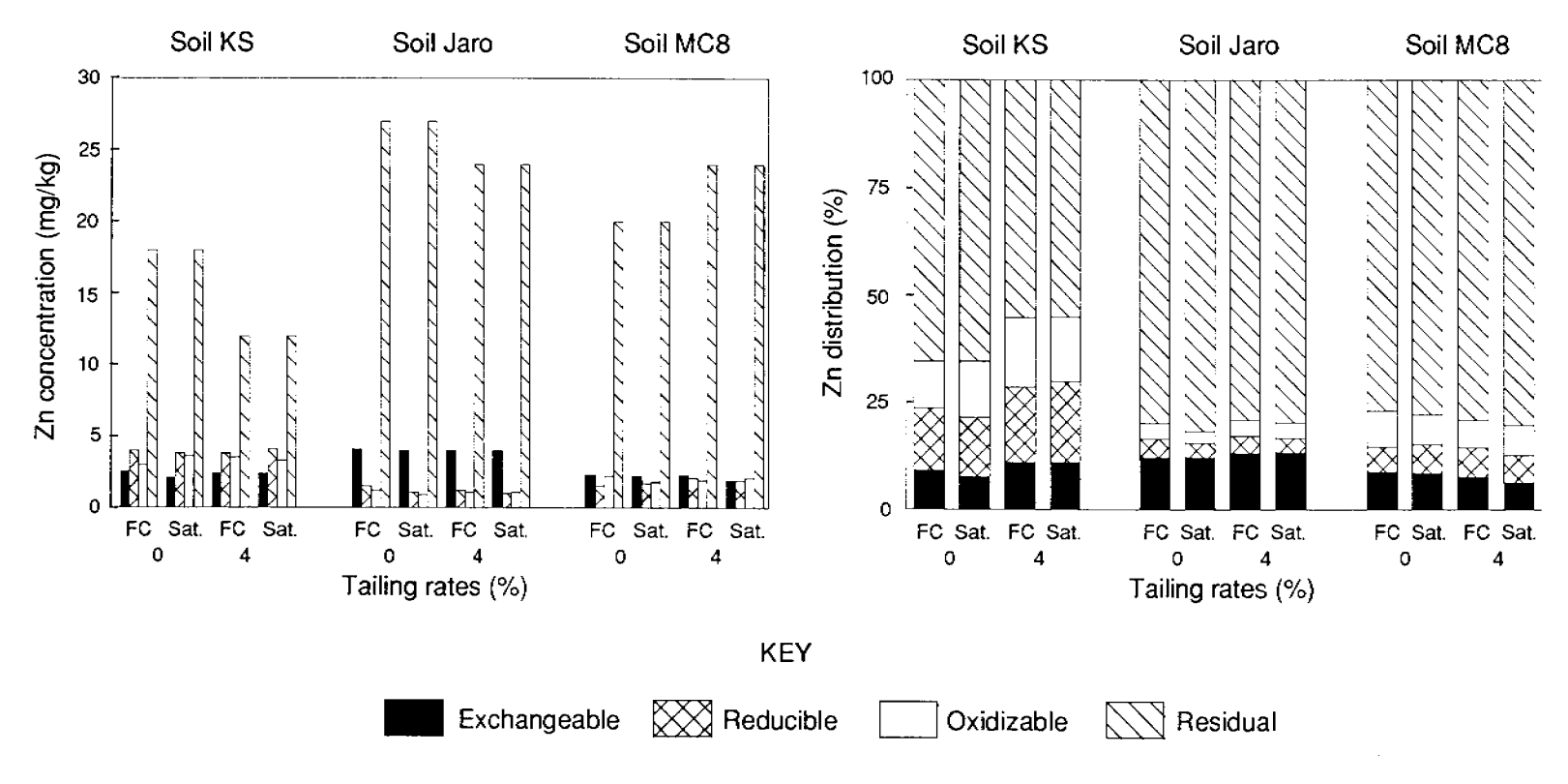


Figure 7.16 Effects of saturation on zinc fractions and their distribution

CHAPTER 8. FUTURE IMPACT ON THE MAGELA PLAIN OF SEDIMENT DERIVED FROM THE MINE SITE – SUMMARY OF MAJOR CONCLUSIONS

8.1 THE PROJECT RECONSIDERED

The summary in Chapter 1 of the background to and origins of this research project can be reduced to two questions:

- 1. Can tailings be safely stored above grade so that they have minimal impact on the Magela Plain?
- 2. Will the erosion of sediments other than tailings from the Mine Site have any serious impact on the Plain?

The second question cannot be readily answered because the nature of sources and rates of erosion on the Mine Site has not been documented. But the tools used in this report to answer the first question can eventually be used in addressing the second question.

In what follows, the major conclusions of this report will be set out. These conclusions include those bearing on the management options for the tailings and those that provide further understanding of the physical and biological environment of the Magela Plain and its catchment.

8.2 SUMMARY OF CONCLUSIONS RELEVANT TO TAILINGS MANAGEMENT

SEDIMENT ROUTING

Measurements of suspended solids at various points in the catchment and on the Plain of Magela Creek, combined with plausible simplifying assumptions about the sediment delivery system, has allowed the construction of a sediment budget and routing model (Chapter 6). This model has been used to estimate both the mass and proportion of tailings that might arrive on the Magela Plain in each average year over various time periods after erosion of the tailings has begun (section 6.9). The proportion of tailings in the mixture of sediment passing Mudginberri in each future year is a function of the total time taken to erode the tailings. At a rate close to the natural long-term denudation rate, the tailings would constitute less than 1% of the present-day level of suspended sediment passing Mudginberri. As the total erosion time decreases, the proportion of tailings in sediment reaching the Plain increases. If the total erosion time is ≤ 1800 years, then tailings will be $\geq 50\%$ of the sediment reaching the Plain.

If catastrophic erosion of the tailings were to occur, most likely as a result of an intense tropical cyclone, and all of the tailings eroded in only a few years, then the sediment delivery system would be overwhelmed and massive deposition would result. The impact of this deposition in the Plain's catchment, under conditions of either catastrophic erosion of the tailings or (more likely) slow erosion, has not been assessed.

DISTRIBUTION OF THE TAILINGS ON THE PLAIN

Various techniques were used to assess the modern pattern of sedimentation as a guide to the likely dispersal of tailings or other sediment derived from the Mine Site. The sediment budget shows that sedimentation rates on the Plain are approximately constant (section 6.3) within large uncertainties using ≤ 3 years of measured suspended sediment loads. The budget

further shows that the catchments adjacent to the Plain are of equal importance with Magela Creek as sources of sediment. The pattern of particle size fractions in surface sediments of the Plain supports the conclusion that sediments derived from Magela Creek do not dominate the Plain, although this analysis is confounded by large quantities of silt-size biogenic silica (section 6.7).

By far the most convincing demonstration of the contribution to the Plain of sediment derived from Magela Creek comes from the use of radionuclides of the natural U and Th series. Disequilibrium between ²³⁸U and ²²⁶Ra in modern stream sediments carried by Magela Creek is mirrored in the sediments of the upstream part of the Plain. The presence of disequilibrium in the surface sediments marks the area where sediment carried by Magela Creek, rather than smaller streams adjacent to the Plain, is deposited. An equation (6.5.1) was derived to calculate the proportion of Magela Creek sediment deposited on various parts of the Plain. It is clear that 90% of Magela Creek sediment is deposited upstream of Jabiluka Billabong, in an area of about 30 km², or about 15% of the Plain. The rest of the Plain's surface sediment comes from other catchments. This conclusion is consistent with the major disjunction between the upstream and downstream parts of the Plain, defined by biogenic silica and organic content of surface sediments, soil chemistry and morphology.

The equation (6.5.1) describing the depositional pattern of Magela Creek sediment in the Mudginberri Corridor and Upstream Basin, when combined with the equations (6.10.1 to 6.10.5) describing the proportions of tailings likely to arrive on the Plain, allows prediction of the pattern of tailings dispersal with different assumed times of total erosion of the tailings (Fig. 6.22).

APPLICABILITY OF THE PREDICTED DEPOSITIONAL PATTERN AND CONCENTRATION OF TAILINGS

The sediment routing model is derived from ≤ 3 years of measurements, and the radionuclide disequilibrium, upon which is based the identification of the pattern of deposition of Magela Creek sediments, has been found in sediments no more than ~140 years old. The predictions of Fig. 6.22 are likely to apply only to future conditions like those of today and the last two centuries, unless confidence in extrapolation can be gained by showing that the sedimentary system of the Plain has been stable for millennia. It has been shown in section 6.11 that the sedimentation rate over the entire Plain is approximately constant at about 0.2 mm y⁻¹ (Table 6.8). This figure holds for time periods from 0.003 to 3.3 ka, implying considerable stability within the relative uncertainties of 6 to 19%.

Extrapolation of sedimentation rates on the Plain, and application of the predicted tailings dispersal, may be appropriate for the next 1000 years, but only if sea level, climate and the sediment delivery system do not change markedly. Figure 6.22 predicts tailings dispersal for periods up to 1.4 x 10⁵ years, clearly a time period over which prediction is unrealistic.

In section 6.10, consideration was given to the most likely futures for the Plain, against which it might be possible to judge the applicability of the predicted patterns of tailings dispersal. These futures are:

1. If the Earth warms with rising atmospheric greenhouse gases, the ocean will expand and some glacial ice could melt, raising sea level by between 20 and 140 cm by about the middle of next century according to Bolin et al. (1986). At the same time, the Australian monsoon is likely to intensify, and the Wet season duration and rainfall will increase (Pearman 1988). Although by no means certain, ENSO may behave as it has during previous warm periods (section 4.7, 4.8), and so the frequency and intensity of tropical cyclones is likely to increase (Nicholls 1984a; Pittock 1989a).

Sedimentation rates on the Plain are not very sensitive to climate change, as shown by their near constancy over a wide range of time periods during which climate change has been detected. If large cyclones are more frequent, however, the tailings may be eroded more rapidly than would be the case under current conditions.

But the Plain is sensitive to changes of sea level, as shown by the detailed stratigraphic studies reported in Chapters 3 and 4. The key conclusion to emerge from this analysis is that absolute sea level is not the only factor that controls the distribution of saline vegetation and sedimentary environments. Connection to tidal channels is just as important, at least for small shifts in the level of the sea. Although not precise, the best prediction is that a sea level rise would reconnect the old tidal channels of the Downstream Plain and possibly the Central High. But it seems highly unlikely that the Upstream Plain would be connected to tidal flows. This conclusion is reached in the light of the stratigraphic results presented in Fig. 4.21, where a tidal connection persisted to Jabiluka Billabong until 2.3 ka but most of the Plain was only poorly connected to tidal flows. Furthermore, channels of different morphology are still connected from the East Alligator Flood Plain to the Central High, providing the most likely sites for renewed tidal flow. The Central High, first established between 3 and 2 ka, may offer some resistance to tidal inundation of the Upstream Basin. However, a rise of sea level of several metres, brought about by melting of ice sheets, would inundate the entire Plain.

It is important to repeat a conclusion of section 4.10. The sequence of change from mangrove forest sediments to transition conditions to freshwater sediments is not the inevitable sequence that is to be expected in reverse if sea level rises. The sequence recorded in the sediments is the combined result of a sea level rise and climate change. Estimates of future sea level rise indicate a rate between 0.06 cm y⁻¹ and 2.3 cm y⁻¹. The range 0.06 to 0.15 cm y⁻¹ seems most likely (Pittock 1989b), a rate 5 to 13 times slower than the post-glacial sea level rise of 0.8 cm y⁻¹ during the period 8-6.5 ka (see Fig. 4.20). Although the sedimentary sequence deposited on the Plain in the future will not necessarily mirror the sediments of the last 6 ka, because of differences of climate, the relatively slow rate of sea level rise will almost certainly allow time for the establishment of transition-like vegetation and sedimentary environments.

2. Within the next 5 ka the Earth should begin to feel the effects of the next glacial as small insolation variations begin the process of cooling that has repeated itself every ~ 100 ka for the last 700 ka or so. Within the next 5 ka sea level lowering, as glaciers grow, will probably be a few metres at most. It is possible that some shallow incision of the Plain could occur under these conditions, although it is not likely given the very low gradients of the area. A fall of sea level is likely to follow the super-interglacial which a doubling of atmospheric CO_2 will bring about.

Within the next 1 ka, the period during which any tailings impoundment at Ranger must retain its integrity and protect the tailings from erosion of any kind (see section 1.1), the most likely change will be the result of the Greenhouse Effect. It seems highly unlikely that the first effects of the next glacial will be felt in this period.

If global emissions of CO_2 are reduced so that the atmospheric concentration stabilises at twice its pre-industrial value, sea level will probably rise but by less than 1 m. The area of Magela Plain most likely to receive tailings, or other Mine Site detritus, namely the Upstream Plain and Mudginberri Corridor, will probably not be connected to the sea. Furthermore, this area of the Plain will be some 20 ± 13 cm higher than it is in 1000 years time as a result of freshwater sedimentation.

It can be concluded that tailings dispersal on the Plain probably will not be affected by a mild Greenhouse Effect, either by a change of sea level or by climate change directly, other than by the effect of increase cyclone activity on the total time of tailings erosion.

TRANSFORMATIONS OF METALS IN THE TAILINGS

With the currently available data, predictions have been made about the future dispersal of tailings. Following catastrophic erosion, massive deposition of tailings would cause serious problems in the Mine Site catchments for plants and animals, and would have aesthetic implications. Under the more likely conditions of slow erosion of the tailings, the most important effect on the biota will be by mobilisation of metals from tailings.

This mobilisation, or transformation, has been explored by first determining the chemical and mineralogic properties of the tailings, and then reacting under controlled conditions the tailings with the various soil materials of the Plain (Chapter 7). No experiments have been carried out with soil materials of the Mine Site catchments.

The heavy metals left in the tailings, after the extraction processes of the mill, occur as inclusions of minerals in silicate fragments and as minerals of the kind found in or near the ore bodies. These metals are in relatively stable forms and are unlikely to be readily mobilised if mixed with soil materials.

Sequential extraction of metals from the tailings showed that sulfides of Pb, Cu and Fe were mobilised in the oxidisable fraction, suggesting that, in the long term, the metals occurring as sulfides could be mobilised under oxidising conditions. The reducing agent extracted some Mn, Cu and Pb, suggesting that these elements would be mobilised if added to saturated soils.

The experiments to determine metal transformations in mixtures of tailings and soils were carried out using the major soil material types of the Plain. These materials were identified by factor analysis of soil chemical properties in Chapter 5, where their relationship with the geomorphic and sedimentary environments of the Plain was also established (Table 5.5, section 5.6). Two varieties of Dark Brown/Black Clay (soil chemistry factor 2), and one sample each of the jarositic horizon (soil chemistry factor 3), and the pyritic mud (soil chemistry factors 4 and 5, and Blue-Grey Clay) were chosen for experimentation.

These soil material types were chosen because they represent the materials most likely to be exposed to tailings under the various futures identified in section 6.10, and discussed further in this chapter. That is, the Dark Brown/Black Clay is the most likely recipient of tailings during the next 1000 years. If the level of the sea rises substantially, however, there is no material on the Plain that can represent the pedologically unaltered transition sediments that are likely to accumulate and also receive tailings. In the unlikely circumstance that sea level falls sufficiently within the next 1000 years to allow incision of the Plain, the jarositic and pyritic materials may receive tailings and so have been included in the experiments.

The tailings have concentrations of Mn, Pb, U and ²²⁶Ra higher than any of the soil materials chosen for the experiments. The soil materials are typical of their kind, as shown by analyses in Chapter 5. These metals are therefore the most likely to increase in concentration if tailings reach the Plain. Assuming that the tailings will erode at about the natural long-term denudation rate, then 0.4% of tailings will occur in each average year's load of sediment reaching the Plain. This proportion of tailings in any of the soil materials increases only the Pb and ²²⁶Ra concentration in mixtures of soil and tailings.

Assuming a total erosion time of the tailings of 5×10^4 years, a rate 3.5 times faster than the long-term natural rate, then the Plain's surface sediments should contain on average 4% tailings. All metals, apart from Zn, increased in their concentrations in the mixtures in all soil materials when 4% tailings was added. The pollution potential of the tailings is highest for Pb and 226 Ra, and lowest for Zn.

Extraction of metals from aerobically incubated mixtures of tailings and each non-pyritic soil material showed no marked changes after 4 months. Increases in readily exchangeable and bio available forms of the metals that could be ascribed to the tailings were small, except for Mn.

Pyrite oxidation appears to produce more changes to the forms of metals than the addition of tailings. There is greater potential for metal mobilisation from native sources of metals within the pyritic mud than from those added as tailings. It is concluded that, up to a concentration of 4% tailings, the effects on the forms of metals is small, and less than that found during pyrite oxidation.

Decreases in the exchangeability of ²²⁶Ra, and therefore its bioavailability, were shown when tailings were mixed with three soils from the Plain. However, it was mobilized from relatively resistant forms to the exchangeable form in soil MC8. Surface soils similar to MC8 are widespread on the upstream part of the Plain and coincide with the areas where tailings are most likely to be deposited. ²²⁶Ra is therefore most likely to be available in the upper part of the Plain, as far as Mine Valley Billabong, and its availability should decrease rapidly further downstream.

PEDOLOGIC EFFECTS OF SEA LEVEL CHANGE

If sea level rises sufficiently to re-establish tidal connections on the Downstream Plain and Central High, then it is likely that the Upstream Basin will be more poorly drained. The period of inundation of the Basin will increase, aided by a longer Wet season, and aquatic macrophytes will probably become more common.

The detailed study reported in Chapter 5 of soil materials, and the processes producing them, has shown that the acid sulfate process will only operate if the water table falls far enough to allow oxygen to penetrate to the pyritic substratum. This oxidation will be less frequent if the length of the period of inundation increases, and so the rate of chemical and mineralogic differentiation, both vertically and horizontally, will decrease.

Given that most changes to the forms and hence bioavailability of metals in soil material of the Plain occurs as a result of oxidation of pyrite, a decrease in the rate of this process will slow the release of metals to the interstitial waters. The Al content of the future part of the Dark Brown/Black Clay will probably be lower than it is in existing sediment of this unit (see Chapters 3, 4, 5).

TURBIDITY

Explicit account of turbidity has not been taken in this report but it is likely to increase, perhaps markedly, as a result of sediment transport from the Mine Site. Turbidity in the Magela Creek, lesser streams, on the Plain, and in the billabongs is generally very low (N.T. Water Division data), but rises during the Dry season in the billabongs. The biota is presumably adapted to very low turbidity, although light penetration may still be low on the Plain as a result of the dense vegetation of the Wet season. Because of this possible balancing between turbidity, vegetation and light penetration, there is a need to investigate the biologic role of turbidity in an attempt to predict the effect of an increase as a result of increased sediment loads. It is probable, however, that at the natural long-term rate of denundation the tailings would make an undetectable impact on turbidity on the Plain.

PREDICTABILITY OF CLIMATE AND EXTREME EVENTS

If an above-grade tailings impoundment were to erode at a rate similar to the natural denudation rate of the catchment, it is probable that the Plain's biota would be unaffected by tailings deposition. This is a strong argument for building the tailings impoundment to

mimic the natural landscape. To aid this aim, engineers will need sound estimates of the stationarity of climate to allow the estimation of the return period of extreme events. If climate has not been stationary during the last 1-2 ka then we might expect that it will not be stationary over the next 1 ka, especially if the controls on past climate are likely to apply in the future.

The analysis of environmental history provided in Chapter 6 shows that climate changes on a wide range of time scales. Changes over millennia are relatively slow and seem to be driven by variations of solar insolation, caused by changes in orbital geometry of the solar system, and modulated by CO_2 and the oceans. At shorter time scales, variations of solar output are important, along with volcanic eruptions and changes to oceanic circulation. While these relationships are becoming clear as research proceeds, none of them is strictly periodic and therefore predictable over the next 1000 years.

What is clear is that the next 1000 years will almost certainly include another warm period like the Medieval Warm Period, superimposed on the warming resulting from the Greenhouse Effect. It was concluded in Chapter 6 that warm periods are likely to be associated with a more positive Southern Oscillation Index and so are likely to be accompanied by more intense and frequent tropical cyclones. The calculation of the return period of intense rainstorms, caused by tropical cyclones, for the next 1000 years based upon the observations of this century is obviously a hazardous exercise in the face of the almost certain changes just predicted.

The sediments of the Plain do not hold a record of extreme events but, as noted in Chapter 6, records of cyclone frequency appear to exist on offshore islands. These should be investigated to see if, for example, cyclone frequency increased during the Medieval Warm Period. Such information could then be used as a guide to engineering design of the tailings impoundment.

8.3 CONCLUSIONS RELEVANT TO THE PHYSICAL AND BIOLOGICAL ENVIRONMENT OF THE ALLIGATOR RIVERS REGION

The most important conclusions of this report relevant to the general understanding of the natural and human history of the ARR, but not strictly relevant to the problem of sediment management, are sketched below.

AGE OF THE FRESHWATER WETLAND

Pickup et al. (1987) were able to show that the freshwater wetland of the Magela Plain is no more than 2000 years old but could be no more precise. The results reported in Chapters 3 and 4, and by Jones (1985), show that the wetland, in approximately its current form, appeared between 1500 and 1000 years BP as the influence of the post glacial sea level rise waned and the climate became slightly wetter.

The wetlands of the Magela Plain type are seen by many as pristine, affected only by the Asian water buffalo. Yet, the appearance of these wetlands appears to have been the stimulus to a dramatic increase in the population of Aborigines in the vicinity of the Magela Creek and South Alligator River, as judged from the great increase in the number of sites occupied (Jones 1985).

The wetlands provided resources for many more people who, in their turn, appear to have begun to influence the Plain by burning it, as judged from the large increase in charcoal about half-way through its history. The Asian water buffalo arrived towards the end of this rise in numbers of Aborigines. The buffalo may have been on the Magela Plain for as long as one-tenth of its history, although in large numbers for a much shorter period. The idea that a pristine and stable wetland was shocked by the arrival of water-buffaloes late in its

life is not supported by the evidence. Nor is the often quoted link between species rich ecosystems, such as the Magela Plain, and antiquity.

LINKS WITH HUMAN HISTORY

The stimulus to human population growth over the last 1 ka or so has already been described, but there is now the opportunity to make much more detailed comparisons between the history of the Plain as a source of food and natural resources, and human history recorded in archaeological sites. The work of Schrire (1982), Jones (1985) and, more recently, Brockwell (pers. comm.) represents a formidable body of archaeological data. It is also possible to check and fine-tune Chaloupka's (1985) reconstruction of the sequence of rock art in Kakadu National Park.

BIOLOGIC CHANGE

Short term observations of vegetation are valuable as guides to the palaeo-record, as shown in Chapter 4. But they cannot substitute for it. The amplitude of change to be expected over 10^2-10^3 years is not imaginable from a few years of observations. Nutrient cycling and organic matter destruction occur on a variety of time scales, most of which are greater than the few years of traditional biological observations. In Chapter 4, and in Clark and Guppy (1988), the complexity of change to the vegetation has been demonstrated, and some of the ecological principles exposed by this analysis were discussed. There is ample opportunity for further examination of these principles on the Magela Plain.

PEDOLOGY VERSUS SEDIMENTOLOGY

The study of the soils of the Plain (Chapter 5) was initially stuctured around vertical profiles as described in pits and auger/core holes. This is traditional thinking among soil scientists. But the soil chemistry is not completely interpretable unless lateral variations are taken into account. Chapter 5 ends with discussion of these lateral variations, meshed with the sedimentary facies.

As sedimentologists, geomorphologists and soil scientists cross-check each others results and prejudices (e.g. Paton 1978), soils are more and more being interpreted as parts of three-dimensional landscapes.

8.4 CONCLUDING REMARKS

This report contains approaches that can be labelled both science and engineering. The former seeks to get the best possible data, often by going to inordinate lengths and cost. The latter uses data that are either available or can be readily gathered, then makes the most plausible story from them. In reality, scientists do much the same as engineers, but stop short of drawing conclusions from inadequate data.

The sediment budget and routing model upon which so much depends in this report is one example of the engineering approach. Better data are highly unlikely to be available in the foreseeable future, so conclusions were drawn from what are available.

The principle conclusion of the report is that, if a tailings impoundment at Ranger can be designed to erode at a rate that approaches the natural long-term denudation rate of the catchment (\sim 25 t/km²/y), it is probable that the biota of the Magela Plain would be unaffected by tailings deposition. If, however, the tailings impoundment erodes at \geq 4 times the natural long-term rate, increases in the bio-available concentrations of some metals will be observable. The biological and radiological significance of these increases requires assessment.

REFERENCES

- Airey, P.L., Roman, D., Golian, C., Short, S., Nightingale, T., Lowson, R.T. & Calf, G.E. (1982-83). Radionuclide Migration around Uranium Ore Bodies Analogue of Radioactive Waste Repositories. USNRC Contract NRC-04-81-172. (a) Annual Report, AAEC Report C29, 1982. (b) Quarterly Report No. 5, AAEC Report C34, 1982. (c) Quarterly Report No. 6, AAEC Report C37, 1983.
- Allan, R.J. (1985). The Australasian summer monsoon, teleconnections and flooding in the Lake Eyre Basin. South Australian Geographical Papers. No. 2, Royal Geographical Society of Australasia (S.A. Branch) Inc, Adelaide.
- Australian Bureau of Meteorology (1961). Climatology Survey. Region 1: Darwin. Melbourne.
- Aston, A.L. & Duursma, E.K. (1973). Concentration effects on ¹³⁷Cs, ⁶⁵Zn, ⁶⁰Co and ¹⁰⁶Ru sorption by marine sediments, with geochemical implications. *Netherlands J. Sea Res.* 6, 225-40.
- Bartlein, P.J. (1988). Late-tertiary and quaternary palaeoenvironments in B. Huntley and T. Webb (eds), Vegetation History. (Handbook of Vegetation Science: 7) Kluwer Academic, Dordrecht, 113-51.
- Berger, A. (1980). The Milankovitch astronomical theory of palaeoclimates: a modern review. Vistas Astron. 24, 103-22.
- Berner, R.A. (1982). Burial of organic carbon and pyrite sulfur in the modern ocean: its geochemical and environmental significance. Am. J. Sci. 282, 451-73.
- Berner, R.A. (1984). Sedimentary pyrite formation: an update. Geochim. Cosmochim. Acta 48, 605-15.
- Berner, R.A., & Raiswell, R. (1983). Burial of organic carbon and pyrite sulfur in sediments over Phanerozoic time: a new theory. *Geochim. Cosmochim. Acta* 47, 855-62.
- Bettenay, E., Russell, W.G.R. & Mann, A.W. (1981). A description of the regolith at Jabiluka, Northern Territory. CSIRO Land Resources Management Technical Paper. No. 9.
- Bolin, B., Doos, B.R., Jager, J. & Warrick, R.A. (eds.) (1986). The Greenhouse Effect, climatic change and ecosystems. Scope 29, John Wiley, Chichester.
- Braithwaite, R.W. & Werner, P.A. (1987). The biological value of Kakadu National Park. Search 18(6), 296-301.
- Brisbin, Jr, I.L., Beyers, R.J., Dapson, R.W., Geiger, R.A., Gentry, J.B., Whitfield Gibbons, J., Smith, M.H. & Wood, S.K. (1974). Patterns of radiocaesium in the sediments of a stream channel contaminated by productive reactor effluents. *Health Physics* 27, 19-27.
- Burrows, C.J. (1979). A chronology for cool-climate episodes in the Southern Hemisphere 12 000-1000 yr BP. Paleo. Paleo. Paleo. 27, 287-347.
- Calmano, W. & Forstner, U. (1983). Chemical extraction of heavy metals in polluted river sediments in central Europe. Sci. Tot. Environ. 25, 77-90.

- Chaloupka, G. (1985). Chronological sequence of Arnhem Land plateau rock art. in R. Jones, (ed.), Archaeological Research in Kakadu National Park, ANPWS Spec. Publ. 13, 269-80.
- Chappell, J. & Grindrod, J. (1985). Pollen analysis: a key to past mangrove communities and successional changes in North Australian coastal environments. in K.N. Bardsley, J.D.S. Davie & C.D. Woodroffe, (eds), Coasts and tidal wetlands of the Australian monsoon region. North Australian Research Unit, ANU, Darwin, 225-36.
- Chartres, C.J., Walker, P.H., Willett, I.R., East, T.J., Cull, R.F., Talsma, T. & Bond, W.J. (1991). Soils and hydrology of Ranger Uranium Mine sites in relation to application of retention pond water: Technical Memorandum 34, Supervising Scientist for the Alligator Rivers Region. AGPS, Canberra.
- Christian, C.S. & Stewart, G.A. (1953). General report on survey of Katherine-Darwin Region, 1946. Land Research Series No. 1, CSIRO, Melbourne.
- Clark, R.L. & Guppy, J.C. (1988). A transition from mangrove forest to freshwater wetland in the monsoon tropics of Australia. J. Biogeogr. 15, 665-84.
- CLIMANZ (1983). Proceedings of the first CLIMANZ: a symposium of results and discussions concerned with late quarternary climatic history of Australia, New Zealand and surrounding seas. Feb, 1981. Department of Biogeography and Geomorphology, Research School of Pacific Studies, ANU, Canberra.
- Clough, B.F. (ed.) (1982). Mangrove ecosystems in Australia. Structure, function and management. Australian National University Press, Canberra.
- COHMAP Members (1988). Climatic changes of the last 18 000 years: observations and model simulations. Science 241, 1043-52.
- Damon, P.E. (1977). Solar induced variations at one AU. in O.R. White (ed.), The solar output and its variation. Colorado Associated University Press, Boulder, Colorado, 429-45.
- Davie, J.D.S. (1985). The mangrove vegetation of the South Alligator River, Northern Territory. in K.N. Bardsley, J.D.S. Davie & C.D. Woodroffe (eds), Coasts and wetlands of the Australian monsoon region. North Australian Research Unit, ANU, Darwin, 133-51.
- Deutscher, R.L., Mann, A.W. & Gibbin, A.M. (1980). Ground water geochemistry in the vicinity of the Jabiluka deposits. in J. Ferguson, & A.B. Goleby, (eds), Uranium in the Pine Creek Geosyncline, IAEA, Vienna, 477-86.
- Dowling, R.M. & McDonald, T.J. (1982). Mangrove communities of Queensland in B.F. Clough (ed.), Mangrove ecosystems in Australia. Structure, function and management. Australian National University Press, Canberra, 79-93.
- Duggan, K. (1983). Geomorphic response to development in the Alligator Rivers Region. in Environmental Protection in the Alligator Rivers Region. Scientific Workshop held at Jabiru, Northern Territory 17-20 May. Volume 1. Supervising Scientist for the Alligator Rivers Region.
- Duggan, K. (1988). Mining and erosion in the Alligator Rivers Region of northern Australia. PhD thesis, School of Earth Sciences, Macquarie University, Sydney.

- East, T.J., Cull, R.F., Murray, A.S. & Duggan, K. (1988). Fluvial dispersion of radioactive mill tailings in the seasonally-wet tropics, Northern Australia. in R.F. Warner (ed.), Fluvial geomorphology of Australia, Academic Press, Sydney, 303-20.
- Eddy, J.A. (1976). The Maunder Minimum. Science 192, 4245.
- Eddy, J.A. (1977). The case of the missing sunspots. Sci. Am. 236, 80-92.
- Eddy, J.A. (1978). Evidence for a changing sun. in J.A. Eddy (ed.), The new solar physics, Westview Press, Boulder, Colorado, 11-33.
- Enfield, D.B. (1988). Is El Nino becoming more common? Oceanogr. Mag. 1, 23-7, 59.
- Etheridge, D.M. & Morgan, V.I. (1989). The records of air temperature, ice sheet extent and atmospheric trace gas concentrations in ice cores. in T.H. Donnelly & R.J. Wasson (eds) CLIMANZ 3, Proceedings of a Symposium. CSIRO, Division of Water Resources, 107-13.
- Findlater, P.A. & White, L.A. (1984). Distribution of selected heavy metals in clay soils of the Alligator Rivers Region, Northern Territory. in J.W. McGarity, E.H. Hoult & H.B. Son (eds), The properties and utilization of cracking clay soils (Reviews in Rural Science 5), University of New England, Armidale, 261-6.
- Finlayson, C.M., Bailey, B.J. & Cowie, I.D. (1989). Macrophyte vegetation of the Magela Creek Flood Plain, Alligator Rivers Region, Northern Territory. Research Report 5, Supervising Scientist for the Alligator Rivers Region. AGPS, Canberra.
- Finlayson, C.M., Bailey, B.J., Freeland, W.J. & Fleming, M.R. (1988). Wetlands of the Northern Territory. The Conservation of Australian Wetlands. in A.J. McComb & P.S. Lake (eds). Surrey Beatty and Sons, Sydney, 103-26.
- Finlayson, C.M., Cowie, I., Bailey, B. & Armstrong, M. (1985). Recycling of nutrients and heavy metals by floodplain vegetation. Supervising Scientist for the Alligator Rivers Region Research Institute, Annual Research Summary 1984-85, AGPS, Canberra, 35-46.
- Fox, R.W., Kelleher, G.G. & Kerr, C.B. (1976). Ranger Uranium Environmental Inquiry. First Report. AGPS, Canberra.
- Fox, R.W., Kelleher, G.G. & Kerr, C.G. (1977). Ranger Uranium Environmental Inquiry, Second Report. AGPS, Canberra.
- Frye, J.C. & Willman, H.B. (1960). Classification of the Wisconsin stage in the Lake Michigan glacial lobe. Illinois State Geol. Survey Circular No. 285.
- Fujiwara, H., Jones, R. & Brockwell, S. (1985). Plant opals (phytoliths) in Kakadu archeological sites: a preliminary report. in R. Jones (ed.), Archeological research in Kakadu National Park, Australian National Parks and Wildlife Service, Canberra, 155-64.
- Galloway, R.W. (1976). Geology of the Alligator Rivers area. Lands of the Alligator Rivers Area, Northern Territory. Land Research Series No. 38, CSIRO, Australia, 50-1.
- Galloway, R.W. (1976). Geomorphology of the Alligator Rivers area. Lands of the Alligator Rivers Area. Land Research Series No. 38. CSIRO, Australia, 52-70.

- Gascoyne, M. (1982). Geochemistry of the actinides and their daughters. Uranium series disequilibrium: Applications to environmental problems. in M. Ivanovich & R.S. Harmon (eds). Clarendon Press, Oxford, 33-55.
- Goede, A. & Hitchman, M.A. (1984). Late Quaternary climatic change evidence from a Tasmanian speleotherm. in J.C. Vogel (ed.), Late Cainozoic palaeoclimates of the southern hemisphere. A.A. Balkema, Rotterdam/Boston, 221-32.
- Gribbin, J. (ed.) (1978). Climatic change. Cambridge Univ. Press, Cambridge.
- Grindrod, J. & Rhodes, E.G. (1984). Holocene sea level history of a tropical estuary: Missionary Bay, north Queensland. in B.G. Thom (ed.), Coastal geomorphology in Australia. Academic Press, Sydney. 151-78.
- Grove, J.M. (1988). The little Ice Age. Methuen, London/New York.
- Gupta, S.K. & Polach, H. (1985). Radiocarbon dating practices at ANU. ANU Radiocarbon Dating Laboratory Monograph. Australian National University, Canberra.
- Hanor, J.S. & Chan, L.H. (1977). Earth Planet. Sci. Lett. 37(2), 242-50.
- Hart, B.T. & Beckett, R. (1986). The composition of suspended particulate matter from the Magela Creek system, northern Australia. *Environ. Technol. Let.* 7, 613-24.
- Hart, B.T., Currey, N.A. & Jones, M.J. (1992). Biogeochemistry and effects of copper, manganese and zinc added to enclosures in Island Billabong, Magela Creek, northern Australia. J. Hydrobiologia. 230, 93-134.
- Hart, B.T., Davies, S.H.R. & Thomas, P.A. (1982). Transport of iron, manganese, cadmium, copper and zinc by Magela Creek, Northern Territory, Australia. *Water Res.* 16, 605-12.
- Hart, B.T. & McGregor, R.J. (1980). Limnological survey of eight billabongs in the Magela Creek catchment, Northern Territory. Aust. J. Mar. Freshwater Res. 31, 611-26.
- Hart, B.T., Ottaway, E.M. & Noller, B.N. (1986). Nutrient and trace metal fluxes in the Magela Creek system, northern Australia. *Ecol. Modelling* 31, 249-65.
- Hart, B.T., Ottaway, E.M. & Noller, B.N. (1987a). Magela Creek system, northern Australia. I. 1982-83 Wet season water quality. Aust. J. Mar. Freshwater Res. 38 (6), 261-88.
- Hart, B.T., Ottaway, E.M. & Noller, B.N. (1987b). Magela Creek system, northern Australia. H. Material budget for the floodplain. Aust. J. Mar. Freshwater Res. 38(6), 861-76.
- Hendy, C.H. & Wilson, A.T. (1968). Paleoclimatic data from speleotherms. *Nature* 219, 48-51.
- Higgins, R.J., Pickup, G. & Cloke, P.S. (1987). Estimating the transport and deposition of mining waste at Ok Tedi. in C.R. Thorne, J.C. Bathurst & R.D. Hey (eds). Sediment transport in gravel-bed rivers, John Wiley, Chichester, 949-76.
- Holmgren, G.G.S. (1967). A rapid citrate-dithionite extractable iron procedure. Soil Sci. Soc. Amer. Proc. 31, 210-11.

- Hooper, A.D.L. (1969). Soils of the Adelaide-Alligator Area. Lands of the Adelaide-Alligator Area, Northern Territory. Land Research Series No. 25, CSIRO, Melbourne, 95-113.
- Jacquez, J.A. (1972). Compartmental analysis in biology and medicine. Kinetics of distribution of tracer-labeled materials. Elsevier Publishing Company, Amsterdam/London/New York.
- Johnston, A., Murray, A.J., Marten, R., Martin, P. & Hancock, G. (1988). Measurement of sedimentation rates by thorium-radium dating. *in* Supervising Scientist for the Alligator River Region, Alligator River Region Research Institute, Annual Research Summary for 1987-1988. AGPS, Canberra, 22-3.
- Jones, R. (ed.) (1985). Archeological research in Kakadu National Park, Special Publication 13. ANPWS, Canberra.
- Jones, D.L. & Clemensha, S.C. (1981). Australian ferns and fern allies. Reed, Sydney.
- Kaufman, A. & Broeker, W.S. (1965). Comparison of ²³⁰Th and ¹⁴C ages for carbonate materials from lakes Lahontan and Bonneville. J. Geophys. Res. 70, 4039-54.
- Kershaw, A.P. & Nix, H.A. (1989). The use of bioclimatic envelopes for estimation of quantitative palaeoclimatic values in CLIMANZ 3, Proceedings of a Symposium. CSIRO, Division of Water Resources, 78-85.
- Kingston, D. (1981). Northern Territory coastal plains hydrology. Unpublished report to the Department of Transport and Works, Darwin, Northern Territory.
- Kutzbach, J.E. & Guetter, P.J. (1986). The influence of changing orbital parameters and surface boundary conditions on climate simulations for the 18 000 years. J. Atmos. Sci. 43(16), 1726-59.
- Lal, D. & Peters, B. (1967). Cosmic ray produced radioactivity on Earth. Handbuch der Physik 46(2), 551-612.
- Lalou, C. (1982). Sediments and sediment processes. in M. Ivanovich & R.S. Harmon (eds), Uranium series disequilibrium — applications to environmental problems. Clarendon, Press, Oxford, 431-58.
- Lamb, H.H. (1966). The changing climate. Methuen, London.
- Lamb, H.H. (1977). Climate: present, past and future. Volume 2, Climatic history and the future. Methuen, London.
- Landscheidt, T. (1987). Long-range forecasts of solar cycles and climatic change. in M.R. Rampino, J.E. Sanders, W.S. Newman & L.K. Konigsson (eds). Climate history, periodicity and predictability, Van Nostrand Reinhold, New York, 421-45.
- Lau, J.E. (1980). Magela Plains drilling 1980. N.T. Geological Survey Technical Report GS 80/51. Department of Mines and Energy, Darwin.
- Lees, B.G. & Clements, A.M. (1985). Implications of chenier dates in northern Australia. in E. Frankel, J.B. Keene & A.E. Waltho (eds), Recent sediments in eastern Australia: marine through terrestrial, Geological Society of Australia, NSW.

- Lees, B.G & Clements, A. (1987). Climatic implications of chenier dates in northern Australia. Radiocarbon 29(3), 311-17.
- Li, Y.H. & Chan, L.H. (1979). Desorption of BA and RA-226 from river-borne sediments in the Hudson Estuary. Earth Planet. Sci. Lett. 43(3), 343-50.
- Li, Y.H., Mathieu, G.G., Biscaye, P. & Simpson, H.J. (1977). HJ-Flux of RA-226 from estuarine and continental-shelf sediments. *Earth Planet. Sci. Lett.* 37(2), 237-41.
- Libby, L.M. (1987). Evaluation of historic climate and prediction of near-future climate from stable-isotope variations in tree rings. in M.R. Rampino, J.E. Sanders, W.S. Newman & L.K. Konigsson (eds), Climate—history, periodicity and predictability. Van Nostrand Reinhold, New York, 81-9
- Longmore, M.E. (1982). The caesium-137 dating technique and associated applications in Australia a review. in W. Ambrose & P. Duerden (eds). Archaeometry: an Australasian perspective, ANU Press, Canberra, 310-21.
- Longmore, M.E., O'Leary, B.M., Rose, C.W. & Chandica, A.L. (1983). Mapping soil erosion and accumulation with the fallout isotope. Aust. J. Soil Res. 21, 373-85.
- Lustig, L.K. (1965). Clastic sedimentation in Deep Spring Valley, California. US Geol. Survey Prof. Paper. 352-F, 131-90.
- Martin, P. & Hancock, G. (1987). Radionuclide analytical technique development. Alligator Rivers Region Research Report, 1986-87. AGPS, Canberra.
- McAlpine, J.R. (1969). Climate of the Adelaide-Alligator area. Land Research Series No. 25, CSIRO, Australia, 49-55.
- McBride, T.P. & Brady, H.T. (undated). High diatom biomas in tropical freshwater ecosystem. School of Biological Sciences, Macquarie University, N.S.W., (unpublished).
- McBride, J.L. & Nicholls, N. (1983). Seasonal relationships between Australian rainfall and the Southern Oscillation. *Mon. Weather Rev.* 111, 1998-2004.
- McDonald, N.S. & McAlpine, J. (1991). Floods and droughts the northern climate. in C.D. Haynes, M.G. Ridpath & M.A.J. Williams (eds). Monsoonal Australia. Landscape, ecology and man in the northern lowlands. Balkema, Rotterdam. 19-29.
- McKeague, J.A. Brydon, J.E. & Miles, N.M. (1971). Differentiation of forms of extractable iron and aluminium in soils. Soil Sci. Soc. Am. Proc. 35, 33-8.
- Michaelson, J. (1989). Long-period fluctuations in El Nino amplitude and frequency reconstructed from tree-rings. in D.H. Peterson (ed.), Aspects of Climate Variability in the Pacific and Western Americas, Geophysical Monograph 55, American Geophysical Union, Washington, 69-74.
- Mitchell, J.F.B. (1989). The Greenhouse effect and climate change. Rev. Geophys. 27, 115-39.
- Morgan, V.I. (1985). An Oxygen isotope U climate record from the La Dome, Antarctica. Climatic Change 7, 415-26.
- Morley, A.W. (1981). A Review of Jabiluka Environmental Studies. Report to Pancontinental Mining Limited, Volume 11.

- Murray, A.S., Caitcheon, G., Olley, H. & Crockford, H. (1990). Methods for determining the sources of sediments reaching reservoirs: targeting soil conservation. *ANCOLD Bulletin* 85, 61-70.
- Murray, A.S., Marten, R., Johnston, A. & Martin, P. (1987). Analysis for naturally occurring radionuclides at environmental concentrations by gamma spectrometry. J. Radioanal. Nucl. Chem. Articles 115(2), 263-88.
- Nanson, G.C., East, T.J., Roberts, R.G., Clark, R.L. & Murray, A. (1989). Quaternary evolution and landform stability of Magela Creek catchment near the Ranger Uranium Mine, northern Australia. Open File Record 63, Supervising Scientist for the Alligator Rivers Region.
- Needham, R.S. (1976). BMR rotary-percussion and auger drilling in the Cahill and East Alligator 1:100 000 sheet areas, Alligator Rivers Region, 1972-73. Record 1976/43, Bureau of Mineral Resources Geology and Geophysics, Canberra.
- Needham, R.S. (1984). Alligator River, Northern Territory (second edition) 1:250 000 Geological Series Explanatory Notes. AGPS, Canberra.
- Nicholls, N. (1984a). The southern oscillation, sea surface temperature and interannual fluctuations in Australian tropical cyclone activity. J. Climatol. 4, 661-70.
- Nicholls, N. (1984b). A system for predicting the onset of the north Australian wet-season. J. Climatol. 4, 425-35.
- Nicholls, N. (1985a). Impact of the southern oscillation on Australian crops. J. Climatol. 5, 553-60.
- Nicholls, N. (1985b). Predictability of interannual variations of Australian seasonal tropical cyclone activity. Mon. Weather Rev. 113(7), 1144-9.
- Nicholls, N. (1985c). The southern oscillation and Australian tropical cyclones. *Trop. Ocean Atmos. Newsl.* 29, 2+.
- Nicholls, N. (1985d). Towards the prediction of major Australian droughts. Aust. Meteorol. Mag. 33, 161-6.
- Nicholls, N. (1988). More on early ENSOs: evidence from Australian documentary sources. Bull. Amer. Meteorological Society 69, 4-6.
- Nicholls, N., McBride, J.L. & Ormerod, R.J. (1982). On predicting the onset of the Australian Wet season in Darwin. *Mon. Weather Rev.* 107, 14-17.
- Noakes, L.C. (1949). A geological reconnaissance of the Katherine-Darwin region, Northern Territory, with notes on the mineral deposits. Bulletin No. 16, Bureau of Mineral Resources Geology and Geophysics, Canberra.
- Norrish, K. & Chappell, B.W. (1977). X-ray fluorescence spectrometry. in J Zussman (ed.), Physical methods in determinative minerology, Academic Press, London 201-72.
- Northcote, K.H. (1975). A factual key for the recognition of Australian soils. Glenside, Australia.
- Northern Territory Water Division, Dept. of Transport & Water (1979-82). Uranium province hydrology, Vols 1 10 (1979), Vol 11 (1980), Vol 12 (1982), Darwin.

- Paton, T.R. (1978). The formation of soil material. Allen & Unwin, London.
- Pearman, G.I. (ed.) (1988). Greenhouse, planning for climatic change. CSIRO, Melbourne.
- Pickup, G. (1988). Hydrology and sediment models. in M.G. Anderson (ed.), Modelling geomorphic systems, John Wiley, Chichester, 153-216.
- Pickup, G., Wasson, R.J., Warner, R.F., Tongway, D. & Clark, R.L. (1987). A feasibility study of geomorphic research for the long term management of uranium mill tailings. CSIRO Division of Water Resources Research, Divisional Report 87/2, Canberra.
- Pittock, A.B. (1975). Climatic change and the patterns of variation in Australian rainfall. Search 6, 498-504.
- Pittock, A.B. (1989a). The effect of long-term climatic change on water resources, G.C. Dandy & A.R. Simpson (eds), in Proceedings of the National Workshop on Planning and Management of Water Resource Systems: Risk and Reliability. AWRC Conference Series No. 17. AGPS, Canberra, 124-40.
- Pittock, A.B. (1989b). Environment changes and their effects on natural hazards. in J. Oliver & N.R. Britton (eds). Natural hazards and reinsurance, Sterling Offices Australia Ltd. Lidcombe, NSW, 91-106.
- Pittock, A.B. (1989c). The Greenhouse Effect, regional climatic change and Australian agriculture. Preprint Volume 5th. Australian Agronomy Conference, Perth, September 1989, 289-303.
- Quinn, W.H., Neal, V.T. & Antunez de Mayolo, S. (1987). El Nino occurrence over the past four and a half centuries. J. Geophys. Res. 92(14), 449-61.
- Raiswell, R., & Berner, R.A. (1985). Pyrite formation in euxinic and semi-euxinic. Am. J. Sci. 285, 710-24.
- Rasmusson, E.M. & Carpenter, T.H. (1982). Variations in tropical sea surface wind fields associated with the southern oscillation/El Nino. Mon. Weather Rev. 110, 354-84.
- Reiger, W.A. & Olive, L.J. (1988). Channell sediment loads: comparisons and estimation. in R.F. Warner (ed.) Fluvial geomorphology of Australia, Academic Press, Sydney, 69-83.
- Ribes, E., Ribes, J.C. & Barthalot, R. (1987). Evidence for a larger sun with a slower rotation during the seventeenth century. *Nature* 326, 52-5.
- Riley, G.H. (1983). Research function of the Supervising Scientist in the Alligator Rivers Region. in Proceedings of the Scientific Workshop in the Alligator Rivers Region, paper no. 4, Supervising Scientist for the Alligator Rivers Region.
- Ritchie, H.C., McHenry, J.R. & Gill, A.C. (1972). The distribution of ¹³⁷Cs in the litter and upper 10 cm of soil under different cover types in northern Mississippi. *Health Physics* 22, 197-8.
- Röthlisberger, F. (1986). 10 000 Jahre Gletschergeshichte der Erde. Aarau, Verlag Sauerlander.
- Rovner, I. (1983). Plant opal phytolith analysis: major advances in archeobotanical research. Advance Archeol. Method & Theory 6, 225-66.

- Russell-Smith, J. (1985). A record of change: studies of Holocene vegetation history in the South Alligator Rivers Region, Northern Territory. in M.G. Ridpath & L.K. Corbett (eds), Ecology of the wet-dry Tropics, Proceedings of the Ecological Society of Australia. 13, 191-202.
- Sainty, G.R. & Jacobs, S.W.L. (1981). Water plants of New South Wales. Water Resources Commission, New South Wales, Sydney.
- Sanderson, N.T., Koontz, D.V. & Morley, A.W. (1983). The ecology of the vegetation of the Magela Creek flood plain: upper section from Oenpelli Road crossing to Nankeen Billabong. in Proceedings of the Scientific Workshop on Environment Protection in the Alligator Rivers Region, paper no. 4, Supervising Scientist for the Alligator Rivers Region.
- SAS Institute Inc. (1985). SAS users guide: statistics, Version 5 edition. SAS Institute Inc., Cary, North Carolina.
- Scherer, R.P. (1988). Freshwater diatom assemblages and ecology/palaeoecology of the Okefenokee swamp/marsh complex, Southern Georgia, U.S.A. *Diatom Res.* 3(1), 129-57.
- Schneider, S.H. & Mass, C. (1975). Volcanic dust, sunspots and temperature trends. *Science* 190, 741-6.
- Schrire, C. (1982). The Alligator Rivers: prehistory and ecology in western Arnhem Land. Terra Australis 7, Department of Prehistory, Research School of Pacific Studies, ANU, Canberra.
- Schumm, S.A. (1977). The fluvial system. Wiley, New York.
- Shen, G.T., Boyle, E.A. & Lea, D.W. (1987). Cadmium in coral as a tracer of historical upwelling and industrial fallout. *Nature* 328, 794-6.
- Shen, W. (1974). Changes in China's climate. Bull. Am. Meteorol. Soc. 55(11), 1347-50.
- Singh, G. (1981). Late Quaternary pollen records and seasonal palaeoclimates of Lake Frome, South Australia. *Hydrobiologia* 82, 419-30.
- Snelling, A.A. (1980). Uraninite and its alteration products, Koongarra uranium deposit. in J Ferguson & A. Goleby (eds), Uranium in the Pine Creek Geosyncline: Proc. Int. Uran. Symp. Pine Creek Geosyncline, CSIRO Institute Earth Resources and Bureau Mineral Resources, Geology and Geophysics, 487-98.
- Southern, R.O. (1966). A review of weather disturbances controlling the distribution of rainfall in the Darwin-Katherine region, N.T. Australian Meteorological Bureau Working Paper 65/3203.
- Stace, H.C.T., Hubble, G.D., Brewer, R., Northcote, K.H., Sleeman, J.R., Mulcahy, M.J. & Hallsworth, E.G. (1968). A handbook of Australian soils. Rellim Tech. Publ. Co., Glenside, South Australia.
- Steelink, C. (1985). Implications of elemental characteristics of humic substances. in G.R. Aiken, D.M. McKnight, R.L. Wershaw & P. McCarthy (eds), Humic substances in soil, sediment and water. Geochemistry, Isolation and Characteristics. John Wiley, New York, 457-76.

- Stephens, C.G. (1961). The soil landscapes of Australia. CSIRO Division of Soils, Soil Publication 18.
- Story, R., Galloway, R.W., McAlpine, J.R., Aldrick, J.M. & Williams, M.A.J. (1976). Lands of the Alligator Rivers area, Northern Territory. Land Research Series No. 38, CSIRO, Australia, 89-111.
- Story, R., Williams, M.A.J., Hooper, A.D.I., O'Ferral, R.E. & McAlpine, J.R. (1969). Lands of the Adelaide-Alligator area, Northern Territory. Land Research Series No. 25, CSIRO, Australia.
- Stuart-Smith, P.G. (1977). Shallow stratigraphic drilling in the Kapalga 1:100 000 sheet area, Alligator Rivers Region, NT, 1974-76. Department of National Resources, Bureau of Mineral Resources Geology and Geophysics Record 1977/53.
- Stuiver, M. (1980). Solar variability and climatic change during the current millennium. *Nature* 286, 868-71.
- Stuiver, M. & Braziunas, T.F. (1989). Atmospheric ¹⁴C and century-scale solar oscillations. *Nature* 338,405-07.
- Tanor, J.S. & Chan, L.H. (1977). Non conservative behaviour of Barium during mixing of Mississippi River and Gulf of Mexico waters. Earth Planet. Sci. Lett. 37(2), 242-50.
- Taylor, J.A. & Dunlop, C.R. (1985). Plant communities of the wet-dry tropics of Australia: the Alligator Rivers region, Northern Territory. *Proc. Ecol. Soc. Aust.* 13, 83-127.
- Taylor, J.A. & Tulloch, D. (1985). Rainfall of the wet-dry tropics: extreme events at Darwin and similarities between years during the period 1870-1983 inclusive. *Aust. J. Ecol.* 10, 281-95.
- Thomas, D.P. (1983). A limnological survey of the Alligator Rivers Region I. Diatoms (Bacillariophyceae) of the Region. Research Report 3(1), Supervising Scientist for the Alligator Rivers Region. AGPS, Canberra.
- Thompson, L.G., Mosley-Thompson, E., Dansgaard, W. & Grootes, P.M. (1986). The Little Ice Age as recorded in the stratigraphy of the tropical Quelccaya Ice Cap. Science, 234, 361-4.
- Troup, A.J. (1967). Opposition of anomalies of upper tropospheric winds at Singapore and Canton Island. Aust. Meteorol. Mag. 15, 32-7.
- Turekian, K.K.(1971). The rivers, tributaries and estuaries. in D.W. Hood (ed.), Impingement of man on the oceans. Wiley Interscience, New York 9-73.
- Turekian, K.K. & Cochran, J.K. (1978). Determination of marine chronologies using natural radionuclides. *in* J.P. Riley & R. Chester (eds) Chemical oceanography Vol 7, 2nd edition, Academic Press, London, 313-60.
- Van Breemen, N. (1982). Genesis, morphology and classification of acid sulfate soils in coastal plains. in Acid Sulfate Weathering. Soil Science Society of America, Madison, Wisconsin, 95-108.
- Vardavas, I.M. (1988). A simple water balance daily rainfall-runoff model with application to the tropical Magela Creek catchment. *Ecol. Modelling* 42, 245-64.

- Vardavas, I.M. (1989). A water budget model for the tropical Magela flood plain. *Ecol. Modelling* 45, 165-94.
- Wada, H. & Seisuwan, B. (1986). The process of pyrite formation in mangrove soils. in International Institute for Land Reclamation and Improvement, Symposium on acid sulphate soils, Dakar January 1986, ILRI publication No 44, Wageningen, 24-37
- Walker, D. (ed.) (1972). Bridge and barrier: the natural and cultural history of Torres Strait. Research School of Pacific Studies, Department of Biogeography and Geomorphology Publication BG/3, ANU, Canberra.
- Walker, P.H. (1963). A reconnaissance of soils in the Kempsey District, NSW. CSIRO Soils and Land Use Series No. 44.
- Wasson, R.J. (1986). Geomorphology and Quaternary history of the Australian continental dunefields. Geogr. Rev. Japan. 59 (Ser. B), 55-67.
- Wasson, R.J. (1989). Desert dune building, dust raising and paleoclimate in the Southern Hemisphere during the last 280 000 years. in T.H. Donnelly & R.J. Wasson (eds), Climanz 3. Proceedings of the third symposium on the Late Quaternary climatic history of Australasia, Melbourne University, 1987. CSIRO Division of Water Resources, Canberra.
- Wells, A.G. (1982). Mangrove vegetation of northern Australia. in B.F. Clough (ed.) Mangrove ecosystems in Australia: structure, function and management. Australian Institute of Marine Science and ANU Press, Canberra, 57-78.
- Wells, M.R. (1979). Soil studies in the Magela Creek catchment 1979. Land Conservation Unit, Territory Parks and Wildlife Commission, Darwin, N.T. Technical Bulletin 79/1A.
- Whitehead, B.R. & Hickey, S.H. (1980). Sediment sampling at Mayamarleprard waterhole, September 1980. N.T. Geological Survey Report GS 80/42, unpublished.
- Wigley, T.M.L. (1988). The climate of the past 10 000 years and the role of the sun. in F.R. Stephenson & A.W. Wolfendale (eds), Secular solar and geomagnetic variations in the last 10 000 years, Kluwer, Dordrecht, 209-24.
- Wigley, T.M.L. (1989). Possible climate change due to SO₂-derived cloud condensation nuclei. *Nature* 339, 365-7.
- Willett, I.R. (1983). Oxidation-reduction reactions. in Soils: An Australian Viewpoint, CSIRO Division of Soils, Melbourne. Academic Press, London, 417-26.
- Willett, I.R. (1989). Causes and prediction of changes in extractable phosphorus during flooding. Aust. J. Soil Res. 27, 45-54.
- Willett, I.R. & Beech, T.A. (1987). Determination of organic carbon in pyritic and acid sulfate soils. Communications in Soil Science and Plant Analysis 18, 715-24.
- Willett, I.R. & Walker, P.H. (1982). Soil morphology and distribution of iron and sulfur fractions in a coastal flood plain toposequence. Aust. J. Soil. Res. 20, 283-94.
- Williams, A.R. (1979). Vegetation and stream patterns as indicators of water movement on the Magela floodplain: Northern Territory. Aust. J. Ecol. 4, 239-47.

- Williams, A.R. (1984). Changes in *Melaleuca* forest density in the Magela floodplain, Northern Territory, between 1950 and 1975. Aust. J. Ecol., 9, 199-202.
- Williams, M.A.J. (1969a). Geology of the Adelaide-Alligator area. in Land Research Series No. 25, CSIRO, Melbourne, 56-70.
- Williams, M.A.J. (1969b). Geomorphology of the Adelaide-Alligator area. in Land Research Series No. 25, CSIRO, Melbourne, 71-94.
- Williams, M.A.J. (1969c). Prediction of rain splash erosion in the seasonally wet tropics. *Nature* 222, 763-5.
- Williams, M.A.J. (1973). The efficacy of creep and slope wash in tropical and temperate Australia. Aust. Geog. Stud. 11, 62-78.
- Williams, M.A.J. (1976). Erosion in the Alligator Rivers area. in Lands of the Alligator Rivers area, Land Research Series No. 38, CSIRO, Australia, 112-25.
- Williams, M.A.J. (1990). Evolution of the landscape. in C.D. Haynes, M.G. Ridpath & M.A.J. Williams (eds), Monsoonal Australia landscape, ecology and man in the northern lowlands. Balkema, Rotterdam, 5-18.
- Woodroffe, C.D., Chappell, J.M.A., Thom, B.G. & Wallensky, E. (1985a). Geomorphology of the South Alligator tidal river and plains, Northern Territory. in K.N. Bardsley, J.D.S. Davie & C.D. Woodroffe (eds). Coasts and tidal wetlands of the Australian monsoon region, North Australia Research Unit, ANU, Darwin, 3-15.
- Woodroffe, C.D., Chappell, J.M.A., Thom, B.G. & Wallensky, E. (1985b). Stratigraphy of the South Alligator tidal river and plains, Northern Territory. in K.N. Bardsley, J.D.S. Davie & C.D. Woodroffe (eds). Coasts and tidal wetlands of the Australian monsoon region. North Australia Research Unit, ANU, Darwin, 17-30.
- Woodroffe, C.D., Chappell, J.M.A., Thom, B.G. & Wallensky, E. (1986). Geomorphological dynamics and evolution of the South Alligator tidal river and plains, Northern Territory. Australian National University, North Australia Research Unit, Mangrove Monograph No. 3, Darwin.
- Woodroffe, C.D., Thom, B.G. & Chappell, J. (1985). Development of widespread mangrove swamps in mid-Holocene times in Northern Australia. *Nature* 317, 711-13.
- Woodroffe, C.D., Thom, B.G., Chappell, J., Wallensky, E., Grindrod, J. & Head, J. (1987). Relative sea level in the South Alligator River Region, North Australia, during the Holocene. Search 18, 198-200.

SUPERVISING SCIENTIST FOR THE ALLIGATOR RIVERS REGION RESEARCH PUBLICATIONS

Alligator Rivers Region Research Institute Research Report 1983-84
Alligator Rivers Region Research Institute Annual Research Summary 1984-85
Alligator Rivers Region Research Institute Annual Research Summary 1985-86
Alligator Rivers Region Research Institute Annual Research Summary 1986-87
Alligator Rivers Region Research Institute Annual Research Summary 1987-88
Alligator Rivers Region Research Institute Annual Research Summary 1988-90
Alligator Rivers Region Research Institute Annual Research Summary 1989-90
Alligator Rivers Region Research Institute Annual Research Summary 1990-91 (in press)

Research Reports (RR) and Technical Memoranda (TM)

Research Re	ports (RR) and Technical Memoranda (TM)	
RR1	The macroinvertebrates of Magela Creek, Northern Territory. April 1982 (pb, mf-46pp.)	R. Marchant
RR2	Water quality characteristics of eight billabongs in the Magela Creek catchment. December 1982 (pb, mf-60 pp.)	B.T. Hart & R.J. McGregor
RR3	A limnological survey of the Alligator Rivers Region. I. Diatoms (Bacillariophyceae) of the Region. August 1983 (pb, mf-160 pp.)	D.P. Thomas
	A limnological survey of the Alligator Rivers Region. II. Freshwater algae, exclusive of diatoms. (pb, mf-176 pp.)	H.U. Ling & P.A. Tyler
RR4	Ecological studies on the freshwater fishes of the Alligator Rivers Region, Northern Territory. Volume I. Outline of the study, summary, conclusions and recommendations. 1986 (pb, mf-63 pp.)	K.A. Bishop, S.A. Allen, D.A. Pollard & M.G. Cook
	Ecological studies on the freshwater fishes of the Alligator Rivers Region, Northern Territory. Volume II. Synecology. 1990 (pb - 155pp.)	K.A. Bishop, S.A. Allen, D.A. Pollard & M.G. Cook
	Ecological studies on the freshwater fishes of the Alligator Rivers Region, Northern Territory. Volume III. Autocology. (in press)	K.A. Bishop, S.A. Allen, D.A. Pollard & M.G. Cook
RR5	Macrophyte vegetation of the Magela Creek flood plain, Alligator Rivers Region, Northern Territory. March 1989 (pb - 41pp.)	C.M. Finlayson, B.J. Bailey & I.D. Cowie
RR6	Modern sedimentation and late Quaternary evolution of the Magela Creek plain.	R.J. Wasson
RR7	Routine analysis of naturally occurring radionuclides in environmental samples by alpha-particle spectrometry.	P. Martin & G. Hancock
RR8	Transport of naturally occurring radionuclides in the surface waters of the Magela Creek and flood plain, northern Australia. (in press)	A.S. Murray, A. Johnston, P. Martin, G. Hancock, R. Marten & J. Pfitzner

RR9	Fish communities in sandy pools of Magela Creek, Alligator Rivers Region. (in press)	D.J. Woodland & P.J. Ward
TM1	Transport of trace metals in the Magela Creek system, Northern Territory. I. Concentrations and loads of iron, manganese, cadmium, copper, lead and zinc during flood periods in the 1978-1979 Wet season. December 1981 (pb, mf-23 pp.)	B.T. Hart, S.H.R. Davies & P.A. Thomas
TM2	Transport of trace metals in the Magela Creek system, Northern Territory. II. Trace metals in the Magela Creek billabongs at the end of the 1978 Dry season. December 1981 (pb, mf-23 pp.)	S.H.R. Davies & B.T. Hart
ТМЗ	Transport of trace metals in the Magela Creek system, Northern Territory. III. Billabong sediments. December 1981 (pb, mf-24 pp.)	P.A. Thomas, S.H.R. Davies & B.T. Hart
TM4	The foraging behaviour of herons and egrets on the Magela Creek flood plain, Northern Territory. March 1982 (pb, mf-20 pp.)	H.R. Recher & R.T. Holmes
TM5	Flocculation of retention pond water. May 1982 (pb, mf-8 pp.)	B.T. Hart & R.J. McGregor
TM 6	Dietary pathways through lizards of the Alligator Rivers Region, Northern Territory. July 1984. (pb, mf-15 pp.)	C.D. James, S.R. Morton, R.W. Braithwaite & J.C. Wombey
TM7	Capacity of waters in the Magela Creek system, Northern Territory, to complex copper and cadmium. August 1984 (pb, mf-42 pp.)	B.T. Hart & S.H.R. Davies
TM8	Acute toxicity of copper and zinc to three fish species from the Alligator Rivers Region. August 1984 (pb, mf-31 pp.)	L. Baker & D. Walden
TM9	Textural characteristics and heavy metal concentrations in billabong sediments from the Magela Creek system, northern Australia. October 1984. (pb, mf-39 pp.)	P.A. Thomas & B.T. Hart
TM10	Oxidation of manganese (II) in Island Billabong water. October 1984 (pb, mf-11 pp.)	B.T. Hart & M.J. Jones
TM11	In situ experiments to determine the uptake of copper by the aquatic macrophyte Najas tenuifolia R. Br. December 1984 (pb, mf-13 pp.)	B.T. Hart, M.J. Jones & P. Breen
TM12	Use of plastic enclosures in determining the effects of heavy metals added to Gulungul Billabong. January 1985. (pb, mf-25 pp.)	B.T. Hart, M.J. Jones & P. Bek
TM 13	Fate of heavy metals in the Magela Creek system, northern Australia. I. Experiments with plastic enclosures placed in Island Billabong during the 1980 Dry season: heavy metals. May 1985. (pb, mf-46 pp.)	B.T. Hart, M.J. Jones & P. Bek
TM14	Fate of heavy metals in the Magela Creek system, northern Australia. II. Experiments with plastic enclosures placed in Island Billabong during the 1980 Dry season: limnology and phytoplankton. May 1985. (pb, mf-32 pp.)	B.T. Hart, M.J. Jones, P. Bek & J. Kessell

TM15	Use of fluorometric dye tracing to simulate dispersion of discharge from a mine site. A study of the Magela Creek system. March 1978. January 1986. (pb, mf-51 pp.)	D.I. Smith, P.C. Young & R.J. Goldberg
TM16	Diets and abundances of aquatic and semi-aquatic reptiles in the Alligator Rivers Region. July 1986. (pb, mf-57 pp.)	R. Shine
TM17	Plants of the Alligator Rivers Region, Northern Territory. August 1986. (pb, mf-54 pp.)	I.E. Cowie & C.M. Finlayson
TM18	The taxonomy and seasonal population dynamics of some Magela Creek flood plain microcrustaceans (Cladocera and Copepoda). September 1986. (pb, mf-80 pp.)	M.E. Julli
TM 19	Frogs of the Magela Creek system. January 1987. (pb, mf-46 pp.)	M.J. Tyler & G.A. Crook
TM20	Radiation exposure of members of the public resulting from operation of the Ranger Uranium Mine. December 1987. (pb, mf-22 pp.)	A. Johnston
TM21	Interlaboratory comparison of the measurement of uranium in urine. June 1988. (pb - 24 pp.)	T. Anttonen, B.N. Noller & D.A. Woods
TM22	Biology and early development of eight fish species from the Alligator Rivers Region. June 1988. (pb - 68 pp.)	W. Ivantsoff, L.E.L.M. Crowley, E. Howe & G. Semple
TM23	Alien plants in the Alligator Rivers Region, Northern Territory, Australia. September 1988. (pb - 34 pp.)	I.D. Cowie, C.M. Finlayson & B.J. Bailey
TM24	The determination of zinc in Magela Creek water. April 1989. (pb - 26 pp.)	C.A.A. leGras & B.N. Noller
TM25	Element concentrations in the freshwater mussel, Velesunio angasi, in the Alligator Rivers Region. June 1989. (pb - 262 pp.)	H.E. Allison & R.D. Simpson
TM26	A simple computer model for terrestrial and solar radiation transfer. August 1989 (pb - 60 pp.)	I.M. Vardavas & L.M. Cannon
TM27	Annual rainfall statistics for stations in the Top End of Australia: normal and log-normal distribution analysis. (in press)	I.M. Vardavas
TM28	A study of the reproducibility of water conditions between small enclosures and a tropical waterbody. November 1989. (pb - 20 pp.)	B.N. Noller, T.P. McBride, C.W. Hunt & B.T. Hart
TM29	Concentration of radon and radon daughters during semi-dry tailings deposition by QML at Nabarlek (1985-88) December 1989. (pb - 35 pp.)	D.A. Woods
TM30	The development of a regulatory mechanism for the control of water release from Ranger Uranium Mine. June 1990. (pb - 31 pp.)	M.W. Carter
TM31	Investigation of the erosional stability of waste rock dumps under simulated rainfall: a proposal. December 1990 (pb - 56 pp.)	S.J. Riley & T.J. East
TM32	The terrestrial and semiaquatic reptiles (Lacertilia, Serpentes) of the Magela Creek region, Northern Territory. November 1990. (pb - 86 pp.)	R.A. Sadlier
TM33	In vitro dissolution of uranium mill products by the batch replacement method. February 1991 (pb - 24 pp.)	D.R. Stockwell,

		K.W. Bentley & C.B. Kerr
TM34	Soils and hydrology of Ranger Uranium Mine sites in relation to application of retention pond water. October 1991 (pb - 69 pp.)	C.J. Chartres, P.H. Walker, I.R. Willett, T.J. East, R.F. Cull, T. Talsma & W.J. Bond
TM35	The determination of low concentrations of sodium, potassium, magnesium, calcium and strontium in natural waters by graphite furnace AAS. December 1991. (pb - 18 pp.)	C.A.A. leGras & B.N. Noller
TM36	Heavy metals in waterbirds from the Magela Creek flood plain, Alligator Rivers Region, Northern Territory, Australia. February 1992. (pb - 59 pp.)	K.G. Brennan, B.N. Noller, C. leGras, S.R. Morton & P.L. Dostine
TM37	Isolation and culture of five species of freshwater algae from the Alligator Rivers Region, Northern Territory. (in press)	A. Padovan
TM38	Radiotoxicity hazard classification: the basis and development of a new list. (in press)	M.W. Carter, P. Burns & L. Munslow-Davies
TM39	Toxic effects of cyanide on aquatic animals of the Alligator Rivers Region. (in press)	G.D. Rippon, C.A. leGras, R.V. Hyne & P.J. Cusbert